Effects of ageing on the vulnerability of the substantia nigra pars compacta dopaminergic neurons: implications in Parkinson's disease

Yolanda Gómez Gálvez

Doctor of Philosophy in Neuroscience

March 2020

Keele University

Dedicated to my grandmother Carmen

ABSTRACT

The degeneration of dopaminergic neurons (DAn) in the midbrain substantia nigra pars compacta (SNpc) is a definitive feature of Parkinson's disease (PD). Although age has been established as one of the main risk factors, the role that ageing has in the development of the disease is not yet fully understood. The aim of this Thesis, therefore, was to enhance our understanding of how ageing may increase the vulnerability of SNpc DAn.

To achieve this aim, isobaric tags for relative and absolute quantitation (iTRAQ) labelling combined with liquid chromatography tandem mass spectrometry (LC-MS/MS) was used to quantitatively compare the SNpc proteome of rats during ageing. Western blot and immunofluorescence analyses were subsequently conducted to verify some of the differentially expressed proteins from the analysis (e.g., GFAP), while immunohistochemistry analyses were performed to quantitatively and morphologically characterize the DAn of the rat SNpc themselves during ageing. From a total of 1,953 proteins that were identified and quantified in the proteomic study, the expression levels of 66 proteins were altered throughout ageing. Bioinformatic analysis revealed that proteins related to glial cells (e.g., GFAP) and the extracellular matrix (ECM) were differentially expressed in the old rat SNpc. Importantly, an unusual form of the GFAP protein (i.e., GFAPδ) was showed for the first time to be differentially expressed during ageing. In addition to this, the level of tyrosine hydroxylase (TH) expression in the SNpc throughout ageing was maintained. This was somewhat surprising as it appears that, independent of the proteomic changes, there was a general decrease in the density of rat SNpc DAn together with an increase of their soma size with ageing, which might indicate that the remaining DAn are able to maintain the level of tyrosine hydroxylase (TH) expression in the SNpc throughout ageing.

These results were followed by an *in vitro* investigation of the role astrocytes play in the vulnerability of DAn. To do this, primary cultures of embryonic DAn were challenged with the toxin 6-hydroxidopamine (6-OHDA) after reducing the number of astrocytes in the

cultures in a unique way (i.e., by using the anti-mitotic drug paclitaxel). Though the anti-mitotic drug was successful in reducing astrocytes in the cultures, it was difficult to test the effect this had on combating the effects of 6-OHDA on DAn because the toxin also affected the viability of the remaining astrocytes in culture.

Lastly, multiple multi-study proteomic comparisons of published studies on the ageing nervous system and PD demonstrated that metabolism, oxidation-reduction mechanisms, mitochondrial function and immune system were biological processes and pathways enriched in both ageing and PD. Because some of these biological processes were the same as those found differentially expressed in the proteomics study of ageing conducted here, this support the idea that they may be key toward understanding how ageing is involved in the development of PD.

In conclusion, this Thesis showed that ageing alters the metabolic support associated with mitochondrial and oxidation-reduction functions (as it happens in PD) and suggests that this might have considerable repercussions on highly reactive oxygen species (ROS) sensitive neurons such as SNpc DAn. Adding to this, the alteration of proteins related to glial cells (e.g., astrocytes) might affect their protective function in the SNpc during a time when they are become even more essential to the survival of DAn.

TABLE OF CONTENTS

LIST OF FIGURES AND TABLES

CHAPTER 1: GENERAL INTRODUCTION

Figures

CHAPTER 2: MATERIALS AND METHODS

Figures

Tables

CHAPTER 3: A QUANTITATIVE PROTEOMICS ASSESSMENT OF THE AGED SNpc IN RATS

Figures

Tables

CHAPTER 4: QUANTITATIVE AND MORPHOLOGICAL CHARACTERIZATION OF THE SNpc DAn IN RATS AND HUMANS DURING AGEING

Figures

Tables

CHAPTER 6: MULTI-STUDY PROTEOMICS ANALYSES OF THE AGEING AND PD NERVOUS SYSTEM

Figures

Tables

ACKNOWLEDGEMENTS

This PhD has given me the opportunity to live for four years doing something I've always wanted to do: use my brain in a scientific and creative way and be surrounded by people from all around the world. During this period, I've learnt a lot academically, but most importantly personally. Moving to another country with a culture so different to mine was a real challenge. However, I'm very happy to have made that decision, because along the way I've met many beautiful and interesting people.

This journey wouldn't have been possible without my supervisors, Dr. Monte Gates and Dr. Heidi Fuller, who gave me the opportunity to start this PhD. – Thank you so much for sharing with me all your knowledge, for having patience teaching me all the new techniques (especially proteomics!), and for always respecting and considering my personal life.

I would like to thank the wonderful people who worked with me in Professor Javier Fernández Ruiz' lab. Especially, I'm extremely thankful to Dr. María Concepcion García García and Dr. Cristina Palomo Garo, for always supervising and teaching me with a lot of love. – ¡Mil gracias!

My start at Keele would have been much more difficult without the unconditional help of Dr. George Joseph, who gave me the warmest welcome and was always there to help me with the microscope and all my technophobic problems – ευχαριστώ!

I also thank Dr. Tim Goodman, for all the discussions and help in the lab; Dr. Jacqueline Tickle who was always willing to help me whenever I needed it; and Sally L. Shirran and Silvia Synowsky for the mass spectrometry analysis of my samples.

I'm very grateful to David for all the beers after work at crazy hours, the long political conversations, and for simply bringing me a sense of Spain.

For my climbing people, especially to Dave and Nick, I've got no words to explain how much they helped me in recent months and how happy and free I feel around them. – I'm not sure if I had finished this Thesis without going crazy without you, guys! Thank you so much for bringing me to the crags, pushing me to climb harder, and always trying to put a smile on my face!

I want to thank Michele for her positivism, her energy, and all her hugs. – Meeting you is one of the best things that happened to me in Stoke and, without a doubt, you are an incredible example for me.

For being the best office ever (award included), full of brilliant and proactive women, I would like to thank Aina, Emma, Farhana and Jess. The end of my PhD wouldn't be the same without their support, encouragement and inspiration. – I've learnt a lot from all of you, especially about how important it is for women to cooperate with each other and how strong we become when we do it! I hope Catia has the opportunity to learn from you as much as I did.

Once of my deepest gratitude goes to Chris and his family, for sharing his life, thoughts and emotions with me, for taking care of me during a long period of time (I know sometimes it wasn't easy), and for helping me grow and discover my calm side. – Thank you for always being there, even now.

To my second family (Ana, Cybil, Tania and Victor), the family I chose, there probably aren't enough important events in my life to say how much I love you and how lucky I feel for having you as the best friends in the entire world. – Gracias por estar siempre ahí y por quererme tanto aun estando lejos.

Lastly, my greatest thank you go to my family. My sisters (awesome badass women!), Lara and Sandra, for both being an example of improvement, and demonstrating to me that we can achieve whatever we decide. My Dad, for working so hard all his life to give me a better future and always being so proud of me. My Mum, for teaching me that curiosity and education are the most powerful weapons, for bringing me up to become an independent person. I wouldn't be the same without all those values – ¡Millones de gracias! Os quiero mucho.

ABBREVIATIONS

aa: amino acids

AA: ascorbic acid

AD: Alzheimer's disease

ANOVA: Analysis of Variance

AraC: arabinosylcytosine C

BBB: blood-brain barrier

CNS: Central Nervous System

CSF: cerebrospinal fluid

DAn: dopaminergic neurons

DAPI: 4'-6-diamidino-2-phenylindole

DAVID: Database for Annotation, Visualization and Integrated Discovery

DDA: data: data-dependent acquisition

DIA: data-independent acquisition

DOPAL: 3,4-dihydroxyphenylacetaldehyde

DRG: dorsal root ganglion

DIV: days *in vitro*

DMSO: dimethyl sulfoxide

ESI: electrospray ionization

ECM: extracellular matrix

FDR: false discovery rate

FA: formic acid

GDNF: glial cell line-derived neurotrophic factor

GFAP: glial fibrillary acidic protein

GO: Gene Ontology

ICAT: isotope-coded affinity tags

iTRAQ: isobaric tags for relative and absolute quantitation

KEGG: Kyoto Encyclopaedia of Genes and Genomes

LC: liquid chromatography

LCM: laser capture microdissection

MALDI: matrix-assisted laser desorption/ionization

MPTP: 1-methyl-1-4-phenyl-1-1,2,3,6-tetrahydropyridine

MAO-B: monoamine oxidase B

MRI: magnetic resonance imaging

mtDNA: mitochondrial DNA

MW: molecular weight

m/z: mass-to-charge

NM: neuromelanin

O.D.: optical density

PCR: polymerase chain reaction

PD: Parkinson’s disease

PINK1: PTEN-induced putative kinase 1

ROS: reactive oxygen species

RPLC: reversed-phase liquid chromatography

TMT: tandem mass tag

SCX: strong cation exchange

SDS: sodium dodecyl sulfate

SILAC: stable isotope labeling of amino acids in cell culture

SNpc: substantia nigra pars compacta

STRING: Search Tool for the Retrieval of Interacting Genes/Protein

TBS: tris-buffered saline

TH: tyrosine hydroxylase

UPS: ubiquitin proteasome system

VM: ventromedial

VTA: ventral tegmental area

SDS-PAGE: sodium dodecyl sulfate polyacrylamide gel electrophoresis

6-OHDA: 6-hydroxydopamine

Chapter 1.
General introduction

CHAPTER 1: GENERAL INTRODUCTION

OVERVIEW: Parkinson's disease (PD) is the second most common age-related neurodegenerative disease after Alzheimer's disease (AD) (Shulman *et al.*, 2011; Sulzer and Surmeier, 2013; Ascherio and Schwarzschild, 2016; Poewe *et al*., 2017). Understanding the mechanisms behind its occurrence and progression has proven difficult. Therefore, the aim of this Thesis is to understand why the incidence of PD increases with ageing. To achieve that, the region of the brain that degenerates with PD (i.e., the substantia nigra pars compacta, SNpc) will be examined at the cellular and protein level in rats during ageing, using a cutting-edge proteomics approach and other traditional techniques (e.g., immunohistochemistry, immunoblotting). In this General introduction, I will first review the literature related to what characterises PD, including its epidemiology and etiology, its symptoms, its neuropathological features (at anatomical, cellular and molecular level), and the available therapies (section 1.1). Following this, this chapter will provide a review with the main characteristics of dopaminergic neurons (DAn) in the SNpc and the similarities and differences to other DAn within the brain (section 1.2). Subsequently, the relationship between PD and ageing will be reviewed, focusing in the similarities between both processes (section 1.3). Lastly, to illustrate my knowledge on the proteomics technique used in this Thesis, the background information of this approach will be discussed, including its advantages and limitations for neuroscience studies (section 1.4).

1.1. What is Parkinson's disease (PD)?

1.1.1 The epidemiology and etiology of PD: ageing as the principal risk factor

Ageing is considered the main risk factor in PD, affecting more 1.5% of the population over 85 years old, as recently documented in a systematic analysis by the Global Burden of Disease Study 2016, which analyzed 127 epidemiological studies related to PD between 1990 and 2016 (GBD 2016 Parkinson's Disease Collaborators, 2018). They observed that PD was rare before 50 years old, increasing its prevalence around 1.5%

after 85 years of age. Similarly, a systematic review and meta-analysis using 112 studies of the prevalence of PD, including 47 door-to-door survey and random population sample from different regions (i.e., Asia, Europe, Australia, South America and North America), observed an increase of the prevalence from 41 per 100,000 individuals between 40 to 49 years, to 428 per 100,000 between 60 to 69 years, and 1,087 per 100,000 between 70 to 79 years (Pringsheim *et al*., 2014). Individual studies in European countries have revealed similar trends. For instance, an observational study between 2012 and 2018 using the data from different French PD expert centers found 9,454 individuals with PD, 69% of them with an age between 50 and 75 years at diagnosis (Mariani *et al*., 2019). In Spain, a 3-year study analysing 3,823 individuals between 65 to 85 without PD, demonstrated that 30 of them went to develop the disease (Benito-Leon *et al*., 2004). This work also indicated that the incidence of PD increased from 67.5 per 100,000 in individuals between the ages of 65 to 69 years, to 225.3 per 100,000 in individuals between 79 to 74 years, and 365.9 per 100,000 individuals in more than 85 years of age. Similarly, a Swedish cohort of 138 patients for four years identified an incidence of PD of 22.4 per 100,000 between 50–59 years, and 165.6 per 100,000 between 70–79, confirming once again that ageing is a key component in the development of PD (Linder *et al*., 2010). Lastly, a report generated by Parkinson's UK, using the data from PD patients from the Clinical Practice Research Datalink (CPRD) database, showed that the prevalence of the disease was 65.4 people per 100,000 individuals at the age of 50–54. This increased to 482.2 per 100,000 in individuals between 65–69 years, and 1,282 per 100,000 individuals between 74–79 years of age. (Parkinson's UK, 2017). Altogether, body of research shows how ageing increases the prevalence and incidence of PD worldwide, being essential the understanding of its relationship with the disease.

It is important to note that both incidence and prevalence of the disease vary worldwide depending on aspects like geography, ethnicity, environment, lifestyle, but also the methodological differences between clinical studies such as the diagnosis or inclusion criteria for PD (Pringsheim *et al*., 2014; Hirsch *et al*., 2016).

In terms of etiology, PD in most cases has no known cause (i.e., it is 'idiopathic' or 'sporadic'), though exposure to pesticide (Pouchieu *et al*., 2018), heavy metals (Weisskopf *et al*., 2010; Willis *et al*., 2010), high consumption of dairy products (Hughes *et al*., 2017), use of methamphetamines (Curtin *et al*., 2015) or traumatic brain injury (Gardner *et al*., 2018) are considered risk factors. Alternatively, tobacco (Hernan *et al*., 2002; Li *et al*., 2015a), caffeine (Hernan *et al*., 2002; Qi and Li, 2014), anti-inflammatory drugs (Gagne and Power, 2010) and physical activity (Xu *et al*., 2010) have been proven to have a protective effect (Ascherio and Schwarzschild, 2016). Interestingly, such environmental factors might mean that ageing is not necessarily a causal mechanism for PD, but that it occurs in individuals exposed to particular substances for long periods of time.

In addition to unknown and environmental factors, PD can also be linked to genetic components. 'Heritable' or 'familial' forms of the disease do occur due to alterations in genes coding for alpha-synuclein (Polymeropoulos *et al*., 1997), leucine-rich repeat kinase 2 (LRRK2) (Zimprich *et al*., 2004), PTEN-induced putative kinase 1 (PINK1) (Valente *et al*., 2004), parkin (Lucking *et al*., 2000) or DJ-1 (Bonifati *et al*., 2003). When such genetic components are a causative factor, the disease onset is typically much earlier in life, usually occurring before 40–50 years of age (Polymeropoulos *et al*., 1997; Lucking *et al*., 2000; Bonifati *et al*., 2003; Valente *et al*., 2004; Zimprich *et al*., 2004). Currently, it is known that many of these genes encode for proteins that are associated with the maintenance and turnover of mitochondria. For example, Burman *et al*. (2012) demonstrated, using *Drosophila* parkin mutants, that alterations of this protein lead to an accumulation of defective mitochondria specifically in the neurons that degenerate with PD. As it will be explained in more detail in subsequent sections, these neurons are highly dependent on energy, so alterations in their mitochondria increases their vulnerability (Kumar *et al*., 2017).

In summary, ageing is the main risk factor in PD, though it is also considered to be a multifactorial neurodegenerative disease that can be affected by environmental and genetic elements. Ultimately, however, the true etiology of PD is currently unknown.

1.1.2 Movement abnormalities are the main symptoms in PD

Motor symptoms such as tremor, bradykinesia or akinesia, gait, rigidity or postural instability are the main clinical features of PD (Moustafa *et al*., 2016). This is because, as it will describe in more detail in further lines (see subsection 1.1.3.1), the loss of SNpc DAn involves the denervation of the dorsolateral striatum (called caudade-putamen in humans), producing a depletion of dopamine that regulated the basal ganglia circuit, affecting the initiation of voluntary movements (DeLong and Wichmann, 2009; Rizzi and Tan, 2017). In addition to motor abnormalities, the disease causes additional symptoms like constipation, hyposmia, insomnia, anxiety, or depression (Stern *et al*., 2012; Liu *et al*., 2017).

1.1.3 The neuropathology of PD is multifactorial and affects mainly the substantia nigra pars compacta (SNpc)

Overview: The following subsections will attempt to provide a summary of the literature related to the diverse and complex pathophysiological characteristics associated with PD, including the gross neuroanatomical alterations that appear in the brain and, more specifically, in the SNpc. Moreover, it will be presented the molecular changes that appear during the disease in the SNpc DAn (e.g., oxidative stress and mitochondria dysfunction) that in many cases are related to ageing. In general, these features are used to not only provide a *post-mortem* diagnosis of the disease at autopsy, but to help to understand what is happening in the SNpc during the course of the disease and to provide clues about its causes. To note, the known similarities between ageing and PD will be discuss in more detail in the section 1.3.

1.1.3.1 The degeneration of dopaminergic neurons (DAn) in the ventral tier of the SNpc is the main pathological feature of PD

The main pathological hallmark of PD is the loss of DAn in the SNpc (Damier *et al*., 1999) (**Figure 1.1**). Damier and colleagues (1999) observed this in five PD brains compared to five controls by using immunostaining for tyrosine hydroxylase (TH), the rate limiting enzyme in the synthesis of dopamine (Daubner *et al*., 2011). Interestingly, the lack of these SNpc DAn can also be readily visualized in humans because human DAn contain neuromelanin (NM) (Hirsch, 1988), which provides a black color to these neurons that can be seen with the eye without histological processing.

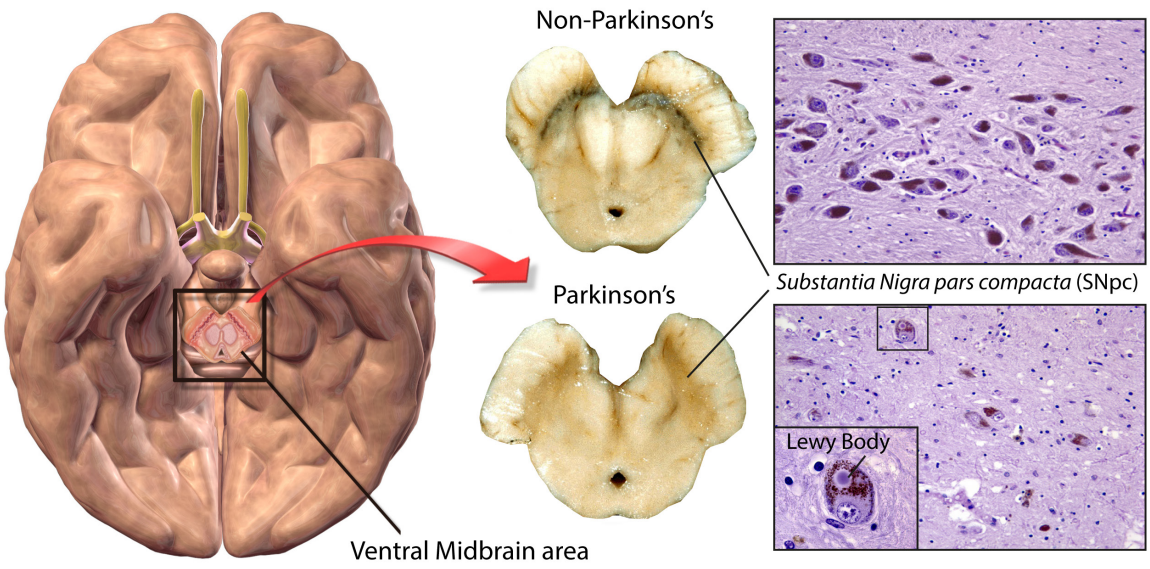

Figure 1.1. The progressive loss of DAn in the SNpc and Lewy bodies are the main pathological hallmarks in PD. The image shows a ventral view of the human brain (left image), with a transverse cut made at the level of the ventral midbrain area, where the SNpc is located. DAn in healthy SNpc have natural black pigmentation due to neuromelanin (NM) that can be viewed without histological processing. However, cells can be stained with cresyl violet for a better visualization (top right image). The loss of DAn in the parkinsonian SNpc produces the lack of this pigmentation (bottom right image). The remaining DAn in the PD SNpc many times contain Lewy bodies, which is an accumulation of alpha-synuclein in the cytoplasm (bottom right image). Extracted from Blausen.com staff, 2014; Neuropathology-web, 2016.

The discovery of the association between the loss of DAn and PD started in 1960, when the first description of a reduction of dopamine in the caudate and putamen of six *post-mortem* adult brains with PD was made (Ehringer and Hornykiewicz, 1960; Hornykiewicz, 2006). In their article, they assumed that the dopamine deficiency found in the caudate and putamen could be related to the reduction of SNpc neurons in PD described previously by Hassler (1938) (Hornykiewicz, 2006). Three years later, Hornykiewicz (1963) analyzed the SNpc of ten PD brains, finding a reduction of dopamine in the SNpc comparable to the lack of dopamine in the striatum, thus contributing to the discovery of the nigrostriatal dopamine pathway (Hornykiewicz, 2006). This discovery had invaluable clinic importance, which was quickly illustrated when Birkmayer and Hornykiewicz (1961) injected 50–150 mg L-3,4-dihydroxyphenylalanine (L-DOPA, levodopa), a precursor of dopamine, into 20 PD subjects and showed a reduction of their symptoms.

In the nigrostriatal dopamine pathway, SNpc DAn mainly project to the GABAergic spiny projection neurons (SPNs) of the striatum or caudate-putamen, adjusting the activity of the basal ganglia circuit **(Figure 1.2**). It is established that the dopamine released by the DAn terminals in the striatum binds to D1 receptors (coupled to a G-protein with a Gs alpha subunit) on the direct-pathway spiny projection neurons (dSPNs), but also to D2 receptors (coupled to a G-protein with a Gi alpha subunit) on indirect-pathway spiny projection neurons (iSPNs) (Gurevich *et al*., 2016). In the direct pathway dopamine activates dSPNs facilitating movement (see **Figure 1.2** for a deeper explanation). On the other hand, in the indirect pathway dopamine inhibits iSPNs that also facilitates movement (see **Figure 1.2** for a deeper explanation) (Yetnikoff *et al.*, 2014; Grillner and Robertson, 2016). In the traditional model, the loss of these DAn reduce the amount of dopamine in the striatum, creating an imbalance in the activity of both pathways and the motor symptoms associated with PD (DeLong, 1990; Mink, 1996). Recent investigations

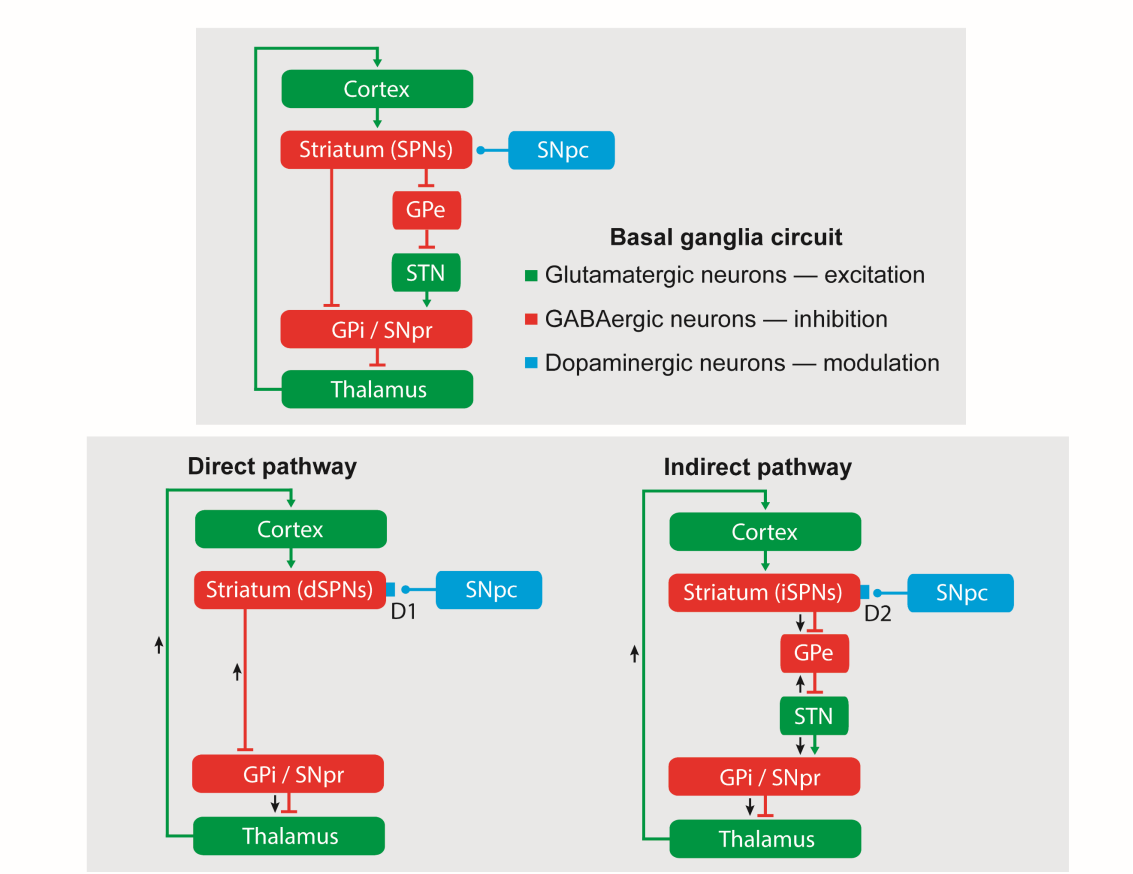

Figure 1.2. Circuit of the basal ganglia with its modulation by DAn from the SNpc. In the nigrostriatal DA pathway, SNpc DAn mainly project to the GABAergic spiny projection neurons (SPNs) of the striatum, adjusting the activity of the basal ganglia circuit (top diagram). In the direct pathway (bottom left diagram), DA binds D1 receptors that activate dSPNs that project to the substantia nigra pars reticulata (SNpr) and globus pallidus interna (GPi), inhibiting the release of GABA by these two nuclei. GPi and SNpr afferents project to the thalamus, which becomes more activated, therefore, activating the cortex and facilitating movement. In the indirect pathway (bottom right diagram), DA binds D2 receptors that inhibit iSPNs that project to the globus pallidus externa (GPe). Thus, the GABAergic functions of the GPe get activated. This produces a major inhibition of the subthalamic nucleus (STN) that reduces the activation of the SNpr and GPi. In turn, the GPi and SNpr reduce their inhibition activity of the thalamus, which produce an increase of the activation of the cortex. In summary, both pathways are mediated by opposite receptors, but the final effect is the same reducing the inhibition of the thalamocortical neurons and facilitating movement. In green, nuclei whose neurons are glutamatergic and produce excitatory synapses (arrowhead). In red, nuclei whose neurons are GABAergic and produce inhibitory synapses (flat ending). In blue, nucleus whose neurons are dopaminergic and produce modulatory synapses (bulb ending). Black arrows indicate if that pathway is more activated (up) or inhibited (down).

have observed the spatial activity of groups of dSPNs and iSPNs in normal mice and mice with a depletion of DAn (Parker *et al*., 2018; Wichmann, 2018). They demonstrated that in normal mice, there were independent clusters of dSPNs and iSPNs that were activated simultaneously with normal movements; while DAn depleted mice showed a parkinsonian phenotype and an increase of iSPNs, because the dSPNs clusters contained less dSPNs and because iSPNs were less clustered.

Although the degeneration of DAn is a hallmark of PD, not all DAn in the brain have the same vulnerability in the course of the disease, with the DAn in the SNpc of the ventral midbrain appearing to be most vulnerable (Damier *et al*., 1999) (see section 1.2). In fact, there are two other dopaminergic nuclei in the ventral midbrain – the ventral tegmental area (VTA) and the retrorubral area (German and Manaye, 1993) – and they seem to be less affected in the disease (German *et al*., 1989; McRitchie *et al*., 1997; Damier *et al*., 1999). This was highlighted by the work by German *et al*. (1989) who investigated the midbrain of five parkinsonian brains and three age-matched controls by staining with cresyl violet. The found that PD brains contained 57% to 86% less DAn than the control group, with the greatest loss appearing in the SNpc compared to the retrorubral area and VTA. Likewise, McRitchie *et al*. (1997) compared the DAn content of seven patients with PD with five controls using cresyl violet staining and TH immunohistochemistry. In their work, they did not observe differences in the number of DAn in the retrorubral area of PD *versus* controls specimens, and only some reduction in TH in the VTA. Similarly, in the five PD brains and five controls examined by Damier *et al*. (1999) using TH immunostaining, there was a significant depletion in the number of DAn only in the SNpc, but not in the retrorubral region or VTA.

Furthermore, the focus of DAn degeneration in PD is not only most associated with the SNpc nucleus, but also appears to be focussed on a precise region within the SNpc: the ventral tier (German *et al*., 1989; Fearnley and Lees; 1992; Damier *et al*., 1999) (**Figure 1.3**). Apart from the already mention findings, German *et al*. (1989) also observed that the ventral part of the SNpc showed the greatest loss of DAn within the SNpc in PD;

whilst Damier and colleagues (1999) also described a preferential degeneration of DAn in the ventral clusters of the SNpc. In accordance, Fearnley and Lees (1992) studied 20 PD brains and 105 controls quantifying the number of DAn, reporting that the ventral tier has a 91% loss of cells, compared to the medial tier (with 71%) or the dorsal tier (with 56%). Thus, as Fearnley and Lees (1992) reported, other regions of the human SNpc (e.g., dorsal, medial) appear to be more resistant in the disease.

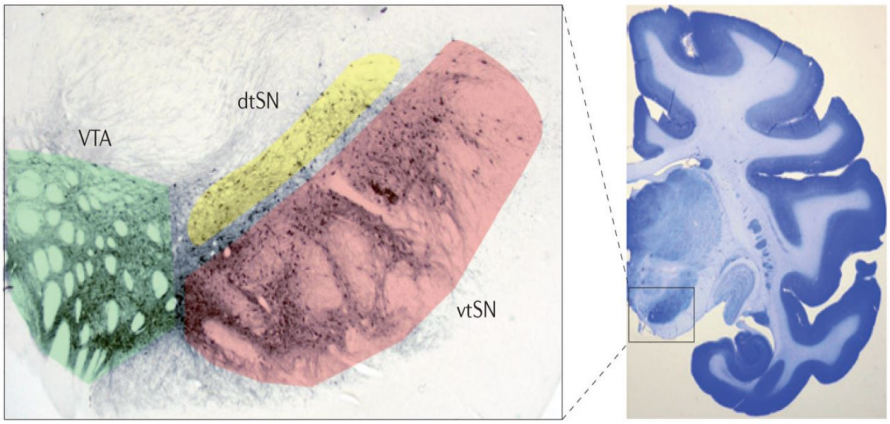

Figure 1.3. DAn of the ventral tier of the SNpc degenerate in PD. On the right is a low-powered image of a coronal hemisection through the rhesus monkey brain stained with cresyl violet. The ventral midbrain area shown on the left is contained in the area highlighted with a square. The left image shows immunostaining for tyrosine hydroxylase and the different DAn regions found in the ventral midbrain: the VTA and the SNpc. DAn of the midbrain area are localized into the VTA and the SNpc. The two main regions of the SNpc are: the dorsal tier (dtSN, shown in yellow) and the ventral tier (vtSN, shown in red). DAn of the ventral tier show more vulnerability and deterioration in PD that those found in the dorsal tier SNpc or VTA. Extracted from Collier *et al*., 2011.

Why the neurodegeneration of DAn is so specific to the ventral tier of the SNpc (in contrast to the rest of the SNpc and other ventral midbrain dopaminergic regions) is something that remains unknown. As it will be explained below in more detail, researchers have been trying to understand what the specific characteristics associated with each DAn subgroup are, why variability exists between them, and if these differences are enough to explain the higher vulnerability of some neurons. This would

not only help to clarify why PD occurs, but also how these differences may combine with ageing to cause the disease and, perhaps, if it is possible to generate new treatments for the disease.

It should be noted, however, that non-DAn areas of the brain also suffer a decline in number in PD. For example, Sasaki *et al*. (2006) found that noradrenergic neurons (which are also NM-positive) in the locus coeruleus from PD patients showed a reduced signal compared to age-matched controls when they were imaged by NM magnetic resonance. Moreover, Halliday *et al*. (1990) demonstrated a loss of serotoninergic neurons in the raphe nuclei in *post-mortem* tissue from parkinsonians by using cresyl violet with haematoxylin/eosin staining. Lastly, Zweig *et al*. (1989) published an immunostaining study where there was a reduction of around 40% of the cholinergic neurons in the pedunculopontine nucleus in PD compared to controls. The degeneration of these non-DAn neurons can be associated with some of the symptoms seen in the disease; such as alteration in gait speed in the case of cholinergic dysfunction (Rochester *et al*., 2012), or a resting tremor when the serotoninergic nucleus is affected (Qamhawi *et al*., 2015). In the future, identifying and comparing all areas of neuronal decline in the brain, and when they occur in the disease, will be relevant as it can help to provide an understanding of the mechanisms that underlie PD degeneration in the SNpc, and the downstream consequences of that degeneration.

In summary, PD is characterized by focal degeneration of DAn of the ventral tier in the SNpc, although other non-DAn are also affected to a lesser extent. It is essential to uncover why this pattern of degeneration occurs and if ageing is involved in this specific loss of neurons.

1.1.3.2 The accumulation of alpha-synuclein into Lewy bodies in the brain, but also in the olfactory bulb and gastric epithelium, is another characteristic of PD

The aggregation of cytoplasmic alpha-synuclein into Lewy bodies in the soma and neuronal processes of DAn has been reported as another feature of PD (reviewed in

Stefanis, 2012; Xu and Pu, 2016) (**Figure 1.1**). Lewy bodies were first described in PD brains by Lewy (1912) as intraneuronal inclusion in the nucleus basalis of Meynert and dorsal motor nucleus of the vagus nerve. Later, Spillantini *et al*. (1997) and Baba *et al.* (1998) discovered that alpha-synuclein was involved in the chemical composition of Lewy bodies. To determine this, Spillantini *et al*. (1997) and Baba and colleagues (1998) explored the SNpc from parkinsonian brain and immunohistochemically stained the tissue with an alpha-synuclein antibody, revealing that this antibody stained Lewy bodies.

Although the physiological function of alpha-synuclein remains unclear, it seems to be related to the storage and release of neurotransmitters. Evidence of this can be found in the work published by Burre *et al*. (2010), where it was demonstrated that alpha-synuclein can bind SNARE complex in mouse brain and HEK293 cells. Thus, alpha-synuclein appears to promote the assemble of proteins that form the SNARE complex to produce vesicle fusion with the membrane to release the neurotransmitter. They concluded that the lack of alpha-synuclein activity, for example by its aggregation in Lewy bodies, would impair SNARE complex generation leading to the neuronal dysfunction in PD. However, it is known that the expression of alpha-synuclein is not limited to the SNpc but appears in the entire Central Nervous system (CNS). Braak *et al*. (2003a), for example, compared alpha-synuclein immunoreactivity in *post-mortem* parkinsonian brains *versus* controls, and showed that the aggregation of alpha-synuclein may start at the level of the olfactory bulb and anterior olfactory nucleus, even before the degeneration of DAn in the SNpc. Braak proposed that this pathological process could self-propagate intercellularly (i.e., prion-like hypothesis), affecting the SNpc and other areas of the brain including the cortex (Braak and Del Tredici, 2017). In addition to this, they also proposed that the gut plays an important role in the initiation of PD. This was suggested from their finding that inclusions of alpha-synuclein occur in the gastric epithelium at different stages of PD (Braak *et al*., 2003b; Braak *et al*., 2006). As Braak and colleagues (2006) hypothesized, the disease could spread from the gastric

myenteric system and submucosa plexus to the CNS through the vagal nerve. Further investigations have begun to support this hypothesis. For example, the work carried out by Sampson *et al*. (2016) shown that transplants of PD-derived gut microbiota into germ-free mice produced similar motor symptoms to that found in PD. Similarly, Unger *et al*. (2016) demonstrated, using real-time quantitative polymerase chain reaction (PCR) of fecal samples, that gut microbiota differences occur in PD patients compared to the age-matched controls and, interestingly, this microbiota change also occurs within a control group with ageing. This point is important to mention for the present Thesis, as it highlights the importance of understanding the relationship of ageing to PD.

In summary, the aggregation of alpha-synuclein in Lewy bodies might alter the function of DAn and affect their viability. In addition, pathological features of cells can be found outside the SNpc at various stages of PD progression, and dysregulation of the gut microbiota might be a contributing or causative factor in the disease. It is important to note that each of these features appear to occur in the normally ageing brain, supporting the idea that ageing may be a contributing factor in PD.

1.1.3.3 An excess of oxidative stress and mitochondria dysfunction, including mtDNA deletions, are associated with parkinsonism

It is normal that our cells produce reactive oxygen species (ROS) during the process of generating energy by oxidative phosphorylation in the mitochondria. However, in physiological conditions these products are buffered by antioxidant mechanisms such as the antioxidant glutathione reducing ROS and free radicals, or the enzyme superoxide dismutase that catalyzes the conversation of superoxide radicals to H_2O_2, which is subsequently degraded by catalases (Angelova and Abramov, 2018). During PD, it is known that the levels of glutathione are reduced, as Perry *et al*. (1982) observed in the SNpc from patients with the disease compared to controls and, interestingly, in the SNpc compared to other areas of the brain such as the cortex, caudate nucleus or cerebellum. The reduction of this antioxidant generates a high vulnerability of the SNpc to oxidative

injury due to the accumulation of ROS that are not neutralized by glutathione. In addition to this, Saggu *et al*. (1989) revealed that the activity of manganese-dependent superoxide dismutase was increased in the SNpc of 11 parkinsonians in comparisons to 11 age-matched controls, while the cerebellum did not show any difference. The increase of the activity of this enzyme may have a protective role, reflecting an excess of oxidative stress in the SNpc, but also may indicate an accumulation of H_2O_2 that can damage the cells. When this antioxidant activity is not adequate, oxidative stress occurs, affecting and inhibiting Complex 1 of the mitochondrial respiratory chain. This results in the generation of more ROS, producing a negative cycle (Blesa *et al*., 2015; Guo *et al*., 2018). The relationship between oxidation and mitochondria in PD was demonstrated by Keeney *et al*. (2006) who looked at the electron transport chain of mitochondria by immunocapture and showed that Complex 1 is damaged by oxidation in the cortex of PD brains compared to age-matched controls. The importance of oxidative stress to the degeneration of DAn in particular, was highlighted in cases where the toxic 1-methyl-1-4-phenyl-1-1,2,3,6-tetrahydropyridine (MPTP) was accidentally ingested by drug users who almost immediately displayed parkinsonian symptoms (Langston *et al*., 1983). Further investigations revealed that MPTP is converted to 1-methyl-4-phenylpyridinium (MPP+) by astrocytes which then inhibits Complex 1 (Ramsay *et al*., 1987; Ransom *et al*., 1987). Currently, the inhibition of the mitochondria and generation of ROS and oxidative stress via this mechanism are so well established and associated with the vulnerability of DAn, that MPTP is extensively used to generate a model of PD in rodents (Meredith and Rademacher, 2011). Added to this, it is important to remember that genetic forms of PD are generally associated with mitochondrial dysfunction (see section 1.1.1), highlighting the relevance of this organelle in the pathogenesis of the disease.

In addition to cellular respiration, Sanders and Timothy Greenamyre (2013) have highlighted how ROS and oxidative stress can produce more general cellular damage. This is because ROS can generate lipid peroxidation, and protein or DNA oxidation. For example, Yoritaka and colleagues (1996) examined the SNpc from seven PD patients

and seven age-matched controls to determine which DAn were positive for 4-hydroxy-2-nonenal. This is important to know because 4- hydroxy-2-nonenal is a product of lipid membrane peroxidation, which reacts with proteins to form adducts and is an indicator of oxidative damage. The results revealed that 58% of DAn from PD brains were positive, while only 9% of DAn were stained in the controls. When the oculomotor nerve from the same samples was evaluated, no differences were found between PD and controls, although there was an increase of the immunostaining in old samples. This indicates that the accumulation of oxidative damage is also an age-related factor. Moreover, Floor and Wetzel (1998) compared the levels of oxidation of proteins in healthy individuals by measuring the carbonyl modification of proteins with a 2,4-dinitrophenylhydrazine assay. They described that in the SNpc there were two times more carbonylated protein than in other areas of the brain such as the frontal cortex, caudate and putamen. This indicates that the SNpc is exposed to higher oxidative stress than other regions of the brain even in physiological conditions, which may contribute to DAn being more vulnerable to PD.

In addition, it seems that mitochondrial DNA (mtDNA) deletions, that could be created by the repair of damaged mtDNA (Krishnan *et al*., 2008), are increased in both PD and ageing. This appears to cause a deficiency in the respiratory chain due to defective encoding of some of the proteins that form this chain (Keeney *et al*., 2006). This was shown in studies using laser capture microdissection (LCM) of the SNpc DAn from *post-mortem* tissue to conduct real-time quantitative PCR assays (Bender *et al*., 2006; Dolle *et al*., 2016). Interestingly, Dolle *et al.* (2016) compared the vulnerability in DAn of PD brain samples with ageing individuals and showed that healthy ageing individuals were able to increase the production of wild-type mtDNA and compensate for mtDNA deletions, while the PD population did not. Thus, an imbalance in the mtDNA homeostasis may be a key point in the specific degeneration of these neurons.

All these findings have contributed to the thought that ROS and oxidative stress might be involved in the degeneration of DAn in PD (Guo *et al*., 2018). Moreover, although the specific mechanisms are not fully understood, some of the characteristics of these

neurons, like the metabolism of dopamine and high metabolic requirements of DAn (see section 1.2), seem to be implicated in the high production of ROS and oxidative stress that can led to the development of the disease.

Finally, due to the fact that an increase of ROS and oxidative stress can accumulate with time (negatively affecting mitochondria in a way that has been associated with DAn degeneration), and considering that the maintenance of functioning mitochondria is crucial to DAn viability, the effect of these processes in the development of PD should continue to be carefully studied.

1.1.3.4 Alterations in the ubiquitin proteasome system and autophagy are also linked to PD

The ubiquitin proteasome system (UPS) and autophagy are two systems involved in the elimination of damage proteins that, as I will explained in the next paragraph, have also been linked to PD (Cook *et al*., 2012). In the UPS, proteins are proteolyzed when they are tagged with ubiquitin (Kleiger and Mayor, 2014), while in chaperone-mediated autophagy proteins are degraded by a selective type of autophagy by the lysosome (Kaushik and Cuervo, 2018). Using Western blot and immunohistochemistry McNaught *et al*. (2003) found in *post-mortem* brain tissue a reduction of members of the UPS in the SNpc DAn of PD compared to healthy controls. Similarly, Alvarez-Erviti *et al*. (2010) discovered a reduction of proteins associated with chaperon-mediated autophagy in the SNpc DAn of parkinsonians. These modifications may produce a failure of both systems in removing impaired proteins like alpha-synuclein (Ebrahimi-Fakhari *et al*., 2011), whose accumulation can affect its role in the regulation of the SNARE complex (see subsection 1.1.3.2). This is important, as Bender *et al*. (2013) and Devi *et al*. (2008) found that the failure to remove alpha-synuclein from the cell in the SNpc and striatum of parkinsonian brains may cause an accumulation in mitochondria, affecting cellular respiration with an elevation of ROS, oxidative stress and mtDNA deletions (see

subsection 1.1.3.3).Taken together, these studies indicate that there is a strong link between alterations in pathways that degrade unwanted proteins in cells, and the mitochondria in PD. This is thought to lead to an accumulation of alpha-synuclein in DAn that, ultimately contributes the degeneration of these neurons.

1.1.3.5 Modifications in glial cells and their functions have been found in the parkinsonian brain

Glial cells (astrocytes, microglia and oligodendrocytes) have an irreplaceable role in the proper functioning of the CNS; giving structural, metabolic, trophic and protective support to neurons (Jakel and Dimou, 2017). Astrocytes, for example, can clearance toxic molecules such as alpha-synuclein in the synaptic cleft (Lee *et al*., 2010), and protect neurons against oxidation by the synthesis and release of glutathione (McBean, 2017). Moreover, astrocytes can protect neurons by releasing trophic factors such as glial cell line-derived neurotrophic factor (GDNF) which enhances the viability of neurons (Sandhu *et al*., 2009). Similarly, microglia, which are considered the immune cell of the CNS, can eliminate pathogens, release anti-inflammatory cytokines, and promote neurogenesis and regeneration (Perry and Teeling, 2013; Troncoso-Escudero *et al*., 2018).

In PD these glial cells can incur modifications and, although it is unclear if this is a cause or consequence of the degeneration of DAn, this can affect their supportive functions (Jakel and Dimou, 2017). In fact, it is well known that mutations associated with DAn in PD (e.g., DJ-1) also occur in astrocytes. Work by Kim *et al*. (2016), for example, has shown that DJ-1 mutant astrocytes have alterations in the assembly of lipid rafts, which impairs the reuptake of glutamate in the synaptic cleft, thereby, increasing neurotoxicity in the extracellular space. However, the literature seems more unclear about the reactive astrogliosis or activation process of astrocytes in PD. Tong and colleagues (2015), for example, did not find differences by quantitative immunoblotting in glial fibrillary acidic protein (GFAP) (a well-known intermediate filament protein that is a characteristic

marker for astrocytes; Eng, 1985) between the PD SNpc and controls. These results were comparable to those found by Mirza *et al.* (2000), where a lack of astrogliosis, including the density of astrocytes and their morphology, was reported similar in the SNpc of PD *versus* healthy individuals. Contrary to this, Song *et al*. (2009) described a mild astrogliosis by immunostaining of the SNpc of parkinsonians compared to age-matched individuals, although the morphology of the astrocytes did not change with the disease. Alternatively, it is well established that activated microglia and neuroinflammation are linked to the disease. For example, positron emission tomography has shown that the intensity of a radiotracer specific for activated microglia was more elevated in the SNpc of humans with PD than in their healthy matches controls (Ouchi *et al.*, 2005). This result agreed with the increase of activated microglia found by immunohistochemistry in the SNpc of parkinsonians (Mirza *et al*., 2000) and humans exposed to MPTP who developed PD (Langston *et al*., 1999). The chronic activation of microglia generates neuroinflammation, that subsequently can provoke the degeneration of DAn (Troncoso-Escudero *et al*., 2018). This has been supported by Koprich *et al*. (2008) who showed that the activation of microglia by a non-toxic dose of lipopolysaccharide (LPS) prompted the release of cytokines, making DAn more vulnerable to 6-hydroxydopamine (6-OHDA), a toxin used to generate a model of PD in rodents.

Other mechanisms, like the accumulation of alpha-synuclein, can also have an impact on glial cells. This can alter their function and, subsequently, damage DAn in an indirect way. Lee *et al*. (2010) demonstrated this effect by co-culturing differentiated SH-SY5Y cells (a characteristic DAn cell line) expressing alpha-synuclein with primary rat astrocytes. Astrocytes in the study accumulated neuron-derived alpha-synuclein, prompting a release of cytokines. Building on this finding, Lindstrom *et al*. (2017) observed in an *in vitro* experiment using primary astrocytes, that aggregates of alpha-synuclein inside the astrocytes impaired their mitochondria, affecting its structure and the production of ATP. Similarly, Liu *et al.* (2018) used transgenic astrocytes in culture

to show that the overexpression of alpha-synuclein caused a breakdown of the Golgi apparatus, and increased apoptosis through stress of the endoplasmic reticulum. This ultimately resulted in the reduction of GDNF release from the astrocytes. On the other hand, alpha-synuclein also plays an important role in the activation of microglia. The overexpression of human alpha-synuclein by a viral vector in the rat SNpc has been shown to activate microglia cells and promote the degeneration or death of neurons (Sanchez-Guajardo *et al*., 2010). Similarly, Xia *et al*. (2019) demonstrated that alpha-synuclein in exosomes derived from PD patients can be phagocytized by a microglia cell line. This accumulation of alpha-synuclein induced an activated phenotype, releasing pro-inflammatory cytokines and nitric oxide, triggering neurotoxicity. Moreover, this alpha-synuclein inhibited autophagy, affecting the removal of alpha-synuclein, increasing its accumulation and release outside the cell. Thus, importantly, microglia were probed to participate in the transmission of alpha-synuclein along the CNS, helping in the progression of PD.

When considered together, these studies demonstrate that glial cells and neuroinflammation are important elements to consider in the pathology of PD, because they cannot only be directly affected by the disease (e.g., accumulation of alpha-synuclein or mutation of their genes, causing alterations in their functions) but can also indirectly aggravate the degeneration of DAn.

1.1.4 The lack of therapies to cure the disease highlight the value of understanding why specific SNpc DAn degenerate in PD

Currently, available therapies seek to decrease the symptoms of the disease by attempting to counteract the low amount of dopamine in the brain through the administration of a precursor of dopamine (i.e., levodopa), dopamine agonists, monoamine oxidase type B (MAO-B) inhibitors and catechol-O-methyltransferase (COMT) inhibitors. Other medications involve anticholinergic drugs or neuroleptics (Connolly and Land, 2014; Cacabelos, 2017). More invasive techniques include

strategies like deep brain stimulation (Connolly and Land, 2014; Cacabelos, 2017; Muthuraman *et al*., 2018) or even cell transplantation (Bjorklund *et al*., 1981). Despite this, many of these treatments are not effective for all patients and, most importantly, they do not stop the degeneration of DAn and the progression of the disease (Cacabelos, 2017).

The absence of long-term treatments that stop or slow the progression of this age-related neurodegenerative disease is of growing importance. As a greater percentage of the population reaches older and older ages, the need to understand the underlying mechanisms behind PD and the implications that ageing has in its course continues to grow.

1.2 The heterogeneity of midbrain DAn as a key point of their vulnerability in PD

Overview: Due to the fact that PD causes a selective degeneration of DAn from the ventral tier of the SNpc, studies have begun to explore what similarities and/or differences may exist between these cells in the midbrain that could explain the selective vulnerability (Vogt Weisenhorn *et al*., 2016; Surmeier *et al*., 2017). The following sections will summarize some of the known similarities and differences within the SNpc, and provide a review of some of the characteristics that can affect the viability of all DAn in the brain. It is important to note that even when similar characteristics are found in all DAn (e.g., they all metabolize dopamine), there are differences that may affect these similar characteristics within subsets of DAn in the brain. Here, to simplify the reading, those similar attributes have been grouped together, explaining specifically how they change in the different populations of DAn.

It is also important to note that specific features within DAn subgroups may be related to the vulnerability and neurodegeneration of DAn (i.e., may contribute to the cause of the disease) but also may be a response to the disease state. Therefore, the existence of a identifying characteristic is not always associated with the susceptibility of the cell to

degeneration, but can be fundamental to protect these neurons against more damage. Understanding which characteristics are directly affecting or preserving these DAn, cause or consequence, and how these characteristics change in ageing and PD is a requisite in order to find a cure for this disease.

1.2.1 Similarities between DAn

1.2.1.1. The metabolism and oxidation of dopamine produces high amounts of oxidative stress and neurotoxicity

The synthesis, storage and release of dopamine in the synapse involve the accumulation of dopamine in vesicles, avoiding an excess of the neurotransmitter in the cytoplasm (Guillot and Miller, 2009). When dopamine is released, it can be removed from the synaptic cleft and degraded thanks to the help of the enzyme monoamine oxidase B (MAO-B), which is found in neurons and astrocytes (Inyushin *et al*., 2012). Interestingly, however, an increase of MAO-B in astrocytes can contribute to the loss of DAn. This event has been investigated by Mallajosyula and colleagues (2008), who found an elevated degeneration of SNpc DAn accompanied by an increase in mitochondrial oxidative stress and microglial activation in mice genetically modified to overexpress astrocytic MAO-B. One explanation for this effect is that the degradation of dopamine by MAO-B generates H_2O_2 (Cohen *et al*., 1997), that can act as ROS (Adams and Odunze, 1991), but also enhance the metabolite 3,4-dihydroxyphenylacetaldehyde (DOPAL), which can be toxic for DAn (Zhang *et al*., 2019). This effect was demonstrated by Burke *et al*. (2003) who injected DOPAL into the ventral midbrain of rats and produced degeneration of DAn in the SNpc and, to a lesser extent, in the VTA. Interestingly, similar work by Burke *et al*. (2008) conducted a Western blot analysis and showed that DOPAL contributed to an increase in aggregates of alpha-synuclein in the SNpc compared to the control groups. In support of the possibility that this process might occur in PD, Goldstein *et al.* (2011) identified by mass spectroscopy that the striatum of *post-mortem*

parkinsonian brains has five times more DOPAL than dopamine when they were compared to healthy controls.

Alternatively, when there is an excess of dopamine in the cytosol of DAn, dopamine is oxidized spontaneously to dopamine-O-quinone and then converted to aminochrome thanks to the cytosolic pH (Herrera *et al*., 2017; Zhang *et al*., 2019). This last metabolic product has cytotoxic effects within the cells, as it has been seen in an experiment performed by Herrera *et al*. (2016) where injecting aminochrome in the rat striatum generated a reduction in the number of DAn, a depletion in the dopamine release, and an increase of mitochondria dysfunction. Moreover, aminochrome is known to cause the same aggregation of toxic alpha-synuclein found in PD (Munoz *et al.,* 2015; Huenchuguala *et al*., 2019). Interestingly, aminochrome is also the precursor of NM, which seems to increase with physiological ageing in DAn to protect them from the accumulation of O-quinones and ROS (see below) (Zecca *et al*., 2002).

In summary, the metabolism and oxidation of dopamine in DAn is becoming an established possible mechanism involved in their vulnerability to degeneration. Understanding if physiological ageing modifies any step in the metabolism and/oxidation of dopamine, therefore will be useful step toward establishing a link between ageing and the occurrence of PD.

1.2.1.2 DAn in the SNpc have the highest concentration of neuromelanin in the ventral midbrain area

As cited previously, NM is a characteristic feature of human DAn, appearing not only in cells in the SNpc but also in the VTA and locus coeruleus (Hirsch, 1988). Other species like primates, horses and sheep express NM (Zecca *et al*., 2001), but interestingly mice and rats, the species more used in research, seem to lack this black pigment (Barden and Levine, 1983). In contrast to this, in a study using electron microscopy, DeMattei and colleagues (1986) described the existence of NM in SNpc DAn of rats, but only when

they were 21-23-month-old. Understanding why these NM differences exist between species and ages is something that is still pending study (Marsden, 1961), but it is important to note that this suggests that the generation of dopamine is not necessarily linked to the production of NM or may be age-dependent (Fedorow *et al*., 2005). In humans, stereological quantification of Nissl-stained SNpc sections showed that NM increased in the SNpc DAn with physiological ageing (Zecca *et al*., 2002; Rudow *et al*., 2008). Conflictingly, recent work by Xing *et al*. (2018), using a neuromelanin-sensitive magnetic resonance imaging (MRI), revealed that the distribution of pigmented neurons increased with adolescence, but decreased from around the fifth decade of age when 134 healthy individuals aged 5-83 were analyzed. Independent of the effect of ageing in the accumulation of NM, DAn of the SNpc contain more NM in comparison to other areas of the ventral midbrain such as the VTA (Hirsch, 1988). This is important to note as multiple studies have determined that SNpc DAn, which contain more NM, are more vulnerable to degenerate in PD (Hirsch, 1988; Zecca *et al*., 2002; Rudow *et al*., 2008). Supporting this line of thought, recent work by Carballo-Carbajal *et al.* (2019) has revealed that an increase in NM in rodents produced a characteristic PD phenotype in the animals, including alterations in their movements, Lewy bodies and DAn degeneration. Interestingly, to generate the rodent model of human NM accumulation, they developed an overexpression of tyrosinase, the enzyme implicated in the production of peripheral melanin, by the injection of a viral vector in the rat SNpc. They described that with ageing, once the accumulation of NM reached a threshold, there was an age-dependent loss of DAn in the SNpc as well as dopaminergic innervation in the striatum. Moreover, they also demonstrated that the overexpression of tyrosinase in SH-SY5Y *in vitro* produced an accumulation of NM, impairing autophagy and UPS proteolysis, creating a negative cascade of cellular effects (including accumulating damaged mitochondria which altered respiration, generating ROS and reduced metabolic support).

The mechanisms by which NM can increase the vulnerability of DAn are manifold. For example (see subsection 1.2.1.1), NM is formed in DAn from aminochrome to avoid the accumulation of toxic O-quinones (Zecca *et al*., 2002). This creates a cytoplasmic substance with a double membrane, that can bind proteins, as well as lipids and metal ions like iron (Zucca *et al*., 2018). For example, it is possible that NM may reduce a less reactive form of iron, generating ROS and, therefore, facilitate degeneration (Swartz *et al*., 1992). Indeed, it is known that an elevated quantity of iron exists in the SNpc of parkinsonians (which might increase the release of ROS in this area), as this was confirmed by a meta-analysis study using thirty-three articles related to *post-mortem* and MRI quantifications of iron levels (Wang *et al*., 2016). Moreover, studies have indicated that the mechanisms by which NM can make DAn from the SNpc more vulnerable to degeneration are linked to neuroinflammation. For example, Zecca *et al*. (2008b) observed that intracerebral NM injections produced an inflammatory microglia response in the cortex and SNpc in rats, as well as the degeneration of DAn. In addition to the works by Zecca *et al.* (2008b) and Carballo-Carbajal (2019) mentioned above, Cebrian *et al*. (2014) revealed that human NM could induce the secretion of the cytokine IFN-γ by microglia, which can cause the expression of MHC-I, in primary cell cultures from the ventral midbrain DAn of postnatal mice. The study also reported that NM could directly activate MHC-I molecule in DAn. Ultimately, this MHC-I could attract cytotoxic T cells causing DAn death. NM can then oxidize or reduce this iron having a protective or toxic function in DAn (Swartz *et al*., 1992).

Finally, NM may have a neuroprotective role buffering the effects of accumulated reactive iron, as shown by Zecca *et al*. (2008a) when looking at the antioxidant effect of human SNpc NM and how the iron-NM complex was able to prevent the production of ROS.

In summary, NM has been identified as a possible causative factor in the degeneration of DAn, either for its connexion to iron or the capacity to increase neuroinflammation.

These studies also indicate that ageing has an important effect in the production of this NM and that it should be investigated to establish if it is a factor that links ageing to PD.

1.2.1.3 DAn in the SNpc have long and ramified axons that require a high production of energy by the mitochondria

As previously mentioned, DAn from the ventral midbrain (SNpc and VTA) have long axons that project rostrally along the medial forebrain bundle. This is exemplified in the work undertaken by Matsuda *et al*. (2009) and Aransay *et al*. (2015), who used a palGFP virus tracer to analyse projections of single-DAn axons from rat SNpc and mouse VTA. Both of these studies highlighted how each DAn has a spread and dense axonal arborization with multiple synapses once reaching their respective targets. However, even though the level of ramification is high in both DAn subpopulation, an *in vitro* study using mouse postnatal SNpc or VTA DAn found that DAn in the SNpc had around 70% more axonal arborizations than the VTA ones (Pacelli *et al*., 2015).

The maintenance of long and highly ramified DAn axons demand a high production of energy by the mitochondria. This has been demonstrated in a study that also claims that there is a higher axonal arborization in SNpc DAn compared to VTA (Pacelli *et al*., 2015). Results from this work compared neurons from the SNpc and VTA and suggest that the more highly arborized neurons from the SNpc show an increase in the number of mitochondria, an elevated consumption of oxygen, and an increase in ROS and ATP production compared to those from the VTA. This possibility is partly supported by a recent study that looked at the density of mitochondria in the axons of remaining DAn in PD tissue compared to controls, finding an increase in the number of mitochondria in parkinsonians when high resolution quantitative immunofluorescence was applied (Reeve *et al*., 2018). As the authors discussed, this result may indicate a compensatory effect by the remaining DAn, that could in turn increase oxidative stress in these neurons. By contrast, Liang *et al*. (2007) published that DAn in the SNpc contained less

mitochondrial density than VTA when they were visualized by electron microscopy in mouse tissue, which would affect the ability to supply all the cell's energy needs.

Despite these conflicting findings, these studies indicate that the morphology and bioenergetic requirements of the SNpc DAn are different in subclasses of DAn and may be a key factor in their susceptibility to PD. In addition to this, the ageing process could also alter the demand for energy or modify the mechanisms that supply it, providing a contributing factor to the neuropathology of PD.

1.2.2 Differences between DAn

1.2.2.1 Subpopulations of DAn have different morphologies in SNpc and VTA

Research has indicated that there are morphological differences between DAn in the ventral midbrain. For instance, two independent studies using immunostaining of mouse and rat ventral midbrain sections observed that DAn from SNpc were bigger in size and with an elongated shape in comparison to those found in the VTA, which were smaller and had an oval shape (Nelson *et al.*, 1996; Thompson *et al.*, 2005). In terms of the population within the SNpc, research has found that (in rats) the dorsal tier expands along 75% of SNpc and is densely stratified into an upper layer with stretched and elongated DAn, and a lower layer with spherical DAn. The ventral tier occupies 10% of the SNpc and contains a low density of small, rounded DAn (Khudoerkov *et al.*, 2014).

Although it is unknown what implications different shapes and sizes can have on the viability of DAn, it is generally considered that the neuronal size can influence, for example, the electrical properties of cells, affect the information they transmit, or the energy they consume (Sengupta *et al*., 2013). Therefore, it appears evident that the morphometric features of DAn and their changes with ageing must be considered to understand whether this links ageing with PD. As Thompson and colleagues (2005) mention in their work, these morphometric differences could be associated with a specific protein profile that may explain differences in the vulnerability of DAn

phenotypes within each area. However, to my understanding, no study has yet directly correlated the morphological characteristics of each DAn subgroup with the expression of any particular proteins, making a link between these characteristics and the distinct degeneration of subphenotypes of DAn in the SNpc.

1.2.2.2 DAn in the SNpc show the highest expression of GIRK2 in the ventral midbrain which might explain their lower levels of excitotoxicity

Along with the potential differences in size and shape of DAn from the SNpc and VTA, it is also possible to find heterogeneity in the expression pattern of some proteins. For instance, G-protein-activated inwardly rectifying potassium channel 2 (GIRK2), an ion channel that allows the entry of K^+ into the cell producing a membrane hyperpolarization and reducing neuronal excitability (Marron *et al*., 2017), was found to be highly expressed in the SNpc (predominantly in the ventral tier) compared to the VTA. Evidence for this has been provided by *in situ* hybridization, LCM, microarray analysis and real-time quantitative PCR in adult mice (Chung *et al.*, 2005), as well as immunostaining in rats (Thompson *et al*., 2005) and humans (Mendez *et al*., 2005). However, a conflicting report by Reyes *et al*. (2012) indicated that there were no qualitative differences by immunostaining between VTA and SNpc, or the ventral and dorsal tier of SNpc, at least in humans and mice.

GIRK2 is associated with D2-autoreceptors, which produce an inhibition of the pacemaking activity when the receptors are activated by an excess of extracellular dopamine. An increase of GIRK2 in a DAn would appear to be associated with a homeostatic function, where excitability of the cell is reduced to lessen instances of excitotoxicity and death. This would explain why SNpc DAn that remain longest in PD show an elevated amount of *Girk2* and D2-autoreceptors mRNA by real-time quantitative PCR (Dragicevic *et al*., 2014).

Being the current literature is so conflicting, it is not currently possible to assign GIRK2 as a definitive marker for differentiating the DAn subgroups in the midbrain. Also, more investigations will need to be conducted to determine if this protein predispose SNpc DAn to degeneration or, alternatively, if it is a physiological response to protect them.

1.2.2.3 DAn in the VTA have an increase of calbindin compared to SNpc and this might protect them from degeneration

Calbindin (CBd28k) is a calcium binding protein implicated in the control of calcium levels within neurons by sequestering these ions and, thereby, protecting them from excitotoxicity (Blesa and Vila, 2019). This protein, too, is currently considered as a possible marker for differentiating the subgroups of DAn in the ventral midbrain. This has been demonstrated in diverse studies in rodents (Thompson *et al*., 2005; Ferreira *et al*., 2008; Fu *et al*., 2012), monkeys (Dopeso-Reyes *et al.*, 2014), and humans (Mendez *et al*., 2005). Each have indicated that there is an increase of calbindin-positive immunostaining in DAn of the VTA compared to cells in the dorsal tier of SNpc and, especially, the ventral part. These findings are in line with research carried out by Chung *et al*. (2005) and Greene *et al*. (2005) where they used LCM and microarray analysis to discover that DAn in the VTA had more *calbindin* transcripts than DAn in the SNpc. This distinction would explain why DAn in the SNpc of parkinsonians that are calbindin-positive are preserved compared to those calbindin-negative neurons (Yamada *et al*., 1990). Despite this possibility, conflicting studies have demonstrated by immunostaining that DAn in SNpc, including the ventral tier, are also calbindin-positive in mouse (Vidyadhara *et al*., 2016) and rats (Liu *et al*., 2010).

More evidence concerning the protective role of this protein, however, have been found in animal models of PD. For instance, in transgenic mice where calbindin is overexpressed, the toxin MPTP seems to produce an increase in the apoptotic caspase-3 and degeneration in wild-type, but not in the transgenic mice (Yuan *et al.*, 2013). In another recent study in monkeys, where immunohistology and imaging analyses were

performed, the overexpression of calbindin in the SNpc by injecting viral vectors encoding calbindin, protected the DAn from MPTP degeneration, especially in the ventral tier of the SNpc (Inoue *et al*., 2019).

As in the case of GIRK2, however, because the literature shows contradictory evidence to link calbindin specifically to VTA DAn, it is necessary to conduct further studies to confirm the expression pattern and role of this protein in protecting VTA DAn.

1.2.2.4 DAn from the ventral tier of SNpc express more ALDH1A1 compared to the dorsal tier, possibly protecting DAn from neurodegeneration

Another protein to consider in the heterogeneity and vulnerability/protection of DAn in the ventral midbrain would be the aldehyde dehydrogenase 1A1 (ALDH1A1), which is responsible for catalyzing the oxidation of aldehydes to carboxylic acids. In DAn, ALDH1A1 can oxidize and detoxify DOPAL, which, as mentioned in a previous section (see subsection 1.2.1.1), promotes the aggregation of alpha-synuclein in the SNpc, linking it to the degeneration of DAn (Marchitti *et al*., 2007a). In humans and mice, Liu and colleagues (2014) revealed that ALDH1A1-positive DAn were found principally in the ventral tier of the SNpc and generated less aggregates of alpha-synuclein. During early stages of PD, however, the same study demonstrated that there is a reduction of 30% of the ALDH1A1 phenotype in DAn from the ventral tier, preceding the degeneration of DAn in late stages of the disease. Thus, ALDH1A1 would be a mechanism to protect DAn of the ventral tier from the high dopamine metabolism and toxic DOPAL. On the other hand, Sgobio and colleagues (2017) have recently shown that ALDH1A1-positive DAn from the ventral tier project striosomes in the dorsolateral striatum in mice, and release less dopamine compared to the striatal matrix. Thus, ALDH1A can regulate the release of dopamine, reducing it in this area of the target region. This means that a reduction of ALDH1A1 will generate an excess of dopamine that might be cytotoxic for the cells, but also that it can be a compensatory mechanism when there is a loss of DAn in PD.

To date, it is unknown why this protein would be reduced in the ventral tier of parkinsonian brains. However, an investigation performed by Fitzmaurice *et al*. (2013) suggested that pesticides could be a possible mechanism of ALDH1A1 inhibition, producing the degeneration of DAn in mesencephalic cultures and in an *in vivo* zebrafish study exposed to the pesticide. These results would support the idea of an epidemiological association between the pesticide and PD.

As with GIRK2 and calbindin, it is still not clear what effect the expression of ALDH1A1 has on the vulnerability or protection of DAn, and if it is a cause or consequence of the disease. It would be necessary in the future to determine not only its contribution, but also the effects that ageing has in its expression and possible new treatments that can be generated linked to it.

1.3 The relation between PD and physiological ageing

Overview: Thus far, it has been described that DAn from the ventral tier in the SNpc present different features that may affect their vulnerability and participate in their degeneration. However, none of these characteristics appear to be a definitive explanation for the death of DAn in PD. As indicated in the first section, ageing is considered the main risk factor to develop parkinsonism, so it seems logical to think that there must be age-related changes in the SNpc linked to the disease. Remarkably, the role that ageing has in the disease (if any) still remains unknown. In this section, the literature surrounding how ageing affects the CNS and, specifically, the SNpc is discussed, along with the current ideas of what implications this has in PD. The possibility of knowing why these DAn are affected with advanced age, as well as which mechanisms would predispose them to degeneration, would provide a basis for understanding why these cells become susceptible to PD at the typical age of disease onset.

1.3.1 Ageing produces global changes in the brain

Current research suggests that morphological and neurochemical alterations in the human CNS occur during physiological ageing (Peters, 2006). That assumption is relevant for the Thesis here because modifications during ageing of the CNS could be affect DAn in the SNpc in particular and, therefore, contribute to the incidence of PD. Moreover, it is important to study ageing in the SNpc in particular because, though the ageing process may affect all areas of the brain equally, these changes, in combination with the factors outlined above might confer a particular susceptibility of the DAn of the SNpc region. This section, therefore, will discuss the major findings associated with ageing in the brain and the SNpc.

1.3.1.1 The volume of the brain is reduced, and the ventricles are expanded with ageing

Both weight and volume are probably the most elementary characteristics of the brain that can be measured in association with ageing. Past research by Scahill *et al*. (2003) has shown an age-dependent decrease in each of these characteristics. Although it is unknown exactly in which region of the brain volume loss occurs, diverse *in vivo* imaging examinations have consistently shown that changes do not affect all brain regions to the same degree. Areas such as the prefrontal cortex (Tisserand *et al*., 2002; Lemaitre *et al*., 2012), amygdala, hippocampus and temporal lobes (Scahill *et al*., 2003; Zanchi *et al*., 2017), or caudate and putamen (Abedelahi *et al*., 2013), have been shown to suffer a reduction of their volume with ageing in healthy humans. Nevertheless, there is no consensus in establishing if this is caused by the deterioration of white (myelinated axons) and/or grey matter (cell bodies) (Peters, 2006). For example, Tang *et al*. (1997) and Piguet *et al*. (2009) found a reduction of 27% and 23% of the white matter with ageing *in post-mortem* analysis of human brains. Another study using combined diffusion tensor imaging (DTI) and MRI showed similar results, with a depletion of white matter in the oldest individuals (Yang *et al*., 2016). On the other hand, using neuroimaging,

Hafkemeijer *et al*. (2014) described an inverse relation between age and the grey matter, but only in specific structures. Meanwhile, Piguet *et al*. (2009) reported no changes in the total or regional volume of grey matter. These differences can be attributed to the different methods used (e.g., *post-mortem* analysis *versus* neuroimaging), but also to the possibility of including individuals in the study with a pre-clinical neuropathological condition (Piguet *et al*., 2009). Regardless of which matter of the brain is reduced, the shrinking of the brain has been associated with mechanical pressure exerted by the enlargement of the ventricles with physiological ageing (Kwon *et al*., 2014).

1.3.1.2 The permeability of the blood-brain barrier (BBB) increases with ageing

Changes in the blood-brain barrier (BBB) are another characteristic of the ageing brain. Because the BBB ensures the correct distribution of blood and nutrients and protects the brain from external toxins, its modification with ageing may cause an imbalance in the homeostasis of the brain and leave it unprotected (Erdo *et al*., 2017). For instance, a recent immunohistochemical study measuring different aspects of the BBB revealed that there was an increase of BBB breaks caused by a reduction of a tight junction protein in aged mice. The importance of this finding was highlighted by the study also showing an increase of serum proteins (indicating the leakage and elevated permeability of the BBB) within old human brains (Goodall *et al*., 2018). These results were similar to those reported by Elahy *et al*. (2015), where there was a decrease of the expression of another tight junction protein in 24-month-old mice compared to 3-month-old by flow cytometry. Furthermore, ultrastructure microscopy showed that the basal membrane, another component of the BBB, increased in thickness in 24-month-old *versus* 6-month-old mice (Ceafalan *et al*., 2019). In this study, the modifications in the membrane size was accompanied by the creation of pockets of lipid accumulation by astrocytic endfeet, which could act as a hydrophobic impediment in the BBB.

1.3.2 The SNpc suffers degenerative changes during ageing that are similar to PD and could affect the vulnerability of DAn

Having mentioned how ageing produces global changes in the CNS (i.e., a decrease of the brain volume and modifications of the BBB), this section will focus on the effect that age has specifically in the SNpc and how this can be associated with PD. This aspect is relevant because, as authors like Collier *et al*. (2017) asserted, age-related modifications in DAn may be comparable to the changes that precede the neurodegeneration of DAn in PD, creating a pre-parkinsonian phenotype. In line with this, Kanaan and colleagues (2008) suggested that there is neuronal dysfunction associated with a slow degeneration during physiological ageing and that genetic predispositions or exposure of individuals to toxic environments would exacerbate this neuronal dysfunction during parkinsonism. The fact that neuronal dysfunction in ageing may appear before the neuronal loss in PD could explain why motor disturbances and pre-motor symptoms such as olfactory, sleep alterations, and mood disorders are a common component in both PD and the elderly (Rodriguez *et al*., 2015).

1.3.2.1 The number of DAn in the SNpc is reduced with ageing, while the soma size increases

Currently, it seems to be a consensus that DAn from the ventral tier of SNpc deteriorate with PD. However, there is controversy in establishing whether this pattern of damage is similar to that seen in the elderly population. Multiple studies have found a reduction of NM-positive neurons and TH-positive neurons in the SNpc from elderly people compared to young (Ma *et al*., 1999; Cabello *et al*., 2002; Rudow *et al*., 2008). Similarly, the work by Buchman *et al.* (2012), using haematoxylin/eosin quantification of SNpc DAn from *post-mortem* tissue, indicated that there was a higher neuronal loss particularly in the ventral part of the SNpc associated with an increase of parkinsonian signs (e.g., bradykinesia or motor alterations) in people above 85 that were not diagnosed with PD. In contrast, early work by Fearnley and Lees (1991), using the same analysis, suggested

that DAn loss was completely different during ageing, affecting mainly the dorsal tier of the SNpc. These authors also reported that the age-related neuronal degeneration would not be enough to provoke parkinsonian symptoms. On the other hand, Di Lorenzo and colleagues (2016), in a stereology study with Nissl staining, established that the number of cells within the SNpc was not altered by ageing, although the total volume of SNpc was reduced. This fact, they discussed, would indicate a higher atrophy of neuronal processes or reduction of neuronal size in the nuclei.

In addition to the more obvious differences in the number of DAn within the SNpc, there are also many studies that have analyzed the size of their soma. This was exemplified in the work undertaken by Cabello *et al*. (2002) and Rudow *et al*. (2008), where it was found a significant increase or hypertrophy of the NM-positive and TH-positive neurons occurred in the SNpc of ageing human brains. They discussed that this hypertrophy might be associated with an accumulation of NM in the cell cytoplasm, as well as a mechanism to compensate the loss of DAn. However, these results would conflict with the already mentioned study by Di Lorenzo *et al*. (2016) reporting a contraction of the SNpc, and the research by Ma *et al*. (1999) where a reduction in DAn cell body with ageing was described.

Other studies in rodents and non-human primates have also found age-associated changes in SNpc DAn number and soma size. For example, in rodents, there was a decrease of TH immunoreactivity between 2-month-old mice and 25-month-old mice (Tatton *et al*., 1991). The reduction in TH neuronal number and an increase in the DAn soma size with age, when comparing young (5-month-old), old (24-month-old) and senile (32-month-old) female rats, seems to be another characteristic of old SNpc (Sanchez *et al*., 2008). This was corroborated by Bardou *et al*. (2014) who found similar results between 3-, 9- and 23-month-old male rats, identifying a decrease in the number of TH-positive neurons in the oldest animals. Also, McCormack *et al*. (2004) found a decrease of this immunoreactivity in squirrel monkeys, and Emborg *et al.* (1998) and Collier *et al*. (2011) described this same depletion in rhesus monkeys.

Despite discrepancies between studies, it seems that there is some consensus that ageing causes a reduction of DAn in the SNpc and an associated increase of their soma size. Nevertheless, it is important to highlight that differences between studies are often caused by the techniques used, and how the study is conducted, which suggest that we must be cautious reviewing the literature and drawing conclusions. Quantification of DAn in most cases employed immunohistochemistry for TH, or simply measured the amount of NM within these cells. This can produce different results. Some authors argue that the number of NM-positive neurons are correlated with the TH-immunoreactive cells (Cabello *et al*., 2002), while others consider that around 18% of melanized DAn lose their TH phenotype in physiological ageing (Kordower *et al*., 2013). This implies that the use of TH as an accurate marker DAn might be difficult in ageing research. Moreover, it is important to note that the brain tissue could undergo some changes during processing *post-mortem,* and that the samples used, such as the number of individuals or sections of each brain, differ greatly between studies (Fearnley and Lees, 1991; Ma *et al.*, 1999; Cabello *et al*., 2002; Rudow *et al*., 2008; Buchman *et al.*, 2012; Di Lorenzo *et al*., 2016).

1.3.2.2 Alpha-synuclein is also increase in the aged SNpc in humans

It has been mentioned that the aggregation of alpha-synuclein as Lewy bodies is an important hallmark in PD. In aged individuals, most of the studies described an increase of alpha-synuclein in the SNpc. An example of this is the work performed by Chu and Kordower (2007), were they tested the expression of alpha-synuclein by immunohistochemistry in humans and rhesus monkeys. They showed an increase in the optical density (O.D.) of alpha-synuclein in the soma of DAn that was associated with a reduction of TH-positive DAn in both species. However, the alpha-synuclein found in these age individuals did not form aggregates, being soluble under protein K digestion. In the study, they speculated that the aggregation of alpha-synuclein due to a lysosomal failure can be key in the degeneration of DAn during PD but not in the ageing process. As Burre *et al*. (2010) identified, alpha-synuclein was involved in the correct assembly

of the SNARE complex to allow fusion of the vesicle with the cell membrane and the release of neurotransmitter. Chu and Kordower (2007) observed an increased with ageing of alpha-synuclein in the soma of the cell, while young individuals presented a positive staining in the neuropils of DAn. Therefore, it is logical to think that the normal function of alpha-synuclein in the aged individuals should not affect the expression of TH. However, it might be possible that in aged SNpc, the only accumulation of alpha-synuclein in the soma without aggregating could be enough to reduce the amount of TH, but not enough to generate the degeneration of DAn as it happens in PD. Furthermore, additional research by Xuan and colleagues (2011) supports the hypothesis that there is an accumulation of alpha-synuclein in the aged SNpc. In this study, they used immunostaining in human samples and found an increase of alpha-synuclein associated with a decrease of TH but also an overexpression of NM. They suggested that this increase of NM might be producing the accumulation of alpha-synuclein in DAn, making them more vulnerable with ageing. Contrary to these findings, a comparison of the expression of alpha-synuclein in the SNpc at different ages in mice (2-month-old, 10-month-old and 20-month-old) by *in situ* hybridization, real-time quantitative PCR and immunohistochemistry revealed that, in rodents, there was a reduction in the RNA and protein expression of alpha-synuclein with ageing, which could implicate a dysregulation of the neurotransmitter release (Mak *et al*., 2009). This was opposite to that seen in humans and primates (Chu and Kordower, 2007; Xuan *et al.,* 2011). The discrepancies between species might suggest different regulation and properties of this protein in different species, which could be important when considering that PD is mostly restricted to humans and primates.

In summary, the literature shows that there is a dysregulation of the expression of alpha-synuclein during ageing in the SNpc, which indicates that the aged brain shares similar mechanisms of vulnerability with PD.

1.3.2.3 Aged SNpc DAn contain an increase of oxidative stress and mtDNA deletions as in PD

As in PD, it seems that the aged SNpc contains high amounts of oxidative stress and mtDNA that can affect the mitochondria and high metabolic requirements of DAn. For instance, Venkateshappa *et al*. (2012) assessed the oxidative damage in *post-mortem* samples of SNpc at different ages, finding a statistically significant increase of protein oxidation with ageing in the SNpc as well as a reduction of the mitochondrial Complex 1 that they associated with an increase of oxidative stress in this area. On the other hand, as it was mentioned in a previous section (see subsection 1.1.3.3), Bender *et al*. (2006) demonstrated by real-time quantitative PCR that mtDNA deletions were increased in the aged human SNpc DAn compared to other regions of the brain like the hippocampus, finding almost the same deletions that in PD individuals. Supporting these results, Kraytsberg *et al*. (2006) observed by single-molecule PCR of individual DAn at different ages that the oldest individuals had the highest amount of mtDNA deletions in the SNpc, while neurons from the cortex, cerebellum or hippocampus were almost absent of these deletions. Unlike PD, however, a higher production of wild-type mtDNA would be counteracting the deletion effect in these old healthy individuals (Dolle *et al*., 2016).

Undoubtedly more investigations are necessary to understand if the main differences between PD and ageing DAn is that in the elderly there are mechanisms to counteract the deficiencies in the respiratory chain produced by oxidative stress and deletions of mtDNA.

1.3.2.4 The number of astrocytes and microglia do not change during the ageing process, although there are modifications in their morphology

In a previous subsection (see subsection 1.1.3.5), it was showed that modifications in glial cells were a hallmark in the neuropathology of PD. During parkinsonism, although it is clear that there is an activation of microglia and an accumulation of alpha-synuclein in glial cells like astrocytes, it seems more ambiguous if exists a reactive astrogliosis.

A similar scenario has been described in the aged SNpc in terms of astroglia. Venkateshappa *et al*. (2012) found an increase of GFAP in the human SNpc with ageing by Western blot, which might indicate an increase in the protein itself, in the number of astrocytes or their reactivity. Likewise, Gao *et al*. (2013) revealed by transcriptomics, together with a real-time quantitative PCR assay and immunohistochemistry, that there was an overexpression of GFAP in the SNpc of 18-month-old mice compared to 2-month-old. However, several studies have failed to demonstrate an increase in reactive astrogliosis. This is the case of Jyothi *et al.* (2015) who observed a reduction of the astroglia processes in the old SNpc in humans by immunohistochemistry, but without an increase in GFAP expression. Kanaan *et al*. (2010) found neither modifications in the number of astrocytes by unbiased stereology or O.D. of GFAP fluorescence in aged SNpc from rhesus monkeys. In fact, the expression of GFAP was reduced from the middle age to the oldest individuals, which might be indicating a failure in the activation of these cells in the elderly.

In the case of microglia in the ageing process, contrary to PD, it is unclear whether there is neuroinflammation associated with a higher density of microglia. This is true not just in the SNpc, but in the rest of the brain as well (Spittau, 2017). According to this, Jyothi *et al.* (2015) and Kanaan *et al*. (2010) noticed no age-related modifications in the number of microglia in the SNpc of humans and rhesus monkeys, respectively, although an increase in the immunoreactivity of the microglia marker in primates was found more intensely in the ventral tier of the SNpc. Furthermore, changes in the morphology of microglia were also described, showing a more activated phenotype characterized by a hyper-ramified ameboid shape that might be associated with a higher production of pro-inflammatory cytokines that can trigger neurodegeneration (Koprich *et al*., 2008).

Altogether, these studies indicate that the neuroinflammatory state of the ageing SNpc is not fully characterized and, in most cases, reveals no changes in the number of glial cells but modifications in their morphology. This could suggest that alterations in the

shape of astrocytes and microglia during ageing precede the microglia activation seen in PD.

1.4 The complex proteome and its study by proteomics

Overview: Probably one of the reasons why classical methods (i.e., histological and cellular studies) have not been able to elucidate the relation between ageing and PD yet is because of the complexity of the brain (Hosp and Mann, 2017) and, more specifically, the SNpc and its DAn. Added to this, the cause of PD seems to be multifactorial, affecting different systems within the cell such as the mitochondria or proteolysis. Moreover, a picture is beginning to emerge that not only DAn are affected by ageing and PD, but other cells in the brain like glial cells are also affected. Therefore, it is essential to understand PD and the ageing process in the SNpc from a wider perspective, exploring the whole SNpc area in its complexity, as a region where everything is connected. Thus, the minimum alteration in the environment or changes in certain cells due to ageing can have repercussions on DAn, making them more susceptible to degenerate in PD as ageing progresses. Over the last two decades, 'omics' approaches such as genomics (McCarroll *et al*., 2014) and transcriptomics (Keil *et al*., 2018) have changed the way neuroscience is explored and have offered new insights into the physiology of the CNS, including possible differences between brain regions and species, and pathological *versus* normal conditions (Geschwind and Konopka, 2009). For example, a study using next generation sequence approaches demonstrated the power of genomics tools by identifying different variants in the non-coding 3 prime untranslated region (3'UTR) involved in a neurodevelopmental disorder related to language impairment (Devanna *et al*., 2018). Transcriptomics methods have been used to specifically establish the transcriptome profile of individual cells in the CNS (e.g., astrocytes, oligodendrocytes, DAn) by combining intact transcriptomes from diverse tissue samples and single-cell RNA-seq data (Menon, 2018; Kelley *et al*., 2018). Ultimately, however, the diverse biological processes that control the brain are mediated by proteins (Freeman and

Hemby, 2004), whose expression and modifications determine not only their own function, but the different cell phenotypes and their interaction with other biomolecules. The combination of all these proteins constitute the proteome of a biological system and, as a whole, regulates the correct activity of the brain (Aebersold and Mann, 2016). Furthermore, protein variations (i.e., isoforms) due to alternative splicing of RNA transcripts (Pan *et al.*, 2008), and post-translational modifications (e.g., phosphorylation, ubiquitination, acetylation, glycosylation or methylation) are involved in the generation of a multitude of 'proteoforms' (Smith *et al*., 2013). These 'proteoforms' act as alternative proteins derived from the same gene, adding another level of complexity to the proteome in biological systems (Freeman and Hemby, 2004). The analysis of the expression of the proteins that form these proteomes, together with the study of protein interactions and post-translational modifications, is carried out by the proteomics process, which is comprised of a large variety of methods and tools to describe and quantify in detail a certain protein profile of cells or tissues (Freeman and Hemby, 2004; Aebersold and Mann, 2016; Hosp and Mann, 2017; Wilson and Nairn, 2018).

1.4.1 Proteomics methods for neuroscience

Among the different methods to identify and quantify proteome changes in neuroscience, traditional gel-based proteomics are and have been a good and cheap option. As an example, 2-dimensional sodium dodecyl sulfate polyacrylamide gel electrophoresis (2D-SDS-PAGE) allows the separation of proteins by their isoelectric point and molecular weight (MW). After the electrophoresis of the samples, the gel can be stained to visualize the proteins within the gel as spots, using different techniques such as visible silver stain, fluorescent Sypro Ruby stain or cyanine dyes (Chevalier, 2010). These spots can be cut and, subsequently, be digested with trypsin to be analyzed by mass spectrometry (Sethi *et al*., 2015). Although this classical method is still used in proteomics and neuroscience, some of the drawbacks of this technique involve that it is time-consuming, has low reproducibility, some of its staining techniques have a limited dynamic range (i.e., the

intensity of more abundant spots is limited) and hydrophobic proteins are difficult to get into the gel (Hayne and Yates, 2000). Moreover, it only allows the researcher to identify a few proteins from a small number of samples at the same time (Freeman and Hemby, 2004). In comparison, gel-free proteomics (i.e., mass spectrometry-based proteomics) can precisely screen simultaneously a vast number of proteins, including proteins from different experimental groups. Making biological sense of the proteomics data is accomplished through the use of bioinformatic software, proteomics databases, and other 'omics' data sets (Aebersold and Mann, 2016).

Two different strategies can be employed in mass spectrometry-based proteomics: 'top-down' and 'bottom-up' approaches. 'Top-down' proteomics analyzes the intact protein or 'proteoform' and can be used to identify all the different modifications that the protein can have at once and detect the MW of a protein (Toby *et al*., 2016). Although promising (due to the absence of protein digestion being less time-consuming), this approach requires a very complex experimental and computational instrumentation because the analysis of an intact protein is more difficult than a peptide (Aebersold and Mann, 2016). On the other hand, 'bottom-up' proteomics (also called shotgun proteomics) characterizes the sequences of the peptides that have been generated from proteins by proteolytic digestion. This identification is possible after a search against protein databases with the help of different algorithms (Zhang *et al*., 2013).

1.4.2 Bottom-up mass spectrometry-based proteomics

During the next subsections, a typical bottom-up mass spectrometry-based proteomics workflow is presented, including the sample preparation, the mass spectrometry analysis and the subsequent analyses of the results.

1.4.2.1 Sample preparation: in solution digestion

Unlike other 'omics' studies, it is important to consider a few points related to the quantity and quality of the sample when working with the identification and quantification of

proteins by proteomics. First, proteins cannot be amplified, unlike the nucleic acids (mRNA) used in transcriptomics studies, which means that the detection of rare proteins that appear in low quantity in the biological samples can be difficult if they are not expressed above a certain threshold (Freeman and Hemby, 2004; Hosp and Mann, 2017; Wilson and Nairn, 2018). Second, during the dissection and preparation of the biological sample, proteases and phosphatases within the sample can modify and degrade proteins, which could affect the full characterization of the proteome in that sample. To avoid this, it is crucial to inhibit these enzymes, work fast, and freezing the sample as soon as possible (Hosp and Mann, 2017).

As mentioned, bottom-up proteomics requires the proteolysis of the proteins to acquire peptides. Initially the biological sample must be homogenized (e.g., mechanically, by ultrasound or pressure, with detergents) in a lysis buffer (i.e., in solution digestion) to rupture the cells and extract the proteins. Extracted proteins are mostly insoluble, aggregating and/or precipitating due to the interactions of disulfide or hydrogen bonds among others. To prevent their aggregation and protein loss from samples, it is essential to solubilize the sample by adding different agents. For example, chaotropes (e.g., urea, thiourea) break hydrogen bonds and hydrophilic interactions. This prevents protein folding. In addition, detergents (e.g., SDS, CHAPS, Triton X-100) disrupt hydrophobic interactions. On the other hand, reducing reagents (e.g., DTT/DTE, TCEP) alter disulfide bonds between cysteines (Bodzon-Kulakowska *et al*., 2007). Finally, proteins can be proteolytically digested to produce peptides (commonly) through the use of the enzyme trypsin, which cleaves specifically C-terminal to arginine and lysine residues (Olsen *et al*., 2004).

1.4.2.2 Peptide fractionation

To manage the complexity of the sample and perform a deep proteome coverage, additional peptide fractionation can be applied by dividing tryptic peptides in different fractions. The reduction of the sample complexity allows more liquid from each different

fraction to be injected in the mass spectrometer, which gives the mass spectrometer more time to analyze the sample and increases the probability of identifying peptides expressed in low quantities (Manadas *et al*., 2010).

There are different methods that can be used for the fractionation of peptides. For instance, strong cation exchange (SCX) chromatography separates peptides according to their ionic positive net charge, which is determined by arginine and lysine residues produced by the tryptic proteolysis in an acidic solution (low pH). Peptides with different net charge will move across a solid stationary phase negatively charged using a salt gradient. More positively charged peptides will bind strongly to the negative stationary phase, while those peptides with more negative charge will move faster and elute first (Mohammed and Heck, 2011). On the other hand, reversed-phase liquid chromatography (RPLC) separates the peptides by their hydrophobic character. In this case, the stationary phase is hydrophobic, in general a column made by silica (e.g., octadecyl carbon chain (C18)), and the mobile phase will contain the peptides in an organic solvent. Therefore, more hydrophilic (polar) peptides from the mobile phase will be repulsed by the stationary column and will elute first, while more hydrophobic (non-polar) peptides will be retained within the column (Molnar and Horvath, 1976). Furthermore, ion-paring reagents (i.e., trifluoroacetic acid (TFA) or formic acid (FA)) can be added to the solvent to retain those ions that are too polar. Ion-paring reagents have a nonpolar tail that bind the column, and a negative end that can bind positive samples, retaining them (Nshanian *et al.*, 2018). Adding to this, a high pH in RPLC will increase the efficiency of separation of the sample changing the hydrophilicity of the peptides. Overall, the advantage of this fractionation method compared to SCX is that the absence of a salt gradient allows the evaporation of the solvent and will increase the concentration of the sample that can be injected into the mass spectrometer (Yang *et al*., 2012).

Alternatively, a high resolution of the sample can be achieved using a multidimensional method separation (i.e., 2D liquid chromatography (LC)) where, for example, SCX is

combined with RPLC, separating the sample by two different resolution methods (Manadas *et al*., 2010).

.

1.4.2.3 Liquid chromatography-tandem mass spectrometry

Before analyzing the sample with the mass spectrometer, the sample must be introduced in the mobile phase of LC attached to the mass spectrometer, which will produce the elution of the peptides in a time dependent manner according to the concentration of the organic solvent (Mitulovic and Mechtler, 2006).

Mass spectrometry is an analytical technique that determines the mass-to-charge (*m/z*) ratio of gas-phase ions. Spectra thus generated are typically represented as a mass spectrum plot of ion quantity (*y*-axis) *versus m/z* (*x*-axis). This implies that the analyte of interest or compound to analyze (peptides in this Thesis), that comes in a liquid solvent from the LC step, must be ionized to be identified and quantified by mass spectrometry. This ionization is generated by an ionization source and, together with the mass analyzer and a detector, form the three main elements of a mass spectrometer (Glish and Vachet, 2003).

The most common ionization approaches to convert compounds/peptides into gas-phase ions are the electrospray ionization (ESI) process, and the matrix-assisted laser desorption/ionization (MALDI) method. During ESI (i.e., the method used in this Thesis), the analyte is dissolved in a solvent solution with water and a volatile compound. Using an electrospray under high voltage, this liquid phase containing the analyte is sprayed, generating droplets. When the solvent evaporates from the droplets, the size of the drops gets reduced and the charge increases, producing a current of multiple-charged ions that move towards the vacuum of the mass analyzer (Fenn *et al*., 1989). On the other hand, ions in MALDI are created by irradiating the sample with a pulsed laser. In this case, the analyte is mixed and crystalized with a light solid matrix that absorbs the light from the laser, producing singly-charged ions (Karas *et al*., 1987). Although both

techniques are considered soft ionization sources, generating very little fragmentation of the analyte, the main difference between them is that ESI can produce multiple-charged ions and can be coupled directly to LC systems (Glish and Vachet, 2003).

Mass analyzers are involved in the selection of ions according to their *m/z*. Two main groups of mass analyzers are found depending on if the ions pass the analyzing field to the detector as a beam (beam analyzers), or if the ions are trapped in the analyzing field (trapping analyzers). Examples of beam analyzers are time-of-flight (ToF) and quadrupole mass filter (QMF) systems; while trapping analyzers are characterized by quadrupole ion trap (QIT), and high-resolution Orbitrap systems (Glish and Vachet, 2003; Savaryn *et al*., 2016).

Finally, the detector of the mass spectrometer can detect the current or image current (in the case of Orbitrap) of the ions when these pass near the detector surface, passing the information on to a computer (Freeman and Hemby, 2004).

1.4.2.4 Tandem mass spectrometry

The ionization of the intact analytes/peptides that has been described so far allows the separation and isolation of these compounds by their *m/z.* However, this first mass spectrometry analysis (MS1) is rarely enough to characterize the sequence of a peptide (Glish and Vachet, 2003). To do that, a second stage is necessary where another MS analysis is applied (MS2), therefore creating a tandem MS (MS/MS). During MS2, isolated ion/peptides that have been selected by their *m/z* in MS1 (parent or precursor ions) are dissociated or fragmented by applying an external stimulus. This reaction generates product/reporter ions or sequence-specific fragments that can be analyzed by MS2, and produces a mass spectrum of all of them (McLafferty, 1981). The advantages of this technique is that it allows fast screening of the sample with high specificity and sensitivity thanks to the digestion of the protein sample in peptides and the so-called parent-ion scan (that have been selected by their specific *m/z*) and fragmentation (that

produces a spectrum of all *m/z* and intensities from all fragments allowing the reliable identification of the amino acids (aa) sequence) (Nesvizhskii, 2007).

There are different methods to dissociate or fragment the parent or precursor ions between MS1 and MS2 by increasing their internal energy to generate product ions (Jones and Cooper, 2011). The most commonly used method in bottom-up proteomics is the collision-induced dissociation (CID) approach, where precursors ions are accelerated to collide with a neutral gas (e.g., helium, nitrogen or argon). When this happens, the kinetic energy generated is transformed to internal vibrational energy. This energy cleaves peptides by the amide-N-Co bond, producing *b* and *y* fragments ions (McLuckey, 1992). Alternatively, ions can collide with a surface in the so-called surface induce dissociation (SID) (Mabud *et al*., 1985). Electron capture dissociation (ECD) is another fragmentation method, where the product ions are irradiated with free electrons. When the electron is added to the ion, energy is liberated. This energy can cleave the peptide in the N-Cα bonds, producing *c* and *z* fragment ions, or disulfide bonds (Zubarev *et al*., 1998). Similar to ECD, during electron transfer dissociation (ETD) peptides are irradiated with radical anions, producing also *c* and *z* fragment ions (Syka *et al*., 2004). Lastly, during photodissociation, the energy is produced when ions absorb a photon that has been produced by visible, UV or infrared lasers (Brodbelt, 2014).

For this Thesis, a TripleTOF 5600+ tandem mass spectrometer (AB Sciex), equipped with a NANOSpray II source (ESI) was used to perform MS/MS analysis. This mass spectrometer is a hybrid tandem quadrupole TOF system formed by a series of quadrupole filters from where ions are passing through until they reach the detector. The first quadrupole (QJet) focusses the ion beam to enter in the next quadrupole (Q0) and improves the sensitivity of the instrument and increases the signal-to-noise ratio. Q0 also focuses the ions in the next quadrupole (Q1). Q1 filters ions towards Q2 (collision cell) by sorting them by a specific *m/z* range (TOF MS scan, all ions are analysed) or choosing a unique ion with a specified *m/z* ratio (TOF MS/MS scan, one selected ion is analysed). Once ions are in Q2, they are fragmented by a CID strategy. The CID increases the

internal energy of the precursors, this vibrational energy is lost by fragmentation to give product ions. The *m/z* of the product ions will be recorded, and these product ions will enter in the TOF region where more MS analysis will be performed (Andrews *et al*., 2011).

1.4.2.5 Acquisition methods

In general, there are three main methods to acquire the proteomics data: data-dependent acquisition (DDA), data-independent acquisition (DIA), and targeted analysis (Aebersold and Mann, 2016).

During the DDA method, in each cycle there is a first scan or survey of spectra from MS1 to determine the intensity (abundance) of parent ions from a determine *m/z*. The algorithm for DDA (TopN) will select those top *n* parent ions with higher intensity to be fragmented and analyzed in MS2. Thus, product ions will be scan by MS2, producing the respective spectrum that will be compared with a pre-defined database. The pitfall of this method is that it is possible that peptides with low intensity (low abundance) can be ignored and not selected after the first scan (Bauer *et al*., 2014; Koopmans *et al*., 2018).

In the DIA method (e.g., sequential window acquisition of all theoretical mass spectra (SWATH)), multiple parent ions from a specific *m/z* range are fragment simultaneously, generating a complex pool of fragments from different precursors. Thus, all peptides in the sample are potentially fragmented and analyzed, generating the entire *m/z* spectrum for the whole proteome (i.e., deeper coverage), in comparison to DDA where only high intensity ions are identified. This means that this technique has the advantage of being a good method to discover new proteins (Gillet *et al*., 2012; Chapman *et al*., 2014).

The third method, targeted analysis (e.g., selected reaction monitoring (SRM)) characterizes known peptides that are preselected by their *m/z* in MS1 to be fragmented and analyzed in MS2 (Picotti and Aebersold, 2012).

1.4.2.6 Peptide and protein identification

The last step in shotgun proteomics is the analysis of the MS/MS spectrum using statistical and computational tools to identify peptide sequences and proteins. All the multiple peptide search engines that can be used are grouped in three main strategies: 'sequence database searching', 'spectral library searching', and '*de novo* peptide sequencing' (Nesvizhskii, 2010).

In the case of 'sequence database searching', the MS/MS spectrum (experimental spectrum) is compared against the theoretical (*in silico*) fragmentation of all the proteins that appear in the database of a specific organism. This *in silico* digestion is performed using a specific protein sequence database (e.g., UniProt/SwissProt, NCBI-nr) based on an established criterion according to the real experiment (e.g., tryptic digestion or chemical modifications) (Nesvizhskii, 2007). The different search engines (e.g., Sequest, Scope, Mascot, ProteinPilot) will use different scoring algorithms to rank all possible peptides based on a database search score. This score will reflect how similar the experimental and theoretical spectrum are and, therefore, how confident the matches are. In general, the top scoring peptide is considered the correct match (Cottrell, 2011).

'Spectral library searching' compares the experimental spectrum with a spectral library (e.g., SpectraSST, Bibliospec) formed by MS/MS spectra that have been identified previously in other experiments. The disadvantage of this technique is that only spectra that are available in the library will be recognized (Frewen *et al*., 2006).

Lastly, '*de novo* peptide sequencing' determines the sequence of peptides directly from MS/MS spectra by knowing which fragmentation methods have been used together with other parameters (e.g., tryptic proteolysis). This approach can compare two fragments ions and calculate the mass difference that corresponds to the mass of an aa residue. This method is very useful to identify proteomes that have not yet been sequence and, therefore, there is not a protein database available. Between the software that can be used, PEAKS is one of the most popular (Valikangas *et al*., 2018).

To avoid errors in the identification of peptides and proteins to add confidence to the quality of the proteomics analyses, a false discovery rate (FDR) can be determine. Peptide-level FDR analyzes the peptide-spectrum matches (PSMs) with their scores that show how confident the matches are. The role of the peptide-level FDR is to reflect the number of false positive PSMs (i.e., incorrect rejection of the null hypothesis) among all PSMs that have been generated from the MS/MS spectra, when a spectrum is assigned to one peptide without being present in the sample (e.g., reversed peptide sequence). The most classical way of generating FDR analysis is with the 'target-decoy' approach, where target (correct sequences) and decoy (wrong sequences determined by reversed or shuffled sequences) databases are analyzed. This 'target-decoy' strategy assumes that when PSMs are positive in the decoy database, they must be false in the target database. Nevertheless, the main aim of proteomics is to identify proteins with the assembly of all peptides that have been determined, which needs another false positive control by establishing a protein-level FDR (The *et al*., 2016).

In this Thesis, ProteinPilot software was used to identify peptides sequences and proteins. This software uses the Paragon™ database search Algorithm, which combines 'sequence database searching' with a 'sequence tag' approach to identify peptides. The algorithm generates small partial sequence tags from the peptide spectrum and then compares these tags with the database. Hence, the sequence with a higher number of tags will be considered as the real answer. For that, tags are compared and mapped over 7-residue segment, generating a Sequence Temperature Value (STV) where the 'hot' STV has the maximum number of tags in that region. Regions with 'hot' STV will be searched in the database, accounting for the possibility of different variations and modifications of the sequence. Then, Pro Group™ Algorithm identifies the proteins by applying the simple assumption that peptides can only be part of one protein. Moreover, the higher the confidence is for each peptide, the more the contribution of this peptide to the protein. For each protein, the algorithm calculates the Total ProtScore (as a total of all found peptides that appear in multiple proteins) and the Unused ProtScore (as

peptides that only appear in one protein). For a protein to be detected, it is necessary to have an Unused ProtScore with the higher confidence (Shilov *et al*., 2007).

1.4.2.7 Quantitative proteomics

Protein quantification allows the comparison of the protein expression or proteomes between different experimental conditions. In order to study the differences between the proteomes of two or more samples, it is possible to chemically label the samples with stable isotopes (i.e., 'label-based' method), or use a 'label-free' approach (Anand *et al*., 2017).

Label-based methods **–** **'**Label-based' quantifications are characterized by labelling each experimental sample with a tag of a different mass. This allows the recognition of the different sample peptides by observing specific changes in their mass. When using this strategy, samples must be labelled first and then pooled before MS analysis is performed. This strategy was developed thanks to the discover of isotope-coded affinity tags (ICAT) by Gygi *et al*. (1999). These tags contain a reactive group that binds cysteinyl residues, a linker segmented with or without eight deuterium isotopes (allowing two different experimental conditions), and a biotin label that can bind avidin to isolate the peptides. After mass spectrometry analysis, the difference in mass between the two linker segments helps to identify the sample from which the peptides came from. Another example of 'label-based' technique is SILAC (stable isotope labeling of amino acids in cell culture), where proteins can be labelled *in vivo* (in general in culture) by using two different media with normal or labeled aa with heavy isotopes. Thus, when cells grow, they will incorporate normal or heavy labeled aa in their new proteins, and generate two proteomes that can be identified based on their peptides having different mass (Mann, 2006). Finally, other 'label-based' methods like tandem mass tag (TMT) and the isobaric tag for absolute and relative quantitation (iTRAQ), use isobaric tags to label the amines of the proteins. TMT allows the quantification of up to 10 different samples, having a total

mass of 305kDa. It is divided into an amine reactive group that binds the N-terminal or lysine of the peptides, a balance group with variable mass (184−192) and a MS/MS reporter group (113−121kDa) that generates a specific reporter ion after fragmentation (Thompson *et al*., 2003). On the other hand, iTRAQ is based on the use of isobaric reagents (from four −4plex− to eight −8plex −), allowing for the analysis of up to eight different samples simultaneously when the tags dissociate during MS/MS analysis. The isobaric labels, with a total mass of 145kDa, are formed by: (a) an amine specific peptide reactive group that binds the lysine and N-terminal of each peptide; (b) a reporter group with a variable mass (114 to 121kDa) to create the mass difference between experimental samples; and (c) a balance group with a variable mass (28 to 31kDa) to maintain the isobaric characteristics of the tag during MS1. After the fragmentation step for the dissociation of ions, the balance group is removed from the tag, which generates differences in the mass between the same peptide from each experimental group in the reporter ions of MS2. This different mass is caused by the distinct reporter groups from each isobaric tag. During MS1 scans, one peak will appear combining the same peptide from each different sample, however, the fragmentation of that peptide will generate the production of reporter ions of different *m/z* in MS2. The specific intensity of these reporter ions will indicate the amount of peptide from each sample, and is used to calculate the relative quantification of each protein by dividing each of the sample groups by the established control as the denominator (Ross *et al*., 2004). The advantage of iTRAQ is the possibility of analyzing up to eight samples in a single MS experiment; although due to the tryptic digestion, the complexity of the sample increases (Wiese *et al*., 2007). Previous studies using iTRAQ, however, have shown its utility in the field of neuroscience using both rodent and human samples. For example, recent work by Xie *et al*. (2018) demonstrated that in a rat model of depression, proteins related to synaptic mitochondria of hippocampal neurons were dysregulated in comparison to their littermates. They speculated that this might indicate an impairment in the production of the energy necessary for synaptic plasticity. Likewise, Adav *et al*. (2019) revealed that

mitochondrial proteins were dysregulated during AD, comparing *post-mortem* human samples (medial frontal gyrus) with AD *versus* healthy control individuals.

In this Thesis, iTRAQ4plex was the method chosen to identify and quantify the samples, allowing the labeling of the four different age groups (see Chapter 2). The relative quantification of each protein was resolved as a fold-change ratio by establishing the oldest group (i.e., old, >21-month-old) as the denominator of each comparison. Thus, MS/MS analyses from the juvenile (postnatal P14), young (8-month-old) and middle age (16-month-old) were compared against the MS/MS analysis obtained from the old samples, generating a relative quantification of each protein expression in comparison to the old age (i.e., juvenile *versus* old; young *versus* old; middle age *versus* old).

Label-free method – 'Label-free' quantifications require independent MS/MS analysis of the different experimental groups, but avoid the use of expensive tags, which reduces the time of preparation of the sample and makes this method cheaper compared to label-based proteomics (Asara *et al*., 2008). One of the ways to generate 'label-free' quantifications is by 'spectral counting' (SpC) of each sample. This works on the principle that proteins with a higher expression produced more peptides (number of spectra) that can be identified. Thus, the quantification and identification of proteins are performed in MS/MS analysis by counting the number of spectra. However, during this strategy it is important to consider that larger proteins will generate more peptides (more spectra) that can be identified, which can affect the estimation of the amount of protein. Therefore, to estimate the amount of protein according to their size, different methods can be used, including 'exponentially modified protein abundance index' (emPAI) or 'normalized spectral index' (SIN) (Arike and Peil, 2014). Another 'label-free' strategy is to quantify the 'area under the curve' (AUC), which reflects the peak intensity of each peptide spectra in MS1. In this process, quantification of the different expression of

peptides/proteins from different samples is performed in MS1, while their identification is done in MS2 (Neilson *et al*., 2011).

1.4.3 Bioinformatics

The production of complex datasets from shotgun proteomics involves the use of bioinformatics tools to understand the biological meaning of the mass spectrometry analysis and observe how a certain proteome changes under different experimental conditions.

Among the different bioinformatic analysis that can be applied, Gene Ontology (GO) annotation analysis allocates proteins in terms or functional groups. These terms are part of three categories – 'biological process', 'molecular function' and 'cellular component' – which indicate the biological function that a specific protein has in that proteome. Moreover, GO enrichment analysis calculates which terms are significantly enriched (overrepresented) over an established dataset (e.g., the whole proteome of the sample) based on the number of proteins associated with various terms (Ashburner *et al.,* 2000). This enrichment analysis can be done directly on the GO project website, using online applications (e.g., Gorilla, AmiGo, Database for Annotation, Visualization and Integrated Discovery (DAVID)) or open-source programming languages such as Python or R (Pomaznoy *et al*., 2018).

Similarly, pathway analysis highlights those biological pathways that are significantly overrepresented in the analyzed proteome. These biological pathways reflect the activity taking place inside the cells by grouping the biological effects of the proteins that have been identified. For that, different databases such as Kyoto Encyclopaedia of Genes and Genomes (KEGG) (Kanehisa and Goto, 2000), Reactome (Matthews *et al.*, 2009) or Ingenuity Pathway Analysis (IPA) (Kramer *et al*., 2014) can be used.

Finally, it is possible to observe what kind of interactions exist between proteins within a certain proteome. This can be illustrated as a protein network where some proteins can be identified as a hub with a high connectivity with a larger portion of the proteome. These association are not just based on experimental data, but also data extracted from the literature. MINT (Chatr-aryamontri *et al*., 2007) or Search Tool for the Retrieval of Interacting Genes/Protein (STRING) (von Mering *et al*., 2003), for example, are some of the software and databases that can be used to perform such an interaction analysis.

In this Thesis, bioinformatics analysis included GO enrichment analysis with DAVID, KEGG and Reactome pathway analyses, and STRING network analysis. More information about each method can be found in Chapter 2.

1.5 Aim and objectives

This chapter has attempted to provide a brief summary of the literature relating to PD, an aged-related neurodegenerative disease characterized by the degeneration of DAn in the ventral tier of the SNpc. Furthermore, this section has tried to review the key aspects that make DAn from the ventral tier SNpc more vulnerable in comparison to more resistant DAn during the disease. Moreover, and because ageing is the main risk factor associated with parkinsonism, it has been described the different changes that the brain and SNpc undergoes with ageing. This literature reveals the attempts that scientists have made so far to try and establish a relationship between ageing and PD. Currently, however, this relationship remains a mystery. To help address this, new cutting-edge techniques, such as the proteomics used here, can help us understand the contribution that ageing make to DAn vulnerability in the SNpc, and provide new insights into how DAn degeneration can be combated during physiological ageing and PD. Therefore, to end this General introduction, an overview of proteomics methods in neuroscience has been described to help the reader better understand the specific methods used.

The aim of this Thesis, therefore, was to enhance our understanding of the role that ageing has in the increased vulnerability of SNpc DAn. The objectives of this Thesis were:

- Objective 1) To analyze the proteome of the SNpc in rats during ageing using a quantitative proteomics approach and bioinformatic tools (Chapter 3).
- Objective 2) To quantitatively and morphologically characterize ageing SNpc DAn in rats and humans (Chapter 4).
- Objective 3) To study the effect that the lack of astrocytes has on the survival and vulnerability of DAn in normal conditions and against the toxin 6-OHDA *in vitro* (Chapter 5).
- Objective 4) To elucidate (through a systematic review) modifications in the proteome of the ageing nervous system and PD and associate these changes with dysregulated proteins found in Chapter 3 (Chapter 6).

Chapter 2.
Materials and methods

CHAPTER 2. MATERIALS AND METHODS

2.1 Studies of the SNpc during ageing in rats

2.1.1 Animals, tissue extraction and sample preparation

Male and female Sprague Dawley rats were used for the study of the rat SNpc during ageing in rats (Chapters 3 and 4). The following four experimental groups were used for comparisons: postnatal day 14 rats ('juvenile'); 8-month-old rats ('young'); 16-month-old rats ('middle age'); and 21-25-month-old rats ('old'). All animal experiments were performed in accordance with European Union Directive 2010/63/EU, were reviewed and approved by the Animal Welfare & Ethical Review Body (AWERB) at Keele University, and conducted under the licensed authority of the UK Home Office (PPL40/3556). Animals were maintained in a room with a controlled light schedule (12-hour light/dark cycle) and temperature (22 ± 1 ^{o}C) with free access to food and water.

Rats were humanely euthanized with an overdose of pentobarbitone anesthetic (0.5 ml/100 g) via an intraperitoneal injection, and transcardially perfused with ice-cold sterile 0.9% sodium chloride (saline) to remove all the blood. Brains were removed rapidly from the skull and cut in half along the sagittal midline. The right hemispheres were used for proteomics and Western blotting analyses (see Chapter 4), while the left hemispheres were kept for immunohistochemistry and immunofluorescence analyses (see Chapter 3 and 4) (**Figure 2.1, Table 2.1**).

The right hemispheres were placed in a petri dish with fresh sterile saline, and the SNpc was removed by careful dissection. Each fresh SNpc sample was placed separately in 1.5 ml aliquots on dry ice and subsequently stored at -80 ^{o}C for proteomics and Western blot procedures (see below).

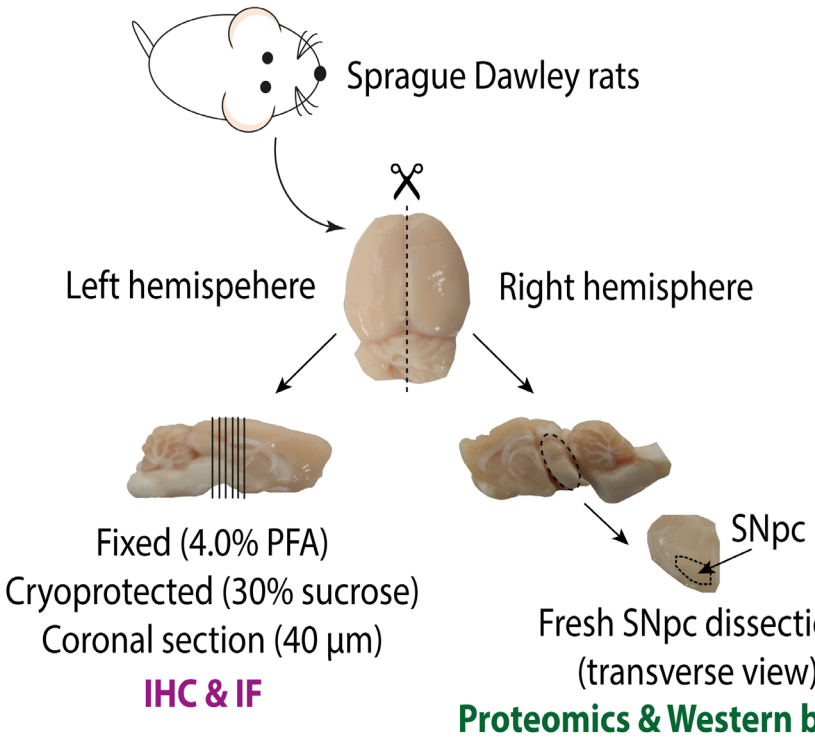

Figure 2.1. **Procedure for tissue extraction and sample preparation for the different analyses.** Rats were transcardially perfused with ice-cold sterile saline and the brains removed. The right hemispheres were used to dissect the midbrain region that contains the SNpc. Subsequently, a sub-dissection of this region was conducted to obtain the fresh SNpc (within the dotted line) for proteomics and Western blotting analyses. The left hemispheres were fixed in 4.0% PFA solution and cryoprotected in 30% sucrose before cutting them in coronal sections (40 µm thickness) for immunohistochemistry (IHC) and immunofluorescence (IF).

The left hemispheres were fixed in 4.0% solution of paraformaldehyde (PFA) in 1X Tris-buffered saline (TBS) overnight. The following day, the hemispheres were submerged in 30% sucrose in TBS until they were completely sunken in the bottom of the solution (this reduces the water content of the tissue to cryoprotect it during freezing). The fixed hemispheres were taken out from the sucrose solution and 40 µm coronal sections were cut through the entire midbrain. To do this, fixed samples were mounted in a microtome (Bright series 8000, Bright Instrument Company) with Bright Cryo-M-Bed embedding compound (Bright Instrument Company) and sliced coronally. Each section was collected consecutively in 6 wells of a plastic plate containing an antifreeze

cryoprotectant solution (30% ethylene glycol, 30% glycerol in 0.2 M phosphate buffer) to store them at -20 ºC for future use.

Table 2.1. Classification of the number of rat samples used in the study of the SNpc during ageing. The study included four experimental groups: postnatal day 14 rats ('juvenile'), 8-month-old rats ('young'), 16-month-old rats ('middle age'), 21-25-month-old rats ('old'). Each age experimental group contained eight rats (*n=8*), except in the old group where there was *n=9*. Both sexes were equally represented in each age group (females, *n=4-5*; males, *n=4*). Left hemispheres (*n=8-9* in each experimental group) were used for immunohistochemistry (IHC) and immunofluorescence (IF) assays. Right hemispheres were dissected to obtain the fresh SNpc for proteomics (SNpc from four rats (*n=4*) pooled together) and Western blotting (WB) analyses (SNpc from four/five rats (*n=4-5*) used individually).

Age group	Sex	IHC & IF	Proteomics (pooled samples)	WB (individual samples)
Juvenile (postnatal day 14)	Female	4	2	2
	Male	4	2	2
	Total	**8**	**4**	**4**
Young (8-month-old rats)	Female	4	2	2
	Male	4	2	2
	Total	**8**	**4**	**4**
Middle Age (16-month-old rats)	Female	4	2	2
	Male	4	2	2
	Total	**8**	**4**	**4**
Old (21-25-month-old rats)	Female	5	2	3
	Male	4	2	2
	Total	**9**	**4**	**5**

2.1.2 Humans, tissue extraction and sample preparation

Fifteen *ex vivo* human brains (9 males and 5 females; **Table 2.2**) were collected from Keele University School of Medicine (Anatomy Facility), regulated by the HTA (Human

Tissue Authority) and with the approval of the School-Student Project Ethics Committee (S-SPEC). All donors were given consent permission for the use of the tissue. Only samples with no brain diseases known were included in the study.

Table 2.2. Details of human midbrain samples containing the SNpc included in the study, *n=15.*

	Human age groups (years)					
Sex	50-59	60-69	70-79	80-89	90-99	100-109
Female	–	1	2	2	–	1
Male	1	–	1	4	3	–
Total	1	1	3	6	3	1

The midbrain containing the SNpc was extracted from each right hemisphere via a horizontal cut (1.2 cm height) from the posterior commissure to the inferior colliculus. The midbrains containing the SNpc were fixed in 4.0% solution of PFA in 1X TBS overnight. The following day, the midbrains were submerged in 30% sucrose in TBS until they were completely sunken in the bottom of the solution. The fixed midbrains were taken out from the sucrose solution and cut 40 µm in transverse sections. To do this, fixed samples were mounted on a microtome (Bright series 8000, Bright Instrument Company) with Bright Cryo-M-Bed embedding compound (Bright Instrument Company) and sliced. Each section was collected consecutively in 6 wells with antifreeze cryoprotectant solution (30% ethylene glycol, 30% glycerol in 0.2 M phosphate buffer) to store them at -20 ^{o}C. In this case, and due to the high amount of material collected, after every 30 sections one sample was kept independently for free-floating immunostaining procedures (i.e., immunohistochemistry).

2.1.3 Protein extraction for proteomics and Western blotting

For quantitative proteomics analysis (Chapter 3), four animals per group were used (*n=4*, 2 males and 2 females) (**Table 2.1**). To minimise sample losses due to the small size of

SNpc tissue, the four samples from each experimental group (juvenile, young, middle age or old) were pooled before the protein extraction. Pooled samples of each experimental group (juvenile, young, middle age or old) were homogenised as previously described (Fuller *et al*., 2014) in 4 volumes (w/v) of 6 M Urea, 2 M thiourea, 2% CHAPS and 0.5% Sodium Dodecyl Sulfate (SDS) using a pellet pestle (20 strokes). Samples were left on ice for 10 minutes, followed by brief sonication. Samples were again left on ice for 10 minutes and then were centrifugated at 13,000 x g for 10 minutes at 4 ºC. The supernatants, containing the extracted proteins, were transferred to a clean tube, and the pellets with all insoluble material were discarded. Subsequently, 6 volumes of ice-cold acetone were added to the supernatants to precipitate the proteins. The tube was inverted three times, to carefully mix the acetone with the extracts, and was incubated overnight at -20 ºC. The following day, the samples with acetone were centrifuged at 13,000 x g for 10 minutes at 4 ºC. The supernatants were removed with care and discarded. Each pellet was then resuspended in 200 µl of 500 mM tetraethylammonium bicarbonate (TEAB) in ultrapure water (Chromasolve). In order to use the same protein concentration from each sample in mass spectrometry analysis, the total protein concentration from each sample was quantified using a Bradford protein assay (see below) (Bradford, 1976).

To validate the proteomics results and test if the changes that appeared in the pooled samples were maintained individually during ageing, Western blotting analyses were conducted (Chapter 3). To do this, the remaining frozen SNpc tissues (*n=4-5* per age group, 2 males and 2-3 females) were extracted individually (without pooling) (**Table 2.1**). Each individual sample was homogenised in 200 µl of cold RIPA buffer (Sigma, #R0278) with Halt™ protease EDTA-free inhibitor cocktail (ThermoFisher Scientific, #87785) using a pellet pestle (20 strokes). Samples were left on ice for 10 minutes, followed by sonication. Samples were placed again on ice for 10 minutes and then were centrifugated at 13,000 x g for 10 minutes at 4 ºC. The supernatants, containing the extracted proteins, were transferred to a clean tube, and the pellets with all insoluble

material were kept in case the protein extraction was not successful. Protein extracts from each individual sample were kept in aliquots at -80 °C for future Western blotting analyses. To ensure the same protein concentration from each sample, the protein concentration from each sample was quantified using a Bradford protein assay (see below) (Bradford, 1976).

2.1.3.1 Bradford protein assay

First, protein standards were produced via serial dilutions from a Protein Standard (Bovine Serum Albumin, BSA; 20 mg/ml) to establish a concentration range from 20–0.312 mg/ml. Subsequently, 5 µl of standard dilutions, protein samples (i.e., proteomics and Western blot) and blanks (500 mM TEAB or RIPA) were diluted in 45 µl of 500 mM of TEAB or RIPA. Next, 1 ml of Bradford protein assay solution (Bio-Rad, #5000006) was added and mixed to the final volume of 50 µl of each sample. Finally, 100 µl of each diluted sample with the Bradford reagent was transfer to a 96-well-plate, measuring the absorbance at 595 nm in a GloMax-Multi+ Detection System plate reader (Promega).

2.1.4 Sample preparation for mass spectrometry analysis [1]

Every step was done following the protocol established by the iTRAQ™ labelling kit (Biotech, 2016; Applied Biosystems, Foster City, CA, USA). This method uses four isobaric (same mass, 145 Da) tags (iTRAQ Reagent 114, 115, 116, 117) that bond covalently to the N-terminus and side-chain amines of peptides from protein digestions. Each tag has a peptide reactive group, a neutral balance group and a unique reporter group, which produces different ions at *m/z* 114, 115, 116 and 117 when peptides are fragmented by MS/MS. This allows one to analyse different samples in a single MS analysis, producing a relative and absolute quantification (Fuller and Morris, 2012).

During iTRAQ labelling preparation, 85 µg of each sample was used, and any remaining protein extract was kept at -80 °C in case they were needed for future use. To each

[1] Sample preparation for mass spectrometry analysis was carried out by Heidi R. Fuller.

sample, 20 µl of Dissolution Buffer was added, followed by 1 µl of 2% SDS to denature the protein extracts. Samples were mixed and, immediately after, 2 µl of the Reducing Reagent (50 mM tris-(2-carboxyethyl)-phosphine (TCEP)) was added and mixed to reduce disulfide bonds. Samples were incubated for 1 hour at 60 °C and the reduced cysteines were blocked by adding 1 µl Cysteine Blocking Reagent (Borges and Sherma, 2014). The tubes were incubated at room temperature for 10 minutes. Proteins were digested with sequencing grade modified trypsin (Promega, #V5113), incubated overnight at 37 °C, using 5 µg of trypsin per 100 µg of protein. The next day, samples were dried down in a centrifugal vacuum concentrator (ThermoSavant, ThermoFisher Scientific) to reduce the volume of the sample digest and maximize labelling efficiency. Subsequently, each iTRAQ Reagent vial with a different tag was transfer to each peptide sample. Peptides were labelled at room temperature for 1 hour with iTRAQ™ Reagents-4plex as follows: 114–juvenile, 115–young, 116–middle age, 117–old. Then, each of the iTRAQ labelled samples (114–juvenile, 115–young, 116–middle age, 117–old) were combined into one tube (**Figure 2.2**).

2.1.5 High pH reverse-phase liquid chromatography (RPLC) fractionation[2]

To reduce the complexity of the samples prior to mass spectrometry analysis, peptides were first separated into fractions by high pH RPLC (**Figure 2.2**). The sample was dissolved in 100 µl of buffer A (10 mM ammonium formate (NH_4HCO_2), 2% acetonitrile (MeCN), pH 10.0). The peptides were then fractionated by RPLC using a C18 column (XBridge C18 5 µm, 4.6 x 100 mm, Waters).

[2] Samples were sent to the BSRC Mass Spectrometry and Proteomics Facility at St. Andrews University (Fife, UK) where the high pH reverse-phase liquid chromatography and mass spectrometry analysis were performed. Details of the methods were provided by Sally L. Shirran and Silvia Synowsky.

The column was rinsed with 96% buffer A at 1 ml/min for 6 minutes until the O.D. on the ultraviolet chromatogram returned to the baseline. The gradient ran from 4–28% of buffer B (10 mM NH_4HCO_2, 90% MeCN, pH 10.0) for 30 minutes to 28–50% buffer B for 6 minutes. The column was rinsed in 80% buffer B for 5 minutes and then was re-equilibrated at initial conditions with 4% buffer B for 11 minutes. Fractions of 0.5 ml were collected every 30 seconds. The UV chromatogram was analysed and the fractions with similar peptide concentration across the elution profile were combined to give 12 fractions. The pooled fractions were concentrated in a vacuum concentrator and resuspended in 30 µl of 0.1% of FA.

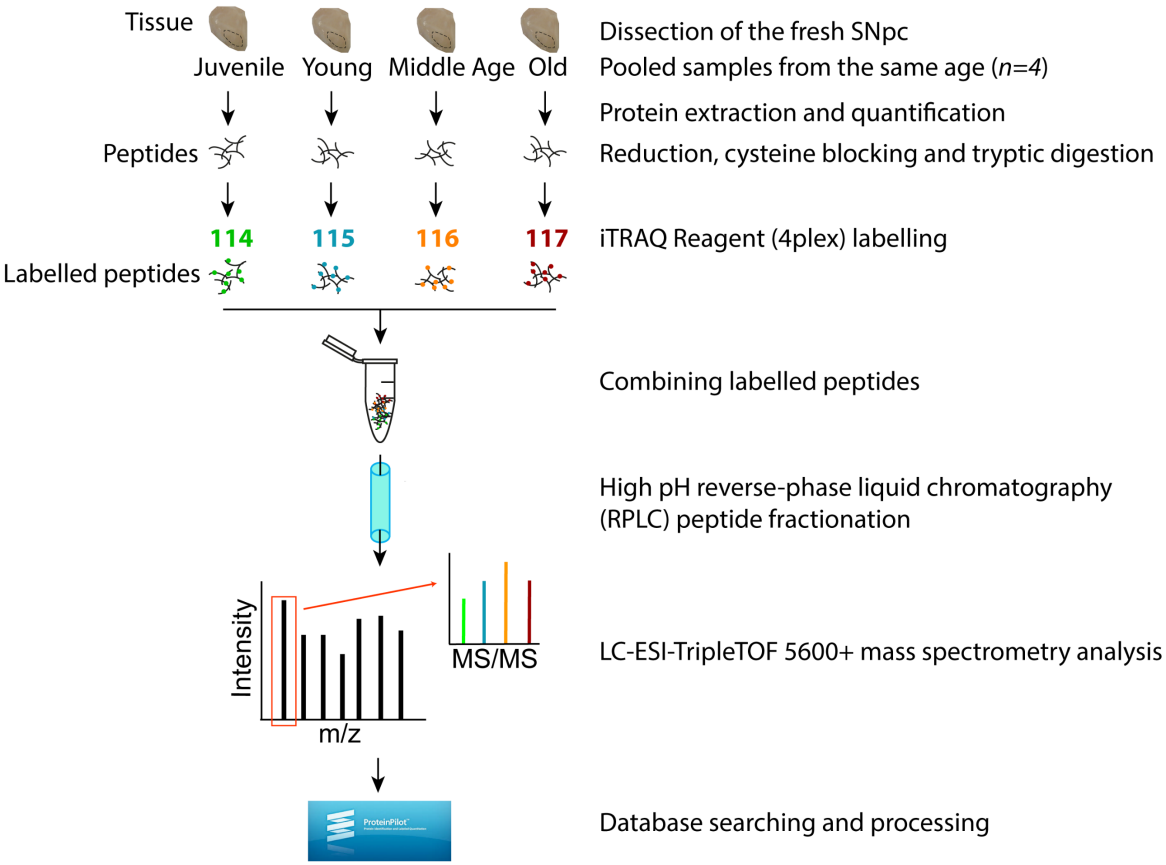

Figure 2.2. Protein extraction from the rat SNpc (within the dotted line) and LC-ESI-TripleTOF 5600+ mass spectrometry proteomics analysis workflow.

2.1.6 Mass spectrometry analysis (LC-ESI-MS/MS)[2]

1/3 of each fraction containing the labelled peptides was analysed by mass spectrometry. First, the peptides were separated by LC using a nanoLC Ultra 2D plus loading pump and nanoLC AS-2 autosampler chromatography system (Eksigent). Peptides were loaded on the column with buffer A (2% MeCN, 0.1% FA in ultrapure water) and bound to an Acclaim PepMap100 trap (100 µm x 2 cm) (ThermoFisher Scientific). The trap was then washed for 10 minutes with buffer A, after which the trap was turned in-line with the analytical column (Acclaim PepMap RSLC column, 75 µm x 15 cm). The analytical solvent system consisted of buffer A and buffer B (98% MeCN, 0.1% FA in ultrapure water) at 300 nl/min flow rate. Peptides were eluted using the following gradient: linear 1–20% of buffer B over 90 minutes, linear 20–40% of buffer B for 30 minutes, linear 40–99% of buffer B for 10 minutes, isocratic 99% of buffer B for 5 minutes, linear 99–1% of buffer B for 2.5 minutes and isocratic 1% buffer B for 12.5 minutes. The eluent was analysed using a TripleTOF 5600+ tandem mass spectrometer (AB Sciex), controlled by Analyst® TF software (AB Sciex). The system was equipped with a NANOSpray II source (ESI) which sprayed the samples into the mass spectrometer (**Figure 2.2**). The mass spectrometer was operated in DDA top20 positive ion mode with 120 mn acquisition time for MS (*m/z* 400–1250) and MS/MS (*m/z* 95–1800), and 15 seconds of dynamic exclusion. MS/MS was conducted with a rolling collision energy (CE) inclusive of present iTRAQ CE adjustments.

2.1.7 Database searching and criteria for identifying differentially expressed proteins

Peptides were identified and quantified using ProteinPilot software, version 5.0.1.0 (Applied Biosystems) (**Figure 2.2**). Once the software converted LC-ESI-MS/MS raw data in peak lists, the Paragon™ database search Algorithm version 5.0.1.0 identified peptides and their isoforms from MS/MS spectra using the UniProtKB/Swiss-Prot FASTA database. Subsequently, the Pro Group™ Algorithm performed a statistical analysis on

the peptides found to accurately determine which proteins had been detected. Proteins that showed a Protein Threshold>5 were used for the Pro Group™ Algorithm to calculate the relative quantification of the protein expression, generating an error factor and p-value. The relative quantification of each protein was produced establishing a ratio between each of the age groups (114–juvenile, 115–young, 116–middle age) in relation to the old age group (117–old). The old group was established as the denominator because it is the focus of this Thesis and the aim was to determine which proteins were differentially expressed in the oldest animals (as this may help to explain or understand why ageing is one of the main risk factors associated with the degeneration of DAn of the SNpc in PD). The general Paragon™ search analysis parameters were: type 'iTRAQ4plex (Peptide Labeled)', cysteine alkylation 'MMTS', digestion 'trypsin' as the cleavage enzyme, instrument 'TripleTOF', and species '*Rattus norvergicus*' for sample parameters; processing parameters were specified as 'quantitative' to determine the relative levels of the protein, 'bias correction' to correct the median ratio to unity eliminating pipette or other errors (ratios of 1.4484 for the 114:117 labels, 1.1639 for 115:117, 1.1788 for 116:117), and 'background correction' to remove the background due to many lower-intensity peptides were selected; 'thorough ID' and 'Biological modifications' to consider biological modifications in the peptides searching were chosen to specify search effort and ID focus parameters. To validate the results, the independence FDR analysis was executed using the Proteomics System Performance Evaluation Pipeline (PSPEP). The local FDR analysis showed the percentages of specific identifications that were incorrect, giving 2,363 proteins (5%) and 2,206 proteins (1%). The protein summary list generated by ProteinPilot included, among others: the accession number, which is a stable identifier for UniProtKB entries or proteins; the number of peptides found for each protein; and the proteins ratios for each different group of age (114–juvenile *versus* 117–old, 114:117; 115–young *versus* 117–old, 115:117; 116–middle age *versus* 117–old, 116:117) with their p-values and error factor.

To eliminate false positives in the protein list generated by ProteinPilot, the following criteria were applied: a) proteins must be non-reversed, based on the reversed database searching to avoid false peptides sequence matches (Feng *et al*., 2007); b) proteins must be identified with at least three peptides with 95% confidence during peptide identification, because a single peptide (denominated 'one-hit wonder') can generate a false protein match by chance (Cottrell, 2011). Thus, reversed proteins and proteins with two or less peptides were eliminated from the protein list.

Next, to produce a robust and confident list of differentially expressed proteins in the old group, other filters were imposed: a) protein fold-change ratios must have a significant p-value ($p<0.05$); and b) in addition to the statistically significant fold-change ratios ($p<0.05$), these ratios must pass an arbitrary 1.25-fold-change cut-off to be sure that the proteins classified as up (ratio ≤0.75) or downregulated (ratio ≥1.25) in the old group were true differences (Jin *et al*., 2009).

2.1.8 Analysis of differentially expressed proteins

Once the differentially expressed protein lists from the three different ratios (114–juvenile:117–old, 115–young:117–old, 116–middle age:117–old) were obtained, the following four independent analysis (subsets) were performed (Chapter 3).

First, a common analysis was conducted using all three differentially expressed protein lists of each ratio (114:117, 115:117, 116:117). This analysis provided the possibility to determine which proteins were differentially expressed in all three groups (juvenile, young and middle age) compared to the old group, in addition to understanding the trending of their expression and distribution along ageing.

Second, the ratio 114:117 (juvenile *versus* old) was removed from the analysis. This step was done to avoid the inclusion of possible changes in the expression of proteins due to development of the brain in the juvenile group.

Third, two sub-groups analyses were executed. The first approach considered only differentially expressed proteins in the ratio 115:117 (young *versus* old), highlighting proteins that changed between the young and the old group but perhaps were not statistically significant and/or with an acceptable cut-off between the middle age and old group. This situation could appear if, for example, modifications in the expression of proteins were gradually changing with increasing age, so variations from the middle age to the old group may not show a significant or acceptable fold-change. These circumstances could be biologically relevant, even though they are not statistically significant in the ratio middle age *versus* old, because they reflect that some modifications in the expression of the proteins related with ageing appear early in the SNpc. The second approach examined proteins that were only differentially expressed in the ratio 116:117 (middle age *versus* old) compared to proteins from the ratio 115:117 (young *versus* old), regardless of whether the protein ratios were statistically significant and/or with an acceptable cut-off or not. This condition could be explained if modifications of the protein expression due to ageing appear, at least significantly, very late in the adult SNpc.

2.1.9 Bioinformatic analyses of proteomic data for biological interpretations

To gain insights into the biological meaning of the data, the four independent subsets of identified proteins in the sub-group analysis were analysed using bioinformatics tools, as described in the following sections.

2.1.9.1 Functional annotation analysis: DAVID

The bioinformatic software to perform all the statistical tests necessaries to accomplish the functional enrichment analysis was DAVID, version 6.8, using the Functional Annotation Clustering Tool (https://david.ncifcrf.gov/). This bioinformatic tool classifies set of proteins using a functional enrichment analysis, which maps large proteins lists in

biological annotations or gene ontology terms, and shows which terms are statistically overrepresented or enriched. This type of large protein list analysis brings the opportunity to successfully identify a biological process associated with a group of related proteins (Huang *et al*., 2007; Huang *et al*., 2009). DAVID uses a unified annotation database (DAVID Gene concept) created by integrating the most popular independent redundant databases (e.g., NCBI or UniProt/SwissProt) using a single-linkage algorithm. This process improves the availability of annotation data and enhance the accessibility to different categories. DAVID determines the statistical significance (p-value) of every single enriched annotation term in the user's protein list (the four different subsets in this case). The statistical method to calculate the enrichment p-value (modified as EASE score) is the Fisher's Exact test. The level of enrichment is generated comparing the sample proteins (or gene list) to an established population background gene. The population background can be the DAVID default one (i.e., genome-wide genes with at least one annotation in the analysing categories) or a customized population background that is submitted to DAVID. Nevertheless, it is important to note that depending on the selections of the population background, the results will differ (Huang *et al*., 2007; Huang *et al*., 2009).

To perform the Functional Annotation analysis the following procedure was undertaken for each of the four subsets of identified proteins (Chapter 3). Each set was submitted independently into the 'Gene List' box within the Functional Annotation Tool as a row list of the corresponding protein accession numbers. The selected identifier was 'uniprot_accesion', and the list type 'gene list'. For the background, the entire list of identified proteins in this study removing the possible false positive matches (**Supplementary Table 2a**) was submitted, regardless of whether they were differentially expressed or not. From the annotation summary result, GO analysis was selected to establish which terms within the following categories were enriched in each dataset: the biological process (BP) in which the proteins are involved, the type of cellular component (CC) to which they belong, and the specific molecular function (MF) that they develop

inside the cell. Also, the KEGG (Kyoto encyclopaedia of genes and genomes) pathway (https://www.genome.jp/kegg/) (Kanehisa and Goto, 2000) was used to determine whether any of the proteins in the dataset map to known biological networks (e.g., metabolism, environmental information processing, human diseases). Each of these functional annotations (BP, CC, MF; KEGG) created a specific Functional Annotation Chart. The chart showed a list of enriched terms, the list of proteins that form each term and their p-value (EASE score). Only terms with a $p<0.05$ and more than two proteins were finally selected.

2.1.9.2 Reactome pathway analysis

The bioinformatic tool Reactome pathway knowledgebase, version 68 (June 2019) (https://reactome.org/) was used for the interpretation, integration, visualization (i.e., using an interactive graphical map) and analysis of the data. Reactome organizes signalling and metabolic molecules called 'entities' that participate together in reactions from biological pathways and processes (e.g., metabolism, transcriptional regulation, disease) (Fabregat *et al*., 2017; Fabregat *et al*., 2018). Reactome is focused on the single species *Homo sapiens*, which means that all non-humans' identifiers or proteins are converted to their human equivalents and, afterwards, they are systematically associated with their molecular functions. To achieve that, the Reactome project recruits expert authors that described pathways in their area with references. Later, a Reactome curator works together with the authors to convert this information into the database structure used in Reactome. Once the module is ready, it is peer-reviewed by another expert in the field, allowing the release of the pathway on the public Reactome website and database. Different databases resources (e.g., Uniprot, NCBI, GO) are cross-referenced by Reactome. The overrepresentation analysis tool determines if the list of proteins provided (i.e., identifiers) by the user are annotated to an entity from the Reactome pathway, using a hypergeometric distribution test that generates a probability score (from 0 to 0.05). In essence, the statistical test calculates if certain Reactome

pathways are overrepresented (enriched) in the submitted dataset, in comparison to what it would be expected by chance. In the case that entities have not been updated as part of a specific Reactome database, identifiers or proteins will not be found or mapped in the Reactome analysis. Reactome pathway analysis (Chapter 3) were performed using the 'Analyze data' tool, placing the list of accession number of each subset of proteins in the big box provided for that. 'Project to human' was selected and the data was analysed.

2.1.9.3 Protein network analysis: STRING

STRING database (https://string-db.org/), version 11.0, was used to predict possible protein networks and understand protein-protein interactions within each subset of results. STRING database collects, scores and integrate publicly available information from online databases (e.g., GO, KEGG, Reactome) related to protein-protein interactions (physical and functional) with computational predictions, and including accessory information such as annotated pathway knowledge or text-mining results (Szklarczyk *et al*., 2019). Proteins that contribute together to a specific biological function (i.e., not only physically) are linked by 'functional association'. Among the different associations, proteins can be related by different 'channels' as follows: genomic context information (i.e., neighbourhood, fusion, gene co-ocurrence), co-expression, text-mining, biochemical//genetic data (i.e., experimental data), protein-complex knowledge (i.e., databases). STRING will generate an interaction score for each channel, which represents not the strength of the interaction but the confidence (from zero to one) to determine if, with the available evidence, the interaction is true. Evidence for each channel is sub-divided into two scores, one represents the evidence from the organism that has been chosen for the analysis, and the other is transfered from other organisms, based on hierarchically arranged orthologous group relations. Scores are computed by combining the probabilities from the evidence that exists from the different channels, being corrected for the probability that a random interaction occurs. For the STRING

analysis (Chapter 3), accession number of each subset of proteins was submitted into the 'List of Names' box within the 'Multiple proteins' tool, and the organism '*Rattus norvegicus*' was selected. The minimum required interaction score was medium (0.400) confidence.

2.1.9.4 Multiple sequence alignment

Clustal Omega multiple sequence alignment (MSA) tool (https://www.ebi.ac.uk/Tools/msa/clustalo/), from the European Bioinformatic Institute part of the European Molecular Biology Laboratory (EMBL-EBI) search (Madeira *et al*., 2019), was used for the alignment of sequences. Clustal Omega generates biologically meaningful MSA of different sequences by using guide trees and HMM profile-profile techniques (Siever *et al*., 2011). In the proteomics study (Chapter 3), sequences from the GFAPα isoform (accession number: P47819), GFAPδ isoform (accession number: P47819-2), and peptides identified in the iTRAQ experiment for GFAP were submitted in a FASTA format.

2.1.9.5 Predicted Molecular Weight (MW) tool

To calculate the MW of a known protein FASTA sequence (in this Thesis, theoretical breakdown products of GFAP by calpain, see Chapter 3), Protein Molecular Weight tool (https://www.bioinformatics.org/sms/index.html) was used. Protein Molecular Weight is a JavaScript application (JavaScript 1.5), part of the Sequence Manipulation Suite (https://sites.ualberta.ca/~stothard/javascript/), which manipulated the submitted sequence by executing in the web browser JavaScript (Stothard, 2000).

2.1.10 Verification of the differentially expressed proteins by Western blotting

Quantitative Western blotting was used to verify the differential expression of several selected proteins of interest from the proteomics study (Chapter 3), loading between three and five independent samples (from individual rats) per group in each gel (**Table**

2.1). Due to the limited amount of total protein from each sample, and the need to include thirteen individual samples onto the same gel, the amount of loaded protein was 7 µg (panGFAP and TH immunoblots) or 14 µg (GFAPδ and calpain-2 immunoblots) (see below).

Samples were kept on ice during the preparation of the sample to avoid protein degradation. 7 µg or 14 µg of each protein extract (7 µg/5 µl or 14 µg/5 µl in extraction buffer) was incubated with an equal volume (5 µl) of 2x loading Laemmli buffer (0.125 M Tris-HCl, 20% glycerol, 4% SDS, 0.004% bromophenol blue, 5% 2-mercaptoethanol in ultrapure water, pH 6.8) for 5 minutes at 95 °C, which left a final concentration of 7 µg/10 µl or 14 µg/10 µl of protein loaded in each well. Samples were centrifugated at 16,000 x g for 1 minute at 4 °C and loaded onto the 4–20% Mini-PROTEAN TGX™ Precast polyacrylamide Protein gels (15-wells, 15 µl/well, Bio-Rad, #4561096). Dual Color Standards (Precision Plus Protein™ Dual Color Standards 10–250 kDa, Bio-Rad, #1610374) were loaded for MW estimations. Proteins were separated by SDS-PAGE in a tank containing running buffer (25 mM Tris, 190 nM glycine, 0.1% SDS in ultrapure water, pH 8.3) at a constant voltage (200 V), between 1 and 3 hours depending on the MW of the protein of interest. The separating gel was removed and a piece of gel without the region containing the protein of interest was cut and stained with Coomassie Brilliant Blue R-250 Staining solution (Bio-Rad, #1610436) to quantify the total amount of protein in each lane (Eaton *et al.*, 2013). After 4 hours, the Coomassie stain was removed and the gel was rinsed with destaining solution (20% methanol, 10% acetic acid in ultrapure water) to remove the background and visualize the lanes. The other part of the gel was soaked in transfer buffer (192 mM glycine, 25 mM Trizma base in ultrapure water – with addition of 0.5 ml 20% SDS for proteins larger than 80 kDa) for 2 minutes to rinse the SDS from the running buffer. Foam pads, Whatman filter papers and a nitrocellulose membrane (0.45 µm, 7 x 8.5 cm, Bio-Rad, #1620145) were also soaked in Transfer buffer for 10 minutes. The transfer sandwich was assembled as follows: the first foam pad was placed in the anode (black part) of the cassette, followed by one filter paper

and the gel, then the nitrocellulose membrane, another filter paper and foam pad. The cassette was placed into a Mini-PROTEAN Tetra Cell tank (Bio-Rad) and filled with transfer buffer. Proteins were electrophoretically transferred to the nitrocellulose membrane at constant milliampere (100 mA) overnight at 4 °C. Membranes were briefly rinsed with 0.1% Tween 20 in 1X TBS (TBST) and stained with Ponceau S solution (Sigma, #P7170) to check the quality of the transfer. Ponceau S stain was rinsed off with 3 washes of TBST for 5 minutes. Membranes were blocked with antibody solution diluted in 5% non-fat dry milk in TBST at room temperature for 30 minutes. Membranes were then incubated with primary antibodies (**Table 2.3**) in antibody solution overnight at 4 °C with shaking. The next day, membranes were washed three times with TBST (5 minutes each wash) and incubated with HRP-conjugated secondary antibodies (**Table 2.4**) diluted in antibody solution at room temperature for 1 hour with shaking. Membranes were washed again three times with TBST and incubated with Clarity Western ECL Substrate (Bio-Rad, #1705061) or SuperSignal West Femto (ThermoFisherScientific, #34094) for 5 minutes. Blots and gels stained with Coomassie were imaged with a CCD system (FluorChem M system, ProteinSimple).

Table 2.3. List of primary antibodies used for immunoblotting.

Antigen	Dilution	Isotype	Raised against	Manufacturer (catalog #)
GFAP	1:1000	Rabbit monoclonal IgG (D1F4Q)	Residues surrounding Asp395 of human GFAP	Cell signalling (12389)
GFAP	1:500	Mouse monoclonal IgG2b (2E1.E9)	Bovine spinal cord homogenate	Biolegend (644701)
GFAPδ	1:100	Rabbit polyclonal IgG	Residues surrounding 350 of mouse GFAP delta	Abcam (93251)
GFAP+1	1:400	Rabbit polyclonal	Epitope DRGDAGWRGH of human origin	Bleeding 070307 (UMC Utrecht)
Calpain-2	1:200	Mouse monoclonal IgG1 (E-10)	Epitope between 2–27 aa (N-terminus) of human origin	SantaCruz (373966)
TH	1:1000	Rabbit polyclonal IgG	Denatured TH from rat pheochromocytoma	Millipore/Merck (ab152)

Table 2.4. List of secondary antibodies used for immunoblotting.

Antigen	Dilution	Isotype	Conjugated	Manufacturer (catalog #)
rabbit	1:1000	Goat polyclonal IgG	HRP	ThermoFisher Scientific (31460)
mouse	1:1000	Goat polyclonal IgG	HRP	ThermoFisher Scientific (31430)

Analysis of the gels stained with Coomassie (total amount of protein) and immunoblotting (membranes with the different protein bands according to the antibody used) were executed in Fiji/ImageJ software (https://imagej.nih.gov/) (National Institute of Health, USA) (Schneider *et al*., 2012). Images were opened on Fiji/ImageJ and the 'rectangle' tool was selected. For the gel, a rectangle was drawn horizontally across all the bands. The first lane was selected (*Analyze>Gels>Select First Lane*) and then that lane was plotted (*Analyze>Gels>Plot Lanes*). This showed a plot with different peaks indicating the intensity of each band. The 'straight' tool was selected, and a horizontal line was drawn at the bottom of each peak, to join the beginning to the end. Once all peaks had a line across their bottom, the 'wand' button was selected, clicking the inside of each peak. The window 'Results' appeared, with a numeric value representing the area for each peak or band. The same procedure was done for the immunoblot. The area of each peak for the gel and immunoblot were copied in Excel. The relative quantification of each protein or densitometry was calculated by dividing the area of the immunoblot from each lane between the area of the total amount of protein in that lane.

2.1.11 Immunofluorescence and immunohistochemistry of rat coronal and human sections

For immunofluorescence (Chapter 3), rat coronal sections (40 µm thickness) were mounted onto slides before the immunofluorescence procedure. Slides were rinsed three times with TBS (5 minutes each) and non-specific binding sites were blocked with blocking solution (0.2% Triton X-100, 3% normal goat serum in TBS) for 20 minutes.

Slides were incubated with the specific primary antibody (anti-GFAP for astrocytes, anti-TH for DAn; **Table 2.5**) in blocking solution overnight at 4 ºC. The day after, sections were washed three times with TBS (5 minutes each) and incubated with the fluorescence secondary antibody (**Table 2.6**) and 4'-6-diamidino-2-phenylindole (DAPI) (1:1000; ThermoFisher, #62247) in TBS for 2 hours at room temperature. Sections were rinsed three times (5 minutes each) and covered with a coverslip using Hydromount mounting media (National Diagnostics, #HS106).

For immunohistochemistry (Chapter 4), rat coronal and human sections (both 40 µm thickness) were kept in wells for free-floating staining. Before immunohistochemistry procedure, slides were rinsed three times with TBS (5 minutes each) and subsequently the endogenous peroxidase was blocked with peroxidase blocking solution (10% methanol, 10% hydrogen peroxide in TBS) for 30 minutes. Sections were then rinsed three times with TBS (5 minutes each) and non-specific binding sites were blocked with blocking solution (0.2% Triton X-100, 3% normal goat serum in TBS) for 20 minutes. Slides were incubated with the primary antibody (anti-TH for DAn; **Table 2.6**) in blocking solution overnight at 4 ºC. The day after, sections were washed three times with TBS (5 minutes each) and incubated with the biotinylated secondary antibody (**Table 2.7**) in TBS for 2 hours at room temperature. After three washes of 5 minutes each, Vectastain Universal ABC Kit detection system (Vector Labs, #PK6101) was applied for 1 hour at room temperature. Slides were washed three times (5 minutes each) and 3,3-diaminobenzidine tetrahydrochloride (DAB, #D8100, Sigma) was used as chromogen. Sections were rinsed several times with TBS and mounted onto slides. Slides were left to dry until the sections were completely stuck to the surface. Samples were then dehydrated in alcohol gradient (70% for 5 minutes, 95% for 5 minutes, 100% for 10 minutes) and immersed in xylene for 10 minutes. Samples were covered with a coverslip using DPX slide mounting medium (ThermoFisher Scientific) for light microscopy analysis.

Table 2.5. List of primary antibodies used for immunofluorescence (IF) and immunohistochemistry (IHC) analysis of the rat SNpc during ageing.

Antigen	Dilution	Isotype	Raised against	Manufacturer (catalog #)
GFAP	1:1000 (IF)	Mouse monoclonal IgG2b (2E1.E9)	Bovine spinal cord homogenate	Biolegend (644701)
TH	1:1000 (IF, IHC)	Rabbit polyclonal IgG	TH from rat pheochromocytoma	Millipore/Merck (ab152)

Table 2.6. List of secondary antibodies used for immunofluorescence (IF) and immunohistochemistry (IHC) analysis of the rat SNpc during ageing.

Antigen	Dilution	Isotype	Conjugated	Manufacturer (catalog #)
mouse	1:500 (IF)	Goat polyclonal IgG	Alexa Fluor® 488	ThermoFisher Scientific (A11001)
rabbit	1:500 (IF)	Goat polyclonal IgG	Alexa Fluor® 594	ThermoFisher Scientific (A11012)
rabbit	1:200 (IHC)	Goat IgG	Biotinylated	Vector Laboratories (PK-6101)

2.1.12 Acquisition and analysis of immunofluorescence and immunohistochemistry images

2.1.12.1 Acquisition and data analysis of immunofluorescence images for proteomics validations

Acquisition – Immunofluorescence images were observed and captured using a Nikon Eclipse 80i microscope and a Hamamatsu fluorescent camera connected to a computer with NiS Elements software, version 2.32 (Nikon Instrument Inc.). Images were taken at 4x, 10x and 20x magnification, using the same exposure setting from each specific antibody between samples. The different magnifications were acquired to have a general view of the slides (4x magnification) and perform qualitative and quantitative analyses (10x, 20x magnifications).

Optical Density (O.D.) measurements of GFAP-positive astrocytes – GFAP O.D. was performed to quantify the density of astrocytes (GFAP-positive) within the SNpc during ageing. This method was chosen because it was not possible to count the number of astrocytes in the 40 µm sections. O.D. measurements allow the calculation of the mean gray value within a section (i.e., sum of the gray values of all pixels in the selection divided by the number of pixels), which correspond to the immunofluorescence intensity (in this case GFAP-positive intensity or staining) (Tickle *et al*., 2015). In essence, with this approach, it is possible to determine in which sections (i.e., age groups) there is more expression of GFAP in an area, although it will not be possible to determine if this is due to an increase of the expression of GFAP within the cell or an increase in the number of astrocytes.

From each animal, one section was selected, ensuring that all sections belonged to the same rostro-caudal level of the SNpc (**Figure 2.3B**). The SNpc was identified thanks in part to the TH-positive labelling of DAn. For quantification, three fields (10x magnification) were selected randomly, without overlap, within the SNpc nuclei. The green channel, corresponding to anti-GFAP astrocytes for O.D. measurements, together with the red (anti-TH DAn) and the blue (DAPI, nuclei) channels, were acquired. Fiji/ImageJ software (https://imagej.nih.gov/) (National Institute of Health, USA) (Schneider *et al*., 2012) was used to assess the GFAP O.D. as follows. ImageJ was calibrated with an O.D. step table (*Analyse* > *Calibrate* > *Function 'roadbard', unit 'O.D.'*). All the images were converted to 8-bit grayscale (*Image* > *Type* > *8-bit*) and inverted (*Edit* > *Invert*). The background was subtracted (*Process* > *Subtract background* > *Rolling ball radius '100 pixels', 'light background'*) and the mean gray value was measured (*Analyse* > *Measure* > *Mean*). Final values from each animal and age group were copied into an Excel spreadsheet for statistical analysis.

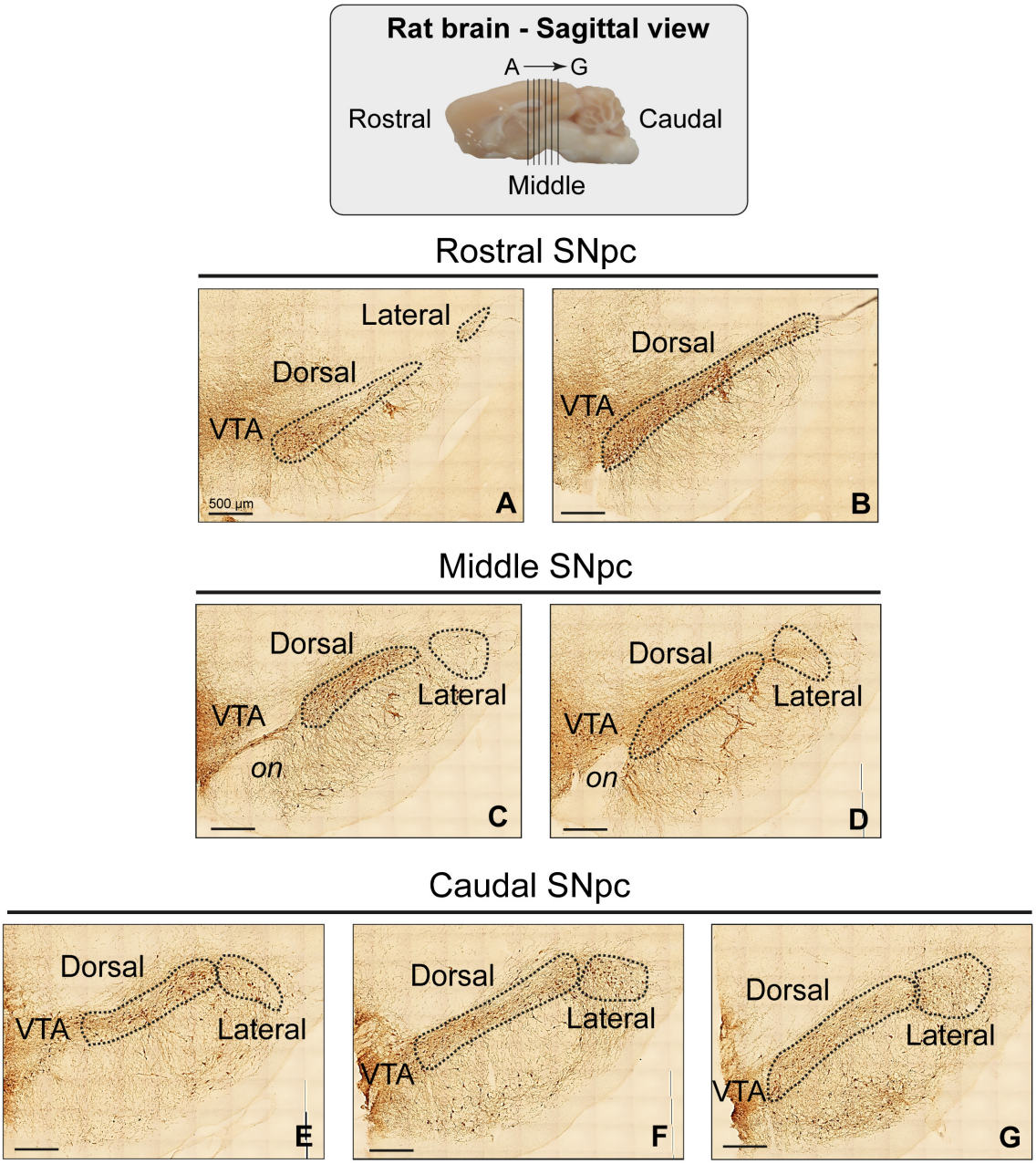

Figure 2.3. Rostro-caudal representation of dorsal and lateral tiers of the SNpc in rats for quantitative and morphometric analyses. Top image shows a sagittal view of a rat adult brain, highlighting the position of the rostral, middle and caudal sections. Square images (**A-G**) represent coronal sections (40 µm thickness) of the TH-positive SNpc and VTA in rats. These sections are organized in (**A, B**) rostral (before the oculomotor nerve, *on*), (**C, D**) middle (where the oculomotor nerve visible), and (**E, F, G**) caudal (after the oculomotor nerve) regions. In turn, the SNpc is also divided into the dorsal and lateral tier.

2.1.12.2 Acquisition and data analysis of immunohistochemistry images for quantitative and morphological characterization of the SNpc DAn in rats and humans during ageing

Acquisition – Immunohistochemistry images were observed and capture using a Nikon Eclipse Ti with automated stage and a Nikon camera also connected to a computer with NiS Elements software, version 2.32 (Nikon Instrument Inc.). To get a high resolution and detailed image of TH-positive DAn for quantitative (i.e., density of DAn in SNpc) and morphometric (i.e., area of DAn soma) analyses, images were taken scanning each slide as a large and a composite image. To do this, smaller images taken at 40x magnification were merged, using the same exposure and light settings between samples. To create this composite image, 'Scan large Image' option was selected, within the 'Acquire' section on NiS Elements software. Once the limits (left, right, bottom and upper) of the SNpc were defined, the 'Start' bottom was pressed, and the composite image was automatically scanned and created.

Quantitative and morphometric measurements of TH-positive DAn – Quantitative analysis (i.e., density of DAn in SNpc) were performed to understand if ageing had an effect on the viability of SNpc DAn in rats and humans; while morphometric analysis (i.e., area of DAn soma) of rat SNpc DAn were conducted to determine if ageing itself or the loss of DAn can modify the size of these cells. DAn were only included in the different analyses if they were TH-positive and if it was possible delimit the soma and proximal processes (McRitchie *et al*., 1996; Schawkat *et al*., 2015).

In the rat tissue, quantitative and morphometric analyses were performed using between six and seven different rostro-caudal sections (each one separated in 240 µm) to represent the whole rat SNpc (**Figure 2.3**). Subsequently, the different sections were grouped as rostral (before the oculomotor nerve; **Figure 2.3A, B**), middle (where the oculomotor nerve was visible; **Figure 2.3C, D**) and caudal (after the oculomotor nerve;

Figure 2.3E-G), analysing the dorsal and lateral tier of each SNpc (**Figure 2.3**). These delimitations, together with the separation of the VTA from the SNpc, were based on previous neuroanatomic and cytoarchitectonic analyses of the SNpc in rodents (Collier *et al*., 2011; Reyes *et al*., 2012; Fu *et al*., 2012; Khudoerkov *et al*., 2014).

For human sections, quantitative analysis was done also using between six and seven different rostro-caudal sections (each one separated in 1,200 μm) to represent the whole human SNpc. However, in this case, the SNpc was analysed entirely because it was more difficult to delimit the different tiers. The delimitation of the SNpc from the VTA was established following previous neuroanatomic and cytoarchitectonic analyses of the SNpc in humans (McRitchie *et al*., 1995; McRitchie *et al*., 1996; McRitchie *et al*., 1997; Damier *et al.,* 1999; Reyes *et al*., 2012).

For both rat and human analyses, NiS Elements software, version 2.32 (Nikon Instrument Inc.) was used. Quantitative analysis was done considering the density of TH-positive neurons (number of TH-positive neurons/μm^2) within a specific region of interest (ROI) of certain size (μm^2) around the SNpc. To do this, a ROI was drawn around the rat SNpc (dorsal and lateral region) (Collier *et al*., 2011; Fu *et al*., 2012; Khudoerkov *et al*., 2014) or all human SNpc (McRitchie *et al*., 1997) and the quantification of TH-positive DAn was performed. In rats, to be sure that the density of neurons did not change because of the size of the brains in the different ages, the area (μm^2) of the hemispheres was also calculated automatically drawing a ROI around its perimeter, using the 'area' tool from the 'Annotation and Measurements' section on NiS Elements software. Morphometric analysis (only in the rat study) was calculated drawing around the profile of each TH-positive cell within the rat SNpc (dorsal and lateral regions). To do this, the 'area' tool was selected from the 'Annotation and Measurements' section on NiS Elements software. Thus, the area (μm^2) represents how big or small the DAn can be. Final values for each analysis from each section/animal and age group were copied into an Excel spreadsheet for statistical analysis.

2.1.13 Statistical analyses

Statistical analyses for Western blot (Chapter 3), immunofluorescence (Chapter 3) and immunohistochemistry (Chapter 4) derived data were performed by GraphPad Prism version 7.01 (La Jolla, USA). In all analysis, normal or Gaussian distribution of the data was tested by D'Agostino-Pearson normality test or Shapiro-Wilk normality test if the *n* was too small. A one-way Analysis of Variance (ANOVA) test was performed if the data showed a Gaussian distribution, followed by a post hoc Tukey's multiple comparison tests to understand the type of differences between groups of age (juvenile, young, middle age and old). If the data did not show a Gaussian distribution, a nonparametric Kruskal-Wallis test was used, followed by a Dunn's multiple comparison test. Significant differences were established when the p-value was less than 0.05 ($p<0.05$), rejecting the null hypothesis. Bar graphs represented the mean of each group, while the error bars indicated the standard deviation (mean ± SD).

2.1.13.1 Statistical analysis of immunoblots from rat SNpc during ageing

For Western blotting (Chapter 3), the relative quantification of each protein (calculated by dividing the area of the immunoblot from each lane between the area of the total amount of protein in that lane) from every individual sample was grouped according to the different ages and the statistical tests were performed. All immunoblots (i.e., panGFAP, GFAPδ, calpain-2, TH) were analyzed with one-way ANOVA test followed by a post hoc Tukey's multiple comparison test.

2.1.13.2 Statistical analysis of the GFAP O.D. immunofluorescence in rat SNpc during ageing

For GFAP immunofluorescence (Chapter 3), the average of the three frames with the GFAP O.D. was calculated in each animal and then grouped in their respective ages to compare if there were modifications in the total expression of GFAP along ageing. A

one-way ANOVA test was performed followed by a post hoc Tukey's multiple comparison test.

2.1.13.3 Statistical analysis of quantifications of SNpc DAn in rats and humans, and morphometric analyses of SNpc DAn in rats

Quantitative (i.e., density of DAn) and morphometric (i.e., area of DAn soma) data obtained by immunohistochemistry procedures in rat tissue (Chapter 4) was analysed independently for the dorsal and lateral tier of the SNpc. For both analyses (i.e., density and area) in each tier (i.e., dorsal and lateral) of the SNpc, three types of analyses were conducted. First, rostral, medial or caudal sections from the same SNpc that belong to the same age group were compared between them (e.g., comparison of the rostral, middle and caudal part of dorsal tier of the SNpc in juveniles), in order to see if there were differences in the characteristics of DAn within the SNpc independent of the ageing process. Second, rostral, middle or caudal regions from one of the SNpc tiers were pooled together according age groups to be compared between them (e.g., comparison of the rostral dorsal tier of SNpc between juvenile, young, middle age and old), in order to investigate if there is more or less degeneration or modifications of DAn with ageing depending on the rostro-caudal region of the SNpc. Third, all rostro-caudal sections from one SNpc tier were grouped in the same age group to be compared between them (e.g., whole dorsal tier of the SNpc from rostro to caudal compared between juvenile, young, middle age and old), in order to see if the two different tiers of the SNpc degenerates or changes with ageing. Moreover, the hemisphere area in rats was compared between age groups. All these data were analysed by one-way ANOVA test followed by a post hoc Tukey's multiple comparison test.

Finally, the quantification of cell counts (i.e., density) generated from each human SNpc section (Chapter 4) were grouped for each individual to be compared in a linear regression test.

2.2 Study of the role of astrocytes in the vulnerability of rat embryonic DAn in cell culture

2.2.1 Reagents and materials for ventromedial cell culture

13 mm glass coverslips (Thermo Scientific, #15757602), 24-well-plates, ethanol, poly-D-lysine (PDL; Sigma, #P6407-5MG), laminin (Sigma, #L2020-1MG), Neurobasal® Medium (1X) solution (Gibco,#12348-017), B-27® Supplement (50X) (Gibco, #17504-044), GlutaMAX™ 100X supplement (Gibco,#35050-038), Fetal Bovine Serum (FBS; Gibco, #10270-106), Antibiotic-Antimytotic Anti-Anti (100X) (Gibco, #15240-096), non-essential aa MEN NEAA (100X) (Gibco, #11140-050), D-(+)-Glucose (Gibco, #15023-021), 0.2 µm pore size filter (Sartorius, #165323-K), trypsin (Sigma), deoxyribonuclease I from bovine pancreas (DNase I; Sigma, D4527), trypan blue stain (0.4%) (Gibco, #15250-061), paclitaxel (Sigma, #T402-1MG), dimethyl sulfoxide (DMSO; Fisher BioReagents, #BP231-100), 6-hydroxydopamine (6-OHDA; Sigma, #H4381-100MG), ascorbic acid (AA; Sigma, #PHR1008-2G), acetone, methanol.

2.2.2 Coating coverslips and plating media

Coverslips, stored in 70% ethanol, were left to dry under a laminar flow hood and subsequently placed in 24-well plates. 600 µl of PDL (0.01 mg/ml in dH_2O) was added to each well, fully covering the coverslip, and the 24-well plate subsequently kept overnight at 37 ºC. The following day, the PDL was removed and 600 µl of laminin (0.5 µg/ml in dH_2O) was added to each well, incubating the coverslips for 2 hours at 37 ºC. Before plating the cells, laminin was removed, trying to dry all the drops, and coverslips were use immediately after this.

Plating media (NBM) was prepared as follows: 1% B-27® Supplement, 1% GlutaMAX™ Supplement, 10% FBS, 1% PSF, 1% MEN NEAA, 1% D-(+)-glucose 30% in Neurobasal® Medium solution. NBM was sterilized using a 0.2 µm pore size filter and stored at 4 ºC. Before using, NBM was warmed up to 37 ºC.

2.2.3 VM cells dissociation and VM cell culture

All animals were housed at the accredited Animal Facility of Keele University. All animal work was performed in agreement with the Animal Welfare & Ethical Review Body (AWERB) at Keele University and conducted under the licensed authority of the UK Home Office (PPL40/3556). Animals were maintained in a room with controlled photoperiod (12 hours light/dark cycle) and temperature (22 ± 1 ^{o}C) with free access to standard food and water.

The ventromedial (VM) area, which is located within the midbrain, includes the SNpc. For primary VM cultures, E14 rat embryos were used, defining the plug date as E0. Sprague Dawley mothers were sacrificed by cervical dislocation and the abdomen was sprayed with 70% ethanol before laparotomy. Embryos were removed from the uterus and decapitated. The heads were rapidly collected in a 50 ml falcon tube with Neurobasal® Medium solution on ice. One by one, the heads were placed on a petri dish to perform the VM dissection (Shimoda *et al*., 1992) under a Leica S6D dissecting microscope (Leica, Germany) in a laminar flow chamber (**Figure 2.4**). All the dissected VM areas were put in a new tube with 1ml of cold Neurobasal® Medium solution. In the meantime, 1 ml of trypsin solution (0.25% Trypsin and 10% DNase I in Neurobasal® Medium solution) was pre-warmed at 37 ^{o}C. After the tissue settled to the bottom of the tube, the Neurobasal® Medium solution was replaced with 1 ml of pre-warmed trypsin solution for 20 minutes at 37 ^{o}C. Trypsin solution was removed carefully, and the tissue was rinsed twice with 500 µl of NBM, deactivating the trypsin with the serum contained in the NBM. Cells were dissociated mechanically using a P100 pipette. Cell viability and density were assessed with a haemocytometer, mixing 10 µl of the dissociated cells and 40 µl of 0.4% trypan blue. The final concentration of VM cells was adjusted to ~7 x 10^6 cells/ml using NBM. A 10 µl 'drop' (~7 x 10^4 cells/well) of the VM dissociated cells were placed in the centre of the coverslips located in the 24-well plate. After incubation for 10 minutes to allow the cells to stick to the surface, 400 µl of the media (with different components; see below) was added carefully to each well. Cells were incubated at 37

ºC in a humidified atmosphere of 5% CO_2 in air. Cells were fed with the respective treatment media (see subsection 2.2.4 and 2.2.5) every two days, changing all medium due to the high amount of debris, until the end of the experiment (7 days *in vitro*, DIV) (**Figure 2.5**).

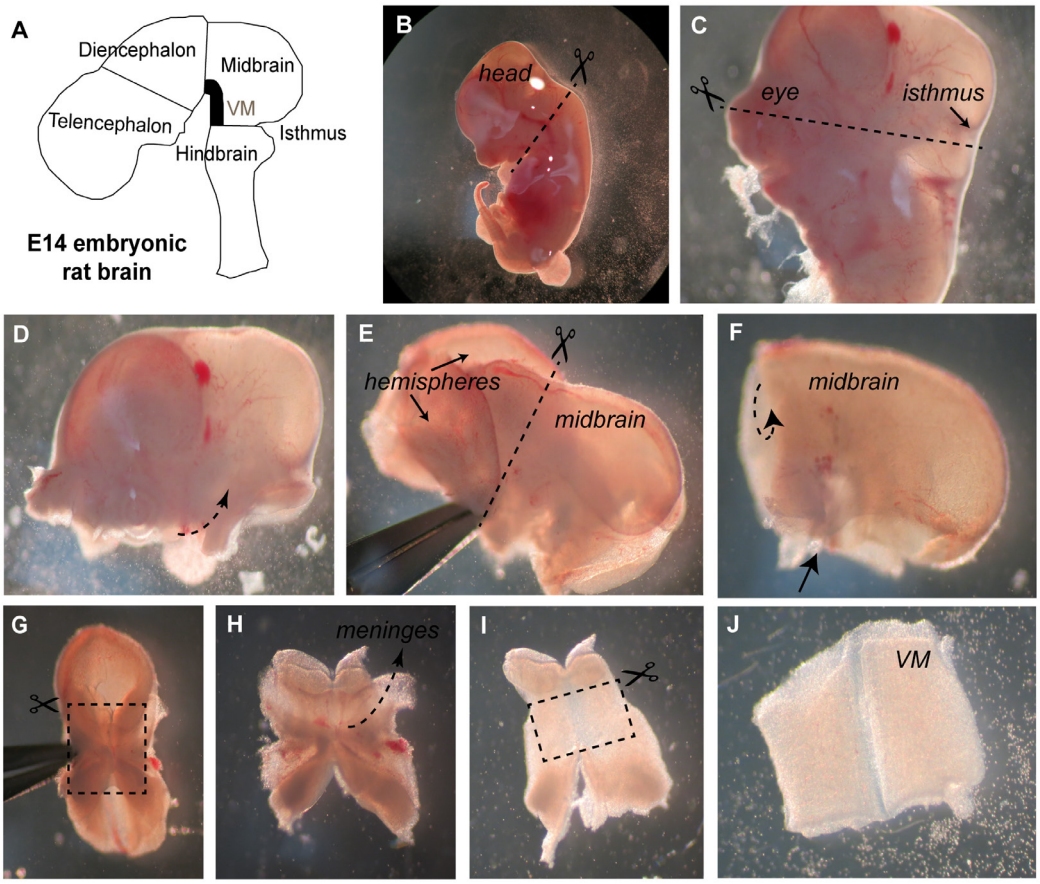

Figure 2.4. Procedure to obtain primary VM cells at embryonic stage E14 in rats. (**A**) SNpc DAn are located in the VM region within the midbrain. (**B, C**) First, heads are cut from the rest of the embryo and a horizontal incision is made from side to side to isolate the brain from the rest of the head. (**D, E**) The skin of the skull is peeled to reveal the brain. A transverse cut is made to remove the hemispheres and leave only the tubular midbrain. (**F, G**) The midbrain is flipped over in order to have a view of the ventral part, which presents a butterfly shape in the middle. This butterfly shape is cut (dotted rectangle) to isolate the region that contains the VM part from the rest of the midbrain. (**H**) Once it is cut, the tissue is flattened, and the meninges are carefully removed from the butterfly shape. (**I, J**) The ventral midbrain (dotted rectangle) is cut from the butterfly shape, trimming the 'wings' of the butterfly. All the procedure is performed under sterile conditions in a petri dish with Neurobasal® Medium solution.

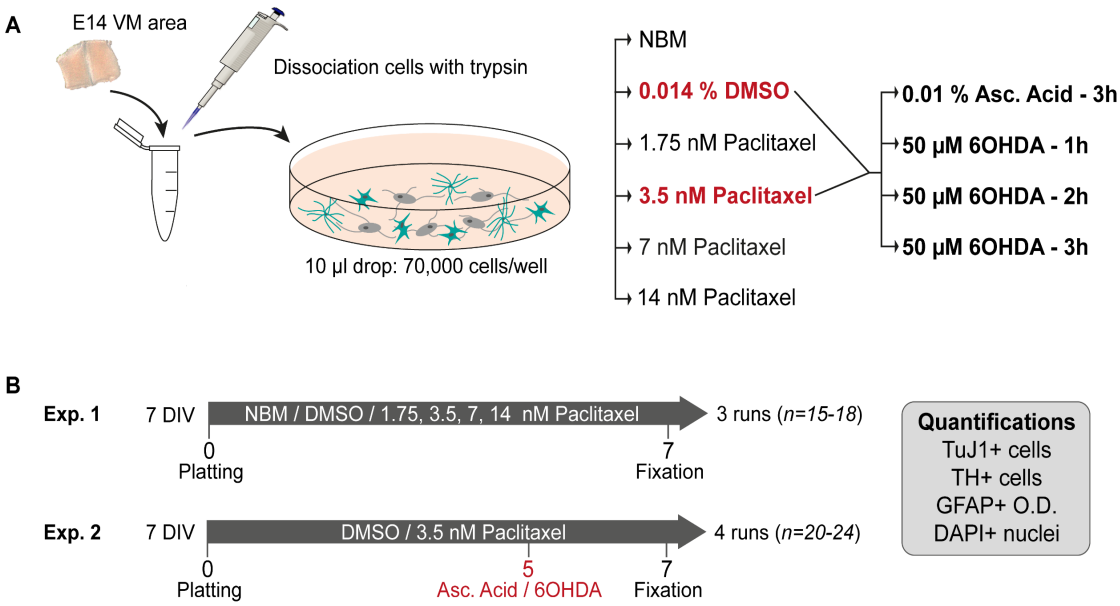

Figure 2.5. Procedure to generate primary VM cultures at embryonic stage E14 in rats. (**A**) The previously dissected VM region (**Figure 2.4**) was dissociated with the help of trypsin. Once VM cells were dissociated, a 10 µl 'drop' (~7 x 10^4 cells/well) was placed in the centre of each coverslip, located in the 24-well plate. Cells were treated with the different concentrations of paclitaxel or 6-OHDA, and the respective controls. (**B**) Diagrams show the timescale of experiment 1 (paclitaxel) and experiment 2 (paclitaxel and 6-OHDA), which have a total duration of 7 DIV. Once the experiment ended, different quantifications were performed, including quantifications of the number of neurons (TuJ1-positive), DAn (TH-positive), and nuclei (DAPI-positive), as well as the O.D. of astrocytes (GFAP-positive).

2.2.4 Paclitaxel treatments: experiment 1

To test the effects of the anti-mitotic drug paclitaxel on astrocyte and DAn viability, different concentrations of paclitaxel (14, 7, 3.5, 1.75 nM) were chosen, based on Sengottuvel *et al*. (2011) who described a non-toxic effect on neurons in comparison to other studies (see **Table 5.1** in Chapter 5). Paclitaxel was diluted in NBM from a stock solution consisting of 100 µM paclitaxel in DMSO (stored at 4 ºC). A solution consisting of 0.014% DMSO in NBM (the same concentration of DMSO contained in 14 nM of paclitaxel, the highest concentration use) was used as a vehicle control. A treatment with only NBM was used to test that the vehicle control (0.014% DMSO) did not have any effect in the culture (**Figure 2.5**).

The different concentrations of paclitaxel, vehicle control (DMSO) or NBM were added to the culture the first day *in vitro* (0 DIV) to stop the division of mitotic cells (i.e., glial cells, astrocytes) from the beginning. The total duration of the treatments with paclitaxel was 7 DIV (finishing the experiment at 7 DIV) because previous studies have shown that at this point DAn are mature, forming networks with developed connections (Gaven *et al*., 2014) (**Figure 2.5**). For this experiment, three 'runs' (three biological replicants) were performed, placing all the experimental groups in one 24-well-plate. For each experimental group, between five and six coverslips were used (total $n=15–18$).

2.2.5 6-OHDA treatments: experiment 2

To challenge DAn viability, cultures previously treated with DMSO or 3.5 nM paclitaxel were exposed to 100 or 50 µM of 6-OHDA in NBM (Ding *et al*., 2004), prepared from a stock (1,000 µM 6-OHDA in 0.1 % AA). A solution of 0.01% AA in NBM was used as a vehicle control. In each experimental set (i.e., DMESO or paclitaxel), a treatment without vehicle control (0.01% AA) or 50 µM 6-OHDA was established to test whether AA was toxic for the cells or not (**Figure 2.5**).

After 5 DIV of treatment with DMSO or 3.5 nM paclitaxel, cultures were incubated with the respective 6-OHDA treatment during 1, 2 or 3 hours. AA treatment was added for 3 hours, as compared to the maximum exposure of this compound with 3 hours of 6-OHDA treatment. After that time, cells were washed twice with warm NBM. Then, the respective DMSO or paclitaxel treatments were added until the end of the experiment (7 DIV) to avoid the proliferation of glial cells. To note, after 6-OHDA or AA treatments (5 DIV), cells were kept two days more in culture (up to 7DIV) to study more than just the acute effect of the drug on the cells (**Figure 2.5**). For this experiment, four 'runs' (four biological replicants) were performed, placing all the experimental groups for DMSO or 3.5 nM paclitaxel in one 24-well-plate. For each experimental group, between five and six coverslips were used (total $n=20–24$).

2.2.6 Fixation of cell cultures and immunofluorescence microscopy

To analyse the different response of cells to paclitaxel and 6-OHDA compared to the respective controls, immunofluorescence microscopic analysis was performed. To prepare the cultures for this procedure and observations, after 7 DIV cultures were rinse once with 400 µl of warm Neurobasal® Medium solution. Then, cells were dehydrated with a mix of acetone and methanol (1:1) for 10 minutes. Once the fixative was removed, every coverslip was left to dry for 30 minutes before proceeding to the immunolabelling.

Briefly, coverslips with the fixed VM cultures were rinsed three times with TBS (5 minutes each). Non-specific binding sites were blocked with a blocking solution (0.2% Triton X-100, 3% normal goat serum in TBS) for 20 minutes. Coverslips were incubated with a specific primary antibody (anti-GFAP for astrocytes, anti-TuJ1 for neurons, anti-TH for DAn; **Table 2.7**) in blocking solution overnight at 4 ºC. The following day, coverslips were washed three times with TBS (5 minutes each) and incubated with the corresponding fluorescence secondary antibodies (**Table 2.8**) and DAPI (1:1000; ThermoFisher, #62247) in TBS for 2 hours at room temperature. Coverslips were rinsed three times (5 minutes each) and mounted onto slides using Hydromount mounting medium (National Diagnostics, #HS106). There were between five and six coverslips stained simultaneously with anti-TuJ1, anti-GFAP and DAPI (in the first experiment), or anti-TH anti-GFAP and DAPI (in the first and second experiment) per each treatment condition.

Table 2.7. List of primary antibodies used for immunofluorescence analysis of VM cultures treated with paclitaxel and 6-OHDA.

Antigen	Dilution	Isotype	Raised against	Manufacturer (catalog #)
GFAP	1:1000	Mouse monoclonal IgG2b (2E1.E9)	Bovine spinal cord homogenate	Biolegend (644701)
GFAP	1:1000	Chicken polyclonal IgY	Native GFAP purified from bovine spinal cord	Biolegend (829401)
TuJ1	1:1000	Mouse monoclonal IgG2a (TUBB3)	Microtubules derived from rat brain	Biolegend (801202)
TH	1:1000	Rabbit polyclonal IgG	Denatured TH from rat pheochromocytoma	Millipore/Merck (ab152)

Table 2.8. List of secondary antibodies used for immunofluorescence analysis of VM cultures treated with paclitaxel and 6-OHDA.

Antigen	Dilution	Isotype	Conjugated	Manufacturer (catalog #)
mouse	1:500	Goat polyclonal IgG	Alexa Fluor® 488	ThermoFisher Scientific (A11001)
mouse	1:500	Goat polyclonal IgG	Alexa Fluor® 594	ThermoFisher Scientific (A11005)
chicken	1:200	Goat polyclonal IgY	Alexa Fluor® 488	ThermoFisher Scientific (A11039)
rabbit	1:500	Goat polyclonal IgG	Alexa Fluor® 594	ThermoFisher Scientific (A11012)

2.2.7 Acquisition and data analysis of immunofluorescence images of VM cultures treated with paclitaxel and 6-OHDA

Acquisition – Images were observed and taken using a Nikon Eclipse 80i microscope and a Hamamatsu fluorescent camera connected to a computer with NiS Elements computer software, version 2.32 (Nikon Instrument Inc.). Images of the coverslips were randomly taken at 10x, 20x and 40x magnification. In the case of 10x magnification, four fields per coverslip were randomly chosen within the 'drop' area where the cells were, moving the coverslip from top to bottom, and from left to right, without overlapping the fields. Each 10x field was used to quantify the number of nuclei (DAPI), neurons (anti-TuJ1), DAn (anti-TH), as well as the O.D. of astrocytes (anti-GFAP). Four fields at 20x and 40x magnification per coverslip were captured to look at the morphology of cells in more detail. Each image was captured with the same exposure settings from each specific antibody, changing the parameters with each magnification.

Quantification of number of neurons, DAn and nuclei – Four 10x magnification images per coverslip were used for quantifications of neurons and nuclei, which were identified thanks to the staining with the corresponding antibody. Images were analyzed with Fiji/ImageJ software (https://fiji.sc/) (National Institute of Health, USA) (Schneider *et al*., 2012), stacking the images of neurons and DAn with their respective images of nuclei

(*Image>Stacks>Stack to images*). Thus, neurons and DAn were counted using its specific staining and the colocalized DAPI nuclei with the help of the 'multi-point' tool. Nuclei were counted as long as they did not present a pyknotic characteristics, represented by a brighter condensation of the chromatic (Wohlan *et al*., 2014). Final values from each frame (and coverslip/treatment) were copied into an Excel spreadsheet for statistical analysis. To determine the effect of the different treatments in the VM cultures and be able to compare between the different biological replicants, data from each experiment was normalised to the vehicle control (DMSO), taking the average of this group as the 100% and calculating the percentage of control for paclitaxel treatments. The vehicle control was normalized using the mean of all its replicates.

Optical Density (O.D.) of GFAP – GFAP O.D. were performed to quantify the density of astrocytes (GFAP-positive). As previously mentioned, this method was chosen because it was difficult to count the number of astrocytes in the coverslips when they were confluent (e.g., under control conditions). Therefore, GFAP O.D. allows the measurements of GFAP immunofluorescence intensity over the whole field, determining in which treatments there is more expression of GFAP (Tickle *et al*., 2015).

Images were analyzed with Fiji/ImageJ software (https://fiji.sc/) (National Institute of Health, USA) (Schneider *et al*., 2012). Four 10x magnification images per coverslip were used for GFAP O.D. analysis as explain in subsection 2.1.12.1. Final mean grey values from each frame (and coverslip/treatment) were copied into an Excel spreadsheet for statistical analysis. To determine the effect of the different treatments in the VM cultures and be able to compare between the different biological replicants, data of each experiment was normalised to the vehicle control (DMSO), taking the average of this group as the 100% and calculating the percentage of control for paclitaxel treatments. The vehicle control was normalized using the mean of all its replicates.

2.2.8 Statistical analysis of immunofluorescence images of VM cultures treated with paclitaxel and 6-OHDA

Quantitative data was analysed using GraphPad Prism version 7.01 (La Jolla, USA). Normal or Gaussian distribution of the data was tested by D'Agostino-Pearson normality test or Shapiro-Wilk normality test where appropriate.

When only two sample means were compared (i.e., effect of DMSO *versus* NBM), unpaired t-test were used if the data showed a normal distribution, while a Mann-Whitney test was applied as a nonparametric test when the populations were non-normally distributed.

For one independent variable with more than two samples (i.e., paclitaxel treatment conditions *versus* DMSO), one-way ANOVA test was performed if the data showed a Gaussian distribution. For two independent variables (i.e., paclitaxel and 6-OHDA treatments *versus* DMSO and AA), two-way ANOVA test was run to elucidate if there were statistically differences. After ANOVA testing, the post hoc Tukey's multiple comparison test was used to determine the type of differences between treatments. If the data did not show a Gaussian distribution, a nonparametric Kruskal-Wallis test was used, followed by a Dunn's multiple comparisons test.

Significant differences were established when the p-value was less than 0.05 ($p<0.05$), rejecting the null hypothesis. Graph bars represented the mean of each group, while the error bars indicated the standard deviation (mean ± SD).

2.3 Multi-study proteomics analyses of the ageing and PD nervous system

2.3.1 Identification and comparison of articles related to the ageing nervous system

To identity articles related to the ageing nervous system for the multi-study comparison, a search was performed in Pubmed combining the terms 'proteom*' AND 'age*' or 'old' AND 'brain' or 'susbtantia nigra'. The search included only articles in English that were related to the ageing process in any area of the nervous system, including the

cerebrospinal fluid (CSF), and were published up to the 10th August 2019. Studies related to diseases (e.g. AD, PD, epilepsy, dementia or Down's syndrome), as well as animal models (e.g., PD, AD, stroke) or animals exposed to food restriction were not considered for examination. This left 75 articles for review that were read in full. However, only 21 articles were kept for further analysis. The reasons to exclude the 54 articles were diverse, including the age of the animals considered 'old' (e.g., postnatal ages), not providing or inaccessibility of the complete results or dataset, and the use of a post-translational proteomics approach in the study. In the articles where multiple regions or species were investigated at the same time, the data was analysed separately as if they were independent studies for comparison. The quantitative proteomics study of the rat SNpc at different ages presented in this Thesis (see Chapter 3), called in this chapter 'Thesis study', was also included in the comparison.

Proteomics datasets from each article were extracted and the differentially expressed proteins from each article copied into a Microsoft Excel spreadsheet. To compare between studies, even when different species were used, all protein names were unified to the official gene name using Uniprot Retrieve/ID mapping or manually searching the identifiers in the NCBI. In general, differentially expressed proteins from each study presented a fold-change comparing the protein expression between the different ages (e.g., young *versus* old). This fold-change was associated with a significant p-value ($p<0.05$) and, most of the time, a fold-change cut-off filter was applied. In cases where no cut-off filter was applied, only proteins whose fold-change was modified by at least 25% with ageing were considered. This filter was chosen because it was the cut-off filter used in the proteomics study of the rat SNpc in this Thesis (see Materials and Methods from Chapter 3, subsection 2.1.7). Moreover, all the gene names were converted to lowercase letters in Microsoft Excel. Subsequently, the list with the gene names from each study was compared using Microsoft Excel's 'pivot table' tool to observe which proteins appeared in numerous studies. From the 4,555 proteins found in total, there were 1,729 proteins that appear in at least two different studies. Therefore, in order to

manage the data, only proteins that appeared in three or more studies (648 proteins in total) and whose expression was conserved between studies (i.e., differentially expressed proteins in the same direction, down- or upregulated) were considered for bioinformatics analyses.

2.3.2 Identification and comparison of articles related to samples from patients with PD

Pubmed searching was done combining the words ‘‘proteom*’ AND ‘parkinson’ to find articles related to multiple regions of the nervous system and other parts of the body (e.g., serum, urine) during PD in humans and PD models (e.g., transgenic, toxins 6-OHDA and MPTP) in other mammals compared to controls without the disease or any type of secondary treatment. *In vitro* studies were excluded from the final comparison, as well as studies that looked at post-translational modifications. Thus, only articles in English that were published up to the 10th July 2019 were considered. In total, 40 studies were found in PD in humans, while 29 articles were found in PD models in mammals. However, only 24 articles were kept in the case of humans and 13 in other mammals. Articles were excluded for different reasons, including lack of controls in the study, not providing or inaccessibility of the complete results or dataset, or the use of a post-translational proteomics approach in the study. As in the ageing multi-study comparison, if there were multiple brain regions investigated at the same time in an article, the data was analyzed separately for comparison as if they were independent studies.

As previously indicated, the differentially expressed proteins from each article were extracted and copied into a Microsoft Excel spreadsheet, unifying the protein name to the official gene name in lowercase letters. If the authors did not apply any filter (e.g., significant p-value $p<0.05$, or fold-change cut-off), a 25% filter was placed, considering only proteins whose fold-change passed that threshold. Gene names from each study were compared using Microsoft Excel’s ‘pivot table’ tool to examine which proteins appeared in numerous studies. Only proteins that appeared in more than two studies

and whose expression was conserved between studies (i.e., differentially expressed proteins in the same direction, down- or upregulated) were considered for bioinformatics analyses. Different comparisons were performed as follows. In the case of humans, first, studies related only to the SNpc were compared. Then, studies performed in other areas of the brain and the SNpc were compared. Moreover, an independent comparison was done using parkinsonian biofluids together with the tear fluid from the eyes and lens fractions. This last tissue was included with biofluids, because it was study with the idea of finding biomarkers in biofluids, and because it was not part of the nervous system (i.e., therefore, it could not be included in the previous comparisons where the brain was analysed). Lastly, a final comparison was done including all studies in humans with PD. In addition, PD models in other mammals (i.e., rodents and monkeys) were compared between them. Finally, to understand the proteomics similarities between the disease in humans and the PD models performed in the lab, humans with PD and PD models in non-human species were also compared.

2.3.3 Comparison of articles related to the ageing nervous system and PD

To gain more insight into the differences or similarities between the proteome of the ageing nervous system and the PD proteome, the final list of proteins that appear in more than two or three studies, respectively, in the PD proteomics comparison and ageing were compared.

2.3.4 Bioinformatic analyses

Bioinformatic analyses (i.e., functional annotation analysis (DAVID), Reactome pathway analysis, and protein network analysis (STRING)) were performed using the differentially expressed proteins that appear conserved (down- or upregulated in the same direction) in more than two or three studies, respectively, in the PD proteomics comparison and ageing.

For each bioinformatic analysis, the same procedure as mentioned before was followed. However, for functional annotation analysis (DAVID) (see subsections 2.1.9.1) and protein network analysis (STRING) (see subsections 2.1.9.3), the '*Homo sapiens*' background was selected. Furthermore, in the case of DAVID, during the submission of the gene list, the selected identifier was 'official_gene_symbol'. For all multi-study proteomic comparisons, an updated version of Reactome pathway knowledgebase (version 69 (August 2019)) (see subsections 2.1.9.2) was used.

2.4 Other figures and diagrams

Venn diagrams and heatmaps in Chapter 3 were produced using GraphPad Prism version 7.01 (La Jolla, USA). Chord diagrams in Chapter 3 were generated using R Studio software, using the 'circlize' package (Gu *et al*., 2014). Montages of all images and drawing of diagrams were done with Adobe Illustrator CC version 17.1.0 (Adobe Inc.).

Chapter 3.

A quantitative proteomics assessment of the aged SNpc in rats

CHAPTER 3: A QUANTITATIVE PROTEOMICS ASSESSMENT OF THE AGED SNpc IN RATS

3.1 Introduction

Overview: This chapter aimed to determine the changes of the rat SNpc proteome during ageing and how this might explain the vulnerability of SNpc DAn in PD. This Introduction will review what is known about the PD proteome in humans and animal models, as well as how the brain and SNpc proteomes change during ageing.

3.1.1 The PD proteome

Overview: Proteomics studies complement histological or genetic analyses and attempt to provide more clues about the causes of the disease by explaining changes that are not perceived at the cellular level. In the case of PD, these investigations have been used to identify differences that exist between the PD proteome compared to healthy controls. This not only facilitated an understanding of the neuropathological mechanisms behind this neurodegenerative disease, but also provides the possibility of identifying biomarkers to diagnose the disease and control its course (Kasap *et al*., 2017). As it will be explained in more detail below, to perform these studies, research has used human samples such as different areas of the brain (including the SNpc), serum, blood, plasma or CSF to find biomarkers for PD. However, it has been difficult so far to draw conclusions that explain the causes of parkinsonism with proteomics, probably due to the complexity of the human brain, the differences found at the protein level between individuals, and the limited availability of fresh *post-mortem* PD brain tissue as well as relevant controls (Li *et al*., 2018a). As stated in the review by Kasap *et al*. (2017), these pitfalls have pushed neuroscientists to use model organisms that mimic the disease, such as rodents, non-human primates, *C. elegans or Drosophila melanogaster*. These animal studies are more experimentally controlled, and the number of the samples can be increased easily, which generates more robust data.

3.1.1.1 Human samples

Brain tissue – Among the numerous types of human samples that can be used for the study of PD by proteomics, the brain is commonly chosen to understand the mechanisms that underlie this disease. Search of the literature revealed a total of 13 proteomics studies using *post-mortem* brains from humans with PD, but only seven of them were performed in the SNpc.

The first research with human SNpc comparing PD and healthy controls was done by Basso *et al*. (2003), using four samples per group for analysis by 2D-SDS-PAGE and peptide mass fingerprinting. However, the results were only able to show that the PD samples had positive spots for alpha-synuclein and anti-ubiquitin, and that there was an increase in superoxide dismutase and dihydropteridine compared to controls. Nevertheless, the same authors subsequently published a more complete study which revealed that from the 44 proteins found by peptide mass fingerprinting, nine proteins related to mitochondria, scavenging oxidative stress, and afferent terminals were dysregulated in PD (e.g., L and M neurofilament decreased; while peroxiredoxin I, mitochondrial Complex 3, ATP synthase D chain, complexin I, profilin, L-type calcium channel delta-subunit, and fatty-acid binding proteins increased). This profile suggests that oxidative stress is prevalent in PD (Basso *et al*., 2004). Similarly, Werner *et al*. (2008) used 2D-SDS-PAGE to compare five SNpc (each) from PD patients and healthy controls, followed by MALDI-MS. From the 37 proteins identified, 16 were differentially expressed between the two groups. The differentially expressed proteins were related to iron metabolism (e.g., ferritin H), glutathione-related redox metabolism (e.g., glutathione S-transferase M3, glutathione S-transferase Pi 1), glial cells (e.g., glial fibrillary acidic protein (GFAP)) or metabolism (e.g., aldehyde dehydrogenase 1 family member A1) among others. Adding to this, Jin *et al*. (2006) analysed SNpc mitochondria-enriched fractions of five parkinsonians compared to five age-matched controls by ICAT and LC-MS. From the 842 proteins identified, 119 were dysregulated in PD compared to the control group, highlighting the depletion of mortalin (a mitochondria stress protein) in

PD. Another example of proteomics analysis of the SNpc of PD tissue was conducted by the same group employing a similar approach, using five samples per group (PD and control) labelled with iTRAQ and analysed by LC-MALDI-TOF/TOF (Kitsou *et al*., 2008). However, they did not provide a detailed dataset in their result section of the differentially expressed proteins between both proteomes, only a list of proteins known to be involved in neurodegeneration. Licker *et al*. (2012) performed a 2D-SDS-PAGE approach to study the SNpc of six parkinsonians and four controls, and detected 32 differentially spots, of which 23 were identified by MALDI-TOF/TOF. Their results showed that expression of proteins related to mitochondrial respiratory chain (e.g., cytochrome b-c1 subunit 2) and metabolism (e.g., fructose-biphosphate aldolase C) was decreased in PD, while the abundance of proteins that protect against free radicals (e.g., superoxide dismutase) were increased. This data indicated that mitochondrial functions directly associated with the production of energy, as well as oxidative stress mechanisms, were affected by PD. Recently, another study compared three samples per group (PD and control) using tandem mass spectrometry and cell culture derived isotope tags (CDITs), with isotope-labelled proteins from SH-SY5Y cells as internal standards (Liu *et al*., 2015). They observed that 11 proteins associated with glial inclusions and white matter were dysregulated between the two experimental groups; six of which were upregulated in SNpc of PD (e.g., alpha-B-crystallin (alpha-crystallin B chain) and hyaluronan and proteoglycan link protein 2), while five were downregulated (e.g., annexin a1).

In addition to the SNpc, other parts of the CNS have been utilized to elucidate what happens in the brain proteome during PD. These areas include the olfactory bulb (Lachen-Montes *et al*., 2019), locus coeruleus (van Dijk *et al*., 2012), anterior cingulate gyrus (Ping *et al*., 2018), and the cortex (Choi *et al*., 2004; Dumitriu *et al*., 2016; Bereczki *et al*., 2018). As described in the General introduction (see Chapter 1), the olfactory bulb is affected by PD, as is evident by inclusions of alpha-synuclein and Lewy Bodies. This is thought to impair the sense of smell of these patients. However, the mechanisms associated with this dysfunction are not known. Therefore, Lachen-Montes *et al*. (2019)

decided to combine label-free quantitative proteomics and MALDI imaging mass spectrometry, where the proteins from the tissue are directly investigated to determine the mass spectra of the surface layer of the sample (Caprioli *et al*., 1997). The study contained olfactory bulbs from eight controls and 21 PD patients and detected 268 differentially expressed proteins between them. The proteins affected by the disease were involved in transport and RNA processing (e.g., nucleotide binding and hydrolase activity), and cell survival and differentiation. On the other hand, an analysis of *post-mortem* locus coeruleus tissue (another area affected by PD) showed 87 differentially expressed proteins when six samples per group (PD and healthy controls) were compared after being analyzed by 1D-SDS-PAGE and LC-MS/MS (van Dijk *et al*., 2012). Bioinformatics analysis revealed that proteins associated with oxidative stress (e.g., aldehyde dehydrogenase X), mitochondria dysfunction (e.g., isoform 1 of acyl-coenzyme A thioesterase 9), cytoskeleaton structure and regulation (e.g., vimentin), inflammation and glial activation (e.g., galectine-3), and synaptic neurotransmission (e.g., gamma-synuclein) were affected by the disease in the locus coeruleus. Lastly, Bereczki *et al*. (2018) compared the cortex of eight PD brains against eight elderly controls by using TMT labelling and LC-MS analysis to understand the mechanisms behind cognitive changes during PD. The results showed 485 differentially expressed proteins, where 286 where upregulated and 199 where downregulated in PD compared to the controls. They demonstrated that there was a loss of proteins related to synapse function (e.g. glutamate ionotropic receptor AMPA type subunit 2, synaptosome associated protein 47, synaptotagmin 2) during the disease.

Biofluids: plasma, CSF, urine and tears – A recent systematic review and meta-analysis selected 27 publications to demonstrate that clinical diagnosis of PD is sometimes inefficient and inaccurate (Rizzo *et al*., 2016). In this study, they concluded that only eight out of ten patients with PD obtained a good diagnosis, especially at early stages of the disease. Due to such findings, researchers have focused on identifying

specific biomarkers in plasma, CSF, urine, or even tears, by using proteomics to diagnose (in a fast and economical way) the neurodegenerative disease. For instance, Kitamura *et al.* (2018) isolated exosomes (small vesicles that contain proteins secreted by cells and, therefore, neurons) from the plasma of 16 patients with PD (eight in early-stage and eight in a more advanced stage) and eight controls, to elucidate if there is any biomarker that could be linked to the severity of the disease. After 2D-SDS-PAGE and MALDI-TOF/TOF analysis, 35 protein spots were observed as differentially expressed between PD and controls. From these, clusterin, complement C1r subcomponent, and apolipoprotein A1 were reduced in PD, and an inverse correlation between apolipoprotein A1 and the severity of the disease was observed. CSF has also been used to attempt to find biomarkers for diagnosing PD. For example, recent research has revealed that 16 metabolites are significantly modified in the CSF of PD patients, when 44 early-stages PD patients were compared to 43 age-matched controls using gas chromatography mass spectrometry analysis (Trezzi *et al*., 2017). The presence of mannose, fructose and threonic acid were significantly increased with PD, while dehydroascorbic acid was reduced, suggesting a depletion in antioxidant activity and an elevation of glycolysis under oxidative stress. In the case of urine, Wang *et al*. (2019) isolated the extracellular vesicles or exosomes in this biofluid from 28 PD and 22 control individuals and analysed them by ion trap mass spectrometry. Both synaptosome associated protein 23 and calbindin were shown to be elevated with PD and useful for predicting the presence of the disease. Finally, tears have also been used as a biofluid to find biomarkers associated with PD. Boerger *et al.* (2019) compared 36 PD individuals and 18 controls by 1D-SDS-PAGE and LC-ESI-MS/MS. They found 21 proteins significantly increased and 19 decreased in PD. This proteome suggested to a dysregulation in immune responses, lipid metabolism and oxidative stress.

3.1.1.2 Animal models

Limited availability of appropriate *post-mortem* material and the lack of experimental controls have led to the use of animal models that mimic the disease in proteomics studies of PD. In these models, a large range of animals, including rodents (Triplett *et al*., 2015; Kim *et al*., 2017a; Maasz *et al*., 2017), primates (Scholz *et al*., 2008), fishes (Visscher *et al*., 2016; Cowie *et al*., 2017; Froyset *et al*., 2018) or *Drosophila melanogaster* (Islam *et al*., 2016) are either exposed to toxins (e.g., MPTP or 6-OHDA) or are genetically modified (e.g., parkin) (Kasap *et al*., 2017). Although the literature shows almost 40 studies combining PD animal models and different approaches in proteomics, here are reviewed the most relevant examples. First, in a previous study performed by our lab few years ago, adult rats were unilaterally lesioned with 6-OHDA in the medial forebrain bundle, producing a denervation of the striatum from SNpc DAn (Fuller *et al*., 2014). After analysis of the striatum at different time points (between 3- and 14-days post-lesion) by iTRAQ labeling and MALDI-TOF/TOF, an elevation of proteins associated with axonal reorganization (e.g., neurofilament polypeptides) were found during the first three days compared to unlesioned rats. These proteins decreased again after denervation of the striatum was complete at 14 days post-lesion. More specifically, the protein guanine deaminase, that regulates dendritic branching, was significantly increased with time after lesion, which may indicate an attempt by the DAn or striatal neurons to re-innervate the area. Likewise, Kuter *et al*. (2016) performed an experiment in which rats were bilaterally injected with 6-OHDA in the medial forebrain bundle, and the mitochondria from both striatum and SNpc were isolated. On this occasion, 2D-SDS-PAGE together with MALDI-TOF/TOF mass spectrometry was used to analyze the samples. Their results were similar to those found by Fuller *et al.* (2014), showing alterations in proteins related to cytoskeleton remodeling, axon outgrowth and regeneration when 6-OHDA was applied. Lastly, in another experiment using the PD animal model of MPTP, 300 zebrafish in total were treated intraperitoneally with MPTP or saline (control) (Sarath Babu *et al*., 2016). After dissecting the entire brain, proteins

were extracted, and peptides were labeled by the iTRAQ method for analysis by tandem mass spectrometry. These results show that, apart from producing a PD-like behavior in the fish, MPTP generated the dysregulation of 78 proteins compared to the control group, with a notable upregulation of the proteins trafficking protein particle complex subunit 8-like, BAH and coiled-coil domain-containing protein 1-like, and hypothetical protein CRE_13172. Pathway analysis suggested that cytoskeleton remodelling of neurofilaments and neurophysiological synaptic vesicle were some of the biological functions altered in this PD model. Altogether, this reflects that proteomics is a useful and valid tool to study the molecular changes that appear in the proteome of animals with induced PD.

3.1.2 The ageing brain and SNpc proteome

Research using a variety of proteomic approaches have been conducted to understand the physiological ageing process in different areas of the brain. In humans, for example, Chen *et al*. (2003) studied how age affected the temporal, frontal and parietal lobes by comparing proteomes from young (23-year-old) and old (73-84-year-old) individuals by 2DE-SDS-PAGE and MALDI-TOF/TOF. This analysis revealed five downregulated proteins (e.g., peroxiredoxin 2, stathmin, apolipoprotein a-I precursor) in old samples, which could have implications on the antioxidant functions of cells and the degeneration of axons. Furthermore, Dominguez *et al*. (2016) looked at the parietal and frontal cortex together with the cingulated gyrus to study the lipoxidation state of the proteins with ageing by comparing five middle age (around 43 years) *versus* old (around 74 years). To do this, they investigated the grade of neuroketals adduction (which causes lipoxidation and aggregation of proteins) by 2D-SDS-PAGE, neuroketal immunolabeling and MS/MS analysis. They found 25 neuroketal-adducted proteins in total in both ages, although the majority of proteins showed a higher lipoxidation in the oldest individuals (e.g., alpha-B-crystallin). The functional analysis of these proteins demonstrated that there were biological functions affected by ageing in these regions, such as energy

metabolism, cytoskeleton structure and proteostasis. Adding to this, Pabba *et al*. (2017) analyzed the orbitofrontal cortex from 15 young (15-43-year-old) and 18 old (62-88-year-old) individuals using LCM to extract the tissue. The mass spectrometry analysis showed 127 differentially expressed proteins, including 65 upregulated (e.g., alpha-B-crystallin, GFAP) and 62 downregulated (e.g., HOMER1), indicating a dysregulation in cell communication, nutrient sensing and proteostasis.

In rodents, Mao and colleagues (2006) used proteomics analysis (2D-SDS-PAGE and MALDI-TOF) to study the mitochondria of the whole mouse brain at six different ages (from newborn to 24-month-old). They described that proteins related to the respiratory chain where either decreased (e.g., complex I and complex IV subunits) or increased (e.g., complex III and complex V) with ageing, which might be indicating a compensatory mechanism for dysfunctional cellular respiration. Alternatively, Gokulrangan *et al*. (2007) used the rat cerebellum at different ages to investigate the nitration state of proteins, which is known to be a marker of oxidative stress. To do this, they dissected the cerebellum from three different groups (5-, 22- and 34-month-old) and performed 2DE-SDS-PAGE followed by immunolabelling of nitrated proteins and an analysis by MS/MS. Although they did not explain the functional consequences of a higher nitration in proteins, they revealed an increase of nitrated proteins with ageing, including ryanodine receptor 3, low density lipoprotein receptor related protein 2, and nebulin-related anchoring protein.

Despite all the proteomic investigations to understand how PD affects proteins from the SNpc and other areas of the CNS, as well as how ageing modifies the proteome of different regions of the brain, to my best knowledge, only a single article exists in the literature (Raghunathan *et al*., 2018) that analyses the ageing process in the rat SNpc. In this publication, the SNpc and striatum proteomes of 3-month-old rats was compared to 20-month-old by LC-MS analysis. However, their main aim was to understand how ageing affects the glycan receptors in the striatum and SNpc. As they explained, the study of these glycan receptors (e.g., heparan sulphate proteoglycans and N-glycans

with terminal galactose) was motivated by the lack of efficacy of adeno-associated viruses (AAV) as vectors for gene therapy during clinical trials in humans. This gene delivery approach seems to work in animal models, therefore, they hypothesized that modifications of these receptors with ageing might be altering the binding of AAV in the striatum and SNpc, which will disrupt the gene delivery. Importantly, although details of the differences found in other proteins in their ageing study was provided as supplementary info in PRIDE public repository, there was not any clear discussion provided for the biological meaning of the proteomic results in ageing. This was, perhaps, a missed opportunity to provide more insight into how ageing affects the proteome of the SNpc and why ageing might be associated with the vulnerability of DAn during PD.

Surprisingly, although most of the proteomics studies in PD used age-matched individuals as controls, it was not possible to find any proteomics research focusing only on healthy SNpc in humans. This is essential because it is necessary to understand the protein profile of the ageing SNpc to comprehend the relationship between ageing and PD. Only recently, it was published a thesis (Steinbach *et al*., 2018) where the proteome of the SNpc in humans was studied in relation to the ageing process. In this pioneering and comprehensive investigation, Steinbach and colleagues not only defined for the first time the proteome of the healthy human SNpc with increasing age, but also the differences that exist between the DAn from dorsal and ventral tier SNpc. First, to analyse the whole human SNpc with ageing, they used the entire SNpc tissue from 36 healthy individuals between 18 to 96 years old and analysed them using an Orbitrap mass spectrometer with a DDA method. Thus, they generated the first spectral library of the healthy human SNpc, containing 5,391 proteins, from which 1,908 were always expressed regardless of the age of this region. Importantly, this data updated the spectral library of the human SNpc presented by Licker *et al.* (2014) that, although it identified 1,795 proteins, was based on SNpc with PD. Furthermore, from the 1,908 proteins, they studied ones which had a correlation with the ageing process, finding that

254 proteins showed a significant correlation when they were analysed at protein and peptide level (135 had a positive correlation, while 119 had a negative correlation). Their GO analysis indicated that these proteins were involved in ‘catalytic activity’, ‘binding’ and ‘structural molecular activity’. Adding to this, their analysis also revealed that 210 proteins were related to mitochondria and 24 of them had a correlation with ageing (e.g., adenylate kinase 2, cytochrome c oxidase subunit NDUFA4). In the same way, from the 20 proteins related to PD, only four of them had a significant correlation with ageing (e.g., protein/nucleic acid deglycase DJ-1, peptidyl-prolyl cis trans isomerase F, ADP/ATP translocase 1, voltage-dependent anion-selective channel protein 1). Secondly, they examined the selective vulnerability of DAn from the dorsal and ventral tier of SNpc, due to their different degeneration during PD. To do this, they isolated by LCM the DAn cell bodies from 15 human SNpc and, after performing an Orbitrap mass spectrometry using a DIA method, they considered only five samples due to the high variability found in the ventral tier. MS/MS analysis reported 2,453 proteins in the dorsal region, and 1,629 proteins in the ventral part. When the proteins of these two areas were compared, they discovered that only five proteins were specific for the dorsal tier (e.g., immunoglobulin heavy constant gamma1, tubulin gamma 1-chain, ADP-ribosylation factor 3, Ras-related protein Rab-11A, aldo-keto reductase family 1 member C1), while four proteins were limited to the ventral tier (e.g., immunoglobulin gamma-1 heavy chain, calmodulin-like protein 3, actin alpha-cardiac muscle 1, ADP-ribosylation factor 1). Moreover, when they checked which proteins were differentially expressed between the two areas, it was found that seven out of a total of nine differentially expressed proteins were upregulated in the dorsal SNpc (e.g., myelin basic protein), and only two had a positive correlation with ageing (e.g., hyaluronan and proteoglycan link protein 2, myelin P2 protein). They concluded that most of the proteins altered with ageing in the SNpc were related with the cytoskeleton of DAn, which might indicate a dysregulation of the maintenance of the cytoskeleton and disruption of the DAn network. In addition, they found alteration in

proteins related to calcium homeostasis, which might affect the respiratory chain of the mitochondria.

In summary, the impact of the ageing process in the SNpc is still unclear and remains a mystery. A proteomics study in the rat SNpc was performed at four different age times to understand how ageing affects the proteome of the SNpc region. This analysis allowed for the first time ever the identification of global proteomic changes in the rat SNpc during the ageing process. The examination of the entire SNpc allows the investigation of possible alterations in proteins related DAn, but also other non-DAn, such as glial cells (e.g., astrocytes, microglia). Ultimately, this is important because ageing can be a direct process that increases the vulnerability of DAn, or an indirect process that first affects other cells (e.g., glial cells) that surround, protect and maintain these DAn. Alteration of these non-neuronal cells could then have indirect effects that contribute to DAn degeneration.

3.1.3 Aim and objectives

The aim of this study was to conduct a quantitative proteomic comparison of the rat SNpc at postnatal day 14, 8-month-old, 16-month-old and >21-month-old to determine whether protein expression levels change during normal physiological ageing. It is hoped that this may provide insights into why SNpc DAn become more vulnerable with increasing ageing and make the occurrence of PD more likely. To do this, a quantitative proteomics assessment of the SNpc, together with bioinformatic, immunoblotting and immunofluorescence analyses were performed.

Based on this, the objectives of this study were:

- Objective 1) To identify and quantify changes in protein expression of the rat SNpc during physiological ageing.

- Objective 2) To identify, through the use of bioinformatic tools, which biological processes and pathways are affected in the most aged SNpc, and if there is any relation or interaction between proteins that change.
- Objective 3) To validate the proteomics results by immunoblotting and immunofluorescence.

3.2 Materials and methods

Details about materials and methods of this experimental chapter can be found in Chapter 2, section 2.1.

3.3 Results

3.3.1 The expression levels of 66 proteins are altered throughout ageing in the adult rat SNpc proteome

A total of 2,986 proteins with a threshold of 5% local FDR were identified in the rat SNpc with the use of ProteinPilot software and UniProtKB/Swiss-Prot FASTA database, considering all three protein comparisons (i.e., juvenile *versus* old; young *versus* old; middle age *versus* old) (**Figure 3.1; Supplementary Table 1**). After removing false positive hits and proteins with two or less peptides to perform reliable quantifications of the data, 1,953 proteins were left (**Figure 3.1; Supplementary Table 2a, 2b**). Subsequently, proteins were included for further analysis only if their fold-change ratios, derived from their comparisons, passed a significant p-value ($p<0.05$) and an arbitrary 1.25-fold-change cut-off (**Figure 3.1; Supplementary Table 2c-e**). This filter was necessary to manage the data, although it is important to indicate that changes in the expression of certain proteins below the 1.25-fold-change cut-off could be relevant biologically. After filtering the data, a total of 631 differentially expressed proteins across all comparisons remained, being distributed as follows: 608 proteins in the juvenile *versus* old comparison (**Figure 3.1, 3.2A; Supplementary Table 2c)**, 43 proteins in the young *versus* old comparison (**Figure 3.1, 3.2B; Table 3.1**), and 28 proteins in the

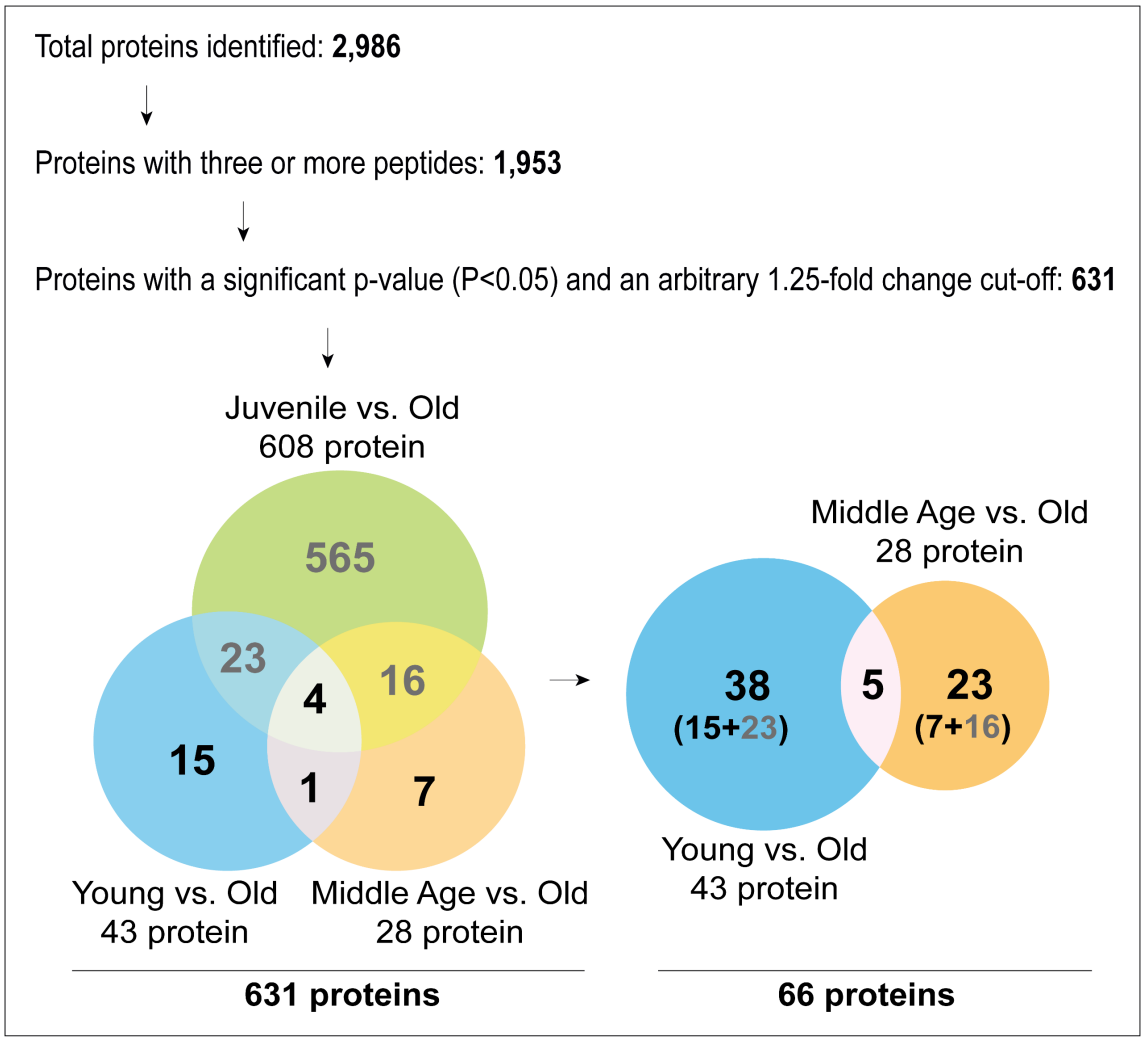

Figure 3.1. The proteome of the aged SNpc in rats. A total of 2,986 proteins were identified in the SNpc with ProteinPilot software and UniProtKB/Swiss-Prot FASTA database. After removing proteins with two or less peptides, 1,953 proteins were left. Protein fold-change ratios with a significant p-value ($p<0.05$) and an arbitrary 1.25-fold-change cut-off was applied to distinguish differentially expressed proteins, leaving 631 proteins in the three different comparisons *versus* old as follows: 608 proteins in juvenile *versus* old, 43 proteins in young *versus* old, and 28 proteins in middle age *versus* old (left Venn diagram). To study only modifications related to the ageing process in adults, the 608 proteins that changed from juvenile to old, that might be implicated in neurodevelopment, were excluded of the final analysis, leaving a final list of 66 differentially proteins in adult stages (young and middle age) compared to the old group (right Venn diagram). In this last diagram, the number of differentially expressed proteins that also appeared in the juvenile *versus* old comparison are presented in grey colour.

middle age *versus* old comparison (**Figure 3.1, 3.2C; Table 3.2**). The distribution of these proteins in a Venn diagram showed that there were four proteins in common between the three comparisons, corresponding to haemoglobin subunit alpha 1 (HBA1), haemoglobin subunit beta (HBB), 3-ketoacyl-CoA thiolase, mitochondrial (ACAA2), and myelin protein P0 (MPZ) (**Figure 3.1; Supplementary Table 2f**).

As mentioned in the Materials and methods section (see Chapter 2), this Thesis focuses on the study of the SNpc proteome related to the adult ageing process. However, at postnatal stages, the brain undergoes protein changes associated with neurodevelopment that might have an impact in the proteome of the juvenile group (see Discussion). Thus, differentially expressed proteins in the comparison juvenile *versus* old might reveal changes in the SNpc proteome linked to neurodevelopment instead of normal physiological ageing. Supporting this consideration, functional annotation analysis by DAVID of the 608 proteins that were differentially expressed in the comparison juvenile *versus* old (**Supplementary Table 2c)** showed that many of the enriched biological processes associated with these proteins were related to neurodevelopment, including terms such as 'substantia nigra development', 'neuron projection development' or 'central neuron system development' (**see Annex 1, Supplementary Table 3a**)**.** To avoid the misinterpretation of the data, the 608 proteins from the comparison juvenile *versus* old were excluded from further examination, leaving a total of 66 differentially expressed proteins in adults ages (young and middle age) compared to old (**Figure 3.1; Supplementary Table 2f**). When these 66 differentially expressed proteins were plotted in a Venn diagram, only five proteins appeared to be in common between these two adult comparisons, corresponding to haemoglobin subunit alpha 1 (HBA1), haemoglobin subunit beta (HBB), 3-ketoacyl-CoA thiolase, mitochondrial (ACAA2), glutathione S-transferase alpha-4 (GST4) and myelin protein P0 (MPZ) (**Figure 3.1; Supplementary Table 2f**). Moreover, these proteins presented the same direction in both comparisons, either increasing or decreasing their expression with the ageing process. Specifically, the expression of two of them (haemoglobin

subunit alpha 1 (HBA1), haemoglobin subunit beta (HBB)) were increased in old animals, while the expression of three proteins (3-ketoacyl-CoA thiolase, mitochondrial (ACAA2), glutathione S-transferase alpha-4 (GST4) and myelin protein P0 (MPZ)) decreased in the old group in comparison to the other two adult ages (i.e., young *versus* old, middle age *versus* old). The rest of the proteins (61 proteins) were differentially expressed only in one of the comparisons – i.e., either in young *versus* old (38 proteins) (**Figure 3.1; Figure 3.2B; Table 3.1**) or middle age *versus* old (23 proteins) (**Figure 3.1; Figure 3.2C; Table 3.2**). From these, considering the 38 proteins from the young *versus* old comparison, 26 proteins were significantly upregulated in the old SNpc, while 12 proteins were downregulated compared to the young age (**Figure 3.2B; Table 3.1**). On the other hand, examining the 23 proteins from the middle age *versus* old comparison, only two proteins were significantly upregulated in the old animals, while 21 were downregulated compared to the middle age group (**Figure 3.2C; Table 3.2**). In addition, some of these differentially expressed proteins in adult ages were also dysregulated in the juvenile group (**Figure 3.1; Supplementary Table 2c-e**). As an example, proteins such as alpha-crystallin B chain (CRYAB), myelin-oligodendrocyte glycoprotein (MOG) or neuromodulin (GAP43) were differentially expressed in both juvenile and young *versus* old; while vimentin (VIM), agrin (AGRN), or glial fibrillary acidic protein (GFAP) were differentially expressed in both juvenile and middle age *versus* old.

Lastly, to check the magnitude of change in the protein expression, the maximum downregulation and upregulation was observed in both comparisons (young *versus* old, middle age *versus* old). The observation of the fold-changes revealed that the expression of the differentially expressed proteins in the SNpc with ageing had a maximum of 0.44 and 2.78-fold-change in the young *versus* old comparison, which corresponded to hyaluronan and proteoglycan link protein 2 (HAPLN2) and myelin protein P0 (MPZ), respectively; while in the middle age group *versus* old comparison the maximum was 0.68 and 2.98-fold-change, which corresponded to sphingosine 1-

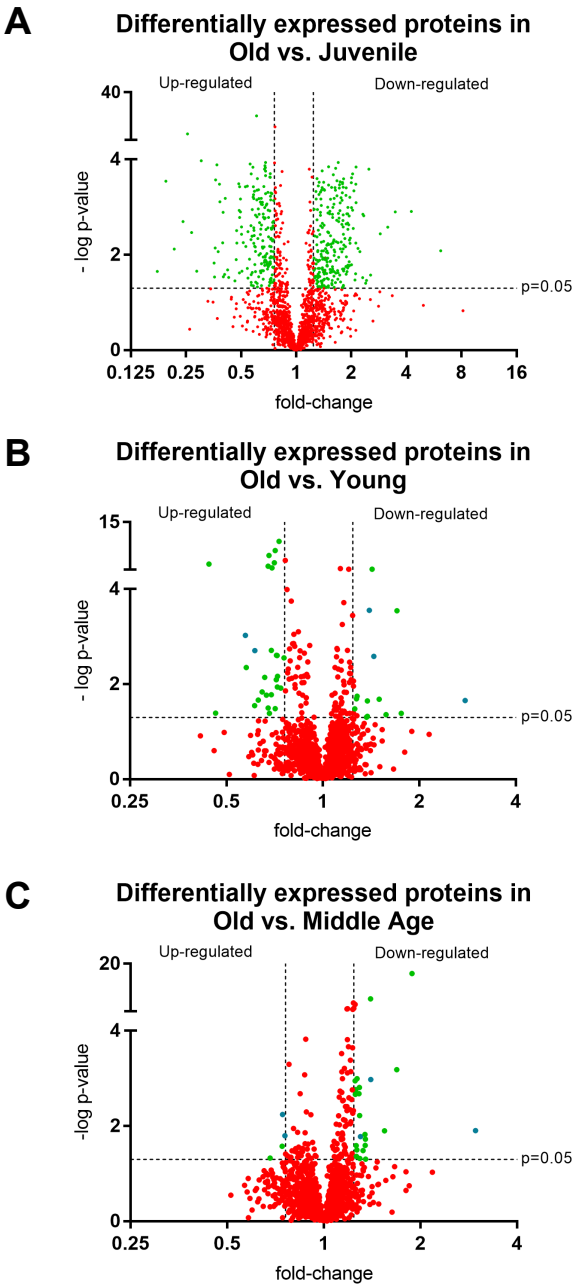

Figure 3.2. Proteins identified in each of the protein comparisons: (A) juvenile *versus* old, (B) young *versus* old, (C) middle age *versus* old. Only proteins with a significant p-value ($p<0.05$) and more than an arbitrary 1.25-fold-change cut-off (green and blue dots) were considered for further analysis. This left **(A)** 608 proteins in juvenile, **(B)** 43 in young, **(C)** and 28 in middle age SNpc compared to old animals. Blue dots indicate proteins in common in the ratios young and middle age *versus* old. In the image, upregulated and downregulated proteins correspond to proteins in the old age compared to the respective age groups. Thresholds ($p<0.05$ and 1.25-fold-change) are presented as dashed lines. Red dots below these thresholds represent proteins with non-significant p-value and non-accepted fold-change, therefore, not included in the analysis.

phosphate receptor 5 (S1PR5) and myelin protein P0 (MPZ), respectively (**Table 3.1; Table 3.2**).

Table 3.1. Differentially expressed protein ratios in the comparison of young *versus* old rat SNpc, showing if their expression is increased (up) or decreased (down) in old age.

Protein name (gen name) [accession number]	iTRAQ ratio [peptides]	p-value
Up in old vs. young		
Hyaluronan and proteoglycan link protein 2 (Hapln2) [Q9ESM2]	0.441 [19]	4.70E-06
Ferritin light chain 1 (Ftl1) [P02793]	0.462 [8]	4.06E-02
Hemoglobin subunit alpha-1/2 (Hba1) [P01946]	0.573 [9]	9.49E-04
Scaffold attachment factor B1 (Safb) [O88453]	0.577 [5]	4.50E-03
Synaptosomal-associated protein 23 (Snap23) [O70377]	0.613 [6]	2.85E-02
Hemoglobin subunit beta-1 (Hbb) [P02091]	0.614 [14]	1.98E-03
Claudin-11 (Cldn11) [Q99P82]	0.628 [29]	2.17E-02
Ribosyldihydronicotinamide dehydrogenase [quinone] (Nqo2) [Q6AY80]	0.646 [6]	1.46E-02
Neurocan core protein (Ncan) [P55067]	0.658 [9]	7.18E-03
Myelin-associated oligodendrocyte basic protein (Mobp) [Q63327]	0.666 [15]	1.70E-02
Transmembrane protein 132A (Tmem132a) [Q80WF4]	0.675 [8]	3.19E-02
Myelin-oligodendrocyte glycoprotein (Mog) [Q63345]	0.675 [31]	1.52E-05
Apolipoprotein E (Apoe) [P02650]	0.679 [47]	4.80E-08
Carboxypeptidase D (Cpd) [Q9JHW1]	0.681 [4]	4.13E-02
Alpha-crystallin B chain (Cryab) [P23928]	0.691 [11]	1.95E-03
Aggrecan core protein (Acan) [P07897]	0.691 [6]	1.66E-02
Dihydropteridine reductase (Qdpr) [P11348]	0.694 [32]	3.89E-05
Carbonic anhydrase 2 (Ca2/Car2) [P27139]	0.706 [50]	2.47E-06
Cytosol aminopeptidase (Lap3) [Q68FS4]	0.710 [32]	3.83E-09
Ubiquitin-conjugating enzyme E2 Z (Ube2z) [Q3B7D1]	0.710 [5]	3.27E-02
Hyaluronan and proteoglycan link protein 1 (Hapln1) [P03994]	0.715 [9]	8.06E-03
Versican core protein (Fragments) (Vcan) [Q9ERB4]	0.716 [25]	2.47E-03
Choline transporter-like protein 1 (Slc44a1) [Q8VII6]	0.720 [8]	2.51E-03
Protein phosphatase 1 regulatory subunit 14A (Ppp1r14a) [Q99MC0]	0.720 [8]	1.15E-02
Aspartoacylase (Aspa) [Q9R1T5]	0.722 [7]	6.83E-03
Contactin-associated protein 1 (Cntnap1) [P97846]	0.730 [44]	2.72E-11
Calcium-regulated heat stable protein 1 (Carhsp1) [Q9WU49]	0.739 [6]	1.22E-02
Sulfated glycoprotein 1 (Psap) [P10960]	0.756 [23]	2.80E-03
Down in old vs. young		
Peptidyl-prolyl cis-trans isomerase FKBP1A (Fkbp1a) [Q62658]	1.257 [21]	3.31E-02
N-acylneuraminate cytidylyltransferase (Cmas) [P69060]	1.273 [6]	2.04E-02
Acetoacetyl-CoA synthetase (Aacs) [Q9JMI1]	1.277 [4]	4.59E-02
Ectonucleotide pyrophosphatase family member 6 (Enpp6) [B0BND0]	1.278 [14]	1.80E-02
Myosin phosphatase Rho-interacting protein (Mprip) [Q9ERE6]	1.369 [3]	4.97E-02
60S ribosomal protein L36 (Rpl36) [P39032]	1.377 [4]	4.76E-02
Glutamate receptor 2 (Gria2) [P19491]	1.377 [9]	2.26E-02
3-ketoacyl-CoA thiolase, mitochondrial (Acaa2) [P13437]	1.395 [17]	2.82E-04
Neuromodulin (Gap43) [P07936]	1.424 [43]	7.13E-05
Glutathione S-transferase alpha-4 (Gsta4) [P14942]	1.442 [11]	2.62E-03
Myristoylated alanine-rich C-kinase substrate (Marcks) [P30009]	1.499 [7]	2.07E-02
Oligophrenin-1 (Ophn1) [P0CAX5]	1.574 [3]	4.39E-02
Transgelin (Tagln) [P31232]	1.703 [13]	2.85E-04
Aldose reductase-related protein 1 (Akr1b7) [Q5RJP0]	1.755 [7]	4.14E-02
Myelin protein P0 (Mpz) [P06907]	2.779 [7]	2.20E-02

Table 3.2. Differentially expressed protein ratios in the comparison of middle age *versus* old rat SNpc, showing if their expression is increased (up) or decreased (down) in old age.

Protein name (gen name) [accession number]	iTRAQ ratio [peptides]	p-value
Up in old vs. middle age		
Sphingosine 1-phosphate receptor 5 (S1pr5) [Q9JKM5]	0.679 [3]	4.72E-02
Agrin (Agrn) [P25304]	0.741 [3]	2.66E-02
Hemoglobin subunit alpha-1/2 (Hba1) [P01946]	0.744 [9]	5.72E-03
Hemoglobin subunit beta-1 (Hbb) [P02091]	0.755 [14]	1.61E-02
Down in old vs. middle age		
Brain-specific angiogenesis inhibitor 1-associated protein 2 (Baiap2) [Q6GMN2]	1.251 [48]	4.38E-07
Neurosecretory protein VGF (Vgf) [P20156]	1.251 [24]	1.13E-03
Acyl-CoA-binding protein (Dbi) [P11030]	1.253 [19]	2.17E-03
Thiomorpholine-carboxylate dehydrogenase (Crym) [Q9QYU4]	1.258 [19]	1.72E-03
Ras-related protein Rab-14 (Rab14) [P61107]	1.262 [23]	2.58E-02
Monoglyceride lipase (Mgll) [Q8R431]	1.264 [5]	4.35E-02
Synaptic vesicle glycoprotein 2B (Sv2b) [Q63564]	1.267 [11]	3.17E-02
Pyridoxal kinase (Pdxk) [O35331]	1.269 [19]	1.02E-03
Glutathione S-transferase Mu 1 (Gstm1) [P04905]	1.286 [34]	2.09E-03
Peroxiredoxin-6 (Prdx6) [O35244]	1.291 [36]	1.55E-03
Calcineurin subunit B type 1 (Ppp3r1) [P63100]	1.292 [26]	6.04E-03
Transgelin-2 (Tagln2) [Q5XFX0]	1.295 [12]	4.81E-02
Glutathione S-transferase alpha-4 (Gsta4) [P14942]	1.300 [11]	1.66E-02
Lysosome-associated membrane glycoprotein 5 (Lamp5) [Q5PPI4]	1.326 [8]	3.28E-02
Sodium channel subunit beta-4 (Scn4b) [Q7M730]	1.343 [7]	1.51E-02
Leucine carboxyl methyltransferase 1 (Lcmt1) [Q6P4Z6]	1.346 [16]	2.56E-02
NAD kinase domain-containing protein 1 (Nadkd1) [Q1HCL7]	1.348 [3]	1.90E-02
Huntingtin (Htt) [P51111]	1.349 [12]	4.99E-02
Vimentin (Vim) [P31000]	1.397 [69]	5.60E-09
3-ketoacyl-CoA thiolase, mitochondrial (Acaa2) [P13437]	1.400 [17]	1.06E-03
Glutathione S-transferase alpha-3 (Gsta3) [P04904]	1.545 [13]	1.26E-02
Keratin, type I cytoskeletal 10 (Krt10) [Q6IFW6]	1.687 [17]	6.55E-04
Glial fibrillary acidic protein (Gfap) [P47819]	1.883 [130]	2.02E-17
Myelin protein P0 (Mpz) [P06907]	2.970 [7]	1.26E-02

In order to gain insights into whether protein expression changes follow a trend with increasing age, the fold-changes of the 66 proteins that were differentially expressed in at least one of the comparisons (i.e., young *versus* old or/and middle age *versus* old) were examined (**Figure 3.3**). To achieve this, the old group was considered as having a ratio of one, and the trends were calculated using the protein fold-changes from the young and middle age group, independent of whether their fold-change ratios were statistically significant or not, or did not pass the arbitrary cut-off. This analysis allowed

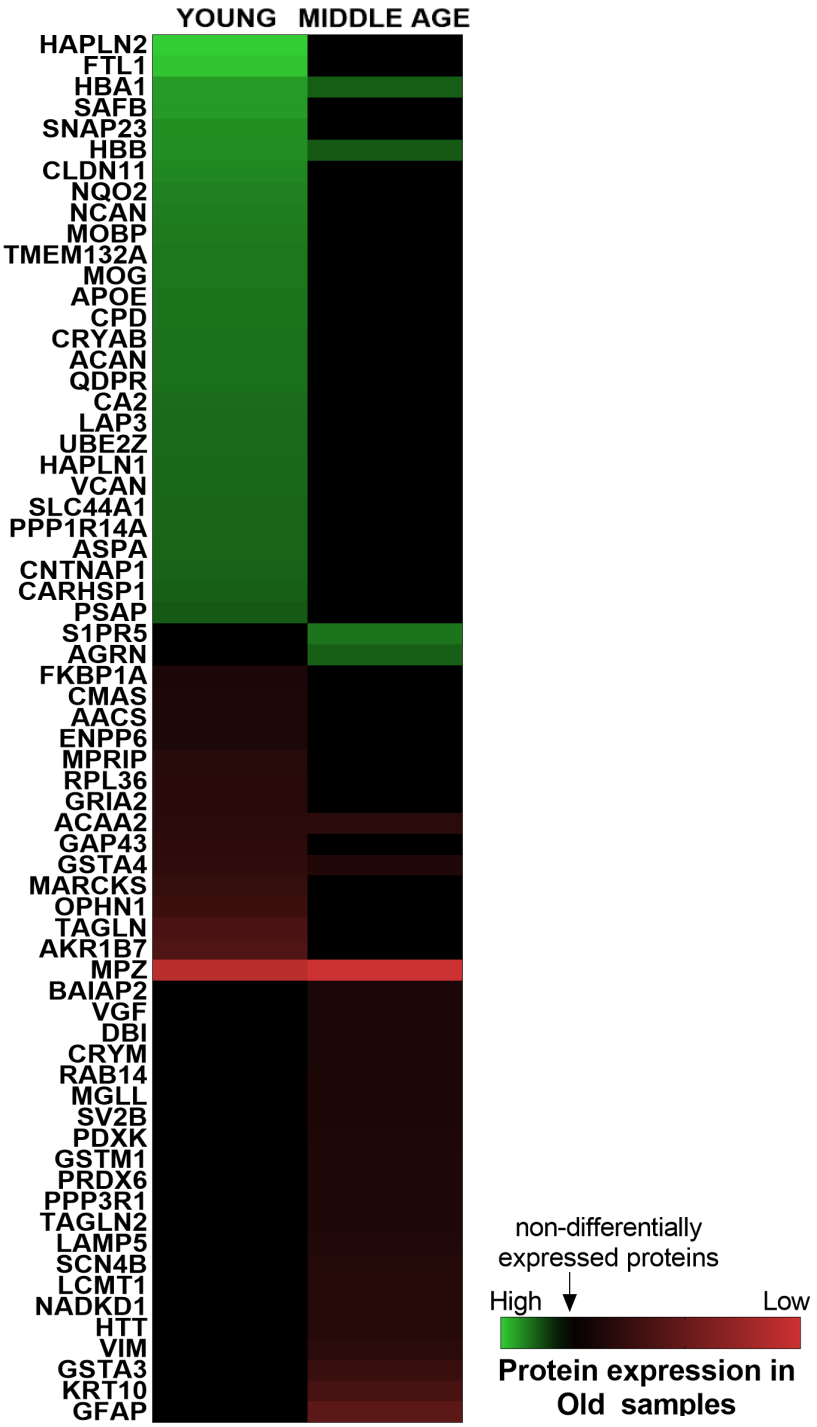

Figure 3.3. Expression of the 66 differentially expressed proteins that change in the adult SNpc with ageing. Heat map of the differentially expressed proteins in the comparison of young *versus* old and middle age *versus* old. Green cells show an increase of the protein expression in the old group, while red cells show a decrease of the protein expression in the old SNpc, in comparison with the young or middle age group. Black cells represent proteins that are not statistically significant or do not pass the established cut-off in both comparisons.

the generation of four different trend groups as follows: a) 27 proteins whose expression increased progressively from young to old (**Figure 3.4A**); b) 11 proteins whose expression decreased progressively from young to old (**Figure 3.4B**); c) four proteins whose expression decreased from young to middle age and increased again from middle age to old (**Figure 3.4C**); and d) 24 proteins whose expression increased from young to middle age group to decrease again in the old (**Figure 3.4D**). Interestingly, most of the differentially expressed proteins whose expression levels changed gradually with increasing age, either increasing (i.e., trend 'a') or decreasing (i.e., trend 'b'), presented fold-change ratios that had an accepted cut-off and were statistically significant only in the comparison young *versus* old, but not in middle age *versus* old. This was true for all proteins in these two trend groups except for haemoglobin subunit alpha 1 (HBA1), haemoglobin subunit beta (HBB), 3-ketoacyl-CoA thiolase, mitochondrial (ACAA2), and glutathione S-transferase alpha-4 (GST4), which were differentially expressed in both comparisons (**Figure 3.4A, B**). Conversely, the trend group 'd' was formed mainly by proteins whose fold-change ratios met the criteria for differential expression based on their fold-change only in the comparison between middle age *versus* old, but not young *versus* old (**Figure 3.4D**).

Altogether, this section revealed that the expression of 66 proteins changed significantly in the rat SNpc proteome with ageing: 38 proteins from young to old, 23 proteins from middle age to old, and five in both comparisons. The examination of the expression trends of these 66 differentially expressed proteins with age demonstrated that, in some cases, the expression increased or decreased progressively from early stages of adult life (i.e., young) until old age. In this scenario, most of the proteins were only differentially expressed and passed the cut-off filter in the young *versus* old comparison, but not middle age *versus* old comparison. On the other hand, most of the proteins that were differentially expressed only in the middle age *versus* old comparison showed a level of expression in the old group similar to the one found in the young age.

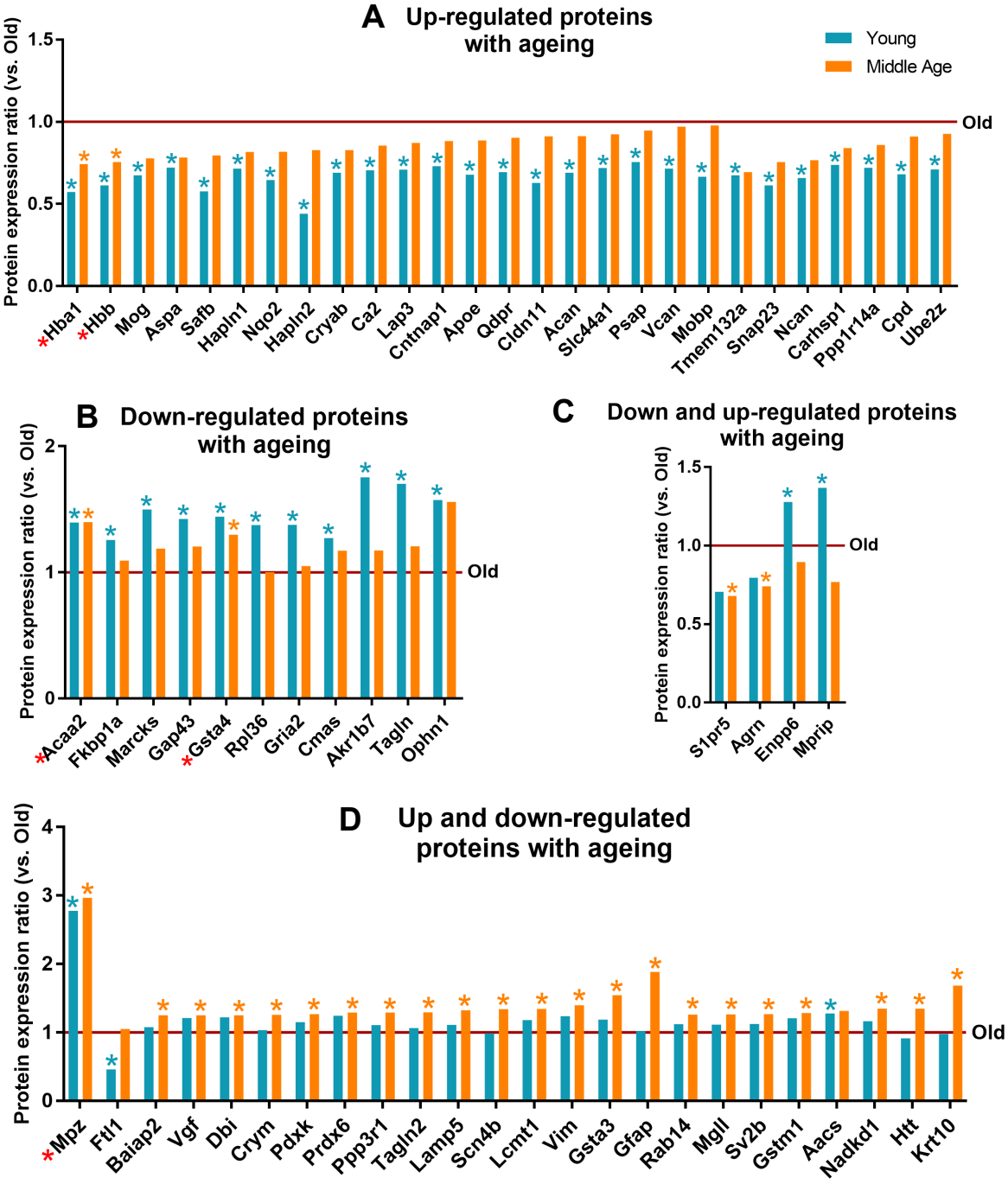

Figure 3.4. Expression of the 66 differentially expressed proteins that change in the adult SNpc with ageing. Trends of expression of proteins whose ratios are statistically significant in at least one of the comparisons (young *versus* old, blue asterisks; middle age *versus* old, orange asterisks; both comparisons, red asterisks). Red line indicates the threshold for old animals (ratio=1). **(A)** Proteins whose expression increases progressively with ageing. **(B)** Proteins whose expression decreases progressively with ageing. **(C)** Proteins whose expression decreases from young to middle age but increases again in the old group. **(D)** Proteins whose expression increases from young to middle age but decreases again in the old group.

3.3.2 Proteins related to cell adhesion, extracellular matrix and detoxification of the environment are dysregulated in the aged SNpc in rats as revealed by Gene Ontology analyses

To obtain a better understanding of the biological meaning of the 66 proteins that were differentially expressed in the old SNpc compared to the young and middle age groups, GO analyses were performed using DAVID software (Huang *et al*., 2007; Huang *et al*., 2009). GO terms were accepted if they had a $p<0.05$ and were assigned to at least two proteins. GO revealed that the three most enriched biological processes in the rat SNpc with ageing were the terms 'cell adhesion', 'central nervous system development' and 'metabolic process' (**Figure 3.5A**). 'Cell adhesion' and 'central nervous system development' were associated almost completely with proteins whose expression increased in the old SNpc, including, for example, versican core protein (VCAN). 'Metabolic process' was related to those proteins whose expression decreased in the old SNpc, for example, glutathione S-transferase alpha-4 (GSTA4). On the other hand, 'myelin sheath', 'extracellular space' and 'extracellular matrix' were the most enriched terms from the cellular component category in the rat aged SNpc (**Figure 3.5B**). The expression of most of the proteins associated with the terms 'myelin sheath' and 'extracellular matrix' increased in the old SNpc, such as alpha-crystallin B chain (CRYAB) and versican core protein (VCAN). Conversely, the term 'extracellular space' was linked to proteins whose expression decreased in the old individuals, including, for example, neurosecretory protein VGF (VGF). Finally, 'hyaluronic acid binding', 'extracellular matrix' and 'structural molecule activity' were the three molecular functions most enriched in the rat SNpc with ageing (**Figure 3.5C**). 'Hyaluronic acid binding' and 'extracellular matrix' were terms associated with proteins whose expression was increased in the old samples, like versican core protein (VCAN); while 'structural molecule activity' was a term linked to proteins whose expression increased in the old SNpc, such as claudin-11 (CLDN11), or decreased, such as glial fibrillary acidic protein (GFAP). Only the 'glutathione metabolism' pathway was determined as an enriched

annotation during the ageing process of the rat SNpc by KEGG pathway analysis (graph not shown).

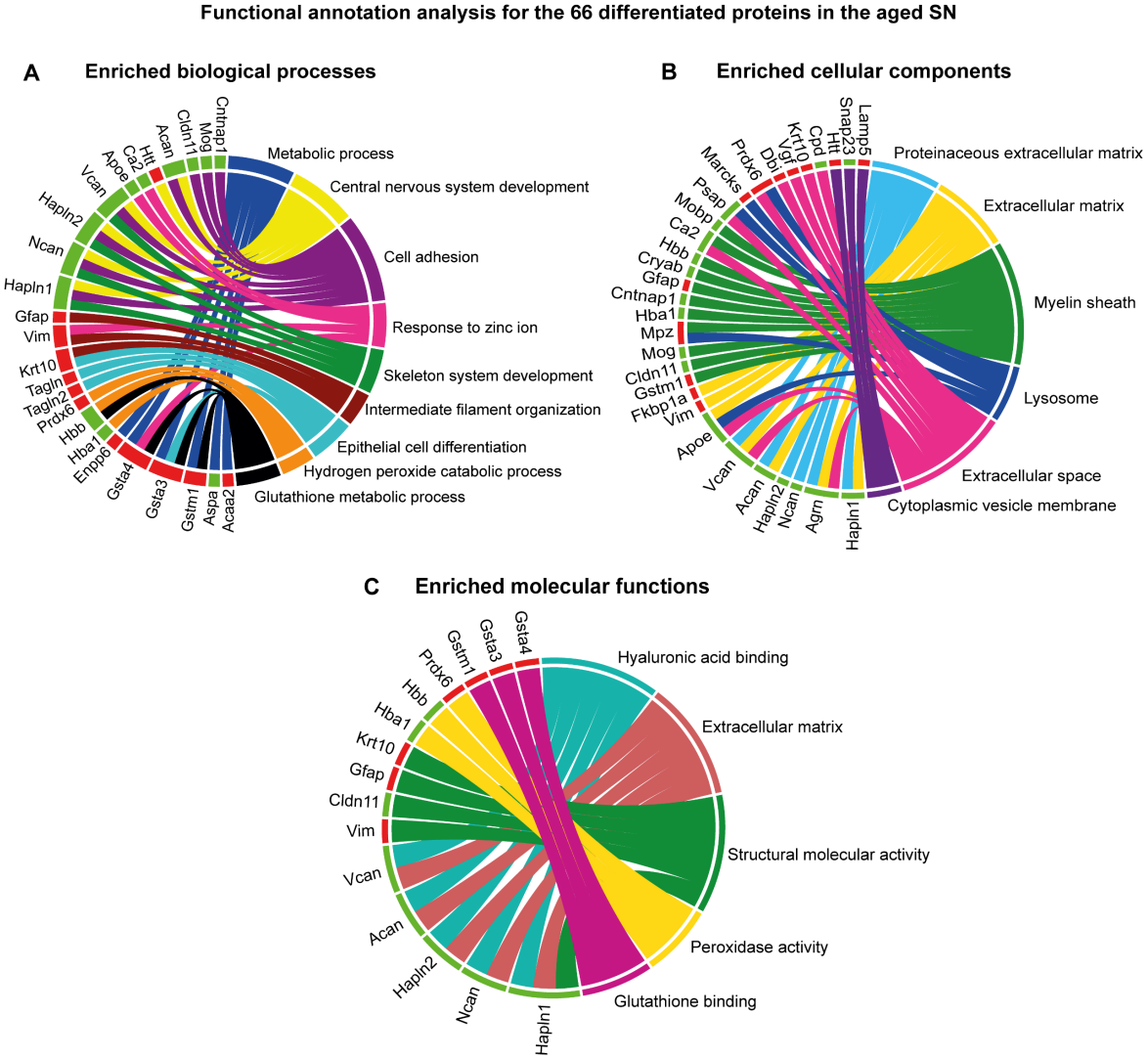

Figure 3.5. Chord diagrams of Functional Annotation analyses (Gene Ontology) of the 66 differentially expressed proteins in the adult SNpc during ageing. DAVID software revealed the enriched terms associated to the 66 proteins dysregulated with ageing, related with **(A)** biological processes, **(B)** cellular components, **(C)** and molecular functions. The right part of each chord diagram represents the terms linked to the differentially expressed proteins (presented with their gene name, see Table 3.1 and 3.2) on the left. Red cells near the protein labels represent proteins whose expression decreases in the old SNpc; while green cells indicate proteins whose expression increases in old animals.

The differentially expressed proteins of each comparison (43 proteins in young *versus* old; 28 proteins in middle age *versus* old) were analysed independently with DAVID software, to gain insights into their biological meaning independently in each comparison. Thus, for the 43 dysregulated proteins in young *versus* old, the most enriched biological processes were 'cell adhesion' and 'central nervous system development', and were both related to upregulated proteins in the old SNpc, including versican core protein (VCAN) or aggrecan core protein (ACAN) (**Figure 3.6A**). 'Myelin sheath' was the most enriched cellular component, associated with dysregulated proteins such as myelin-oligodendrocyte glycoprotein (MOG) or alpha-crystallin B chain (CRYAB), with an increase of their expression in old animals (**Figure 3.6B**). Lastly, 'hyaluronic acid binding' and 'extracellular matrix' were the most enriched molecular functions associated with upregulated proteins in the old SNpc, including versican core protein (VCAN), aggrecan core protein (ACAN) and hyaluronan and proteoglycan link protein 2 (HAPLN2) (**Figure 3.6C**). In the case of the 28 differentially expressed proteins in middle age compared to old, 'metabolic process' and 'glutathione metabolic process' were the more enriched biological processes with almost all their proteins downregulated in the old SNpc, including, for example, glutathione S-transferase alpha-4 (GSTA4) and 3-ketoacyl-CoA thiolase, mitochondrial (ACAA2) (**Figure 3.7A**). 'Intermediate filament organization' and 'cytoplasmic vesicle membrane' were the only terms that appeared enriched in the category of cellular components, and were linked to proteins whose expression was decreased in the old group, such as glial fibrillary acidic protein (GFAP) and huntingtin (HTT) (**Figure 3.7B**). In terms of the molecular function category, the most enriched term was 'protein homodimerization activity', which was associated with proteins whose expression was reduced in the old SNpc, including, for example, glutathione S-transferase alpha-4 (GSTA4) (**Figure 3.7C**). Finally, pathways related to 'glutathione metabolism' and 'metabolism of xenobiotics by cytochrome P45' were enriched with ageing in the rat SNpc, with a reduction of the expression of their related proteins, such as glutathione S-transferase alpha-4 (GSTA4) (**Figure 3.7D**).

In summary, processes related to cell adhesion, extracellular matrix, extracellular space, myelin sheath or glutathione metabolic process are altered in the rat SNpc with ageing. More specifically, the terms that are enriched when the young group is compared to the old age group are associated with proteins whose expression is increased in the old SNpc. On the other hand, the terms that are enriched when the middle age is compared to the old group are linked to proteins whose expression is reduced in the old SNpc.

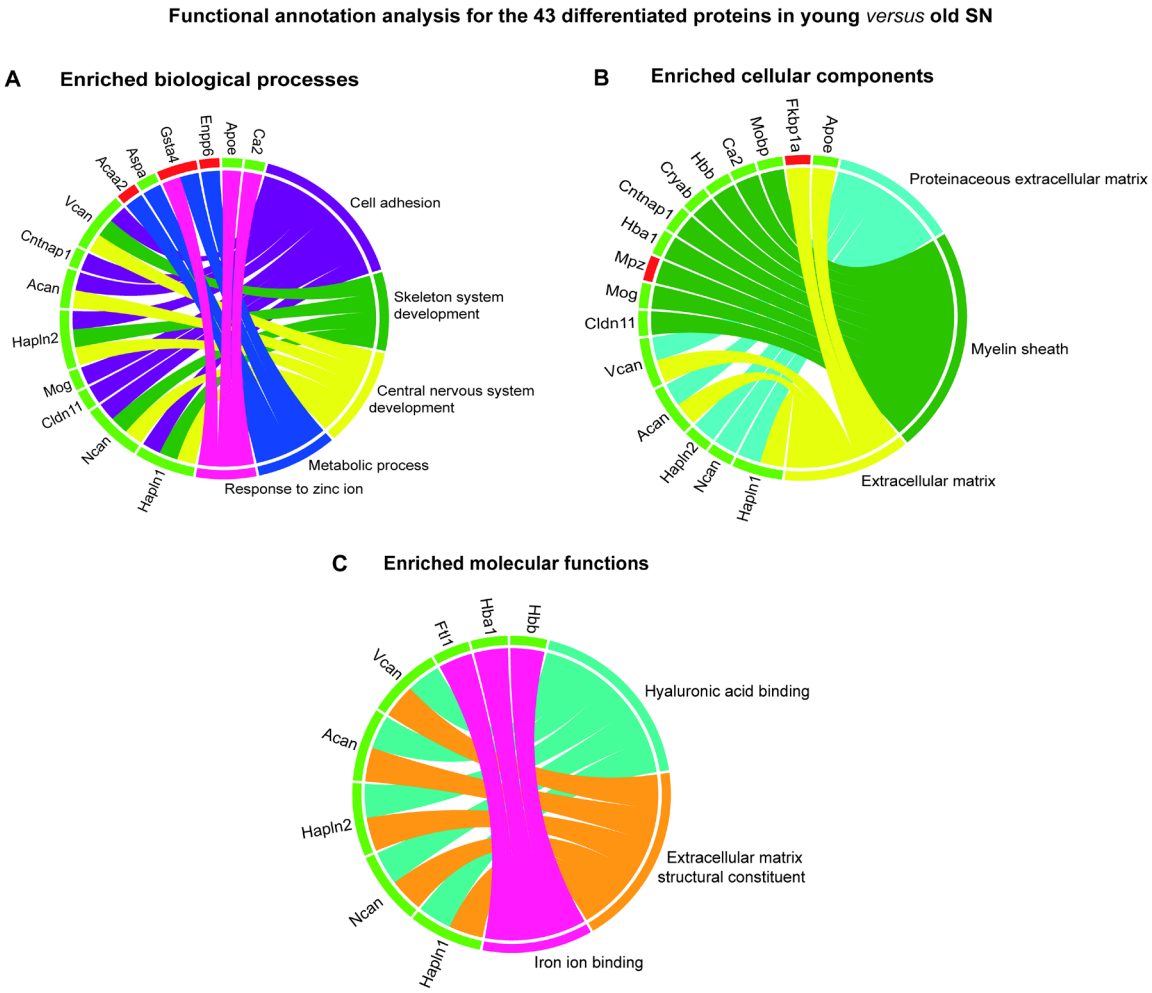

Figure 3.6. Chord diagrams of Functional Annotation analyses (Gene Ontology, GO) of the 43 differentially expressed proteins in the young SNpc compared to old. DAVID software revealed the enriched terms associated to the 43 proteins dysregulated with ageing between young and old animals, related with **(A)** biological processes, **(B)** cellular components, **(C)** and molecular functions. The right part of each chord diagram represents the terms linked to the differentially expressed proteins (presented with their gene name, see Table 3.1 and 3.2) on the left. Red cells near the protein labels represent proteins whose expression decreases in the old SNpc; while green cells indicate proteins whose expression increases in old animals.

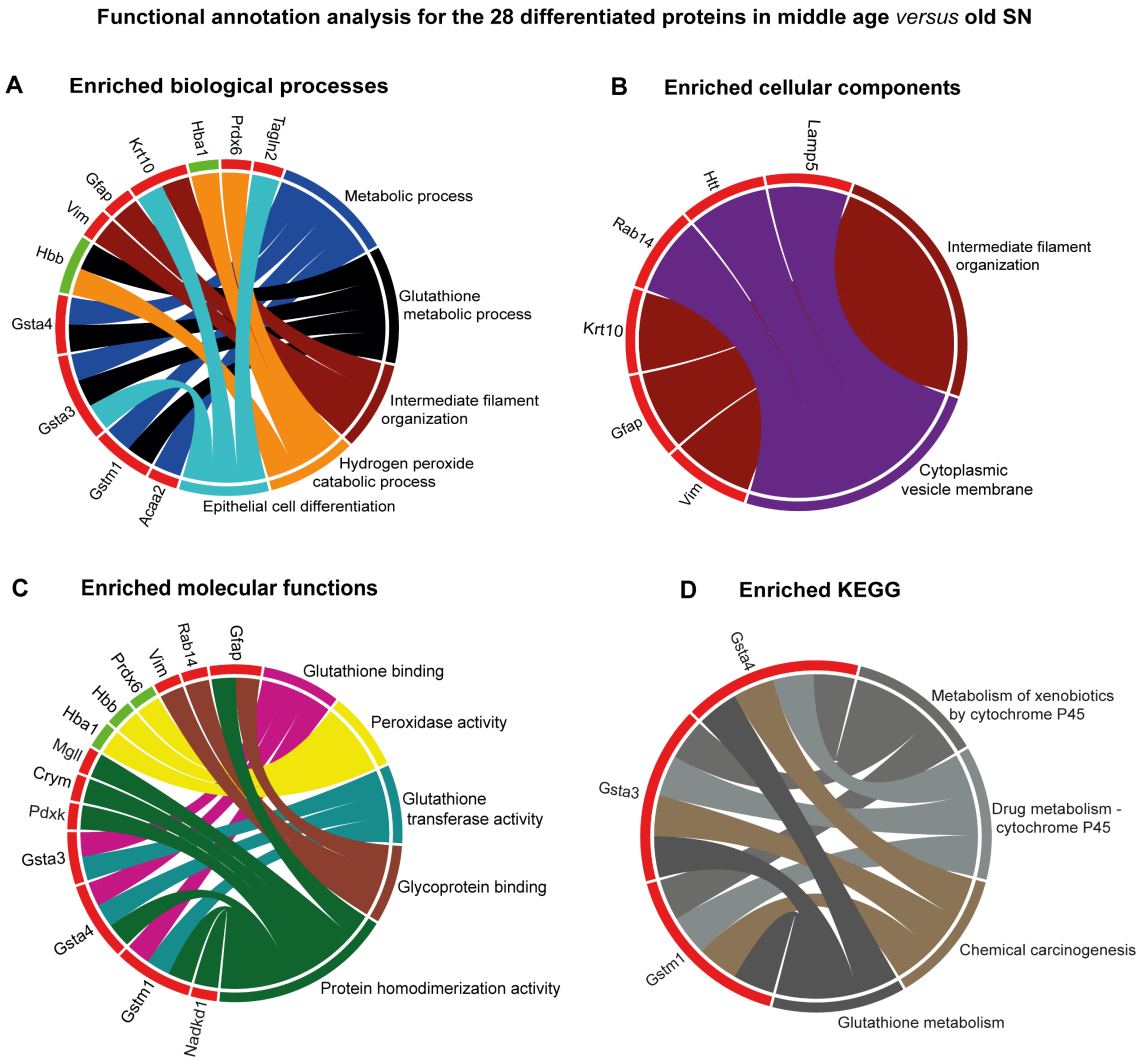

Figure 3.7. Chord diagrams of Functional Annotation analyses (Gene Ontology and KEGG of the 28 differentially expressed proteins in the middle age SNpc *versus* old. DAVID software revealed the enriched terms associated to the 28 proteins dysregulated with ageing, related with **(A)** biological processes, **(B)** cellular components, **(C)** molecular functions, **(D)** and KEGG. The right part of each chord diagram represents the terms linked to the differentially expressed proteins (presented with their gene name, see Table 3.1 and 3.2) on the left. Red cells near the protein labels represent proteins whose expression decreases in the old SNpc; while green cells indicate proteins whose expression increases in old animals.

3.3.3 Reactome pathway analysis showed dysregulation in metabolism, metabolism of proteins and extracellular matrix organization in the aged rat SNpc

Reactome pathway analysis (Fabregat *et al*., 2017; Fabregat *et al*., 2018) of the 66 dysregulated proteins in the old SNpc was conducted to determine which molecular pathways they may be related to. Reactome found 47 out 66 proteins related to 170 pathways that were overrepresented (enriched). In addition, 19 identifiers were either not found or were not mapped to any entity (biological molecule) in Reactome, including proteins that were identified by GO analysis by DAVID. This happened because these entities are not updated as part of a pathway in the Reactome database yet. Some of these 19 missed proteins were glutathione S-transferase alpha-4 (GSTA4), glutathione S-transferase alpha-3 (GSTA3), and glutathione S-transferase mu-1 (GSTM1) associated with the GO term 'glutathione metabolic process'; or glial fibrillary acidic protein (GFAP) and huntingtin (HTT) associated with the GO term 'intermediate filament organization'. The most relevant pathway based on the most statistically significant p-value (in terms of its overrepresentation among the 47 proteins) was 'ECM proteoglycans' (R-RNO-3000178) (**Table 3.3**). This pathway was associated with the following five entities or proteins: versican core protein (VCAN), aggrecan core protein (ACAN), neurocan core protein (NCAN), agrin (AGRN), and hyaluronan and proteoglycan link protein 1 (HAPLN1). Moreover, this 'ECM proteoglycans' (R-RNO-3000178) pathway belongs to the top-level pathway 'extracellular matrix organization' (R-RNO-1474244), which is also enriched in the old SNpc.

These results complement the findings provided by GO analysis by DAVID, where the term 'extracellular matrix' was also enriched. On the other hand, the genome-wide view offered an overview of the overrepresented pathways (Sidiropoulos *et al*., 2017), including other pathways or terms that did not appear in DAVID analysis; such as 'post-translational protein phosphorylation' (R-RNO-8957275), 'chondroitin sulfate/dermatan sulfate metabolism' (R-RNO-1793185), or 'glycosaminoglycan metabolism' (R-RNO-

Table 3.3. 25 most enriched pathways sorted by the most statistically significant p-values, using the 66 differentially expressed proteins in the old SNpc. 'Entities' refers to Uniprot accession numbers, showing the number of entities found in the analysis from the total in that pathway.

Pathway name	Entities	
	found/total	p-value
ECM proteoglycans	5/47	0.00001
Erythrocytes take up carbon dioxide and release oxygen	3/23	0.0004
O2/CO2 exchange in erythrocytes	3/23	0.0004
A tetrasaccharide linker sequence is required for GAG synthesis	3/29	0.0008
Erythrocytes take up oxygen and release carbon dioxide	2/10	0.0018
Dermatan sulfate biosynthesis	2/13	0.0031
Post-translational protein phosphorylation	4/11	0.0054
Chondroitin sulfate/dermatan sulfate metabolism	3/68	0.0093
Regulation of Insulin-like Growth Factor (IGF) transport and uptake by Insulin-like Growth Factor Binding Proteins (IGFBPs)	4/13	0.0102
Chondroitin sulfate biosynthesis	2/25	0.0111
CS/DS degradation	2/26	0.0120
Heparan sulfate/heparin (HS-GAG) metabolism	3/78	0.0135
Glycosaminoglycan metabolism	4/16	0.0200
Extracellular matrix organization	5/30	0.0430
Activation of AMPA receptors	1/7	0.0433
Binding and Uptake of Ligands by Scavenger Receptors	3/12	0.0469
Chylomicron clearance	1/9	0.0554
Calcineurin activates NFAT	1/10	0.0613
Lysosphingolipid and LPA receptors	1/10	0.0613
Caspase-mediated cleavage of cytoskeletal proteins	1/11	0.0673
CLEC7A (Dectin-1) induces NFAT activation	1/12	0.0732
Retinoid metabolism and transport	2/71	0.0747
Glycerophospholipid catabolism	1/13	0.0790
Arachidonate production from DAG	1/13	0.0790
Activation of BAD and translocation to mitochondria	1/14	0.0848

1630316) (**Figure 3.8; Table 3.3**). These pathways complement DAVID results because they are related to the metabolism of the proteins that form the extracellular matrix; such as versican core protein (VCAN) and other proteins such as agrin (AGRN), neurocan core protein (NCAN), apolipoprotein E (APOE) or neurosecretory protein VGF (VGF). Interestingly, the Reactome analysis revealed two new pathways that did not appear with DAVID. These pathways were 'activation of AMPA receptors' (R-RNO-399710), associated with glutamate receptor 2 (GRIA2); and 'binding and Uptake of Ligands by Scavenger Receptors' (R-RNO-2173782), linked to apolipoprotein E (APOE),

haemoglobin subunit alpha 1 (HBA1) and haemoglobin subunit beta (HBB) (**Figure 3.8; Table 3.3**).

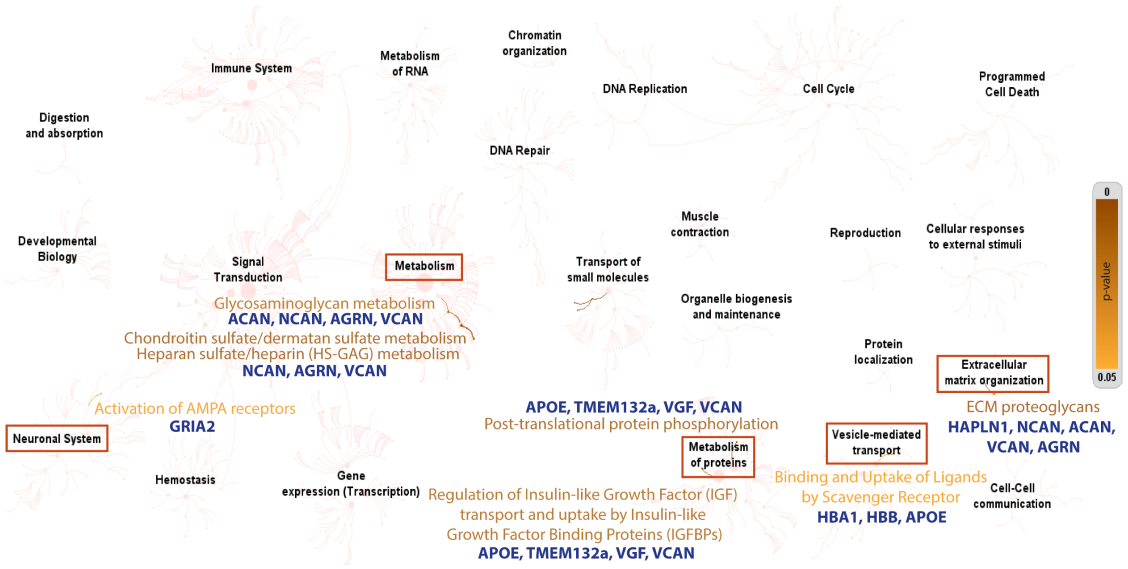

Figure 3.8. Genome-wide overview of the Reactome pathway analysis (Sidiropoulos *et al*., 2017) of the 66 differentially expressed proteins in the old SNpc. Each top-level pathway has a centre from which other pathways of lower hierarchy start. Top-level overexpressed pathways are emphasized with a red rectangle (e.g., 'extracellular matrix organization'), while secondary overexpressed pathways (e.g.,'ECM proteoglycans') linked to them are highlighted using a colour-scale that indicates p-value (right-hand side). Proteins associated to each pathway appear in blue. Light grey pathways are not significantly overrepresented.

3.3.4 GFAP, a protein characteristic of astrocytes, appears as the main connector of many of the dysregulated proteins in the aged SNpc in protein-protein interaction analysis

STRING database (Szklarczyk *et al*., 2019) was performed to identify any known protein-protein interactions among the 66 proteins that were differentially expressed with ageing in the rat. This protein networks analysis identified GFAP, an intermediate filament protein that is a marker for astrocytes (Eng, 1985), as the central or core protein of the network, with the largest number of direct associations (13 in total) with other differentially expressed proteins. GFAP was linked directly or indirectly to other proteins

that were significantly changed in the middle age *versus* old comparison (e.g., agrin (AGRN), vimentin (VIM)), as well as in the young *versus* old comparison (e.g., alpha-crystallin B chain (CRYAB), glutamate receptor 2 (GRIA2), and hyaluronan and proteoglycan link protein 2 (HAPLN2)) (**Figure 3.9; Figure 3.4A-D**). As described above, these proteins are involved in functions that comprise the extracellular matrix, but also cellular adhesion. Therefore, this protein network analysis highlights the possibility that GFAP might be related with these pathways as well. In addition, both comparisons (young *versus* old, middle age *versus* old) were analysed independently by STRING (**Figure 3.10A, B**). This step was taken to understand if differentially expressed proteins whose expression was changed in the same comparison were related or not. As expected, most of the connected proteins appeared to have biological functions or pathways in common. For example, as previously seen, versican core protein (VCAN) was connected to other proteins related to the 'extracellular matrix' term, such as apolipoprotein E (APOE) and aggrecan core protein (ACAN).

3.3.5 GFAP immunostaining increases in the rat SNpc with ageing, and immunoblotting shows extra bands that are different from the canonical isoform

Astrocytes are glial cells in the CNS, taking part, for example, in metabolic and structural functions and, therefore, are essential for the viability of neurons (Yang and Wang, 2015). With this in mind, and as GFAP was a core protein in the network protein analysis above, it was studied further by immunofluorescence and Western blot (see Chapter 2).

First, the immunofluorescence expression of GFAP in the rat SNpc at different ages was measured by O.D., using the TH-positive expression (a marker for DAn) to define the area of the SNpc (**Figure 3.11A**). The results revealed that between the young (0.02781 ± 0.0022), middle age (0.02949 ± 0.0014) and old (0.03267 ± 0.0056) groups, there was

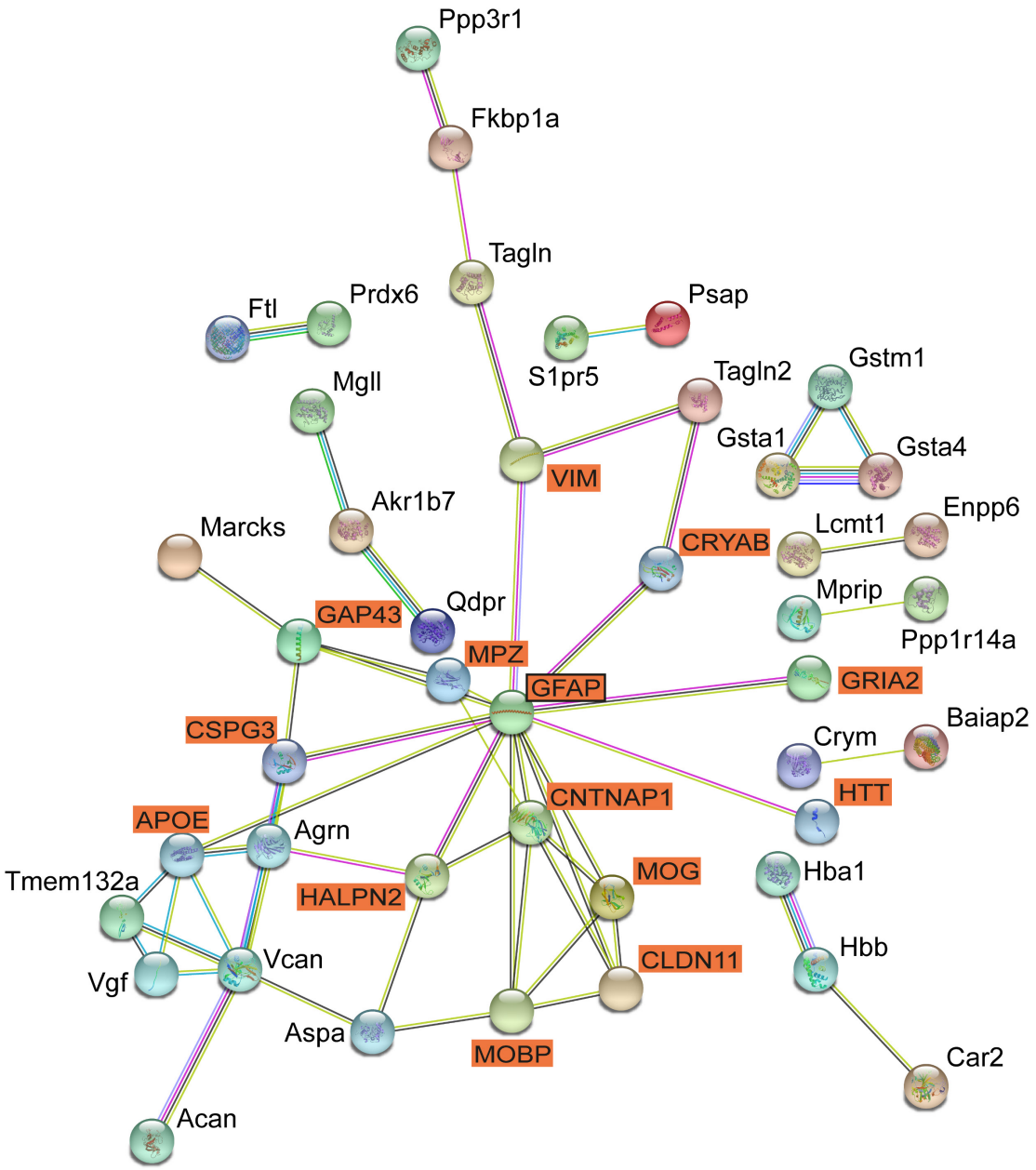

Figure 3.9. Protein network analysis with STRING database of the dysregulated proteins in the rat SNpc with ageing. Protein-protein interactions of the total 66 proteins dysregulated in the SNpc with ageing. In orange boxes with black border, proteins show the larger number of associations; while orange boxes indicate their protein associated. The network displays only proteins with interactions, hiding those proteins that are disconnected. The coloured lines indicate the type of interaction between proteins (light blue, associated in curated database; pink, experimental or biochemical determined; green, gene neighbourhood; black, co-expression; grey, protein homology; lime, co-mentioned in Pubmed abstracts).

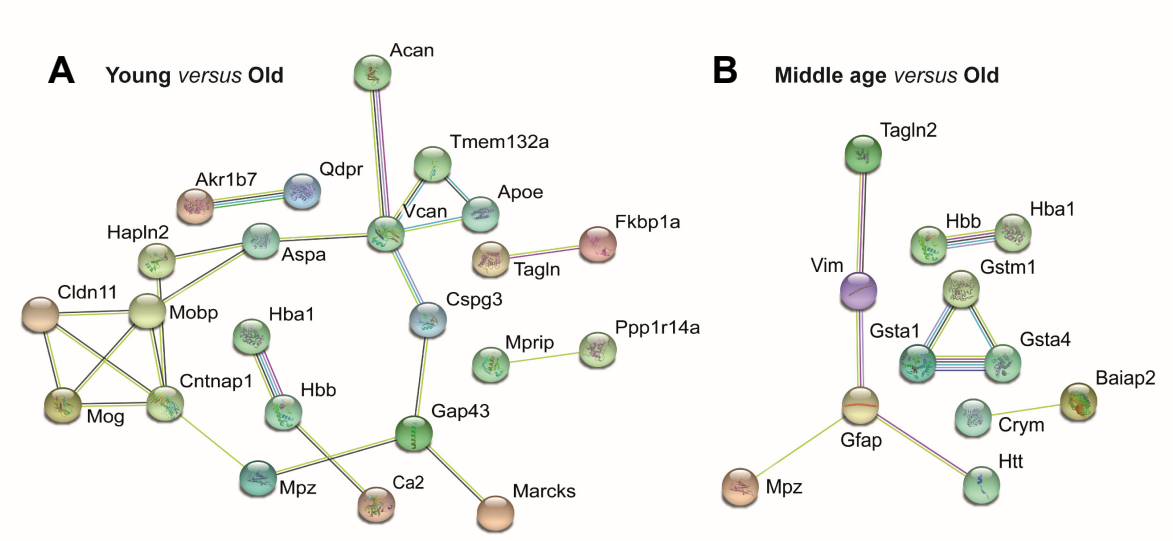

Figure 3.10. Protein network analysis with STRING database of the dysregulated proteins in the rat SNpc with ageing. (A) Protein-protein interactions of the 43 differentially expressed proteins in the young SNpc *versus* old. **(B)** Protein-protein interactions of the 28 differentially expressed proteins in the middle age SNpc *versus* old. The network displays only proteins with interactions, hiding those proteins that are disconnected. The coloured lines indicate the type of interaction between proteins (light blue, associated in curated database; pink, experimental or biochemical determined; green, gene neighbourhood; black, co-expression; grey, protein homology; lime, co-mentioned in Pubmed abstracts).

a statistically significant (p=0.0357) increase of 17% of the O.D. for GFAP between the young and the old group. However, no significant differences were observed between young SNpc and middle age (p=0.6304); or middle age and old (p=0.2086) (**Figure 3.11B**).

The results obtained from the analysis of GFAP by immunofluorescence (increase of GFAP O.D. in the rat SNpc with ageing), surprisingly, did not match the proteomics findings, where the trend of GFAP expression showed an increase from the young to the middle age that decreased again in the old group (**Figure 3.4D**). Consequently, it was not possible to validate the proteomics results by immunofluorescence. Western blotting was performed next to understand more about the protein expression trend of

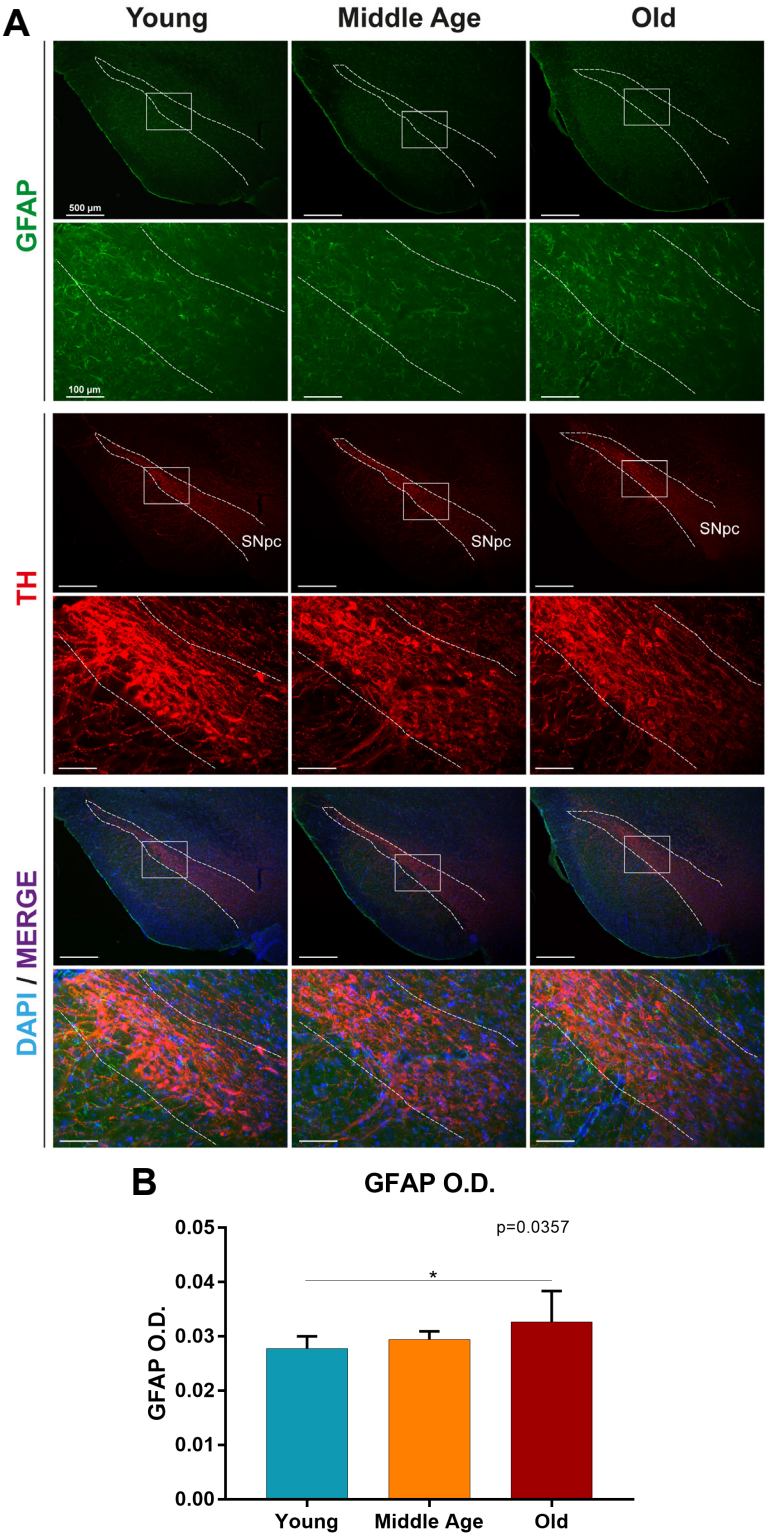

Figure 3.11. The O.D. for GFAP increases in the rat SNpc from the young to the old age. Measurements of the O.D. of GFAP in the SNpc region at different ages in rats. **(A)** Immunofluorescence images for GFAP, TH and DAPI (including merge images) in the young, middle age and old SNpc. TH-positive images were selected in order to indicate the level of the SNpc where measurements of GFAP O.D. were done. **(B)** Quantification of GFAP O.D. showed a statistically significant increase of 17% from young to old samples (p=0.0357). Error bars represent standard deviation. *p<0.05.

GFAP. This was done to determine whether the proteomics results could be verified, but also to comprehend if there was any alteration in the protein (e.g., proteolytic cleavage) not visible in the different methods (i.e., proteomics, immunofluorescence) that could justify the lack of consensus between techniques.

Western blot analysis of the individual samples using a rabbit monoclonal GFAP antibody from Cell Signalling Technology (#12389) showed a main band in all samples at 50kDa, which is the predicted MW for GFAP (**Figure 3.12**). Added to this, some extra bands of lower MW between 48kDa and 37kDa also appeared, being more intense in the old SNpc (**Figure 3.12A**). The measurement of the integrated density of GFAP at 50kDa normalised to the total amount of protein (Coomassie stained gel) revealed that its expression followed a similar trend that the results found by proteomics for GFAP, but they were not statistically significant. Thus, the increase of GFAP between the young (1.226 ± 0.2672) and the middle age (1.719 ± 0.3412) group was not statistically significant ($p=0.0571$); and the decreased of GFAP between the middle age and old (1.342 ± 0.1277) group was not statistically significant either ($p=0.0571$). Moreover, there were no statistically significant differences when GFAP at 50kDA from the young age was compared with the old animals ($p=0.8791$) (**Figure 3.12B**). When all GFAP bands were analysed, from the young (0.634 ± 0.1325) to the old (1.138 ± 0.2615) group there was a statistically significant ($p=0.0221$) increase of 79% of GFAP in the old SNpc, similar to the results found by GFAP immunofluorescence. However, the comparison of GFAP in young (0.634 ± 0.1325) *versus* middle age (0.8972 ± 0.2437), or middle age (0.8972 ± 0.2437) *versus* old (1.138 ± 0.2615), showed that there were no statistically significant differences between them ($p=0.3382$; $p=0.3659$, respectively) (**Figure 3.12C**). Similarly, when the band for GFAP at 48kDa was measured and normalized with the total amount of protein, the integrated density for GFAP in young (0.1662 ± 0.07953) compared to the old (1.184 ± 0.3263) showed a statistically significant ($p=0.0452$) increase of 612% with ageing. On the other hand, when GFAP at 48kDa was compared

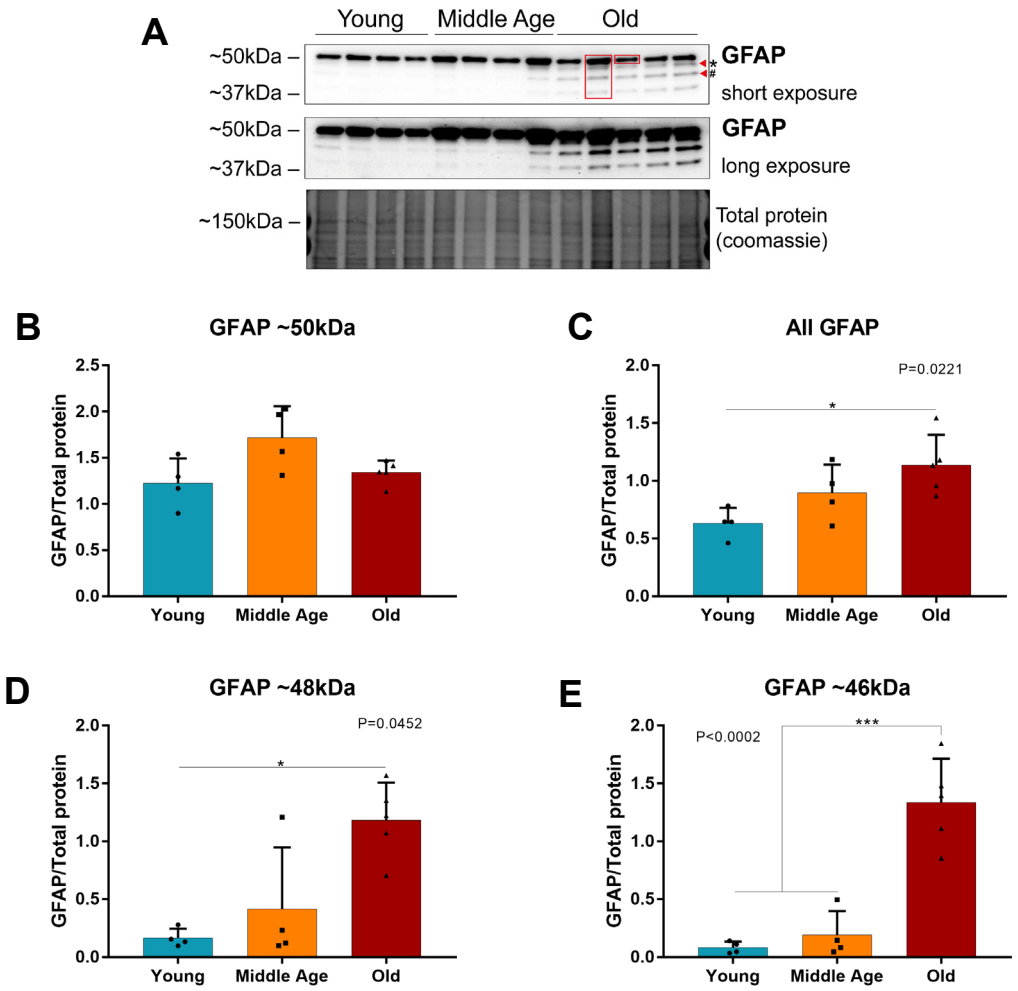

Figure 3.12. Western blot analysis of GFAP expression in the SNpc during ageing in rats. (A) Immunoblots showing the expression levels of GFAP in the SNpc of young (*n=4*), middle age (*n=4*) and old (*n=5*) rats, using a rabbit monoclonal GFAP antibody from Cell Signalling Technology (#12389). A main band at 50kDa was detected in all ages, together with some extra bands of lower MW between 48kDa and 37kDa that were more intense in the old SNpc samples. Coomassie stained gel shows the total amount of protein in each sample used to normalise the integrated density of measured GFAP. **(B)** Measurements of GFAP at 50kDa (small red rectangle in (A)) showed the same trend than in the proteomics results for GFAP but without being statistically significant in the increase from young to middle age (p=0.0571), or a decrease from middle age to old (p=0.1398). **(C)** Measurements of all GFAP bands (big red rectangle in (A)) revealed a statistically significant increase of 79% between the young and old samples (p=0.0221). **(D)** Measurements of GFAP at 48kDa (red arrow and * in (A)) revealed a statistically significant increase of 672% between the young and old samples (p=0.0452). **(E)** Measurements of GFAP at 46kDa (red arrow and # in (A)) revealed a statistically significant increase of 595% and 1512%, respectively, between young and old samples (p<0.0001), as well as the middle age and old (p<0.0002) group. Error bars represent standard deviation. *p<0.05; ***p<0.0001.

between the young (0.1662 ± 0.07953) and the middle age (0.416 ± 0.5322) group, as well as the middle age *versus* the old (1.184 ± 0.3263) SNpc, there were no statistically significant differences in any of these comparisons (p>0.9999; p=0.1217, respectively) (**Figure 3.12D**). Lastly, the integrated density for GFAP at 46kDa in the young (0.083 ± 0.05088) and middle age (0.1924 ± 0.2061) compared to the old (1.338 ± 0.3764) group increased significantly with ageing (p<0.0001; p<0.0002, respectively) by 595% and 1,512%, respectively, despite the lack of statistically significant differences (p=0.9217) between the young (0.083 ± 0.05088) and the middle age (0.1924 ± 0.2061) SNpc (**Figure 3.12E**).

To ensure that the extra bands were not detected because of a cross-reaction of the Cell Signalling Technology GFAP antibody, another GFAP antibody was tested. Thus, Western blot analysis with the same individual samples were performed using a mouse monoclonal GFAP antibody from Biolegend (#644701) (**Figure 3.13**). The results revealed also a main band in all ages at 50kDa, and the additional bands of lower MW between 48kDa and 37kDa with a higher intensity in the old SNpc (**Figure 3.13A**). Similar to the first GFAP antibody results, the analysis of the integrated density of GFAP 50kDa normalised with the total amount of protein (Coomassie stained gel) showed a similar expression of GFAP than the proteomics results for GFAP, but without being statistically significant. Hence, no statistically significant differences were found in the increase of GFAP from young (2.185 ± 0.4607) to middle age (3.092 ± 0.4711) (p=0.1562), and in the decrease of GFAP from middle age to old (2.23 ± 0.6276) (p=0.2218), or when the young and the old samples were compared (p=0.9993) (**Figure 3.13B**). Measurements of all GFAP bands between the young (1.482 ± 0.2892), middle age (1.963 ± 0.2613) and old (2.027 ± 0.2881) samples showed the same trend as the previous antibody with an increase of GFAP with ageing. However, these results were not statistically significant in any of the comparisons (i.e., young *versus* old (p=0.1119), middle age *versus* old (p=0.9908); or young *versus* middle age (p=0.1691)) (**Figure 3.13C**).

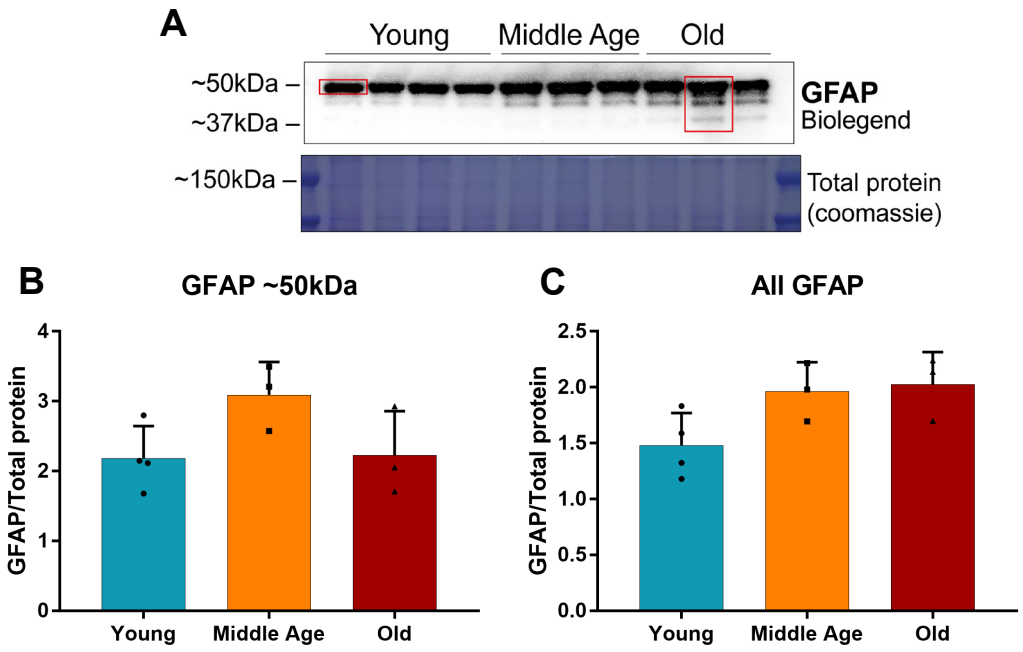

Figure 3.13. Western blot analysis of GFAP expression in the SNpc during ageing in rats with a different GFAP antibody. (A) Immunoblot showing the expression levels of GFAP in the SNpc of young (*n=4*), middle age (*n=3*) and old rats (*n=3*), using a mouse monoclonal GFAP antibody from Biolegend (#644701). Similar to Figure 3.12A, a main band at 50kDa was detected in all samples, together with some extra bands of lower MW between 48kDa and 37kDa that were more intense in the old SNpc samples. Coomassie stained gel shows the total amount of protein in each sample used to normalise the integrated density of measured GFAP. **(B)** Measurements of GFAP at 50kDa (small red rectangle in (A)) showed the same trend that was seen in the proteomics results for GFAP but without being statistically significant in the either the increase from young to middle age (p=0.1562), or decrease from middle age to (p=0.2218). **(C)** Measurements of all GFAP bands (big red rectangle in (A)) revealed a similar trend than Figure 3.12C, but in this case the increase between the young and the middle age or old SNpc was not statistically significant (p=0.1691; p=0.1119, respectively). Coomassie stained gel shows the total amount of protein in each sample. Error bars represent standard deviation.

The detection of extra bands of lower MW generated two questions: a) what is happening to GFAP in the SNpc of old animals to produce these extra bands by Western blot (i.e., are these extra bands different isoforms produced by alternative splicing or breakdown

products from degradation or cleavage by proteolysis?)?, and b) did ProteinPilot software identify and quantify only the sequence from GFAP at 50kDa (top band) or identify and quantify the sequences from the extra bands within the proteomics analysis?

As mentioned before, GFAP is an intermediate filament of astrocytes (Eng, 1985). In general, most of the articles that have cited GFAP were focused on the main isoform called GFAPα (i.e., isoform 1), which is the most abundant isoform in the brain and whose mRNA was the first identified (Middeldorp and Hol, 2011). Lewis *et al*. (1984) were the first authors to generate the sequence of a cDNA clone for mouse GFAP, by screening a cDNA expression library created from 15-21-day-old mouse brain mRNA with a GFAP-polyclonal antiserum. After this, cDNA clones were produced from cerebral hemispheres of rats (Feinstein *et al*., 1992), glioblastoma-derived cell line HTB17 and adult brain white matter of humans (Reeves *et al*., 1989). These studies characterized the nucleotide sequence for the three species of animals used, and predicted that the protein length of GFAP is 432 aa in humans and 430 aa in rats and mouse, with a MW of approximately ~50kDa. Thus, the top band at ~50kDa found for GFAP in the rat SNpc in this Thesis would correspond to the main or canonical isoform GFAPα (i.e., isoform 1). As described in detail below and in the Discussion, the existence of other extra bands between 48kDa and 37kDa has been already described in other GFAP sequencing and immunoblotting analysis, as an indication of GFAP isoforms or breakdown products from the proteolysis of GFAP. In this Result section, firstly, the possibility of defining these extra bands as GFAP isoforms is addressed, followed by the feasibility of finding these extra bands as breakdown products from degradation or cleavage by proteolysis.

3.3.6 The expression of the GFAPδ isoform in the rat SNpc increases significantly in middle age compare to young and old ages

To determine if the extra bands from the GFAP immunoblot in Thesis belonged to other GFAP isoforms (**Figure 3.12A**), the first step was to review the literature to understand which isoforms might match their MW (between 48kDa and 37kDa) (see **Figure 3.14**).

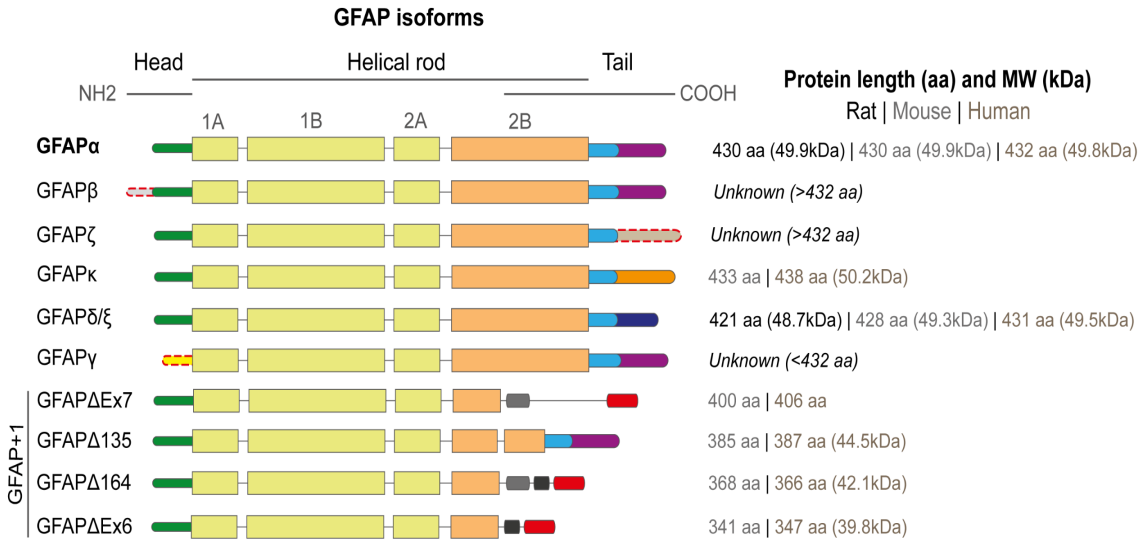

Figure 3.14. The modification of the sequence of the canonical isoform for GFAP produces different isoforms. GFAP is an intermediate filament protein considered a marker for astrocytes, a type of glia cell (Eng, 1985). As the diagram shows, the canonical isoform for GFAP, called GFAPα (isoform1), has a MW of approximately 50kDa and its structure is formed by 3 domains (head, α-helical rod and tail). The head domain contains the exon 1. The rod domain is divided in 4 subregions [1A (exon 2), 1B (exon 3), 2A (exon 4), 2B (exons 5 and 6)], separated by linker regions (black lines). The tail domain contains exons 7 to 9. Apart from GFAPα, nine more isoforms have been described, presented in the diagram below GFAPα with their respective modifications. GFAPβ includes a longer 5' region before exon 1. GFAPβ protein length is unknown (red dash line), existing only evidence of the partial mRNA sequence in rat (Condorelli *et al.*, 1999a; Condorelli *et al.*, 1999b). GFAPζ includes the last 284 bp of intron 8-9. GFAPζ protein length is also unknown (red dash line), existing only partial evidence at transcript level in mouse (Zelenika *et al.*, 1995; Kamphuis *et al.*, 2012). GFAPκ has an alternative exon 7b that replaces exon 8 and 9 (Blechingberg *et al.*, 2007; Kamphuis *et al.*, 2012; Kamphuis *et al.*, 2014; Hol and Pekny 2015). GFAPδ/ε (isoform 2) has an alternative exon 7a that replaces exon 8 and 9 (Condorelli *et al.*, 1999a; Condorelli *et al.*, 1999b; Roelofs *et al.*, 2005). Differences between GFAPδ and GFAPε are controversial in the literature due to their similar open reading frames (ORF), although Blechingberg and colleagues (2007) establish that, unlike GFAPδ, GFAPε is polyadenylated in exon 7a. GFAPγ excludes exon 1 but adds the last 126 bp of intron 1. GFAPγ protein length is also unknown (red dash line), existing only partial evidence at transcript level in mouse (Zelenika *et al.*, 1995). GFAP+1 (GFAPΔEx7, GFAPΔ135, GFAPΔ164, GFAPΔEx6) undergoes different frameshift mutations in exon 6 and 7 (Kamphuis *et al.*, 2012; (*cont. next page*)

(*cont. Figure 3.14*) Kamphuis *et al.*, 2014; Hol and Pekny 2015). Only the known (e.g., published or database) protein length (aa) and MW (kDa) for each isoform in rat (black), mouse (light grey) and/or human (dark grey) are shown. Notice again that the exact protein length and MW in some of the proteins remain unknown.

According to the literature (**Figure 3.14**), there are two different isoforms (i.e., GFAPβ, GFAPζ) whose MW is unknown but whose protein length (aa) is bigger than the canonical isoforms GFAPα, suggesting that their MW, although unknown, had to be higher than 50kDa. There is also evidence of GFAPκ which has an alternative exon 7b that replaces exon 8 and 9, with a final MW of 50.2kDA in humans. Hence, these three isoforms (i.e., GFAPβ, GFAPζ, GFAPκ) were excluded as possible candidates for the detected extra bands, as they were all lower than 50kDa. Nevertheless, there were other isoforms (i.e., GFAPδ/ε, GFAPγ, GFAP+1 – GFAPΔEx7, GFAPΔ135, GFAPΔ164, GFAPΔEx6 –) with smaller protein length (aa) than GFAPα and, therefore, with MW below 50kDa. Thus, GFAPδ/ε (isoform 2) has a final MW of 48.7kDa in rats, and, although the final protein length for GFAPγ is unknown (existing only as partial evidence at the transcript level in mouse), because it has less aa than the canonical isoforms GFAPα, it is assumed that its MW is lower than 50kDa. Lastly, GFAP+1, which includes GFAPΔEx7, GFAPΔ135, GFAPΔ164, and GFAPΔEx6, has a MW between 39kDa and 44kDa in humans. Thus, the isoforms GFAPδ/ε, GFAPγ, GFAP+1 – GFAPΔEx7, GFAPΔ135, GFAPΔ164, GFAPΔEx6 – were considered as possible candidates for the extra bands detected between 48kDa and 37kDa (**Figure 3.12**).

The review of the literature related to GFAP isoforms led to the question of if the ProteinPilot software identified exclusively GFAPα (isoform 1), the main isoform with a MW of ~50kDa, or if it was possible that it also recognized the other isoform GFAPδ (isoform 2). This GFAPδ isoform was chosen between the possible candidates because it was the only one with a completed published sequence in rats, which made it possible

to use it to perform a multiple sequence alignment (**Figure 3.15**). Therefore, the multiple sequence alignment of the FAST sequence of rat GFAPα and GFAPδ from UniProtKB (accession numbers P47819-1 and P47819-2, respectively) was performed and this alignment was compared to the protein sequence coverage detected for GFAP by the iTRAQ experiment (**Figure 3.15**). This comparison demonstrated that the peptides identified in the iTRAQ experiment matched almost entirely to the isoform alpha and also the homologous regions in GFAPδ. Moreover, the alignment revealed that the head and the tail of GFAPα, modified in other isoforms like GFAPδ (**Figure 3.14**), were detected by the proteomics analysis (**Figure 3.15**).

```
GFAP alpha      MERRRITSARRSYASSETMVRGHGPTRHLGTIPRLSLSRMTPPLPARVDFSLAGALNAGF 60
GFAP delta      MERRRITSARRSYASSETMVRGHGPTRHLGTIPRLSLSRMTPPLPARVDFSLAGALNAGF 60
                ************************************************************

GFAP alpha      KETRASERAEMMELNDRFASYIEKVRFLEQQNKALAAELNQLRAKEPTKLADVYQAELRE 120
GFAP delta      KETRASERAEMMELNDRFASYIEKVRFLEQQNKALAAELNQLRAKEPTKLADVYQAELRE 120
                ************************************************************

GFAP alpha      LRLRLDQLTTNSARLEVERDNLTQDLGTLRQKLQDETNLRLEAENNLAVYRQEADEATLA 180
GFAP delta      LRLRLDQLTTNSARLEVERDNLTQDLGTLRQKLQDETNLRLEAENNLAVYRQEADEATLA 180
                ************************************************************

GFAP alpha      RVDLERKVESLEEEIQFLRKIHEEEVRELQEQLAQQQVHVEMDVAKPDLTAALREIRTQY 240
GFAP delta      RVDLERKVESLEEEIQFLRKIHEEEVRELQEQLAQQQVHVEMDVAKPDLTAALREIRTQY 240
                ************************************************************

GFAP alpha      EAVATSNMQETEEWYRSKFADLTDVASRNAELLRQAKHEANDYRRQLQALTCDLESLRGT 300
GFAP delta      EAVATSNMQETEEWYRSKFADLTDVASRNAELLRQAKHEANDYRRQLQALTCDLESLRGT 300
                ************************************************************

GFAP alpha      NESLERQMREQEERHARESASYQEALARLEEEGQSLKEEMARHLQEYQDLLNVKLALDIE 360
GFAP delta      NESLERQMREQEERHARESASYQEALARLEEEGQSLKEEMARHLQEYQDLLNVKLALDIE 360
                ************************************************************

GFAP alpha      IATYRKLLEGEENRITIPVQTFSNLQIRETSLDTKSVSE---GHLKRNIVVKTVEMRDGE 417
GFAP delta      IATYRKLLEGEENRITIPVQTFSNLQIRGGKSTKEGEGHKVTRHLKRLT-IQVIPIQALA 419
                ****************************  .  .:. ..    ****   ::.: ::

GFAP alpha      VIKESKQEHKDVM     430
GFAP delta      RL----------      421
                 :
```

Figure 3.15. Multiple sequence alignment of rat GFAPα (isoform 1) and GFAPδ (isoform 2). The alignment of rat GFAPα and GFAPδ sequences, using Clustal Omega multiple sequence alignment (MSA) tool, shows that the peptides identified in the iTRAQ experiment for GFAP (highlighted in grey) correspond to the isoform alpha. Notice that GFAPδ differs from the canonical sequence of GFAPα between the last 389 and 430 aa.

Altogether, this indicated that ProteinPilot identified the canonical isoform of GFAPα, based on the peptides that were specific only for that isoform (i.e., head and tail). However, the alignment results revealed that was not possible to exclude the presence of GFAPδ, even though specific peptides were not found, because of the identified homologous regions. Due to this uncertainty, the expression pattern of GFAPδ was examined in the aged rat SNpc samples by immunoblotting, to determine whether it was possible or not to observe the expression of this isoform that may help to explain the extra bands that were previously detected.

The analysis of GFAPδ of the individual samples by Western blot using a rabbit polyclonal antibody specific for GFAPδ from Abcam (#93251). showed a band at approximately 50kDa in all ages that was more intense in the middle age group, but no extra bands between 48kDa and 37kDa (**Figure 3.16A**). Measurements of the integrated density of GFAPδ, normalised with the total amount of protein (Coomassie stained gel), revealed that comparing the middle age (2.141 ± 0.3445) *versus* the young (0.7601 ± 0.1823), and old (1.091 ± 0.2393) age there were changes in the expression of GFAPδ, with a statistically significant (p=0.0002) increase of 182% from young to middle age, and a statistically significant (p=0.0008) decrease of 49% from middle age to old (**Figure 3.16B**).

Importantly, these Western blot results demonstrated that, even though the proteomics study did not identify any peptide specifically for the isoform GFAPδ, the rat SNpc contains this alternative isoform. Notably, to my understanding, this is the first time that a specific GFAP isoform (GFAPδ) has been detected and expression levels measured within the SNpc, showing that its expression changes along ageing. This finding could have important implications in the phenotype and functions of astrocytes and, therefore, in the vulnerability of DAn (see Discussion). Moreover, the immunoblotting band at 50kDa of this GFAPδ isoform did not explain the rest of the bands between 48kDa and 37kDa, which makes the investigation of other isoforms essential to determine whether

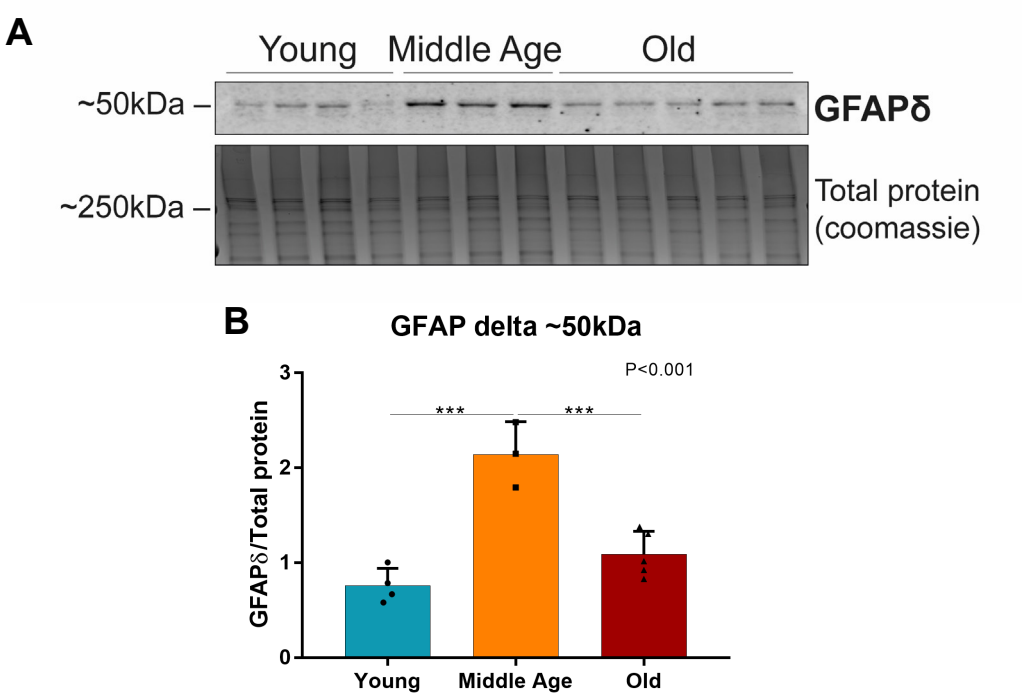

Figure 3.16. Western blot analysis of GFAPδ expression in the SNpc during ageing in rats. (A) Immunoblot showing the expression levels of GFAPδ in the SNpc of young (*n=4*), middle age (*n=3*) and old rats (*n=5*), using a rabbit polyclonal GFAPδ antibody from Abcam (#93251). **(B)** Measurements of the integrated density of GFAPδ at 50kDa, normalised to total protein (Coomassie stained gel), showed a statistically significant increase of 182% in the middle age samples compared to young (p=0.0002) and a statistically significant decrease of 49% from middle age to old samples (p=0.0008). Error bars represent standard deviation. ***p<0.001.

the extra bands belong to them. Finally, the trend of expression for GFAPδ revealed that there was an increase in the rat SNpc during middle age compared to the young and the old age, while the expression in the young and old age was similar. This trend was comparable to the trend found previously for GFAPα at 50kDa (**Figure 3.12B**), which might indicate that GFAPδ has a contribution to the band at 50kDa in the GFAPα immunoblotting. Why this increase in the GFAPδ expression appeared in the SNpc from the middle group is something that will be discussed in the Discussion section.

To gain a better idea about where GFAPδ was expressed within the SNpc, assuming to find it in astrocyte-like cells, immunofluorescence for GFAPδ in the rat SNpc at different ages (similar to **Figure 3.11**) was also performed. However, the staining was very faint and difficult to observe (images not shown), therefore, it was not possible to establish any conclusion from these results.

Due to the identification of an isoform by Western blot (i.e., GFAPδ) that was not recognized by the proteomics study, as well as the lack of verification of the extra bands as part of GFAPδ, immunoblotting was organised to identify other possible candidates for which suitable antibodies were available. The aim of such an analysis was to understand if other isoforms, apart from GFAPα and GFAPδ, were also expressed in the rat SNpc during the ageing process. However, it was not possible to find any antibody available for rat GFAPγ, and the immunoblot for GFAP+1, using a human antibody generated and kindly provided by the group from the Netherlands led by Dr. EM Hol, did not show any bands when the SNpc samples at different ages were analysed (immunoblot not shown).

3.3.7 The low MW extra bands found in the immunoblotting for GFAP might be related to the production of GFAP breakdown products after its proteolysis by the enzyme calpain

The first requirement to understand if the alternative hypothesis, related to the enzymatic degradation of GFAP with the generation of breakdown products, could explain the extra bands between 48kDa and 37kDa in the GFAP immunoblots, was to gain a deeper understanding of the literature around this topic. As **Figure 3.17** details, the proteolysis of GFAP (assumed, in this case, as GFAPα) by calpain or caspase produces breakdown products that could be detected in immunoblots. Calpain cuts GFAPα around its head (69–70 aa) and tail (386–384 aa), generating breakdown products with MW between 44kDa and 38kDa (Fujita *et al*., 1998; Lee *et al*., 2000; Zhang *et al*., 2014) (**Figure 3.17**).

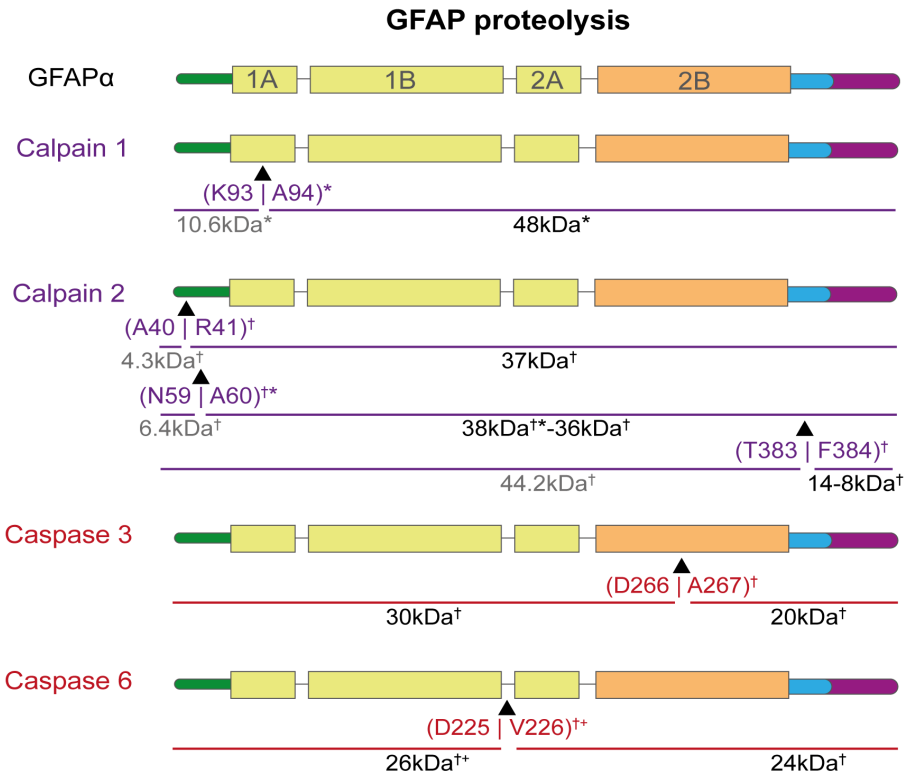

Figure 3.17. GFAPα undergoes proteolytic digestion with calpain and caspase at different cleavage sites, producing various breakdown products of diverse MW. Diagram of the GFAPα fragmentation generating breakdown products of different MW (kDa). MW in black show the specific experimental fragments of GFAPα from rat (*), mouse (+), or human (†) origin found in the literature using calpain 1 (Lee *et al*., 2000), calpain 2 (Fujita *et al*., 1998; Zhang *et al*., 2014), caspase 3 (Mouser *et al*., 2006) or caspase 6 (Chen *et al*., 2013a). The MW of other breakdown products that were not mentioned in the literature (MW in grey) were calculated with the use of the 'Protein Molecular Weight' tool, using the part of the GFAPα sequence (rat or human) that was left before the cleavage site, without considering post-translational modifications (e.g., phosphorylation), which could increase the final MW of the fragment.

Thus, the MW of these breakdown products would have the same size that the extra lower MW bands found in the immunoblot for GFAP in this Thesis. To fully understand the implications that the effect of calpain has in GFAPα and the possible MW of breakdown products, the unknown MW was calculated using a 'Protein Molecular Weight' tool and the GFAPα sequences (rat or human) that were left before the cleavage site, without considering post-translational modifications (e.g., phosphorylation), which

could increase the final MW of the fragment. With this method, potential breakdown products of approximately 42kDa, 11kDa, 6kDa and 4kDa were calculated (**Figure 3.17**). At least one of these new breakdown products (42kDa) would have the same size that the extra bands found in the immunoblot for GFAP in this Thesis. On the other hand, caspase cuts GFAPα around the core of the protein, around 78–79 aa and 266–267 aa, producing smaller breakdown products with MW between 30kDa and 20kDa (Mouser *et al*., 2006; Chen *et al*., 2013a) (**Figure 3.17**). In this case, the MW of these breakdown products would be too small to explain any of the extra bands found in the immunoblot for GFAP in this Thesis, although that does not invalidate the presence of caspase in the SNpc samples and the production of GFAP breakdown products of low MW that, perhaps, have not been detected by immunoblot.

The literature showed that calpain is an enzyme that was able to produce GFAP breakdown products with a MW between 44kDa and 38kDa, similar to the MW of the extra bands found in the GFAP immunoblot. On the other hand, caspase can also cleavage GFAP generating breakdown products of low MW that might not have been detected in the GFAP immunoblot. Therefore, the possibility of characterizing the extra bands as GFAP breakdown products was explored. To do this, the first step was to corroborate the existence of the proteolytic enzymes (i.e., caspase and calpain) in the SNpc samples. To achieve that, proteomics results were analyzed to detect the presence or absence of calpain and caspase. The evaluation of the data showed that calpain-2 (CAPN2), calpain-1 (CAPN1), calpain small subunit 1 (CAPNS1) and caspase-3 (CASP3) were presented in the samples (**Supplementary Table 2b**). Because calpain-2 seems to be the most abundant calpain in brain (Singh *et al*., 2014) and it is expressed in astrocytes (Li et *al.*, 1995; Li *et al*., 1996), this enzyme was quantified by Western blot, although the proteomics data did not show any significant difference in its expression between ages (**Supplementary Table 2b**; **Figure 3.18**).

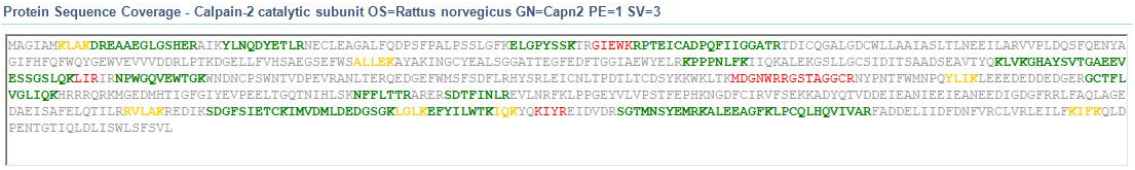

Figure 3.18. Protein Sequence Coverage for calpain-2 by ProteinPilot software. The areas in grey represent portions of the sequence with no spectral evidence. Low confidence peptides are red, moderate confidence peptides are yellow and high confidence peptides are green.

The decision of exploring calpain-2 despite the lack of significant differences in its expression was taken because the activity of calpain-2 may not necessarily be accompanied by increased expression. Whilst it is not possible to directly measure activity by Western blot, it might, however, be possible to detected activated calpain 2 that would be evidenced by a proteolytically cleaved protein product with a shorter length and smaller MW (Brown and Crawford, 1993; Azuma *et al*., 1997; Chou *et al*., 2011). Consequently, this reduction of its sequences may be detected by Western blot but not by iTRAQ quantifications (see Discussion). Hence, Western blot analysis of the individual samples using a mouse monoclonal calpain-2 antibody from Santa Cruz (#373966) revealed a strong band at 78kDa, but also a faint band at approximately 43kDa in all samples (**Figure 3.19A**). The quantification of the calpain-2 band at 78kDa, normalised to total protein (Coomassie stained gel), showed that comparing young (3.273 ± 0.39), middle age (2.97 ± 0.274) and old (3.274 ± 0.5439) samples there were no statistically significant differences between any of the comparisons, including young *versus* middle age (p=0.6240) or old (p>0.9999) (**Figure 3.19B**). Similarly, the quantification of the calpain-2 band at 43kDa, normalised to total protein (Coomassie stained gel), revealed that its expression in young (1.185 ± 0.225), middle age (1.122 ± 0.075) and old (1.633 ± 0.316) did not change significantly between young and middle age (p=0.9318) or old (p=0.0828) (**Figure 3.19C**). Nevertheless, all this indicated that there is not enough evidence to assume that the extra band belongs to the calpain-2

breakdown products due to its proteolysis during activation, therefore, it is difficult to establish if calpain-2 is activated or not in the SNpc samples.

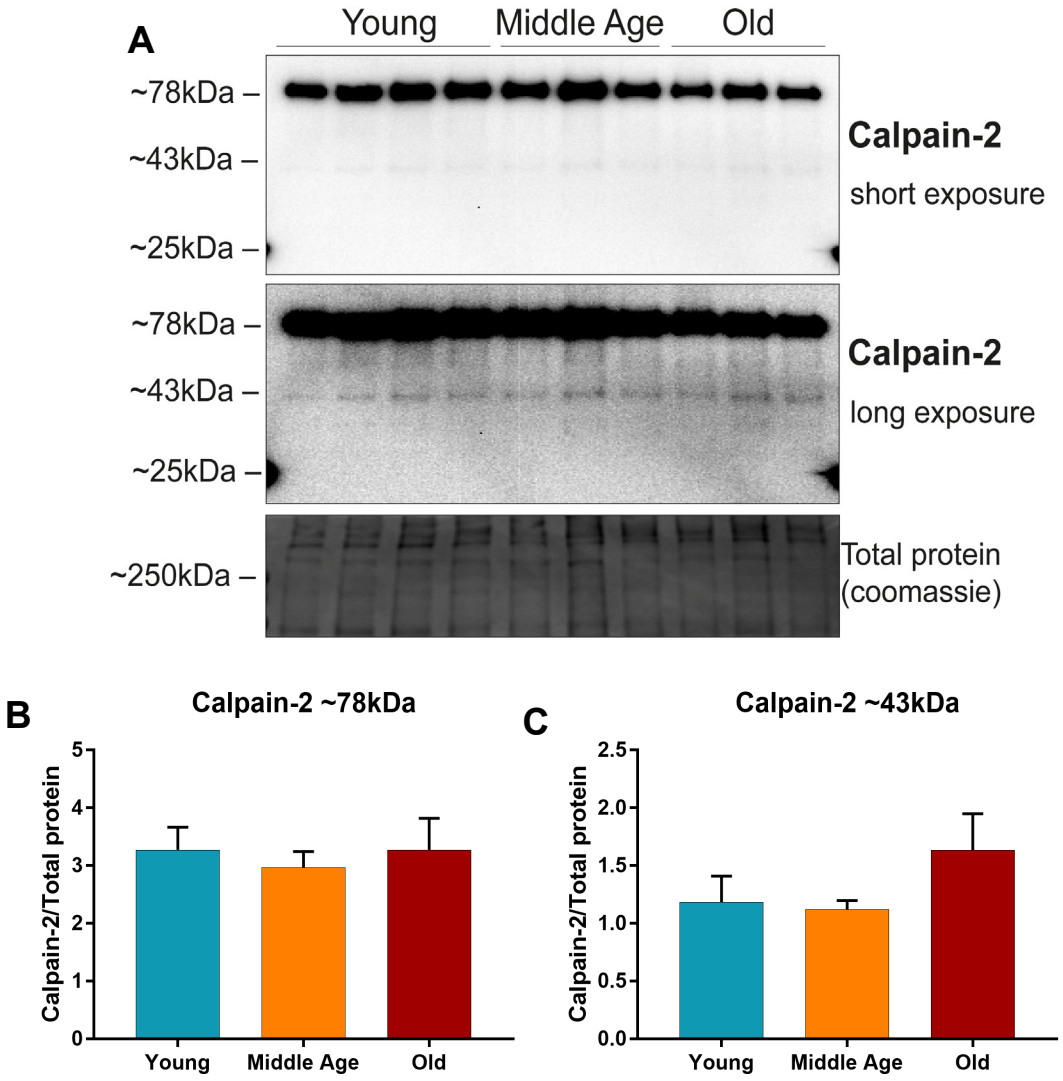

Figure 3.19. Western blot analysis of calpain-2 expression in the SNpc during ageing in rats. (A) Immunoblot showing the expression levels of calpain-2 in the SNpc of young (*n=4*), middle age (*n=3*) and old rats (*n=3*), using a mouse monoclonal calpain-2 antibody from Santa Cruz (#373966). **(B)** Measurements of the integrated density of calpain-2 at 78kDa, normalised to total protein (Coomassie stained gel), did not show statistically differences between young and middle age (p=0.6240) or old (p>0.9999) SNpc. **(C)** Measurements of the integrated density of calpain-2 at 43kDa, normalised to total protein (Coomassie stained gel), showed no statistically differences between young and middle age (p=0.9318) or old (p=0.0828) SNpc. Error bars represent standard deviation.

Adding to this, the other enzyme found in the SNpc samples by proteomics (i.e., caspase-3) was also tested by Western blot. To do this, a mouse monoclonal caspase-3 antibody from Santa Cruz (#56053) was used. However, in this case, no bands were detected (immunoblot not shown).

3.3.8 The expression of TH, a marker for DAn, showed no statistically significant differences in the rat SNpc with increasing age

Tyrosine hydroxylase (i.e., tyrosine 3-monooxygenase, TH) is the enzyme of the dopamine synthesis in SNpc DAn, therefore, the observation of its expression indicates the presence of DAn in the sample. The existence of the TH protein was confirmed in the iTRAQ study, which suggested that there were no statistical differences in its expression in the rat SNpc during the ageing process (**Supplementary Table 2b**). Subsequently, these results were validated by Western blot using a rabbit polyclonal TH antibody from Millipore (#ab152) in independent SNpc samples (**Figure 3.20**). The immunoblot detected a strong band at 62kDa in all ages (**Figure 3.20A**). Measurements of the integrated density of TH at 62kDa, normalised to total protein (Coomassie stained gel), demonstrated that the expression of TH in the young (0.5606 ± 0.083), middle age (0.676 ± 0.1575) and old (0.6654 ± 0.2035) was not statistically different with ageing in any comparison (young *versus* middle age (p=0.5867) or young *versus* old (p=0.6121) (**Figure 3.20B**).

In summary, the results in this chapter show that during the ageing process the proteome of rat SNpc undergoes changes in the expression of 66 proteins from a total of 1,953 proteins identified. Some of these changes appeared at early stages of the adult life (i.e., young), while others emerged later (i.e., middle age). GO functional annotation analysis and protein pathways revealed that these proteins were involved in biological functions such as the extracellular matrix, cell adhesion, intermediate filament organization, detoxification of the environment or metabolism, suggesting that these functions were

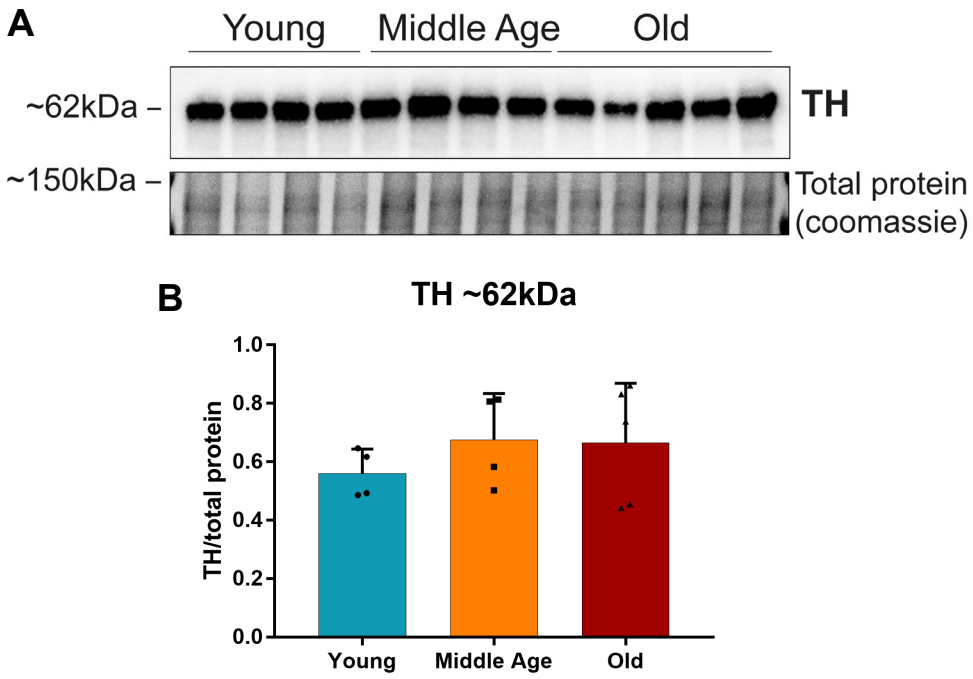

Figure 3.20. Western blot analysis of TH expression in the SNpc during ageing in rats. (A) Immunoblot showing the expression levels of TH in the SNpc of young (*n=4*), middle age (*n=4*) and old rats (*n=5*), using a rabbit polyclonal TH antibody from Millipore (#ab152). **(B)** Measurements of the integrated density of TH at 62kDa, normalised to total protein (Coomassie stained gel), showed non-statistically changes between young and middle age (p=0.5867) or old (p=0.6121) SNpc. Error bars represent standard deviation.

dysregulated in the aged SNpc of rats. Moreover, protein network analysis situated GFAP, a protein that characterizes astrocytes (a type of glial cells), as a core protein in the network, being associated with other dysregulated proteins. Due to the importance of GFAP in astrocytes, GFAP was chosen for further investigations. The expression of GFAP by immunofluorescence increased with ageing, while the immunoblot reported extra bands apart from the canonical form. The study of these extra bands led to the discovery of the presence of GFAPδ in the samples, with a higher expression in the middle age, and the existence of calpain-2, a proteolytic enzyme that might be involved in the cleavage of GFAP producing breakdown products. Lastly, the expression of TH by immunoblot did not change significantly in the rat SNpc during the ageing process.

3.4 Discussion

In this chapter, a quantitative proteomics approach was used to examine the proteome of the rat SNpc at four different stages of life (postnatal P14, 8-month-old, 16-month-old and >21-month-old) to determine whether protein expression levels change during normal physiological ageing, which may give insights into why SNpc DAn become more vulnerable to PD with increasing age. From a total of 1,953 proteins that were identified and quantified, 608 proteins in juvenile, 43 in young, and 28 in middle aged were differentially expressed compared to the old SNpc.

3.4.1 Proteomics changes in the postnatal SNpc in rats are related to neurodevelopment

The results from the functional annotation analysis of the 608 differentially expressed protein in the rat SNpc from the comparison juvenile *versus* old showed multitude of dysregulated biological processes related to neurodevelopment of the brain and SNpc. During the postnatal period, the brain is very dynamic, and is affected by a multitude of modifications. For example, the postnatal rat brain grows due to changes in the cellular composition (Bandeira *et al*., 2009), and also undergoes a peak of myelination at P10 (Downes and Mullins, 2014). Moreover, proteomics studies have reported significant changes in the expression of certain proteins related to the synaptosome and mitochondria (McClatchy *et al*., 2012), as well as cytoskeletal organization, microtubule dynamics and neurite outgrowth (Fuller *et al.,* 2015). Therefore, a variation in the CNS proteome between juvenile and old ages, although potentially affecting similar proteins in both neurodevelopment and the ageing processes, must be interpreted with caution because it might be associated with two different scenarios with different implications within the cell. To avoid the misinterpretation of the data, these 608 differentially expressed proteins were excluded from future analysis. Nevertheless, it is important to note that the identification and quantification of the rat SNpc at postnatal stages in comparison to adult individuals has generated an extensive set of data. This dataset

provides an excellent and free resource for future investigations for the understanding of the neurodevelopment process in the rat SNpc (**see Annex 1**), which could help to clarify the characteristics of DAn and why they are more vulnerable than other neurons of the brain.

3.4.2 Changes in the expression of certain proteins as ageing progresses in the rat SNpc might be associated with translational modifications or proteolysis

The exclusion of the 608 proteins from the juvenile *versus* old comparison left a total of 66 differentially expressed proteins in the rat SNpc along the three adult ages (young, middle age and old). The observation of their fold-changes revealed that their expression changed a maximum of 0.44 and 2.78-fold-change in the young *versus* old comparison, while in the middle age group *versus* old comparison the maximum was 0.68 and 2.98-fold-change. These changes in the expression, although appear small, can be enough to alter the function of a protein or affect an entire proteome. Thus, small changes in individual proteins that are part of the complex SNpc proteome might have a major biological impact in the homeostasis of the cells and brain, leading to disease (Karve and Cheema, 2011).

Most of the 38 differentially expressed proteins in the young *versus* old comparison showed an expression trend that was increasing or decreasing progressively with age. Interestingly, in this case, when the same proteins were observed in the middle age *versus* old comparison, their expression did not show any statistically significant change, with the exception of haemoglobin subunit alpha 1 (HBA1), haemoglobin subunit beta (HBB), 3-ketoacyl-CoA thiolase, mitochondrial (ACAA2) and, glutathione S-transferase alpha-4 (GST4). The lack of statistical differences in the expression of these proteins between middle age and old animals might be simply explained because of the progressive increase or decrease of their expression with ageing, starting at young stages. Consequently, the expression of these proteins in middle age would be more similar to the old group, not presenting statistical differences between them.

Furthermore, it might happen that the progressive decrease of the expression of certain proteins as ageing increases is the consequence of their post-translational modifications or truncations. These alterations change the mass of the protein, affecting its identification and quantification by proteomics, and could contribute to a false sense of depletion in its expression. It is essential to consider this possibility, because post-translational modifications can affect the structure of the protein and its function, which could have a negative effect (including degeneration) on the cell (Santos and Lindner, 2017). For example, it has been described by immunohistochemistry that the phosphorylation and nitration of alpha-synuclein increases in SNpc DAn of aged monkeys, and that this could exacerbate the neuroinflammatory response and degeneration of these neurons (McCormack *et al*., 2012).

On the other hand, there were 23 proteins whose expression only changed significantly in the middle age *versus* old comparison but not in young *versus* old. Interestingly, most of the expression of these proteins increased from young to middle age, but afterwards decreased in the old SNpc. This situation might also be explained by post-translational modifications or proteolysis of some of these proteins in the old SNpc after an increase of the expression in the middle age. It is probable that a decrease in the expression detected by this proteomics study did not always indicate a biological reduction of the protein, but changes in its structure and function by adding temporary post-translational modifications. In the future, it would be interesting to explore this possibility by creating a proteomics analysis of specific post-translational modifications. There is an extensive variety of post-translational modifications that can be studied, including phosphorylation, sumoylation, glycosylation, ubiquitylation or acetylation (Santos and Lindner, 2017). However, the SNpc is characterized by an increase of oxidative stress with ageing, which produces a rise in the number of oxidized proteins as Venkateshappa *et al*. (2012) demonstrated in the human SNpc by Oxiblot. To study possible oxidation of the differentially expressed proteins in the rat SNpc with ageing, a similar approach can be used. To do this, carbonyl (i.e., oxidized) groups from the proteins can be tagged with

dinitrophenylhydrazine (DNP) and, after immunoprecipitation by anti-DNP antibody, LC-MS/MS analysis can be performed, searching the data for the possible modifications associated with oxidation of the protein (Kristensen *et al*., 2004). Another possible explanation for the drop in expression of certain proteins in the old group after an increase in middle age, is that the rat SNpc has a higher proteolytic activity during ageing, or that the aged SNpc is more prone to proteolysis during the dissection process. This option will be discussed more in the context of GFAP in a subsequent section of this Thesis.

3.4.3. The dysregulation of GFAP in the rat SNpc with ageing may be related to alterations of astrocytes that, in turn, modify the ECM or *vice versa*

Bioinformatic analysis of the 66 differentially expressed proteins identified enriched processes and pathways related to cell adhesion, extracellular matrix, and intermediate filament organization, among others. Interestingly, protein network analysis demonstrated that from the 66 proteins, glial fibrillary acidic protein (GFAP) was the main connector associated with the highest number of differentially expressed proteins. The GFAP protein is a class-III intermediate filament that characterises and forms part of the cytoskeleton of mature astrocytes (Eng, 1985). In the adult CNS, GFAP has been also found in Bergmann glia (specialized astroglia with radial processes in cerebellum) (Kril *et al*., 1997) and neural stem cells (Filippov *et al*., 2003); while in the adult peripheral nervous system GFAP has been described in non-myelin-forming and dedifferentiated Schwann cells after axonal injury and regeneration (Jessen *et al*., 1990; Mancardi *et al*., 1991). The exact function of GFAP in astrocytes is not fully understood (Hol and Capetanaki, 2017), but as with other class-III intermediate filament, this protein gives structural support to the astrocyte, regulating the cell membrane that interacts with other cells and the extracellular matrix (ECM) (Middeldorp and Hol, 2011). Other functions associated with GFAP are cell motility, morphology and proliferation (Elobeid *et al*., 2000), exocytosis of vesicles to release different substances (e.g., gliotransmitters)

(Potokar, 2007), and regulation of the integrity of the BBB and myelination (Liedtke *et al*., 1996). Furthermore, an increase of the expression of GFAP, together with the increase of other proteins like vimentin, is characteristic of reactive astrocytes and is accompanied by a hypertrophy of their morphology (Bignami and Dahl, 1976; Pekny *et al*., 2014; Liddelow and Barres, 2017). However, the whole implications that these changes produce in astrocytic function and, therefore, in the CNS remain unknown (Kamphuis *et al*., 2015). Astrocytes play an irreplaceable role in the CNS in maintaining and regulating the BBB when wrapping with their endfeet on endothelial cells that form the blood capillaries in the brain (Janzer and Raff, 1987). They also modulate myelination (Sorensen *et al*., 2008), and providing metabolic support and energy to neurons (Camandola, 2018). Therefore, it seems likely that the differential expression of GFAP found in the ageing SNpc is associated with astrocytes. Considering all the functions in which GFAP is involved, such as the interaction with the ECM (Middeldorp and Hol, 2011), the dysregulation of GFAP in the rat SNpc with ageing might indicate an impairment not only of these astrocytes, but in all the processes astrocytes are related to. This would change the expression of the proteins related to these processes, which would justify the high number of connections that GFAP has with other dysregulated proteins in the protein network. Altogether, this could create a hostile environment for DAn, promoting their degeneration. In addition, it could be possible that changes in GFAP occur to counteract degeneration, in an attempt to protect neurons against an insult in the brain, or as the consequence of alterations in other proteins.

Among the proteins that were dysregulated and associated with GFAP, some of them (e.g., aggrecan (AGRN), versican (VCAN), neurocan (NCAN), hyaluronan and proteoglycan link protein 1 and 2 (HPLN1, HPLN2)) were increasing their expression with ageing and were part of the ECM. The ECM is an accumulation of proteins in the extracellular space and can be found around some cell bodies and dendrites in the form of so-called perineuronal nets (Carulli *et al*., 2006). These perineuronal nets can inhibit plasticity by stabilizing the connection between neurons (Pizzorusso *et al*., 2002; de Vivo

et al., 2013). Likewise, perineuronal nets can also protect neurons against oxidative stress due to the capacity of its charge structure to bind redox ions (Morawski *et al*.,2004). Thereby, two possible implications associated with the increased expression of these proteins related to the ECM with ageing might be stabilizing the connection between DAn or other cells in the SNpc (e.g., astrocytes), or have a protective effect against oxidative stress in the SNpc, which is known to generate a high amount of ROS and be harmful for DAn (see General introduction in Chapter 1). This last option might also be related to the reduction of glutathione-S-transferases in the SNpc with ageing shown in this Thesis. Glutathione-S-transferases detoxify xenobiotics (e.g., drugs, pesticides, carcinogens) and products of oxidative stress (e.g., hydroperoxides, quinones), catalysing the conjugation of glutathione to these substrates (Mannervik and Danielson, 1988). Therefore, the depletion of this system reduces the detoxification function and increase of oxidative stress in the SNpc. Hence, it might happen that the decline of glutathione-S-transferases forced other mechanisms around the cells (i.e., ECM) to increase in order to counteract and reduce the oxidative damage.

It is known that the ECM components such as aggrecan, versican, neurocan, hyaluronan and proteoglycan link protein 1, which were upregulated with ageing in this Thesis, can be expressed or generated by all cells in the brain. For example, neurocan is expressed in neurons (Engel *et al.,* 1996), while versican is highly expressed in oligodendrocyte lineage cells of an injured area of the CNS, inhibiting the axon growth of neurons in that region (Asher *et al*., 2002). Astrocytes can also produce or express some of these components, including aggrecan (Asher *et al*., 1995; Afshari *et al*., 2010), versican (Beggah *et al*., 2005), neurocan (Asher *et al*., 2000; Carulli *et al*., 2007; Meng *et al*., 2012), and link proteins as hyaluronan and proteoglycan link protein 1 (Cahoy *et al*., 2008). When an injury or a lesion appears in the CNS, the production of these ECM components by reactive astrocytes increases inhibiting axon regeneration. This has been proved by Jones *et al*. (2003) and Moon *et al*. (2002) who demonstrated an increase of neurocan and versican after spinal cord injury or axotomy of the nigrostriatal

pathway. Thus, it is possible that the increase of ECM proteins in the aged SNpc might be suggesting a certain level of damage occurs in SNpc, generated as a result of an increase of GFAP in the middle age in astrocytes. Conversely, ECM proteins can affect different aspects of astrocytes themselves, including the expression of GFAP during development (Domowicz *et al*., 2008). In this Thesis, an increase of ECM proteins such as aggrecan appeared in the middle age, which coincided with an increase of GFAP during that age. Although the regulation of astrocytes by proteoglycans seems to happen in embryonic and postnatal stages, associated with an overexpression of GFAP (Domowicz *et al*., 2008), it seems plausible that during a traumatic event the adult ECM and the increase of proteoglycans would have the capability to also affect the expression of GFAP. This would alter some of the functions which GFAP is involved with (see above) and impact their viability and the support role they play in the brain.

Regardless of the cause-effect relationship between ECM proteins and astrocytes/GFAP, the alteration of the ECM with ageing appears to be an event not restricted to the SNpc. An example of this is the proteomics study carried out by Smidak *et al*. (2017) who observed that during the ageing process the rat dentate gyrus had an increase of aggrecan, neurocan, versican, and hyaluronan and proteoglycan link protein 1 and 2. However, contrary to the results in this Thesis, they did not observe any change in the expression of GFAP. This could suggest that changes in the ECM precede modifications in the astrocytes, but also that astrocytes in the SNpc are more susceptible to alterations of the ECM compared to other areas of the brain. In relation to PD in particular, proteins associated with the ECM have been shown to be dysregulated in the SNpc in both human PD and models of PD. This is the case of the hyaluronan and proteoglycan link protein 2, which is highly expressed in SNpc DAn of PD patients and rats lesioned intrastriatally with the toxin 6-OHDA (Liu *et al*., 2015; Wang *et al*., 2016). The results of these studies agree with the increase of expression of hyaluronan and proteoglycan link protein 2 during ageing in the rat SNpc shown here. Interestingly, Wang *et al*. (2016) demonstrated that the overexpression of this protein can sequestrate

and aggregate alpha-synuclein, which suggest that hyaluronan and proteoglycan link protein 2 and other proteoglycans during ageing might contribute to the accumulation of alpha-synuclein in DAn and a higher susceptibility to PD.

Lastly, it is important to mention another possibility that could justify the changes in the expression of proteins related to ECM and GFAP between the different age groups. This simply be related to the fact that the third oculomotor cranial nerve crosses the SNpc. This nerve is considered part of the peripheral nervous system, having axons myelinated by Schwann cells (Hagan *et al*., 2012). As it was mentioned before, Schwann cells can express GFAP after axonal degeneration and the consequent regeneration, reorganizing the cytoskeleton of the Schwann cells and the surrounded ECM (Triolo *et al*., 2006). Therefore, the increase of the expression of GFAP in the middle age could be produced by changes in Schwann cells after axonal disruption of the oculomotor nerve with ageing. In fact, Sharma *et al*. (2009) identified a reduction of the total amount of myelinated fibres together with an increase of myelin thickness and modification of the ECM in human oculomotor cranial nerve with ageing, which might affect the morphology of Schwann cells. Interestingly, the alteration of these Schwann cells would explain as well why the expression of proteins related to the ECM were increased with the ageing process. In line with this, it is important to highlight the fact that the dissection of the SNpc contained more or less oculomotor nerve in certain samples. This could explain why myelin protein P0 (MPZ), a protein also expressed in Schwann cells (Bai *et al*., 2011), appeared enhanced in young and middle age compared to old individuals. Although the extraction of the SNpc tissue in all ages was performed with the same care, the SNpc is a small structure within the midbrain and its dissection was a challenge. Consequently, the possibility cannot be excluded that the dissection of the SNpc from the old group included less oculomotor nerve and, therefore, less myelin protein P0. On the other hand, it may happen that, independently of technical difficulties, the oculomotor nerve in old individuals contain less myelin protein P0 because of the effect of ageing, which could also have an impact in the ECM composition and GFAP expression. Nevertheless,

it seems improbable that the differences in the composition of the sample (with less or more oculomotor nerve) has a direct effect in the expression of ECM proteins and GFAP, because there is a lack of correlation between the changes of myelin protein P0 with ageing and the rest of proteins already mentioned. In the future, it would be useful to generate a new experiment with a higher number of SNpc samples for each experimental group. This would reduce the chance of differences because of technical issues.

3.4.4 The increase of expression of GFAP in the ageing SNpc of rats may indicate an expansion in the number of astrocytes or an increase of GFAP expression in each cell

Using immunofluorescence, a significant increase of the O.D. for GFAP was found with ageing in the SNpc region. Surprisingly, the immunofluorescence results for GFAP did not match the proteomics findings, where the expression of GFAP decreased in the oldest group after an increase in middle age individuals. As it was mentioned before, GFAP is an intermediate filament protein closely related to astrocytes, and it is involved in multitude of functions within these cells. The alteration of GFAP might affect the function of the astrocytes in the CNS, and, ultimately, have implications in the maintenance and viability of DAn (see above). Thus, understanding how the astrocytic activity changes with ageing is fundamental to gaining new insight into relationship between ageing and neurodegenerative disease, and might help in the generation of new treatments (Bernal and Peterson, 2011). However, as cited in the General introduction of this Thesis (see Chapter 1), increases in the expression of GFAP with ageing in the SNpc have so far been controversial (Kanaan *et al*., 2010; Gao *et al*., 2013; Jyothi *et al*., 2015). Nevertheless, interestingly, Kanaan *et al*. (2010) has reported (in a study where no differences were found in the number of astrocyte or GFAP intensity) that when the morphology of astrocytes was observed, only a few animals of the middle age group showed an activated hypertrophic phenotype, returning to a resting state

similar to young individuals in the old group. These data were consistent with the proteomics results for GFAP found in this Thesis, where an increase of the expression of GFAP appeared in the middle age compared to the young and old groups. In their discussion, they proposed that this U-shape response of GFAP with ageing may be indicating the failure of the activation of astrocytes in the old age, which might have implications in the vulnerability of DAn. This possibility has been also exemplified by Rodriguez *et al.* (2014) who found a broad heterogeneity of the GFAP expression between different areas of the brain (hippocampus and entorhinal cortex) with ageing (from 3- to 24-month-old).

Altogether, this shows a lack of consensus across the literature concerning changes in GFAP expression in the SNpc during ageing. In all of them, immunohistochemistry was the technique applied, however, the methods they used to measure and quantify the expression of GFAP varied between publications (e.g., densitometry or unbiased stereology), which might justify the differences between results. It is necessary to be critical with the measurements of the O.D. for GFAP in this Thesis, where it was difficult to distinguish individual astrocytic cells and where an increase of GFAP O.D. can mean either an increase of the number of astrocytes or an increase of the expression of GFAP in each astrocyte. Consequently, this highlights the urgent need for more investigations where the study of the expression of GFAP is analysed in different species in a similar way by a combination of techniques (i.e., PCR, immunofluorescence, immunoblotting and proteomics). This requires a pause to reconsider whether reactive astrogliosis is truly a normal and well-established process during ageing in the whole brain and, more specifically, in the SNpc. This may open up the possibility of discovering more specific, subtle changes in astrocytes that can be detrimental for them and to certain neuropathologies.

3.4.5 Ageing generates alternative variations of the canonical isoform GFAPα in the rat SNpc

The disagreement between results using immunofluorescence and proteomics here led to an additional analysis of the expression of GFAP by Western blot. Intriguingly, Western blots for GFAP with two different antibodies revealed that, apart from the main band at 50kDa, there were extra bands of a lower MW between 48kDa and 37kDa that were strongly expressed in the old SNpc. To date, it is believed that the main band of 50kDa is associated with the canonical isoform of GFAP, GFAPα, which is often what the literature is referring to when it mentions 'GFAP' (Reeves *et al*., 1989; Middeldorp and Hol, 2011). Although the two different antibodies showed the low MW bands, corroborating that these bands belonged to GFAP, differences between immunoblots were also described. This can be explained due to the different epitopes that these two antibodies recognize (see Chapter 2), and that in many cases are not fully detected or described by the manufacturers. For example, in the case of the Biolegend GFAP antibody, the only information supplied by the manufacturer is that the antibody has been 'raised by immunization of whole spinal cord homogenates'; while the Cell Signalling GFAP antibody has been produce by 'immunizing animals with a synthetic peptide corresponding to residues surrounding Asp395 of human GFAP protein'. As will be discussed later, GFAP is a protein that can undergo changes in its sequence, which alters its MW. Thus, the lack of information around what part of the protein these antibodies recognize makes it extremely difficult to determine alternative patterns of staining.

Nevertheless, when all bands (from 50kDa to 37kDa) were measured together by Western blot, the results were similar to the immunofluorescence findings; while measurements of the band at 50kDa alone reflected the proteomics results but without showing significant differences. The absence of statistical differences by Western blot might be explained by a variety of reasons, including low sample numbers, the high background of the gels to quantify the total amount of protein, some variability between

individual samples, or the small fold-change for the expression of GFAP. Western blot is a semiquantitative technique that, although showing good results for the presence and absence of proteins, it has some limitations in accurately measuring small changes in the expression of proteins (Gassmann *et al*., 2009). Altogether, these results demonstrated that by combining multiple approaches (i.e., immunofluorescence, immunoblotting and proteomics), different observations of the expression of one protein (in this case GFAP) can be done to understand the full story, revealing diverse characteristics of one protein, which might have implications in its structure and function.

The detection of these extra bands generated two possible explanations linked to modifications of GFAPα, which include the production of new isoforms of the protein and/or breakdown products due to its proteolysis.

3.4.5.1 GFAPδ is a unique GFAP isoform in the rat SNpc whose expression changes with ageing

As mentioned previously, GFAPα (isoform 1) is the canonical GFAP isoform and the most abundant in the CNS. The length of the protein is 432 aa in humans and 430 aa in rats and has a MW of approximately 50kDa (Reeves *et al*., 1989; Middeldorp and Hol, 2011). As in others intermediate filaments, the structure of GFAPα is formed by three main domains, including a N-terminal head, a helical rod, and C-terminal tail (Reeves *et al*., 1989), knowing that the head must be preserved in order to assemble GFAP in filaments (Chen and Liem, 1994). Due to this, post-translational modifications, including phosphorylation in the head and tail domain, seems to have an effect on the assembly of the protein (Sihag *et al*., 2007).

Apart from GFAPα, nine isoforms have been described so far, including GFAPβ, GFAPζ, GFAPκ, GFAPδ/ε, GFAPγ and GFAP+1 (GFAPΔEx7, GFAPΔ135, GFAPΔ164, GFAPΔEx6) (reviewed in Hol and Capetanaki, 2017). These isoforms are generated by alternative splicing, generally changing the C-terminal of the protein (see Result section

for more detail of each isoform, **Figure 3.14**). Moreover, it seems that these isoforms are related to a specific subpopulation of astrocytes that, in some cases, are associated with neurodegenerative diseases. For example, a study using a mouse model of AD showed an increase of GFAP isoforms (GFAPα, GFAPβ, GFAPζ, GFAPκ, GFAPδ and GFAPγ) at the transcript level in the cortex compared to controls (Kamphuis *et al*., 2012). However, from all these proteins, only GFAPδ was identified at the protein level by Western blot and immunofluorescence, overlapping with one of the bands and the staining produced using a panGFAP antibody. In addition, *post-mortem* hippocampal tissue from humans with AD revealed that the same isoforms were upregulated at the transcript level, with a correlation of expression accorded to the progression of the disease (Kamphuis *et al*., 2014). In the same article, the authors observed a positive immunostaining for GFAPδ and GFAP+1. The expression of GFAPδ was higher in reactive astrocytes of AD brains, while GFAP+1 was characteristic of a specific subgroup of non-reactive astrocytes in AD and control groups. Moreover, by immunoblotting, they demonstrated that a panGFAP antibody was able to recognize all GFAP isoforms, producing a blot with multiple bands between 39kDa and 50kDa. When they tested specific antibodies for GFAPδ, GFAPκ and GFAP+1, the bands for these antibodies appeared at approximately at 49kDa, 50kDa and 44–39kDa, respectively, which could match some of the bands found in this Thesis.

The examination of GFAPδ by Western blot in the rat SNpc revealed a band of approximately 50kDa that was significantly increased in middle age compared to the other two ages. GFAPδ differs from the canonical sequence GFAPα in the last 42 aa, from 389 to 430 aa (Roelofs *et al*., 2005), therefore, the GFAPδ antibody (which recognizes residues surrounding 350 aa of mouse GFAPδ) identifies only this variant and no other isoforms (e.g., GFAPα). However, because the band appeared at 50kDa, it was not possible to justify the origin of the other bands below 50kDa. Importantly, this reveals that panGFAP antibodies, which produces a main band for GFAPα at 50kDa, might be recognizing other isoforms, such as GFAPδ, very near the same MW. Thus,

the use of panGFAP antibodies might be hiding the expression of other splice forms, as it does with GFAPδ. Altogether, this indicates that we must be critical with the conclusions from previous investigations that handle GFAP as a stable and unique protein, and without considering other isoforms that might have been included and treated as GFAPα.

Notably, to the best of my knowledge, this is the first time that someone mentions the expression of GFAPδ in the SNpc region and in connection with the ageing process in this area. However, other authors have reported the existence of this isoforms in the CNS. For example, Roelofs *et al*. (2005) found GFAPδ-positive astrocytes or ependymal cells in subpial and subependimal regions. When they investigated the implications that the expression of GFAPδ had in the astrocyte, they discovered that the low expression of GFAPδ together with a high expression of GFAPα allowed the astrocyte to form a normal and stable cytoskeleton with a star morphology. However, high concentrations of GFAPδ produced perinuclear failure that interrupted the formation of the cytoskeleton due to the modification of the C-terminal in the isoform, necessary for the correct assemble of intermediate filaments. They speculated that, because GFAPδ surrounds the nucleus and is associated with a smaller cytoskeleton, this isoform might have a role controlling the volume or cellular location of the cytoskeleton within the astrocyte, which can have implications in the motility of these cells. Another example of the implications that GFAPδ has in the correct assembly of intermediate filaments in astrocytes has been reported by Perng *et al.* (2008), who studied the *in vitro* assembly of GFAPδ and GFAPα by electron microscopy. They demonstrated that GFAPδ expression was always associated with a major expression of GFAPα, therefore, presenting a normal intermediate filaments assembly and being involved in the normal function of astrocytes. However, when GFAPδ represented more than 10% of the total GFAP expression, the filaments tended to aggregate. Hence, GFAPδ exists as a permissible relative in an appropriate ratio with GFAPα before the GFAP network is compromised. In relation to

this Thesis, it would be very useful to know what the ratio of GFAPδ over GFAPα was in the SNpc samples, in order to understand if the expression of GFAPδ can have an impact in the cytoskeleton of astrocytes in the SNpc. Sadly, it was not possible to test this by Western blot due to the same MW of both isoforms (approximately 50kDa). Moreover, immunofluorescence approaches did not show any staining for this GFAPδ protein, which could be due to a lower affinity of the antibody for the epitope in tissue samples, being impossible to characterize the type of cells that contain this protein. Furthermore, the proteomics assay did not provide any clues about GFAPδ and, therefore, the ratio of both isoforms. Multiple sequence alignment of the sequences of both GFAPα and GFAPδ, together with the protein sequence coverage detected for GFAP by ProteinPilot software, demonstrated that the proteomics study did not identified any specific peptide for the isoform GFAPδ. Therefore, it should be noted that this proteomics approach can miss relevant results for certain proteins. For instance, it can happen that if the number of peptides from one isoform is very low, these can be difficult to detect and distinguish among the peptides from the main and more abundant isoform. Likewise, it is possible that ProteinPilot algorithm associates the common peptides (e.g., peptides from the protein core) with the main isoform by probability, instead of to the other isoforms. In the future, it would be useful to create a proteomics experiment to identify and quantify the possible different isoforms, measuring the specific peptides associated with each isoform by the Multiple Reaction Monitoring (MRM) method for peptide absolute quantitation.

On the other hand, Perng and colleagues (2008) demonstrated that the high expression of GFAPδ increased the interaction and association with the cytoplasmic protein alpha-crystallin B chain a protein that, interestingly, increases its expression with ageing in the rat SNpc. Alpha-crystallin B chain is a heat-shock chaperone that appears upregulated in conditions of stress within the cell (e.g., pH extreme changes, hypoxia, oxidative stress), avoiding the aggregation of other proteins by binding exposed hydrophobic sites and promoting their refolded (Derham and Harding, 1999). Alpha-crystallin B chain can

regulate GFAP filament and have a protective role within the astrocyte when a high expression of GFAP appears, avoiding its aggregation and reactive gliosis, reducing its stress and having an anti-apoptotic function thanks to an increase of alpha-crystallin B chain (Ousman *et al*., 2007; Hagemann *et al*., 2009; Klopstein *et al*., 2012). Surprisingly, an upregulation of alpha-crystallin B chain has been seen in reactive astrocytes and degenerated astrocytes in the SNpc of a mouse MPTP model of PD and parkinsonians compared to age-matched controls by quantitative proteomics analysis (Liu *et al*., 2015). All this together might indicate that, in the ageing SNpc, the increase of alpha-crystallin B chain is trying to avoid the aggregation of GFAP and the degeneration of astrocytes.

Why GFAPδ increases in the middle age in the first place is something that must be assessed in the future to determine if changes in its expression has a physiological purpose or appears as a pathological hallmark. To do this, a knock-in transgenic mice could be created, overexpressing GFAPδ in order to study *in vivo* the implications of its increased expression in astrocytes on the SNpc and their DAn. Moreover, to see the effect of this GFAPδ overexpression with ageing, astrocytes at different age points can be compared. Either way, the high expression of GFAPδ might increase the association of proteins like alpha-crystallin B chain that, simultaneously, would be working to avoid the aggregation of GFAP, protecting the astrocyte from degeneration. Moreover, it is fundamental to understand why there is a reduction of GFAPα in old individuals and if this reduction is associated with the production of other isoforms or, as it will discuss below, breakdown products.

So far, this work has demonstrated the existence of GFAPδ in the rat SNpc, but it was not possible to probe the presence of other isoforms because of the lack of available GFAPγ antibodies for rat tissue or because the immunoblot for GFAP+1 did not show any band for that antibody used. This last finding could indicate that there was not enough protein expression in the samples to be detected by Western blot, that the affinity of the antibody did not bind the epitope,or that GFAP+1 was not expressed in the SNpc samples. These options, however, would not justify why the bands appear with the

panGFAP antibody. Another possibility is that the GFAP+1 antibody (raised against the human isoform) was not able to detect the rat sequence, although this seems improbable because the antibody recognizes the C-terminal of the protein that in humans and rats is conserved.

3.4.5.2 GFAP might be truncated in the ageing SNpc samples

Countering the information mentioned above, the proteolysis of GFAP was also explored in the literature as a mechanism to generate some of the extra bands that were found. Seminal work by Dahl and others demonstrated that GFAP from bovine, rodent and human brains could be affected by *post-mortem* proteolysis if they were not rapidly frozen, producing breakdown products that were more soluble in an aqueous solution, and with lower MW between 46 and 39kDa (Dahl and Bignami, 1975; Dahl 1976). This suggests that the SNpc samples used here may not have frozen rapidly enough after the dissection, producing the breakdown products that can be observed as extra bands. However, because all samples were extracted in the same conditions, it seems unlikely that only the oldest samples suffered the process of proteolysis, unless that the characteristics of the tissue from the old individuals are implicated in an increase in proteolysis. In fact, Smith *et al*. (1984) visualized that the production of breakdown products in rat spinal cord homogenates depended on the age of the tissue. Hence, samples from older individuals (18-month-old) showed higher degradation of GFAP compared to younger ones (15 and 50 days), indicating that in old tissue either the substrate is more susceptible to proteolysis or there is a higher activity of the enzyme.

In the past, authors noticed an increase in the cleavage of GFAP after an increase of calcium in the media (Schlaepfer and Zimmerman, 1981; DeArmond *et al*., 1983; Ciesielski-Treska *et al*., 1984), corroborating that behind the breakdown of GFAP must be a calcium-dependent cysteine protease. Currently, it is well established that calpain is the protease implicated in the disruption of GFAP in astrocytes (Li *et al*.,1995; Li *et al*.,

1996). Adding to this, Lee e*t al.* (2000) suggested that reactive astrogliosis might be mediated by the proteolysis of GFAP by calpain. Thus, the activation of calpain would be cleaving GFAP in Asp94, producing an increase of a band at 48kDa. This might expose more GFAP antigens compared to the full-length protein, showing a stronger signal by immunolabelling with a panGFAP antibody. If that interpretation is correct, it could offer one explanation for why an increase of GFAP was found with ageing in the SNpc samples by immunofluorescence, and at the same time a decrease of GFAP 50kDa (GFAPα) in the oldest group by proteomics and Western blot. The proteolysis of GFAP might be generating breakdown products, represented as extra bands that were not identified by proteomics but that were visualized by immunoblot.

Interestingly, the proteolysis of GFAP by calpain with the production of bands of lower MW than 50kDa has been observed previously in several diseases. For instance, calpain has been seen to produce GFAP breakdown products bands between 35kDa and 48kDa associated with a reduction of GFAP 50kDa in spinal cord from patients with Amyotrophic Lateral Sclerosis (ALS) compared to matched controls (Fujita *et al*., 1998). Similar to the results in this Thesis, when all GFAP bands were quantified, an increase of GFAP appeared in ALS subjects. Moreover, multiple studies related to Traumatic Brain Injury (TBI) have revealed an increase of the proteolysis of GFAP due to calpain. This is exemplified by the work produced by Zoltewicz *et al.* (2012) and Papa *et al*. (2012) where *post-mortem* brains and plasma from TBI individuals showed an increase of GFAP breakdown products between 38kDa and 42kDa. Similarly, Zoltewicz and colleagues (2013) demonstrated in a TBI rat model an increase of the cleaved GFAP at 45kDa after 7 days post lesion in brain, CSF and plasma. Work published by Guingab-Cagmat *et al*. (2012) identified an increase of GFAP breakdown products with calpain, specifically at 38kDa, in a TBI model using rat cortical cultures.

To know if the extra bands belonged to breakdown products produced by calpain, information on calpain expression in the proteomics samples was sought. The data showed that different calpain isoforms were detected and identified by ProteinPilot

software. Calpain-2 was the isoform chosen for Western blot validations because this calpain is the most abundant in the rat brain (Singh *et al*., 2014), but also because it apparently plays an important role in astrocytic differentiation (Santos *et al*., 2012). Furthermore, the activity of calpain-2 seems to increase with ageing in the rat brain, breaking neurofilament proteins faster (Benuck *et al.*, 1996). Added to this, it has been published that the immunoreactivity of calpain-2 is overexpressed in SNpc DAn of parkinsonians compared to controls (Mouatt-Prigent *et al.*, 1996), and that the administration of an inhibitor for calpain reduced the death of SNpc DAn in a PD model of MPTP in mice (Crocker *et al*., 2003), thus, corroborating that calpain has an important detrimental role in the midbrain. However, they did not demonstrate if calpain belonged to neurons or to other cells in the midbrain such as astrocytes. Therefore, it is difficult to determine if the inhibitor of calpain was affecting, for example, glial cells by reducing their reactive astrogliosis or maintaining their protective function. Neither the proteomics data nor Western blot in this Thesis revealed an increase of calpain-2 expression with ageing to explain the increase of GFAP breakdown products in the old SNpc.

Nevertheless, as will be explained in further detail later, the activity of calpain-2 might not be associated with its expression, but by the lysis of the structure (Brown and Crawford, 1993; and Azuma *et al*., 1997; Chou *et al*., 2011).Therefore, an elevation of active calpain-2 might exist in the old individuals without seeing an increase of its expression by proteomics or immunoblotting, but finding extra bands of lower MW than the expected band at 80kDa. There are two main theories in the literature that try to explain how calpain changes to its active form. First, the autolytic theory is defended by authors such as Brown and Crawford (1993) and Azuma *et al*. (1997) who argued that calpain-2 (form by a catalytic and a regulatory subunit) self-digest itself when calcium binds the C-terminal of the protein *in vitro*. This auto-lysis process removes the first 9 aa from the N-terminal (anchor helix) in the catalytic subunit (80kDa), activating the proteins and reducing its MW up to 76–78kDa. This fact would make extremely difficult to observe changes in the immunoblot between the inactive form (80kDa) and the active form

(78kDa), because the band at 80–78kDa can be a representation of both forms or only one of them. Both authors demonstrated by immunoblot that, after a while, the active form of calpain-2 was degraded, producing fragments of 43kDa, 24kDa and 23kDa. During this degradation, sequences from the C-terminal with different sizes are eliminated, which might cause the loss of the proteolytic activity due to the fact that this region is the calcium binding site. On the other hand, Chou *et al*. (2011) defended that calpain-2 is activated without autolysis, when the anchor helix is released in presence of calcium, forming the active catalytic cleft site. The authors justified this theory because, apparently, the 9 aa that are removed from the anchor helix in the N-terminal are not long enough to be self-digest by the catalytic cleft site. Once calpain-2 was active and the catalytic cleft site was form, the autolysis generated 40kDa and 20kDa fragments, reducing the expression of the protein at 80kDa *in vitro*.

The lack of consensus about the activation of calpain-2, with most of the experiments performed *in vitro*, suggests that it is necessary to be cautious how the results for calpain-2 are interpreted both with proteomics and Western blot. The protein sequence coverage for calpain-2 showed that the last 9 aa from the N-terminal were not identified, therefore, with the proteomics analysis it was not possible to distinguish if there was any type of activation of the enzyme through auto-lysis and/or if the software identified the inactive or active form. On the other hand, in the hypothetical case that calpain-2 was active because of a change in its anchor helix, the proteomics study does not help either to understand those type of modifications in the protein. Despite the proteomics results being validated by Western blot, not seeing statistical differences in calpain-2 with ageing means the question remains whether the immunoblot illustrates whether or not any type of activation of the enzyme is occurring. The calpain-2 antibody used in this experiment recognizes an epitope between 2–27 aa at the N-terminal of human origin, therefore, if the auto-lysis hypothesis of the cleavage of 9 aa is correct, the immunoblot should recognize the active and inactive form at 80kDa and 78kDa, which would not be possible to distinguish. By contrast, if the autolysis generated a product of 43kDa, that

would explain why a faint band with that MW was found in the SNpc samples. However, because the band was very faint, it was difficult to gauge if those results were a reliable representation of each age group or not. The absence of available antibodies for active calpain-2, together with the lack of unanimity along the literature, reflect the urgent need to produce new antibodies for the active form, to comprehend the mechanism of activation of capain-2 in the brain, and, ultimately, to understand how its proteolysis function affects itself and other proteins like GFAP.

3.4.6 The expression of TH does not change in rat SNpc as ageing progresses

Lastly, and due to the importance of the DAn system in this Thesis, the levels of TH found in proteomics were validated by Western blot, finding no differences among ages. As mentioned in the General introduction (see Chapter 1), there is a great controversy in establishing whether DAn from the SNpc degenerates with ageing and if the pattern of degeneration is similar or not to PD (Fearnley and Lees, 1991; Tatton *et al*., 1991; Emborg *et al*., 1998; Ma *et al*., 1999; Cabello *et al*., 2002; McCormack *et al*., 2004; Rudow *et al*., 2008; Sanchez *et al*., 2008; Collier *et al*., 2011; Buchman *et al*., 2012; Bardou *et al*., 2014; Di Lorenzo *et al*., 2016). In terms of soma size, the discrepancies are maintained, with some authors describing an increase or hypertrophy of SNpc DAn that might be indicating a mechanism to compensate the loss of DAn (Cabello *et al*., 2002; Rudow *et al*., 2008; Sanchez *et al*., 2008), while others support a reduction of the soma size (Ma *et al*., 1999; Di Lorenzo *et al*.,2016).

Nevertheless, it seems that at least in rodents ageing causes the reduction of DAn in the SNpc associated with an increase of their soma size. As it will be explained in the next chapter (see Chapter 4), the lack of differences in the expression of TH with ageing could be generated by compensatory mechanisms after a reduction in the number of DAn. Therefore, it is necessary that cellular characterizations of SNpc DAn is conducted in order to understand if there is a reduction or not in the number of these cells, and if exist

any morphological change (e.g., size of the soma) that can justify the lack of differences of the TH expression by proteomics and Western blot.

3.5 Conclusions

In summary, the results from this study demonstrate that proteins related to ECM and GFAP undergo changes in their expression in the SNpc during the ageing process. However, it remains unknown if these changes are related, or are a cause or consequence of each other. It might be the case that these modifications appear as normal adaptation to counteract the effects that physiological ageing has in GFAP-positive cells (e.g., astrocytes or Schwann cells) or DAn, or that alterations in the ECM due to ageing is changing the expression of GFAP. It is possible that ageing is negatively affecting astrocytes and their functions, and may fail in the maintenance of DAn, making these neurons more vulnerable. Moreover, more investigations are necessary to understand specifically if the changes found for GFAP correspond to astrocytes or other type of cells; as well as the implications, if any, that alterations in the ECM has in astrocytes and *vice versa*. Very importantly, this Thesis has characterized the expression of the isoform GFAPδ in the SNpc for the first time, finding differences of its expression across different ages. Thus, it is essential to perform future experiments to elucidate the repercussions that an increase of this isoform has in astrocytes and in the SNpc. The production of breakdown products was an alternative that could justify the results found in Western blot for GFAP, although it was not possible to find an increase of activity of one of the enzymes that might be involved in the proteolysis of GFAP. Knowing how different isoforms and the proteolysis of GFAP take part in the function of astrocytes, or even how the proteolysis can affect diverse isoforms, are questions that neuroscientist will have to tackle if they want to fully understand the complete picture of astrocytes, our brain and neurodegenerative diseases. Future experiments, for instance, can include the excision of the bands from the immunoblot to perform a LC/MS and identify their sequences. In addition, this work has highlighted the urgent need of

producing well defined and characterized antibodies, especially for GFAPα, the canonical isoform. As it was noted before, this Thesis has also demonstrated the power that the combination of different techniques has, producing complementary results that, otherwise, would be hidden. Finally, these gaps open a multitude of new possibilities in this field, starting from the assumption that, perhaps, talking about GFAP is not enough to characterize and show the complexity of astrocytes and their function.

Chapter 4.

Quantitative and morphological characterization of the SNpc DAn in rats and humans during ageing

CHAPTER 4: QUANTITATIVE AND MORPHOLOGICAL CHARACTERIZATION OF THE SNpc DAn IN RATS AND HUMANS DURING AGEING

4.1 Introduction

To understand the impact that ageing has on the incidence of PD, researchers have tried to identify which degenerative changes are common in both processes (see General introduction). The most evident modification in PD, the loss of DAn in the ventral tier of SNpc (Damier *et al*., 1999; Ma *et al*., 1999) has led to an investigation of whether the same pattern of neuronal degeneration appears in the ageing population. Although it is not well established in humans if the same areas of the SNpc are affected with ageing, there is some evidence that age can significantly alter DAn populations in the SNpc similar to the changes observed in PD. For example, physiological ageing can produce a reduction in the number of DAn and increase their soma size (Fearnley and Lees, 1991; Ma *et al*., 1999; Cabello *et al*., 2002; Rudow *et al*., 2008; Buchman *et al*., 2012; Di Lorenzo *et al*., 2016). Additionally, experiments in rodents and primates have also shown a decrease in DAn density along with an increase in the size of their cell bodies (Tatton *et al*., 1991; Emborg *et al*., 1998; McCormack *et al*., 2004; Sanchez *et al*., 2008; Collier *et al*., 2011; Bardou *et al*., 2014). Moreover, modifications in the morphology of astrocytes in humans (Jyothi *et al*., 2015) and microglia in monkeys (Kanaan *et al*., 2010) have been identified, although the neuroinflammation and activation of these glial cells in the aged SNpc is rather controversial. Changes in the morphology, however, might indicate a higher production of pro-inflammatory cytokines that can be destructive for DAn (Koprich *et al*., 2008).

Other alterations described during physiological ageing and PD include the accumulation of alpha-synuclein in DAn, the increase in the level of oxidative stress and mtDNA deletions. In relation to alpha-synuclein, an increase of this protein has been seen in the aged SNpc from humans and rhesus monkeys (Chu and Kordower, 2007; Xuan *et al*., 2011). Because alpha-synuclein promotes SNARE complex assembly

(which mediates vesicle fusion and neurotransmitter release in the extracellular space) (Burre *et al*., 2010), its dysregulation might affect the release of dopamine, keeping it inside the cells. In turn, this might trigger the degeneration of DAn due to the increase of oxidative stress during the metabolism and oxidation of dopamine (see General introduction). In addition, high amounts of protein oxidation associated with oxidative stress (Venkateshappa *et al*., 2012), together with mtDNA deletions (Bender *et al*., 2006; Kraytsberg *et al*., 2006) have been observed in the aged SNpc. These affect the mitochondrial respiratory chain complex and the generation of ATP in cells. Because DAn require a lot of energy to maintain their axons, an imbalance of energy could affect their susceptibility to death (Pissadaki and Bolam, 2013). Nevertheless, the role that ageing has in the development of the disease, is not yet fully understood. Thus, it is fundamental to keep investigating the implications that ageing has on SNpc DAn.

A basic approach to characterize patterns of neurodegeneration in various conditions is to quantify the presence of DAn in the SNpc (Nelson *et al.*, 1996; McRitchie *et al.*, 1997; Damier *et al.*, 1999; Chu *et al.*, 2002; McCormack *et al.*, 2004; Collier *et al.*, 2007; Kanaan *et al.*, 2007; Nair-Roberts *et al.*, 2008), and analyse possible differences in the number of these neurons in physiological conditions *versus* PD (McRitchie *et al*., 1995; Damier *et al*., 1999; Ma *et al*., 1999; Kordower *et al*., 2013) and the aged brain (Fearnley and Lees, 1991; Ma *et al*., 1999; Cabello *et al*., 2002; Rudow *et al*., 2008; Buchman *et al.*, 2012; Di Lorenzo *et al*., 2016) (see General introduction). However, other methods, such as the study of the morphology of cells (Ma *et al*., 1999; Cabello *et al*., 2002; Rudow *et al*., 2008; Sanchez *et al*., 2008; Werner *et al*., 2008; Di Lorenzo *et al*., 2016) and modifications in the expression of proteins in the SNpc (Basso *et al*., 2004; Kasap *et al*., 2017) have been essential to providing new insights into the similarities between ageing and PD.

The analysis of the rat SNpc proteome using a quantitative proteomics assessment presented in this Thesis (see Chapter 3) allowed the study of the proteome of this area with ageing, identifying changes related to glial cells and the ECM. However, the protein

expression of TH, the enzyme implicated in the synthesis of dopamine and, therefore, a marker for DAn, was unchanged during ageing in rats in the SNpc. This result, however, did not fully probe alterations of SNpc DAn in the aged brain. For instance, it could be possible that a reduction in the number of SNpc DAn is compensated for by an increased expression of TH in the neurons that have not degenerated. This scenario would produce the same amount of TH in the SNpc and might be interpreted as no differences in the DAn population with proteomics results alone. Due to this, a fundamental approach was adopted to discover whether there were any gross morphological or numerical changes in DAn during ageing and if those changes (if any) could be involved in the increased vulnerability if these neurons.

4.1.1 Aim and objectives

The aim of this study was to understand if there were fundamental alterations in DAn (e.g., number of cells, soma size and shape) during ageing, that would not be possible to detect using proteomics and Western blotting analyses alone.

To this end, the number (density) and morphology (area of the soma) of DAn in the rat SNpc were analyzed at different ages to determine whether changes in these variables occur as ageing progressed. This analysis was performed either in the dorsal tier or lateral tier of the SNpc (see **Figure 2.3** in Chapter 2). Moreover, because the shape of the SNpc changes along its rostro-caudal axis (see Discussion), analysis on the nuclei was conducted using three rostro-caudal locations (rostral, middle and caudal). In this chapter, I will first present two main sets of results for the analysis of the rat SNpc, with information on whether there is a change in the density and soma size of DAn from the dorsal tier or the lateral tier of the SNpc. For each tier (dorsal and lateral), I will show the modifications that exist between the rostral, middle and caudal part, without considering an effect of ageing (i.e., whether there are differences within an age group). Afterwards, I will describe how these three areas change with ageing (e.g., how the rostral part

changes between the juvenile, young, middle age and old group). Lastly, I will pool the three rostro-caudal areas together to see if there are modifications of each tier (i.e., the dorsal and lateral as a whole) as ageing progresses (e.g., comparing the entire dorsal SNpc between the juvenile, young, middle age and old group).

Moreover, I will also conduct similar quantifications in human DAn in *post-mortem* tissue taken at different ages to determine if there are similar effects of ageing across species. However, it should be noted that the data generated with the human tissue was very limited due to the lack of access to samples with a substantially different age range.

On this basis, the objective of this study was:

- Objective 1) To determine if there are changes in the number of DAn in both rat and human SNpc at different ages by immunohistochemistry analysis.
- Objective 2) To determine if there were changes in the morphology of DAn in rats by immunohistochemistry analysis.

4.2 Materials and methods

Details about materials and methods of this experimental chapter can be found in Chapter 2, section 2.1.

4.3 Results

4.3.1 The rat midbrain increases significantly in size with ageing

Because possible modifications in the SNpc (density and soma size of DAn) can be produced by modifications in the whole brain, the size or area of the left midbrain (in mm^2), where the SNpc is located, was measured. As might be expected, the midbrain (*n=8-9* per group) from juvenile rats (12.54 ± 1.47) were statistically different from all the the adult ages (young, 17.42 ± 1.61; middle age, 17.56 ± 1.28; old, 18.20 ± 1.44; $p<0.0001$) (**Figure 4.1**). Specifically, the midbrain increased in size up to 39%, 40% and

45% when comparing the juvenile age to the young, middle age and old age, respectively. When the midbrain from adult individuals were compared, only the young (17.42 ± 1.61) and old hemispheres (18.20 ± 1.44) showed significant differences (p=0.0444), with an increase of 4% as ageing progressed.

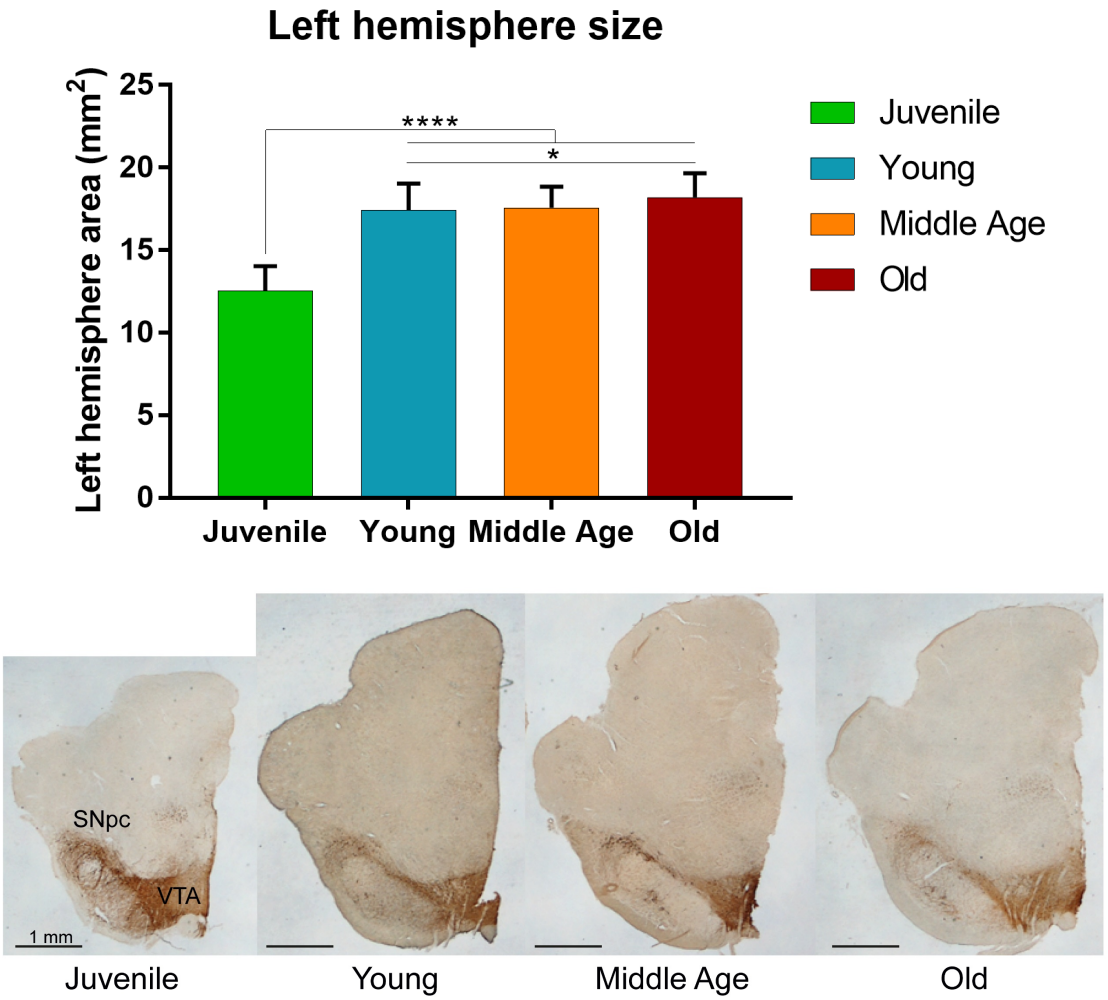

Figure 4.1. The size of the midbrain increases with ageing. The midbrain region, where DAn (TH-positive in image) are located within the SNpc and VTA, showed a statistically significant increase in area (mm^2) from juvenile to adult (young, middle age and old) (39%, 40% and 45%, respectively; p<0.0001), but also an increase of 4% between young and old samples (p=0.0444). Error bars represent standard deviation. *p<0.05; ****p<0.0001.

4.3.2 Analyses of the dorsal SNpc of rats

4.3.2.1 The density of DAn, but not area of the soma, changes rostro-caudally in the dorsal tier of the SNpc in rats when the effect of ageing is not considered

The density (number of DAn / area of the SNpc in mm^2) and the area of the soma (in μm^2) of DAn may differ along the rostro-caudal axis of the SNpc. Thus, before establishing if ageing has an impact in the degeneration of the dorsal tier of the SNpc DAn, the density and area of the soma of DAn was quantified in the rostral, middle and caudal part of dorsal tier of the SNpc independently in each group age. This allowed for a study of, for example, whether these cellular features changed in the rostral, middle part and caudal parts of the SNpc in the juvenile age, and whether this was the same with the other ageing groups.

Measurement of the density (number of DAn / area of the SNpc in mm^2) of DAn in the dorsal tier of the SNpc from the juvenile group revealed that the rostral (662 ± 36) compared to middle (928 ± 228) or caudal (507 ± 134) parts showed no statistical differences in any of the comparisons ($p=0.2888$; $p=0.9372$, respectively). However, quantification of the density of DAn in the middle (928 ± 228) *versus* the caudal (507 ± 134) region showed significant differences ($p<0.0001$) between them, with a decrease of 45% from the middle to the caudal region (**Figure 4.2A**). A similar situation appeared in the young group, where the density of DAn in rostral (490 ± 172) *versus* middle (490 ± 157) or caudal (324 ± 116) areas were not statistically significant ($p>0.9999$; $p=0.0556$, respectively); although the density of DAn from the middle (490 ± 157) to the caudal (324 ± 116) region were significantly different ($p=0.0353$), decreasing 33% in the most caudal part of the dorsal tier of the SNpc (**Figure 4.2B**). Quantifications of DAn in the middle age group indicated that the density in rostral (333 ± 99) compared to the middle (317 ± 100) or caudal (171 ± 70) parts were not statistically different ($p>0.999$; $p=0.1301$, respectively). Even when the density from the middle (317 ± 99) was compared to the caudal (171 ± 70) region no statistical differences ($p=0.0911$) appeared (**Figure 4.2C**). Lastly, the density of DAn in the old group from the rostral (403 ± 130) *versus* the middle

(372 ± 151) or caudal (229 ± 90) parts showed no statistically differences (p>0.9999; p=0.1040, respectively); although the density from middle (372 ± 151) to caudal (229 ± 90) regions was significantly different (p=0.0115), decreasing up to 38% in the caudal region (**Figure 4.2D**).

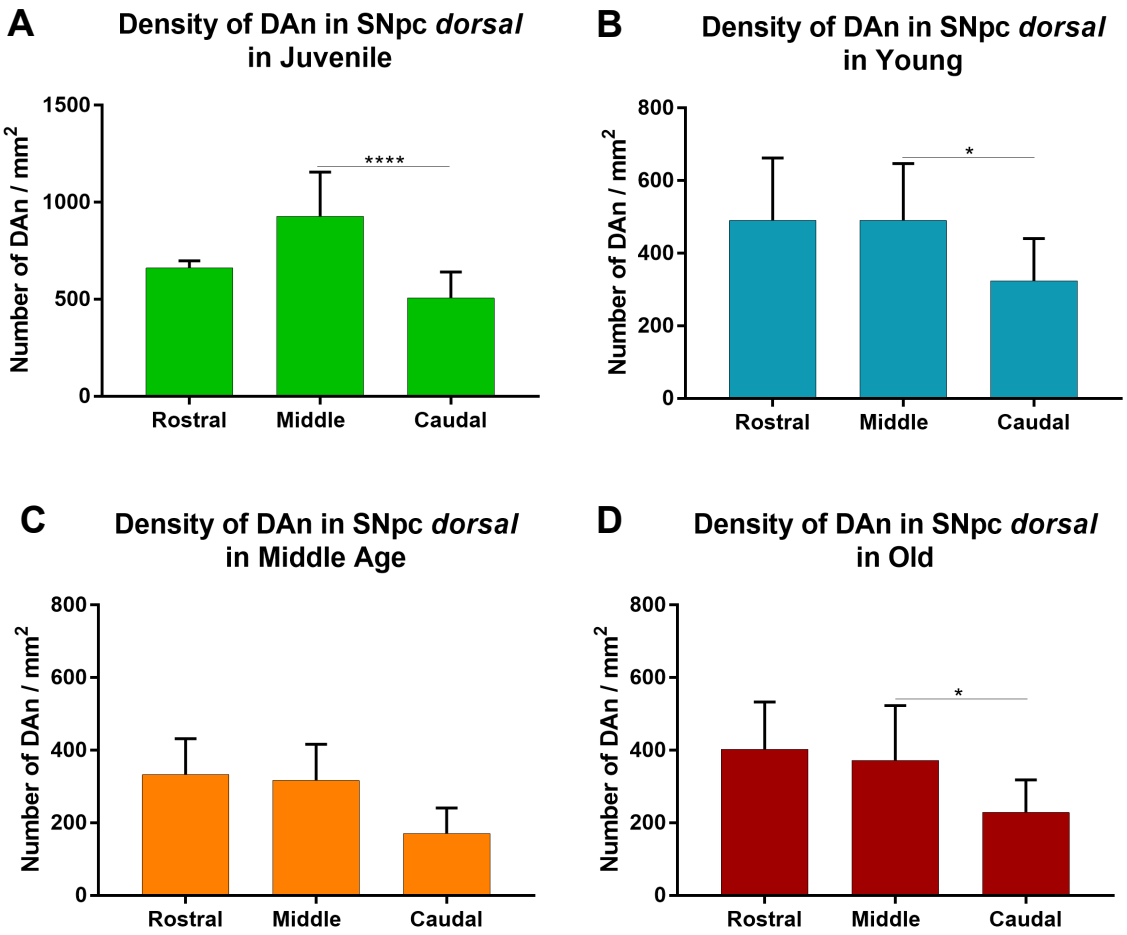

Figure 4.2. The density of DAn changes rostro-caudally in all ages, except in the middle age group. Rostro-caudal quantifications of the density (number of DAn / area of the SNpc in mm^2) of DAn in dorsal tier of the SNpc in rats independently in each group of age showed a significant reduction between the middle and caudal part in juvenile **(A)**, young **(B)** and old **(D)** of 45%, 33% and 38%, respectively, except in the middle age group **(C)**. Notice the difference scale in the juvenile group. Error bars represent standard deviation. *p<0.05; ****p<0.0001.

On the other hand, measurements of the area (in μm^2) of DAn cell body in the juvenile group demonstrated that DAn somas from the rostral (277.86 ± 11.69) *versus* the middle

(232.60 ± 39.11) or caudal (262.41 ± 30.87) parts did not show a significant change (p=0.9455; p>0.9999, respectively); nor when the middle (232.60 ± 39.11) *versus* the caudal (262.41 ± 30.87) region was compared (p=0.6188) (**Figure 4.3A**). When the area of DAn was analyzed in the young age group, a similar trend appeared. From the rostral (195.52 ± 31.93) to the middle (185.78 ± 26.77) or caudal (170.77 ± 24.46) parts, the area of DAn did not change significantly (p>0.9999; p=0.8958, respectively); as was the case when the area of DAn from middle (185.78 ± 26.77) to caudal (170.77 ± 24.46) regions were compared (p=0.9967) (**Figure 4.3B**). The soma of DAn from the middle

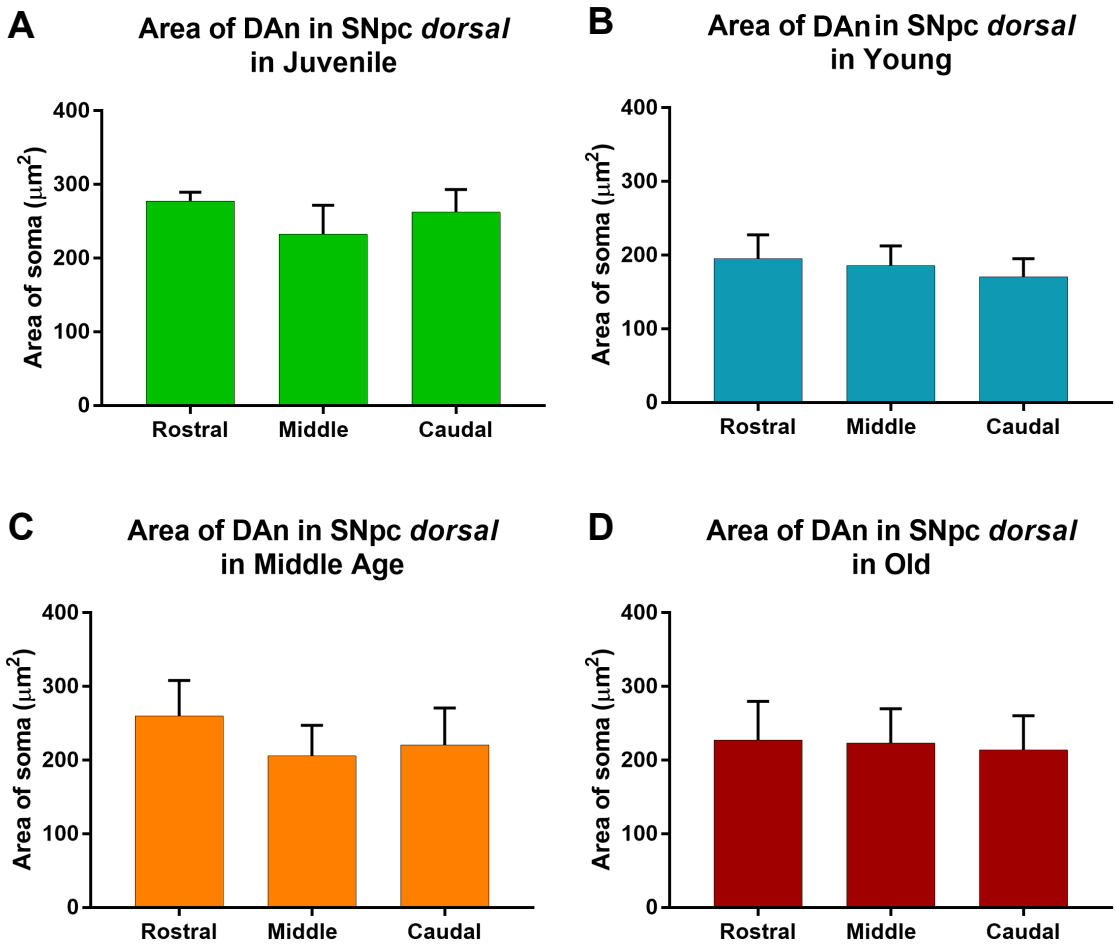

Figure 4.3. The area of the soma of DAn does not change rostro-caudally in any of the age groups. Rostro-caudal quantifications of the area of the cell body (in μm^2) of DAn in the dorsal tier of the SNpc in rats independently in each group of age showed no significant changes between the rostral, middle and caudal region in the juvenile **(A)**, young **(B)**, middle age **(C)** and old **(D)**. Error bars represent standard deviation.

age had a similar size from the rostral (260.24 ± 47.94) to the middle (205.87 ± 41.26) or caudal (220.79 ± 49.88) areas, with no statistical differences between them (p=0.0500; p=0.4092, respectively); or from the middle (205.87 ± 41.26) to the caudal (220.79 ± 49.88) region (220.79 ± 49.88) (p=0.9960) (**Figure 4.3C**).

Finally, the rostro-caudal study of the area of DAn cell bodies in old animals revealed that the size of neurons in the rostral (227 ± 52.46) compared to medial (223.24 ± 46.66) or caudal (213.71 ± 46.43) regions was not significantly different (p>0.9999; p=0.9954, respectively). No differences were found either from the medial to caudal (p=0.9998) region in the old SNpc (**Figure 4.3D**).

4.3.2.2 Ageing in rats decreases the density of DAn in some rostro-caudal regions of the dorsal tier of the SNpc, and increases the soma size in the caudal region

In the previous section, it was demonstrated that the density of DAn changed rostro-caudally when the middle part of the dorsal tier of the SNpc was compared to the caudal part in all ages except the middle age group (**Figure 4.2**). On the other hand, the area of the soma of DAn did not show significant changes rostro-caudally (**Figure 4.3).** This new section will explore the effect that ageing has in the density and area of the soma of DAn in the different rostro-caudal regions (i.e., rostral, middle or caudal) from the dorsal tier of the SNpc. For instance, the rostral region from the dorsal tier of the SNpc will be compared between the four age groups, and the same will be done for the middle and caudal part.

The density (number of DAn / area of the SNpc in mm^2) of DAn in the rostral part in juvenile (662 ± 36) and middle age (333 ± 99), showed significant differences (p=0.0243), with a reduction of 49% in the number of DAn within the dorsal tier of the SNpc as age increased (**Figure 4.4A**). In the case of the middle region, the density of DAn in juveniles (928 ± 228) compared to young (490 ± 157), middle age (317 ± 99) and old (372 ± 151) rats showed significant differences (p<0.0001), with a 47%, 66%, and

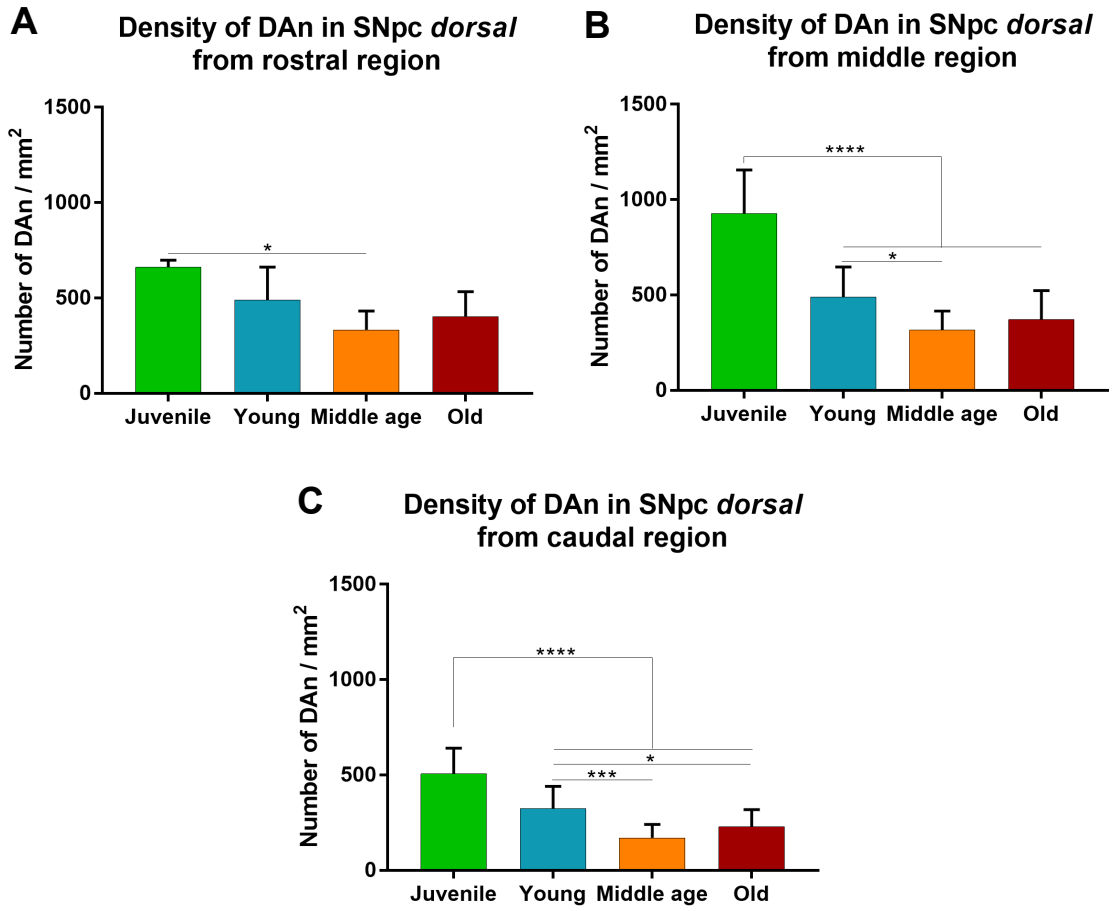

Figure 4.4 The density of DAn changes in each rostro-caudal region with ageing. Quantifications of the density (number of DAn / area of the SNpc in mm^2) of DAn in the dorsal tier of the SNpc in rats independently in each rostro-caudal region showed a significant reduction in the rostral region **(A)** only from the juvenile to middle age group by 49%. The density of DAn in the middle region **(B)** decreases from juvenile to adult ages by 47% (young), 66% (middle age) and 60% (old); and between young and middle ages by 35%. Lastly, the density in the caudal region **(C)** was reduced by 36% in the case of young, 66% for middle age, and 54% in old compared to juvenile; while the middle age and old group have a depletion in the density of 47% and 29%, respectively, from the young age. Error bars represent standard deviation. *p<0.05; ***p<0.001; ****p<0.0001.

60% depletion of DAn from the juvenile to the oldest ages, respectively. In addition, the density of DAn in the middle part in young (490 ± 157) *versus* the middle age (317 ± 99) was significantly different (p=0.0350), having a 35% reduction in the density of DAn from young to middle age (**Figure 4.4B**). Lastly, when the density of DAn from the caudal part was compared between ages, juvenile (507 ± 134) compared to the young (324 ± 116),

middle age (171 ± 70) and old (229 ± 90) groups were statistically different ($p<0.0001$), with the density of DAn being reduced by 36%, 66% and 54%, respectively. In line with this, the young (324 ± 116) group *versus* the middle age (171 ± 70) and old (229 ± 90) showed significant differences ($p=0.0004$; $p=0.0357$, respectively), indicating a reduction of the density of DAn from young individuals by 47% in middle age and 29% in old (**Figure 4.4C)**.

Measurements of the cell size (in μm^2) of DAn in the rostral region with ageing in juvenile (277.86 ± 11.69) *versus* young (195.52 ± 31.93), middle age (260.24 ± 47.94) or old (227 ± 52.46) groups showed no statistical differences ($p=0.9144$; ; $p=0.4162$; $p=0.5398$, respectively) between them. Similarly, when adult ages were compared, the rostral region from young (195.52 ± 31.93) *versus* middle age (260.24 ± 47.94), young *versus* old (227 ± 52.46), or middle age *versus* old, revealed no significant changes ($p=0.0621$, $p=0.0875$, $p=0.9870$ respectively) in the size of DAn (**Figure 4.5A**). Furthermore, analysis of the area of the soma of DAn in the middle part of the dorsal tier of the SNpc showed that the soma in juvenile (232.60 ± 39.11) and young (185.78 ± 26.77) were significantly different in size ($p=0.0112$), with a decrease of 20% of the soma size as ageing progressed from juvenile to young (**Figure 4.5B**). Finally, the size of DAn in the caudal part of the dorsal tier of the SNpc in the juvenile (262.41 ± 30.87) age *versus* young (170.77 ± 24.46) and middle age (220.79 ± 49.88) decreased significantly ($p<0.0001$) by 34% and 21%, respectively. The size of DAn in the caudal part of juvenile (262.41 ± 30.87) and old (213.71 ± 46.43) also changed significantly ($p=0.0002$), showing a decrease of 18% in the density of DAn in the oldest animals. When the area of the cell bodies of DAn in the caudal part where compared within the adult individuals, the young (170.77 ± 24.46) and the old (213.71 ± 46.43) ages revealed significant changes ($p=0.0081$), with an increase of 19% as ageing progressed (**Figure 4.5C**).

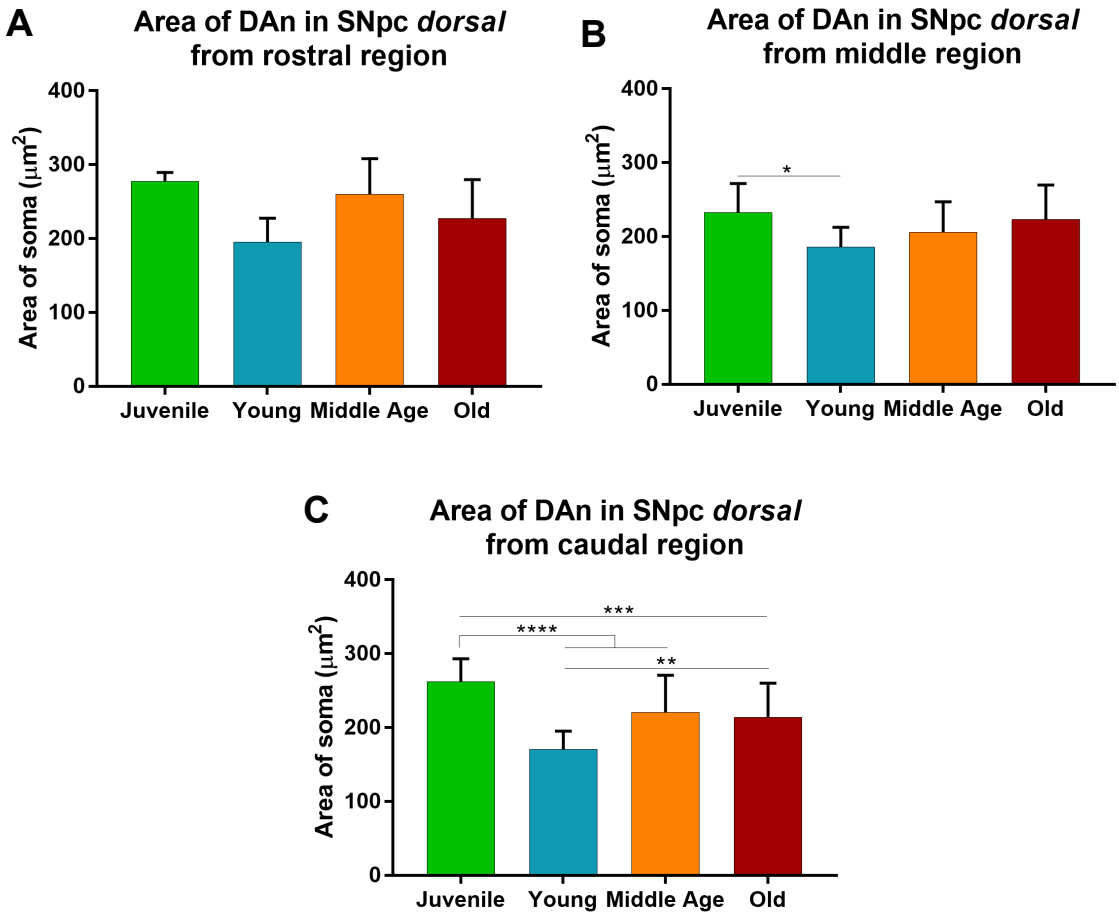

Figure 4.5 The area of the soma of DAn changes in the middle and caudal region during ageing. Quantifications of the area of the soma (in µm^2) of DAn in the dorsal tier of the SNpc in rats independent of age showed no significant differences in the rostral region **(A).** However, ageing had an effect in the middle **(B)** and caudal part **(C)**. Thus, there was a 20% decrease in the size of the soma between juvenile *versus* young ages in the middle part of the dorsal SNpc. The caudal area showed a significant decrease from juvenile to young (34%), middle age (21%) and old (18%), but also an increase of the size within the adult groups between the young and middle age (19%). Error bars represent standard deviation. *p<0.05; **p<0.01; ***p<0.001; ****p<0.0001.

4.3.2.3 The density of DAn in the whole dorsal tier of the SNpc decreases with ageing in rats, while the soma size of DAn increases

To understand if the entire dorsal tier of the SNpc was losing DAn and if there were modifications in the soma of these neurons with ageing, the different rostro-caudal regions (i.e., rostral, middle and caudal) were grouped together and the effect of ageing

analyzed. When the entire dorsal tier of the SNpc was grouped together (i.e., pooling the rostral, middle and caudal regions) to see the effect that ageing had, the density (number of DAn / area of the SNpc in mm^2) of DAn in the juvenile group (711 ± 281) compared to the young (413 ± 169), middle age (264 ± 117), and old (325 ± 148) was statistically different ($p<0.0001$). Thus, there was a decrease of density of DAn in the dorsal tier of the SNpc from the juvenile age by 42%, 63% and 54% in the young, middle age and old individuals, respectively. Moreover, measurements of the density of DAn in the dorsal tier of the SNpc in young (413 ± 169) *versus* middle age (264 ± 117) showed changes that were statistically significant ($p=0.0009$), with a reduction of the density with advanced ageing from young to middle age (**Figure 4.6**).

When the area of the soma (in μm^2) of DAn from the entire dorsal tier of the SNpc was analysed, the juvenile group (223 ± 42.94) compared to young (164 ± 35.89), middle age (198.3 ± 51.85), and old (201. ± 50.53) showed significant changes ($p<0.0001$; $p=0.0083$; $p=0.0160$, respectively) in relation to ageing. This represents a reduction of the cell size by 26%, 11% and 10% from the juvenile group compared to young, middle age and old individuals. When comparing adult samples alone, the area of the soma of DAn in young (164 ± 35.89) *versus* middle age rats (198.3 ± 51.85) and old (201. ± 50.53) was significantly different ($p<0.0001$), with an increase in the size of 21% and 23% from young to middle and old animals, respectively. However, from middle age (198.3 ± 51.85) to old (201. ± 50.53) there was no statistical differences ($p=0.9824$) in the size of the soma (**Figure 4.7**).

4.3.3 Analyses of the lateral SNpc of rats

4.3.3.1 Density of DAn increases from middle to caudal in the lateral tier of the SNpc in rats, while the soma size remains the same without considering the effect of ageing

Similar to the histological study of the dorsal tier of the SNpc (above), quantification and statistical analyses of DAn within the lateral tier of the SNpc were conducted to

understand if the density (number of DAn / area of the SNpc in mm^2) and size of the soma (in μm^2) of DAn changed in the rostro-caudal axis from the medial to the caudal part without the effect of ageing, but within each age group.

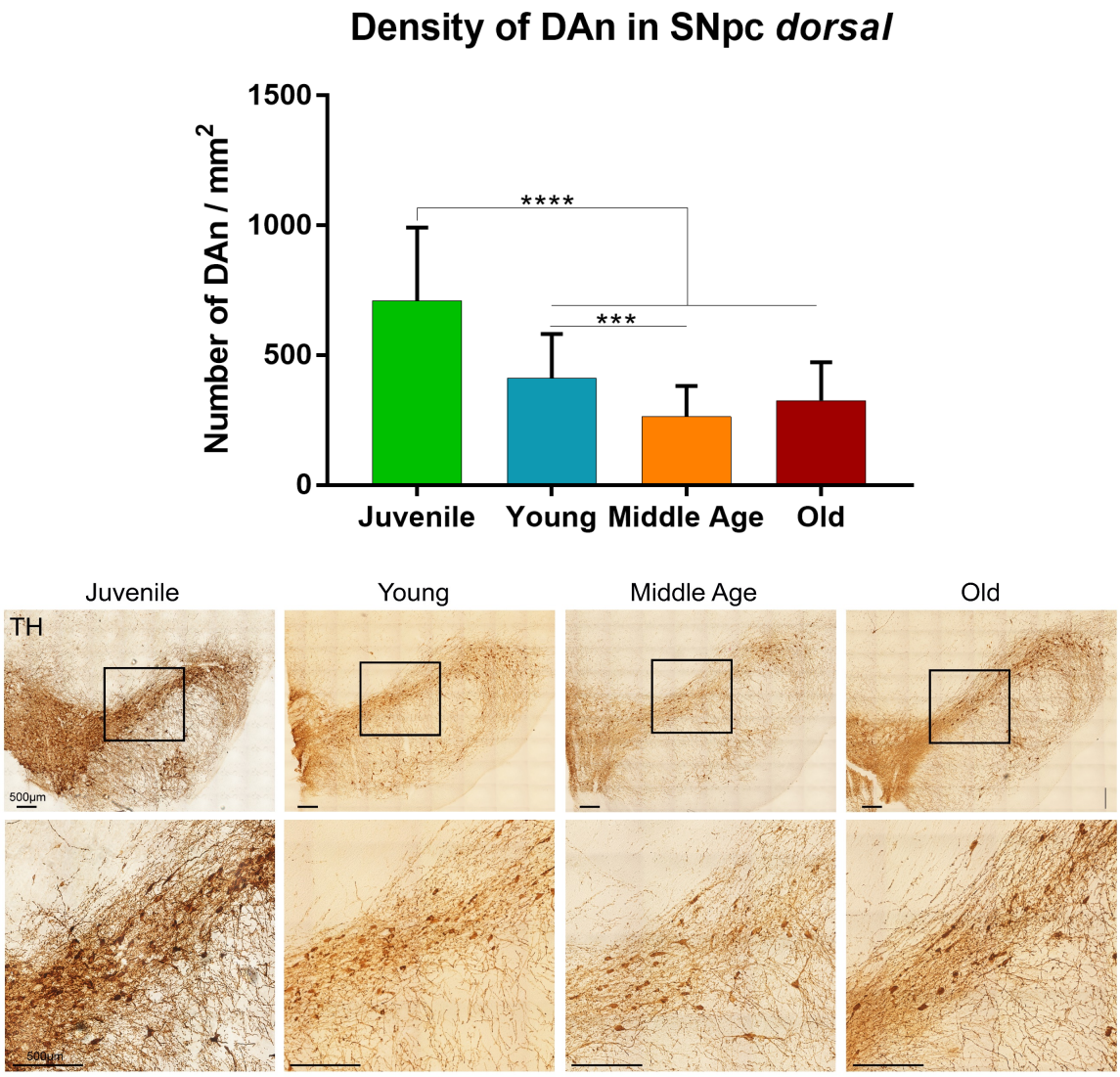

Figure 4.6. The density of the whole dorsal tier of the SNpc is reduced with ageing in rats. The number of DAn decreased from the juvenile age to the adult ages by 42% (young), 63% (middle age) and 54% (old). Within adults, there is only a significant decrease of the density from young to middle age by 36%. Error bars represent standard deviation. *p<0.05; ***p<0.001; ****p<0.0001. TH-positive staining of DAn in the SNpc nuclei of rat transversal sections in each age group (top images). High magnification photomicrographs (bottom images) show more detail of the DAn.

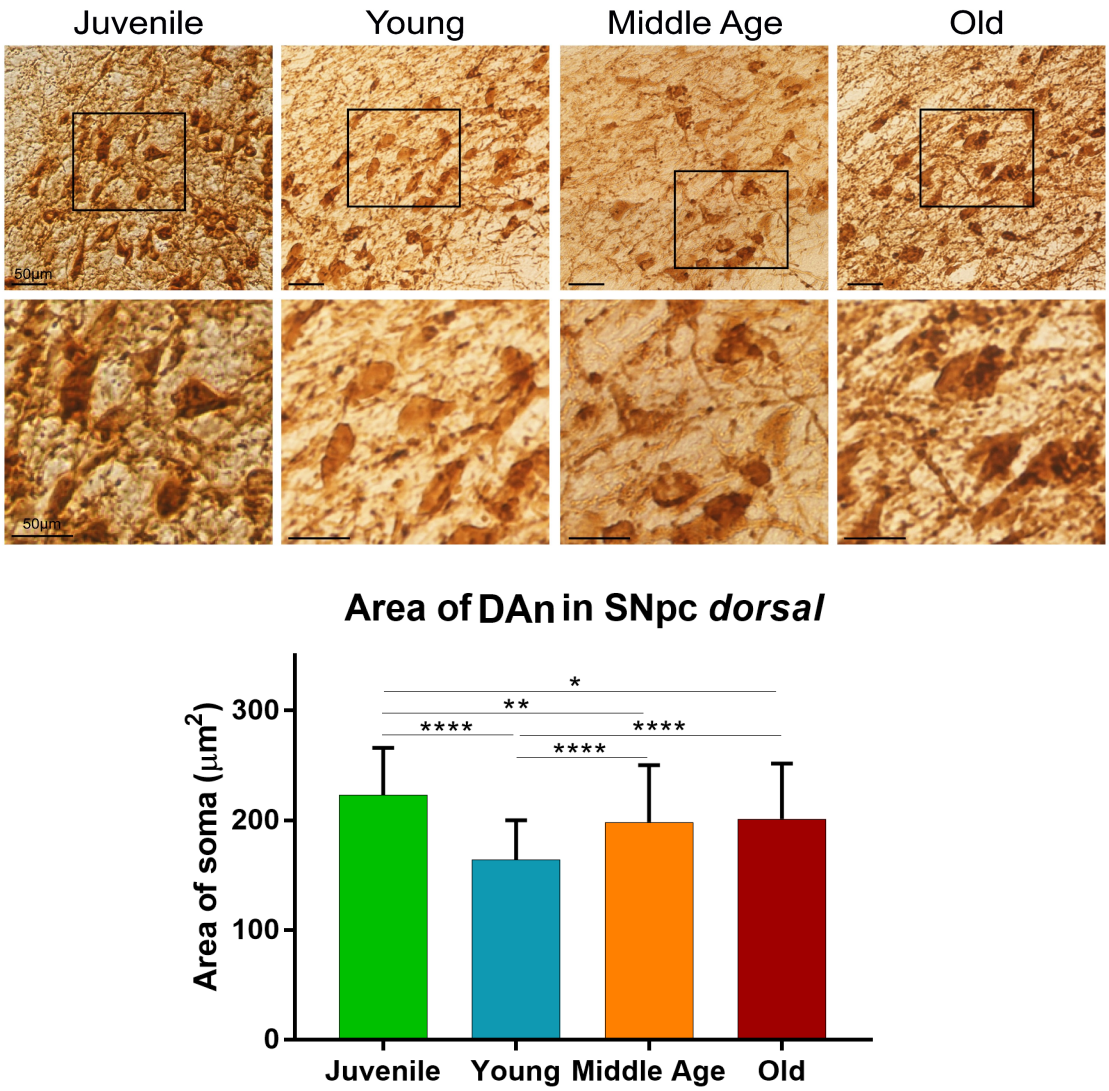

Figure 4.7. The area of the soma of DAn is reduced from juvenile to adult individuals, but increases in the adult groups with ageing. Measurements of the area of the soma of DAn in the dorsal tier of the SNpc at different ages in rats showed a reduction of their soma from juvenile to the young, middle age and old age groups by 26%, 11% and 23%, respectively. On the other hand, within the adult populations, the area of the soma increases from young to middle age and old by 21% and 23%, respectively. Error bars represent standard deviation. *p<0.05; **p<0.01; ****p<0.0001. TH-positive staining of DAn in the SNpc nuclei of rat transversal sections in each age group (top images). High magnification photomicrographs (bottom images) show more detail of the DAn.

Quantifications of the density (number of DAn / area of the SNpc in mm^2) of DAn in the lateral tier of the SNpc in the juvenile group showed that the middle (7 ± 1) *versus* caudal

(12 ± 4) regions did not have statistical differences (p=0.9410) (**Figure 4.8A**). However, measurements of the density of DAn in the lateral tier of the SNpc in the young group revealed that from the middle (5 ± 1) to the caudal (8 ± 2) area the density varied significantly (p=0.0485), increasing by 60% in the most caudal part (**Figure 4.8B**). In the case of the middle age group, the number of DAn within the lateral tier of the SNpc changed from middle (4 ± 1) to caudal (6 ± 2), although this change in density was not significant (p=0.5010) (**Figure 4.8C**). Lastly, the density of DAn in the lateral tier of the

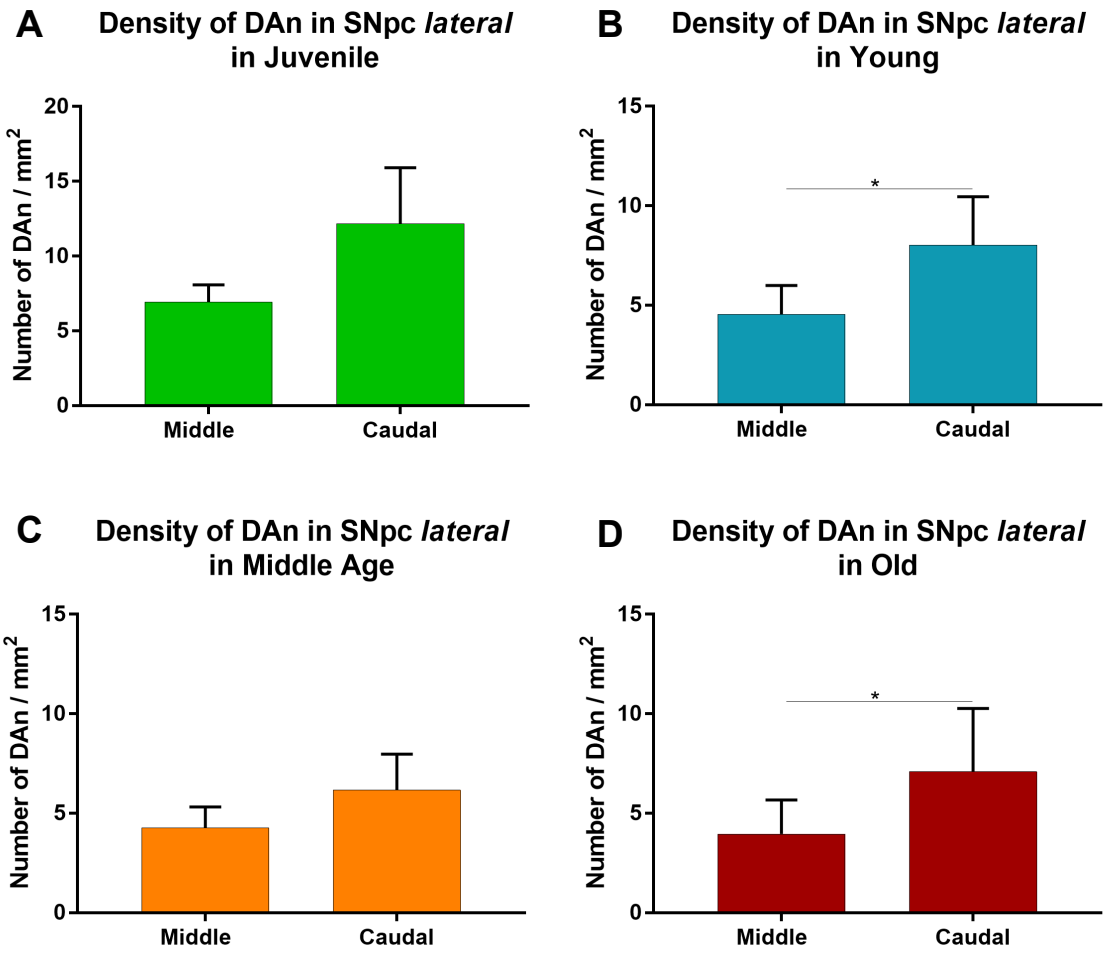

Figure 4.8. The density of DAn in young and old animals increases significantly between the middle and caudal regions of the lateral tier of the SNpc. Rostro-caudal quantifications of the density (number of DAn / area of the SNpc in mm^2) of DAn in the lateral tier of the SNpc in rats in each age group independently showed a significant increase between the middle and caudal part in young **(B)** and old **(D)** by 60% and 75%, respectively, but not in the juvenile **(A)** and middle age group **(C)**. Notice the difference scale in the juvenile group. Error bars represent standard deviation. *p<0.05.

SNpc in old animals changed significantly (p=0.0253) from middle (4 ± 2) to caudal (7 ± 3), with an increase of 75% in the caudal region (**Figure 4.8D**).

To determine if the size of the cell body (in μm^2) of DAn was modified within the different regions of the lateral tier of the SNpc, measurements of the area of the soma were performed. The results showed no statistically significant differences between the middle and caudal part in any of the four age groups (juvenile: middle 256.99 ± 53.17 *versus* caudal 269.57 ± 38.43, p=0.9697; young: middle 194.94 ± 48.68 *versus* caudal 188.26 ± 44.15, p>0.9991; middle age: middle 238.18 ± 46.46 *versus* caudal 213.05 ± 42.79, p=0.3976; old: middle 227.30 ± 51.52 *versus* caudal 226.00 ± 52.48, p>0.9999) (**Figure 4.9A, B, C, D**).

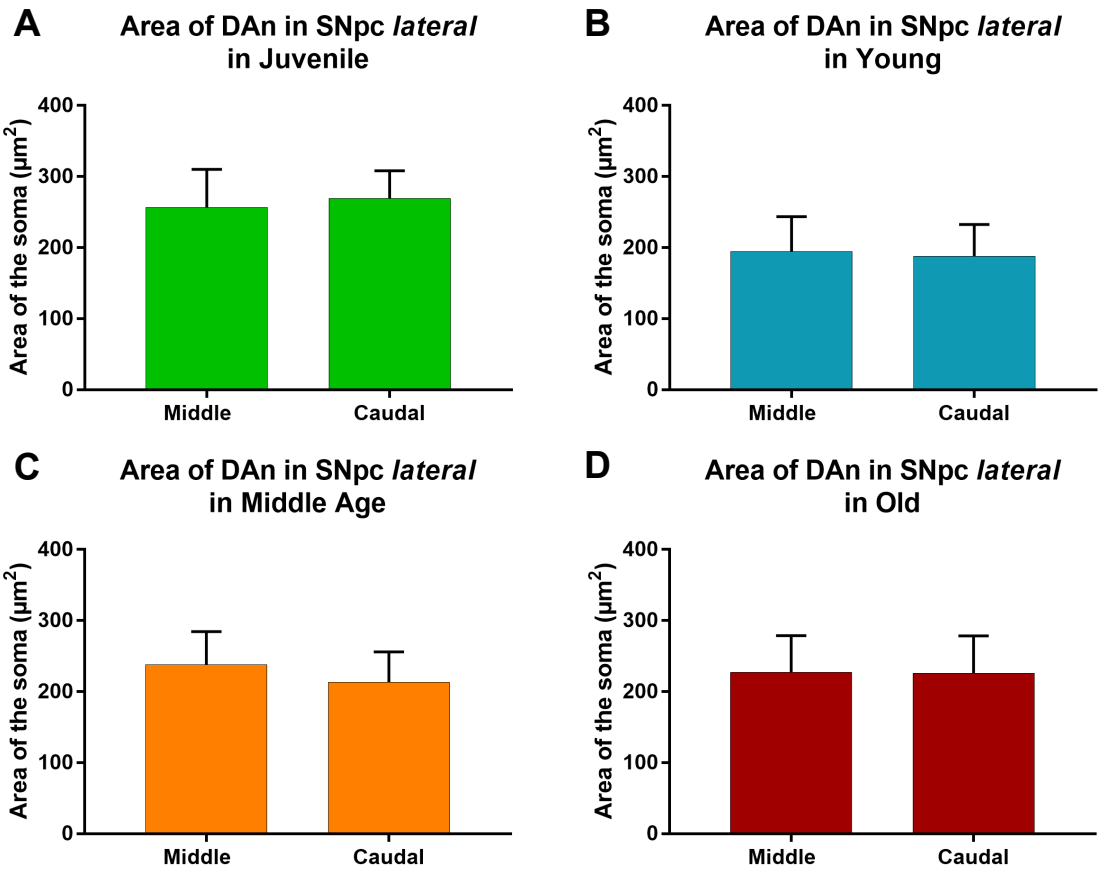

Figure 4.9. There are no statistical differences in the soma size in the lateral tier of the SNpc between the middle and caudal regions. Rostro-caudal quantifications of the area of the cell body (in μm^2) of DAn in SNpc lateral in rats in each age group independently showed no significant differences between the middle and caudal regions in the juvenile **(A)**, young **(B)**, middle age **(C)** and old **(D)**. Error bars represent standard deviation.

4.3.3.2 DAn change in density in the caudal part of the lateral tier of the SNpc in rats with ageing, while the soma size increases in both middle and caudal regions

To identify if the effect of ageing produces any modification in the middle or caudal part of the lateral tier of the SNpc, the density and soma size of DAn in each region was studied and compared between age groups.

Measurements of the density (number of DAn / area of the SNpc in mm^2) of DAn within the lateral tier of the SNpc showed that in the middle region the density of DAn in the juvenile (7 ± 1) age *versus* the other adult groups (young, 5 ± 1; middle age, 4 ± 1; old, 4 ± 2) was not significantly different (p=0.8340; p=0.3772; p =0.1791, respectively). When only adult ages were compared, the density of DAn from the lateral tier of the SNpc in the middle region from young (5 ± 1) to middle age (4 ± 1) or old (4 ± 2) did not show any significant modification (p>0.9999); and a similar scenario was found when the middle age was compared to the old group (p>0.9999) (**Figure 4.10A**). However, when the caudal part in the lateral tier of the SNpc was studied along ageing, the density of DAn in juvenile (12 ± 4) *versus* the young (8 ± 2), middle age (6 ± 2) and old (7 ± 3) revealed significant changes between them (p=0.0113; p<0.0001; p<0.0001, respectively); with a decrease in 35%, 58% and 51% of the number of neurons, respectively. In addition, the caudal region between adult ages (young *versus* middle age, young *versus* old, middle age *versus* old) did not show significant modifications in any of the comparisons (p=0.2434; p=0.9430; p=0.9356, respectively) **(Figure 4.10B).**

Analysis of the area (in μm^2) of DAn in the middle region of the lateral tier of the SNpc demonstrated that the juvenile (256.99 ± 53.17) *versus* the young (194.94 ± 48.68) age changed significantly (p=0.0001), finding a decrease of the area of the soma of DAn by 24% with ageing from juvenile to young. Alternatively, when the area of the soma was compared between the juvenile (256.99 ± 53.17) and the middle age (238.18 ± 46.46) or old (227.30 ± 51.52) group, no statistical differences (p=0.5309; p=0.0827, respectively) were found. Furthermore, soma size of DAn from the middle region in young (194.94 ± 48.68) compared to middle age (238.18 ± 46.46) or old (227.30 ± 51.52)

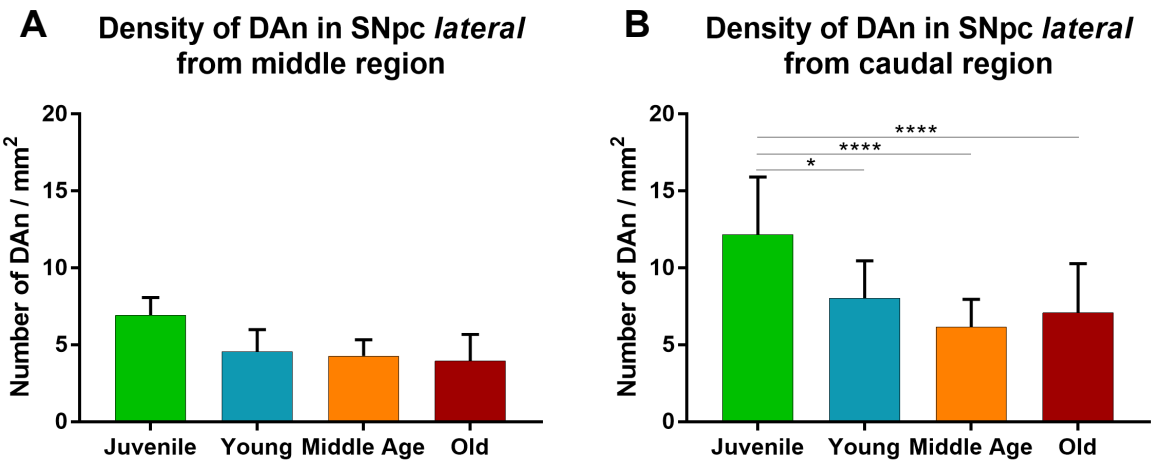

Figure 4.10. The density of DAn in the lateral tier of the SNpc is reduces in the caudal region with ageing. Rostro-caudal quantifications of the density (number of DAn / area of the SNpc in mm^2) of DAn in the lateral tier of the SNpc in rats in the middle **(A)** region showed no statistical changes. However, when the caudal **(B)** region was analysed, there was a significant decrease by 35%, 58% and 51% in the number of DAn from juvenile to young, middle age and old, respectively. Error bars represent standard deviation. *p<0.05; ****p<0.0001.

was significantly modified (p=0.0122; p=0.0488, respectively). Thus, there was an increase of 22% and 16% in the soma size during ageing from young to middle age and old, respectively. However, no significant changes were observed between middle age and old age (p=0.8158) (**Figure 4.11A**). Similarly, the area of DAn from the lateral tier of the SNpc in the caudal part, changed from juvenile (269.57 ± 38.43) to young (188.26 ± 44.15), middle age (213.05 ± 42.79) and old (226.00 ± 52.48) significantly (p<0.0001, p<0.0001, p=0.0026, respectively), decreasing by 30%, 21% and 16% as ageing occurs. In addition, the size of DAn from the caudal part in young (188.26 ± 44.15) *versus* the old (226.00 ± 52.48) age increased significantly (p=0.0070), with an expansion of 20% in their area when they became old; while from young to middle age (213.05 ± 42.79) and middle age to old (226.00 ± 52.48) the differences were not statistically significant (p=0.0606; p=0.6885, respectively) (**Figure 4.11B**).

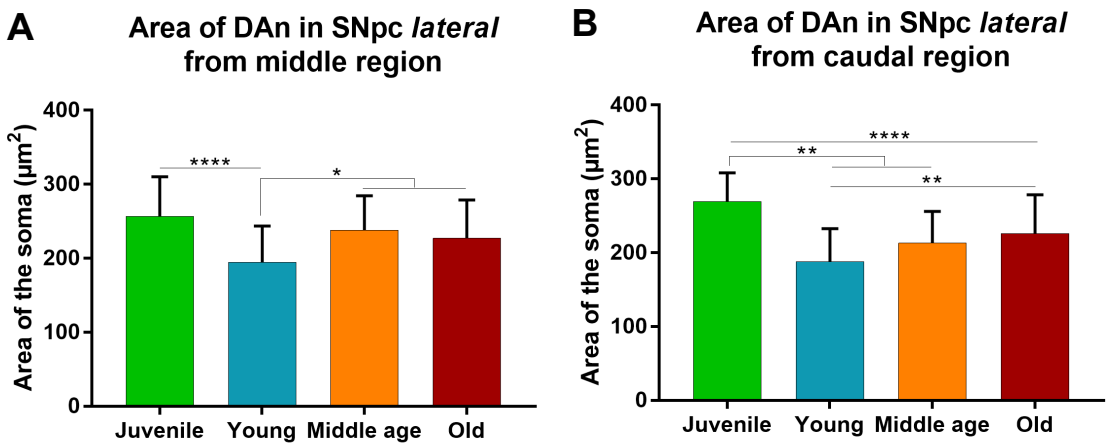

Figure 4.11. The size of the soma of DAn from the lateral tier of the SNpc changes in the middle and caudal region. Quantifications of the area of the soma (in μm^2) of DAn in the lateral tier of the SNpc in rats in the middle region **(A)** showed a decrease in their size by 24% at juvenile ages, but this was recovered afterwards with an increase of their area by 22% and 16% in middle and old ages, respectively. In addition, DAn soma size from the caudal **(B)** region in the lateral SNpc decreases from juvenile to young by 30%, to middle age by 21% and to old by 16%. Between adults, the soma in old aged animals were increased by 20% *versus* the young ages. Error bars represent standard deviation. *p<0.05; **p<0.01; ****p<0.0001.

4.3.3.3 The density of DAn in the lateral tier of the SNpc in rats decreases only between juvenile to adults ages, but the soma size of DAn collectively changes during ageing

Similar to the analysis of the dorsal tier of the SNpc (above), the entire lateral tier was analyzed, grouping the rostro-caudal regions together, to understand the effect of ageing in the density and soma size of DAn. Also, the juvenile group was subsequently excluded to identified changes only in adult stages.

Thus, the density of DAn from the whole lateral tier of the SNpc changed significantly from the juvenile (12 ± 4) age to young (7 ± 3), middle age (6 ± 2) and old (6 ± 3) groups (p=0.0020; p<0.0001; p<0.0001, respectively), with a decrease in the density of DAn by 36%, 54%, 53% from the juvenile to the rest of adult stages, respectively. When adult

ages were compared in isolation, the density of DAn in the entire lateral tier of the SNpc did not change significantly in any of the comparisons (young *versus* middle age, p=0.2935; young *versus* old, p=0.3673; middle age *versus* old, p>0.9999) **(Figure 4.12**).

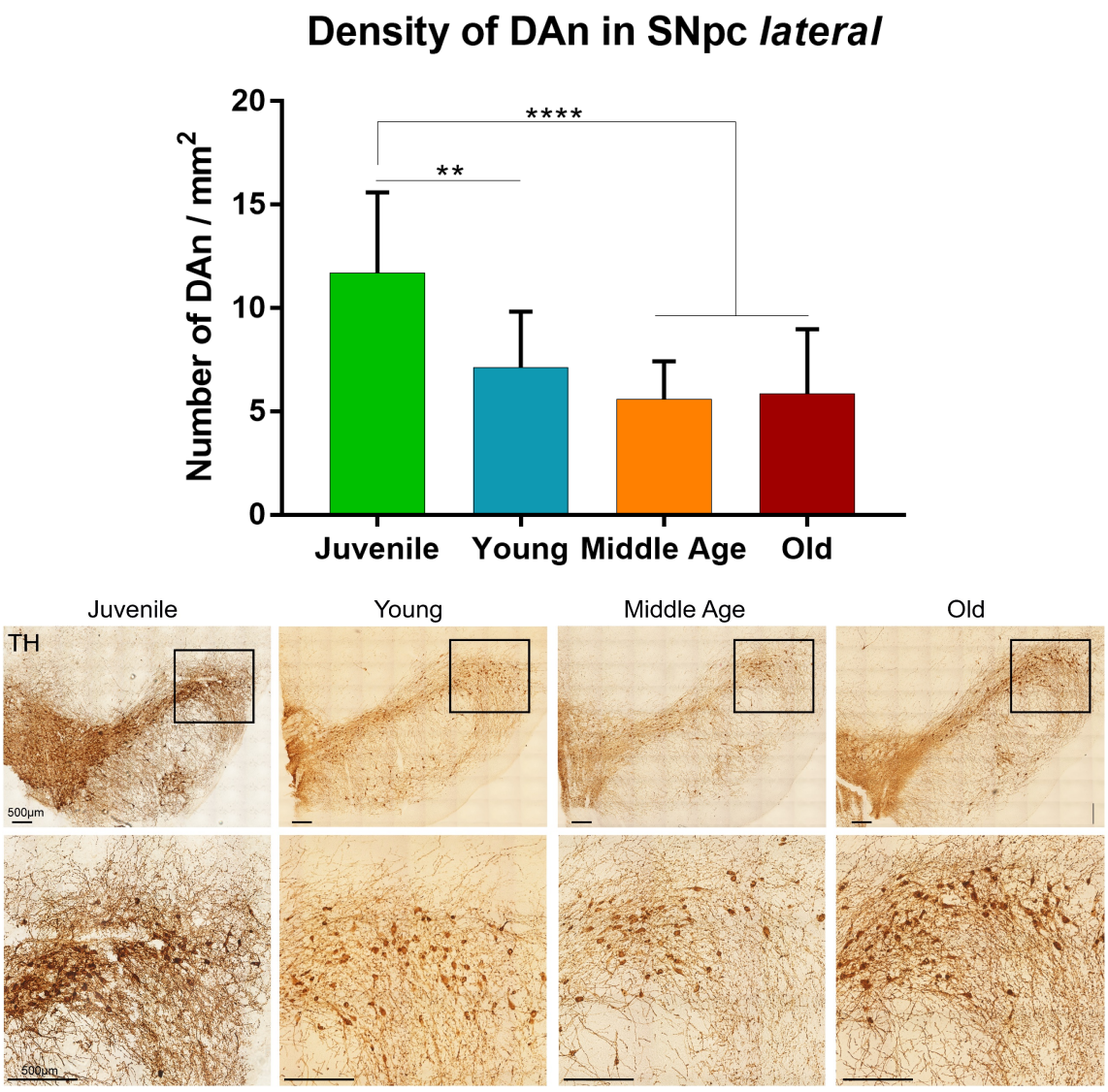

Figure 4.12. The density of the whole lateral tier of the SNpc is reduced with ageing in rats. The number of DAn decrease from the juvenile age to the young age by 36%, and to the middle age and old by 54% and 53%, respectively. Error bars represent standard deviation. **p<0.01; ****p<0.0001. TH-positive staining of DAn in the SNpc nuclei of rat transversal sections in each age group (top images). High magnification photomicrographs (bottom images) show more detail of the DAn.

Lastly, measurements of the soma of DAn of the entire lateral tier of the SNpc were compared across age groups. The size of the area of DAn in the lateral tier of the SNpc

in the juvenile (252.1 ± 52) group compared to young (196.9 ± 52.42), middle age (225.3 ± 51.68) and old (227.5 ± 52.83) animals was significantly different ($p<0.0001$; $p<0.0001$; $p=0.0018$, respectively), with a reduction in soma size by 22%, 11% and 10% during ageing from the juvenile age to the other adult ages. The area of DAn in the lateral tier of the SNpc from the young age (196.9 ± 52.42) to the middle age (225.3 ± 51.68) and old (227.5 ± 52.83) revealed significant modifications ($p<0.0001$; $p=0.0001$, respectively), expanding with ageing by 14% from young to middle age and by 16% from young to old. However, the area of the cell between the middle age and the old group were not statistically different ($p=0.9792$) (**Figure 4.13**).

4.3.4. A comparison of both tiers of SNpc shows the dorsal tier contains a higher density of DAn but with small somas compared to the lateral part

Comparisons of both density and soma size of DAn in the dorsal and lateral tier of SNpc revealed clear differences between these two areas along all ages.

First, the number of DAn in the dorsal tier (711 ± 281) *versus* the lateral tier (12 ± 4) changed significantly ($p<0.0001$) in the juvenile group, having a reduction by 98% of the density of cells in the lateral part. Similarly, the dorsal tier (413 ± 169) compared to the lateral tier (7 ± 3) was significantly different ($p<0.0001$), also showing a reduction by 98% of the density of DAn in the lateral part. In the middle age group, the dorsal tier (264 ± 117) presented a significantly higher density of DAn in comparison to the lateral tier (6 ± 2) part ($p<0.0001$) with a decrease of the density by 97% in the lateral area. Lastly, the dorsal tier (325 ± 148) in the old age *versus* the lateral tier (6 ± 3) was significant ($p<0.0001$) modified, with a 98% reduction in the density of DAn in the lateral part (**Figure 4.14A**).

Secondly, the soma size of DAn in the juvenile group changed between the dorsal (223 ± 42.94) and the lateral tier (252.1 ± 52) significantly ($p=0.0046$), with an increase of the area of 13% in the lateral tier. In line with this, the young group revealed the same

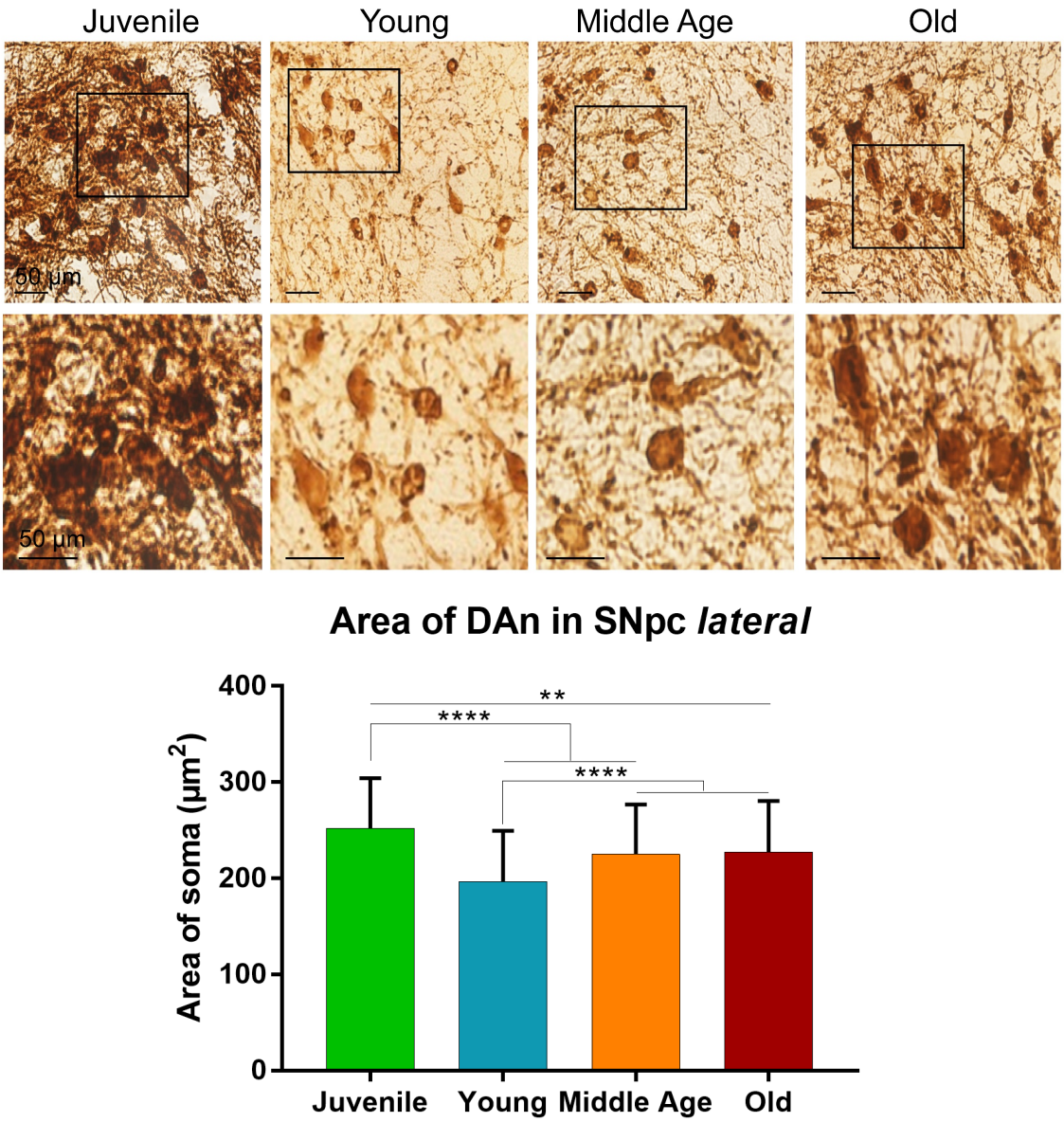

Figure 4.13. The area of the soma of DAn in the lateral tier of the SNpc is reduced from juvenile to adult individuals but increases in the adult groups with ageing. Measurements of the area of DAn in the lateral tier of the SNpc at different ages in rats revealed a reduction from juveniles to young (22%), middle age (11%) and old (11%). However, within the adult populations, the area of the soma increases from young to middle age and old by 14% and 16%, respectively. Error bars represent standard deviation. **p<0.001; ****p<0.0001. TH-positive staining of DAn in the SNpc nuclei of rat transversal sections in each age group (top images). High magnification photomicrographs (bottom images) show more detail of the DAn.

characteristics between the dorsal (164 ± 35.89) and lateral (196.9 ± 52.42) SNpc, showing a significant (p=0.0002) increase in the area of lateral DAn of 19 %. In the middle age, the soma of DAn in the dorsal tier (198.3 ± 51.85) of the nigra were different to the lateral tier (225.3 ± 51.68), being significantly bigger (p=0.0015) by 14% in the lateral tier of the SNpc. Finally, DAn from the dorsal (201. ± 50.53) SNpc in old animals compared to the lateral (227.5 ± 52.83) revealed significant (p=0.0038) differences in the soma size, being 13% bigger in the lateral tier (**Figure 4.14B**).

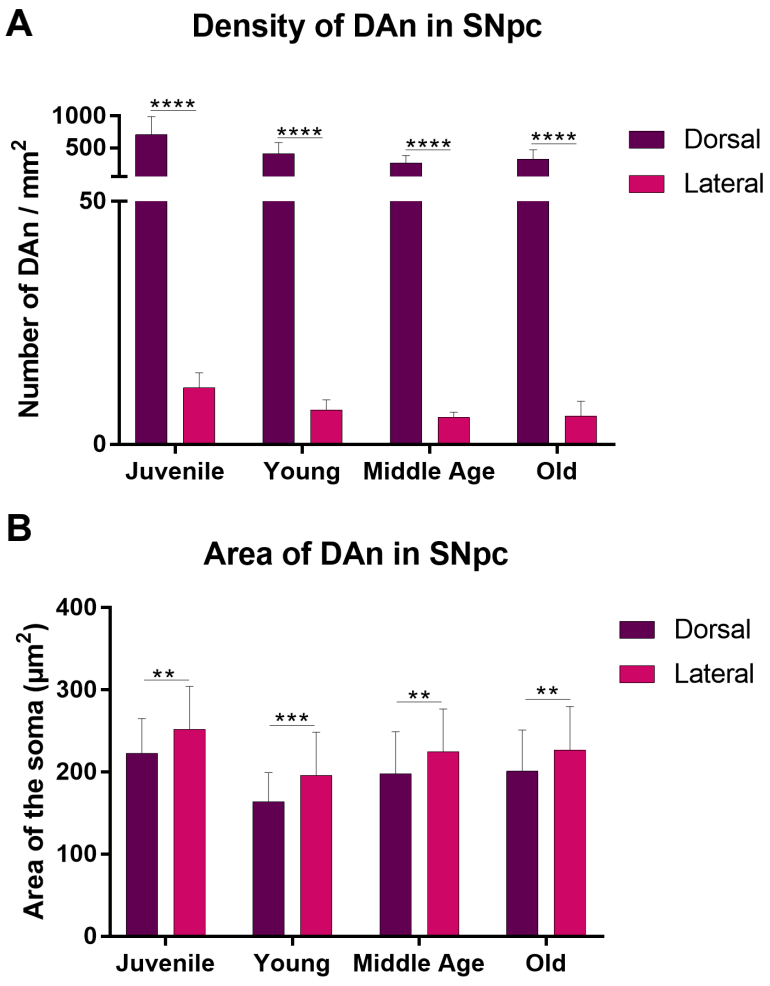

Figure 4.14. The density of DAn and their soma size are different between the dorsal and lateral tiers of the SNpc. (A) The density of DAn in the lateral part is significantly reduced compared to the dorsal tier in all age groups (juvenile, 98%; young, 98%; middle age, 97%; old, 98%). **(B)** In contrast, the area of the soma significantly increases in the lateral tier *versus* dorsal tier along all ages (juvenile, 13%; young, 19%; middle age, 14%; old, 13%). Error bars represent standard deviation. **p<0.01; ***p<0.001; ****p<0.0001.

4.3.5 There is no correlation between the density of DAn in the human SNpc and ageing using a limited sample of age range

In an attempt to determine if the density of DAn in the SNpc changed with ageing in humans, the number of DAn was quantified in fifteen brains from subjects aged between 50 and 109 years old. Afterwards, a linear regression analysis was performed, plotting each SNpc DAn density against the age of the individual where the SNpc comes from. The analysis showed that there was no significant correlation (r=0.2415, p=0.3859) between the density of DAn in the human SNpc and ageing (**Figure 4.15**).

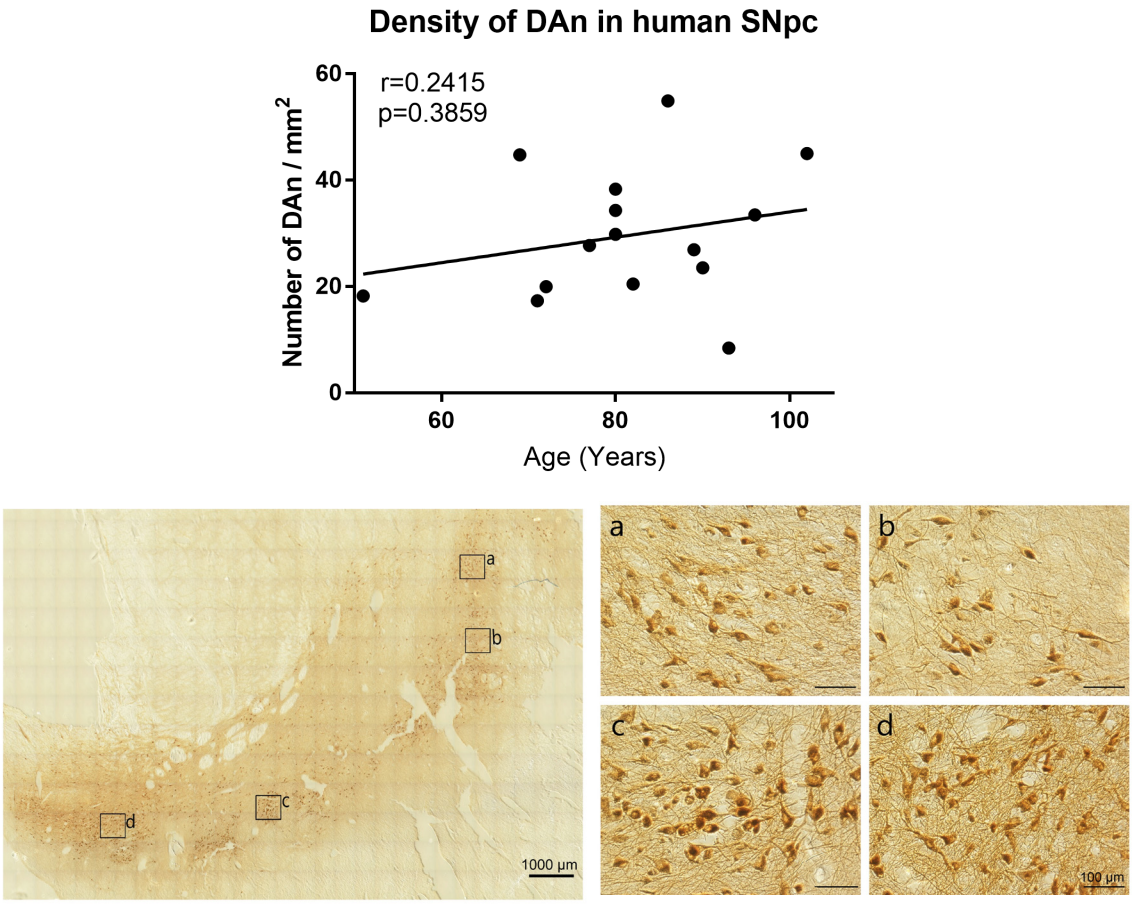

Figure 4.15. There is not a significant correlation between ageing and the density of DAn in the SNpc in humans. Linear regression between the density of DAn in the human SNpc *versus* the age of the correlated individuals revealed no significant changes with ageing in the human SNpc. TH-positive staining of DAn in the SNpc nuclei of human transversal sections (left image). High magnification photomicrographs (a-d, right images) show more detail of the DAn.

4.4 Discussion

This chapter has attempted to provide information about whether there are histological changes in rat and human DAn from the SNpc in response to ageing. Because ageing adds a substantial risk factor for the occurrence of PD (Tysnes and Storstein, 2017; Poewe *et al.*, 2017), it is important to analyse if during the physiological ageing process DAn from the SNpc undergo any type of natural degeneration or modification that could explain their vulnerability to the disease as we get older. In a previous chapter (see Chapter 3), the proteomics analyses revealed that the expression of TH in the rat SNpc did not change significantly between the different age groups. This raised the question of whether other fundamental characteristics of DAn within the SNpc was also maintained during ageing or, on the other hand, if the normal level of TH expression masked alterations in other characteristics. Here, analyses of the number and morphology of DAn were performed to assess the basic integrity of the SNpc. It was found that the midbrain increases in size during ageing in rats. While the DAn of the dorsal tier of the SNpc in rats changed in terms of density rostro-caudally but not in cell size within age groups; there was a reduction in the number of neurons in some rostro-caudal regions together with an increase of the soma size across ageing. Similar analysis of the lateral tier of the SNpc in rats revealed an increase in the density of DAn from the middle to the caudal area without modifications in the size of the cells. In addition, the caudal region of the lateral tier had a reduction of the density of DAn with ageing without an alteration of the soma size. Overall, this demonstrated that the dorsal tier contained more DAn with small somas compared to the lateral tier when ageing was not considered as a factor. In humans, no correlations were established between density of DAn and age, due to the limitation in the number of samples across ages (i.e., there was no comparable ‘juvenile’, ‘young’ and ‘middle age’ tissues available).

4.4.1 Ageing increases the size of the rat midbrain

The area of the midbrain in the different age groups of rats was measured in order to know if the midbrain, and eventually the entire rat brain, experienced any modification with ageing. This analysis was done because alterations in the SNpc with ageing could be derived from general transformations in the CNS. The results showed that the midbrain increased significantly during ageing, especially from the juvenile to the young group. These findings corroborated a previous study using MRI and histology techniques, where there was an increase in the volume of the whole rat brain between the early postnatal period and 6-month-old due in part to a higher myelination during development (Mengler *et al*., 2014). Likewise, Bandeira *et al*. (2009), using the isotropic fractionator method, highlighted an increase in brain mass during the first three postnatal months in rat brains likely due to an increase in the number of glial cells and expansion of neuronal soma. However, results here only show a significant growth of the midbrain between the young (6-month-old) and the old (>21-month-old) animals in adult ages, but not between middle age (16-month-old) and old. This would be in line with the data presented by Mortera and Herculano-Houzel (2012), who showed, using the isotropic fractionator method, an increase in the rat brain mass between 1- to 22-month-old. Interestingly, they also determined that after the first 4-month-old of life up to 22-month-old, there was a 20–30% reduction in the number of neuronal cells, while the number of glial cells remained stable. However, because this article used a Spearman correlation between ages and brain mass to see if there were statistical differences in the brain weight, it was difficult to conclude if any significant changes occurred between middle age and the oldest brains. Nevertheless, other investigations also show that between middle age and old rats there are no age-related changes in the volume of the brain. Work of Hamezah *et al*. (2017), for example, compared 14- and 27-month-old rat brains by MRI and showed that, even finding an increase in the volume of lateral ventricles, prefrontal cortex and hippocampus with ageing, other areas such as the striatum, cerebellum or the whole brain remained stable. Discrepancies in these results may be a

product of the different techniques used (e.g., isotropic fractionator, MRI, histology) to estimate the size of the brain along ageing. In the study presented here, for example, digital measures using histological sections were used to analyse the area of the midbrain specifically, while the articles cited from the literature looked at volume or mass of the whole brain. What is notable about these results is that ageing in the rat has the opposite effect on brain volume of the human brain, which shows a reduction of its size (Scahill *et al*., 2003). These contrasting effects might be explained by the different proportion of cells found in the brains of rats and humans, and the more specialised regions of the human brain (that the rat does not have) that might suffer degeneration. Hence, rodents need to increase the size of their brains if there is an expansion in cell numbers, while humans (and primates in general) can increase the number of cells without their brains expanding (Herculano-Houzel, 2007; Herculano-Houzel *et al*., 2007; Azevedo *et al*., 2009; Herculano-Houzel, 2009). It is possible that physiological ageing produces an increase in the number of certain cells like oligodendrocytes in the brain of rodents but not in humans, therefore increasing the size of the rat brain (Lasiene *et al*., 2009). Adding to this, it is plausible that because human brains contain relatively more cells in a smaller space, any degeneration may affect more cells in humans than in rodents, leading to a more evident shrinkage of the brain. Another possibility not related with the cell number is that ageing rat brains contain more ECM (making them bigger), as the proteomics study of this Thesis has provided evidence for (see Chapter 3).

4.4.2 When conducting within age group comparisons, the dorsal tier of the SNpc shows heterogeneity in the density of DAn rostro-caudally, but the soma size is unchanged

The dorsal tier of the SNpc was analysed, quantifying the density of DAn within this region and measuring the size of their soma along the rostro-caudal axis within each age independently. The difference in the density of DAn in the SNpc along the rostro-caudal axis has been previously mentioned by other authors (Panneton *et al*., 2010; Gao

et al., 2011; Tapia-Gonzalez *et al*., 2011; Fu *et al*., 2012), although only Gao *et al*. (2011) in rats and Tapia-Gonzalez *et al*. (2011) in mice described clearly how the number of DAn had a significant increase in the middle part compared to the caudal region (similar to the results here). Different densities of DAn might be associated with different degrees of vulnerability within the SNpc, independent of the effect of ageing. Although I have not found any research that proves this *in vivo*, it might happen that regions with a greater density of DAn could be more resistant or susceptible to degeneration than other areas with less density. For example, different densities of neurons can change their morphological properties, affecting the distribution of their dendrites and with that their synaptic connectivity with other cells in that region. That could change the electrophysiological properties of the network, as Ivenshitz and Segal (2010) demonstrated in a hippocampal culture experiment where the spontaneous network activity was assessed. In their work, they revealed that sparse cultures had fewer synapses, and that the amplitude and duration of the signal was higher compared to the denser cultures. This can result in longer and larger calcium bursts that can cause neurotoxicity within cells. Interestingly, to my knowledge, it is still unexplored if this rostro-caudal diversity in DAn density is linked to any functional distinction and the possible implications of this heterogeneity in degeneration. With that said, Damier *et al*. (1999) found a major loss of DAn in the caudal part of SNpc in human PD, followed by the middle and rostral regions. This might indicate specific characteristics associated with each area that either prevent or accelerate the degeneration of DAn. Moreover, when the density of DAn across the rostro-caudal axis was compared within the different age groups, the density of DAn was reduced from the middle to caudal in all age animals except in the middle age. This might suggest that the middle age group has less DAn in the middle region of the dorsal tier of the SNpc than it should have. Physiological ageing is a multifactorial complex process that can affect individuals differently (Tosato *et al*., 2007). Therefore, one explanation for these results is that some of the animals from the middle age group experienced the ageing process in the SNpc at earlier stages

compared to the other ages. Another option is that these animals had less DAn *per se* from young ages, and because the comparisons cannot be done in the same animals at different ages, it is impossible to draw either conclusion. The possibility that animals started life with differences in neuronal number is supported by a study performed by Herculano-Houzel *et al*. (2015) in mice. In their work, they demonstrated that different individuals can have the same brain mass, but a different number of neurons and density. In fact, this appeared to be associated with a change in their soma size (i.e., more density generates a reduction of the soma size and *vice versa*).

In terms of the size of the DAn soma, the data reported here showed a similar area of the cell bodies within the same age group in the rostral, middle and caudal part. This was in contrast to previous findings in mice where the area of the soma of DAn appeared bigger in the caudal part (Fu *et al*., 2012). This discrepancy could be attributed to the different species of rodents used in each study.

4.4.3 Ageing affects mainly the density and soma size of DAn in the caudal region of the dorsal tier of the SNpc

When the effect of ageing was assessed in the dorsal tier of the SNpc, the middle and caudal areas were the regions with a higher depletion of DAn density between juvenile and adult animals. A possible and simple explanation for these results may be the fact that the juvenile brains are smaller than adults (see Results). Therefore, DAn were more packed and denser within the SNpc in early postnatal stages compared to young, middle age and old groups. Because the same thickness (40 μm) was applied in the coronal sections of both juvenile and adult brains, a section from a juvenile individual will contain more DAn in a smaller SNpc area, showing a higher density. Another possibility to justify the drop in density of DAn from juvenile to adults can be the programmed cell death by apoptosis associated with neurodevelopment. This is thought to occur so that a balance is maintained between the number of neurons, their functions, and the minimum size of

the CNS (Dekkers *et al*., 2013; Pfisterer and Khodosevich, 2017). In fact, the cell death of immature DAn in the SNpc appears in two different stages of early life; between postnatal day 0 and 6 (P0–6), and at postnatal day 14 (P14) (Oo and Burke, 1997), which coincides with the age of the juvenile group in this study. In adult rats, the caudal region showed more DAn degeneration when comparing the young *versus* middle age and old age groups. This matches closely to the area of the SNpc that suffers major degeneration in PD (Damier *et al*., 1999). Contrary to these findings, however, Gao *et al.* (2011) described in rats a significant depletion in the number of DAn with ageing in the rostral part of the SNpc (instead of the caudal). In their experiment, they used ten rats per age group (including 5-month-old and 24-month-old), and they collected 6 µm sections every five slides for immunohistochemistry analysis. This discrepancy between studies may be due to differences in the thickness of the sections used (40 µm *versus* 6 µm) and the number of slices collected (every six *versus* every five) that obviously can change the distribution of number of neurons rostro-caudally. Moreover, the fact that this study analysed the density rather than the total number of DAn makes a comparison more difficult. Taken together, this suggests that we must be cautious about making too many conclusions about which rostro-caudal region degenerates more in the dorsal tier of the SNpc during physiological ageing, reinforcing the idea that more studies are necessary to clarify those discrepancies. A possible study to clarify this point could be a full characterization through digital reconstruction of the SNpc, taking for example sections of 10 µm thickness, and analysing every single slide with the use of stereology to avoid the quantification of the same neuron. Clearly, this study would be time consuming, but as computational approaches improve, manual quantifications are giving way to more accurate automatic analysis that can help us to fully understand the anatomical and physiological features of the brain. A good example of this becoming a reality is the reconstruction of the neocortex of rats performed by Markram *et al.* (2015) under the Blue Brain Project, where they not only estimated the number of neurons and its

composition but revealed the connectivity and electrophysiological activity of the whole region.

Though the study here indicates that DAn from the caudal part of the dorsal tier of the SNpc showed a significant decrease in their soma size between the juvenile age and in adulthood, authors like Tepper and colleagues (1994) or Park *et al.* (2000) have indicated that the size of the cell bodies in these regions do not change from postnatal to adults in rats. The observed lack of change in the soma size in these studies might be attributed to the age at which they used as adult, which corresponds to P75 or over P75 (without specifying the exact age). The first adult age (young) in this Thesis was 8-month-old (P240), therefore, it is possible that the observed differences here illustrate effects of more advanced ageing. In fact, as Sengupta (2013) indicated, P75 in rats would correspond to 5 years of age in humans, while P240 would be around 18 years old. Nevertheless, the same article showed that rats are considered young adults around P70 during the peak of sexual maturity. However, they claimed that this sexual maturity indicates the beginning of adolescence, but not adulthood, a period where like in humans the increase of social activity can regulate changes in the brain (Spear, 2000). Moreover, Tepper *et al*. (1994) choose sections at the level of the oculomotor nerve (which corresponds to the middle part in this study) and only showed a slight significant change in the soma size from juvenile to young. In terms of the significant increase in the soma size of DAn from young to middle age or old, Sanchez *et al*. (2008) also revealed that DAn expanded their cell bodies with ageing. However it is important to note that they measured the area of the soma of DAn within the rostral part, which in this Thesis seemed not to change significantly between adult individuals.

4.4.4 The density of DAn in the whole dorsal tier of the SNpc is reduced during ageing, which may be generating the increase of the soma size of DAn

As in the previous section, when the dorsal tier of the SNpc was analyzed as a whole, the density of DAn was reduced during ageing from juvenile to old, while the soma size decreased from juvenile to adults, but increased again between the young and old age. As it was mentioned before, these differences are produced by alterations of the caudal part, which correspond to the SNpc after the oculomotor nerve. In my opinion, this shows how relevant it is to study the entire SNpc before drawing conclusions, and the implications that this heterogeneity can have, for example, in models of PD. According to the data presented here, a PD model will be more severe if it is applied in the caudal part of rat SNpc, depending on the age of the rat, because there is an added effect of the ageing process that produces neurodegeneration without any toxin being used. This could, in essence, aggravate the effect of any lesion in the caudal part of the SNpc. On the other hand, if the toxin is applied in the middle region, where the differences are not as evident, the age of the individuals will not matter because in this area the degeneration would be produced only by the toxin. Overall, this means that when studies are compared it is necessary to really understand the age of the animals and the region of the SNpc that has been chosen to not introduce confounding variables to the experiment. It is also essential to understand why DAn increase their soma size during physiological ageing and the impact this has in the vulnerability of these neurons. It seems logical to consider that a reduction in the number or density of neurons will give more space to these neurons to expand, as the opposite happens when there is a high density (Herculano-Houzel *et al*., 2015). However, to my knowledge, the mechanisms that regulate this process have not been explored in ageing and is lacking in the literature. Nevertheless, investigations with drugs of abuse (nicotine and cocaine) have found that DAn in the VTA increase their soma size when the level of dopamine is increased in the extracellular space (Collo *et al*., 2012; Collo *et al*., 2013). It might happen that an increase in the size of the cell affects the structural composition of DAn

in the SNpc. If a reduction of the number of neurons is compensated for by a high expression of TH by each neuron, an increase in the production of dopamine in the extracellular space can appear, generating an increase of the cell soma. Though it is speculative, any increase in dopamine in the extracellular space could increase oxidative stress in the region and leads to neurotoxicity among DAn (see Chapter 1; Adams and Odunze, 1991; Cohen *et al*., 1997; Zhang *et al*., 2019).

4.4.5 The lateral tier of the SNpc has a higher density of DAn in the caudal part, but the soma size is the same rostro-caudally

The same analysis was done in the lateral tier of the SNpc, which could be considered separately from the rest of SNpc because it has a higher expression ratio of calbindin/TH (Fu *et al*., 2012). Unlike the dorsal region, the lateral part contains a greater density of DAn in the caudal part. Although Khudoerkov *et al*. (2014) did not described the regions rostro-caudally in their article (they referenced the sections according to distance from bregma), it appears they too demonstrated that the higher density of DAn in the lateral tier appeared more caudally than in the case of the dorsal tier. Why DAn in the lateral part, as in the middle region in the case of dorsal tier of the SNpc, are denser caudally is something that, to my knowledge, has not been studied. Moreover, Khudoerkov and colleagues (2014) also showed that the dorsal tier of the SNpc contained a greater number of DAn than the lateral part, as it has been described in this chapter. In support of this, Damier *et al*. (1999) also found a major density of DAn in the dorsal part of the SNpc compared to the lateral tier.

In terms of cell morphology, the soma size does not change from rostral to caudal in the lateral region. This is important to note because it demonstrates that without the effect of ageing, the soma size of DAn remains the same, no matter if the density of DAn changes or not, along the rostro-caudal axis. Nevertheless, when the soma size from DAn in the lateral tier was compared to the dorsal tier, the lateral DAn had bigger cell

bodies, which could be attributed to the fact that in this area the density of DAn is lower. Therefore, within the same SNpc region (dorsal or lateral), even though the density of DAn can change rostro-caudally, DAn have a similar soma size. But if the regions (dorsal *versus* lateral) are compared, the differences in the density of DAn seem to be associated inversely to the size of the neurons.

4.4.6 During ageing, only the density of DAn in the caudal region of the SNpc is affected, as is seen by their changing the size of their soma

As it happens in the dorsal tier of the SNpc, the caudal region in the lateral tier was more affected by the ageing process. In this area there was a reduction from juveniles to adult stages that could be explained by the same reasons that was provided for the dorsal part (i.e., small brains and programmed cell death). Comparisons between adult animals in this region are difficult to find in the literature, probably because studies have focused on the dorsal tier of the SNpc. In addition, as it occurs in the dorsal tier, changes in the density seems to be linked to a modification of the cell body, increasing while less neurons appear in the lateral SNpc. The reasons why the remaining DAn expand is unknown. Interestingly, however, in the lateral tier, the DAn from the middle part also increased their size during the ageing process in adults, without having a significant change in the density of DAn. Thus, there is an increase in the soma size without having a decrease in the number of cells. One of the possibilities to explain this result is that in the middle region of the lateral tier the density of DAn is so low that it is difficult to visualize a depletion of the number of cells. Moreover, it is possible that the increase of cell size is not directly related to the reduction of the number of neurons, therefore, all DAn increase size with ageing no matter the tier where they are located. Lastly, alternatively, the increase of the size of DAn in this region could be compensating the reduction of neurons in the dorsal tier.

The analysis of the lateral tier of the SNpc as a whole diluted the differences found in the caudal part related to the density of DAn, although the differences between ages in the soma size remained. This, again, highlights the necessity of more studies to elucidate if the pattern of degeneration in the caudal part is maintained or not, why and how DAn change the size of their somas, and what are the implications of this in ageing. As in the dorsal tier, a more in-depth characterization and reconstruction of this region using new computational tools allowing for automated analysis, using all slides from the entire SNpc, and including a high number of rats with a range of age (more than 24-month-old), would help us to understand if the differences in the caudal part are a real effect of the ageing process or not.

4.4.7 The SNpc in rats is a heterogeneous structure in the midbrain that changes with ageing

This chapter has attempted to understand if the lack of change in the expression of TH in the SNpc during ageing is reflected in the density or soma size of DAn in this region of the brain. In most of the regions where there are changes in the density of DAn, it was found that there was an increase of the area of the DAn cell bodies. This could indicate a compensatory mechanism to express a higher quantity of TH to produce more dopamine in those neurons that remain. Other studies analyzing divisions of the SNpc in dorsal and lateral tiers or along the rostro-caudal axis (Damier *et al*., 1999; Gao *et al*., 2011; Fu *et al*., 2012) have showed differences both in density and soma size between the different areas of the SNpc without considering the effect of ageing. However, these authors only mentioned the differences in the morphology of DAn, but without explaining possible causes for the increase of their size. Therefore, the interpretation that an increase of the production of TH is pushing neurons to expand their size is only speculative and must be interpreted with caution because of the lack of literature to support it. Moreover, it is true that other markers, apart from TH, are necessary to really delimit the different areas in the SNpc and conclude if DAn in each region are part of

different subgroups with a specific morphology and, perhaps, diverse functions and grades of degeneration. Saying this, another simple possibility is that the diverse distribution and morphology of the SNpc is arbitrary, due to the neuroanatomical organization of the brain, and does not have any implication or effect in the function, characteristics or vulnerability of DAn.

On the other hand, the modification of the SNpc during physiological ageing is something that remains, surprisingly, unclear. While some authors suggest that the ventral tier of the SNpc has a reduction of DAn with ageing (Ma *et al*., 1999; Cabello *et al*., 2002; Rudow *et al*., 2008; Buchman *et al.* ,2012); others, including Fearnley and Lees (1991), suggest that the dorsal tier is the part that is most affected. However, it is fair to say that because DAn in the ventral tier in rats appeared very disperse and in a very low number, it was difficult to quantify them consistently in the different samples, so these analyses were not considered. In terms of size, it has been already indicated that the literature does not agree on this point either (see Chapter 1). Di Lorenzo and colleagues (2016), for example, speculated that the soma size of DAn should be reduced with ageing due to a reduction of the SNpc. That would disagree with the increase of cell body found in this study. Similar to the findings of this Thesis, other authors have described a hypertrophy of the soma in DAn (Cabello *et al*., 2002; Rudow *et al*., 2008; Sanchez *et al*., 2008). It could be possible that the increase of the size of the brain with ageing described at the beginning of this section would be producing the increase in the soma size, however, the lack of a significant change in the cell bodies with ageing in all the rostro-caudal regions suggests this is less likely. The different techniques used and the way of counting cells (e.g., observationally, manually, computationally or stereologically) in each of the different studies, along with the difficulty in maintaining consistency in the samples and the statistical methods applied, contribute to the variability of the data, getting heterogeneous results and making very difficult to draw final conclusions (Brichta and Greengard, 2014; Giguere *et al*., 2018).

4.4.8 The reduce number of human samples made it impossible to draw conclusions about how ageing affects the SNpc

Because changes in the rat SNpc were found with ageing, it was logical to think that these changes would appear in humans as well. However, the corroboration of this hypothesis faced the problem of a reduced number of samples in humans, with only one sample below 60 years old (the time where PD onset usually starts) together with a high diversity in the density of DAn. These differences in the density could be caused by tissue processing, which often was damaged because of the difficult maintenance of the frozen sample while cutting. This is important because it could give false results if it was considered, for example, that a section of a certain age had fewer neurons, but only because tissue was missing. Due to these factors, a significant correlation between ageing and the density of DAn in the SNpc was not possible to determine and, therefore, it was not possible to compare these results with previous publications. Moreover, it was also difficult to identify and separate the VTA from the SNpc in the human samples because of the lack of good markers to delimit each area, which clearly can affect the final outcome.

In the future, more investigations are necessary in the human SNpc to comprehend the ageing process, increasing the number and quality of samples and characterising the different subgroups of DAn with better markers. Because DAn in the SNpc in humans contain NM, these neurons can be detected by MRI (Sulzer *et al*., 2018). As Adler *et al*. (2018) demonstrated characterizing the human hippocampus in ageing, high resolution *ex vivo* MRI scans can be used to generate a well-defined 3D reconstruction of an area of the brain. Together with the MRI analysis of the *post-mortem* tissue, they histologically processed in slides some of the samples to be imaged by MRI afterwards, generating a more accurate 3D reconstruction. A similar approach could be applied to characterize NM-positive DAn from the whole SNpc in humans and compare them between a high number of individuals at different ages. This type of study, however, should be combined with other methods to characterize possible differences between subgroups of DAn,

establishing the real regions (if any) of each area. To do that, a cell-type-specific proteomics method like LCM (Steinbach *et al*., 2018; Wilson and Nairn, 2018) would be a good alternative to isolate specifically human DAn and study the proteome of these neurons, understanding if different subgroups can be found and, after that, validate those results by immunohistochemistry procedures.

4.5 Conclusions

In summary, the data reported here appear to support the assumption that a decrease in the density of DAn is associated with an increase of the soma size with ageing, probably to maintain the same amount of TH, which would corroborate the proteomics findings (see Chapter 3).

Chapter 5.

The role of astrocytes in the vulnerability of DAn: a cell culture study

CHAPTER 5: THE ROLE OF ASTROCYTES IN THE VULNERABILITY OF DAn: A CELL CULTURE STUDY

5.1 Introduction

As discussed in Chapter 3, the alteration of ECM proteins and GFAP might be related to a dysregulation of astrocytes due to the direct effect of the ageing process in these cells or as a response to reduce the damage that ageing causes to DAn. It was speculated that the proteolysis of GFAP might be involved in the dysregulation of these astrocytes with ageing. On the other hand, a reduction of the density of SNpc DAn, as well as an increase of their soma size as ageing progresses, were found in the rat SNpc. Thus, a dysfunction of astrocytes and alteration of the ECM might be implicated in the reduced density and bigger soma size of DAn or *vice versa*.

As it will detailed later in this chapter, although there are studies that have tried to understand what implications altered astrocytic characteristics and functions have on the vulnerability of DAn, it is not well understood how crucial fully functioning astrocytes are to the ongoing viability of DAn. The chapter presented here arose from the need to gain a better understanding of the supportive function that astrocytes have in the viability of DAn, not only in physiological conditions but also when DAn are challenged by a toxic event (i.e., exposure to 6-OHDA).

5.1.1 Astrocytes in health and disease: implications for the SNpc in ageing and PD

5.1.1.1 Functions of astrocytes in the healthy brain

Astrocytes have indispensable roles maintaining the correct function of the CNS. For instance, astrocytes regulate and integrate the BBB (Janzer and Raff, 1987). They also modulate myelination by cell-cell contact and the secretion of glia factors (Sorensen *et al*., 2008), and produce some of the components of the ECM such as versican, aggrecan or neurocan (Asher *et al*., 1995; Asher *et al*., 2000; Beggah *et al*., 2005; Carulli *et al*., 2007; Cahoy *et al*., 2008; Afshari *et al*., 2010; Meng *et al*., 2012). In addition, astrocytes reduce and neutralize ROS from the environment by using antioxidants (McBean, 2017),

remove molecules that can be toxic for neurons such as alpha-synuclein by phagocytosis (Lee *et al*., 2010), and release trophic factors like GDNF (Sandhu *et al*., 2009). Moreover, glial cells control the extracellular concentration of ions like K^+ produced by neurons (Halnes *et al*., 2013), neurotransmitters like glutamate (Tanaka *et al*., 1997), and water homeostasis in the synaptic gap by using the water channel protein aquaporin-4 (Haj-Yasein *et al*., 2011). Furthermore, glial cells provide metabolic support and energy to neurons (Voutsinos-Porche *et al*., 2003), produce calcium waves between astrocytes (Navarrete *et al*., 2013), and modulate and support synaptic activity and plasticity of neurons with the release of glutamate, ATP or D-serine in the tripartite synapse (Henneberger *et al*., 2010; Chen *et al*., 2013b; De Pitta and Brunel, 2016).

5.1.1.2 Loss of astrocytic functions during disease

Pathological conditions can change the characteristics of astrocytes, which might result in the loss of some of their supportive functions (Vasile *et al*., 2017). This is evident in the case of transgenic arctic β-amyloid (arcAβ) mice, a model of AD characterized by a strong angiopathy associated with Aβ plaques (Merlini *et al.*, 2011). In this AD model, there was a retraction of the astrocytic endfeet that destabilized the neurovascular interface and caused leakage of the BBB and the impairment of the cerebral metabolism. Similarly, Gu *et al*. (2010) revealed that transgenic expression of alpha-synuclein in astrocytes in a mouse model of PD produced aggregation of alpha-synuclein in astrocytes, affecting the BBB, and producing degeneration of SNpc DAn. Likewise, transgenic expression of alpha-synuclein in astrocytes in culture revealed that the overexpression of this protein produced a breakdown of the Golgi apparatus, along with an increase of apoptosis mediated by stress of the endoplasmic reticulum, and a concomitant reduction of GDNF release (Liu *et al*., 2018). Another example of what happens when glia become dysfunctional can be seen in the work presented by Peng *et al*. (2019) where a lentivirus was used to knockdown the protein DJ1 in astrocytes. The knockdown of DJ1 (which provides an antioxidant function) increased neuronal

degeneration in an ischemia/reperfusion model *in vivo* and *in vitro*. They speculated that this result was likely due to the reduction of the expression of glutathione, which neutralizes ROS. Finally, Piacentini *et al*. (2017) have recently published that astrocytes can accumulate tau protein from AD patients *in vitro*. The misfolding and accumulation of tau is a characteristic of neurons in AD and thought to facilitate their degeneration. In this work, they observed that tau can rapidly accumulate in astrocytes, producing a disruption of intracellular calcium and, therefore, affecting the release of gliotransmitters such as ATP.

It is important to note that the loss of functions in astrocytes might be particularly relevant in a neurodegenerative diseases like PD, where DAn can be characterised, for example, by a high amount of ROS, oxidative stress and neurotoxicity due to the metabolism and oxidation of dopamine (Cohen *et al*., 1997) (see Chapter 1). In essence, the alteration of astrocytic functions, such as the scavenger of ROS, might aggravate the vulnerability of these neurons in ageing and PD.

5.1.1.3 Reactive astrogliosis during disease

Pathological conditions such as neurodegenerative diseases or brain injury might activate the state of the astrocyte, producing reactive astrogliosis that can be beneficial or detrimental for the brain area (e.g., by releasing anti-inflammatory or pro-inflammatory cytokines, respectively; Sofroniew, 2009). As Sofroniew (2009) stated, this reactive astrogliosis would be characterized by an astrocytic response similar to a CNS insult, which would generate changes in the protein expression of the astrocyte (e.g., increase of the expression of GFAP and/or vimentin), and cause cellular hypertrophy and altered function. Consequently, astrogliosis can affect other cells around them, including neurons and microglia. If the CNS insult is severe, it will show a proliferation of astrocytes together with the formation of a glial scar that can serve to protect the tissue and preserve its function. This consequence of the glial scar was demonstrated by Faulkner *et al*. (2004) using a SCI model, where the ablation of reactive astrogliosis by the antiviral

agent ganciclovir produced a disruption of BBB repair, the infiltration of leukocytes, and demyelination and cell death. This was in opposition to a group of animals where the tissue and BBB were repaired, and inflammation was reduced and cell death was not produced.

Reactive astrogliosis can be triggered by multiple factors, causing in turn the release of molecules that mediate the response of reactive astrocytes. For example, activated microglia have been showed to induce reactive astrogliosis *in vitro* by releasing the cytokines tumour necrosis factor (TNF) and interleukin 1α (IL-1α) (Liddelow *et al.,* 2017). These reactive astrocytes called A1 showed a reduced maintenance of synapses and phagocytic function, causing a reduction and weakening of synapses between retinal ganglion cells and an accumulation of myelin debris. Liddelow and colleagues (2017) also demonstrated that these A1 reactive astrocytes were toxic for cortical neurons, motoneurons, DAn and oligodendrocytes. Moreover, it was found that there was an increase of these reactive astrocytes in *post-mortem* tissue from brains with neurodegenerative disease (e.g., AD, PD), which might be related to the progression of the diseases. On the other hand, Nahirnyj *et al*. (2013) showed that molecules related to oxidative stress (like ROS; which was generated by adding paraquat or H_2O_2 in the culture) can induce reactive astrogliosis in primary retinal astrocytes. In turn, astrocytes will release pro-inflammatory cytokines that can be toxic for cells.

Nevertheless, the literature surrounding the potential for a reactive astrogliosis in the SNpc during ageing and PD (as was mentioned in Chapter 1) is more ambiguous. Some authors report a lack of astrogliosis in human PD brains (Mirza *et al*., 2000; Tong *et al*., 2015), while others observed a mild astrogliosis (Song *et al*., 2009). Similarly, astrogliosis during ageing of the SNpc remains controversial. Recent research, for example, has shown that a reactive astrogliosis is not apparent in humans (Jyothi *et al.*, 2015) and a reduction of astrocyte reactivity may occur in monkeys (Kanaan *et al*., 2010), while others found an increase of reactive astroglia in humans and mice (Venkateshappa *et al*., 2012; Gao *et al*., 2013). These differences between studies are probably

generated because the different ways of characterizing astrogliosis (either measuring the increase of GFAP immunostaining or quantifying the number of astrocytes) as well as possible ageing differences between species.

5.1.1.4 Senescence of astrocytes during the ageing process

Astrocyte can undergo cellular senescence with the ageing process, which might have implications for the course of neurodegenerative diseases (Cohen and Torres, 2019). Senescent astrocytes are associated with an arrest of the cell cycle, increased beta-galactosidase activity, expression of cell cycle inhibitor p21, secretion of pro-inflammatory cytokines and ROS, and dysfunction of the mitochondria. A good illustration of the potential to combat neurodegeneration by addressing astrocyte activity is seen in HIV-1 patients where cognitive impairments associated with the disease can be successfully treated with antiretroviral therapy that causes a senescence of astrocytes (Cohen *et al*., 2017). Interestingly, however, senescent astrocytes seem to share a lot of the characteristics seen in reactive astroglia. Recent research by Clarke *et al*. (2018) compared astrocytes from hippocampus, cortex and striatum at different ages (ten weeks *versus* two years). They found that aged astrocytes presented a reactive transcriptomic phenotype similar to A1 reactive astrocytes, which could enhance neurodegeneration during ageing similar to that seen in PD.

In the SNpc itself, recent studies looking at *post-mortem* SNpc from PD patients showed that they contained astrocytes positive for cell cycle inhibitor p16, protease MMP-3, pro-inflammatory cytokines IL-6, IL-1α and IL-8, and a reduce expression of lamin B1, all of which are characteristics of senescent astrocytes (Chinta *et al*., 2018). Moreover, the same study found that cultured human astrocytes exposed to paraquat, a herbicide strongly linked to the development of PD, stop proliferating and showed a senescence phenotype, with an increase of senescence-associated beta-galactosidase activity, p16 and cytokine IL-6. The conditioned media produced by these senescent astrocytes

caused the death of DAn and suppressed the proliferation and migration of neural progenitor cells.

5.1.2 The supportive role of astrocytes in the maintenance and viability of dopaminergic neurons in culture

5.1.2.1 In vitro *dopaminergic cultures*

Recently, organotypic cultures have gained in popularity in order to mimic *in vivo* circumstances in a petri dish and maintain the synaptic connections and microenvironment between cells (Daviaud *et al*., 2014). Thus, organotypic cultures at postnatal stage P0–P3 can contain in the same slice DAn from the SNpc connected to other areas of the brain (e.g., striatum and globus pallidus) (Cavaliere *et al*., 2010; Ullrich *et al*., 2011). However, these organotypic cultures are difficult to generate and keep viable, particularly at adult stages where there is a higher amount of cell death as the age of the animals increases (Humpel, 2015).

To understand the characteristics and functions of DAn in isolated conditions, different cell culture methods can be used to challenge these neurons against stress conditions and study neuroprotective effects of multiple molecules (di Porzio *et al*., 1980; Gaven *et al*., 2014; Weinert *et al*., 2015; Lautenschlager *et al*., 2018; Marton and Ioannidis, 2019; Taylor-Whiteley *et al*., 2019). However, although cell culture is a very useful and easy method to gain new insights into DAn viability and function that is relevant for *in vivo* conditions, the drawback of this approach is that cell to cell and synaptic connections are disrupted, altering the microenvironment of the tissue. Nevertheless, these cell culture studies allow an easy replication of experiments, using a reduced number of animals compared to *in vivo* or organotypic studies (Humpel, 2015).

Among the many cell culture approaches that can be performed, immortalized cell lines (e.g., human-derived neuroblastoma SH-SY5Y) can be a good option for the better understanding of DAn without any other type of cell (e.g., glial cells) in the culture (Taylor-Whiteley *et al*., 2019). SH-SY5Y cells can be differentiated into a DAn-like phenotype,

expressing TH and dopamine transporter (DAT), when retinoic acid and BDNF is added to the media. Moreover, stem cells (SCs), including mesenchymal (MSCs), embryonic (ESCs) or induce pluripotent stem cells (iPSCs), can be used for the study of DAn when they are differentiated into a DAn-like phenotype (Marton and Ioannidis, 2019). Although iPSCs, in particular, can be expensive and adds certain ethical issues, one of the advantages is that experiments can be conducted using the same genetic background as the patient. In general, the main disadvantage of these two cell culture options is that cells must be differentiated into DAn, which is arduous, expensive and time consuming (Yang *et al*., 2019).

Primary cell cultures from postnatal or embryonic brains are alternatives to investigate the properties of DAn and their relationship with other cells (e.g., astrocytes) within the CNS. In the case of postnatal cultures, primary cells can be obtained from the mesencephalic region around P0–P2, including post-mitotic DAn (Lautenschlager *et al*., 2018). Although postnatal neurons are more difficult to produce and keep than embryonic cultures, it makes the distinction between VTA and SNpc possible, which is useful to understand the degenerative differences associated with these two dopaminergic groups. In embryonic stages, primary cells can be dissected easily from the VM region between E12.5–E14.5 in rodents to generate post-mitotic DAn (see below) (di Porzio *et al*., 1980; Gaven *et al*., 2014; Weinert *et al*., 2015). At this phase of development, DAn have not developed axons yet, which enhances their survival because there is no stress from axotomy. However, it is not possible to distinguish between DAn from the SNpc and VTA in embryonic tissues. Though the VM region from rat brains are easier to dissect and more DAn can be obtained compared to mice, the use of mice allows for the integration of transgenic models into the culture which can be useful to mimic some characteristics of PD.

Embryonic primary cell cultures, however, can easily generate differentiated DAn, and other glial cells such as astrocytes or microglia (Weinert *et al*., 2015). On the one hand, this characteristic creates a great opportunity to study the relationship between

astrocytes and DAn, for example, investigating what happens to DAn in physiological and stress conditions when there is less support by astrocytes, or their functions are affected. An example of this is the work presented by Datta *et al*. (2018), where it was demonstrated that a high density of VM astrocytes from postnatal rats (P0–P3), co-cultured in transwells with primary VM cells, protected more DAn against the toxic effect of 75μM of 6-OHDA compared with a low density of astrocytes or the control group without co-cultured astrocytes. On the other hand, the inclusion of other non-neuronal cells (e.g., astrocytes) within the embryonic primary culture can cause difficulties if the aim of the work is to comprehend the relation between neurons and their functions without introducing the influence of glial cells, or if other mechanisms like the effect of aged astrocytes in DAn is a subject to be investigated. In such a situation, it would be necessary to reduce or eliminate the embryonic astrocytes first, to generate a DAn-enriched culture to, for example, add afterwards adult astrocytes from different ages.

5.1.2.2 Generating neuron-enriched cell cultures

Neuroscientists have attempted multiple methods to generate embryonic primary cell cultures with a large number of neurons and synapses, reducing or eliminating astrocytes either to study the consequences of this reduction in neurons or to generate neuron-enriched (i.e., purified) cultures. These methods include reducing the plating density of the culture (Lucius and Mentlein, 1995; Yang *et al*., 2010), creating co-cultures using the sandwich technique or coating the coverslips with astrocyte conditioned medium (Lucius and Mentlein, 1995; Wang and Cynader, 1999; Kaneko and Sankai, 2014), and using serum-free media (Wang and Cynader, 1999; Kaneko and Sankai, 2014; Zuchero, 2014; Hui *et al*., 2016). In addition, different antimitotic drugs, such as 5-Fluoro-2'-deoxyuridine (FdU) or arabinosylcytosine C (AraC), can be added to the culture with the intention of directly attacking the process of division of non-neuronal cells (Gonzalez-Burguera *et al*., 2016; Hui *et al*., 2016; Schwieger *et al*., 2016), also in primary VM cultures (Gaven *et al*., 2014; Lautenschlager *et al*., 2018). In the case of

AraC, it is a structural analog and competitive inhibitor of 2'-deoxycytidine, a component of deoxyribonucleic acid, interfering with the synthesis of DNA during the S phase (Wallace and Johnson, 1989); FdU, on the other hand, inhibits thymidylate synthase, an essential enzyme to produce 2'-deoxythymidine-5'monophosphate for DNA biosynthesis (Uchikubo *et al*., 2002). One final possibility to control neuron and astrocyte numbers in cultures is through the use of flow cytometry (i.e., fluorescence-activated cell sorting, FACS) where DAn can be isolated by injecting a fluorescent dye in the embryonic rat striatum that is retrogradely transported to the SNpc DAn (Kerr *et al*., 1994), or using transgenic mice where the TH gene is tag with a GFP reporter, genetically tagging midbrain DAn (Donaldson *et al.*, 2005).

However, some of these modifications make it very difficult to maintain the healthy cultures (Kaneko and Sankai, 2014). For example, plating cells at low density showed a reduction in the viability of rat embryonic neurons from different regions such as the SNpc, striatum or hippocampus after 4 DIV (Brewer, 1995). Additionally, it has been published that serum deprivation affects the viability of DAn, with less than 1.0% surviving after 7 DIV, probably because of the suppression of astrocyte proliferation (Takeshima *et al*., 1994). Moreover, antimitotic drugs are often applied together with a serum-free medium (Hui *et al*., 2016) which can also be harmful for certain neurons like DAn. This effect was first observed *in vivo* in patients with leukemia treated with AraC, who had developed ataxia because of the degeneration of cerebellar Purkinje neurons (Winkelman and Hines, 1983). Later, it was demonstrated that AraC at 200 μM during 4 DIV was able to kill 50% of post-mitotic dorsal root ganglion (DRG) neurons or postmitotic ciliary parasympathetic ganglion neurons (Wallace and Johnson, 1989); while 50 μM AraC during 4 DIV reduced the number of sympathetic neurons from the cervical ganglia by half (Martin *et al*., 1990) by a mechanism that might involve the blockage of the response to trophic factors. Embryonic cortical neurons, cerebellar granule cells, and postnatal hippocampal neurons have also been described to be affected by AraC (Geller *et al*., 2001; Ahlemeyer *et al*., 2003; Leeds *et al*., 2005). In the

case of cortical neurons, 3 μM of AraC for 24 hours affected 50% of these post-mitotic cells by increasing the production of ROS, which caused the break of DNA strands and provoked their death by apoptosis (Geller *et al*., 2001). Hippocampal neurons die due to excitatory damage caused by the release of glutamate by reactive astrocytes when 1 μM of AraC was added to the culture for 2 DIV (Ahlemeyer *et al*., 2003); while cerebellar granule cells from newborn rats die by apoptosis when 300 μM of AraC was added to the media (Leeds *et al*., 2005). Lastly, although FdU seems to be less toxic for post-mitotic cells than AraC (Wallace and Johnson, 1989; Martin *et el*., 1990), it has also been reported that FdU can produce damage in embryonic cortical neurons when they are treated with 5 μM of this drug for 14 DIV, but not with 1 or 2 μM for 2 hours (Hui *et al*., 2016). In fact, during my Thesis I tested the effect of FdU as an option to reduce the number of astrocytes, following the article published by Hui *et al.* (2016). However, although it was found to decrease the density of astrocytes, the number of DAn was very low (data not shown), which might be related to the lack of basic compounds in the FdU media and that might be essential for the viability of DAn.

Altogether, these studies show that it is necessary to seek new strategies to generate neuron-enriched cultures with a reduction of glial cells. In the process, the maintenance of healthy DAn must be ensured while controlling the astrocyte numbers and replicating the special characteristics of primary DAn in different states (e.g., elevate degeneration associated with an increase of oxidative stress production).

5.1.3 Paclitaxel as a drug to generate neuron-enriched cultures

5.1.3.1 Mechanism of action of paclitaxel

Paclitaxel or Taxol is an anti-mitotic agent that comes from the bark of the Pacific Yew tree *Taxus brevifolia* and it is used to treat diverse types of cancers such as lung, ovarian or breast (Weaver, 2014). Therefore, its characteristics as anti-mitotic drug make it a good candidate to reduce the number of astrocytes and produce neuron-enriched cultures, as will be explained here. In 1980, Schiff and Horwitz demonstrated, by using electron microscope and immunofluorescence, that 10 μM of paclitaxel for 22 hours

inhibited the replication of human HeLa cells and mouse fibroblasts, due to the arrest of G_2 and M phases of the cell cycle by stabilizing their microtubules. These microtubules are tubular structures within the cytoplasm of the cell that can be self-assembled by αβtubulin subunits (Nogales and Wang, 2006). Microtubules are very dynamic thanks to their polymerization or depolymerization, adding or removing, respectively, tubulin subunits. To polymerize, it is necessary that they are stabilised by adding a cap of GTP-bound tubulin dimers; while to depolymerize, GTP must be hydrolysed to GDP, making GDP-tubulin subunits very instable, losing the cap and disassembling the microtubule. When paclitaxel is added, it binds βtubulin, which blocks the depolymerization and stabilizes the microtubule, but also enhances its polymerization without the participation of GTP (Nogales *et al*., 1995). Microtubules have a significant role in the replication of the genome during mitosis ensuring the correct distribution of the chromosomes (Mitchison and Kirschner, 1984). Therefore, the final consequence of adding the microtubule-targeting agent paclitaxel is the alteration (e.g., slippage or arrest) of the mitosis (Magidson *et al*., 2016). After mitotic slippage or arrest, in most of the cases, the cell will die (Bolgioni *et al*., 2018).

5.1.3.2 Paclitaxel in primary VM cultures from the mesencephalic region

Embryonic mammalian brains contain multipotent neural precursor cells (NPCs) that can divide and differentiate into specific neurons, astrocytes or oligodendrocytes. However, during embryonic development, only the differentiation of neurons is promoted, generating neuronal precursors and young neurons, and inhibiting the creation of astrocytes until the end of gestation (Namihira *et al.,* 2009). As Namihira *et al.* (2009) explained, to switch from neurogenesis to gliogenesis, differentiated neuronal precursors and young neurons express Notch ligands, which activates the Notch signal in surrounded NPCs. The activation of Notch signal will generate the expression of the transcription of the nuclear factor I that can bind the promoter of astrocytic genes to

demethylate them. This demethylation will unblock astrocytic-specific genes, allowing the production of astrocytes.

More specifically, in the case of VM cells from the mesencephalic region, cutting-edge single cell RNAseq analyses have recently corroborated the timeframe for the formation of DAn in the mouse brain, finding that DAn progenitors appear at E10.5 and post-mitotic DAn around E12.5, expressing the enzyme TH involved in dopamine synthesis (La Manno *et al*., 2016; Kee *et al*., 2017). From that embryonic stage, these post-mitotic DAn will not divide anymore, generating the perfect circumstances to, theoretically, use paclitaxel in VM mesencephalic cultures without killing these neurons. In addition, the peak of proliferation of radial glial cells, the cell precursors for astrocytes that express the protein GFAP, is produced between E13.5 and P3, as Tien *et al*. (2012) and Seki *et al*. (2014) observed in the mouse spinal cord and hippocampus, respectively. Consequently, astrocytes will divide occupying the brain during the two first postnatal weeks, limiting their ability to proliferate in adult stages to certain areas of the brain such as the cortex or corpus callosum (Ge and Jia, 2016; Zhang *et al*., 2016). Thus, these glial cells would keep their division capacity during the production of VM mesencephalic cultures, allowing the anti-mitotic drug paclitaxel to eliminate them.

In sum, the advantages of combining embryonic VM mesencephalic cultures and paclitaxel to generate DAn-enriched cultures seemed evident: paclitaxel will affect the mitosis and viability of glial cells because they can still divide, but not DAn because they are post-mitotic and they have lost their division ability.

5.1.3.3 The effect of paclitaxel in astrocytes

Paclitaxel has been extensively studied *in vitro* for its potential to treat glioblastomas. For example, Silbergeld and colleagues (1995) demonstrated that 0–250 nM of paclitaxel reduced the survival of human and rat glioblastoma cells, but increased the mobility of these cells, suggesting that paclitaxel might enhance the progression or

metastasis of the glioblastoma *in vivo*. Similarly, Tseng *et al*. (1999) showed that paclitaxel had better effects against three different human glioblastoma cell lines when the drug was applied for more than 24 hours in a concentration between 4 to 18 nM. Moreover, additional research established that the treatment of paclitaxel at different concentrations (0.05 µg/ml, 0.1 µg/ml, 0.2 µg/ml, 0.5 µg/ml) for 24 hours inhibited human glioma cells migration into pig brain slices in a dose-dependent manner, although in this case the concentration applied did not have a direct cytotoxic effect and the viability of the glioma cells was not affected (Schichor *et al*., 2005). Lastly, paclitaxel has been conjugated with nanoparticles in order to improve the crossing of the BBB, finding that different concentrations of paclitaxel (0.5 µg/ml, 1 µg/ml) reduced the volume of the tumour in the U87 MG glioma cell line when was applied for 7 DIV, with an improvements of the effect when paclitaxel was loaded in angio-pep-conjugated nanoparticles (Xin *et al*., 2012).

Moreover, the effect that paclitaxel has in cultured astrocytes has been also studied in relation to its ability to change the morphology of astrocytes. Goetschy and colleagues (1986), for instance, analysed the effect of 500 nM of paclitaxel in cortical astrocytes for 4 hours, finding that astrocytes changed their morphology to a flattened and non-symmetric shape, with large and thick prolongations. Likewise, Abe and Saito (1999) reported that adding 500 nM of paclitaxel for 1 hour had the potential to rearrange the cytoskeleton of cortical astrocytes, changing the stellated shape to a flat structure.

Interestingly, to my understanding, it has not been published yet any article of paclitaxel in relation to its possible function to reduce the number of astrocytes in embryonic primary cultures or to generate neuronal-enriched cultures. Therefore, the work presented here is the first of its type, offering a new tool to control the astrocytic expansion or the division of glial cells in culture.

5.1.3.4 The effect of paclitaxel in neurons

Though the mechanism of action of paclitaxel should not affect cells that are non-dividing (such as post-mitotic neurons), cancer patients treated with this drug develop sensory axonal neuropathy, whose symptoms are dose and time dependent and include sensory loss, and decreased of proprioception or burning pain (Tofthagen *et al*., 2013). This effect is thought to be produced because paclitaxel does not cross the BBB and affects mainly the Peripheral Nervous System when a neurotoxic dose is reached in distal sensory axons (Park *et al*., 2011). To understand the mechanisms that underlie this paclitaxel-induced degeneration in the Peripheral Nervous System, researchers have studied the effects of paclitaxel *in vitro* (see **Table 5.1**), as well as *in vivo* by injecting paclitaxel into rodents (Cavaletti *et al*., 1995; Cliffer *et al*., 1998; Authier *et al*., 2000; Peters *et al*., 2007; Xiao *et al*., 2011; Li *et al*., 2015b; Li *et al*., 2018b). The results, summarized in **Table 5.1**, have revealed that its toxicity mainly affects the sensory DRG neurons, and it is time and dose dependant. Moreover, apart from the sensory neurons, the effect of paclitaxel *in vitro* has been also investigated in other neurons from the CNS (**Table 5.1**). *In vivo*, Mercado-Gomez *et al*. (2004) observed paclitaxel-induced neurotoxicity in the hippocampus when paclitaxel was injected there at different concentrations (25 nM, 50 nM, 100 nM) after 3 hours, 12 hours, 24 hours or 7 days. Thus, they reported that the extension of the lesion was dose-dependent, finding that 25 nM of paclitaxel did not show damage, while the highest doses produced pyknotic neurons with fragmented nuclei and cell death after 12 and 24 hours, respectively. Moreover, a notable reduction of microtubule-associated proteins after 100 nM injection was found, while an increase of reactive astrogliosis with hypertrophic astrocytes was evident after 7 days. Investigations of how paclitaxel affects neurons are relevant because, although this drug cannot pass the BBB and affect the CNS, its use is being explored with new therapies that combine paclitaxel with nanoparticles to increase its permeability through the BBB and reach the brain. Therefore, it is essential to understand the effect that this microtubule-targeting agent has in non-dividing post-

mitotic neurons. Neurons have long stable microtubules, giving structural support and providing axonal transport (Gornstein *et al*., 2014). However, as Gornstein and colleagues (2014) suggested, the dynamic characteristics of microtubules in neurons are still necessary, so an overstabilization of these microtubules by paclitaxel might be detrimental for them. On the other hand, microtubule stabilization could also be good for neurons depending on the extent of stabilization associated with lower doses of paclitaxel and the situation of the neurons (e.g., promoting axon outgrowth for regeneration of CNS after injury) (**Table 5.2**).

The literature review (summarized in **Table 5.1** and **5.2**) demonstrates that the effect that paclitaxel has in DAn *in vitro* (or *in vivo*) has not been established. Therefore, it will be essential to elucidate first the best concentration and exposure time of paclitaxel to avoid neurotoxicity, especially considering the sensitivity of these DAn and the variability that seems to exist in terms of cytotoxicity between different type of neurons previously studied (e.g., hippocampal neurons *versus* DRG neurons).

The results of this study will show if it is possible to generate DAn-enriched cultures with the drug paclitaxel, without reaching cytotoxicity and/or affecting the viability of DAn. This would be very beneficial in the future to perform isolated investigations of this neuronal group that degenerates in PD. Furthermore, this research will allow the understanding of the effect of a reduction of astrocytes in DAn cultures in both physiological conditions and against the toxin 6-OHDA. Finally, the reduction of astrocytes in DAn might generate an opportunity to co-culture embryonic DAn with astrocytes at different ages, which may help us to comprehend the role that astrocytes play in the SNpc and whether ageing *per se* affects their functions.

Table 5.1. Summary of the detrimental effect of paclitaxel at different concentrations and exposure times in culture, using various cell types from multiple species and age. DRG: Dorsal Root Ganglion. h: hours. min: minutes. sec: seconds Primary cell cultures from the CNS in bold.

Reference	Cell culture	Concentration	Exposure time	Results
Letourneau and Ressler, 1984	DRG neurons from chick embryos	3.5 µM, 70 µM, 23 µM, 70 nM, 7 nM	4 h	Concentrations above 7 nM of paclitaxel produced shorter and broader neurites that did not elongate, with neurofilaments aggregated in bundles
Figueroa-Masot *et al*., 2001	**Cortical neurons from new-born rats**	**10, 50, 100, 250 nM**	**24-48 h**	**Paclitaxel reduced cell viability producing nuclear fragmentation and condensation, a characteristic of apoptosis**
Wang *et al*., 2002	DRG neurons from new-born mice	0.7 µM, 2.3 µM, 12 µM	4, 8, 10 days	Paclitaxel caused a dose-dependent loss of axonal length
Nicolini *et al*., 2003	SH-SY5Y human neuroblastoma cells	10 µM, 1 µM, 100 nM, 10 nM	24 h–48 h	1 µM of paclitaxel induced cell death with DNA fragmentation by apoptosis
Mironov *et al*., 2005	Pre-Botzinger complex neurons from P3-7 mice	10 µM	10 min	Paclitaxel stabilized and disrupted microtubules, which opened the pores of the mitochondria by the interaction with proteins of the membrane, depolarizing mitochondria and releasing calcium
Boehmerle *et al*., 2006	SH-SY5Y human neuroblastoma cells	937 nM	40 sec	Paclitaxel induced an increase of intracellular calcium with an oscillatory pattern, while binding to a calcium binding protein NCS-1 that opens the calcium inositol receptor in the endoplasmic reticulum
Scuteri *et al*., 2006	DRG neurons from E15 Sprague-Dawley rats	10 µM, 1 µM, 100 nM, 10 nM	24–48 h	Paclitaxel reduced neurite length in a dose-dependent manner, and it was cytotoxic inducing cell death by necrosis and not by apoptosis
Boehmerle *et al*., 2007	SH-SY5Y human neuroblastoma cells; DRG neurons from Pi-P3 rats	937 nM	6 h	Paclitaxel activated µ-calpain, which degraded the calcium binding protein NCS-1, attenuating the calcium inositol receptor. Contrary to acute exposure to the drug, there was no spontaneous activity or calcium oscillations
Jang *et al*., 2008	**Cortical cells from E14-E15 mice**	**30-1000 nM**	**24 h**	**Paclitaxel provoked chromatin condensation, nuclear fragmentation characteristics of apoptosis, and neuronal cell death by enhancing the activity of NADPH oxidase and**

				production of ROS. Astrocytes were not affected (data not showed in the article)
Yang *et al*., 2009	DRG neurons from E15 rats	30 nM	24 h	Paclitaxel produced a decrease in the length of axons and degeneration when it was applied directly to the axon, but did not affect them if the drug was applied in the cell body
Shemesh and Spira, 2010	Neurons B1, B2 and bifurcated neurons from *Aplysia californica*	100 or 10 nM	27–72 h	Paclitaxel caused polar reconfiguration of microtubules and impaired organelle transport
Ustinova *et al*., 2013	DRG neurons from 6-to-8-week-old mice	0.1, 0.5, 1, 10, 100 nM	48 h	Low concentrations of paclitaxel (0.1–0.5 nM) did not affected neuronal growth in culture. Paclitaxel at concentrations of more than 1 nM reduced the number of neurons, and the number and length of axons. The disruption of neurites growth is mediated by toll-like receptor 4 (TLR4)
Tanimukai *et al*., 2013	SK-N-SH cells	1, 10, 50, 100 µM	24 h	Paclitaxel induced endoplasmic reticulum stress and apoptosis in a dose-dependent manner
Gornstein and Schwarz, 2017	**DRG neurons from 8-to 10-week-old mice; hippocampal neurons from E18 rats**	**10–50 nM**	**72 h**	**Paclitaxel produced dose-dependent increase of axon swellings and retraction bulbs with local microtubule hyperstabilization on the distal axon. However, these doses did not produce cell death. Hippocampal neurons are more sensitive than DRG neurons against 50 nM paclitaxel, with fragmented microtubules**
Huehnchen *et al*., 2017	**NSCs from 2- to 4-week-old mice; hippocampal neurons from E14 mice**	**3 pm–3 µM**	**2 h**	**Paclitaxel generates cytotoxicity in NSCs. Hippocampal neurons were less susceptible to paclitaxel. 30 nM reduced the viability of NSCs in 50% compared to vehicle controls due to apoptosis by activation of caspases**
Imai *et al*., 2017	Schwann cells from P1-P4 rats	0.01, 0.1 µM	24–48 h	Paclitaxel reduced the viability of Schwann cells in a time and dose-dependent manner, finding a high toxicity with 0.01 µM after 48 h. Paclitaxel also induced morphological changes, with a decrease of myelin protein MBP
Li *et al*., 2017	**Hippocampal neurons from neonatal rats**	**10 nM, 100 nM, 1 µM, 10 µM**	**24 h**	**1–10 µM paclitaxel generated apoptosis of 50% of the neurons, with shrunk bodies and short axons**

Table 5.2. Summary of the positive effect of paclitaxel at different concentrations and exposure times, using various cell types from multiple species and age. h: hours.

Reference	Cell or tissue culture	Concentration	Exposure time	Results
Erturk *et al*., 2007	Cerebellar Granule neurons from P9 rats	10 nM	18 h	Paclitaxel enhanced axonal growth when they were platted on an inhibitory surface
Witte *et al*., 2008	Hippocampal neurons from E18 rats	3-10 nM	48 h	Paclitaxel increased neurite outgrowth and the formation of multiple axons and dendrites due to the stabilization of microtubules that formed neuronal networks
Sengottuvel *et al*., 2011	Retinal ganglion cells; PC12 cells; primary astrocytes from P4 mice Crushed optic nerve from adult rats	0.5, 1, 3, 10, 50, 100 nM 1, 10, 100, 1000 µM	24-72 h	Paclitaxel enhanced neurite extension below 10 nM and compromised the inhibition of the neurite length by neurocan or myelin in retinal ganglion cells and PC12 cells. In the crushed optic nerve, paclitaxel increased axonal sprouting and delayed macrophages and gliosis activation. Paclitaxel delayed the expansion of astrocytes in scratch injury

5.1.4 Aim and objectives

The aim of this chapter was to perform an *in vitro* study using embryonic VM mesencephalic cultures, exposed to different concentration of the anti-mitotic drug paclitaxel (1.75, 3.5, 7, 14 nM) for 7 DIV, to elucidate whether it is possible to generate DAn-enriched cultures and the consequence that a reduction of astrocytes has in the viability of DAn in physiological conditions and in presence of the toxin 6-OHDA.

The objectives of this chapter were:

- Objective 1) To determine what is the best concentration of paclitaxel to reduce or eliminate the number of astrocytes without affecting the viability of neurons or DAn or produce neurotoxicity in embryonic VM mesencephalic cultures.
- Objective 2) To study the response of DAn to the toxin 6-OHDA when cultures of these cells have been treated previously with paclitaxel and there is a reduction of the number of astrocytes.
- Objective 3) To analyze the viability of DAn once the population of astrocytes has been reestablished with astrocytes of different ages, including when 6-OHDA is added to the culture.[3]

5.2 Materials and methods

Details about materials and methods of this experimental chapter can be found in Chapter 2, section 2.2.

5.3 Results

5.3.1 DMSO does not affect the viability of astrocytes or DAn in vitro

Because DMSO was used as a vehicle for paclitaxel, it was necessary to assess its toxicity alone on astrocytes and DAn from VM cultures. The concentration of DMSO (i.e., 0.014%) present in the highest concentration of paclitaxel used (i.e., 14nM) was set as

[3] Notice that this objective was not achieved as explained in the Conclusions section.

a vehicle control for experiments. This was added to the culture media to compare its effect with the culture media solution (NBM) alone (**Figure 5.1)**. Both cells exposed to DMSO and NBM were treated at the same time as part of the same culture run. After 7 DIV, the number of DAn treated either with NBM (45.5 ± 28; normalized 100 ± 61.03) or DMSO (52.5 ± 24.5; normalized 114.8 ± 58.68) did not show any statistically significant difference (p=0.1865) (**Figure 5.1A, C**). Likewise, when the O.D. of astrocytes treated with NBM (546.35 ± 145.75; normalized 100 ± 26.94) or DMSO (569.91 ± 129.26; normalized 104.8 ±23.89) were compared, no significant differences (p=0.3898) were found (**Figure 5.1B, C**).

These results demonstrated that DMSO was a good vehicle control for paclitaxel, as it did not affect the number of DAn or the O.D. of GFAP.

5.3.2 Paclitaxel has a different effect in embryonic VM cultures depending on the type of cell studied: neurons, DAn or astrocytes

To determine the optimal concentration of paclitaxel to reduce the density of astrocytes (GFAP-positive) without affecting the viability of neurons (TuJ1-positive) and particularly DAn (TH-positive), different concentrations (1.75, 3.5, 7, 14 nM) of the anti-mitotic drug were added to the media during the first 7 DIV.

Initial observations of cells growing in culture at 4 DIV (i.e., approximately halfway through the experiment) using Phase contrast microscopy suggested that the total number of cells appeared reduced in a dose-dependent (**Figure 5.2**).

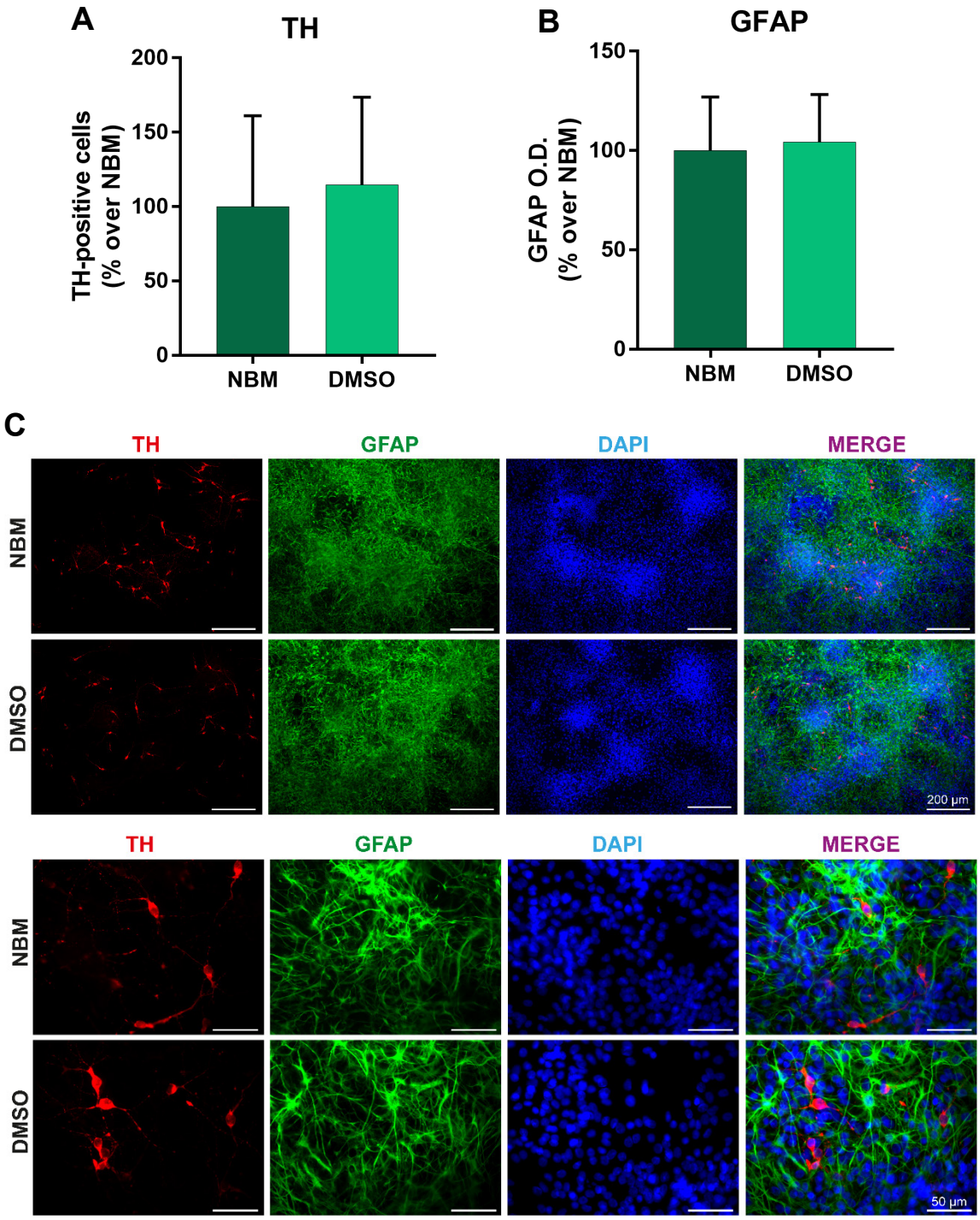

Figure 5.1. DMSO does not affect the viability of astrocytes or DAn from rat E14 VM cultures. (A) Quantifications of the number of DAn in ventromedial cultures treated with NBM or DMSO showed no statistically significant differences between treatments. **(B)** The optical density (O.D.) of astrocytes treated with DMSO showed no statistically significant differences compared to astrocytes treated with NBM. **(C)** Immunofluorescence images at low magnification (top panel) and high magnification (bottom panel), including images of DAn (TH-positive), astrocytes (GFAP-positive), nuclei (DAPI-positive) from both NBM and DMSO treatment groups. Error bars represent standard deviation.

Figure 5.2. The total number of cells appeared reduced in a dose-dependent manner with paclitaxel in living VM cultures at 4 DIV. Rat E14 VM living cultures treated with different doses of paclitaxel (1.75, 3.5, 7, 14 nM) observed by Phase contrast microscopy at 4 DIV revealed that the number of cells seemed to be reduced in a dose-dependent manner, which was representative of these cultures at this stage.

5.3.2.1 Paclitaxel reduces the density of astrocytes and changes their morphology in a dose-dependent manner

When the O.D. of GFAP of cultures treated with DMSO (0.072 ± 0.010; normalized 100 ± 10.72) was compared to the cultures treated with different concentrations of paclitaxel after 7 DIV, the analysis showed that in comparison to 3.5 nM paclitaxel (0.035 ± 0.007; normalized 53.58 ± 11.89), 7 nM paclitaxel (0.012 ± 0.002; normalized 18.88 ± 4.35), and 14 nM paclitaxel (0.007 ± 0.003; normalized 11.56 ± 6.08) there was a statistically significant reduction in GFAP O.D. of 47% ($p=0.0006$), 81% ($p<0.0001$) and 88% ($p<0.0001$), respectively (**Figure 5.3, 5.4**). However, the lowest dose of paclitaxel of 1.75 nM (0.061 ± 0.012; normalized 92.97 ± 21.12) did not produce any significant difference in the O.D. of GFAP compared to DMSO control group ($p=09357$) (**Figure 5.3, 5.4**).

Among the groups treated with paclitaxel, when 1.75 nM cultures (0.061 ± 0.012; normalized 92.97 ± 21.12) were compared to 3.5 nM (0.035 ± 0.007; normalized 53.58 ± 11.89), 7 nM (0.012 ± 0.002; normalized 18.88 ± 4.35), and 14 nM (0.007 ± 0.003; normalized 11.56 ± 6.08) groups, there was a statistically significant reduction of 43% (p=0.0008), 80% (p<0.0001) and 87% (p<0.0001), respectively (**Figure 5.3, 5.4**). Likewise, the GFAP O.D. was significantly reduced between VM cultures treated with 3.5 nM (0.035 ± 0.007; normalized 53.58 ± 11.89) or 7 nM (0.012 ± 0.002; normalized 18.88 ± 4.35) in 65% (p=0.0028) and 14 nM (0.007 ± 0.003; normalized 11.56 ± 6.08) in 78% (p=0.0004). No differences were found when 7 nM and 14 nM were compared (p=0.8825) (**Figure 5.3, 5.4**).

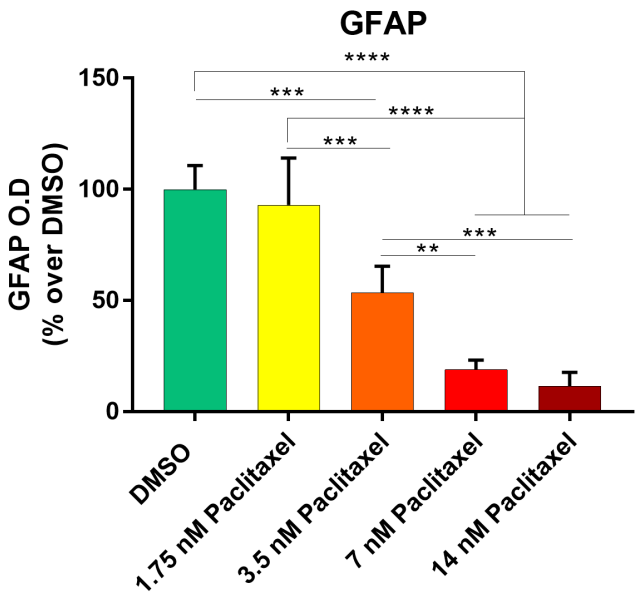

Figure 5.3. Paclitaxel reduces the O.D. of GFAP in a dose-dependent manner. The comparison of the O.D. of GFAP between VM cultures treated with DMSO or different concentrations of paclitaxel (1.75, 3.5, 7, 14 nM) demonstrated that GFAP O.D. was reduced by 47%, 81% and 88% when the DMSO group control was compared to 3.5 nM, 7 nM and 14 nM paclitaxel, respectively. There were differences between the doses of paclitaxel, finding that 7 nM and 14 nM reduced GFAP O.D. in 65% and 78% compared to 3.5 nM paclitaxel. Error bars represent standard deviation. **p<0.01; ***p<0.001; ****p<0.0001.

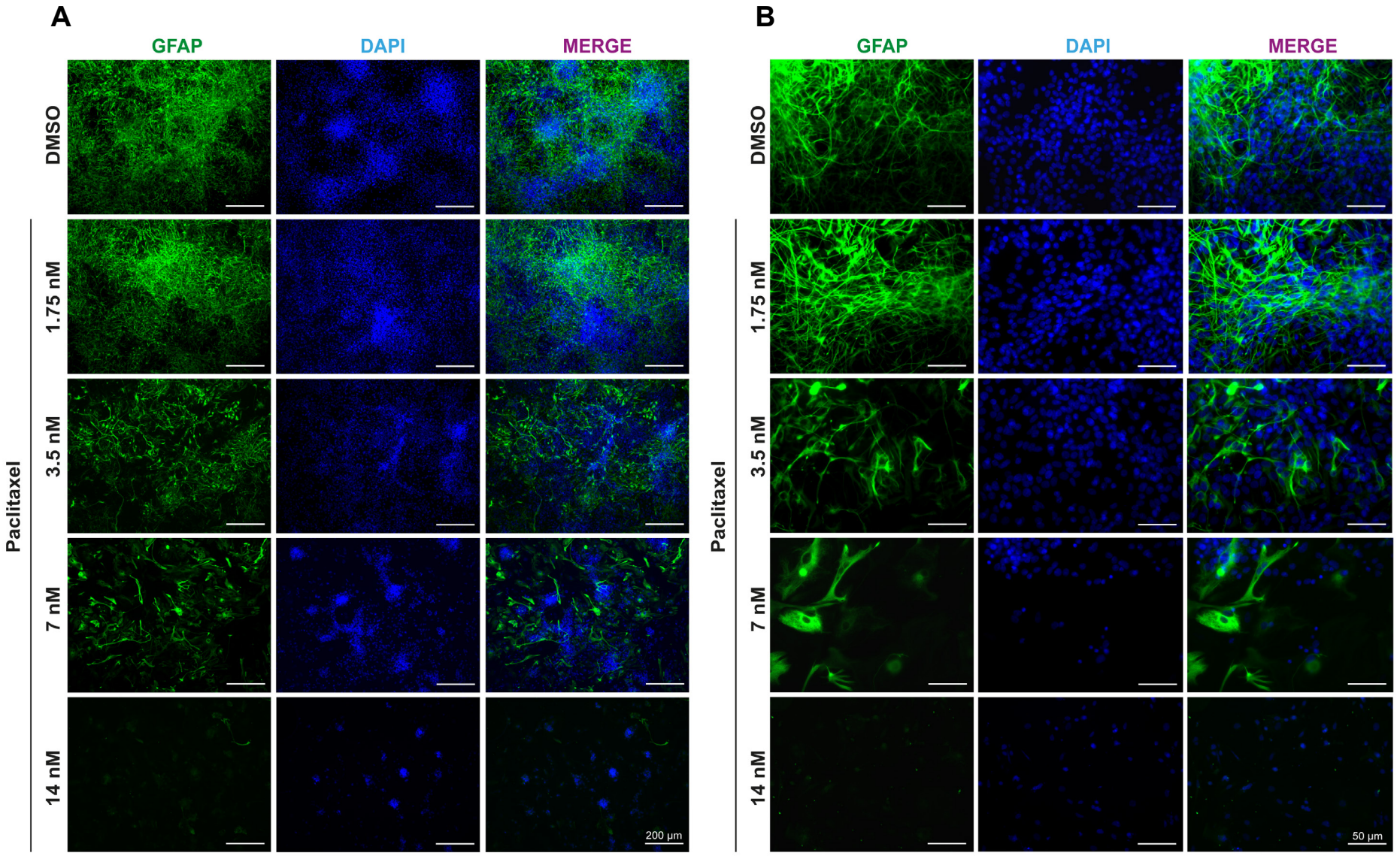
A
GFAP
DAPI
MERGE
DMSO
1.75 nM
3.5 nM
7 nM
14 nM
Paclitaxel
200 µm
B
GFAP
DAPI
MERGE
DMSO
1.75 nM
3.5 nM
7 nM
14 nM
Paclitaxel
50 µm

◄ Figure 5.4. Paclitaxel reduces the O.D. of GFAP in a dose-dependent manner. **(A)** Low magnification immunofluorescence images of VM cultures treated with DMSO or different doses of paclitaxel show a reduction in the density of astrocytes as the dose of the drug is increased. **(B)** High magnification immunofluorescence images of VM cultures treated with DMSO or different doses of paclitaxel show more detail of the different morphology of astrocytes as the concentration of the drug increases. Without paclitaxel or with a low concentration of the drug, astrocytes are fibrous with long processes; while they become flatter and egg-shaped with high doses of paclitaxel.

In VM cultures that were not treated with paclitaxel or with low doses of the drug (**Figure 5.4**), the high confluency of astrocytes made it difficult to differentiate individual cells, which was a pitfall to performing quantitative analysis of these cells and to compare their morphology between different treatments. However, qualitative observations of the cultures suggested that the morphology of astrocytes also changes in a dose-dependent manner. Astrocytes presented fibrillar characteristics, with long and thin processes when cultures were treated with DMSO and/or the low dose of paclitaxel of 1.75 nM (**Figure 5.4**). In contrast, with the increase of paclitaxel concentrations, many astrocytes displayed a flat and egg-like morphology, which was more evident when astrocytes were isolated (**Figure 5.4)**.

Together these experiments indicate that paclitaxel reduces the density of dividing astrocytes in a dose-dependent manner in rat embryonic VM cultures compared to DMSO, and that there is a potential alteration of the morphology of these cells in these culture conditions.

5.3.2.2 The highest dose of paclitaxel compromises the viability of neurons

Pan-neuronal staining with TuJ1 revealed that the highest dose of paclitaxel (i.e., 14 nM) (188 ± 46; normalized 53.7 ± 14.09) produced a significant ($p<0.0001$) reduction in the total number of neurons compared to DMSO by 46% (351 ± 37; normalized 100 ± 11.39) (**Figure 5.5, 5.6**). When comparing the number of neurons from the control DMSO (351

± 37; normalized 100 ± 11.39) with those grown in 7 nM paclitaxel (288 ± 72; normalized 82.2 ± 21.9), there was a reduction of 18% but this was not statistically significant (p=0.2187) (**Figure 5.5, 5.6**). Interestingly, although the low doses of paclitaxel of 1.75 nM (388 ± 65; normalized 110.5 ± 19.9) and 3.5 nM (417 ± 39; normalized 118.9 ± 12) did not have a significant effect on the number of neurons compared to DMSO (351 ± 37; normalized 100 ± 11.39), there was a trend of increasing their survival by 10% (p=0.7093) and 19% (p=0.1682), respectively (**Figure 5.5, 5.6**). When the number of

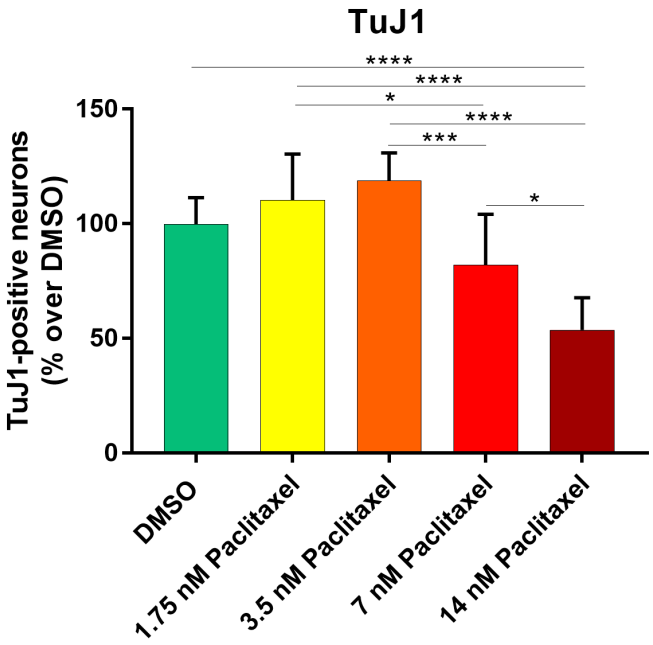

Figure 5.5. Paclitaxel reduces the number of neurons but only with the highest dose of 14 nM. The comparison of the number of TuJ1-positive neurons between VM cultures treated with DMSO or different concentrations of paclitaxel (1.75, 3.5, 7, 14 nM) demonstrated that the number of neurons was significantly reduced in 46% between the control group DMSO and 14 nM of the drug. Differences were also observed when 1.75 nM paclitaxel was compared to 7 nM and 14 nM, finding a significant reduction of the number of neurons of 25% and 52%, respectively; while the number of neurons decrease 30% and 55% when 3.5 nM paclitaxel was compared to 7 nM and 14 nM, respectively. Error bars represent standard deviation. *p<0.05; ***p<0.001; ****p<0.0001.

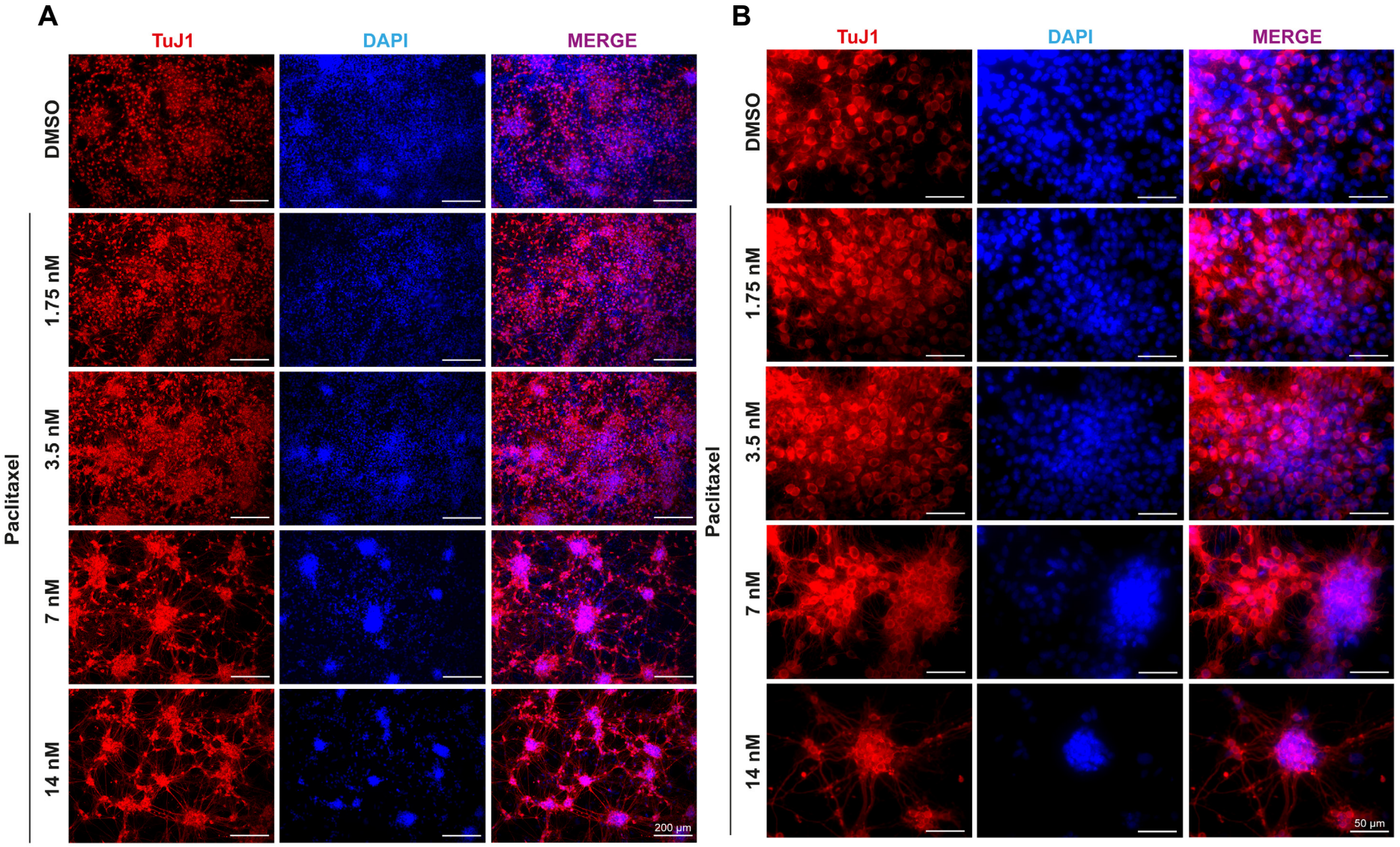
A
TuJ1
DAPI
MERGE
DMSO
1.75 nM
3.5 nM
7 nM
14 nM
Paclitaxel
200 µm
B
TuJ1
DAPI
MERGE
DMSO
1.75 nM
3.5 nM
7 nM
14 nM
Paclitaxel
50 µm

◄ Figure 5.6. Paclitaxel reduces the number of neurons but only with the highest dose of 14 nM. (A) Low magnification immunofluorescence images of VM cultures treated with DMSO or different doses of paclitaxel, where it can be observed the clusters of neurons connected between them by long axons that appear when high doses paclitaxel (7 and 14 nM) are added to the cultures. **(B)** High magnification immunofluorescence images of VM cultures treated with DMSO or different doses of paclitaxel, where it can be observed that the morphology of neurons appear similar along the different treatments. TuJ1 is a marker for neurons, while DAPI shows their nuclei.

neurons was compared among the different concentrations of paclitaxel, significant differences in the number of neurons between treatments were found. Thus, there were significant differences between 1.75 nM (388 ± 65; normalized 110.5 ± 19.9) *versus* 7 nM (288 ± 72; normalized 82.2 ± 21.9) and 14 nM (188 ± 46; normalized 53.7 ± 14.09), showing a reduction of the total number of neurons by 25% ($p=0.0126$) and 52% ($p<0.0001$), respectively (**Figure 5.5, 5.6**). Between 1.75 nM (388 ± 65; normalized 110.5 ± 19.9) and 3.5 nM (417 ± 39; normalized 118.9 ± 12), no statistically significant differences were reported ($p=0.8397$), although the trend indicated an increase in the number of neurons of 7% with the highest concentration (**Figure 5.5, 5.6**). In the case of 3.5 nM paclitaxel (417 ± 39; normalized 118.9 ± 12) compared to 7 nM (288 ± 72; normalized 82.2 ± 21.9) and 14 nM (188 ± 46; normalized 53.7 ± 14.09), a statistically significant reduction of 30% ($p=0.0007$) and 55% ($p<0.0001$) in the number of neurons was observed as the concentration of the drug increased (**Figure 5.5, 5.6**). Lastly, there was a significant ($p=0.0115$) reduction of 35% in the number of neurons from 7 nM (288 ± 72; normalized 82.2 ± 21.9) to 14 nM (188 ± 46; normalized 53.7 ± 14.09) (**Figure 5.5, 5.6**).

Qualitative observations of the culture showed that with the highest doses of paclitaxel (i.e., 7 and 14 nM), most neurons that remained in the culture were distributed in clusters of cells, but not alone. In this situation, it was possible to visualize an integrated network

between the neuronal clusters, connected by long axons (**Figure 5.6A**). Nevertheless, the size and morphology of neuronal somas appeared similar between the vehicle control DMSO and the different treatments of paclitaxel (**Figure 5.6B**).

These results show that doses of paclitaxel equal to or below 3.5 nM do not affect the viability of neurons and, in fact, it might enhance their survival.

5.3.2.3 Low doses of paclitaxel allows the survival of DAn

There was a statistically significant reduction in the number of DAn of 31% (p=0.0133) and 56% (p=0.0085) when primary cultures were exposed to 7 nM (45.5 ± 31.5; normalized 74.68 ± 57.24) and 14 nM (28 ± 14; normalized 47.28 ± 27.18) paclitaxel, respectively, but only when these treatments were compared to 3.5 nM (63 ± 28; normalized 108.3 ± 49.26) paclitaxel (**Figure 5.7, 5.8A**). However, when the vehicle control DMSO (59.5 ± 28; normalized 100 ± 49.66) or the lowest dose of paclitaxel 1.75 nM (56 ± 24; normalized 95.78 ± 42.05) were analyzed, no statistically significant differences were found in any of the other comparisons (**Figure 5.7, 5.8A**). Nevertheless, although not statistically significant (p>0.9999), there was a trend of increasing by 5% the number of DAn in the 3.5 nM (63 ± 28; normalized 108.3 ± 49.26) group compared to DMSO (59.5 ± 28; normalized 100 ± 49.66), a trend similar to what was observed when the total number of neurons was quantified (**Figure 5.7, 5.8A**).

In addition, while TH-positive neurons in culture treated with DMSO and doses of paclitaxel between 1.75 nM and 7 nM presented a normal soma, those grown in 14 nM of paclitaxel appeared disrupted, generating some debris (**Figure 5.8B**).

Altogether, this indicates that, as with total neurons, sub-maximal doses of paclitaxel did not have an effect on the viability of DAn above vehicle controls.

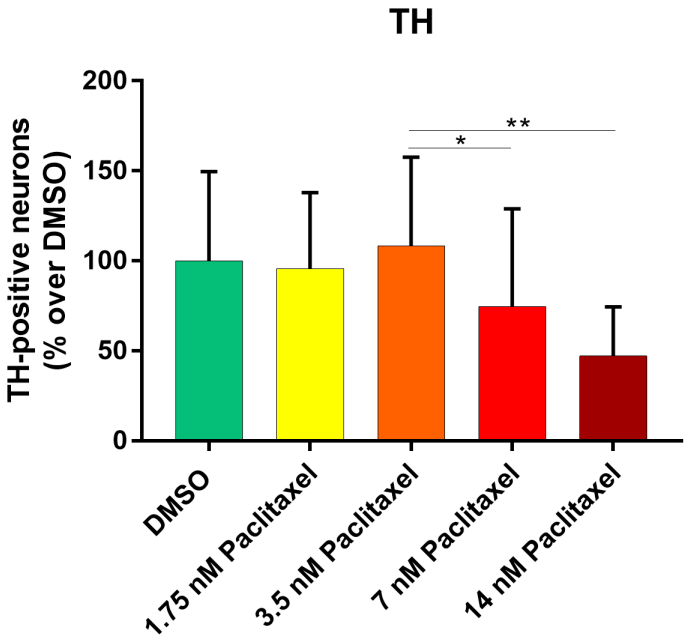

Figure 5.7. The lowest dose of paclitaxel does not affect the viability of DAn. The comparison of the number of TH-positive DAn between VM cultures treated with DMSO or different concentrations of paclitaxel (1.75, 3.5, 7, 14 nM) demonstrated that the number of DAn was significantly reduced by 31% and 56% when 3.5 nM paclitaxel was compared to 7 nM and 14 nM, respectively. Error bars represent standard deviation. *p<0.05; **p<0.01.

5.3.3 Previous treatment with paclitaxel increases the toxic effect of 6-OHDA in astrocytes but not in DAn from VM cultures

5.3.3.1 6-OHDA at a concentration of 50 μM reduces by almost half the number of DAn

In order to evaluate the effect that the toxin 6-OHDA had in VM cultures, and more specifically in DAn, the first step was to establish the best sub-toxic concentration of 6-OHDA to add into the media, in order to challenge DAn without killing all of them. Hence, two different concentrations (50 μM and 100 μM) of 6-OHDA were added to the culture for 1 hour to be compared with 0.01% AA as vehicle control (**Figure 5.9**). These two concentrations were chosen based on previous research found in the literature (see

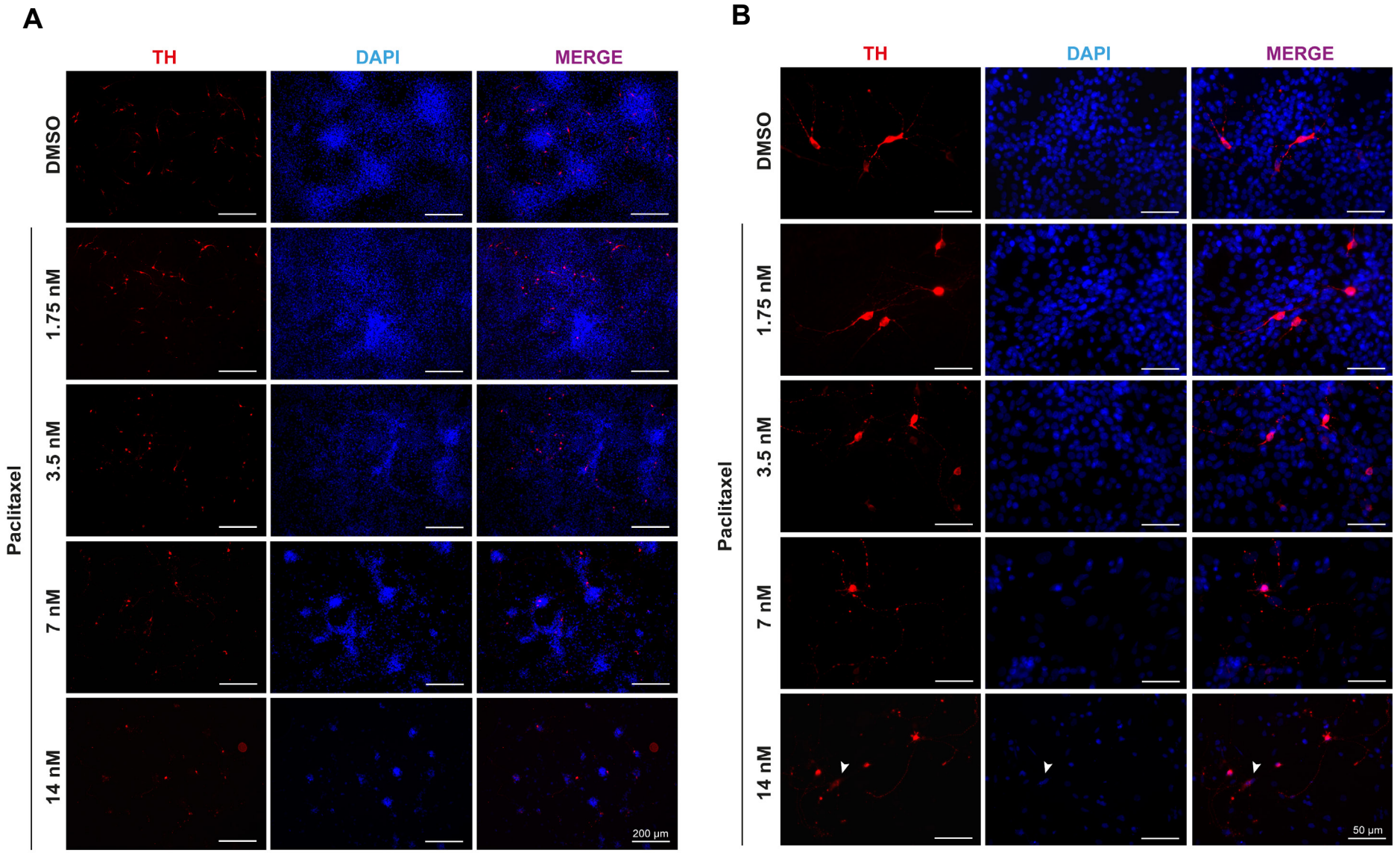
A
TH
DAPI
MERGE
DMSO
1.75 nM
3.5 nM
7 nM
14 nM
Paclitaxel
200 µm
B
TH
DAPI
MERGE
DMSO
1.75 nM
3.5 nM
7 nM
14 nM
Paclitaxel
50 µm

◄ **Figure 5.8. The lowest dose of paclitaxel does not affect the viability of DAn.** **(A)** Low magnification immunofluorescence images of VM cultures treated with DMSO or different doses of paclitaxel, where it can be observed the reduction in the number of DAn **(B)** High magnification immunofluorescence images of VM cultures treated with DMSO or different doses of paclitaxel, where it can be observed that 14 nM paclitaxel induced the disruption to the soma, generating debris (arrow). TH indicated DAn, while DAPI shows their nuclei.

Chapter 2). Quantification of TH-positive neurons showed that the number of DAn surviving in cultures treated with AA (59.5± 7; normalized 100 ± 9.32) was reduced by 43% and 98% in cultures with 50 µM 6-OHDA (35 ± 10.5; normalized 57.62 ± 14.76) and 100 µM 6-OHDA (4 ± 1; normalized 2.20 ± 0.67), respectively. This reduction in the 6-OHDA treated cultures was statistically significant (p=0.0001; p<0.0001, respectively) (**Figure 5.9A**). Furthermore, there were also significant differences (p<0.0001) between

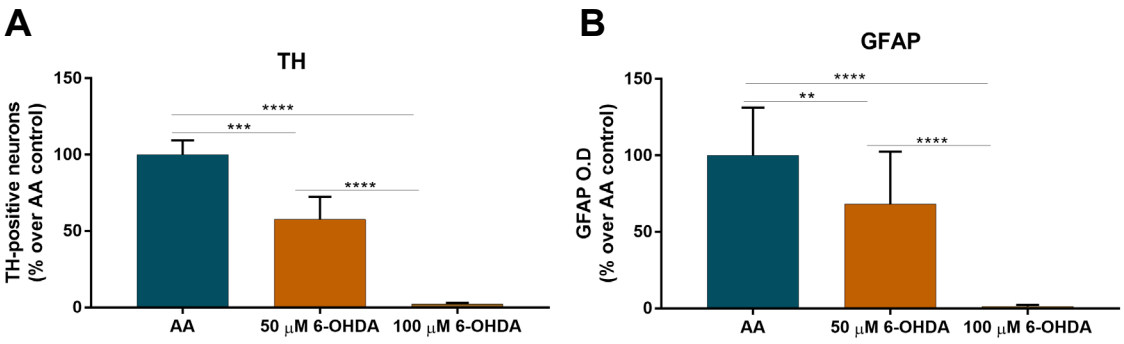

Figure 5.9. Treatment VM cultures with 6-OHDA reduces the number of DAn and O.D. of GFAP in a dose-dependent manner. **(A)** The administration of 50 µM 6-OHDA for 1 hour reduced the number of DAn by 43% compared to the control group treated with 0.01% AA, while 100 µM 6-OHDA almost killed all DAn. **(B)** Similarly, 50 µM 6-OHDA for 1 reduced the O.D. for GFAP by 32% compared to the control group, and 100 µM 6-OHDA has a depletion of 98%. Error bars represent standard deviation. **p<0.01, ***p<0.001; ****p<0.0001.

the two different 6-OHDA treatments, with a decrease in the number of DAn of 96% when 100 μM 6-OHDA (4 ± 1; normalized 2.20 ± 0.67) was added in comparison to 50 μM 6-OHDA (35 ± 10.5; normalized 57.62 ± 14.76) (**Figure 5.9A**). This suggested that 50 μM 6-OHDA was better low-toxic concentration for future experiments.

On the other hand, due to the aim of this chapter being the reduction of astrocytes by paclitaxel, the effect of 6-OHDA on astrocytic cells in the VM cultures was also evaluated to elucidate if 6-OHDA itself might reduce the density of astrocytes. Interestingly, similar results to the effects on the number of DAn were found. Thus, when the O.D. for GFAP in cultures treated with AA (0.0579 ± 0.0181; normalized 100 ± 31.28) alone was compared with 50 μM 6-OHDA (0.0395 ± 0.0198; normalized 68.26 ± 34.27) or 100 μM 6-OHDA (0.0007 ± 0.0005; normalized 1.33 ± 0.96) treated cultures. This showed a reduction of 32% ($p=0.0019$) and 98% ($p<0.0001$), respectively (**Figure 5.9B**). Likewise, there was a statistically significant ($p<0.0001$) depletion of GFAP O.D. between 50 μM 6-OHDA (0.0395 ± 0.0198; normalized 68.26 ± 34.27) and 100 μM 6-OHDA (0.0007 ± 0.0005; normalized 1.33 ± 0.96) of 98% (**Figure 5.9B**).

These results demonstrate that while 100 μM of 6-OHDA for 1 hour killed all the examined cells (DAn and astrocytes) from embryonic VM cultures, 50 μM of 6-OHDA for 1 hour only reduced the number of DAn and the O.D. of GFAP compared to AA.

5.3.3.2 6-OHDA reduces the number of DAn in VM cultures, an effect that is not exacerbated with paclitaxel

To evaluate the effect that 50 μM 6-OHDA had in DAn when there was a previous reduction of the density of astrocytes with paclitaxel, this drug was added to VM cultures for three different lengths of time (1, 2 and 3 hours) after 5 DIV of treatment with 3.5 nM paclitaxel or DMSO (**Figure 5.10, 5.11**). This concentration of paclitaxel was chosen because, as it was seen in previous experiments, it was able to significantly reduce the density of astrocytes without affecting the total number of neurons and/or DAn (see above). As a control, 0.01% AA (vehicle for 6-OHDA) was added for a maximum of 3

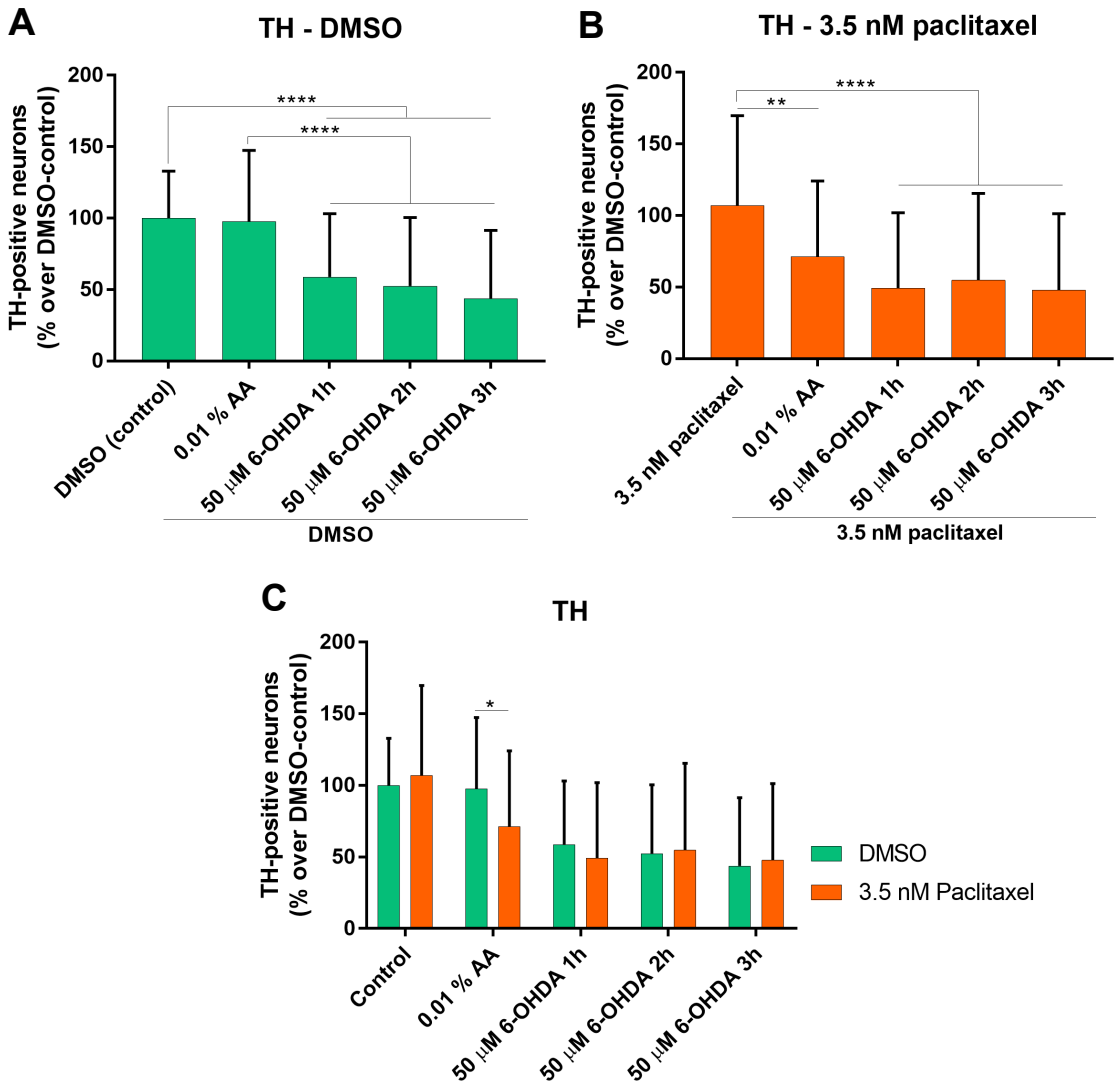

Figure 5.10. The treatment of 50 µM 6-OHDA reduces the number of DAn in cultures treated previously with DMSO or paclitaxel. (A) VM cultures treated with DMSO for 5 DIV showed a reduction in the number of DAn by 42%, 48% and 57% when the cultures were exposed to 1 hour, 2 hours or 3 hours of 6-OHDA, respectively. Similarly, a decrease of 40%, 46%, 55% was found in the number of DAn when AA treatments were compared to 1 hour, 2 hours and 3 hours of 6-OHDA, respectively. **(B)** VM cultures previously treated with 3.5 nM paclitaxel for 5 DIV showed a decrease in the number of DAn when they were compared to cells treated with 6-OHDA 1 hour (40%), 2 hours (35%), and 3 hours (42%), but also with AA (34%). **(C)** When cultures treated previously with DMSO and paclitaxel were compared, only the group AA showed statistically significant differences, with a reduction of 26% when the anti-mitotic drug was added earlier to the culture. Error bars represent standard deviation. *p<0.05; **p<0.01; ****p<0.0001.

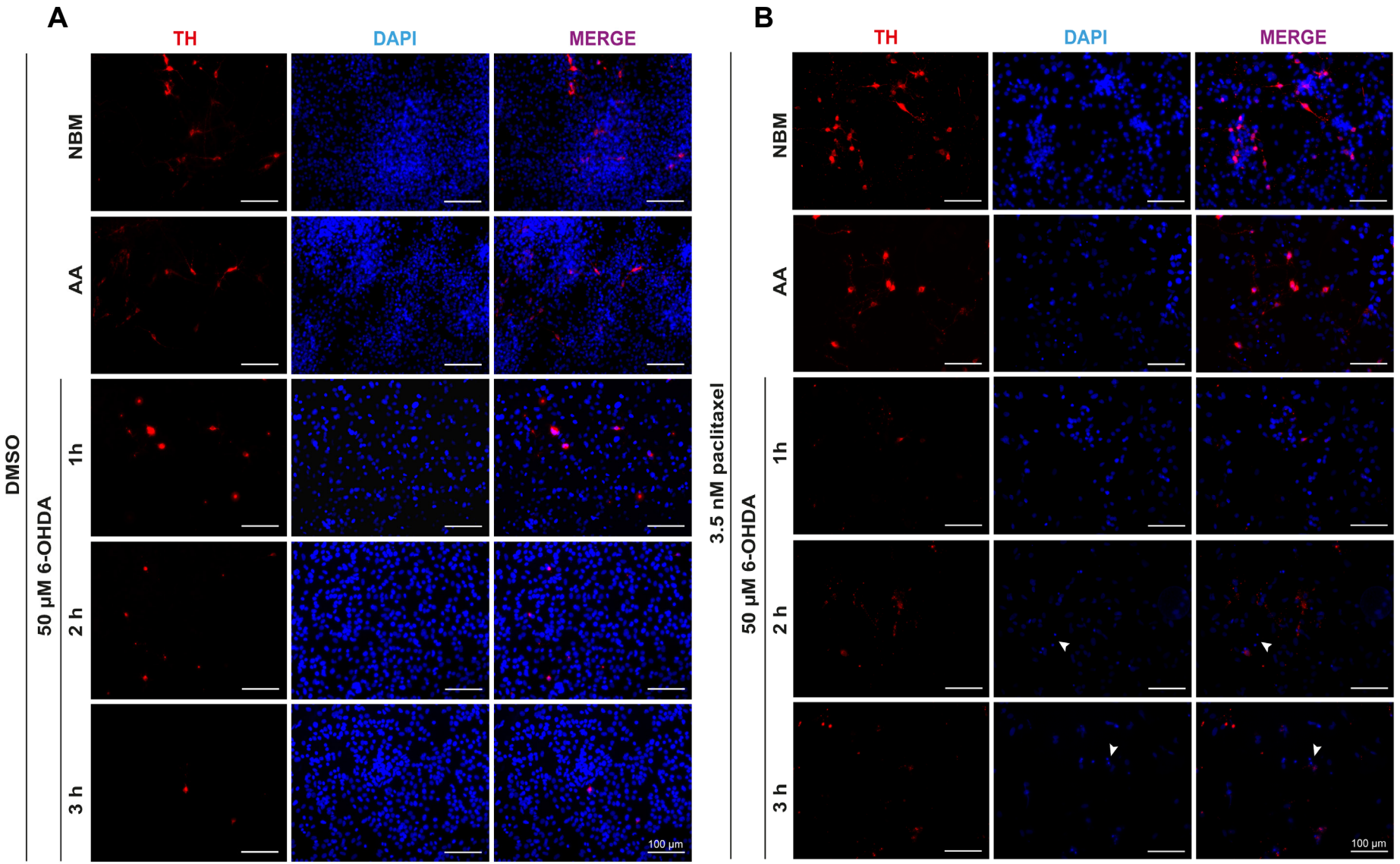
A
TH
DAPI
MERGE
DMSO
NBM
AA
50 µM 6-OHDA
1h
2 h
3 h
100 µm
B
TH
DAPI
MERGE
3.5 nM paclitaxel
NBM
AA
50 µM 6-OHDA
1h
2 h
3 h
100 µm

◄ Figure 5.11. The treatment of 50 µM 6-OHDA reduces the number of DAn in cultures treated previously with DMSO or paclitaxel. (A) VM cultures earlier treated with DMSO or AA for 5 DIV showed a reduction in the number of DAn (TH-positive) when they were expose to 1 hour, 2 hours or 3 hours of 6-OHDA. **(B)** VM cultures previously treated with 3.5 nM paclitaxel for 5 DIV showed a decrease in the number of DAn when they were compared with cells challenged with 6-OHDA (1 hour, 2 hours, and 3 hours) and AA.TH indicated DAn, while DAPI shows their nuclei.

hours to determine if the vehicle had any effects on DAn viability in paclitaxel and control cultures.

In cultures treated previously only with DMSO (**Figure 5.10A, 5.11A**), the results showed that when the number of DAn from the control group treated only with DMSO (76 ± 30; normalized 100 ± 30.32) was compared to the different exposure times of 6-OHDA, including 1 hour (46 ± 35; normalized 58.76 ± 44.39), 2 hours (43 ± 41; normalized 52.47 ± 47.97), or 3 hours (35 ± 39; normalized 43.76 ± 47.59), there was a statistically significant reduction of 42% ($p<0.0001$), 48% ($p<0.0001$) and 57% ($p<0.0001$), respectively (**Figure 5.10A, 5.11A**). Similarly, when cultures treated with AA (72 ± 41; normalized 97.79 ± 49.60) were compared with 1 hour 6-OHDA (46 ± 35; normalized 58.76 ± 44.39), 2 hours (43 ± 41; normalized 52.47 ± 47.97), or 3 hours (35 ± 39; normalized 43.76 ± 47.59) statistically significant differences were found, with the number of DAn decreasing by 40% ($p<0.0001$), 46% ($p<0.0001$), and 55% ($p<0.0001$). No statistically significant differences ($p=0.9989$) were found between the group treated only with DMSO (76 ± 30; normalized 100 ± 30.32) and AA (72 ± 41; normalized 97.79 ± 49.60) (**Figure 5.10A, 5.11A**). The different exposure times of 6-OHDA did not produced changes in the number of DAn between treatments either. Thus, the comparison of the number of DAn with 1 hour 6-OHDA (46 ± 35; normalized 58.76 ± 44.39) *versus* 2 hours (43 ± 41; normalized 52.47 ± 47.97) or 3 hours (35 ± 39; normalized 43.76 ± 47.59) did not show statistically significant differences ($p=0.9179$; $p=0.2650$, respectively); and the same appeared when 2 hours 6-OHDA (43 ± 41;

normalized 52.47 ± 47.97) was compared to 3 hours (35 ± 39; normalized 43.76 ± 47.59) (p=0.7299) (**Figure 5.10A, 5.11A**).

On the other hand, when cultures treated previously with 3.5 nM paclitaxel were treated and compared with different exposure times of 6-OHDA or AA (**Figure 5.10B, 5.11B**), the data showed that there was a reduction in the number of DAn from the group only treated with paclitaxel (83 ± 45; normalized 107.45 ± 62.62) in comparison to 1 hour 6-0HDA (42 ± 48; normalized 49.19 ± 52.76), 2 hours 6-OHDA (44 ± 50; normalized 54.93 ± 60.54), or 3 hours 6-OHDA (42 ± 52; normalized 47.95 ± 53.35). Thus, the number of DAn significantly decreased by 40%, 35%, and 42% comparing the paclitaxel group with 1 hour ($p<0.0001$), 2 hours ($p<0.0001$), or 3 hours ($p<0.0001$) of 6-OHDA, respectively (**Figure 5.10B, 5.11B**). In the case of the group treated with AA (55 ± 46; normalized 71.17 ± 52.91), comparing cultures where 6-OHDA was added, no statistically significant differences were found in the number of DAn in 1 hour (42 ± 48; normalized 49.19 ± 52.76) (p=0.0913), 2 hours 6-OHDA (44 ± 50; normalized 54.93 ± 60.54) (p=0.3387), or 3 hours 6-OHDA (42 ± 52; normalized 47.95 ± 53.35) (p=0.0313) (**Figure 5.10B, 5.11B**). However, the number of DAn was different between the group treated only with paclitaxel (83 ± 45; normalized 107.45 ± 62.62) and AA (55 ± 46; normalized 71.17 ± 52.91), showing a statistically significant (p=0.0026) reduction of 34% (**Figure 5.10B, 5.11B**). Lastly, no changes in the number of DAn were found between treatments of 6-OHDA at different exposure times, comparing 1 hour (42 ± 48; normalized 49.19 ± 52.76) with 2 hours 6-OHDA (44 ± 50; normalized 54.93 ± 60.54) (p=0.9658) or 3 hours 6-OHDA (42 ± 52; normalized 47.95 ± 53.35) ($p>0.9999$) (**Figure 5.10B, 5.11B**).

Finally, both VM cultures treated previously with DMSO and paclitaxel, including the treatments with AA or 6-OHDA, were compared between them (**Figure 5.10C, 5.11A, B**), in order to understand if there were differences when paclitaxel was added previously to the media and cultures were challenged with AA and 6-OHDA. Interestingly, only VM cultures treated with paclitaxel and AA (55 ± 46; normalized 71.17 ± 52.91) seemed to differ to those cultures treated only with DMSO and AA (72 ± 41; normalized 97.79 ±

49.60). Thus, there was a statistically significant (p=0.0284) reduction in the number of DAn of 26% in cultures treated with paclitaxel and AA *versus* DMSO and AA (**Figure 5.10C, 5.11A, B**).

Together, these results show that in cultures previously treated with DMSO or 3.5 nM paclitaxel for 5 DIV, the subsequent exposure to 50 µM 6-OHDA for different times (1 hour, 2 hours, 3 hours) showed a reduction in the number of DAn compared to those cells only treated with DMSO or paclitaxel, respectively. Moreover, in the group treated with DMSO for 5 DIV, differences were also observed between cells treated with AA and 6-OHDA, while these differences were eliminated in the paclitaxel group. Nevertheless, in the paclitaxel group, there was a reduction in the number of DAn compared cultures treated only with paclitaxel or paclitaxel and AA. This fact generated differences between the two groups (DMSO and paclitaxel) treated with AA, finding a reduction of the number of DAn when paclitaxel and AA were added to the culture.

5.3.3.3 The density of astrocytes is reduced with 6-OHDA and paclitaxel exacerbates this effect

As it was mentioned before, 6-OHDA reduced the O.D. of GFAP compared to those VM cultures treated with AA (**Figure 5.9B**). Therefore, the next step was to elucidate if different exposure times were able to produce a different effect in cultures previously treated with DMSO or 3.5 nM paclitaxel (**Figure 5.12, 5.13**).

When the DMSO control group (0.1115 ± 0.0347; normalized 100 ± 39.45) was compared with 6-OHDA, only the treatment for 1 hour (0.0598 ± 0.0284; normalized 67.47 ± 35.23) and 3 hours (0.0612 ± 0.0347; normalized 69.76 ± 39.83) showed differences in the O.D. of GFAP (**Figure 5.12A, 5.13A**). Thus, there was a statistically significant decrease of the O.D. by 33% (p=0.0003) in those cultures treated for 1 hour with 6-OHDA, and 31% (p=0.0005) in those cultures treated for 2 hours with 6-OHDA. However, although the O.D. for GFAP was reduced by 20% with 2 hours 6-OHDA (0.0712 ± 0.0436; normalized 80.63 ± 49.15) compared with DMSO (0.1115 ± 0.0347;

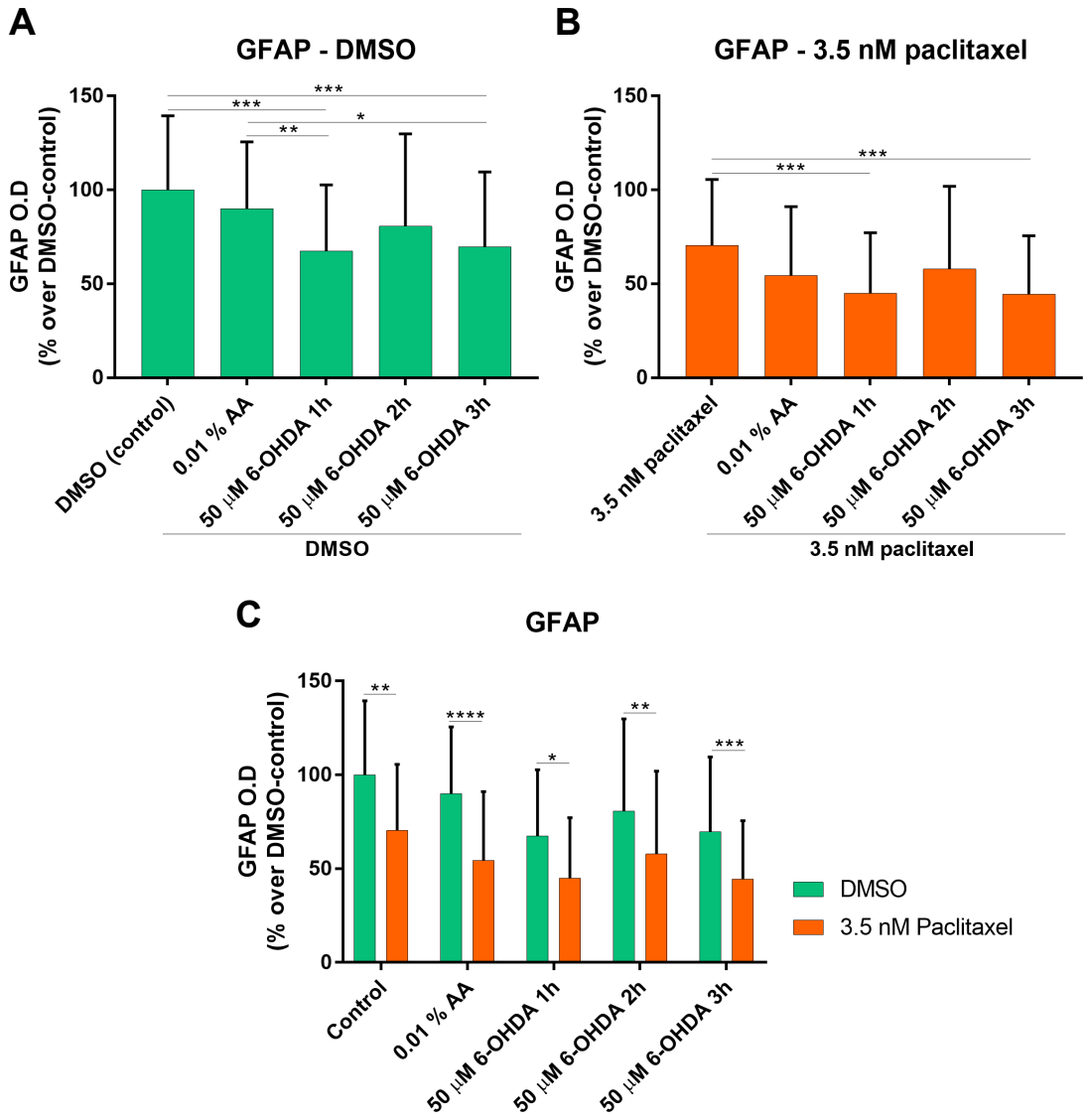

Figure 5.12. The treatment of 50 μM 6-OHDA reduces the O.D. of GFAP in cultures treated previously with DMSO or paclitaxel. (A) VM cultures treated with DMSO for 5 DIV showed a reduction in the GFAP O.D. by 33% and 31% when the cultures were exposed to 1 hour and 3 hours of 6-OHDA, respectively. Similarly, a decrease of 25% and 23% was found in the GFAP O.D. when AA treatments were compared to 1 hour and 3 hours of 6-OHDA, respectively. **(B)** VM cultures previously treated with 3.5 nM paclitaxel for 5 DIV showed a decrease in the O.D. of GFAP but only when they were compared to cells treated with 6-OHDA 1 hour (36%) and 3 hours (37%). **(C)** When cultures treated previously with DMSO and paclitaxel were compared between them, all experimental groups showed statistically significant differences, with a reduction of the O.D. GFAP when the anti-mitotic drug was added earlier to the culture as follows: control (30%), AA (40%), 1 hour 6-OHDA (33%), 2 hours 6-OHDA (30%) and 3 hours 6-OHDA (35%). Error bars represent standard deviation. *p<0.05; **p<0.01; ***p<0.001; ****p<0.0001.

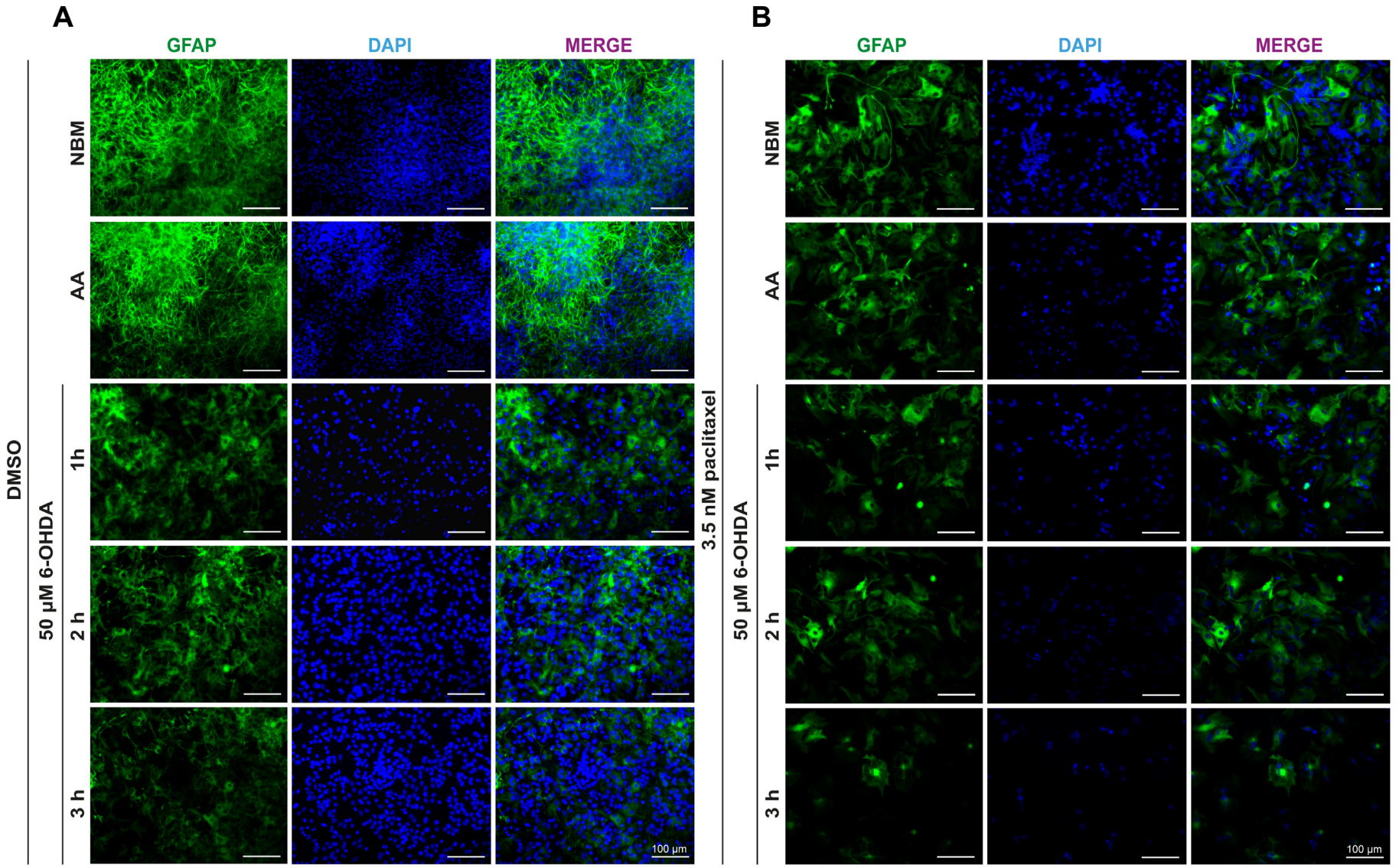
A
GFAP
DAPI
MERGE
DMSO
NBM
AA
50 µM 6-OHDA
1h
2 h
3 h
3.5 nM paclitaxel
100 µm
B
GFAP
DAPI
MERGE
NBM
AA
50 µM 6-OHDA
1h
2 h
3 h
100 µm

◄ Figure 5.13. The treatment of 50 µM 6-OHDA reduces the O.D. of GFAP in cultures treated previously with DMSO or paclitaxel. (A) VM cultures previously treated with DMSO or AA for 5 DIV showed a reduction in the O.D. GFAP (astrocytes) when they were exposed to 1 hour and 3 hours of 6-OHDA. **(B)** VM cultures previously treated with 3.5 nM paclitaxel for 5 DIV showed a decrease in O.D. GFAP when they were compared with cells challenged with 6-OHDA (1 hour, or 3 hours). GFAP is a marker for astrocytes, while DAPI shows their nuclei.

normalized 100 ± 39.45), this difference was not statistically significant (p=0.0663) (**Figure 5.12A, 5.13A**). No statistically significant differences (p=0.6543) were found in O.D. GFAP either comparing the group control DMSO (0.1115 ± 0.0347; normalized 100 ± 39.45) with AA (0.0801 ± 0. 0.0311; normalized 90.01 ± 35.51) (**Figure 5.12A, 5.13A**). In the case of the O.D GFAP of cultures treated with AA (0.0801 ± 0. 0.0311; normalized 90.01 ± 35.51), there was a significant depletion of this O.D. in 25% (p=0.0061) and 23% (p=0.0105) when it was compared against 1 hour (0.0598 ± 0.0284; normalized 67.47 ± 35.23) and 3 hours (0.0612 ± 0.0347; normalized 69.76 ± 39.83), respectively; but not against 2 hours 6-OHDA (0.0712 ± 0.0436; normalized 80.63 ± 49.15) (p=0.5557) (**Figure 5.12A, 5.13A**). Ultimately, no differences where reported between the multiple exposure times of 6-OHDA, comparing 1 hour (0.0598 ± 0.0284; normalized 67.47 ± 35.23) with 2 hours 6-OHDA (0.0712 ± 0.0436; normalized 80.63 ± 49.15) (p=0.2680) or 3 hours (0.0612 ± 0.0347; normalized 69.76 ± 39.83) (p=0.9968) (**Figure 5.12A, 5.13A**).

On the other hand, the O.D. of GFAP was examined in cultures treated previously with 3.5 nM paclitaxel and exposed to AA or 6-OHDA (**Figure 5.12B, 5.13B**). The results showed that there was a significant decrease of GFAP O.D. in 36% and 37% only when cultures were compared between 3.5 nM paclitaxel (0.0623 ± 0.0311; normalized 70.49 ± 35.05) and 1 hour 6-OHDA (0.0400 ± 0.0285; normalized 45.01 ± 32.19) (p=0.0008) and 3 hours 6-OHDA (0.0391 ± 0.0267; normalized 44.62 ± 30.97) (p=0.0006), respectively, but not against 2 hours of 6-OHDA (0.0507 ± 0.0392; normalized 57.88 ± 44.07) (p=0.2788) (**Figure 5.12B, 5.13B**). On this occasion, there were not statistically

significant differences in the O.D. GFAP from AA (0.0481 ± 0.0320; normalized 54.43 ± 36.66) cultures and other cells treated with 6-OHDA (1 hour, p=0.4494; 2 hours, p=0.9719; 3 hours, p=0.3948) (**Figure 5.12B, 5.13B**). The O.D. GFAP of cultures treated only with 3.5 nM paclitaxel (0.0623 ± 0.0311; normalized 70.49 ± 35.05) or AA (0.0481 ± 0.0320; normalized 54.43 ± 36.66), were not statistically significant (p=0.0888) either (**Figure 5.12B, 5.13B**). Lastly, no statistically significant differences were found comparing the three exposure times of 6-OHDA, including 1 hour (0.0400 ± 0.0285; normalized 45.01 ± 32.19) *versus* 6-OHDA 2h (0.0507 ± 0.0392; normalized 57.88 ± 44.07) (p=0.1505) or 6-OHDA 3h (0.0391 ± 0.0267; normalized 44.62 ± 30.97) (p=0.1213) (**Figure 5.12B, 5.13B**).

Finally, when these two sets of data (DMSO and 3.5 nM paclitaxel) were compared with each other to see how an earlier treatment with paclitaxel affected the O.D. of GFAP when astrocytes are challenged with 6-OHDA or AA (**Figure 5.12B, 5.13A, B**), the statistical analysis showed that there were significant differences between the VM cultures treated with DMSO or paclitaxel in all the experimental groups. Hence, when the O.D. of GFAP was compared from cultures treated only with DMSO (0.1115 ± 0.0347; normalized 100 ± 39.45) against the O.D. of GFAP of cultures treated only with paclitaxel (0.0623 ± 0.0311; normalized 70.49 ± 35.05), as it was expected, there was a significant (p=0.0055) reduction in 30% (**Figure 5.12C, 5.13A, B**). Likewise, in astrocytes challenged with AA, there was a significant decrease (p<0.0001) in 40% of the O.D. GFAP when cultures were treated previously with paclitaxel (0.0481 ± 0.0320; normalized 54.43 ± 36.66) in comparison to DMSO (0.0801 ± 0. 0.0311; normalized 90.01 ± 35.51) (**Figure 5.12C, 5.13A, B**). In line with this, in all cultures treated with 6-OHDA, the reduction in the O.D. of GFAP was higher in those cultures treated with paclitaxel. Thus, in 1 hour 6-OHDA, there was a statistically significant (p=0.0142) decrease of 33%, at 2 hours (p=0.0046) the reduction was 30%, and at 3 hours (p=0.0009) there was a depletion of 35% (**Figure 5.12C, 5.13A, B**).

In summary, these results show that 50 μM 6-OHDA was able to reduce the O.D. of GFAP when cultures were treated with DMSO or 3.5 nM paclitaxel the previous 5 DIV compared with those cultures only treated with DMSO or paclitaxel, respectively. Furthermore, in the DMSO group, there were also differences between cultures treated with AA and 6-OHDA. As a whole, the reduction of O.D. GFAP was always exacerbated when cultures were previously exposed to paclitaxel, regardless of whether they were treated afterwards with AA or 6-OHDA.

5.4 Discussion

5.4.1 Paclitaxel treatment can enrich the number of DAn in primary cultures from the VM region

5.4.1.1 Paclitaxel reduces the density of astrocyte and changes in their morphology

In this chapter, the effect that a reduction of astrocytes, measured by the O.D. of GFAP, has on the viability of DAn was evaluated. To asses this, different concentrations (1.75, 3.5, 7, 14 nM) of the anti-mitotic drug paclitaxel was added to the culture for 7 DIV, in order to kill the cells that were able to divide. The results of these experiments showed that paclitaxel, using the vehicle control of DMSO, seemed to reduce the total number of cells while growing in cultures at 4 DIV. When quantitative statistical analyses were performed using immunofluorescence at 7 DIV, it was observed that paclitaxel was able to decrease GFAP O.D. in a dose-dependent manner. In addition to this, qualitative observations suggested a change in morphology of the GFAP-positive cells from a star like shape to a flatter and egg-shape. The expression of the GFAP intermediate filament is usually very high in cultures of primary astrocytes (Tawfik *et al*., 2006), because these astrocytes are considered reactive due to the stresses suffered during their dissection (Lange *et al*., 2012). Therefore, a reduction of this protein by O.D. with paclitaxel would indicate a reduction in the density of these cells.

As described in the Introduction, paclitaxel has been extensively investigated *in vitro* to treat glioblastomas at doses below 250 nM and even 18 nM, producing a cytotoxic effect that destroys glioma cells (Silbergeld *et al*., 1995; Tseng *et al*., 1999). These results would be in agreement with the data presented in this chapter, supporting the idea that paclitaxel can reduce the density of astrocytes when used below a concentration of 14 nM. The destructive effect of the anti-mitotic drug likely involves stabilizing the microtubule of astrocytes and affecting their reorganization during mitosis, which causes mitosis arrest and the death of the cell (Nogales *et al*., 1995; Magidson *et al*., 2016).

The changing morphology of astrocytes surviving paclitaxel treatment would match previous research using the compound. This response has been described previously by Goetschy and colleagues (1986) and Abe and Saito (1999), who both used 500 nM of paclitaxel and reported a flatter morphology in cortical astrocytes. Hence, this chapter shown, for the first time using VM astrocytes, that even lower doses of the anti-mitotic compound can produce this effect. The morphology of astrocytes *in vivo* presents heavily branched processes that interact with blood vessels, other glial cells and neuronal synapses; remodelling these branches through plasticity of their cytoskeleton in response to neuronal activation (Schweinhuber *et al*., 2015). This has been shown in experiments applying *in vivo* whisker stimulation to mice. This produces an increase in the coverage of bouton-spine interface with an expansion of the perimeter of the astrocytic membrane in the cortex (Genoud *et al*., 2006). However, studies in cultures have demonstrated that astrocytes *in vitro* typically develop a stellate morphology characterized by thin and long processes (Schweinhuber *et al*., 2015). Astrocytes can become flatter and more polygonal in the presence of certain compounds, as Safavi-Abbasi *et al*. (2001) showed using cortical cultures from P2 rats. In their study, they observed that the addition of lysophosphatic acid, a stimulator of RhoA pathway, generated flat astrocytes without processes without affecting the amount of βtubulin. In contrast, Ren *et al*. (2017) have determined that 1 μM paclitaxel in renal cell carcinomas increased the levels of GTP-RhoA protein expression, which caused the reorganization

of tubulin and microtubules; changing from being widely distributed in the cytoplasm to compactly surrounding the nucleus. This suggests that the stabilization of microtubules by paclitaxel might be mediated by RhoA activation, which may explain why this drug causes flatter shape astrocytes.

5.4.1.2 Paclitaxel at low doses does not affect the viability of neurons and DAn

Although paclitaxel should not have caused DAn death in primary cultures from E14 rats due to the fact that they are post-mitotic, the results from the experiments here showed that 7 nM and 14 nM paclitaxel reduced both the total number of neurons and DAn. A possible explanation for this is the demonstrated ability of paclitaxel to induce neurotoxicity, producing short axons and a "dying back" reaction (see Introduction, **Table 5.1**). However, the concentrations of paclitaxel used in those experiments (e.g., 1–10 μM in hippocampal neurons) were much greater that the doses used in this study (7 nM and 14 nM). The ability to generate neurodegeneration at such a low dose could be due to differences in neurotoxicity according to the neural types used. Thus, neurons from the VM area, including DAn, might be more sensitive to the exposure to paclitaxel than DRG neurons (Scuteri *et al*., 2006; Gornstein and Schwarz, 2017) or cortical neurons (Jang *et al*., 2008; Figueroa-Masot *et al*., 2001). Indeed, as Gornstein and Schwarz (2017) have demonstrated that hippocampal neurons were more sensitive than DRG neurons, with hippocampal neurons displaying fragmentation of their axons, something that did not occur in DRG neurons. It is also important to bear in mind that in almost all primary cultures from the CNS where the neurotoxicity of paclitaxel was investigation, they did not observe the effect that the drug had on astrocytes within the culture (see **Table 5.1**). Only one article (Jang *et al*., 2008) reported no changes in astrocytes with 30–1000 nM paclitaxel, although the data was not shown. This implies that the degeneration seen in neurons cultured at high dosages of paclitaxel might be mediated or reinforced by a reduction of astrocytes and their functions.

In the experiments here, a high depletion of the density of astrocytes was found with 7 nM and 14 nM of paclitaxel. Consequently, another reason that could be involved in the decline of neurons is the high dependence that these cells have on astrocytes, generating neuronal death once these astrocytes have died. As it was cited in the Introduction, astrocytes are involved in the maintenance and support of neurons, regulating the BBB (Janzer and Raff, 1987), modulating myelination (Sorensen *et al*., 2008), reducing and neutralizing ROS (McBean, 2017), and providing metabolic support and energy (Voutsinos-Porche *et al*., 2003). Therefore, less astrocytes and a decrease of their functions would be detrimental for the survival of neurons, proving the main hypothesis of this chapter. Furthermore, another simple possibility is that, unlike *in vivo* where astrocytes form a complex 3D network along with other cells and neurons, 2D cultured astrocytes form a flat monolayer (Lange *et al*., 2012), having thus the ability to attach neurons by providing a good substrate for the extension of their processes (Powell *et al*., 1997). Moreover, as Aebersold *et al.* (2018) demonstrated, providing a cellulose fibre matrix of astrocytes for neurons to grow increased their viability and neurite outgrowth even when neurons were plated at a low-density. In this way, it is possible that if astrocytes degenerate, neurons will lose their physical ability to be attached to the culture surface, forcing those neurons to detach from the coverslip and die. This situation would explain why the neurons that were kept alive at high doses of paclitaxel are those neurons that form islands of cells, without a lot of astrocytes nearby that can trigger neuronal detachment. These group of neurons might have the capacity to support each other, preventing the lack of astrocytic support.

On the other hand, the results of this chapter showed that doses below 3.5 nM paclitaxel did not affect the viability or morphology of total neurons or DAn, and in fact, there was a trend of increasing their number with 3.5 nM paclitaxel compared to the control group. It was noticed in the Introduction (see **Table 5.2**) that a concentration below 10 nM of paclitaxel can promote axon outgrowth with the formation of active neuronal networks (Witte *et al*., 2008). Actually, the formation of more or longer axons has been seen to

promote neuronal survival in embryonic cortical neurons that were compared with individual cells with a low number of connections (Aebersold *et al.*, 2018). Although the number and length of axons in these VM cultures were not analysed, it would be reasonable in the future to explore this possibility. Furthermore, the hypothetical increase of the number of neurons by longer axons and the establishment of a more stable neuronal network might be justified by the reduction of astrocytes found at 3.5 nM paclitaxel. The depletion of astrocytes as a deleterious mechanism for neurons has been discussed so far in this section. However, it is important to remember that a harmful scenario for neurons might also be created if the opposite situation (i.e., an excess of astrocytes) appears in cultures. Hence, it is known that the glial scar that is formed after injury of the CNS and contains high number of reactive astrocytes (Moeendarbary *et al*., 2017), stops neuronal regeneration and inhibits neurite growth, as Wanner *et al*. (2008) reported generating a glial scar model with cortical astrocytes and DRG neurons. This has been shown in organotypic VM cultures from E12 and E14 rats by af Bjerken *et al*. (2008), using different concentrations of AraC (0.5–5 μM) to reduce the density of astrocytes and their mobility. This promoted the growth of long axons from primary neurons. Therefore, paclitaxel, reducing the density of astrocytes, might be eliminating the 'glial scar' situation in these primary cultures, allowing the extension of neurites and the formation of more networks. Supporting this assumption, is the work by Sengottuvel *et al.* (2011), where the administration of 1 μM paclitaxel *in vivo* in an injured rat optic nerve improved axon regeneration by the interrupting glial scar formation, and treatment with different doses of paclitaxel (3, 10, 50, 100 nM) reduced the expansion of astrocytes in a primary astrocyte culture with a scratch injury.

In summary, it might be possible that with low doses of paclitaxel (i.e., 3.5 nM), there is a perfect balance between the density of astrocytes and neurite outgrowth, which would generate an increment in the survival of neurons. To be true, 3.5 nM paclitaxel would be a very good tool to control the population of astrocytes *in vitro* and generate healthier and more enriched neuronal cultures.

5.4.2 Initial treatment with paclitaxel increases the toxic effect of 6-OHDA in astrocytes but not in DAn

The second objective of this chapter was based on the hypothesis that after a reduction of the density of astrocytes, DAn challenged with a toxin would be more vulnerable to the cytotoxic effect due to the lack of support of astrocytes. For that, 3.5 nM paclitaxel was the selected dose chosen, because at this concentration the density of astrocytes was reduced without affecting the viability of DAn. To challenge DAn, 50 μM 6-OHDA, a specific toxin widely used to damage DAn *in vitro* (Ding *et al*., 2004) and generate PD models *in vivo* (Ungerstedt, 1968; Fuller *et al*., 2014) was added to the culture after 5 DIV. That concentration of 6-OHDA was determined after observing that, at that dose, 6-OHDA was able to kill approximately half of DAn compared to the control AA; and after seeing that that 100 μM 6-OHDA was killing all cells.

5.4.2.1 6-OHDA reduces the number of DAn in VM cultures, but paclitaxel does not exacerbate this effect

6-OHDA is a hydroxylated analog of dopamine which allows its recapture by the dopamine transporter DAT (Hernandez-Baltazar *et al*., 2017). Although its mechanism of action is not fully understood, it is known that it is related to its high oxidation, a process that can happen inside or outside the cell. This is thought to increase the production of H_2O_2 and ROS, elevating the oxidative stress with the consequence being cell death (Blum *et al*., 2001). The data presented in this Thesis showed that independent of the exposure time (1 hour, 2 hours or 3 hours), there was a reduction of DAn of approximately 50% when cells were challenged with 6-OHDA in both cultures treated previously either with DMSO or paclitaxel. The lack of differences in the number of DAn between the multiple exposure times of 6-OHDA can be due to an ‘all or nothing’ effect of this toxin within the cell, where once the toxin is recaptured in the DAn during the first hour, this time is enough to generate ROS. Similar to these findings, Barkats *et al*. (2002)

reported, in an identical investigation treating E14 VM cultures with 50 μM 6-OHDA for 2 hours, a reduction of the number of DAn by 65%.

However, the effect of paclitaxel did not exacerbate the degeneration of DAn by 6-OHDA, which indicated that the depletion of astrocytes when paclitaxel was applied did not increase the vulnerability of these neurons against the toxin. It is possible that regardless of the density of astrocytes in the DMSO treatment, this toxin affects the DAn without astrocytes having enough of defensive role in the process. It seems possible that 6-OHDA could generate an increase of oxidative stress inside the DAn, not allowing the astrocytes to have access to the ROS molecules to buffer them with the antioxidants release by these cells (McBean, 2017). Moreover, as discussed below, astrocytes were affected by 6-OHDA, as there was a reduction of their density not only with paclitaxel but also in controls. This means that if astrocytes were also damaged by 6-OHDA, they might not maintain their support properties, and might directly impair their antioxidant capabilities.

Interestingly, the effect of paclitaxel did not exacerbate the degeneration of DAn when it was added in combination with 6-OHDA but produced an increase of death of DAn when these neurons were treated with AA. AA is an antioxidant that has been commonly used as a vehicle of 6-OHDA to avoid its oxidation (Holtz and O'Malley, 2003; Ding *et al*., 2004). However, a recent publication has demonstrated that 0.15% AA enhanced the toxicity of 25−100 μM 6-OHDA when they were added in combination in SH-SY5Y cells for 15 minutes, an effect that was mediated by an increase of calcium influx within the cells (Wang *et al*., 2017). Although this effect will not explain the reduction of the number of DAn only with AA, it is essential to have this in mind for future experiments, because the effect found with 6-OHDA might be mediated and intensified with AA. Nevertheless, the lack of degeneration within the group that was only treated with AA and DMSO corroborated that AA, at least on its own, was not toxic for DAn. Regardless of this effect, AA has been seen to stabilize the microtubules in endothelial cell cultures, promoting their assembly and polymerization (Parker *et al.*, 2016). As earlier mentioned in the

Introduction, although neurons have long and stable microtubules, their dynamic features are necessary for axonal transport and survival (Gornstein *et al*., 2014). Therefore, it might be possible that an overstabilization of the microtubules in DAn when paclitaxel and AA are added together could alter some of the vital neuronal functions that also need depolymerization of the microtubules, which would cause the degeneration of these neurons.

5.4.2.2 The reduction of the density of astrocytes found with 6-OHDA was aggravated with paclitaxel

Apart of the degeneration of DAn with 6-OHDA, astrocytes were also affected by 6-OHDA in the DMSO and paclitaxel group, observing that this effect was aggravated when cultures were previously treated with paclitaxel.

Theoretically, the effect of 6-OHDA should be selective to DAn, however studies have shown that 6-OHDA can also produce the degeneration of non-DAn. For example, Michel and Hefti (1990) reported that 10–100 μM of 6-OHDA for 24 hours caused the death of GABAergic neurons in embryonic VM cultures. Likewise, Kramer *et al.* (1999) observed by phase contrast microscopy that 10–50 μM 6-OHDA for 30 minutes produced a remarkable decrease in overall cell viability. In the case of astrocytes, different concentrations of 6-OHDA (30, 60, 120 μM) have been proven to cause cell death in primary astrocyte cultures and in rat and human astrocytoma cell lines (Raicevic *et al*., 2005). This study reported DNA fragmentation and apoptosis linked to an increase of oxidative stress, due to the auto-oxidation of 6-OHDA outside the cell, generating H_2O_2. Hence, a similar mechanism might be happening in the VM cultures here, where an increase of ROS in the media by auto-oxidation of 6-OHDA induces the degeneration of astrocytes. This effect, added to the fact that the density of astrocytes is reduced with paclitaxel, would help to explain why the effect of paclitaxel exacerbates the effect of 6-OHDA on astrocytes.

5.5 Conclusions

In summary, although this chapter proved that paclitaxel was a drug that can be used to reduce or control the density of astrocytes in VM cultures, generating more enriched DAn cultures, it was not possible to eliminate almost completely the density of astrocytes without affecting the number of DAn. In the objective 3, this chapter wanted to assess what happened when DAn-enriched cultures (from VM cultures where an elimination of embryonic astrocytes was performed) were co-culture with adult SNpc astrocytes from young and old individuals. However, the lack of elimination of embryonic astrocytes in this study means that these adult astrocytes had to be co-culture together with embryonic astrocytes, which would make very difficult the interpretation of the data without knowing which astrocytes (e.g., embryonic or adult) are giving the support to DAn. Moreover, it was demonstrated that 6-OHDA reduced the number of DAn but also the density of astrocytes. Along with this, the low density of astrocytes with paclitaxel did not have an effect in the viability of DAn when these were exposed to 6-OHDA. This suggests that in the hypothetical case of testing the susceptibility of DAn against 6-OHDA with adult astrocytes, it might not have any effect between young and old astrocytes because 6-OHDA can also affect glial cells. These two situations compromised the objective 3 of this chapter, which was not examined at the end.

Chapter 6.

Multi-study proteomics analyses of the ageing and PD nervous system

CHAPTER 6: MULTI-STUDY PROTEOMICS ANALYSES OF THE AGEING AND PD NERVOUS SYSTEM

6.1 Introduction

Overview: It has been demonstrated in Chapter 3 that proteomics is a powerful technique to identify which molecular pathways are dysregulated during the ageing process in the nervous system. As explained in detail in the Introduction of the Chapter 3, research has focused on the study of the PD proteome by using diverse human samples, including different areas of the brain such as the SNpc (Basso *et al*., 2003; Basso *et al*., 2004; Choi *et al*., 2004; Jin *et al*., 2006; Kitsou *et al*., 2008; Werner *et al*., 2008; Licker *et al*.; 2012; van Dijk *et al*., 2012; Dumitriu *et al*., 2016; Liu *et al*., 2015; Bereczki *et al*., 2018; Ping *et al*., 2018; Lachen-Montes *et al*., 2019), and biofluids such as serum, CSF or urine (Trezzi *et al*., 2017; Kitamura *et al*., 2018; Boerger *et al.*, 2019; Wang *et al*., 2019). In addition, neurotoxic (e.g., 6-OHDA, MPTP) and genetically modified animal models, that replicate the disease under controlling conditions in the lab, have also been used in proteomic studies to gain more insight into the disease process (Scholz *et al*., 2008; Triplett *et al*., 2015; Islam *et al*., 2016; Visscher *et al*., 2016; Cowie *et al*., 2017; Kasap *et al*., 2017;Kim *et al*., 2017a; Maasz *et al*., 2017; Froyset *et al*., 2018). In general, the biological functions that were dysregulated during PD were related to metabolism, oxidative stress, as well as axonal and cytoskeleton remodeling, among others. To help understand why PD is generally associated with the elderly, a wide range of proteomic studies have also been performed in the nervous system during the physiological ageing process, with the idea of gaining a deeper understanding of the consequences that ageing has in neurodegenerative diseases. These proteomic investigations, using samples from both humans (Chen *et al*., 2003; Dominguez *et al*., 2016; Pabba *et al*., 2017) and rodents (Mao *et al*., 2006; Gokulrangan *et al*., 2007; Raghunathan *et al*., 2018), have revealed that ageing affects biological processes related to energy metabolism, cytoskeleton structure or proteostasis. Thus, based on the description of the narrative literature, it seems that proteomics studies in both PD and

ageing are showing dysregulation in similar biological processes (e.g., metabolism, cytoskeleton). Importantly, this could indicate that proteomic changes during ageing precede or have a direct implication in the development or course of the disease, although more systematic analysis, as the one presented in this Thesis chapter, are necessary to corroborate these findings.

6.1.1 Multi-study proteomic comparisons to understand common dysregulated molecular pathways in the ageing nervous system and PD

During proteomic analyses, independent studies produce large sets of proteomics data that, many times, are deposited in public-domain repositories (Vizcaino *et al*., 2010). In general, from these big datasets, only a few proteins are interrogated and validated in each single study. Nevertheless, despite the undeniable value of this type of proteomic approach, the exclusion of most of the proteins for further examination can lead to an underestimation of the implications that certain proteins, and their associated molecular pathways, have on the proteome in question. To avoid this, precise systemic reviews (or multi-study proteomic comparisons) from similar proteomes can be executed by extracting and collecting the secondary data of each single study in order to find common dysregulated targets or proteins (Uman, 2011). The results of these comparisons, which can be further examined by different bioinformatics analyses, help to draw more powerful and robust conclusions associated with the research questions, and provide an effective tool to unravel the complex molecular mechanisms that define them. In fact, the advantages of using this approach have been demonstrated previously, as Soltic and colleagues (2018) proved using a comparative analysis of proteomic studies related to spinal muscular atrophy (SMA) and amyotrophic lateral sclerosis (ALS). As a result, they found common differentially expressed proteins between both diseases that might be useful for creating new therapies in the future.

Given that the interest of this Thesis is the ageing process and its relation to PD, finding common dysregulated proteins between independent proteomic studies related to the

ageing nervous system or PD can help to generate a reference proteome for both PD and ageing. This could help establishing pathological mechanisms that might explain the causes of this disease. Moreover, these ageing and PD proteomes can be compared with each other to elucidate the molecular and protein implications that ageing has in PD. In addition, the ageing reference proteome is a useful database to understand if the proteomic changes found in the rat SNpc during ageing (see Chapter 3) are exclusive of this area of the brain (which would explain the higher vulnerability to degeneration of the SNpc) or, on the other hand, if they are conserved in the entire nervous system during ageing. This last possibility might indicate that other processes, apart from ageing, are necessary to explain the degeneration of SNpc DAn, but also it could mean that the SNpc has more demanding requirements and dependency for certain proteins expressed in the whole brain compared to other regions of the CNS. Lastly, the PD reference proteome will shed on which proteins and molecular pathways (if any) are conserved between PD and the ageing SNpc in rats.

6.1.2 Aim and objectives

The aim of this study was to compare the data of published proteomic studies related to the ageing nervous system, as well as PD, observing which differentially expressed proteins were common in both and in order to generate a well-defined reference proteome related to ageing and PD. It is expected that this multi-study proteomic comparison, together with bioinformatics analyses, might help to understand the mechanism(s) that underlie the disease and the implications that ageing has on its development.

Based on this, the objectives of this chapter were:

- Objective 1) To identify the common differentially expressed proteins in proteomic studies related to the ageing nervous system (including the

dysregulated proteins from the rat SNpc found in the Chapter 3 of this Thesis) and the biological meaning of these changes in the proteome.

- Objective 2) To determine the common differentially expressed proteins in PD proteomic studies and the biological implications of this dysregulation.
- Objective 3) To establish the common differentially expressed proteins (and their biological meaning) between the reference PD proteome and the reference ageing nervous system proteome, focusing in the ageing rat SNpc.

6.2 Materials and methods

Details about materials and methods of this experimental chapter can be found in Chapter 2, section 2.3.

6.3 Results

6.3.1 Examination of ageing nervous system proteomic studies

Over the 75 articles reviewed, a total of 21 studies related to the ageing process in the nervous system were suitable for comparison (**Table 6.1**). From these, articles that used label-free or quantitative proteomics (based on labelling methods such as super-SILAC or TMT) showed the highest number of differentially expressed proteins compared with 2DE gel electrophoresis procedures (**Table 6.1**). As described in **Table 6.1**, five articles used human and non-human primate samples; 16 articles, including the proteomic study performed in this Thesis (see Chapter 3), examined rodents; and one was done in sheep. The areas that were analyzed combined different regions of the brain such as the cortex, hippocampus, striatum, or cerebellum, but also included mitochondria and nuclear fractions from the entire CNS, and CSF.

Table 6.1. Proteomic studies of the ageing nervous system (brain and cerebrospinal fluid, CSF) included in the comparison. Each article has associated a reference that has been used to identify each article in the result sections. In the case that an article showed results for more than one region of the brain or species, more than one reference was added to that article. In the case than an article analysed the protein expression at different time points in the same region, the same reference is allocated but with 'a' or 'b'. The table shows the species, type of sample, and age in each study. Moreover, the number of differentially expressed proteins identified in each study is presented, together with the number of proteins that have been used for the comparison. In the case some proteins were removed, the reasons were: ‡ Proteins not identified or repeated. † After applying a 25% filter because a fold-change cut-off was not applied previously. * It was only possible to obtain the ten most differentially expressed proteins. Analysis platform and protein database used in each study appear in the last column.

Article	Ref.	Sample (age compared)	Differentially expressed proteins (included in comparison)	Analysis platform and protein database
Arguelles *et al.*, 2011	[1]	Rat hypothalamus (3 months *vs.* 24 months)	8 (8)	2DE GE, MALDI-TOF/TOF NCBInr database
Chadwick *et al.*, 2012	[2]	Rat hypothalamus (2-3 months *vs*. 24 months)	147 (147)	Cy3/Cy5 dye labelling, Panorama Cell signalling Array chip (Sigma)
Chen *et al.*, 2003	[3]	Human temporal, frontal and parietal lobes (23 years *vs.* 73 years)	5 (3)‡	2DE GE, Micromass MALDI-TOF (Micromass) or Bruker autoflex MALDI-TOF (Bruker Daltonics) Swiss-prot or NCBInr database
Chen *et al.*, 2018	[4]	Sheep CSF (1-2 years *vs*. 3-6 years *vs*. 7-10 years)	70 (70)	iTRAQ4plex labelling, 4800 MALDI-TOF/TOF (Applied Biosystems) Mammal NCBInr database
Cutler *et al.*, 2017	[5]	Mouse whole brain, nuclear isolation (3 months *vs*. 24 months)	32 (32)	Label-free, Orbitrap Fusion (ThermoFisher Scientific) Mouse Uniprot database
Duda *et al.*, 2018	[6]	Mouse cerebellum (1 months *vs.* 12 months)	219 (219)	Label-free, Q-Exactive HF Orbitrap (ThermoFisher Scientific)
	[7]	Mouse cortex (1 months *vs.* 12 months)	97 (97)	

	[8]	Mouse hippocampus (1 months *vs.* 12 months)	256 (256)	
Flowers *et al*. 2017	[9]	Mouse whole brain, primary microglia culture (3-4 months *vs.* 20-24 months)	271 (158)†	Super-SILAC labelling, Q-Exactive Orbitrap plus (ThermoFisher Scientific) *Mus musculus* Uniprot database
Graham *et al*., 2019	[10]	Human occipital cortex (18-25 years *vs*. 40-45 years *vs*. +70 years)	1145 (1145)	Label-free, LTQ-Orbitrap (ThermoFisher Scientific) IPI-*Macaca mullata* and IPI-*Homo sapiens databases*
	[11]	Human hippocampus (18-25 years *vs*. 40-45 years *vs*. +70 years)	1044 (1044)	
	[12]	Rhesus monkey occipital cortex (9.5 years *vs*. 15.6 years *vs*. 23 years)	1423 (1423)	
	[13]	Rhesus monkey hippocampus (9.5 years *vs*. 15.6 years *vs*. 23 years)	1269 (1269)	
Hamezah *et al*., 2018	[14]	Rat hippocampus (14 months *vs*. 18 months *vs*. 23 months *vs.* 27 months)	97 (5)†	2DE-GE, Q-Exactive HF Orbitrap (ThermoFisher Scientific) *Rattus norvegicus* Uniprot database
	[15]	Rat striatum (14 months *vs*. 18 months *vs*. 23 months *vs.* 27 months)	5 (1)†	
Mao *et al.*, 2006	[16]	Mouse whole brain, mitochondria fraction (2 weeks *vs.* 24 months)	6 (6)	2DE-GE, Bruker Reflex IV MALDI-TOF (Bruker Daltonics) NCBInr database
McGinn *et al*., 2012	[17]	Rat subventricular zone (1 month *vs*. +24 months)	7 (7)	2DE-GE, LCQ Deca XP Plus (ThermoFinnigan) MASCOT database
Pabba *et al*., 2017	[18]	Human orbitofrontal cortex (15-43 years *vs*. 62-68 years)	127 (127)	Label-free, Orbitrap Elite (ThermoFisher Scientific)
Pollard *et al*., 2016	[19]	Mouse whole brain, mitochondria fraction (4-11 weeks *vs*. 20 months)	4 (4)	2-DE-GE, Q-TOFII (Waters) Swissprot and NCBInr databases
Poon *et al.*, 2004	[20]	SAMP8 mouse whole brain (4 months *vs*. 12 months)	5 (5)	2-DE-GE, Finnigan LCQ 'classic' quadrupole ion trap (Finnigan) NCBInr database
Poon *et al.*, 2006	[21]	Mouse whole brain (6 weeks *vs.* 20 months)	4 (4)	2DE-GE, TofSpec 2E MALDI-TOF (Micromass) NCBI database
Smidak *et al*., 2017	[22]	Rat dentate gyrus (17 weeks *vs*. 22 months)	153 (153)	TMT10plex labelling, Q-Exactive Plus Orbitrap (ThermoFisher Scientific) *Rattus norvegicus* Uniprot database

Wille *et al.*, 2015	[23]	Rat cerebellum (3 months *vs.* 21 months)	21 (21)	2DE-GE, 4700 MALDI-TOF/TOF (Applied Biosystems) *Rattus norvegicus* Uniprot database
Stauch *et al.*, 2015	[24a]	Mouse whole brain, mitochondria fraction (12 months *vs*. 24 months)	519 (519)	Super-SILAC labelling, AB Sciex TripleTOF (TTOF) 5600 (Applied Biosystems)
	[24b]	Mouse whole brain, mitochondria fraction (5 months *vs.* 24 months)	553 (553)	
Zeccaa	[25]	Human hippocampus (22-49 years *vs*. +70 years)	60 (60)	TMT4plex labelling, Thermo Q-Exactive Orbitrap Benchtop (ThermoFisher Scientific) Human FASTA Uniprot database
Xu *et al.*, 2016b	[26a]	Human temporal lobe (34 years *vs*. 62 year)	64 (10)*	TMT4plex labelling, Thermo Q-Exactive Orbitrap Benchtop (ThermoFisher Scientific) Human FASTA Uniprot database
	[26b]	Human temporal lobe (34 years *vs*. 84 years)	91 (10)*	
	[26c]	Human temporal lobe (34 years *vs.* 95 years)	70 (10)*	
Yang *et al.*, 2008	[27]	Mouse whole brain (3 months *vs.* 6 months *vs*. 12 months *vs*. 15 months)	39 (39)	2DE-GE, Bruker autoflex MALDI-TOF (Bruker Daltonics) Rodent NCBI database
'Thesis study'	[28a]	Rat substantia nigra (16 months *vs.* +21 months)	28 (28)	iTRAQ4plex labelling, TripleTOF 5600 (AB Sciex) UniProtKB/Swiss-Prot FASTA database
	[28b]	Rat substantia nigra (8 months *vs.* +21 months)	43 (43)	

6.3.2 The ageing process generates conserved protein changes in the nervous system

The comparison of the differentially expressed proteins that change with ageing in the 21 articles reviewed left a total of 648 proteins that were independently observed in at least three different studies as being altered in ageing. From these, 147 proteins changed in the same direction (44 proteins were always upregulated with ageing, while 103 proteins were always downregulated with ageing), and 501 proteins showed contrary directions depending on the study. Among the downregulated proteins, dihydropyrimidinase like 3 (*dpysl3*) was the protein that appeared repeated in the highest number of articles, being presented in six different studies (**Table 6.2; Table S1 Annex 2; Supplementary Table 4**). In the case of the upregulated proteins, alpha-crystallin B chain (*cryab*) appeared in eight independent studies, followed by hyaluronan and proteoglycan link protein 2 (*hapln2)* and palmitoyl-protein thioesterase 1 *(ppt1)* both in seven studies, and sulphated glycoprotein 1 *(psap)* in six studies (**Table 6.3; Table S2 Annex 2; Supplementary Table 4**). Lastly, glial fibrillary acidic protein (*gfap*, GFAP), versican core protein (*vcan*) and aggrecan core protein (*acan*) were the non-conserved (different direction of expression) proteins presented in more studies (seven in total), including the rat SNpc proteomic study; while MARCKS-related protein (*marcksl1*) and calreticulin (*calr*) were also two proteins that were presented in seven studies without including the rat SNpc proteomic study (**Table 6.4; Table S3 Annex 2; Supplementary Table 4**). In most cases, versican core protein (*vcan*), aggrecan core protein (*acan*) and GFAP were upregulated with ageing, without existing a pattern in the direction of the expression of these proteins according to the species or region of the brain study (see **Table 6.1**). For example, in the case of GFAP, it was upregulated in rhesus monkey hippocampus, subventricular zone in rats, orbitofrontral cortex and hippocampus in humans, and when the whole mouse brain was examined; while it was downregulated in the occipital cortex of rhesus monkeys (Graham *et al*., 2019) and in the rat SNpc proteome (see **Table 6.1**). When the proteins from the proteomic study of the rat SNpc

presented in this Thesis (Chapter 3) were compared with the rest of the articles analyzed, only one protein, monoglyceride lipase (*mgll*) was also downregulated in two different areas (i.e., hippocampus and occipital cortex) in rhesus monkeys (Graham *et al*., 2019) (**Table S1 Annex 2; Supplementary Table 4**), while six proteins were also upregulated in other studies, including alpha-crystallin B chain (*cryab*), hyaluronan and proteoglycan link protein 2 (*hapln2*), sulphated glycoprotein 1 *(psap*), myelin-associated oligodendrocyte basic protein *(mobp*), apolipoprotein E (*apoe*) and haemoglobin subunit alpha 1 (*hba1*) (**Table 6.3; Table S2 Annex 2; Supplementary Table 4**). Thus, alpha-crystallin B chain (*cryab*) was also upregulated in mouse cortex and hippocampus, human hippocampus and orbitofrontal cortex, rhesus monkey occipital cortex and hippocampus, and rat dentate gyrus (**Table 6.1**). Hyaluronan and proteoglycan link protein 2 (*hapln2*) was upregulated in mouse cerebellum, cortex and hippocampus, but also the hippocampus of humans and rhesus monkeys, and rat dentate gyrus (**Table 6.1**). There was an increase of sulphated glycoprotein 1 *(psap)* in sheep CSF, rhesus monkey occipital cortex and hippocampus, human orbitofrontal cortex, and rat dentate gyrus (**Table 6.1**). Interestingly, myelin-associated oligodendrocyte basic protein *(mobp*) was only upregulated in mice, in the areas of the cerebellum, cortex, hippocampus and when the whole brain was studied (**Table 6.1**). Apolipoprotein E (*apoe*) increased in the whole brain of mice, and the hippocampus of humans and rhesus monkeys; while haemoglobin subunit alpha 1 (*hba1*) was upregulated in human hippocampus and occipital cortex of monkeys (**Table 6.1**). Nevertheless, as **Table 6.1** shows, it is important to note that the articles where these proteins were found represent the studies where more proteins were identified in total, based on the used proteomic approaches (e.g., label-free and quantitative proteomics). Lastly, in the case of proteins expressed in opposite directions, 29 proteins from the rat SNpc proteome in ageing, including GFAP, versican core protein (*vcan*), and aggrecan core protein (*acan*) (already mentioned in this subsection) were also dysregulated in other independent studies (**Table 6.4; Table S3 Annex 2; Supplementary Table 4**).

Table 6.2. Differentially expressed proteins that change in the same direction (downregulated) in at least three different proteomic studies related to the ageing nervous system. Only proteins that are expressed in four or more studies are presented. The rest of the list can be found in **Table S1** (**Annex 2**) The first column shows the gene name of the 44 proteins downregulated (red cells) with ageing. Numbers indicate the reference numbers of each article, which can be checked in **Table 6.1**.

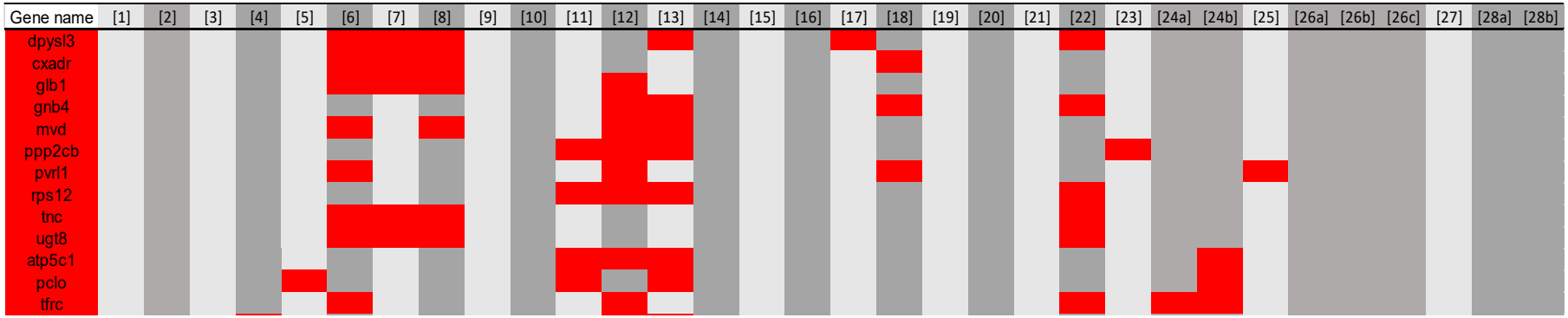

Table 6.3. Differentially expressed proteins that change in the same direction (upregulated) in at least three different proteomic studies related to the ageing nervous system. Only proteins that are expressed in four or more studies are presented. The rest of the list can be found in **Table S2** (**Annex 2**) The first column shows the gene name of the 103 proteins upregulated (green cells) with ageing. Numbers indicate the reference number that can be checked in **Table 6.1**.

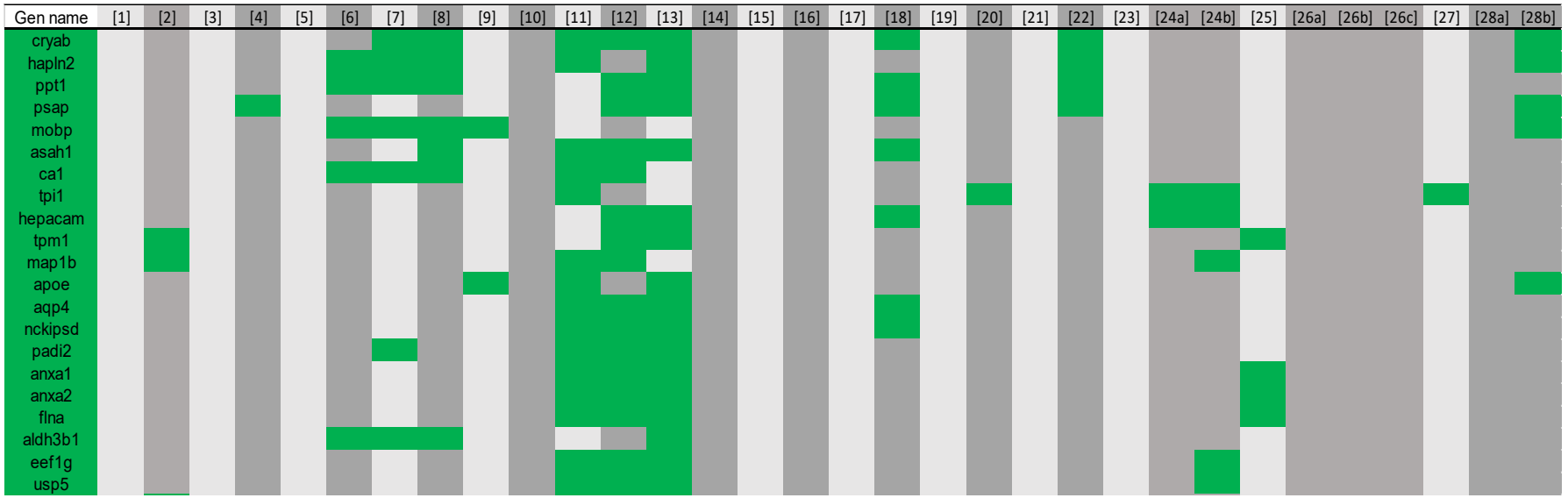

Table 6.4. Differentially expressed proteins that change in different direction (down- and upregulated) in at least three different proteomic studies related to the ageing nervous system. Only proteins that are expressed in six or more studies are presented. The rest of the list can be found in **Table S3** (**Annex 2**) The first column shows the gene name of the 501 proteins downregulated (red cells) or upregulated (green cells) with ageing. Numbers indicate the reference number that can be checked in **Table 6.1**.

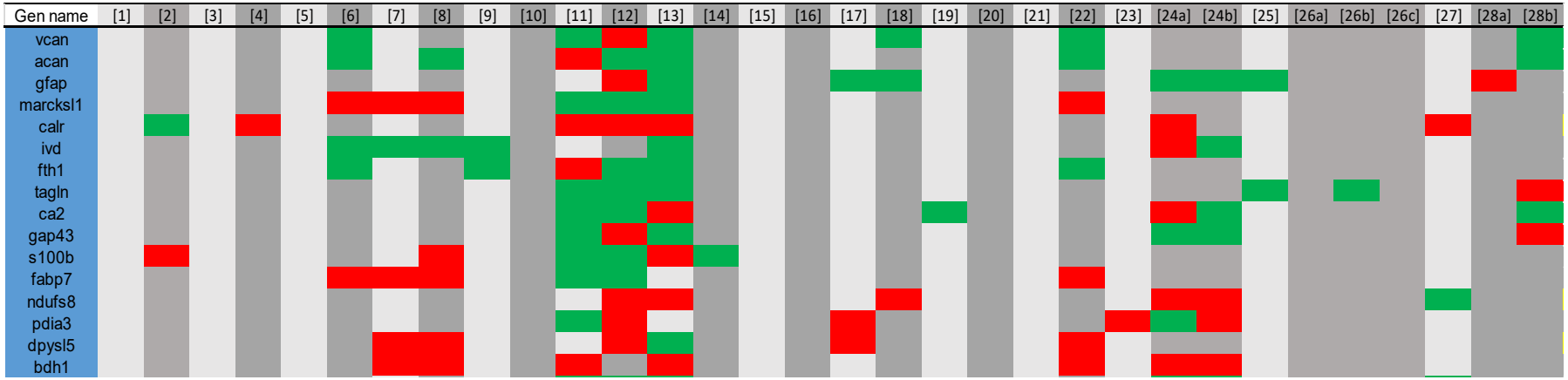

6.3.3 Proteins related to mitochondrial energy metabolism, oxidation-reduction process and cell adhesion are dysregulated in a conserved manner in the nervous system during ageing as revealed by Gene Ontology analysis

GO analysis using DAVID software (Huang *et al*., 2007; Huang *et al*., 2009) were performed to obtain a better understanding of the biological meaning of the 147 proteins that were differentially expressed in the same direction in the ageing nervous system. For that, the 44 downregulated and 103 upregulated conserved proteins were analysed independently, accepting GO terms if they had a $p<0.05$ and were assigned to at least two proteins. GO showed that the most enriched biological processes using the 44 downregulated proteins (**Table 6.2; Table S1 Annex 2; Supplementary Table 4**) were the terms 'mitochondrial ATP synthesis coupled proton transport, 'ATP synthesis coupled proton transport' and 'ATP biosynthesis process' (**Figure 6.1A, Table S4 Annex 2**). The top four most enriched terms from the cellular component category linked to downregulated proteins in the ageing nervous system were 'extracellular exosome', 'membrane', 'mitochondrial inner membrane' and 'mitochondrion' (**Figure 6.1B, Table S4 Annex 2**). 'Poly(A) RNA binding' and 'proton-transporting ATP synthase activity, rotational mechanism' were the top two molecular functions most enriched, related to conserved downregulated proteins in the ageing nervous system (**Figure 6.1C, Table S4 Annex 2**). Lastly, three pathways ('metabolic pathway', 'oxidative phosphorylation', and 'Parkinson's disease') were determined as enriched with the downregulated proteins in the ageing nervous system by the KEGG pathway analysis (**Figure 6.1D, Table S4 Annex 2**).

On the other hand, when the 103 upregulated proteins that were conserved in the ageing nervous system (**Table 6.3; Table S2 Annex 2; Supplementary Table 4**) were examined, GO analysis revealed that the terms 'oxidation-reduction process', 'cell-cell adhesion' and 'negative regulation of apoptotic process' were the top three enriched biological processes (**Figure 6.2A, Table S5 Annex 2**).

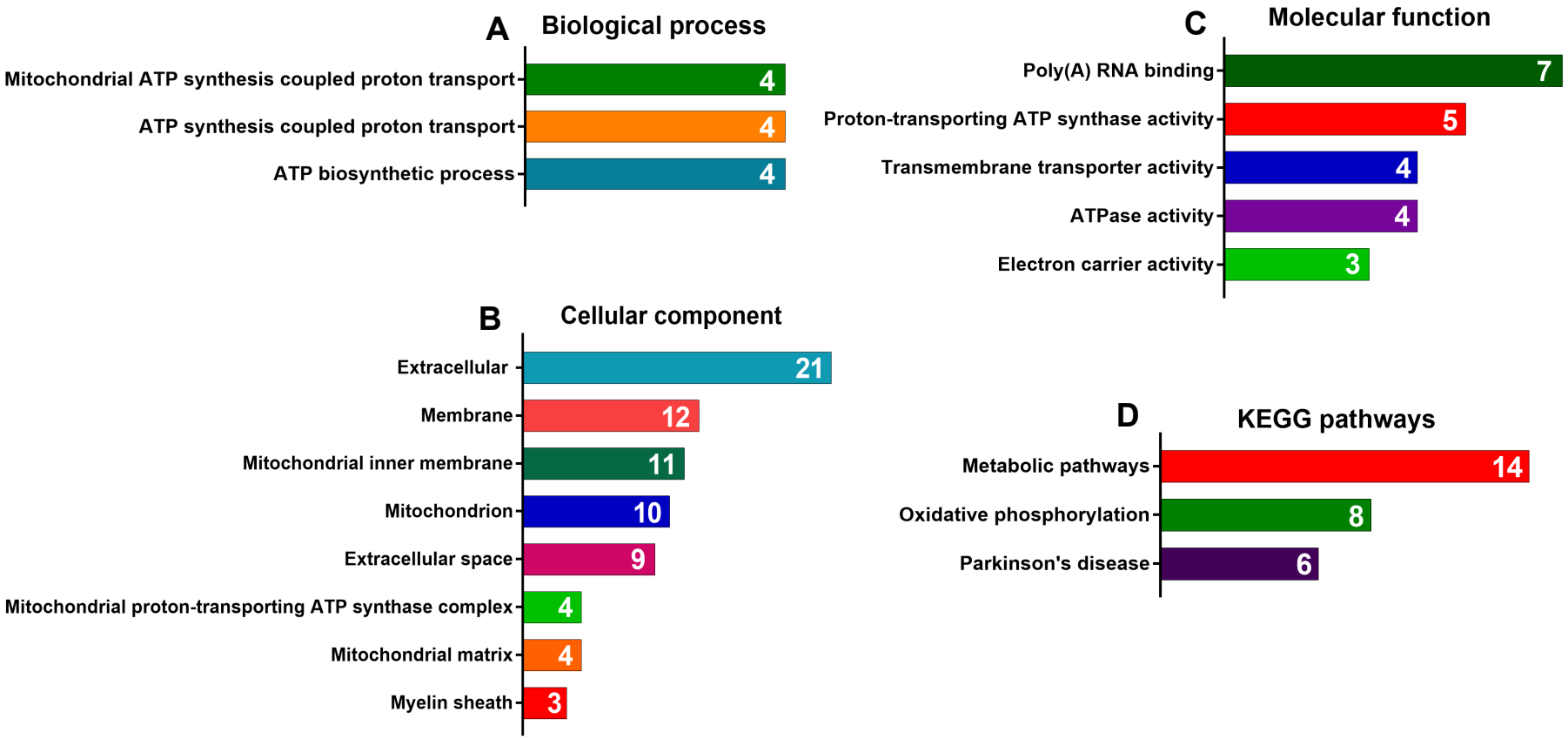

Figure 6.1. Summary of Functional Annotation analyses (Gene Ontology and KEGG) of the 44 downregulated proteins conserved in the ageing nervous system proteome. DAVID software revealed the enriched terms related to **(A)** biological processes, **(B)** cellular components, **(C)** molecular functions, **(D)** and KEGG pathways. In the graphs, the number of annotated proteins is indicated by a white number. The name of annotated proteins for each term and the entire list of terms can be checked in **Table S4** (**Annex 2**).

As cellular components, 'extracellular exosome', 'cytoplasm', and 'cytosol' were by far the terms with the highest number of upregulated proteins associated with them (**Figure 6.2B, Table S5 Annex 2**). In the case of molecular functions, 'cadherin binding involved in cell-cell adhesion', 'identical protein binding' and oxidoreductase activity' were the overrepresented terms when the upregulated proteins were used (**Figure 6.2C, Table S6 Annex 2**). Finally, KEGG analysis showed that 'metabolic pathway', 'lysosome' and 'glycolysis/gluconeogenesis' were the enriched terms associated with upregulated proteins (**Figure 6.2D, Table S5 Annex 2**).

6.3.4 Reactome pathway analysis showed a conserved dysregulation of metabolism, metabolism of proteins and immune system pathways in the ageing nervous system

To extract more information about the biological meaning associated with the 147 dysregulated proteins that were conserved in the ageing nervous system, Reactome pathway analyses (Fabregat *et al*., 2017; Fabregat *et al*., 2018) were performed, examining downregulated and upregulated proteins independently.

In the case of the downregulated proteins (**Table 6.2; Table S1 Annex 2; Supplementary Table 4**), Reactome found 32 out of 44 proteins, generating 297 pathways that were hit by at least one of these proteins. This left 12 downregulated proteins that were not found or mapped to any Reactome entity. Nevertheless, some of these unmappable proteins were identified by DAVID during the GO analysis, including cell adhesion molecule 4 precursor (CADM4), chloride intracellular channel protein 6 (CLIC6) and 2',3'-cyclic-nucleotide 3'-phosphodiesterase precursor (CNP) which were linked to the GO term 'extracellular exosome'; and mitochondrial carrier homolog 1 (MTCH1) and protein piccolo (PCLO) which were associated with the term 'membrane'.

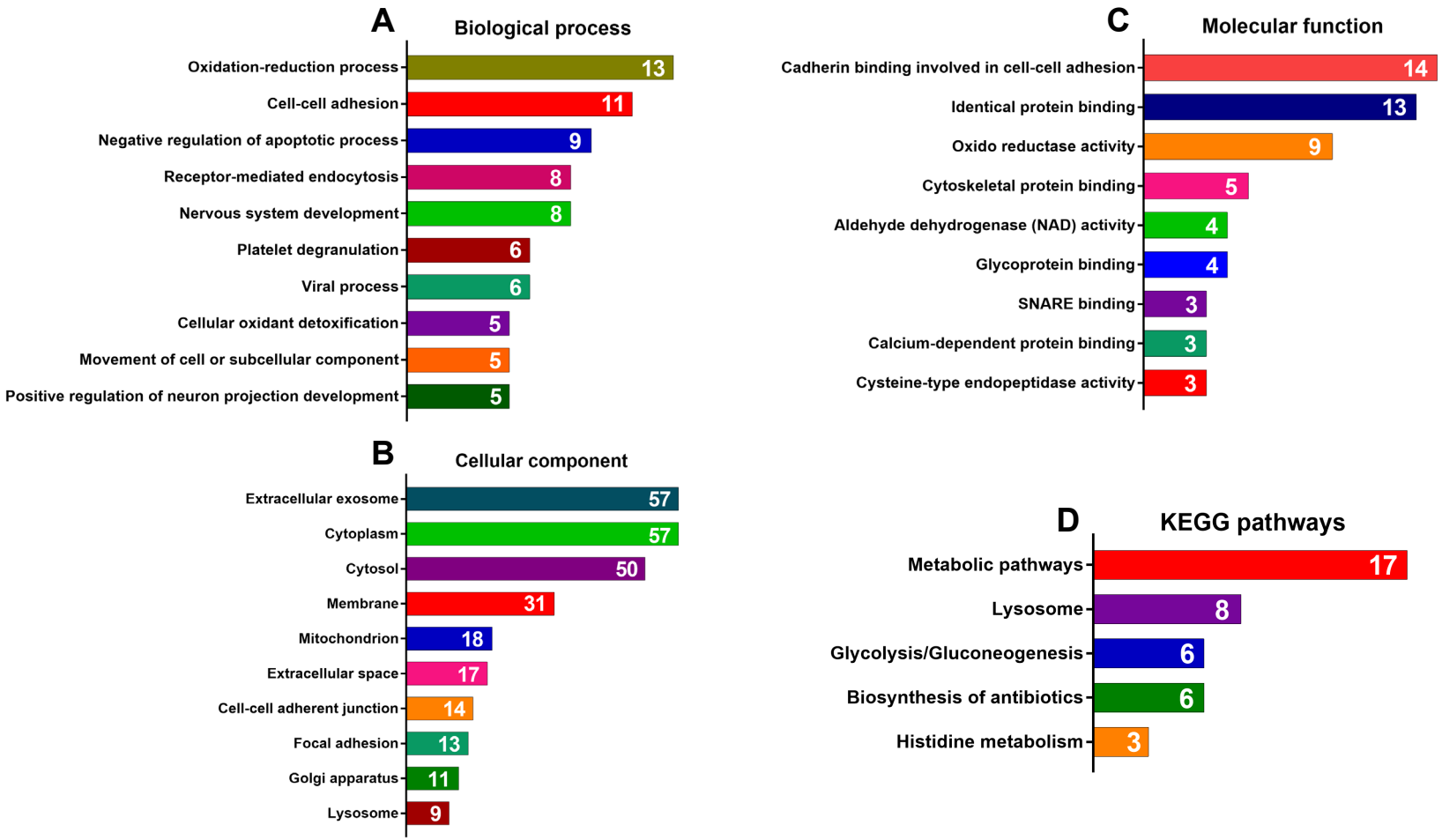

Figure 6.2. Summary of Functional Annotation analyses (Gene Ontology and KEGG) of the 103 upregulated proteins conserved in the ageing nervous system proteome. DAVID software revealed the enriched terms associated with **(A)** biological processes, **(B)** cellular components, **(C)** molecular functions, **(D)** and KEGG pathways. In the graphs, only the top ten terms are shown as bars, with the number of annotated proteins indicated with a white number. The name of annotated proteins to each term and the entire list of terms can be checked in **Table S5** (**Annex 2**).

Table 6.5. The 25 most enriched pathways sorted by the most statistically significant p-values, using the 44 conserved downregulated proteins in the ageing nervous system. 'Entities' refers to Uniprot accession numbers, showing the number of entities found in the analysis from the total in that pathway.

Pathway name	Entities	
	found/total	p-value
Respiratory electron transport, ATP synthesis by chemiosmotic coupling, and heat production by uncoupling proteins	8 / 146	3.93e-08
The citric acid (TCA) cycle and respiratory electron transport	8 / 229	1.16e-06
Formation of ATP by chemiosmotic coupling	4 / 23	1.39e-06
Cristae formation	4 / 31	4.48e-06
Respiratory electron transport	4 / 115	6.87e-04
Mitochondrial biogenesis	4 / 127	9.91e-04
Keratan sulfate degradation	2 / 22	0.003
Iron uptake and transport	3 / 83	0.003
Glycosphingolipid metabolism	3 / 86	0.003
Metabolism	21 / 3,639	0.007
Transferrin endocytosis and recycling	2 / 39	0.008
Phase 2 - plateau phase	2 / 42	0.009
Triglyceride catabolism	2 / 42	0.009
HS-GAG degradation	2 / 44	0.01
MPS IV - Morquio syndrome B	1 / 4	0.014
Keratan sulfate/keratin metabolism	2 / 52	0.014
Complex I biogenesis	2 / 57	0.017
Sphingolipid metabolism	3 / 157	0.017
Translation initiation complex formation	2 / 62	0.02
Activation of the mRNA upon binding of the cap-binding complex and eIFs, and subsequent binding to 43S	2 / 66	0.022
Triglyceride metabolism	2 / 66	0.022
Phase 0 - rapid depolarisation	2 / 68	0.023
Nectin/Necl trans heterodimerization	1 / 7	0.024
Activation of gene expression by SREBF (SREBP)	2 / 70	0.025
Defective NEU1 causes sialidosis	1 / 8	0.027

The Reactome pathway with the most statistically significant p-value was 'respiratory electron transport, ATP synthesis by chemiosmotic coupling, and heat production by uncoupling proteins' (R-HAS-163200) (**Table 6.5**). This pathway was associated with eight proteins: ATP synthase subunit gamma, mitochondrial (ATP5C1), ATP synthase subunit O, mitochondrial (ATP5O), succinate dehydrogenase [ubiquinone] iron-sulfur subunit, mitochondrial (SDHB), ATP synthase subunit d, mitochondrial (ATP5H), NADH dehydrogenase [ubiquinone] 1 alpha subcomplex subunit 12 (NDUFA12), cytochrome b-c1 complex subunit 1, mitochondrial (UQCRC1), ATP synthase subunit g, mitochondrial (ATP5L), and protein arginine methyltransferase NDUFAF7, mitochondrial (NDUFAF7). In addition, the genome-wide view offered an overview of the

overrepresented pathways (Sidiropoulos *et al*., 2017), revealing that the 'respiratory electron transport, ATP synthesis by chemiosmotic coupling, and heat production by uncoupling proteins' pathway was part of the top-level pathway 'metabolism' (R-SHA-1430728) (**Figure 6.3A**). This 'metabolism' pathway, included in the top 25 most enriched pathways associated with the downregulated proteins in the ageing nervous system, was a top-level pathway of another 12 relevant pathways (**Table 6.5, Figure 6.3A**). Altogether, these results corroborate and complement the findings generated by GO analysis, where biological processes associated with ATP metabolism such as 'mitochondrial ATP synthesis coupled proton transport, 'ATP synthesis coupled proton transport' and 'ATP biosynthesis process' were also enriched with the conserved downregulated proteins of the ageing nervous system.

On the other hand, using the 103 upregulated proteins (**Table 6.3; Table S2 Annex 2; Supplementary Table 4**), Reactome analysis found 85 out of 103 upregulated proteins in the ageing nervous system, producing 572 pathways where at least one identified protein was present, and leaving 18 upregulated proteins that were not found or mapped to any Reactome entity. Similar to the downregulated proteins, some of these unmappable upregulated proteins in the Reactome analysis were identified during the GO analysis. This was the case of hepatocyte cell adhesion molecule (HEPACAM) and microtubule-associated protein 1B (MAP1B) linked to the term 'cytoplasm'; as well as sorting nextin-1 (SNX1) and STE20/SPS1-related proline-alanine-rich protein kinase (STK39) associated with the term 'extrinsic component of membrane'. The Reactome pathway with the most statistically significant p-value was 'antigen presentation: folding, assembly and peptide loading of class I MHC' (R-SHA-983170) associated with 21 entities linked to the HLA class I histocompatibility antigen (HLA-A). This 'antigen presentation: folding, assembly and peptide loading of class I MHC' pathway belonged to the top-level pathway 'immune system' as the genome-wide view (Sidiropoulos *et al*., 2017) showed (**Table 6.6, Figure 6.3B**). This top-level pathway was also included in the top 25 most relevant pathways and comprised another 15 enriched Reactome pathways

(**Table 6.6, Figure 6.3B**). Importantly, this Reactome result revealed new pathways that were not discovered by GO analysis, highlighting a dysregulation in the immune system associated with proteins that were upregulated in the ageing nervous system.

Table 6.6. 25 most enriched pathways sorted by the most statistically significant p-values, using the 103 conserved upregulated proteins in the ageing nervous system. 'Entities' refers to Uniprot accession numbers, showing the number of entities found in the analysis from the total in that pathway.

Pathway name	Entities	
	found/total	p-value
Antigen Presentation: Folding, assembly and peptide loading of class I MHC	21 / 102	1.11e-16
Endosomal/Vacuolar pathway	21 / 82	1.11e-16
ER-Phagosome pathway	22 / 165	1.11e-16
Antigen processing-Cross presentation	23 / 187	1.11e-16
Interferon alpha/beta signaling	22 / 184	1.11e-16
Interferon gamma signaling	22 / 250	6.05e-14
Immunoregulatory interactions between a Lymphoid and a non-Lymphoid cell	21 / 316	4.27e-11
Class I MHC mediated antigen processing & presentation	25 / 465	4.48e-11
Interferon Signaling	23 / 392	5.38e-11
Immune System	60 / 2,803	2.46e-08
Cytokine Signaling in Immune system	34 / 1,245	3.90e-07
Adaptive Immune System	29 / 998	9.75e-07
Neutrophil degranulation	19 / 480	1.24e-06
Interleukin-12 family signaling	7 / 96	9.37e-05
Gene and protein expression by JAKSTAT signaling after Interleukin-12 stimulation	6 / 73	1.58e-04
Interleukin-12 signaling	6 / 84	3.33e-04
XBP1(S) activates chaperone genes	6 / 95	6.33e-04
IRE1alpha activates chaperones	6 / 101	8.67e-04
Transcriptional regulation by the AP-2 (TFAP2) family of transcription factors	4 / 52	0.003
Surfactant metabolism	4 / 53	0.003
Defective CSF2RB causes pulmonary surfactant metabolism dysfunction 5 (SMDP5)	2 / 8	0.004
Defective CSF2RA causes pulmonary surfactant metabolism dysfunction 4 (SMDP4)	2 / 8	0.004
Platelet degranulation	6 / 137	0.004
Innate Immune System	25 / 1,324	0.004
Neurofascin interactions	2 / 9	0.004

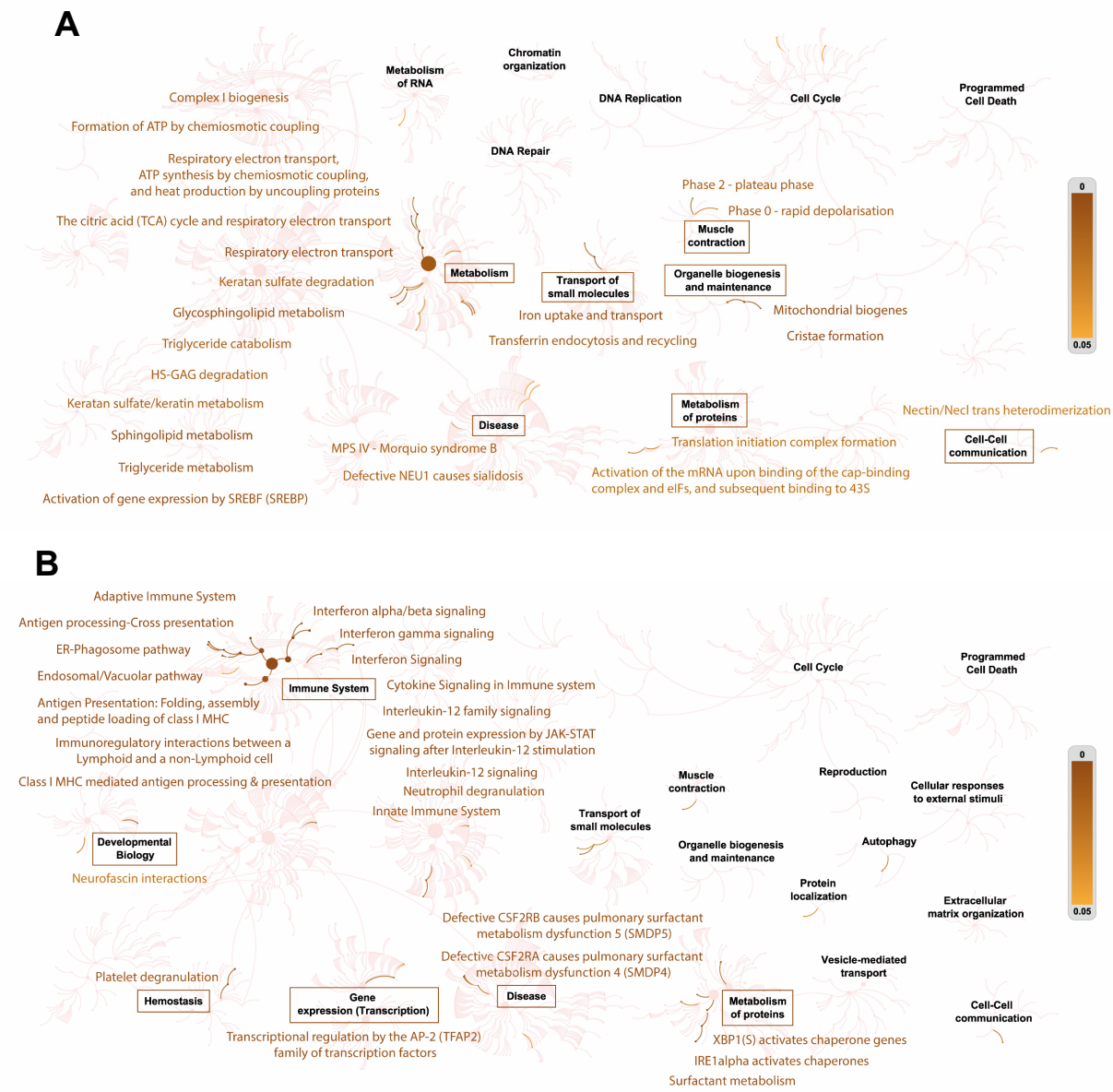

Figure 6.3. Genome-wide overview of the Reactome pathway analysis (Sidiropoulos *et al*., 2017) of the 147 conserved differentially expressed proteins in the ageing nervous system. (A) Genome-wide overview of the Reactome pathway analysis of the 44 conserved downregulated proteins. **(B)** Genome-wide overview of the Reactome pathway analysis of the 103 conserved upregulated proteins. Each top-level pathway has a centre from which other pathways of a lower hierarchy start. Top-level overexpressed pathways are emphasized with a red rectangle (e.g., 'metabolism', 'immune system'), while secondary overexpressed pathways (e.g., 'complex I biogenesis') linked to them are highlighted using a colour-scale that indicates p-value (right-hand side). Light grey pathways are not significantly overrepresented.

6.3.5 Proteins related to mitochondrial ATP metabolism and immune system are the main hubs in the protein network of the conserved downregulated and upregulated proteins in the ageing nervous system

To identify protein-protein interactions between the conserved dysregulated proteins, STRING database (Szklarczyk *et al*., 2019) was performed, executing independent analyses of the 44 downregulated and the 103 upregulated proteins found of the multi-study comparison of the ageing nervous system.

For the 44 downregulated proteins (**Table 6.2; Table S1 Annex 2; Supplementary Table 4**), three proteins (ATP synthase subunit g, mitochondrial (ATP5L), ATP synthase subunit O, mitochondrial (ATP5O), and succinate dehydrogenase [ubiquinone] iron-sulfur subunit, mitochondrial (SDHB)) showed the larger number of associations (eight in total each) with other downregulated proteins (**Figure 6.4**). These three proteins were part of the enriched biological process 'mitochondrial ATP synthesis coupled proton transport, 'ATP synthesis coupled proton transport' and 'ATP biosynthesis process' (**Figure 6.1A, Table S4 Annex 2**), as well as the enriched Reactome pathways related to the top-level 'metabolism' pathway and the second pathways overexpressed associated with it (**Figure 6.3A**). These three proteins were associated between them and also to four proteins downregulated (ATP synthase subunit gamma, mitochondrial (ATP5C1), ATP synthase subunit d, mitochondrial (ATP5H), NADH dehydrogenase [ubiquinone] 1 alpha subcomplex subunit 12 (NDUFA12), and cytochrome b-c1 complex subunit 1, mitochondrial (UQCRC1)). In addition, ATP synthase subunit g, mitochondrial (ATP5L) was associated with V-type proton ATPase subunit S1 (ATP6AP1) and ferrochelatase, mitochondrial (FECH); ATP synthase subunit O, mitochondrial (ATP5O) was associated with V-type proton ATPase subunit S1 (ATP6AP1) and mitochondrial carrier homolog 1 (MTCH1); while succinate dehydrogenase [ubiquinone] iron-sulfur subunit, mitochondrial (SDHB) was linked to ferrochelatase, mitochondrial (FECH) and glycerol-3-phosphate dehydrogenase, mitochondrial (GPD2) (**Figure 6.4**).

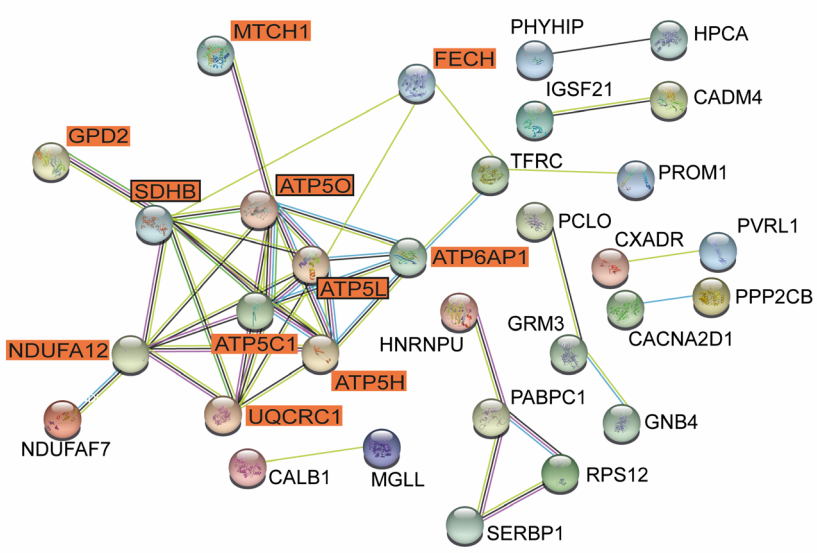

Figure 6.4. Protein network analysis with the STRING database of the 44 conserved downregulated proteins in the ageing nervous system. In orange boxes with black border, proteins show the larger number of associations; while orange boxes alone indicate their protein associations. The network displays only proteins with interactions, hiding those proteins that are disconnected. The coloured lines indicate the type of interaction between proteins (light blue, associated in curated database; pink, experimental or biochemical determined; green, gene neighbourhood; black, co-expression; grey, protein homology; lime, co-mentioned in Pubmed abstracts).

Among the protein network of the 103 upregulated proteins (**Table 6.3; Table S2 Annex 2; Supplementary Table 4**), the receptor protein-tyrosine kinase (EGFR) was the proteins with a larger number of association (18 in total) (**Figure 6.5**). This protein was involved in GO biological processes such as 'negative regulation of apoptosis process', 'receptor mediated endocytosis', and 'positive regulation of phosphorylation' (**Figure 6.2A, Table S6 Annex 2**). This receptor protein-tyrosine kinase (EGFR) was also linked to the top-level 'immune system' enriched pathway in Reactome and other secondary pathways associated with it such as 'cytokine signalling in immune system' (**Figure 6.3B**). The 18 proteins networking with receptor protein-tyrosine kinase (EGFR) were:

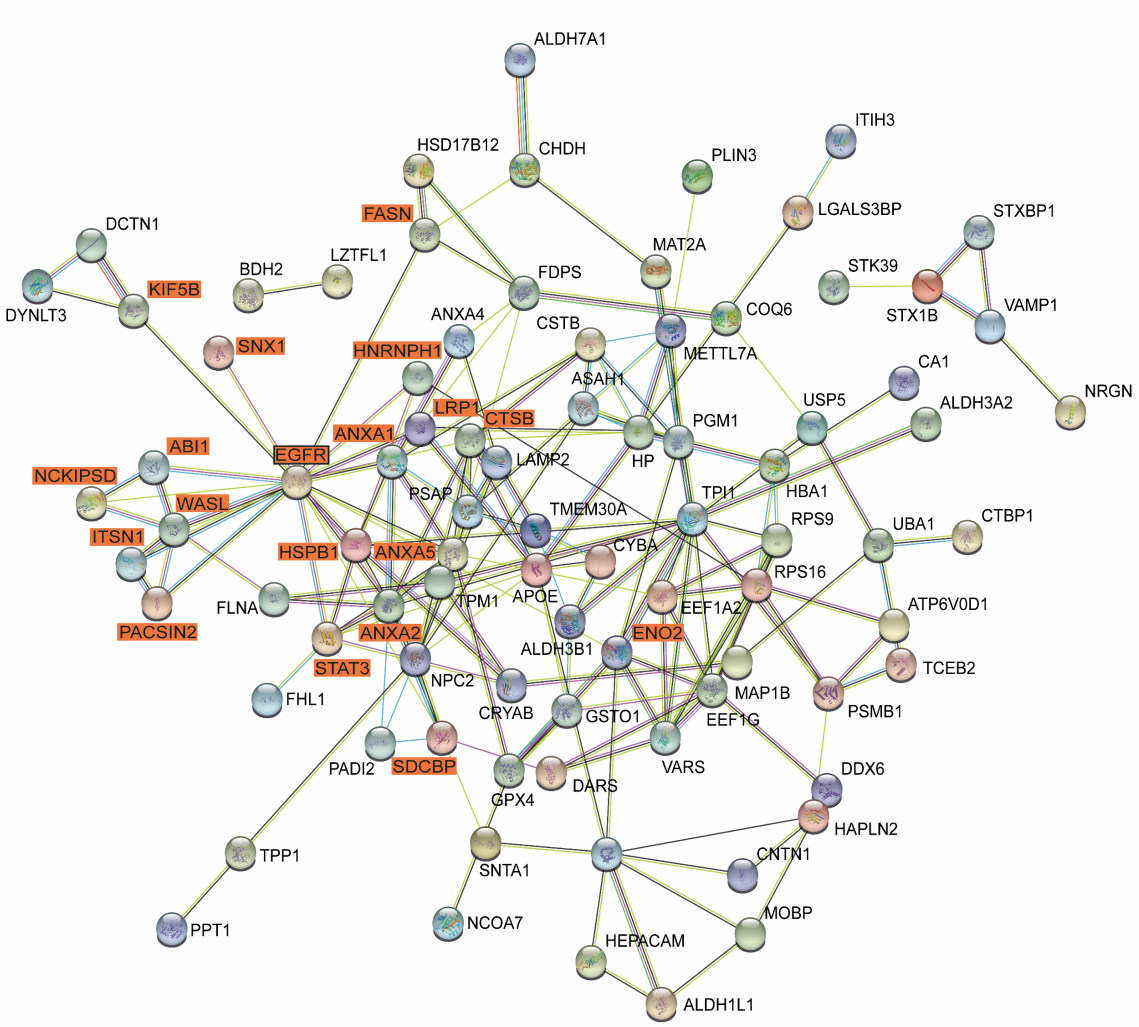

Figure 6.5. Protein network analysis with the STRING database of the 103 conserved upregulated proteins in the ageing nervous system. In orange boxes with black border, proteins that show the larger number of associations; while orange boxes alone indicate their protein associations. The network displays only proteins with interactions, hiding those proteins that are disconnected. The coloured lines indicate the type of interaction between proteins (light blue, associated in curated database; pink, experimental or biochemical determined; green, gene neighbourhood; black, co-expression; grey, protein homology; lime, co-mentioned in Pubmed abstracts).

Abl interactor 1 (ABI1), annexin A1 (ANXA1), annexin A2 (ANXA2), annexin A5 (ANXA5), cathepsin B (CTSB), gamma-enolase (ENO2), fatty acid synthase (FASN), heterogeneous nuclear ribonucleoprotein H (HNRNPH1), heat shock protein beta-1 (HSPB1), intersectin-1 (ITSN1), kinesin-1 heavy chain (KIF5B), prolow-density lipoprotein receptor-related protein 1 (LRP1), NCK-interacting protein with SH3 domain

(NCKIPSD), protein kinase C and casein kinase substrate in neurons protein 2 (PACSIN2), syntenin-2 (SDCBP), sorting nexin-1 (SNX1), signal transducer and activator of transcription 3 (STAT3), and neural Wiskott-Aldrich syndrome protein (WASL) (**Figure 6.5**).

In summary, bioinformatic analysis of the differentially expressed proteins, obtained when proteomic studies of the ageing nervous system were compared, has revealed that mitochondrial ATP metabolism, oxidation-reduction process, cell adhesion and immune system are biological processes that are altered in this proteome.

6.3.6 Examination of PD proteomic studies

In total, 40 studies were found in PD in humans, while 29 articles were found in PD models in mammals. However, only 24 were used in the multi-study comparison in humans (**Table 6.7**) and 13 in PD models (**Table 6.8**). The proteomes that were examined by label-free and TMT labelling proteomics showed the highest number of differentially expressed proteins compared to those proteomes analyzed by 2DE gel electrophoresis (**Table 6.7, Table 6.8**). As referenced in **Table 6.7**, considering only the human studies with PD, six of them examined the SNpc; while another six investigated other areas of the brain, including the prefrontal cortex, locus coeruleus, olfactory bulbs, and subventricular zone. The remaining 11 articles observed different biofluids from parkinsonians such as tears, blood/serum/ plasma, CSF, and urine; and one looked at the rinsing fluids and lenses fractions of parkinsonians in order to find new biomarkers (therefore, this last study was also included in the biofluid comparison). In the case of PD models, as **Table 6.8** shows, four looked at the SNpc of rodents under different toxins such as 6-OHDA, MPTP, or adenoviral injection of PARIS (a substrate of parkin that produce the degeneration of DAn). Nine studies examined the striatum, under conditions of lesioning with 6-OHDA, MPTP, methamphetamine, maneb/paraquat, and adenoviral injection of PARIS. From these, only one study was performed using monkeys and the

Table 6.7 Proteomic studies of PD in humans included in the comparison. Each article has an associated reference that has been used to identify each article in the result section. The table shows the species, type of sample and age in each study. Moreover, the number of differentially expressed proteins identified in each study is presented, together with the number of proteins that have been used for the comparison. In the case some proteins were removed, the reasons were: † It was possible only to obtain the list of the synaptic proteins differentially expressed. ‡ After applying a 25% filter because a fold-change cut-off was not applied previously. * Proteins not identified or repeated. Analysis platform and protein database use in each study appear in the last column. IPI: International Protein Index. VTA: ventral tegmental area.

Article	Ref.	Human sample (age-matched controls)	Differentially expressed proteins (included in comparison)	Analysis platform and protein database
Bereczki *et al*., 2018	[1]	PD with dementia prefrontal cortex (72-89 years) *vs*. controls (65-96 years)	485 (5)†	TMT10plex labelling, Q-Exactive (ThermoFisher Scientific) Huma Swiss-Prot database
Van Dijk *et al*., 2012	[2]	PD locus coeruleus (77 years) *vs.* controls (77 years)	87 (78)‡	1DE GE, LTQ-FT hybrid (ThermoFisher Scientific) Human IPI database
Licker *et al.*, 2014	[3]	PD susbtantia nigra (72 years) *vs.* controls (79 years)	204 (38)‡	TMT6plex labelling, LTQ Orbitrap XL (Thermo Electron) *Homo sapiens* UniProt Swiss-Prot database
Boerger *et al*., 2019	[4]	PD tear fluids (66 years) *vs*. control (63 years)	40 (40)	1DE GE, LTQ Orbitrap XL (ThermoFisher Scientific) *Homo sapiens* UniProt Swiss-Prot database
Lachen-Montes *et al*., 2019	[5]	PD olfactory bulbs (77 years) *vs.* controls (79 years)	268 (268)	Label-free, AB Sciex TripleTOF (TTOF) 5600 (Applied Biosystems) *Homo sapiens* UniProt Swiss-Prot database
Kitamura *et al*., 2018	[6]	PD exosomes from plasma (65 years) *vs.* controls (62 years)	3 (3)	2DE GE, 4800 Plus MALDI-TOF/TOF (Sciex) Uniprot database
Magdalinou *et al*., 2017	[7]	Atypical parkinsonism cerebrospinal fluid (66 years) *vs*. controls (59 years)	26 (26)	TMT6plex labelling, Q-Exactive (ThermoFisher Scientific) UniProtKB Swiss-Prot database

Klettner *et al*., 2017	[8]	PD rinsing fluid and lens fractions (72 years) *vs*. controls (71 years)	1 (1)	2DE GE, Thermo Q-Exactive plus (ThermoFisher Scientific) FAST human database
Chiu *et al*., 2016	[9]	PD serum (62 years) *vs*. controls (61 years)	20 (20)	2DE GE, MS/MS (Bruker Daltonics) SwissProt or NCBInr databases
Xing *et al*., 2015	[10]	PD monocluclear cells from cerebrospinal fluid (57 years) *vs*. controls (56 years)	9 (9)	2DE GE, 4307 MALDI-TOF (Voyager)
Dumitriu *et al*., 2016	[11]	PD prefrontal cortex (76 years) *vs*. controls (79 years)	283 (5)‡	TMT6plex labelling, LTQ Orbitrap Velos (ThermoFisher Scientific) Human IPI database
Liu *et al*., 2015	[12]	PD substantia nigra (78 years) *vs*. control (74 years)	11 (11)	CDIT labelling, Tandem (ThermoFisher Scientific)
Wang *et al*., 2019	[13]	PD urinary extracellular vesicles (63 years) *vs*. controls (66 years)	15 (15)	NuPAGE GE, Thermo Orbitrap Velos Pro (ThermoFisher Scientific) UniRef100 database
Donega *et al*., 2019	[14]	PD subventricular zone (78 years) *vs*. controls (80 years)	90 (90)	2DE GE, TripleTof 5600 (Sciex) Human UniProt database
Alberio *et al*., 2012	[15]	PD blood T-lymphocytes (54 years) *vs.* controls (60 years)	20 (14)*	2DE GE, Esquire 6000 (Burker Daltonics) NCBInr database
Licker *et al*., 2012	[16]	PD substantia nigra (81 years) *vs.* controls (83 years)	23 (23)	2DE GE, LTQ Orbitrap XL (ThermoFisher Scientific) or MALDI-TOF/TOF (Applied Biosystems) *Homo sapiens* UniProt Swiss-Prot database
Zhang *et al*., 2012	[17]	PD serum *vs*. controls	26 (24)‡*	iTRAQ3plex labelling, Qstar XL (Applied Biosystems) Human IPI database
Zhao *et al*., 2010	[18]	PD serum (71 years) *vs*. controls (64 years)	13 (13)	2DE GE, Micromass-ESI-Q-TOD Ultima (Waters) NCBI database
Sinha *et al*., 2009	[19]	PD cerebrospinal fluid (59 years) *vs*. controls (46 years)	6 (4)*	2DE GE, Bruker Ultraflex MALDI-TOF and 2D Nano LC-ESI-Trap (Agilent) NCBI and Swiss-Prot databases

Werner *et al*., 2008	[20]	PD substantia nigra (84 years) *vs.* controls (77 years)	16 (3)‡	2DE GE, Voyager DE Pro (Perseptive Biosystems) NCBI and SwissProt databases
Abdi *et al*., 2006	[21]	PD cerebrospinal fluid (63 years) *vs.* controls (67 years)	72 (53)*	iTRAQ4plex labelling, 4700 Proteomcis analyser (Applied Biosystems) IPI and Celera Discovery System databases
Basso *et al*., 2004	[22]	PD substantia nigra (75 years) *vs.* controls (70 years)	9 (9)	2DE GE, Reflex III MALDI-TOF (Bruker Daltonics) Swiss-Prot database
Choi *et al*., 2004	[23]	PD frontal cortex (72 years) *vs*. controls (76 years)	1(1)	2DE GE, Voyager DE Pro (Perseptive Biosystems) and Finnigan LTQ ion trap (ThermoFisher Scientific) Protein Prospector databases
Jin *et al*., 2006	[24]	PD substantia nigra mitocondrias *vs.* controls	119 (105)*	ICAT labelling, LTQ (ThermoFisher Scientific) Human IPI database

Table 6.8. Proteomic studies of PD models in mammals included in the comparison. Each article has an associated reference that has been used to identify each article in the result section. In the case of an article showing results for more than one region of the brain, more than one reference was added to that article. The table shows the species, type of sample and how much time passed after the dissection (if applicable) in each study. Moreover, the number of differentially expressed proteins identified in each study is presented, together with the number of proteins that have been used for the comparison. In the case some proteins were removed, the reasons were as follow: ‡ After applying a 25% filter because a fold-change cut-off was not applied previously, or p-value (<0.05) filter. * Proteins not identified or repeated. Analysis platform and protein database used in each study appear in the last column. IPI: International Protein Index. KO: Knock-out. WT: wild-type. AAV: adeno-associated viral vectors. VTA: ventral tegmental area. 6-OHDA: 6-hydroxydopamine. MPTP: 1-methyl04-phenyl-1,2,3,4-tetrahydropyrdine. METH: methamphetamine. MB+PQ: maneb and paraquat.

Article	Ref.	Mammal sample (dissection time after lesion or treatment, if applicable)	Differentially expressed proteins (included in comparison)	Analysis platform and protein database
Triplett *et al*., 2015	[1]	PINK1 KO mouse whole brains *vs.* WT controls	23 (23)	2DE GE, LTQ Orbitrap XL (ThermoFisher Scientific) Swiss-Prot database
Kim *et al*., 2017a	[2]	Mouse cortex injected with AAV-PARIS (after 4 weeks) *vs*. AAV-GFP control	48 (48)	2DE GE, LTQ ion-trap (ThermoFisher Scientific) Uniprot database
	[3]	Mouse striatum injected with AAV-PARIS (after 4 weeks) *vs*. AAV-GFP control	61 (61)	
	[4]	Mouse substantia nigra injected with AAV-PARIS (after 4 weeks) *vs*. AAV-GFP control	15 (15)	
Maasz *et al*., 2017	[5]	Substantia nigra from rats treated with unilateral 6-OHDA injection in substantia nigra (after 14 days) *vs*. contralateral controls	1 (1)	2DE GE, Bruker Amazon SL ion trap (Bruker Daltonics) Rat NCBI and Swiss-Prot databases
Stauch *et al*., 2016	[6]	PINK1 KO rat striatum, synaptic mitochondria fraction *vs*. WT controls	69 (69)	SWATH-5600 TripleTOf (Sciex) *Rattus norvegicus* Uniprot database

Kuter *et al*., 2016	[7]	Substantia nigra from rats treated bilateral 6-OHDA injection in the medial forebrain bundle (after 4 weeks), mitochondria fraction *vs*. sham operated controls	47 (15)‡	2DE GE, MALDI-TOF/TOF Ultraflex I (Bruker Daltonics) and Voyager DE-Pro BioSpectrometry and Voyager Data Explorer (Applied Biosystems) *Rattus norvegicus* Uniprot and NCBI databases
Xiong *et al*., 2014	[8]	Striatum from rats treated with unilateral 6-OHDA in striatum (1-month) *vs*. sham operated controls	76 (69)*	2DE GE, 6538 series ESI-Q-TOF (Agilent) Rat Swiss-Prot database
Fuller *et al*., 2014	[9]	Striatum from rats treated with unilateral 6-OHDA injection in medial forebrain bundle (after 14 days) *vs.* unlesioned controls	34 (31)*	iTRAQ labelling4plex, 4800 MALDI-TOF/TOF (applied Biosystems) NCBI database
Lessner *et al*., 2010	[10]	Striatum from rats treated with unilateral 6-OHDA injection in medial forebrain bundle (after 3-months) *vs.* controls	100 (100)	2DE GE, Reflex III MALDI-TOF (Bruker Daltonics) Swiss-Prot and TrEMBL databases
Jeon *et al*., 2008	[11]	Substantia nigra from mice treated with intraperitoneal MPTP injection (after 7 days) *vs.* saline controls	22 (22)	2DE GE, Ettan MALDI-TOF (Amersham Biosciences) Swiss-Prot and NCBI databases
Scholz *et al*., 2008	[12]	Striatum from monkeys treated with intravenous MPTP injection *vs.* vehicle controls	8 (6)*	2DE GE, ESI-LTQ (Thermo Electron) *Homo sapiens* Uniprot database
Chin *et al*., 2008	[13]	Striatum from mice treated with intraperitoneal MPTP injection (after 7 days) *vs.* saline control	86 (70)‡	16O/18O labelling, FTICR Accurate and time tag database
	[14]	Striatum from mice treated with intraperitoneal METH injection (after 7 days) *vs.* saline control	86 (51)‡*	
Patel *et al*., 2007	[15]	Striatum from mice treated with intraperitoneal MB+PQ injection (after 6 and 9 weeks of treatment) *vs.* saline controls	3 (3)	2DE PAGE, Bruker Ultraflex MALDI-TOF/TOF (Bruker Daltonics)
Pierson *et al*., 2004	[16]	Striatum from rats treated with unilateral 6-OHDA injection in medial forebrain (after 21 days) *vs*. controls	4 (1)*	Voyager DE-STR MALDI TOF (Applied Biosystems) Mascot database search tool

rest used rodents (i.e., rats and mice). The cortex was also investigated with an adenoviral injection of PARIS. Lastly, two proteomics investigations were the samples were transgenic mice (PINK KO) were included in the comparison

6.3.7 The proteome changes found in humans with PD are not observed in animal PD models

The examination of the PD proteome in humans revealed that, when the six studies from the SNpc were compared, from the final list of 179 dysregulated proteins only eight proteins appeared in at least two different studies (**Table 6.9, Supplementary Table 5**). Half of them changed in the same direction with PD, finding two proteins (neurocan core protein (*ncan*), pyruvate kinase PKM *(pkm*)) downregulated in two studies, while the two other proteins (integrin beta-1 precursor (*itgb1*), ferritin light chain (*ftl*)) were always upregulated. Conversely, the other half (four of them) had opposing dysregulation patterns. Only one protein, ferritin light chain (*ftl*) was differentially expressed in three studies, while the other seven proteins appeared dysregulated only in two different studies.

Table 6.9. Differentially expressed proteins in the human SNpc with PD in at least two different proteomic studies. The first column shows the gene name of the dysregulated proteins in the human SNpc. Numbers indicate the reference number that can be found in **Table 6.7**. Red cells represent proteins that change in the same direction (downregulated) with PD, while green cells show upregulated proteins with PD. Blue cells are proteins that change in different directions (down- and upregulated) depending on the study.

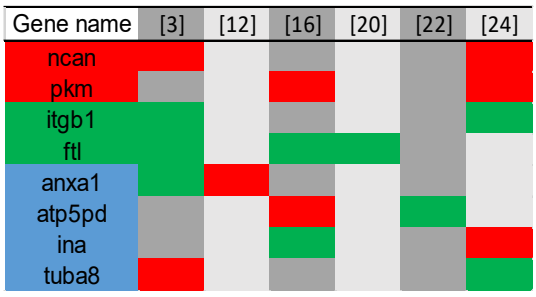

A similar approach was performed, observing six new studies in other areas of the brain together with the six studies from the SNpc. This generated a list of 596 differentially expressed proteins, although only 35 appeared simultaneously in two or more studies (**Table 6.10, Supplementary Table 5**). Seventeen of these 35 proteins changed in the same direction (six were always downregulated with PD, while 11 were always upregulated during the disease). All these 17 proteins were dysregulated with PD in only two articles simultaneously, except in the case of the upregulated protein ferritin light chain (*ftl*) that was differentially expressed in the three studies related to the SNpc. The rest of the 18 proteins were dysregulated with PD in contrary directions. As in previous cases, proteins appeared only in two different articles, except mitochondrial ornithine aminotransferase (*oat*) that was downregulated in two studies and upregulated in one.

The investigation of biofluids and rinsing fluids and lenses fractions from patients with PD revealed 157 proteins that were differentially expressed in 12 articles. When these proteins were compared, only 19 were dysregulated in two or more studies (**Table 6.11, Supplementary Table 5**). From these 19 proteins, five were changed in a conserved way with PD, with four of them downregulated and one (transthyretin precursor (*ttr*)) upregulated. Similar to above, all these proteins appeared only dysregulated in two different studies. Among the 14 proteins whose expression was not conserved between studies, haptoglobin (*hp*) was the protein that was repeated in the highest number of articles (five).

Finally, the comparison of the total 766 dysregulated proteins found in the 24 articles related to PD in humans revealed 68 proteins repeated in at least two different studies. Twenty-eight were conserved between articles (15 downregulated and 13 upregulated with PD), whilst 40 showed opposing directions of differential expression (**Table 6.12, 6.13, 6.14; Supplementary Table 5**). Interestingly, even in this comparison, most of the conserved proteins (except ferritin light chain (*ftl*)) were only differentially expressed in two different studies. Haptoglobin (*hp*) was the protein that was identified in the highest number of articles, all of them associated with the five articles related to biofluids.

Table 6.10. Differentially expressed proteins in the human brain with PD in at least two different proteomic studies. The first column shows the gene name of the dysregulated proteins in the human brain with PD. Numbers indicate the reference number that can be found in **Table 6.7**. Red cells represent proteins that change in the same direction (downregulated) with PD, while green cells show upregulated proteins with PD. Blue cells are proteins that change in different direction (down- and upregulated) depending on the study.

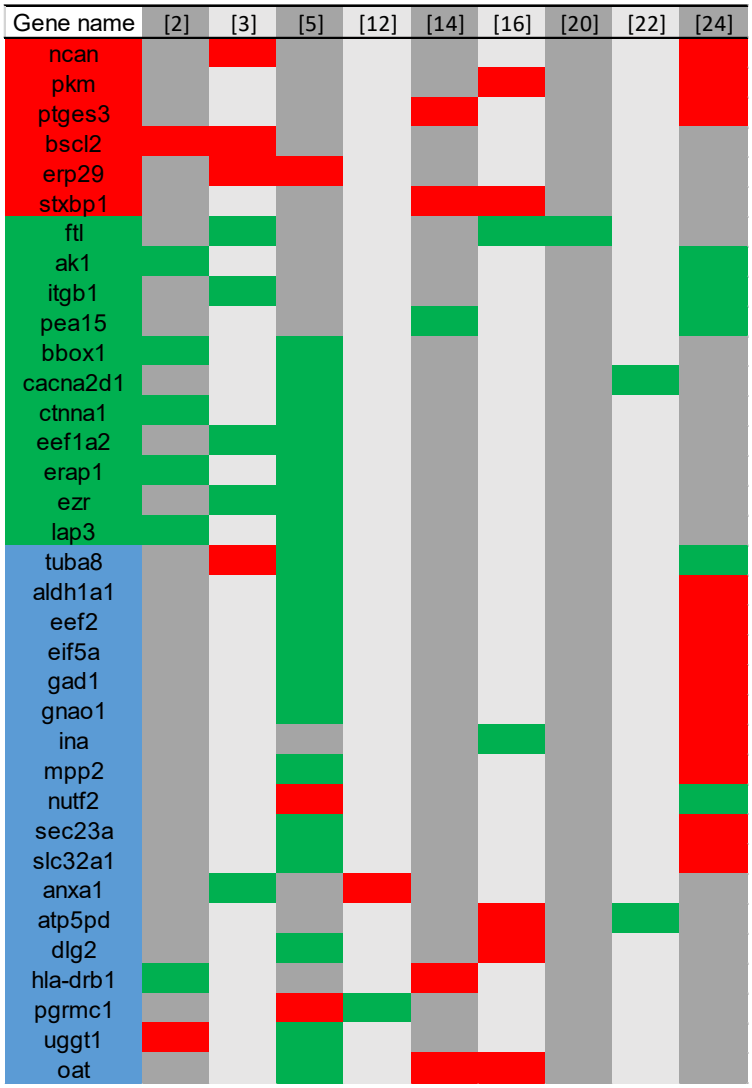

Table 6.11. Differentially expressed proteins in human biofluids with PD in at least two different proteomic studies. The first column shows the gene name of the dysregulated proteins in human biofluids with PD. Numbers indicate the reference number that can be found in **Table 6.7**. Red cells represent proteins that change in the same direction (downregulated) with PD, while green cells show upregulated proteins with PD. Blue cells are proteins that change in different direction (down- and upregulated) depending on the study.

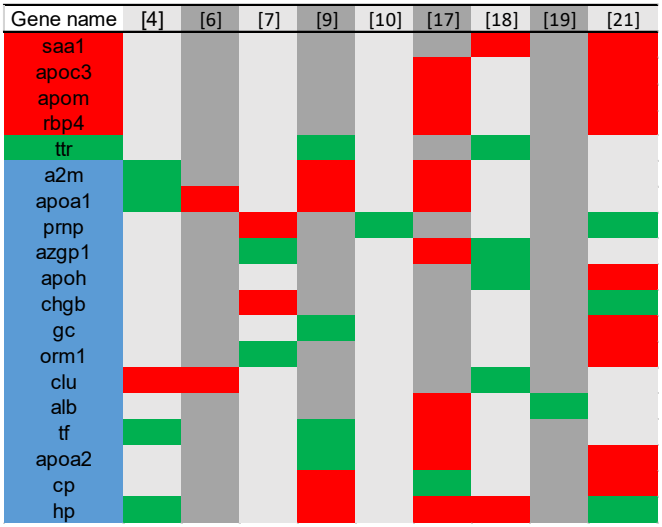

Table 6.12. Differentially expressed proteins that change in the same direction (downregulated) in at least two different proteomic studies related to humans with PD. The first column shows the gene name of the 15 proteins downregulated (red cells) with PD in humans. Numbers indicate the reference number that can be found in **Table 6.7**.

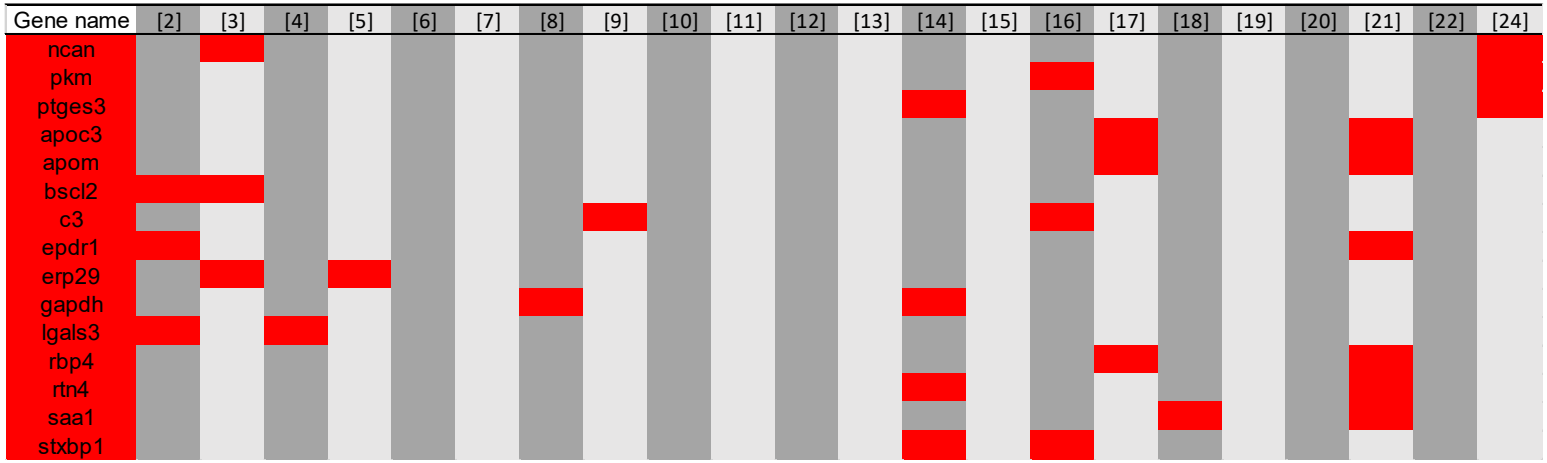

Table 6.13. Differentially expressed proteins that change in the same direction (upregulated) in at least two different proteomic studies related to humans with PD. The first column shows the gene name of the 13 proteins upregulated (green cells) with PD in humans. Numbers indicate the reference number that can be found in **Table 6.7**.

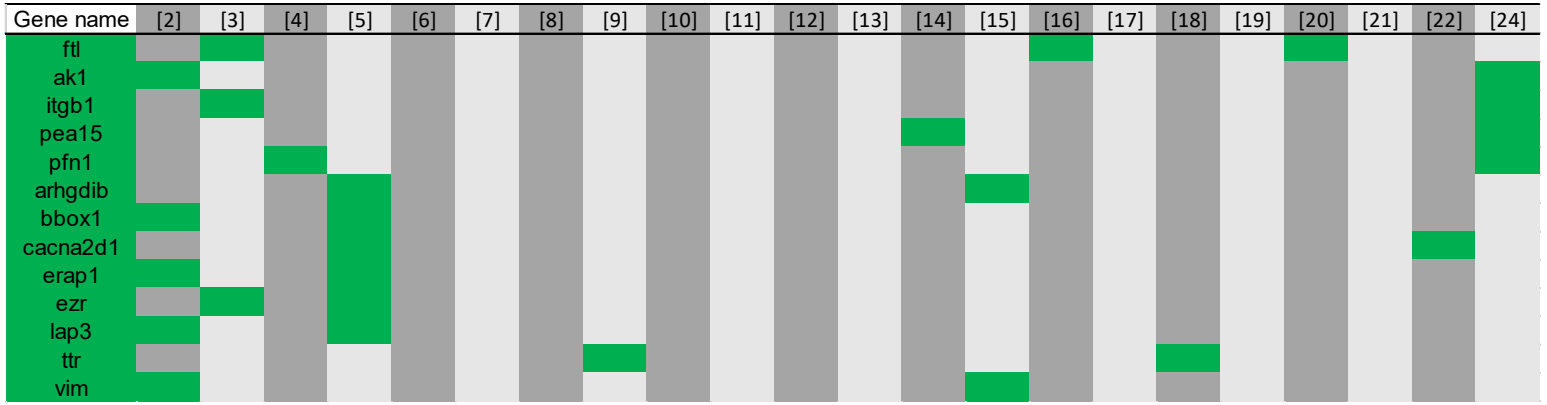

Table 6.14. Differentially expressed proteins that change in different directions (down- and upregulated) in at least two different proteomic studies related to humans with PD. The first column shows the gene name of the 40 proteins downregulated (red cells) and upregulated (green cells) with PD in humans. Numbers indicate the reference number that can be found in **Table 6.7**.

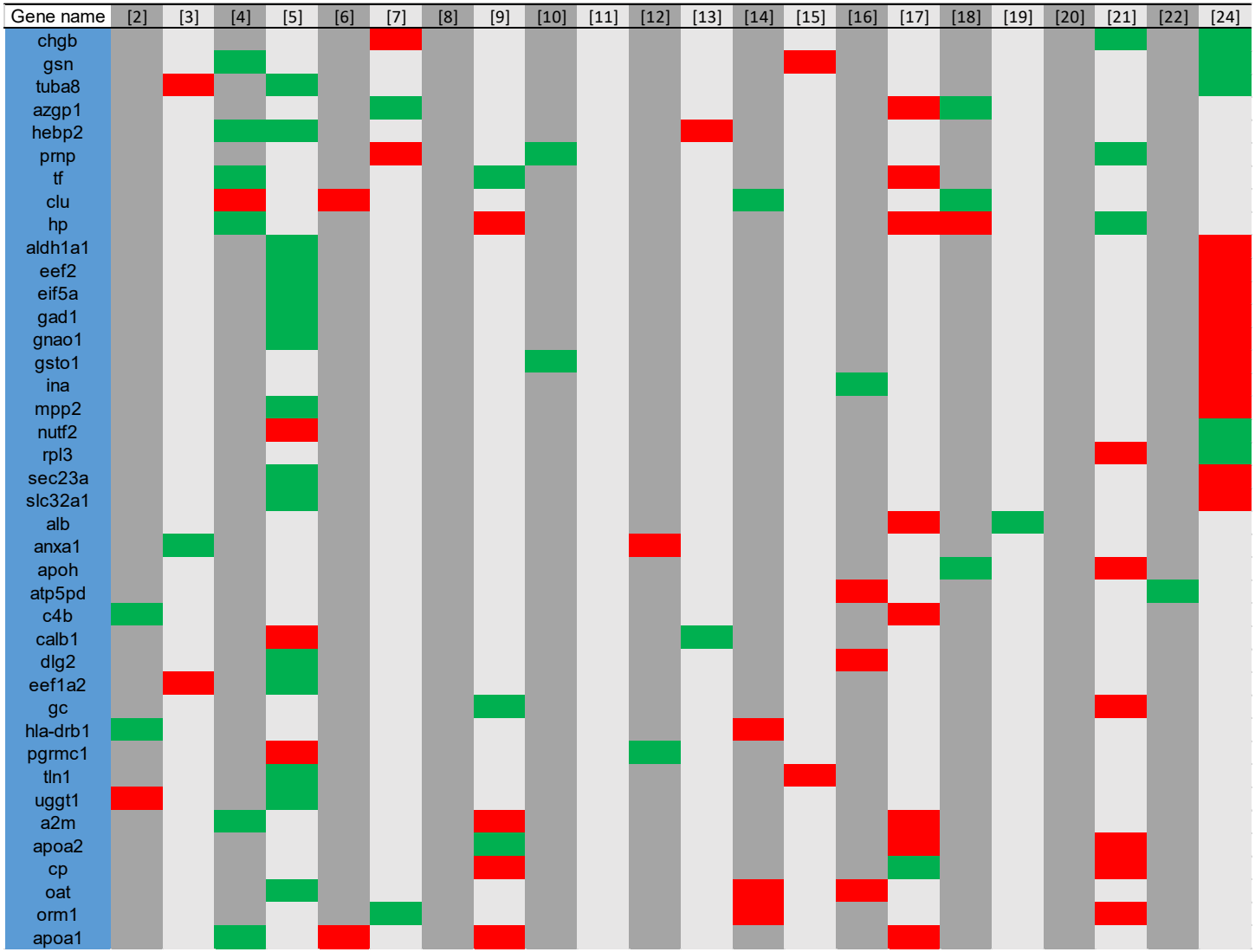

On the other hand, the search of studies related to PD modes in mammals, including rodents and monkeys, led to the finding of 13 different articles where the SNpc, striatum, cortex and whole brain were examined under different toxic (e.g., 6-OHDA, MPTP) or genetic conditions that mimic the disease. In total, 443 proteins were differentially expressed, and from these 113 were repeated in two or more studies). There were 76 proteins whose expression was conserved in the same direction (43 were downregulated and 33 were upregulated), while the 37 proteins left were expressed in opposite the different studies (**Table 6.15, 6.16, 6.17; Supplementary Table 5**). There were three downregulated proteins (enoyl-CoA hydratase, mitochondrial precursor (*echs1*), neuronal membrane glycoprotein M6-b (*gpm6b*), phosphodiesterase (*pde10a*)), and one upregulated protein (vimentin (*vim*)) that were expressed in the highest number of articles. As **Table 6.8** indicates, conserved changes were not associated with any particular model of PD, finding for example that phosphodiesterase (*pde10a*) was downregulated in striatum of rats treated with 6-OHDA, but also mice treated with MPTP and methamphetamine. Similarly, different PD models, including mouse treated with and injection of PARIS and 6-OHDA, generated an increase of vimentin (*vim*), Adding to this, glial fibrillary acidic protein (*gfap,* GFAP) was differentially expressed in five articles, related to mice treated with an injection of PARIS, injections of 6-OHDA in rats, and mice exposed to MPTP and methamphetamine. However, the direction of change was not conserved in these five studies.

Table 6.15. Differentially expressed proteins that change in the same direction (downregulated) in at least two different proteomic studies related to PD models. The first column shows the gene name of the 43 proteins downregulated (red cells) in PD models. Numbers indicate the reference number that can be found in **Table 6.8**.

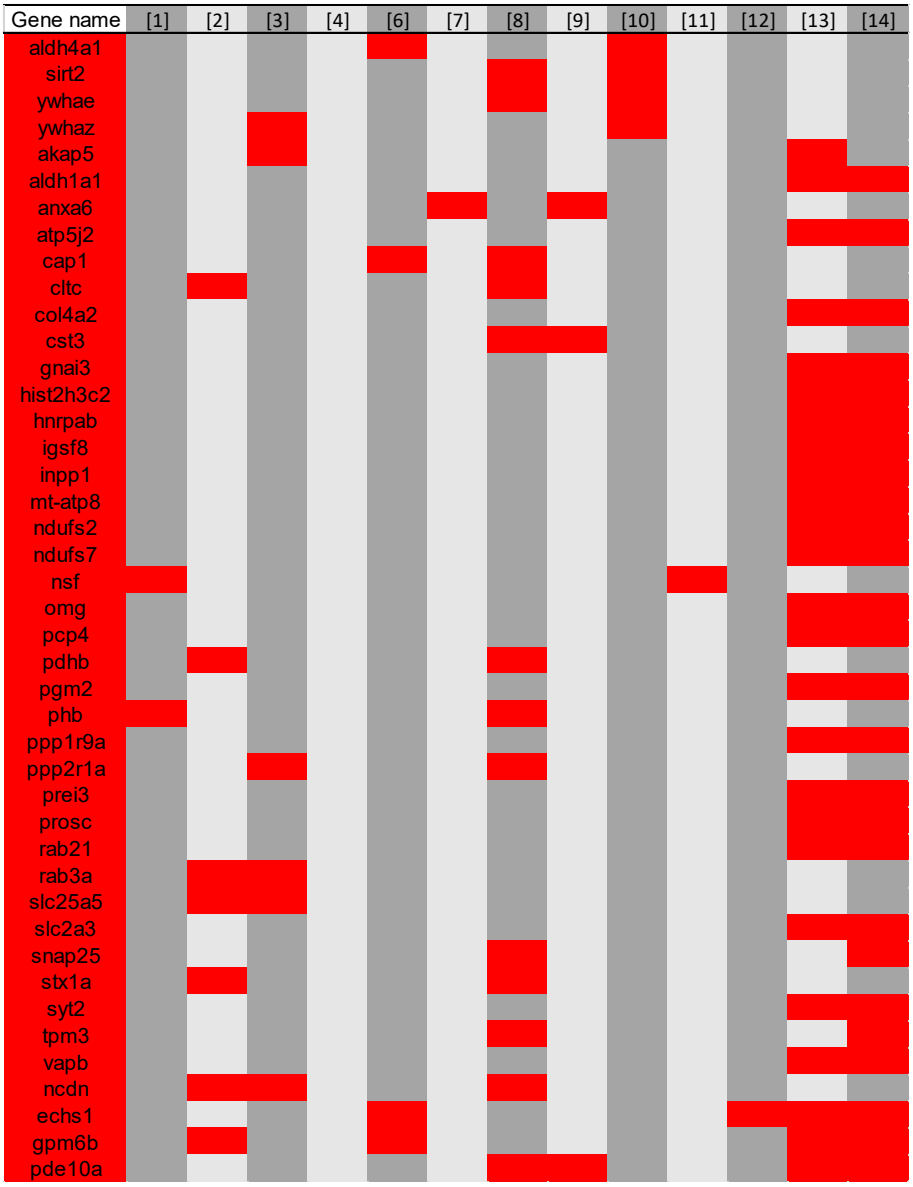

Table 6.16. Differentially expressed proteins that change in the same direction (upregulated) in at least two different proteomic studies related to PD models. The first column shows the gene name of the 33 proteins upregulated (green cells) in PD models. Numbers indicate the reference number that can be found in **Table 6.8**.

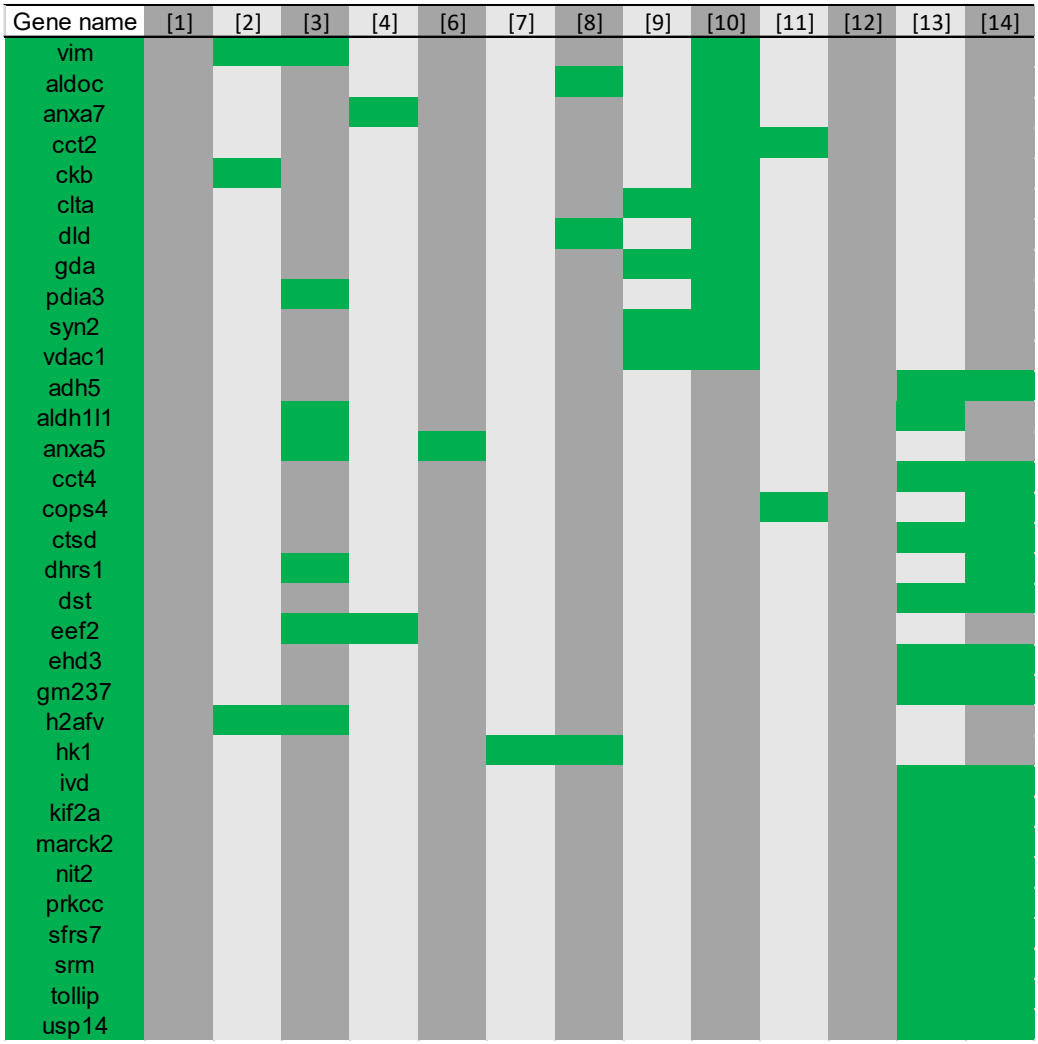

Table 6.17. Differentially expressed proteins that change in different directions (down- and upregulated) in at least two different proteomic studies related to PD models. The first column shows the gene name of the 37 proteins downregulated (red cells) and upregulated (green cells) in PD models. Numbers indicate the reference number that can be found in **Table 6.8**.

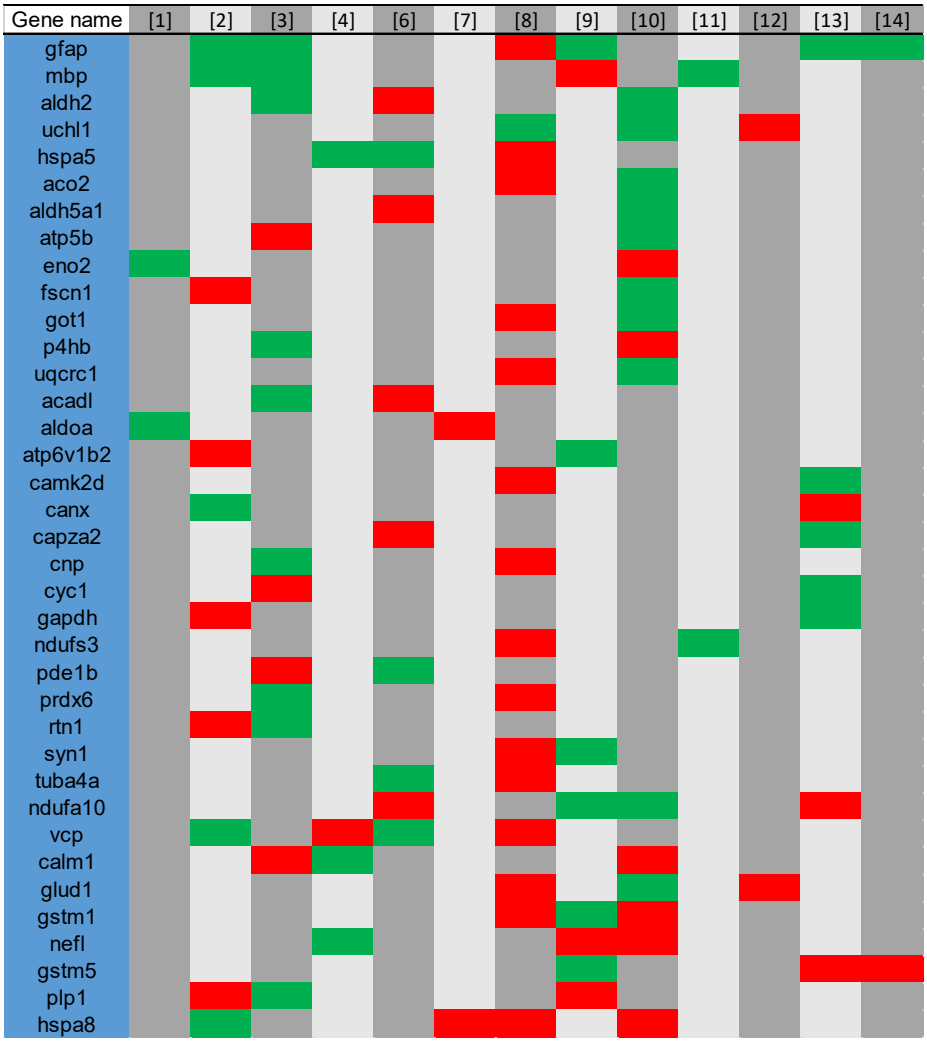

Lastly, a final comparison was done to observe which differentially expressed proteins were in common between PD in humans and PD models. Interestingly, when the 68 proteins that appeared in more than two studies in humans with PD and the 113 proteins from PD models were compared only four proteins appeared to be expressed simultaneously in both proteomes (**Figure 6.6A, Table S1 Annex 3, Supplementary Table 5**). These proteins were retinal dehydrogenase 1 A1 (ALDH1A1), elongation factor 2 (EEF2), glyceraldehyde-3-phosphate dehydrogenase (GAPDH), and vimentin (VIM). In the case of retinal dehydrogenase 1 A1 (ALDH1A1), it was found in olfactory bulb and mitochondrial fraction from SNpc of parkinsonians, as well as striatum of mice treated with MPTP and methamphetamine (**Table 6.14, Table 6.15**). Elongation factor 2 (EEF2) was dysregulated in the olfactory bulb mitochondrial fraction from SNpc of parkinsonians, as well as the striatum and SNpc of mice treated with a viral injection of PARIS (**Table 6.14, Table 6.16**). Moreover, glyceraldehyde-3-phosphate dehydrogenase (GAPDH) was differentially expressed in the rinsing fluids and lenses of parkinsonians, the subventricular zone of PD patients, the cortex of mice treated with PARIS, and the striatum of MPTP models (**Table 6.12, Table 6.17**). Lastly, vimentin (VIM) was upregulated in the locus coeruleus and blood of parkinsonians, but also in in the cortex and striatum of mice treated with PARIS and the striatum of rats under a 6-OHDA model (**Table 6.13, 6.16**).

6.3.8 PD and ageing express common differentially expressed proteins

To gain a deeper understanding of the association of PD and ageing at the protein level, the 648 differentially expressed proteins found in the ageing nervous system proteome were compared to the 177 dysregulated in the entire PD proteome, combining humans and PD models. The results showed that 70 proteins were commonly expressed in both proteomes **(Figure 6.6B, Table S2 Annex 3, Supplementary Table 5***)*. However, this further analysis found that there were not any patterns in terms of the sample where

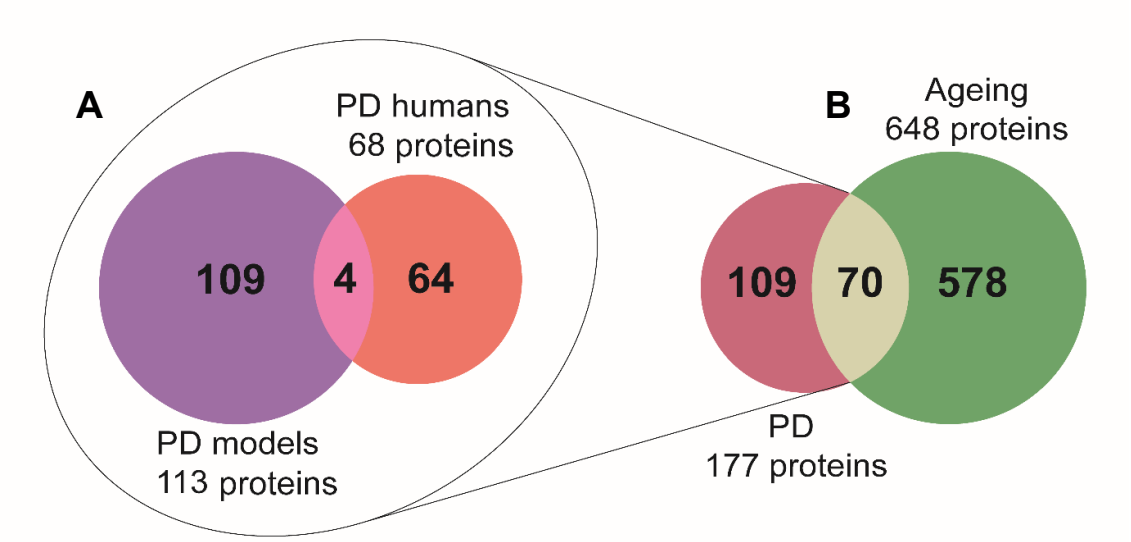

Figure 6.6. Venn diagrams showing the differentially expressed proteins in common between (A) PD in humans and PD models, and (B) between PD and ageing. (A) Proteins that were differentially expressed in two or more proteomic studies related to PD in humans were compared with differentially expressed proteins in PD models, showing that four proteins appeared in both proteomes simultaneously. **(B)** All the proteins in PD proteomic studies that were differentially expressed in at least two articles were compared with proteins that were differentially expressed in three or more studies in the ageing nervous system. This revealed that 70 proteins were differentially expressed in both proteomes.

these proteins were dysregulated in both ageing and PD. Thus, for example, glyceraldehyde-3-phosphate dehydrogenase (GAPDH) was differentially expressed in rat hypothalamus, human hippocampus and monkey occipital cortex during the ageing process; while, as mentioned before, this protein was dysregulated in the rinsing fluids, lenses and the subventricular zone of parkinsonians, the cortex of mice treated with PARIS, and the striatum of MPTP models. Thus, it seems that the only pattern these dysregulation follows is related to the number of proteins identified in each study due to the proteomic approach used (**Table 6.1, 6.7, 6.8, Supplementary Table 4, 5**). Additionally, the 177 dysregulated proteins with PD were compared with the 66 differentially expressed proteins found in the proteomic study of the rat SNpc with ageing performed in this Thesis. This showed that six proteins (vimentin (VIM), glial fibrillary

acidic protein (GFAP), glutathione S-transferase Mu1 (GSTM1), cytosol aminopeptidase (LAP3), neurocan core protein (NCAN), peroxiredoxin-6 (PRDX6)) were commonly expressed in both proteomes. From these, glutathione S-transferase Mu1 (GSTM1) appeared always differentially expressed in the striatum of PD models treated with 6-OHDA and the aged rat SNpc. Interestingly, neurocan core protein (NCAN) was the only protein that appeared dysregulated in the SNpc of both parkinsonians and ageing rats. However, when the expression of this protein was observed in the rest of studies related to the ageing nervous system, other regions such as the human hippocampus, rat dentate gyrus and sheep CSF showed a dysregulation of neurocan core protein (NCAN) (**Supplementary Table 4, 5**)

6.3.9 Gene Ontology analysis shows that differentially expressed proteins associated with the extracellular space, neurotransmitter secretion, binding process, and metabolic functions are conserved in the PD proteome

In order to better understand the biological meaning of the conserved dysregulated proteins with PD in humans, GO analyses of the 15 downregulated and 13 upregulated proteins were executed using DAVID software (Huang *et al.*, 2007; Huang *et al.*, 2009). There was only one enriched biological process ('retinoid metabolic process') assigned to three proteins; and four enriched cellular components ('extracellular exosome', 'extracellular region', 'extracellular space', 'extracellular matrix') when the downregulated proteins were investigated (**Figure 6.7, Table S3 Annex 3**).

On the contrary, when the upregulated proteins were analyzed, there were six terms linked to cellular components that were enriched ('extracellular exosome', 'cytosol', cytoplasm', 'membrane', 'focal adhesion', 'cytoskeleton'), while there were three molecular functions ('identical protein binding', 'actin binding' and 'cadherin binding involved in cell-cell adhesion') overrepresented (**Figure 6.8, Table S4 Annex 3**). Additionally, it is important to notice that GO analyses were also performed independently for the conserved dysregulated proteins found in the human PD SNpc,

PD brains and PD biofluids, but these analyses did not show any satisfactory result due to the low number of proteins in the input.

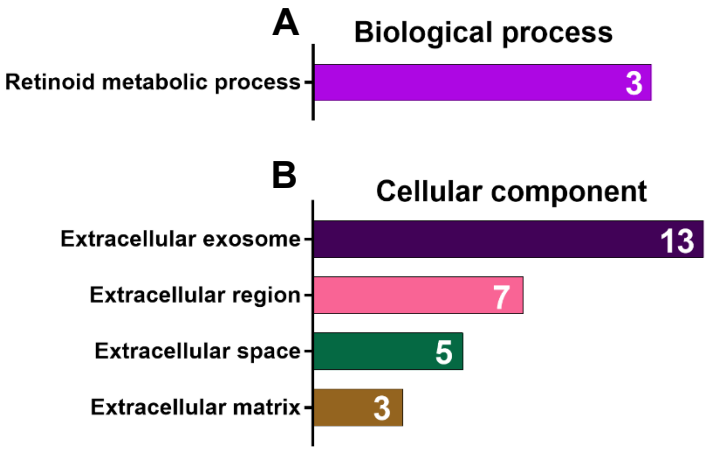

Figure 6.7. Summary of Functional Annotation analyses (Gene Ontology) of the 15 downregulated proteins conserved in the human PD proteome (SNpc, brain, biofluids). DAVID software revealed the enriched terms associated with **(A)** biological processes, and **(B)** cellular components. In the graphs, the number of annotated proteins is indicated with a white number. The name of annotated proteins for each term and the entire list of terms can be found in **Table S3** (**Annex 3**).

On the other hand, GO analyses of the 43 downregulated and 33 upregulated proteins in PD models showed a multitude of enriched terms associated with all the GO categories and KEGG pathways. Thus, downregulated proteins were assigned to six biological processes, where the most enriched term was ‘neurotransmitter secretion’. In the case of cellular components, ‘extracellular exosome’ and ‘cytosol’ were the most enriched terms, while ‘protein binding’ was by far the most enriched molecular function being associated with 29 proteins. The most overrepresented KEGG pathway was ‘metabolic pathways’, although ‘synaptic vesicle cycle’ and ‘Parkinson’s disease’ were also enriched (**Figure 6.9, Table S5 Annex 3**). Likewise, upregulated proteins in PD models were assigned to different biological processes, including ‘epithelial cell differentiation’ or ‘antigen processing and present’. The most enriched cellular components were ‘extracellular exosome’ and ‘cytosol’; while the most enriched

molecular function was 'protein binding'. KEGG pathway analysis revealed that, as in the case of downregulated proteins, 'metabolic pathways' was the most enriched KEGG term in PD models (**Figure 6.10, Table S6 Annex 3**). Ultimately, GO analysis were also performed for the four commonly expressed proteins in humans with PD and PD models, revealing that only the category of cellular component had enriched terms such as 'extracellular exosome', 'cytosol', 'cytoplasm' and 'extracellular matrix' (**Figure 6.11, Table S7 Annex 3**).

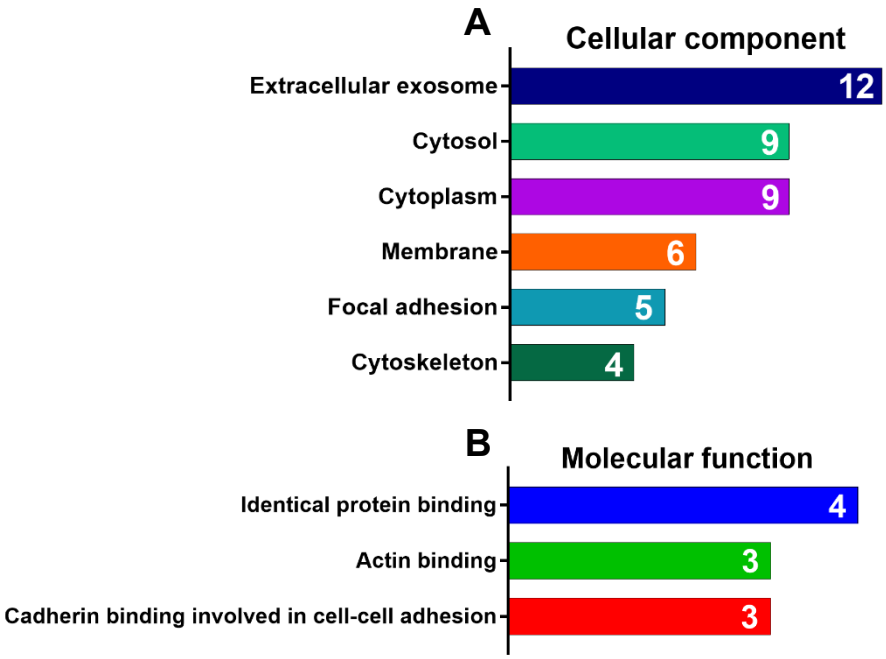

Figure 6.8. Summary of Functional Annotation analyses (Gene Ontology) of the 13 upregulated proteins conserved in the human PD proteome (SNpc, brain, biofluids). DAVID software revealed the enriched terms associated with **(A)** cellular components, and **(B)** molecular functions. In the graphs, the number of annotated proteins is indicated with a white number. The name of annotated proteins for each term and the entire list of terms can be found in **Table S4** (**Annex 3**).

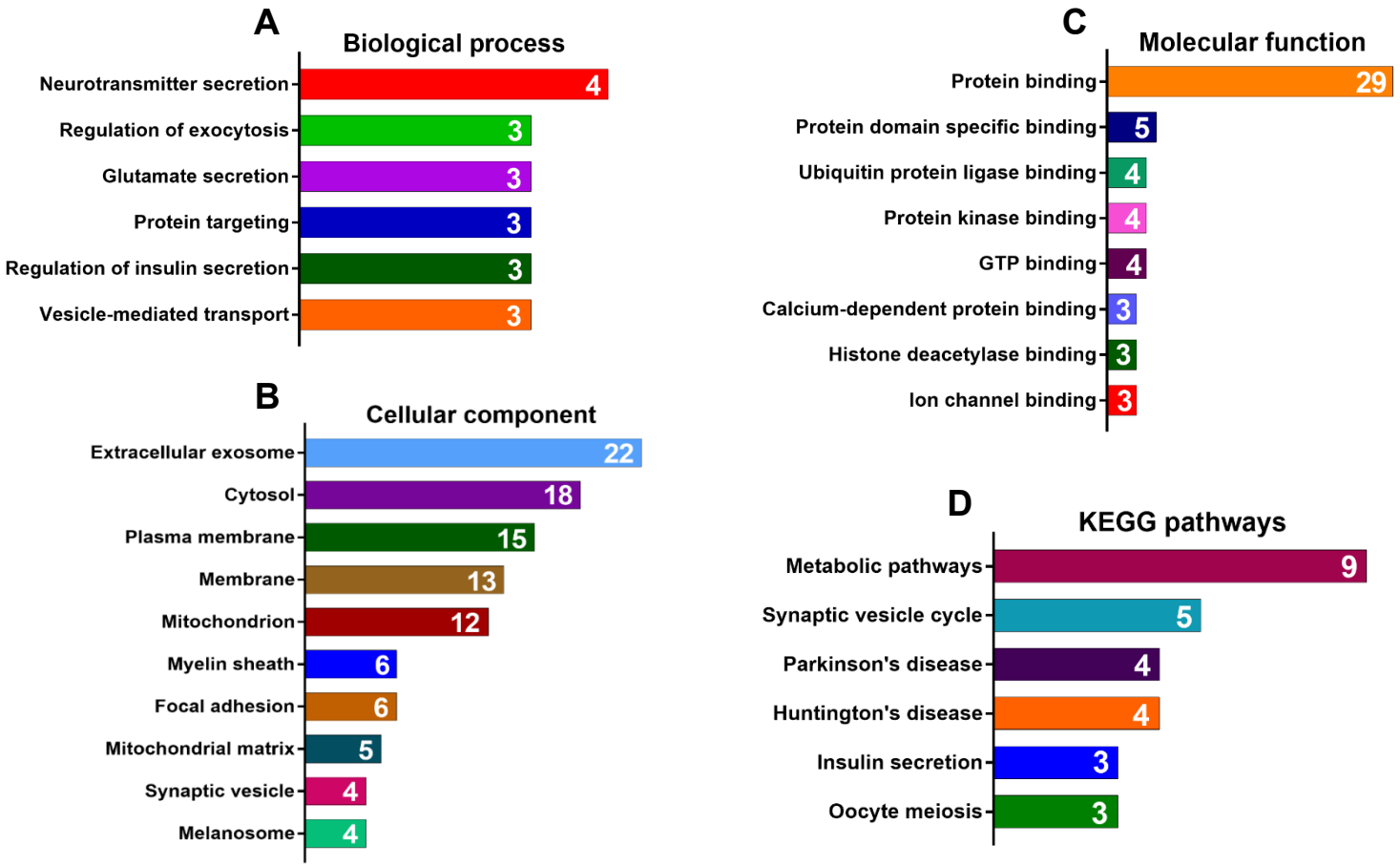

Figure 6.9. Summary of Functional Annotation analyses (Gene Ontology and KEGG) of the 43 downregulated proteins conserved in PD models. DAVID software revealed the enriched terms associated with **(A)** biological processes, **(B)** cellular components, **(C)** molecular functions, **(D)** and KEGG pathways. In the graphs, only the top ten terms are shown as bars, with the number of annotated proteins indicated with a white number. The name of annotated proteins for each term and the entire list of terms can be found in **Table S5** (**Annex 3**).

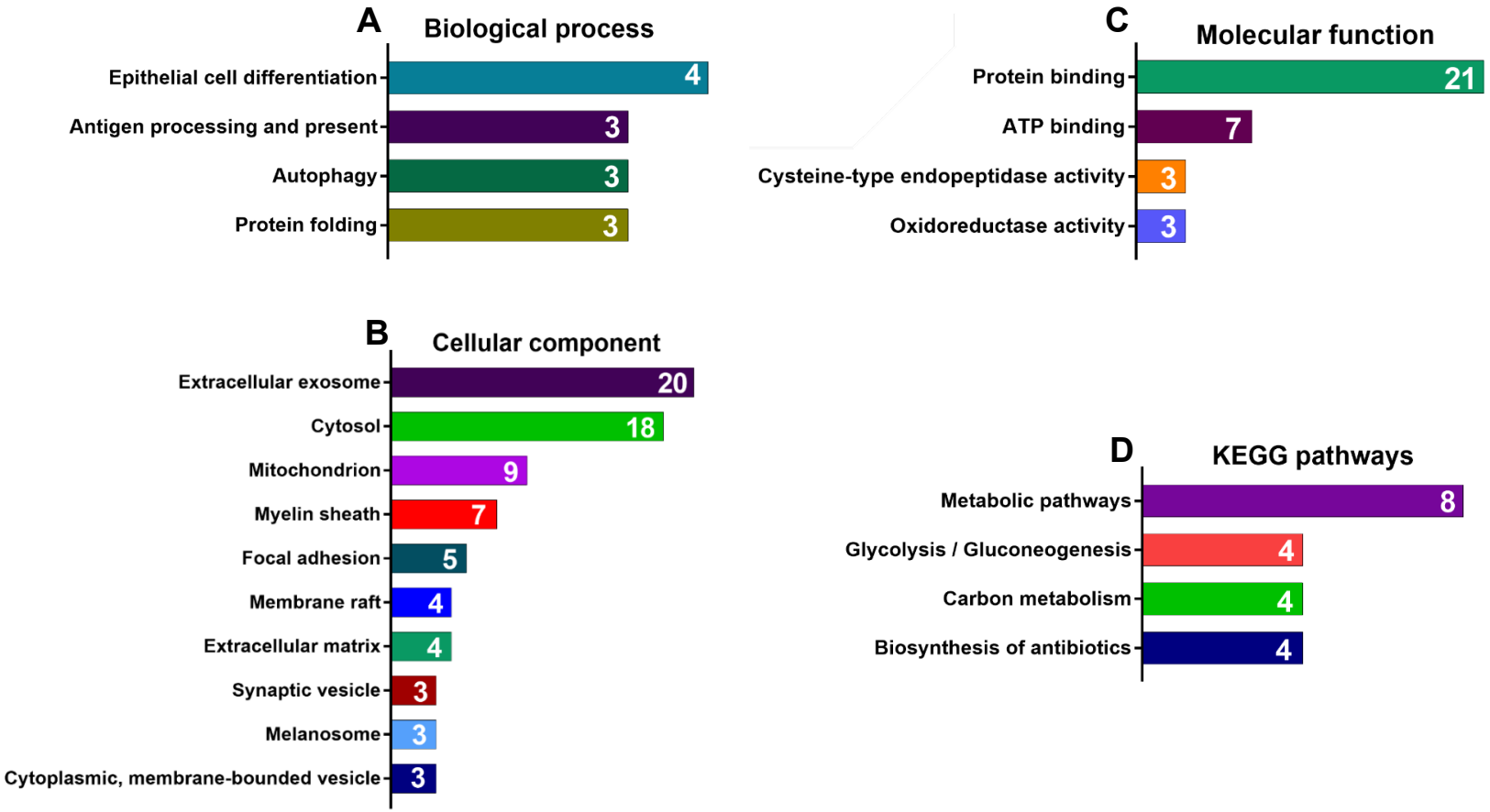

Figure 6.10. Summary of Functional Annotation analyses (Gene Ontology and KEGG) of the 33 upregulated proteins conserved in PD models. DAVID software revealed the enriched terms associated with **(A)** biological processes, **(B)** cellular components, **(C)** molecular functions, **(D)** and KEGG pathways. In the graphs, only the top ten terms are shown as bars, with the number of annotated proteins indicated with a white number. The name of annotated proteins for each term and the entire list of terms can be found in **Table S6** (**Annex 3**).

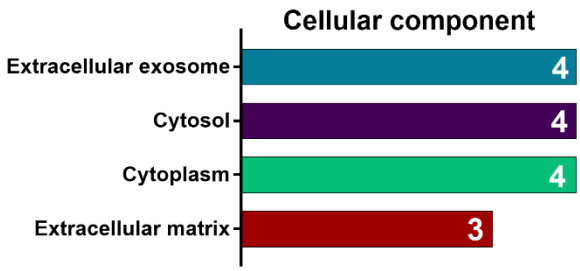

Figure 6.11. Summary of Functional Annotation analyses (Gene Ontology) of the four common proteins between human PD proteomic studies and PD model proteomic studies (Figure 6.6A). DAVID software revealed the enriched terms associated with cellular components. In the graphs, the four terms are shown as bars, with the number of annotated proteins indicated with a white number. The name of annotated proteins to each term and the entire list of terms can be found in **Table S7** (**Annex 3**).

6.3.10 Gene Ontology analysis indicates that dysregulated proteins that are common between the PD proteome and the ageing nervous system proteome are linked to the development of the substantia nigra, oxidation-reduction and metabolic processes, and protein binding

An additional GO analysis was performed with the 70 common proteins that were differentially expressed in the PD proteome and in the ageing nervous system proteome. The two most enriched biological processes were ‘substantia nigra development’ and ‘oxidation-reduction process’; while the ‘extracellular exosome‘ term was the cellular component more overrepresented. In terms of molecular function, ‘protein binding’ was the term with the highest number of proteins associated with it. Furthermore, ‘metabolic pathways’ was the most enriched KEGG pathway (**Figure 6.12, Table S8 Annex 3**).

6.3.11 Reactome pathway analysis shows that the conserved dysregulated proteins in PD are linked to immune system, metabolism and neurotransmitter release pathways

Reactome pathway analysis (Fabregat *et al*., 2017; Fabregat *et al*., 2018) were performed to observe if other overrepresented biological pathways exist that are associated with the dysregulated proteins in PD. As in previous analyses, the 15 downregulated and 13 upregulated proteins from the PD human proteome were examined first; and afterwards the same procedure was taken for the 43 downregulated and 33 upregulated proteins in PD models.

In the case of the 15 downregulated human proteins in PD, 12 out of 15 identifiers were found in the Reactome, where 145 pathways were associated with at least one of these proteins. The three proteins that were not found or mapped were seipin (BSCL2), mammalian ependymin-related protein 1 (EPDR1) and endoplasmic reticulum resident protein 29 (ERP29), which were identified by DAVID in GO analysis except in the case of seipin (BSCL2). 'RUNX2 regulates genes involved in differentiation of myeloid cells' (R-HSA-8941333) was the pathway with the most statistically significant p-value (**Table 6.18**) associated with the protein galectin-3 (LGALS3). The overview of the overrepresented pathways by the genome-wide view (Sidiropoulos *et al*., 2017) showed that most of the overrepresented secondary pathways belonged to the top pathway 'metabolism' (**Figure 6.13A**). Thus, the Reactome analysis corroborated the disruption that appears in metabolic processes during PD found by the GO analysis, but also revealed that the downregulated proteins in the disease in humans were linked to pathways associated with the production of myeloid cells.

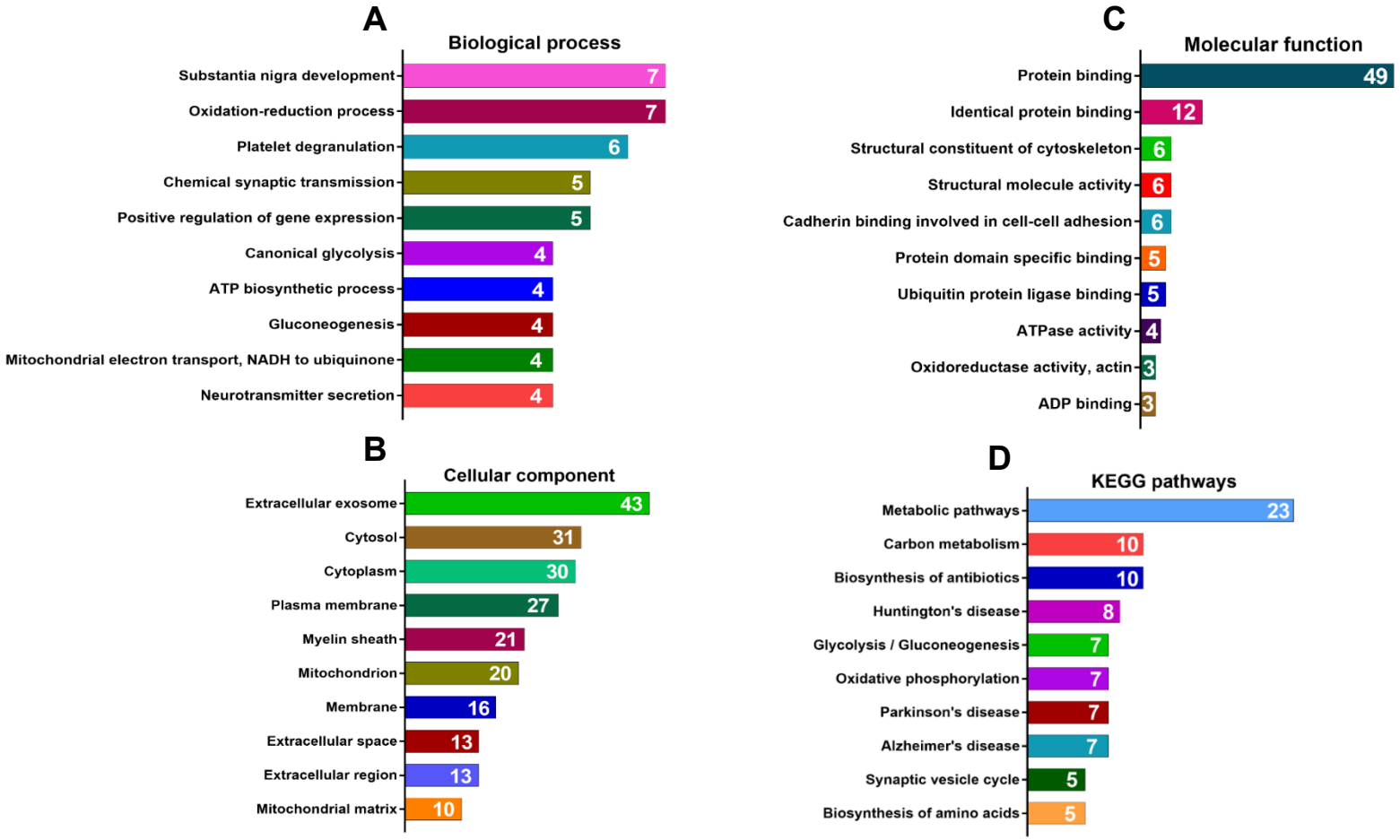

Figure 6.12. Summary of Functional Annotation analyses (Gene Ontology and KEGG) of the 70 common proteins between PD proteomic studies and ageing of the nervous system (Figure 6.6B). DAVID software revealed the enriched terms associated with **(A)** biological processes, **(B)** cellular components, **(C)** molecular functions, **(D)** and KEGG pathways. In the graphs, only the top ten terms are shown as bars, with the number of annotated proteins indicated with a white number. The name of annotated proteins for each term and the entire list of terms can be found in **Table S8** (**Annex 3**).

The Reactome pathway analysis of the 13 upregulated proteins in humans with PD revealed that 12 out of 13 identifiers were found in the Reactome (only cytosol aminopeptidase (LAP3) was not found or mapped), with a link to 99 different pathways. 'Interleukin-4 and interleukin-13 signaling' (R-HSA-6785807) was the pathway more overrepresented, and was associated with the proteins vimentin (VIM) and integrin beta-1 (ITGB1) (**Table 6.19**), both of them identified by GO analysis.

Table 6.18. The 25 most enriched pathways sorted by the most statistically significant p-values, using the 15 conserved downregulated proteins in the proteome of humans with PD. 'Entities' refers to Uniprot accession numbers, showing the number of entities found in the analysis from the total in that pathway.

Pathway name	Entities	
	found/total	p-value
RUNX2 regulates genes involved in differentiation of myeloid cells	2 / 6	4.51e-05
RUNX1 regulates transcription of genes involved in differentiation of myeloid cells	2 / 11	1.51e-04
Retinoid metabolism and transport	3 / 79	2.82e-04
Advanced glycosylation end product receptor signaling	2 / 16	3.17e-04
Metabolism of fat-soluble vitamins	3 / 94	4.68e-04
Glycolysis	3 / 110	7.37e-04
Glucose metabolism	3 / 141	0.002
G alpha (i) signalling events	5 / 567	0.002
Visual phototransduction	3 / 168	0.002
Metabolism of vitamins and cofactors	4 / 385	0.003
Retinoid metabolism disease events	1 / 2	0.003
Metabolism of carbohydrates	4 / 457	0.006
Neutrophil degranulation	4 / 480	0.007
Alternative complement activation	1 / 6	0.01
Protein-protein interactions at synapses	2 / 93	0.01
Activation of C3 and C5	1 / 7	0.011
Aryl hydrocarbon receptor signalling	1 / 8	0.013
Defective CHST14 causes EDS, musculocontractural type	1 / 9	0.015
Defective CHST3 causes SEDCJD	1 / 9	0.015
Defective CHSY1 causes TPBS	1 / 10	0.016
Axonal growth inhibition (RHOAactivation)	1 / 11	0.018
Formyl peptide receptors bind formyl peptides and many other ligands	1 / 11	0.018
p75NTR regulates axonogenesis	1 / 12	0.019
Dermatan sulfate biosynthesis	1 / 13	0.021 0
Chylomicron assembly	1 / 14	0.022

Table 6.19. The 25 most overrepresented (enriched) pathways sorted by the most statistically significant p-values, using the 13 conserved upregulated proteins in the proteome of humans with PD. 'Entities' refers to Uniprot accession numbers, showing the number of entities found in the analysis from the total in that pathway.

Pathway name	Entities	
	found/total	p-value
Interleukin-4 and Interleukin-13 signaling	4 / 211	1.00e-04
RHO GTPases Activate Formins	3 / 149	7.08e-04
Phase 2 - plateau phase	2 / 42	0.001
Signaling by Rho GTPases	4 / 457	0.002
Non-integrin membrane-ECM interactions	2 / 61	0.002
Signaling by Interleukins	5 / 836	0.002
Phase 0 - rapid depolarisation	2 / 68	0.003
Muscle contraction	3 / 256	0.003
Iron uptake and transport	2 / 83	0.004
Localization of the PINCH-ILKPARVIN complex to focal adhesions	1 / 4	0.005
MET interacts with TNS proteins	1 / 5	0.006
RHO GTPase Effectors	3 / 326	0.007
Fibronectin matrix formation	1 / 7	0.008
Immune System	8 / 2,803	0.01
L1CAM interactions	2 / 130	0.01
CHL1 interactions	1 / 10	0.012
Cytokine Signaling in Immune system	5 / 1,245	0.013
Caspase-mediated cleavage of cytoskeletal proteins	1 / 12	0.014
Presynaptic depolarization and calcium channel opening	1 / 15	0.018
Cardiac conduction	2 / 175	0.018
Platelet Adhesion to exposed collagen	1 / 16	0.019
Other semaphorin interactions	1 / 19	0.023
Cell-extracellular matrix interactions	1 / 19	0.023
Carnitine synthesis	1 / 22	0.026
Signal transduction by L1	1 / 25	0.03

In turn, the genome-wide view (Sidiropoulos *et al*., 2017) showed that 'immune system' top pathway, included also in the 25 top most enriched pathways, was comprised of three secondary pathways that were the most overrepresented (**Figure 6.13B**). These results would complement the data found by GO analysis, where no biological processes were found.

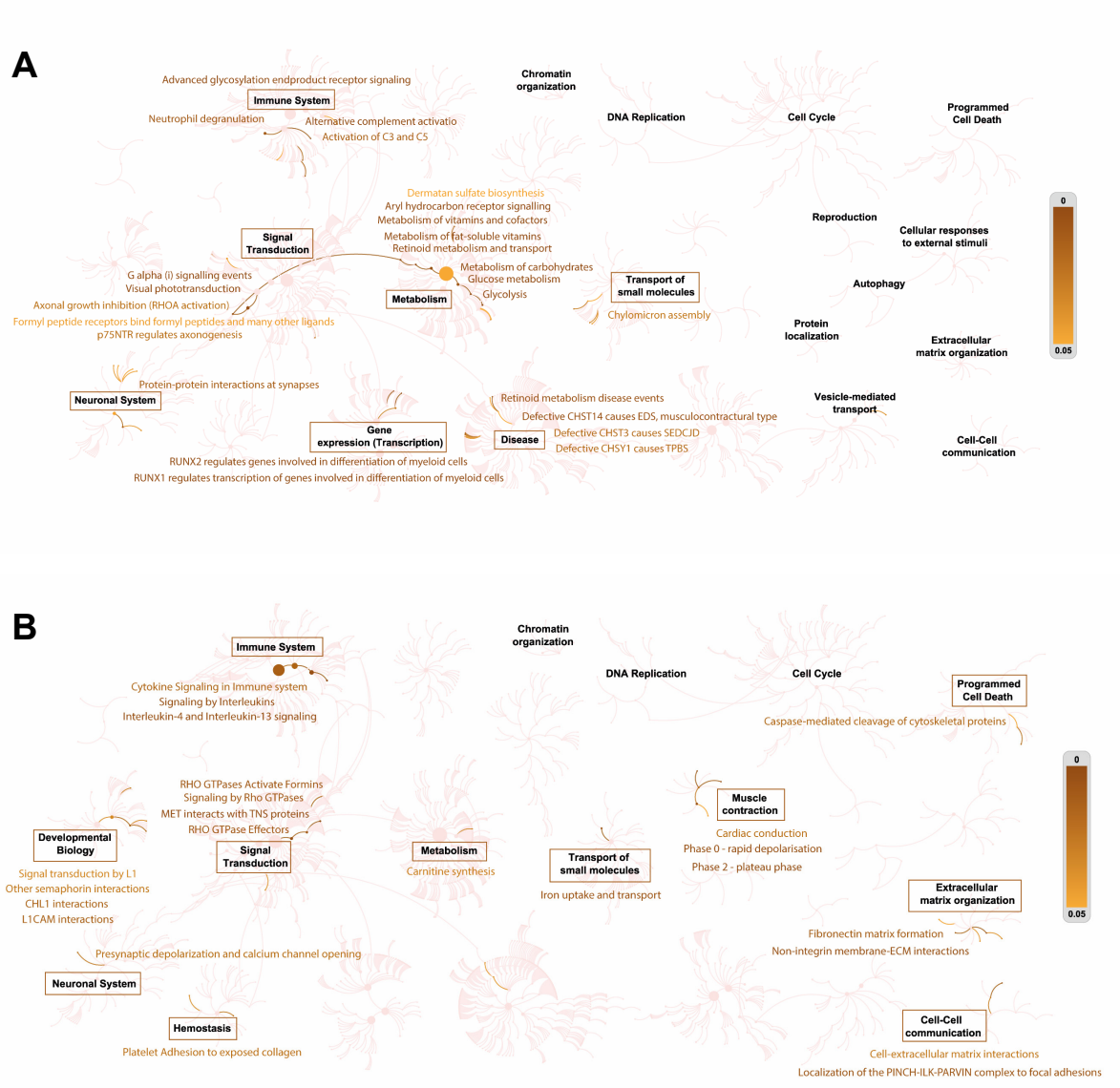

Figure 6.13. Genome-wide overview of the Reactome pathway analysis (Sidiropoulos *et al*., 2017) of the 28 conserved differentially expressed proteins in humans with PD. (A) Genome-wide overview of the Reactome pathway analysis of the 15 conserved downregulated proteins. **(B)** Genome-wide overview of the Reactome pathway analysis of the 13 conserved upregulated proteins. Each top-level pathway has a centre from which other pathways of a lower hierarchy start. Top-level overexpressed pathways are emphasized with a red rectangle (e.g., 'metabolism', 'immune system'), while secondary overexpressed pathways (e.g., 'glycolysis') linked to them are highlighted using a colour-scale that indicates p-value (right-hand side). Light grey pathways are not significantly overrepresented.

Additionally, the Reactome analysis of the 43 downregulated proteins in PD models mapped and found 34 of these proteins, producing 383 pathways where at least one of these proteins appeared. The nine remaining identifiers that were not found nor mapped by the Reactome were neuronal membrane glycoprotein M6-b (GPM6B), heterogeneous nuclear ribonucleoprotein A/B (HNRPAB), immunoglobulin superfamily member 8 (IGSF8), neurochondrin (NCDN), calmodulin regulator protein PCP4 (PCP4), neurabin-1 (PPP1R9A), MOB-like protein phocein (PREI3), pyridoxal phosphate homeostasis protein (PROSC) and NAD-dependent protein deacetylase sirtuin-2 (SIRT2). All these downregulated proteins were identified by GO analysis, with the exception of heterogeneous nuclear ribonucleoprotein A/B (HNRPAB) and MOB-like protein phocein (PREI3).The most enriched pathway associated with these downregulated proteins in PD models was ‘serotonin neurotransmitter release cycle’ (R-HSA-181429), which had three proteins assigned (Ras-related protein Rab-3A (RAB3A), synaptosomal-associated protein 25 (SNAP25), and syntaxin-1A (STX1A)) (**Table 6.20**). Additionally, genome-wide view (Sidiropoulos *et al*., 2017) corroborated the findings by GO analysis, where secondary pathways related to neurotransmitter release (associated with the top pathway ‘neuronal system’) as well as the top pathway ‘metabolism’ were overrepresented (**Figure 6.14A, Table 6.20**).

On the other hand, the analysis of the 33 upregulated proteins in PD models by Reactome analysis revealed that 28 of these proteins were mapped or found, and 242 pathways contained at least one of the upregulated proteins. Three of the five proteins that were not mapped by Reactome (annexin A7 (ANXA7), dehydrogenase/reductase SDR family member 1 (DHRS1), protein kinase C gamma type (PRKCC)) were found in GO analysis, while two of them (aminoethanethiol dioxygenase (GM237), hypothetical protein (MARCK2)) were not associated with any biological function or pathway in both analyses. In terms of which pathways were more enriched, ‘MHC class II antigen presentation’ (R-HSA-2132295), contained the proteins clathrin light chain A (CLTA), cathepsin D (CTSD), and kinesin-like protein KIF2A (KIF2A), and showed the highest p-

value (**Table 6.21**). However, the overview of genome-wide view (Sidiropoulos *et al*., 2017) showed that the top term 'metabolism of proteins' included most of the 25 top enriched terms (**Figure 6.114B, Table 6.21**). Therefore, Reactome pathways analysis complement the GO analysis, where terms associated with protein binding were overrepresented.

Table 6.20. The 25 most enriched pathways sorted by the most statistically significant p-values, using the 43 conserved downregulated proteins in the proteome of PD models. 'Entities' refers to Uniprot accession numbers, showing the number of entities found in the analysis from the total in that pathway.

Pathway name	Entities	
	found/total	p-value
Serotonin Neurotransmitter Release Cycle	3 / 23	9.43e-05
Vpr-mediated induction of apoptosis by mitochondrial outer membrane permeabilization	2 / 4	1.09e-04
Acetylcholine Neurotransmitter Release Cycle	3 / 26	1.35e-04
Dopamine Neurotransmitter Release Cycle	3 / 28	1.68e-04
Neurotoxicity of clostridium toxins	3 / 28	1.68e-04
Norepinephrine Neurotransmitter Release Cycle	3 / 30	2.05e-04
Glutamate Neurotransmitter Release Cycle	3 / 32	2.48e-04
GABA synthesis, release, reuptake and degradation	3 / 35	3.22e-04
Toxicity of botulinum toxin type C(BoNT/C)	2 / 7	3.31e-04
Smooth Muscle Contraction	3 / 55	0.001
Chk1/Chk2(Cds1) mediated inactivation of Cyclin B: Cdk1 complex	2 / 15	0.001
Uptake and actions of bacterial toxins	3 / 60	0.002
The citric acid (TCA) cycle and respiratory electron transport	5 / 229	0.002
Transmission across Chemical Synapses	6 / 352	0.002
Neutrophil degranulation	7 / 480	0.002
Integration of energy metabolism	4 / 144	0.002
RAB geranylgeranylation	3 / 68	0.002
Respiratory electron transport, ATP synthesis by chemiosmotic coupling, and heat production by uncoupling proteins.	4 / 146	0.002
Activation of BAD and translocation to mitochondria	2 / 19	0.002
Neuronal System	7 / 498	0.002
Membrane Trafficking	8 / 665	0.003
Vesicle-mediated transport	9 / 824	0.003
Formation of ATP by chemiosmotic coupling	2 / 23	0.003
Glycogen synthesis	2 / 26	0.004
Cellular hexose transport	2 / 28	0.005

Table 6.21. 25 most enriched pathways sorted by the most statistically significant p-values, using the 33 conserved upregulated proteins in the proteome of PD models. ‘Entities’ refers to Uniprot accession numbers, showing the number of entities found in the analysis from the total in that pathway.

Pathway name	Entities	
	found/total	p-value
MHC class II antigen presentation	6 / 148	5.68e-06
Factors involved in megakaryocyte development and platelet production	5 / 194	3.00e-04
Folding of actin by CCT/TriC	2 / 13	7.41e-04
Kinesins	3 / 68	0.001
BBSome-mediated cargo-targeting to cilium	2 / 24	0.002
Signaling by Nuclear Receptors	5 / 317	0.003
Amplification of signal from unattached kinetochores via a MAD2 inhibitory signal	3 / 94	0.003
Amplification of signal from the kinetochores	3 / 94	0.003
Mitochondrial calcium ion transport	2 / 27	0.003
Neutrophil degranulation	6 / 480	0.003
Ethanol oxidation	2 / 28	0.003
Prefoldin mediated transfer of substrate to CCT/TriC	2 / 29	0.004
Formation of tubulin folding intermediates by CCT/TriC	2 / 30	0.004
COPI-dependent Golgi-to-ER retrograde traffic	3 / 107	0.004
Mitotic Spindle Checkpoint	3 / 110	0.005
Cooperation of Prefoldin and TriC/CCT in actin and tubulin folding	2 / 37	0.006
Association of TriC/CCT with target proteins during biosynthesis	2 / 40	0.007
Lysosome Vesicle Biogenesis	2 / 43	0.008
Resolution of Sister Chromatid Cohesion	3 / 134	0.008
Cooperation of PDCL (PhLP1) and TRiC/CCT in G-protein beta folding	2 / 45	0.008
Defective HK1 causes hexokinase deficiency (HK deficiency)	1 / 3	0.009
Golgi-to-ER retrograde transport	3 / 148	0.01
RHO GTPases Activate Formins	3 / 149	0.01
Estrogen-dependent gene expression	3 / 154	0.011
Cargo trafficking to the periciliary membrane	2 / 55	0.012

Lastly, a similar approach was conducted to understand the biological meaning of the four dysregulated proteins in common between the proteomes of humans with PD and PD models. These four proteins were found by Reactome in at least one of the 39 pathways describe by the software. ‘Interleukin-4 and interleukin-13 signaling’ (R-HSA-6785807) was the most-enriched pathway, associated with vimentin (VIM) (**Table 6.22**). The overview of genome-wide view (Sidiropoulos *et al*., 2017) showed that this overrepresented pathway was part of the ‘immune system’ top pathway (also part of the 25 most enriched pathways) (**Figure 6.15A, Table 6.22**). Moreover, ‘metabolism’

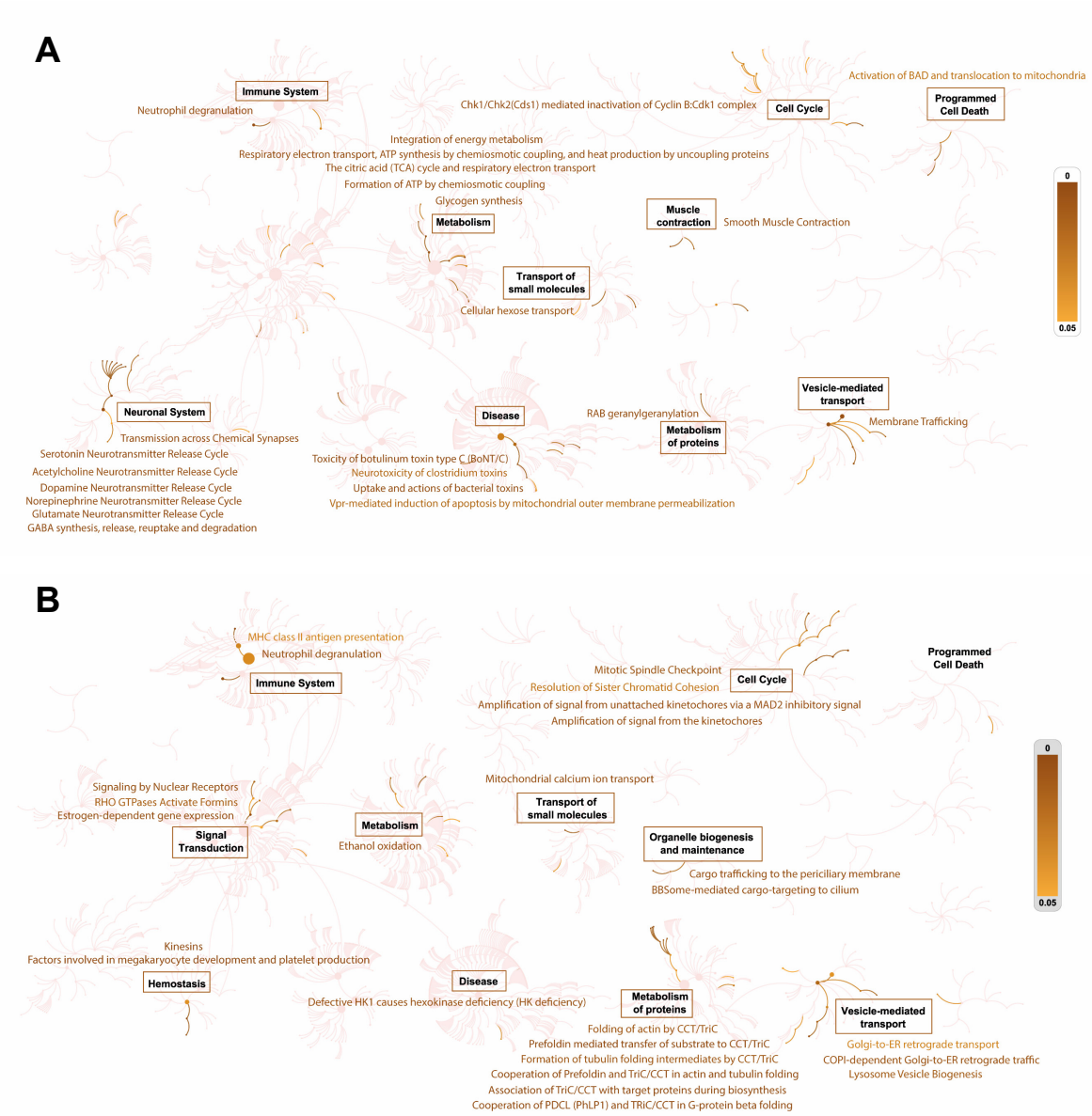

Figure 6.14. Genome-wide overview of the Reactome pathway analysis (Sidiropoulos *et al.*, 2017) of the 76 conserved differentially expressed proteins in PD models. (A) Genome-wide overview of the Reactome pathway analysis of the 43 conserved downregulated proteins. **(B)** Genome-wide overview of the Reactome pathway analysis of the 33 conserved upregulated proteins. Each top-level pathway has a centre from which other pathways of a lower hierarchy start. Top-level overexpressed pathways are emphasized with a red rectangle (e.g., 'metabolism', 'immune system'), while secondary overexpressed pathways (e.g., 'ethanol oxidation') linked to them are highlighted using a colour-scale that indicates p-value (right-hand side). Light grey pathways are not significantly overrepresented.

included multiple overrepresented pathways, which would complement the results generated by GO analysis where no biological functions (only cell components) were found.

Table 6.22. The 25 most enriched pathways, sorted by the most statistically significant p-values, using the four common proteins between the proteomes of parkinsonians and PD models. 'Entities' refers to Uniprot accession numbers, showing the number of entities found in the analysis from the total in that pathway.

Pathway name	Entities	
	found/total	p-value
Interleukin-4 and Interleukin-13 signaling	2 / 211	0.002
Uptake and function of diphtheria toxin	1 / 10	0.004
Caspase-mediated cleavage of cytoskeletal proteins	1 / 12	0.004
Synthesis of diphthamide-EEF2	1 / 15	0.005
Protein methylation	1 / 19	0.007
Fructose catabolism	1 / 20	0.007
Fructose metabolism	1 / 27	0.009
Metabolism of carbohydrates	2 / 457	0.01
Ethanol oxidation	1 / 28	0.01
Apoptotic cleavage of cellular proteins	1 / 38	0.013
RA biosynthesis pathway	1 / 39	0.014
Striated Muscle Contraction	1 / 40	0.014
Apoptotic execution phase	1 / 54	0.019
Uptake and actions of bacterial toxins	1 / 60	0.021
Gluconeogenesis	1 / 67	0.023
Gamma carboxylation, hypusine formation and arylsulfatase activation	1 / 69	0.024
Signaling by Retinoic Acid	1 / 72	0.025
Signaling by Interleukins	2 / 836	0.031
Peptide chain elongation	1 / 97	0.034
Eukaryotic Translation Elongation	1 / 102	0.035
Glycolysis	1 / 110	0.038
Glucose metabolism	1 / 141	0.049
Immune System	3 / 2,803	0.056
Apoptosis	1 / 187	0.064
Cytokine Signaling in Immune system	2 / 1,245	0.064

-

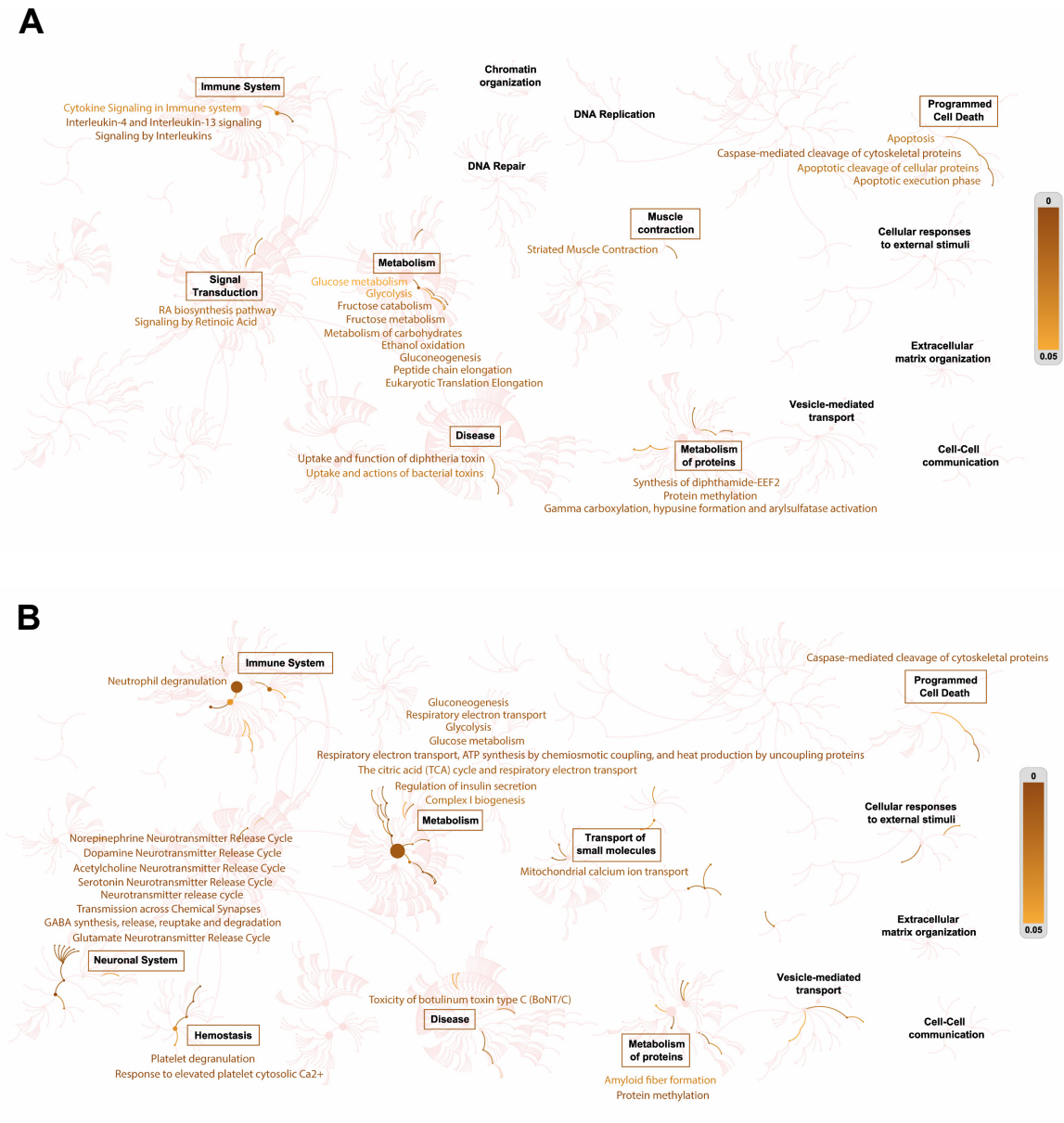

Figure 6.15. (A) Genome-wide overview of the Reactome pathway analysis (Sidiropoulos *et al.*, 2017) of the four common proteins between the proteomes of parkinsonians and PD models. (B) Genome-wide overview of the Reactome pathway analysis of the 70 common proteins between the PD proteome and the proteome of the ageing nervous system. Each top-level pathway has a centre from which other pathways of a lower hierarchy start. Top-level overexpressed pathways are emphasized with a red rectangle (e.g., 'metabolism', 'immune system'), while secondary overexpressed pathways (e.g., 'complex I biogenesis') linked to them are highlighted using a colour-scale that indicates p-value (right-hand side). Light grey pathways are not significantly overrepresented.

6.3.12 Reactome pathway analyses demonstrated that neuronal system and metabolism pathways are common dysregulated in both PD and ageing

As mentioned previously, the 70 common dysregulated proteins between the PD proteome and the ageing nervous system were investigated by Reactome pathway analysis, finding that 59 of these proteins were mapped to 346 pathways. The 11 proteins that were missing were 2',3'-cyclic-nucleotide 3'- phosphodiesterase (CNP), endoplasmic reticulum resident protein 29 (ERP29), neuronal membrane glycoprotein M6-b (GPM6B), immunoglobulin superfamily member 8 (IGSF8), alpha-internexin (INA), cytosol aminopeptidase (LAP3), neurochondrin (NCDN), nuclear transport factor 2 (NUTF2), myelin proteolipid protein (PLP1), reticulon-1 (RTN1) and NAD-dependent protein deacetylase sirtuin-2 (SIRT2), all of them were found associated with at least one term in the GO analysis. As **Table 6.23** shows, 'the citric acid (TCA) cycle and respiratory electron transport' (R-HSA-1428517) was the most overrepresented pathway, finding ten identifiers linked to it: ATP synthase subunit beta, mitochondrial (ATP5B), ATP synthase subunit f, mitochondrial (ATP5J2), cytochrome c1, heme protein, mitochondrial (CYC1), dihydrolipoyl dehydrogenase, mitochondrial (DLD), NADH dehydrogenase [ubiquinone] 1 alpha subcomplex subunit 10, mitochondrial (NDUFA10), NADH dehydrogenase [ubiquinone] iron-sulfur protein 2, mitochondrial (NDUFS2), NADH dehydrogenase [ubiquinone] iron-sulfur protein 7, mitocondrial (NDUFS7), pyruvate dehydrogenase E1 component subunit beta, mitochondrial (PHDB), cytochrome b-c1 complex subunit 1, mitochondrial (UQCRC1), and voltage-dependent anion-selective channel protein 1 (VDAC1). The genome-wide view (Sidiropoulos *et al*., 2017) revealed that this pathway was part of the top 'metabolism' pathway, which included, together with the top pathway 'neuronal system', most of the top 25 overrepresented pathways (**Figure 6.15B, Table 6.23**). Altogether, this Reactome analysis corroborated the finding by GO analysis where 'metabolism pathways', 'substantia nigra development 'and 'oxidation-reduction processes' were enriched.

Table 6.23. The 25 most enriched pathways sorted by the most statistically significant p-values, using the common 70 proteins between the PD proteome and the ageing nervous system proteome. 'Entities' refers to Uniprot accession numbers, showing the number of entities found in the analysis from the total in that pathway.

Pathway name	Entities	
	found/total	p-value
The citric acid (TCA) cycle and respiratory electron transport	10 / 229	2.14e-06
GABA synthesis, release, reuptake and degradation	5 / 35	3.39e-06
Respiratory electron transport, ATP synthesis by chemiosmotic coupling, and heat production by uncoupling proteins	7 / 146	4.36e-05
Neutrophil degranulation	12 / 480	5.35e-05
Platelet degranulation	6 / 137	2.54e-04
Protein methylation	3 / 19	2.59e-04
Glucose metabolism	6 / 141	2.96e-04
Neuronal System	11 / 498	3.25e-04
Response to elevated platelet cytosolic Ca2+	6 / 144	3.31e-04
Transmission across Chemical Synapses	9 / 352	4.15e-04
Neurotransmitter release cycle	5 / 99	4.47e-04
Serotonin Neurotransmitter Release Cycle	3 / 23	4.52e-04
Acetylcholine Neurotransmitter Release Cycle	3 / 26	6.44e-04
Glycolysis	5 / 110	7.17e-04
Mitochondrial calcium ion transport	3 / 27	7.18e-04
Dopamine Neurotransmitter Release Cycle	3 / 28	7.97e-04
Respiratory electron transport	5 / 115	8.73e-04
Gluconeogenesis	4 / 67	9.24e-04
Toxicity of botulinum toxin type C (BoNT/C)	2 / 7	9.49e-04
Norepinephrine Neurotransmitter Release Cycle	3 / 30	9.71e-04
Glutamate Neurotransmitter Release Cycle	3 / 32	0.001
Amyloid fiber formation	4 / 88	0.002
Caspase-mediated cleavage of cytoskeletal proteins	2 / 12	0.003
Regulation of insulin secretion	4 / 106	0.005
Complex I biogenesis	3 / 57	0.006

6.3.13 Proteins related to the extracellular exosome, binding process, neurotransmitter secretion or metabolism form protein networks in the PD proteome

STRING database analyses (Szklarczyk *et al*., 2019) were conducted to visualize the protein-protein interactions between the different conserved dysregulated proteins in humans with PD and PD models, as well as the common proteins between them. In the case of the 15 downregulated proteins in humans with PD, four of these proteins (apolipoprotein C-III (APOC3), apolipoprotein M (APOM), serum amyloid A-1 protein (SAA1), and complement C3 (C3)) showed the highest number of associations (**Figure**

6.16A). There was not only an associatiation between them (as the network shows in **Figure 6.16A**), but two of them were also linked to retinol-binding protein 4 (RBP4). These proteins were associated with the biological term 'retinoid metabolic process', as well as cellular components related to the 'extracellular exosome' (**Table S3 Annex 3).** In addition, these proteins were found associated with Reactome pathways such as **'**retinoid metabolism and transport (R-HSA-975634) or 'G alpha (i) signalling events' (R-HSA-418594). On the other hand, the protein network analysis of the 13 upregulated proteins in parkinsonians showed that ezrin (EZR) and integrin beta-1 (ITGB1) were the proteins with the highest number of connections (two each) (**Figure 6.16B)**. These proteins were part of enriched molecular functions such as 'actin binding' and 'cadherin binging involved in cell-cell adhesion' (**Table S4 Annex 3**), as well as one of the top 25 Reactome pathways ('L1CAM interactions' (R-HSA-373760)).

When the 43 downregulated proteins in PD models were analyzed by STRING, clathrin heavy chain 1 (CLTC) was the protein with the maximum number of connexions (seven in total), including vesicle-fusing ATPase (NSF), prohibitin (PHB), serine/threonine-protein phosphatase 2A 65kDa regulatory subunit A alpha isoform (PPP2R1A), synaptotagmin-2(SYT2), tropomyosin alpha-3 chain (TPM3), 14-3-3 protein epsilon (YWHAE), and 14-3-3 protein zeta/delta (YWHAZ) (**Figure 6.17A**). GO analysis found these proteins involved in 'vesicle-mediated transport', 'myelin sheath' or 'focal adhesion' (**Table S5 Annex 3**), while Reactome pathway analysis revealed that these proteins were a part of pathways such as 'membrane trafficking' (R-HSA-199991) or 'vesicle-mediated transport' (R-HSA-5653656).

On the other hand, only one upregulated protein (protein disulfide-isomerase A3 (PDIA3)) appeared to be a connection hub, associated with the seven dysregulated proteins annexin A5 (ANXA5), T-complex protein 1 subunit beta (CCT2), creatine kinase B-type (CKB), dihydrolipoyl dehydrogenase, mitochondrial (DLD), elongation factor 2 (EEF2), voltage-dependent anion-selective channel protein 1 (VDAC1), and vimentin (VIM) (**Figure 6.17B**). In terms of which enriched terms these proteins were associated,

'extracellular exosome', 'mitochondrion' or 'metabolic pathways' were some of the cellular components and pathways that GO analysis identified (**Table S6 Annex 3**). However, although many of these proteins were identified by Reactome pathway analysis, most of them did not belong to the top 25 most enriched pathways. Nevertheless, pathways such as 'neutrophil degranulation' (R-HSA-6798695) or 'signaling by nuclear receptors' (R-HSA-9006931) were pathways associated with some of these proteins.

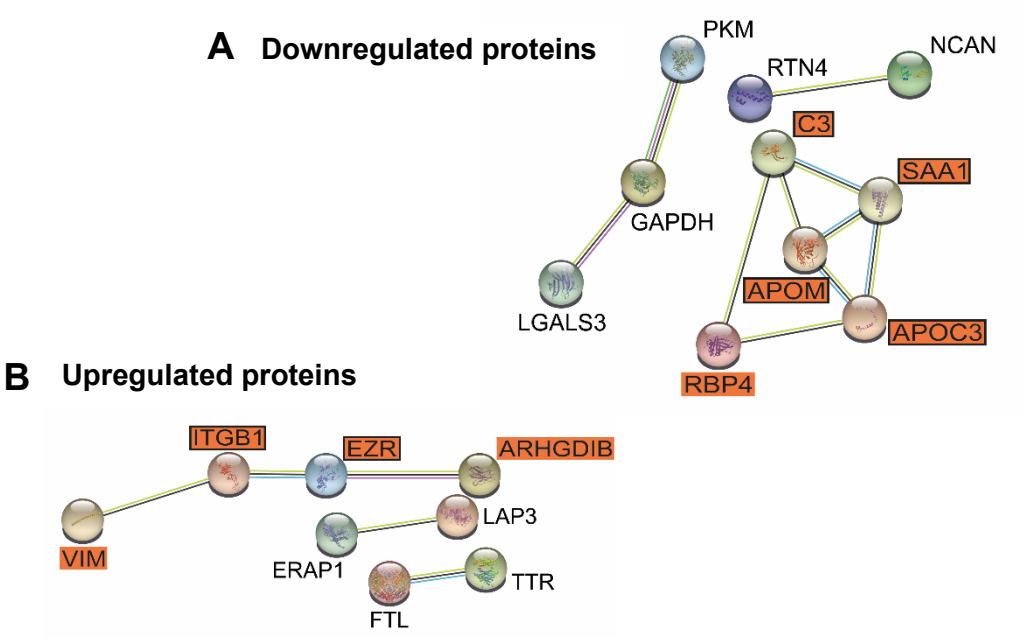

Figure 6.16. Protein network analysis with the STRING database of the conserved dysregulated proteins in the human PD proteome. Protein-protein interactions of the total 28 dysregulated proteins that are conserved in the human PD proteome. **(A)** Protein network of the 15 conserved downregulated proteins. **(B)** Protein network of the 13 conserved upregulated proteins. In orange boxes with black border, proteins show the larger number of associations; while orange boxes alone indicate their protein associations. The network displays only proteins with interactions, while those proteins without connections were hidden. The coloured lines indicate the type of interaction between proteins (light blue, associated in curated database; pink, experimental or biochemical determined; green, gene neighbourhood; black, co-expression; grey, protein homology; lime, co-mentioned in Pubmed abstracts).

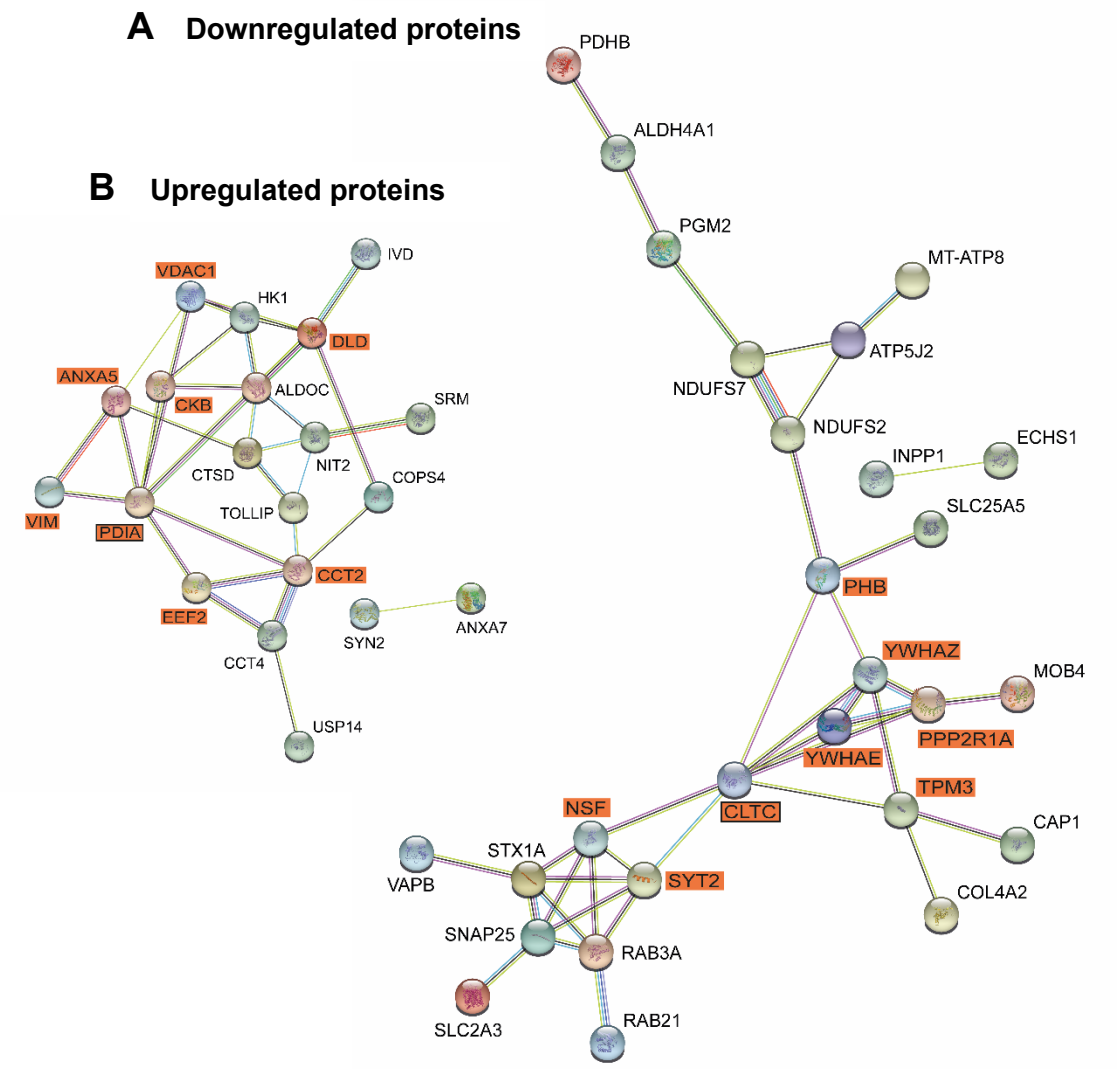

Figure 6.17. Protein network analysis with STRING database of the conserved dysregulated proteins in the proteome of PD models. Protein-protein interactions of the total 76 dysregulated proteins that are conserved in the proteome of PD models. **(A)** Protein network of the 43 conserved downregulated proteins. **(B)** Protein network of the 33 conserved upregulated proteins. In orange boxes with black border, proteins show the larger number of associations; while orange boxes alone indicate their protein associations. The network displays only proteins with interactions, those proteins that are not connected to the network are hidden from view. The coloured lines indicate the type of interaction between proteins (light blue, associated in curated database; pink, experimental or biochemical determined; green, gene neighbourhood; black, co-expression; grey, protein homology; lime, co-mentioned in Pubmed abstracts).

Finally, the protein glyceraldehyde-3-phosphate dehydrogenase (GAPDH) is the dysregulated protein with more interaction than is commonly expressed in the proteome of humans with PD and PD models (**Figure 6.18A**), as well as the ageing nervous system (**Figure 6.18B**). In the first case, glyceraldehyde-3-phosphate dehydrogenase (GAPDH) connects with three different proteins (retinal dehydrogenase 1 (ALDH1A1), elongation factor 2 (EEF2), and vimentin (VIM)) (**Figure 6.18A**), while in the second comparison glyceraldehyde-3-phosphate dehydrogenase (GAPDH) is linked to 34 different proteins (**Figure 6.18B**). Adding to this, GO analysis showed that this hub protein was implicated in multiple biological processes such as 'canonical glycolisis', or 'metabolic pathways' (**Table S8 in Annex 3**), while 'metabolism of carbohydrates' (R-HSA-71387)', 'gluconeogenesis' (R-HSA-70263) or 'glycolysis' (R-HSA-70171) were the Reactome pathways more enriched.

Altogether, bioinformatic analyses demonstrated that biological functions such as metabolism, neurotransmitter secretion, extracellular matrix, protein binding or immune system are commonly dysregulated across samples from PD patients and models of PD.

6.4 Discussion

In this chapter, a multi-study proteomic comparison was performed with the purpose of determining which biological and molecular mechanisms are commonly affected during the ageing process in the nervous system, as well as during PD, and between these two processes. To achieve this, differentially expressed proteins from published proteomic articles related to the ageing nervous system or PD were compared independently, identifying proteins commonly expressed in at least three or two articles, respectively.

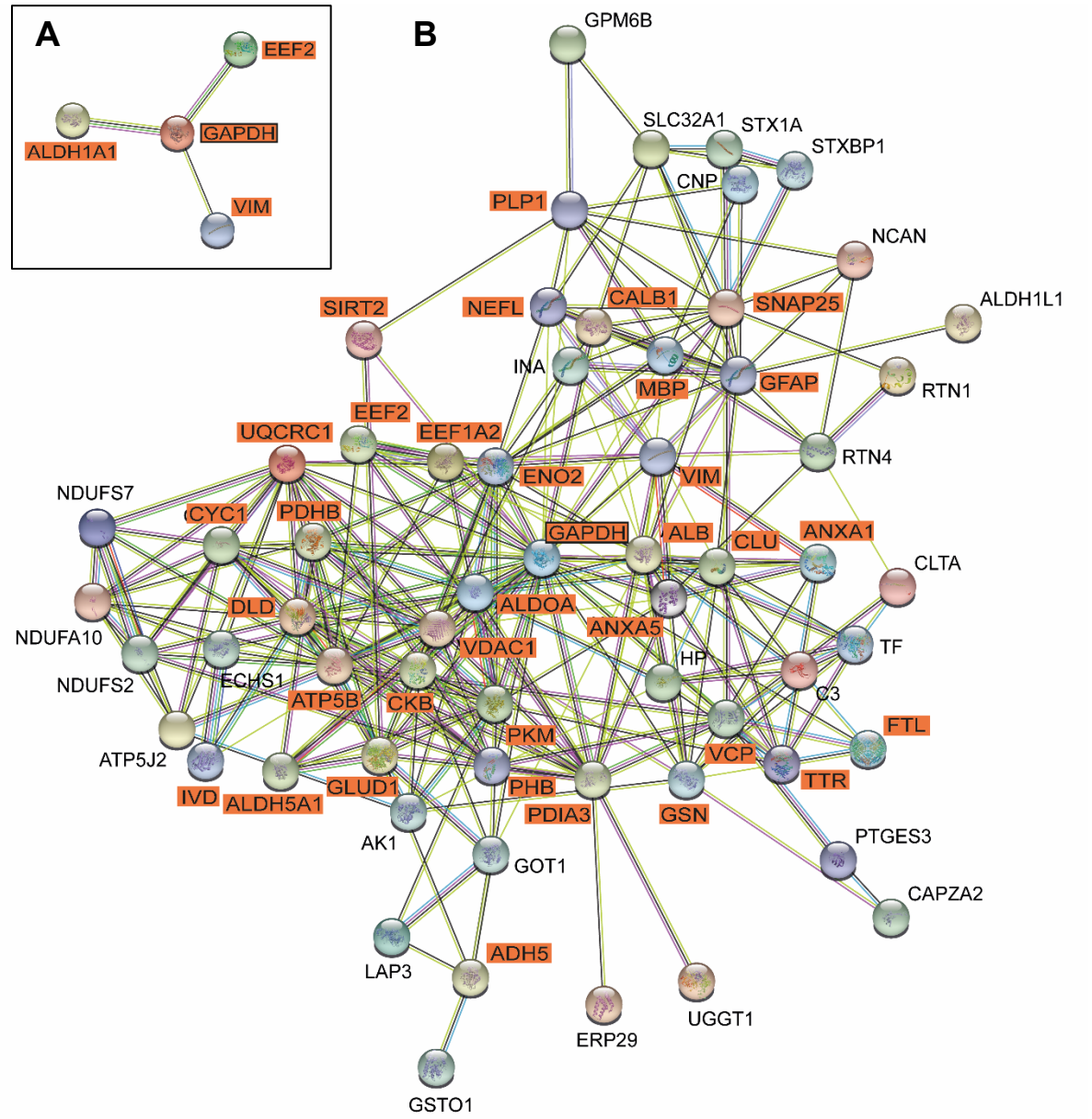

Figure 6.18. Protein network analysis with STRING database of the 4 common proteins between the proteomes of parkinsonians and PD models (A) and 70 common proteins between the PD proteome and the proteome of the ageing nervous system (B). In orange boxes with black border, proteins show the larger number of associations; while orange boxes alone indicate their protein associations. The network displays only proteins with interactions and those proteins that are not connected are hidden. The coloured lines indicate the type of interaction between proteins (light blue, associated in curated database; pink, experimental or biochemical determined; green, gene neighbourhood; black, co-expression; grey, protein homology; lime, co-mentioned in Pubmed abstracts).

6.4.1 The ageing brain is characterized by a reduction of metabolism-associated proteins together with mitochondrial dysfunction, and an increase of the immune system response

The comparison of the differentially expressed proteins from published proteomic articles related to the ageing nervous system revealed 648 proteins simultaneously expressed across three or more independent studies, finding 147 dysregulated in the same direction. Alpha-crystallin B chain (*cryab*), hyaluronan and proteoglycan link protein 2 (*hapln2)*, palmitoyl-protein thioesterase *1 (ppt1)* and glial fibrillary acidic protein (*gfap*, GFAP) were the proteins that appeared in the highest number of studies. Notably, most of the proteins that showed dysregulation of proteins were related to proteomics approaches based on label-free and quantitative proteomics. Therefore, it is possible that the common dysregulation found between studies are not associated with areas of the nervous system but with more sensitive techniques. Thus, only a few proteins were identified in samples that have been examined with 2DE gel electrophoresis, which would indicate a bias in the comparison results in favour of those areas where more proteins in total have been found. In essence, this highlights the necessity in the future of performing new analysis of different samples using the same technique in order to compare them and avoid technical limitations or bias.

Moreover, 36 of the 66 dysregulated proteins in the ageing SNpc in rats presented in this Thesis (see Chapter 3) were also found dysregulated in other areas of the ageing nervous system. Bioinformatic analyses of these proteins showed that biological pathways such as ‘mitochondrial ATP synthesis coupled proton transport’, ‘metabolic pathways’, ‘oxidative phosphorylation’, ‘respiratory electron transport, ATP synthesis by chemiosmotic coupling, and heat production by uncoupling proteins’, and ‘Parkinson’s disease’ were associated with the commonly downregulated proteins in ageing; while the terms and pathways that were overrepresented for the upregulated proteins included ‘oxidation-reduction process’, ‘cell-cell adhesion’, and ‘immune system’.

Importantly, the fact that the same proteins were dysregulated in the ageing SNpc in rats, but also in other regions of the nervous system, indicates that the changes and the molecular mechanisms associated with the ageing SNpc are not exclusive of this region but are part of the general ageing process in the nervous system. This means that, at least in rats, the ageing process by itself will not be enough to explain the specific vulnerability to degeneration of SNpc DAn. However, it is also possible that protein changes across the nervous system affect different regions differently, with the SNpc possibly being more sensitive to these changes and therefore, needing less time to show neurodegeneration. For example, during the General introduction of this Thesis, it was explained that SNpc DAn are high energy demanding and produce high amount of ROS and oxidative stress. Thus, alteration in proteins that affect the metabolism or try to counteract the oxidative stress can be an issue for DAn but not for other neurons. Nevertheless, the proteins that are simultaneously dysregulated in more studies (including the rat SNpc) are proteins related to glial cells (e.g., astrocytes), such as GFAP and alpha-crystallin B chain (CRYAB) (Eng, 1985; Ousman *et al.*, 2007; Hagemann *et al.*, 2009; Klopstein *et al.*, 2012), which highlights the role that astrocytes have during ageing. Previously (see Chapter 3), it was noted the important function that alpha-B-crystallin has in stopping the aggregation of GFAP filaments to avoid the degeneration of astrocytes by apoptosis (Derham and Harding, 1999; Ousman *et al.*, 2007; Hagemann *et al.*, 2009; Klopstein *et al.*, 2012). This increase in the expression of alpha-crystallin B chain (CRYAB) might be conserved in the entire nervous system during ageing, including the SNpc, as a mechanism to counteract the decline of astrocytes. However, the lack of consensus in the expression of GFAP in different brain regions, being downregulated in the SNpc, might indicate that this mechanism is not enough to preserve the expression of GFAP in certain regions, which may generate astrocytic dysfunction. As it was mentioned before (see Chapter 3), an impairment of astrocytes in the SNpc (but not in most of the other areas of the CNS) might affect their functions, which could cause a hostile environment for DAn, promoting their degeneration.

The alteration of the mitochondria and reduction of metabolism with ageing has been described previously. Indeed, previous findings suggest that dysfunction of the mitochondria, which produces ATP by oxidative phosphorylation (Spinelli and Haigis, 2018), is the cause of ageing. For example, the mtDNA mutator mouse characterized by multiple mtDNA mutations, develops a natural ageing phenotype due to the alteration of the mitochondrial respiratory chain caused by substitution of aa (Kujoth *et al*., 2005; Edgar *et al*., 2009). Moreover, defects in the mitochondria lead to oxidative phosphorylation deficiency, as shown by Pickrell *et al*. (2011) in a transgenic mouse with mtDNA depletion. The deficiency of the oxidative phosphorylation function produced neurodegeneration in the striatum and a phenotype associated with abnormal motor behaviours, which highlights the importance of the mitochondria in neurodegenerative diseases, and the relation between ageing and neurodegeneration. In fact, it seems that the brain is very vulnerable during the ageing process. This has been demonstrated recently by Kim and colleagues (2018), studying the mitochondrial characteristics from fibroblast-to-induced neuron (iNS) from people of different ages. In their results, they saw a 70% reduction of mitochondrial genes in old iNS, including those related to the respiratory chain; but also mitochondria fragmentation, lower accumulation of mitochondria in axons, a reduction in the production of ATP, and a high rate of oxidized protein damage. Interestingly, old fibroblasts from which iNS were derived did not possess these characteristics, indicating that brain cells are more susceptible to the ageing process in comparison to other cells in the body.

On the other hand, the increase of different aldehyde dehydrogenases with ageing, related to the oxidation-reduction process, might indicate a mechanism against oxidative stress (Singh *et al.,* 2013). Aldehyde dehydrogenases oxidize and detoxify aldehydes, which can be generated by oxidative stress and be cytotoxic for the cell (Kim *et al*., 2017b). Supporting this, Marchitti *et al*. (2007b) published that HEK293 cells transfected with ALDH3B1 (an aldehyde dehydrogenase that was upregulated in the ageing nervous system comparison) were protected against a lipid peroxidation product, reducing the

cytotoxicity and increasing the survival of the cells. Interestingly, the cytochrome b-245 light chain (CYBA) protein (another proteins that it is upregulated in the ageing nervous system) it is involved in the production of ROS by NADPH oxidase (Djordjevic *et al*., 2005), forming part of the phagosome pathway in microglia (Bodea *et al*., 2014). These microglia are immune cells in the brain that can phagocyte and degraded cellular components (e.g., dying cells, unfolded proteins) due to the production of ROS (Martinez *et al*., 2015; Arcuri *et al*., 2017). Therefore, it is possible that the increase of ROS and oxidative stress, generated firstly by microglia to protect the brain, might trigger the upregulation of aldehyde dehydrogenases during ageing in order to reduce cytotoxicity. Moreover, this increase of ROS might be deleterious for the mitochondria, due to its role in the damage and degradation of mtDNA (Shokolenko *et al*., 2009).

6.4.2 The human brain during PD is characterized by a reduction in the expression of metabolism-related proteins, and an increase in the expression of proteins related to interleukin signaling

The different comparisons of the differentially expressed proteins in humans with PD revealed that, in the SNpc, only eight proteins appeared dysregulated in at least two different studies. Nevertheless, these eight proteins might represent ‘core’ proteins related to molecular features that are systematically altered during PD, which would be good to explore with more detail in the future. Likewise, when the whole brain was considered, 35 proteins appeared simultaneously in two or more studies, and from these, 17 were dysregulated in the same direction. In the case of PD biofluids, from the 19 dysregulated proteins across two articles or more, only five were dysregulated in a conserved way during the disease. Lastly, during the comparison of the whole human PD proteome, 68 proteins were dysregulated in more than two studies, finding 28 of them conserved. Bioinformatic analyses of the conserved downregulated proteins in the proteome of parkinsonians showed that terms such as ‘metabolism’, including ‘glucose

metabolism' and 'glycolysis' were overrepresented. Oppositely, conserved upregulated proteins were linked to the pathway 'interleukin-4 and interleukin-13 signalling'.

It is important to mention the low number of common differentially expressed proteins within the six studies related to the PD SNpc in humans (one of them focused on mitochondrial fraction), where only eight proteins were dysregulated simultaneously in two studies. In essence, this technical characteristic will affect the final results found in the comparison. A reason to explain this lack of consistency can be the low number of proteins identified in four of the articles, based on the proteomic approach used (e.g., 2DE gel electrophoresis), but also it might indicate other technicalities such as the way of preparing the sample, the instrument used to identified the proteins, or the different strategies to process the data.

Moreover, with the data that it was possible to examine from the different studies, TH was only identified (being downregulated) in one study of the PD SNpc in humans (Licker *et al*., 2014). Although it would be expected to find a reduction of its expression in all the studies, due to the characteristic degeneration of DAn associated with PD (Damier *et al*., 1999), this event might be produced by the limitations of the number of proteins found in each sample, as well as the use of mitochondrial fractions which would not contain the enzyme. Furthermore, the fact that most of the proteins were only expressed in SNpc, brain or biofluids, without finding proteins in common, suggest that during PD the alterations in the proteome found in different parts of the body differ. Nevertheless, as previously noted, these differences can be produced by the proteomic techniques used in each case as well as other technicalities and highlights the necessity to reproduce these studies with more powerful and similar approaches to be able to compare them.

A reduction in glucose metabolism has been observed in two independent studies using positron emission tomography in PD patients with cognitive decline (Meles *et al*., 2015; Firbank *et al*., 2017). Meles and colleagues (2015) found a metabolic decrease during PD in caudate-putamen, thalamus, supplementary motor area, cingulate cortex and parietal regions of the brain; while Firbank *et al*. (2017) described a reduction of the

metabolic rate in the parietal lobes of early diagnosed PD patients compared to controls. Interestingly, although previous research has showed that glycolysis increases in PD blood mononuclear cells, associated with a high levels of mitochondria dysfunction and ROS production (Smith *et al.*, 2018), the multi-study comparison showed the opposite effect with the disease. However, this effect can be due to other roles that glyceraldehyde-3-phospahye dehydrogenase (GAPDH), the protein linked to this pathway, is related to. Thus, it has been described that glyceraldehyde-3-phospahye dehydrogenase (GAPDH), as a part of its metabolic function, when it is in the form of protofibrils can also interact with alpha-synuclein oligomers, scavenging their toxicity (Avila *et al.,* 2014). Therefore, it is possible to speculate that a reduction of glyceraldehyde-3-phospahye dehydrogenase (GAPDH) with PD is triggering the accumulation of toxic alpha-synuclein oligomers within the cells.

On the other hand, interleukin 4, produced by microglia after a treatment with the inflammatory toxin lipopolysaccharide, is involved in the degeneration of DAn *in vivo* (Bok *et al.*, 2018). Moreover, another study has shown that the increase of interleukin 13 (in microglia and SNpc DAn of a mouse model of chronic stress) participated in the degeneration of DAn (Mori *et al.*, 2017). Altogether, this might indicate that the release of cytokines (e.g., interleukin 4 and 13) by microglia during PD might have an impact in the vulnerability of DAn.

6.4.3 The proteome of PD models showed dysregulation of processes related to neurotransmitter secretion, synaptic vesicle cycling and metabolism of proteins

The multi-comparison analysis in PD models revealed 113 dysregulated proteins in two or more studies, 76 of them were conserved in the direction of expression. Once again, GFAP was one the proteins that appeared in the highest number of studies, while TH did not appear as one of the dysregulated proteins in more than two studies simultaneously. Bioinformatics analyses indicated that the most enriched term associated with downregulated proteins were ’neurotransmitter secretion’, ‘synaptic

vesicle cycle' and 'Parkinson's disease', whilst upregulated proteins were linked to 'metabolism of proteins', including 'folding of actin by CCT/TriC'.

Alterations in the proteins that regulate neurotransmitter SNARE-mediated exocytosis have been proven to be reduced in immortalized embryonic mesencephalic cells treated with the PD neurotoxin 6-OHDA (Stepkowski *et al*., 2015). Moreover, Choi *et al*. (2013) discovered that alpha-synuclein oligomers, found extensively in PD (see General introduction), have a detrimental effect on the assemble of the SNARE complex avoiding the vesicle lipid mixing. This generates a reduction of exocytosis, as demonstrated by the same authors in PC12 cells exposed to alpha-synuclein oligomers. Conversely, other authors have described that a dysfunction in SNARE assembly shows a reduction in neurotransmitter release and triggers the aggregation of alpha-synuclein in presynaptic terminals in the striatum (Nakata *et al.,* 2012). Although I did not find any article suggesting a mechanism of action by which PD toxins (e.g., 6-OHDA) affect the SNARE complex, it seems quite clear that PD models might mimic the disease through the dysfunction of the SNARE-mediated exocytosis process. Therefore, it is not surprising to find the 'Parkinson's disease' pathway overrepresented in this proteome.

Chaperonins, such as those upregulated in PD models (e.g., chaperonin Containing TCP1 Subunit 2 and 4 (CCT2, CCT4)) as part of the 'folding of actin by CCT/Tric' pathway, ensure the proper folding of essential proteins, such as actin and tubulin (Llorca *et al*., 2000; Balchin *et al*., 2018). PD models such as 6-OHDA have been shown to produce microtubule disruption by fragmentation of tubulin in DAn cultures (Lu *et al*., 2014). As they proved, this fragmentation affects axonal transport, including mitochondrial synaptic vesicle motility, which causes retrograde degeneration. Hence, it could happen that an increase in the metabolism of proteins such as chaperonins appear as a mechanism by the cell to neutralize this harmful effect.

6.4.4 The proteomic changes found in human PD and PD models reveal that both proteomes differ

To understand how well PD models reflected the human disease at the proteomic level, a comparison of both proteomes was performed. Very surprisingly, only four proteins (related between them in a protein network) were differentially expressed simultaneously in both proteomes.

Aldehyde dehydrogenase 1A1 (ALDH1A1) is involved in the oxidation of reactive DOPAL in a less toxic DOPAC, which it is essential for the cell to avoid the aggregation of cytotoxic alpha-synuclein promoted by DOPAL (Marchitti *et al*., 2007a). Previous research by Liu *et al*. (2014), using alpha-synuclein transgenic mice and PD human samples, has shown that a reduction of aldehyde dehydrogenase 1A1 (ALDH1A1) in SNpc, as it was found in this PD multi-study comparison, is linked to a higher accumulation of alpha-synuclein aggregates and neurodegeneration. Thus, a dysregulation of this protein, together with glyceraldehyde-3-phospahye dehydrogenase (GAPDH) might be affecting the scavenging of cytotoxic alpha-synuclein oligomers (Avila *et al.,* 2014). Nevertheless, it is difficult to corroborate this hypothesis because in the present multi-study analyses alpha-synuclein was only found in one article, being downregulated in the striatum of mice treated with MPTP (Chin *et al*., 2008). This could indicate that alpha-synuclein is not dysregulated in PD, although it is more likely that the proteomics approaches used (most of them using 2DE gel electrophoresis) did not identify it.

This emphasizes the necessity of performing new analyses of both proteomes using more robust and similar proteomic approaches to comprehend if the lack of common proteins is due to real proteomic differences or limitations in the technique. In the hypothetical case that real proteomic differences are found, that would mean that research needs to reconsider these PD models as a successful way to mimic the disease. Moreover, GAPDH is used for many researchers as a loading control for

Western blot (Pan *et al*., 2019), therefore, if it is true that it is dysregulated during PD, its use for this application should be avoided.

6.4.5 Oxidation-reduction pathways and metabolism are common pathways in ageing and PD

Seventy differentially expressed proteins were simultaneously dysregulated in PD and ageing. Adding to this, six of the proteins dysregulated in the rat SNpc proteome during ageing (some of them already described as part of glial cells and ECM, see Chapter 3) were part of those 70 common proteins in ageing and PD. Although the ageing process cannot alone explain the degeneration of SNpc, the conserving changes in proteins related to glial cells and ECM suggests that its impact in the disease is important. Bioinformatic analyses revealed conserved enriched pathways associated with 'substantia nigra development', 'oxidation-reduction process' and 'metabolism pathways'.

Throughout this Thesis, it has been mentioned that during neurodevelopment the CNS undergoes important proteomic changes related to cytoskeletal organization, microtubule dynamic and mitochondria (McClatchy *et al*., 2012; Fuller *et al*., 2015). However, the expression of these proteins in a specific time window is important to avoid pathological consequences. For example, one dysregulated protein found in this multi-study comparison, alpha-internexin (ina), is an intermediate filament protein highly expressed in postmitotic neurons in the developing CNS and has a low expression in adult brains (Fliegner *et al*., 1994). However, if this protein aggregates in adults, it produces the abnormal accumulation of other intermediate filaments, axonal swelling, neurodegeneration and astrogliosis (Ching *et al.,* 1999; Cairns *et al*., 2004). Another common dysregulated protein, sirtuin-2 (SIRT2), has been seen to accumulate in the ageing brain and has a role deacetylating microtubules (Maxwell *et al*., 2011). Recently, it has been described that this protein can also deacetylate alpha-synuclein, generating its aggregation (de Oliveira *et al*., 2017). Thus, the overexpression of sirtuin-2 (SIRT2)

increases the toxicity produced by alpha-synuclein and, in fact, its deletion protects SNpc DAn from MPTP toxicity *in vivo*.

Finally, 'oxidation-reduction process' and 'metabolism pathways' are two other processes that are commonly altered in PD and ageing. As it was reviewed in detail in the General introduction of this Thesis (see Chapter 1), DAn need high amounts of energy for survival, which produces high amounts of ROS (Pacelli *et al*., 2015). Furthermore, the metabolism and oxidation of dopamine produces ROS and other metabolites (e.g., DOPAL) that can be toxic for the cells (Adams and Odunze, 1991; Zhang *et al*., 2019). In addition, the dysregulation and production of excessive ROS can affect the mitochondria (e.g., deficiencies in respiratory chain and mtDNA deletions) (Bender *et al*., 2006; Venkateshappa *et al*., 2012). This event would affect the production of energy and have consequences on the high metabolic demand of neurons such as SNpc DAn, but not in other areas of the brain.

6.5 Conclusions

In summary, the results of this multi-study proteomic comparisons demonstrate that during the ageing process, the nervous system has a dysregulation of metabolism probably due to an alteration of mitochondrial function, as well as an increase of the immune system response.

On the other hand, there are differences between the PD proteome in humans and PD models, although it is difficult to conclude if these differences are due to the multiple proteomic approaches used where low number of proteins were identified or associated with real proteomic differences. Nevertheless, metabolism and interleukin signaling are the pathways enriched in human PD proteome, while defects in the neurotransmitter secretion pathways related to metabolism and oxidation-reduction and metabolism of proteins are found in PD models.

Finally, the multi-study proteomic comparison between ageing and PD produced here corroborates previous findings where metabolism and oxidation-reduction processes are dysregulated in the ageing brain and affected during PD.

Chapter 7.
Final discussion and future perspectives

CHAPTER 7: FINAL DISCUSSION AND FUTURE PERSPECTIVES

It is well established that ageing is the principal risk factor in PD, a neurodegenerative disease characterized by the loss of DAn from the SNpc (Damier *et al*., 1999; GBD 2016 Parkinson's Disease Collaborators, 2018). However, the role that the physiological ageing process plays in the development of this disease remains elusive. Thus, with the aim of gaining more insight into how becoming older might increase the vulnerability of DAn to PD, one of the objective of this Thesis was to use a cutting-edge proteomic approach, together with bioinformatic analysis, and molecular and cellular techniques to investigate the rat SNpc as it ages.

Proteomics results showed that GFAP, the main intermediate filament of astrocytes (Eng, 1985), as well as proteins from the ECM, were dysregulated in the rat SNpc during ageing. This Thesis also showed that, although changes in the proteomic expression of TH were not found, the density of SNpc DAn was reduced whilst the size of their somas increased. Such changes in the number and morphology of these neurons may affect the proteomic composition of the ECM, in an attempt to stabilize these DAn in the SNpc or to reduce possible oxidative stress caused by the death of these neurons (Pizzorusso *et al*., 2002; Morawski *et al*.,2004; de Vivo *et al*., 2013). Interestingly, astrocytes can produce some of these ECM proteins, such as the dysregulated proteins in the SNpc aggrecan or versican (Asher *et al*., 1995; Beggah *et al*., 2005; Afshari *et al*., 2010). Therefore, one possibility is that during this process astrocytes might also undergo cytoskeleton changes in order, for example, to adapt to the modifications found in the ECM. Though still speculative, it appears that the main canonical isoform of GFAP (i.e., GFAPα) within astrocytes is reduced during ageing, which might implicate a concomitant increase of other isoforms already described in the literature or new ones that have not been discovered yet. This Thesis demonstrated for the first time the existence of the isoform GFAPδ in the rat SNpc, thus, it is not unthinkable to believe that other isoforms might exist in this region of the brain during ageing that are not yet possible to identify by proteomics or Western blot analysis. The high expression of GFAPδ is associated

with the aggregation of intermediate filaments, which in turn affects the function of the astrocyte (Roelofs *et al*., 2005; Perng *et al.,* 2008). Therefore, other isoforms or changes in GFAP might have the same effect, further aggregating these intermediate filaments, which would explain why there is an increase of the chaperone alpha-crystallin B chain in the oldest samples (i.e., to combat the accumulation of intermediate filaments and protect these glial cells; Derham and Harding, 1999; Ousman *et al*., 2007; Perng *et al*., 2008; Hagemann *et al*., 2009; Klopstein *et al*., 2012). The multi-study comparison of the ageing nervous system also showed that the increase of proteins related to the ECM (e.g., hyaluronan and proteoglycan link proteins 2) and alpha-crystallin B chain were upregulated in the elderly, which suggests that something similar to this speculative process must be conserved across the whole nervous system but that the SNpc is more vulnerable to these changes.

The increased sensitivity of SNpc DAn are likely due to their characteristically high amount of ROS production and oxidative stress due to the metabolism and oxidation of dopamine (Cohen *et al*., 1997). In addition, the multi-study proteomic comparisons of the ageing nervous system and PD revealed that metabolic and mitochondrial functions are altered in both ageing and PD, which suggests that the disruption of these processes plays a major role in the vulnerability of DAn. Adding to this, astrocytic dysfunction through modifications of their cytoskeleton might exacerbate this vulnerability, because astrocytes provide metabolic support and energy to neurons, and reduce and neutralize ROS from the environment by using antioxidants (Voutsinos-Porche *et al*., 2003; McBean, 2017).

Lastly, in the attempt to understand the important role that astrocytes have in protecting DAn, the neurons were challenged by exposure to low concentration of the drug 6-OHDA *in vitro*. However, it was not possible to show how important glial cells were in supporting DAn during such a challenge because the toxin also affected astrocytes. Nevertheless, it is still possible that the damaging effects of 6-OHDA to DAn was due to the fact that astrocytes were also impaired. 6-OHDA inhibits the mitochondrial respiratory chain and

forms free radicals (Glinka *et al*., 1997), effects that astrocytes combat through their support of metabolic activity and the neutralization of ROS (Voutsinos-Porche *et al*., 2003; McBean, 2017). Thus, the degeneration of astrocytes might aggravate the direct toxic effect of 6-OHDA on DAn. Bearing this in mind, it will be very important to consider this effect in the future when the impact of this widely used drug is assessed in DAn, because part of the effect might be associated by the lack of viable astrocytes and their functions.

This Thesis has demonstrated the strength of cutting-edge proteomic analysis combined with traditional techniques and bioinformatic examinations to gain insight into the complex proteome of the SNpc and obtain a better understanding of physiological processes that emerge during ageing. This Thesis has highlighted the necessity of producing better antibodies for more specific characterizations of astrocytes, beyond the general idea of 'GFAP', and understanding the effect that different isoforms have in astrocytes and their functions. In the future, this might be addressed with label-free proteomic approaches to define the proteome of astrocytes, and to reveal the changes that appear in this proteome in processes such as ageing. Moreover, after understanding the proteomic changes that are conserved with ageing in the brain and the SNpc, it would be important to investigate further the proteome of the extracellular space in these areas with ageing to elucidate the implications that a dysregulation of this proteome has in the protection or vulnerability of neurons. In addition, more effort is needed to comprehend the relationship between neurons and astrocytes in culture, and to generate enriched neuronal cultures that allow for the study of the ageing process in neurons *in vitro* on their own. Finally, this Thesis has shown the value of comparing published proteomic studies and how important it is to examine again certain samples with more sensible proteomic techniques in order to identified more proteins and obtain more robust results.

References

REFERENCES

Abdi F, Quinn JF, Jankovic J, McIntosh M, Leverenz JB, Peskind E, Nixon R, Nutt J, Chung K, Zabetian C, Samii A, Lin M, Hattan S, Pan C, Wang Y, Jin J, Zhu D, Li GJ, Liu Y, Waichunas D, Montine TJ, Zhang J (2006) Detection of biomarkers with a multiplex quantitative proteomic platform in cerebrospinal fluid of patients with neurodegenerative disorders. J Alzheimers Dis 9:293-348.

Abe K, Saito H (1999) Astrocyte stellation induced by tyrosine kinase inhibitors in culture. Brain Res 837:306-308.

Abedelahi A, Hasanzadeh H, Hadizadeh H, Joghataie MT (2013) Morphometric and volumetric study of caudate and putamen nuclei in normal individuals by MRI: Effect of normal aging, gender and hemispheric differences. Pol J Radiol 78:7-14.

Adams JD,Jr, Odunze IN (1991) Oxygen free radicals and Parkinson's disease. Free Radic Biol Med 10:161-169.

Adav SS, Park JE, Sze SK (2019) Quantitative profiling brain proteomes revealed mitochondrial dysfunction in Alzheimer's disease. Mol Brain 12:8-019-0430-y.

Adler DH, Wisse LEM, Ittyerah R, Pluta JB, Ding SL, Xie L, Wang J, Kadivar S, Robinson JL, Schuck T, Trojanowski JQ, Grossman M, Detre JA, Elliott MA, Toledo JB, Liu W, Pickup S, Miller MI, Das SR, Wolk dopamine, Yushkevich PA (2018) Characterizing the human hippocampus in aging and Alzheimer's disease using a computational atlas derived from ex vivo MRI and histology. Proc Natl Acad Sci U S A 115:4252-4257.

Aebersold MJ, Thompson-Steckel G, Joutang A, Schneider M, Burchert C, Forro C, Weydert S, Han H, Voros J (2018) Simple and Inexpensive Paper-Based Astrocyte Co-culture to Improve Survival of Low-Density Neuronal Networks. Front Neurosci 12:94.

Aebersold R, Mann M (2016) Mass-spectrometric exploration of proteome structure and function. Nature 537:347-355.

af Bjerken S, Marschinke F, Stromberg I (2008) Inhibition of astrocytes promotes long-distance growing nerve fibers in ventral mesencephalic cultures. Int J Dev Neurosci 26:683-691.

Afshari FT, Kwok JC, White L, Fawcett JW (2010) Schwann cell migration is integrin-dependent and inhibited by astrocyte-produced aggrecan. Glia 58:857-869.

Ahlemeyer B, Kolker S, Zhu Y, Hoffmann GF, Krieglstein J (2003) Cytosine arabinofuranoside-induced activation of astrocytes increases the susceptibility of neurons to glutamate due to the release of soluble factors. Neurochem Int 42:567-581.

Alberio T, Pippione AC, Zibetti M, Olgiati S, Cecconi D, Comi C, Lopiano L, Fasano M (2012) Discovery and verification of panels of T-lymphocyte proteins as biomarkers of Parkinson's disease. Sci Rep 2:953.

Alvarez-Erviti L, Rodriguez-Oroz MC, Cooper JM, Caballero C, Ferrer I, Obeso JA, Schapira AH (2010) Chaperone-mediated autophagy markers in Parkinson disease brains. Arch Neurol 67:1464-1472.

Anand S, Samuel M, Ang CS, Keerthikumar S, Mathivanan S (2017) Label-Based and Label-Free Strategies for Protein Quantitation. Methods Mol Biol 1549:31-43.

Andrews GL, Simons BL, Young JB, Hawkridge AM, Muddiman DC (2011) Performance characteristics of a new hybrid quadrupole time-of-flight tandem mass spectrometer (TripleTOF 5600). Anal Chem 83:5442-5446.

Angelova PR, Abramov AY (2018) Role of mitochondrial ROS in the brain: from physiology to neurodegeneration. FEBS Lett 592:692-702.

Aransay A, Rodriguez-Lopez C, Garcia-Amado M, Clasca F, Prensa L (2015) Long-range projection neurons of the mouse ventral tegmental area: a single-cell axon tracing analysis. Front Neuroanat 9:59.

Arcuri C, Mecca C, Bianchi R, Giambanco I, Donato R (2017) The Pathophysiological Role of Microglia in Dynamic Surveillance, Phagocytosis and Structural Remodeling of the Developing CNS. Front Mol Neurosci 10:191.

Arguelles S, Cano M, Machado A, Ayala A (2011) Effect of aging and oxidative stress on elongation factor-2 in hypothalamus and hypophysis. Mech Ageing Dev 132:55-64.

Arike L, Peil L (2014) Spectral counting label-free proteomics. Methods Mol Biol 1156:213-222.

Asara JM, Christofk HR, Freimark LM, Cantley LC (2008) A label-free quantification method by MS/MS TIC compared to SILAC and spectral counting in a proteomics screen. Proteomics 8:994-999.

Ascherio A, Schwarzschild MA (2016) The epidemiology of Parkinson's disease: risk factors and prevention. Lancet Neurol 15:1257-1272.

Ashburner M, Ball CA, Blake JA, Botstein D, Butler H, Cherry JM, Davis AP, Dolinski K, Dwight SS, Eppig JT, Harris MA, Hill DP, Issel-Tarver L, Kasarskis A, Lewis S, Matese JC, Richardson JE, Ringwald M, Rubin GM, Sherlock G (2000) Gene ontology: tool for the unification of biology. The Gene Ontology Consortium. Nat Genet 25:25-29.

Asher RA, Morgenstern dopamine, Fidler PS, Adcock KH, Oohira A, Braistead JE, Levine JM, Margolis RU, Rogers JH, Fawcett JW (2000) Neurocan is upregulated in injured brain and in cytokine-treated astrocytes. J Neurosci 20:2427-2438.

Asher RA, Morgenstern dopamine, Shearer MC, Adcock KH, Pesheva P, Fawcett JW (2002) Versican is upregulated in CNS injury and is a product of oligodendrocyte lineage cells. J Neurosci 22:2225-2236.

Asher RA, Scheibe RJ, Keiser HD, Bignami A (1995) On the existence of a cartilage-like proteoglycan and link proteins in the central nervous system. Glia 13:294-308.

Authier N, Gillet JP, Fialip J, Eschalier A, Coudore F (2000) Description of a short-term Taxol-induced nociceptive neuropathy in rats. Brain Res 887:239-249.

Avila CL, Torres-Bugeau CM, Barbosa LR, Sales EM, Ouidja MO, Socias SB, Celej MS, Raisman-Vozari R, Papy-Garcia D, Itri R, Chehin RN (2014) Structural characterization of heparin-induced glyceraldehyde-3-phosphate dehydrogenase protofibrils preventing alpha-synuclein oligomeric species toxicity. J Biol Chem 289:13838-13850.

Azevedo FA, Carvalho LR, Grinberg LT, Farfel JM, Ferretti RE, Leite RE, Jacob Filho W, Lent R,Herculano-Houzel S (2009) Equal numbers of neuronal and nonneuronal cells make the human brain an isometrically scaled-up primate brain. J Comp Neurol 513:532-541.

Azuma M, Fukiage C, David LL, Shearer TR (1997) Activation of calpain in lens: a review and proposed mechanism. Exp Eye Res 64:529-538.

Baba M, Nakajo S, Tu PH, Tomita T, Nakaya K, Lee VM, Trojanowski JQ, Iwatsubo T (1998) Aggregation of alpha-synuclein in Lewy bodies of sporadic Parkinson's disease and dementia with Lewy bodies. Am J Pathol 152:879-884.

Bai Q, Sun M, Stolz DB, Burton EA (2011) Major isoform of zebrafish P0 is a 23.5 kDa myelin glycoprotein expressed in selected white matter tracts of the central nervous system. J Comp Neurol 519:1580-1596.

Balchin D, Milicic G, Strauss M, Hayer-Hartl M, Hartl FU (2018) Pathway of Actin Folding Directed by the Eukaryotic Chaperonin TRiC. Cell 174:1507-1521.e16.

Bandeira F, Lent R, Herculano-Houzel S (2009) Changing numbers of neuronal and non-neuronal cells underlie postnatal brain growth in the rat. Proc Natl Acad Sci U S A 106:14108-14113.

Barden H, Levine S (1983) Histochemical observations on rodent brain melanin. Brain Res Bull 10:847-851.

Bardou I, Kaercher RM, Brothers HM, Hopp SC, Royer S, Wenk GL (2014) Age and duration of inflammatory environment differentially affect the neuroimmune response and catecholaminergic neurons in the midbrain and brainstem. Neurobiol Aging 35:1065-1073.

Barkats M, Millecamps S, Bilang-Bleuel A, Mallet J (2002) Neuronal transfer of the human Cu/Zn superoxide dismutase gene increases the resistance of dopaminergic neurons to 6-hydroxydopamine. J Neurochem 82:101-109.

Basso M, Giraudo S, Corpillo D, Bergamasco B, Lopiano L, Fasano M (2004) Proteome analysis of human substantia nigra in Parkinson's disease. Proteomics 4:3943-3952.

Basso M, Giraudo S, Lopiano L, Bergamasco B, Bosticco E, Cinquepalmi A, Fasano M (2003) Proteome analysis of mesencephalic tissues: evidence for Parkinson's disease. Neurol Sci 24:155-156.

Bauer M, Ahrne E, Baron AP, Glatter T, Fava LL, Santamaria A, Nigg EA, Schmidt A (2014) Evaluation of data-dependent and -independent mass spectrometric workflows for sensitive quantification of proteins and phosphorylation sites. J Proteome Res 13:5973-5988.

Beggah AT, Dours-Zimmermann MT, Barras FM, Brosius A, Zimmermann DR, Zurn AD (2005) Lesion-induced differential expression and cell association of Neurocan, Brevican, Versican V1 and V2 in the mouse dorsal root entry zone. Neuroscience 133:749-762.

Bender A, Desplats P, Spencer B, Rockenstein E, Adame A, Elstner M, Laub C, Mueller S, Koob AO, Mante M, Pham E, Klopstock T, Masliah E (2013) TOM40 mediates mitochondrial dysfunction induced by alpha-synuclein accumulation in Parkinson's disease. PLoS One 8:e62277.

Bender A, Krishnan KJ, Morris CM, Taylor GA, Reeve AK, Perry RH, Jaros E, Hersheson JS, Betts J, Klopstock T, Taylor RW, Turnbull DM (2006) High levels of mitochondrial DNA deletions in substantia nigra neurons in aging and Parkinson disease. Nat Genet 38:515-517.

Benito-Leon J, Bermejo-Pareja F, Morales-Gonzalez JM, Porta-Etessam J, Trincado R, Vega S, Louis ED (2004) Incidence of Parkinson disease and parkinsonism in three elderly populations of central Spain. Neurology 62:734-741.

Benuck M, Banay-Schwartz M, DeGuzman T, Lajtha A (1996) Changes in brain protease activity in aging. J Neurochem 67:2019-2029.

Bereczki E, Branca RM, Francis PT, Pereira JB, Baek JH, Hortobagyi T, Winblad B, Ballard C, Lehtio J, Aarsland D (2018) Synaptic markers of cognitive decline in neurodegenerative diseases: a proteomic approach. Brain 141:582-595.

Bernal GM, Peterson dopamine (2011) Phenotypic and gene expression modification with normal brain aging in GFAP-positive astrocytes and neural stem cells. Aging Cell 10:466-482.

Bignami A, Dahl D (1976) The astroglial response to stabbing. Immunofluorescence studies with antibodies to astrocyte-specific protein (GFA) in mammalian and submammalian vertebrates. Neuropathol Appl Neurobiol 2:99-110.

Birkmayer W, Hornykiewicz O (1961) Der L-Dioxyphenylalanin (=DOPA)-Effekt bei der Parkinson-Akinese. Wien Klin Wochenschr 73:787-788.

Bjorklund A, Stenevi U, Dunnet SB, Iversen SD (1981) Functional reactivation of the deafferented neostriatum by nigral transplants. Nature 289: 497-499.

Blausen.com staff Medical gallery of Blausen Medical 2014. WikiJournal of Medicine 1 2014:(2): 10.

Blechingberg J, Holm IE, Nielsen KB, Jensen TH, Jorgensen AL, Nielsen AL (2007) Identification and characterization of GFAPkappa, a novel glial fibrillary acidic protein isoform. Glia 55:497-507.

Blesa J, Trigo-Damas I, Quiroga-Varela A, Jackson-Lewis VR (2015) Oxidative stress and Parkinson's disease. Front Neuroanat 9:91.

Blesa J, Vila M (2019) Parkinson disease, substantia nigra vulnerability, and calbindin expression: Enlightening the darkness? Mov Disord 34:161-163.

Blum D, Torch S, Lambeng N, Nissou M, Benabid AL, Sadoul R, Verna JM (2001) Molecular pathways involved in the neurotoxicity of 6-OHDA, dopamine and MPTP: contribution to the apoptotic theory in Parkinson's disease. Prog Neurobiol 65:135-172.

Bodea LG, Wang Y, Linnartz-Gerlach B, Kopatz J, Sinkkonen L, Musgrove R, Kaoma T, Muller A, Vallar L, Di Monte dopamine, Balling R, Neumann H (2014) Neurodegeneration by activation of the microglial complement-phagosome pathway. J Neurosci 34:8546-8556.

Bodzon-Kulakowska A, Bierczynska-Krzysik A, Dylag T, Drabik A, Suder P, Noga M, Jarzebinska J, Silberring J (2007) Methods for samples preparation in proteomic research. J Chromatogr B Analyt Technol Biomed Life Sci 849:1-31.

Boehmerle W, Splittgerber U, Lazarus MB, McKenzie KM, Johnston DG, Austin DJ, Ehrlich BE (2006) Paclitaxel induces calcium oscillations via an inositol 1,4,5-trisphosphate receptor and neuronal calcium sensor 1-dependent mechanism. Proc Natl Acad Sci U S A 103:18356-18361.

Boehmerle W, Zhang K, Sivula M, Heidrich FM, Lee Y, Jordt SE, Ehrlich BE (2007) Chronic exposure to paclitaxel diminishes phosphoinositide signaling by calpain-mediated neuronal calcium sensor-1 degradation. Proc Natl Acad Sci U S A 104:11103-11108.

Boerger M, Funke S, Leha A, Roser AE, Wuestemann AK, Maass F, Bahr M, Grus F, Lingor P (2019) Proteomic analysis of tear fluid reveals disease-specific patterns in patients with Parkinson's disease - A pilot study. Parkinsonism Relat Disord

Bok E, Cho EJ, Chung ES, Shin WH, Jin BK (2018) Interleukin-4 Contributes to Degeneration of Dopamine Neurons in the Lipopolysaccharide-treated Substantia Nigra in vivo. Exp Neurobiol 27:309-319.

Bolgioni AF, Vittoria MA, Ganem NJ (2018) Long-term Live-cell Imaging to Assess Cell Fate in Response to Paclitaxel. J Vis Exp (135). doi:10.3791/57383.

Bonifati V, Rizzu P, van Baren MJ, Schaap O, Breedveld GJ, Krieger E, Dekker MC, Squitieri F, Ibanez P, Joosse M, van Dongen JW, Vanacore N, van Swieten JC, Brice A, Meco G, van Duijn CM, Oostra BA, Heutink P (2003) Mutations in the DJ-1 gene associated with autosomal recessive early-onset parkinsonism. Science 299:256-259.

Braak H, de Vos RA, Bohl J, Del Tredici K (2006) Gastric alpha-synuclein immunoreactive inclusions in Meissner's and Auerbach's plexuses in cases staged for Parkinson's disease-related brain pathology. Neurosci Lett 396:67-72.

Braak H, Del Tredici K (2017) Neuropathological Staging of Brain Pathology in Sporadic Parkinson's disease: Separating the Wheat from the Chaff. J Parkinsons Dis 7:S71-S85.

Braak H, Del Tredici K, Rub U, de Vos RA, Jansen Steur EN, Braak E (2003a) Staging of brain pathology related to sporadic Parkinson's disease. Neurobiol Aging 24:197-211.

Braak H, Rub U, Gai WP, Del Tredici K (2003b) Idiopathic Parkinson's disease: possible routes by which vulnerable neuronal types may be subject to neuroinvasion by an unknown pathogen. J Neural Transm (Vienna) 110:517-536.

Bradford MM (1976) A rapid and sensitive method for the quantitation of microgram quantities of protein utilizing the principle of protein-dye binding. Anal Biochem 72:248-254.

Brewer GJ (1995) Serum-free B27/neurobasal medium supports differentiated growth of neurons from the striatum, substantia nigra, septum, cerebral cortex, cerebellum, and dentate gyrus. J Neurosci Res 42:674-683.

Brichta L, Greengard P (2014) Molecular determinants of selective dopaminergic vulnerability in Parkinson's disease: an update. Front Neuroanat 8:152.

Brodbelt JS (2014) Photodissociation mass spectrometry: new tools for characterization of biological molecules. Chem Soc Rev 43:2757-2783.

Brown N, Crawford C (1993) Structural modifications associated with the change in Ca2+ sensitivity on activation of m-calpain. FEBS Lett 322:65-68.

Buchman AS, Shulman JM, Nag S, Leurgans SE, Arnold SE, Morris MC, Schneider JA, Bennett dopamine (2012) Nigral pathology and parkinsonian signs in elders without Parkinson disease. Ann Neurol 71:258-266.

Burke WJ, Li SW, Williams EA, Nonneman R, Zahm DS (2003) 3,4-Dihydroxyphenylacetaldehyde is the toxic dopamine metabolite in vivo: implications for Parkinson's disease pathogenesis. Brain Res 989:205-213.

Burman JL, Yu S, Poole AC, Decal RB, Pallanck L (2012) Analysis of neural subtypes reveals selective mitochondrial dysfunction in dopaminergic neurons from parkin mutants. Proc Natl Acad Sci U S A 109:10438-10443.

Burre J, Sharma M, Tsetsenis T, Buchman V, Etherton MR, Sudhof TC (2010) Alpha-synuclein promotes SNARE-complex assembly in vivo and in vitro. Science 329:1663-1667.

Cabello CR, Thune JJ, Pakkenberg H, Pakkenberg B (2002) Ageing of substantia nigra in humans: cell loss may be compensated by hypertrophy. Neuropathol Appl Neurobiol 28:283-291.

Cacabelos R (2017) Parkinson's Disease: From Pathogenesis to Pharmacogenomics. Int J Mol Sci 18:10.3390/ijms18030551.

Cahoy JD, Emery B, Kaushal A, Foo LC, Zamanian JL, Christopherson KS, Xing Y, Lubischer JL, Krieg PA, Krupenko SA, Thompson WJ, Barres BA (2008) A transcriptome database for astrocytes, neurons, and oligodendrocytes: a new resource for understanding brain development and function. J Neurosci 28:264-278.

Cairns NJ, Zhukareva V, Uryu K, Zhang B, Bigio E, Mackenzie IR, Gearing M, Duyckaerts C, Yokoo H, Nakazato Y, Jaros E, Perry RH, Lee VM, Trojanowski JQ (2004) Alpha-Internexin is Present in the Pathological Inclusions of Neuronal Intermediate Filament Inclusion Disease. Am J Pathol 164:2153-2161.

Camandola S (2018) Astrocytes, emerging stars of energy homeostasis. Cell Stress 2:246-252.

Caprioli RM, Farmer TB, Gile J (1997) Molecular imaging of biological samples: localization of peptides and proteins using MALDI-TOF MS. Anal Chem 69:4751-4760.

Carballo-Carbajal I, Laguna A, Romero-Gimenez J, Cuadros T, Bove J, Martinez-Vicente M, Parent A, Gonzalez-Sepulveda M, Penuelas N, Torra A, Rodriguez-Galvan B, Ballabio A, Hasegawa T, Bortolozzi A, Gelpi E, Vila M (2019) Brain tyrosinase overexpression implicates age-dependent neuromelanin production in Parkinson's disease pathogenesis. Nat Commun 10:973-019-08858-y.

Carulli D, Rhodes KE, Brown DJ, Bonnert TP, Pollack SJ, Oliver K, Strata P, Fawcett JW (2006) Composition of perineuronal nets in the adult rat cerebellum and the cellular origin of their components. J Comp Neurol 494:559-577.

Carulli D, Rhodes KE, Fawcett JW (2007) Upregulation of aggrecan, link protein 1, and hyaluronan synthases during formation of perineuronal nets in the rat cerebellum. J Comp Neurol 501:83-94.

Cavaletti G, Tredici G, Braga M, Tazzari S (1995) Experimental peripheral neuropathy induced in adult rats by repeated intraperitoneal administration of taxol. Exp Neurol 133:64-72.

Cavaliere F, Vicente ES, Matute C (2010) An organotypic culture model to study nigro-striatal degeneration. J Neurosci Methods 188:205-212.

Ceafalan LC, Fertig TE, Gheorghe TC, Hinescu ME, Popescu BO, Pahnke J, Gherghiceanu M (2019) Age-related ultrastructural changes of the basement membrane in the mouse blood-brain barrier. J Cell Mol Med 23:819-827.

Cebrian C, Zucca FA, Mauri P, Steinbeck JA, Studer L, Scherzer CR, Kanter E, Budhu S, Mandelbaum J, Vonsattel JP, Zecca L, Loike JD, Sulzer D (2014) MHC-I expression renders catecholaminergic neurons susceptible to T-cell-mediated degeneration. Nat Commun 5:3633.

Chadwick W, Martin B, Chapter MC, Park SS, Wang L, Daimon CM, Brenneman R, Maudsley S (2012) GIT2 acts as a potential keystone protein in functional hypothalamic networks associated with age-related phenotypic changes in rats. PLoS One 7:e36975.

Chapman JD, Goodlett DR, Masselon CD (2014) Multiplexed and data-independent tandem mass spectrometry for global proteome profiling. Mass Spectrom Rev 33:452-470.

Chatr-aryamontri A, Ceol A, Palazzi LM, Nardelli G, Schneider MV, Castagnoli L, Cesareni G (2007) MINT: the Molecular INTeraction database. Nucleic Acids Res 35:D572-4.

Chen CPC, Preston JE, Zhou S, Fuller HR, Morgan DGA, Chen R (2018) Proteomic analysis of age-related changes in ovine cerebrospinal fluid. Exp Gerontol 108:181-188.

Chen MH, Hagemann TL, Quinlan RA, Messing A, Perng MD (2013a) Caspase cleavage of GFAP produces an assembly-compromised proteolytic fragment that promotes filament aggregation. ASN Neuro 5:e00125.

Chen J, Tan Z, Zeng L, Zhang X, He Y, Gao W, Wu X, Li Y, Bu B, Wang W, Duan S (2013b) Heterosynaptic long-term depression mediated by ATP released from astrocytes. Glia 61:178-191.

Chen W, Ji J, Xu X, He S, Ru B (2003) Proteomic comparison between human young and old brains by two-dimensional gel electrophoresis and identification of proteins. Int J Dev Neurosci 21:209-216.

Chen WJ, Liem RK (1994) The endless story of the glial fibrillary acidic protein. J Cell Sci 107 (Pt 8):2299-2311.

Chevalier F (2010) Highlights on the capacities of "Gel-based" proteomics. Proteome Sci 8:23-5956-8-23.

Chin MH, Qian WJ, Wang H, Petyuk VA, Bloom JS, Sforza DM, Lacan G, Liu D, Khan AH, Cantor RM, Bigelow DJ, Melega WP, Camp DG,2nd, Smith RD, Smith DJ (2008) Mitochondrial dysfunction, oxidative stress, and apoptosis revealed by proteomic and transcriptomic analyses of the striata in two mouse models of Parkinson's disease. J Proteome Res 7:666-677.

Ching GY, Chien CL, Flores R, Liem RK (1999) Overexpression of alpha-internexin causes abnormal neurofilamentous accumulations and motor coordination deficits in transgenic mice. J Neurosci 19:2974-2986.

Chinta SJ, Woods G, Demaria M, Rane A, Zou Y, McQuade A, Rajagopalan S, Limbad C, Madden DT, Campisi J, Andersen JK (2018) Cellular Senescence Is Induced by the Environmental Neurotoxin Paraquat and Contributes to Neuropathology Linked to Parkinson's Disease. Cell Rep 22:930-940.

Chiu CC, Yeh TH, Lai SC, Weng YH, Huang YC, Cheng YC, Chen RS, Huang YZ, Hung J, Chen CC, Lin WY, Chang HC, Chen YJ, Chen CL, Chen HY, Lin YW, Wu-Chou YH, Wang HL, Lu CS (2016) Increased Rab35 expression is a potential biomarker and implicated in the pathogenesis of Parkinson's disease. Oncotarget 7:54215-54227.

Choi BK, Choi MG, Kim JY, Yang Y, Lai Y, Kweon DH, Lee NK, Shin YK (2013) Large alpha-synuclein oligomers inhibit neuronal SNARE-mediated vesicle docking. Proc Natl Acad Sci U S A 110:4087-4092.

Choi J, Levey AI, Weintraub ST, Rees HD, Gearing M, Chin LS, Li L (2004) Oxidative modifications and down-regulation of ubiquitin carboxyl-terminal hydrolase L1 associated with idiopathic Parkinson's and Alzheimer's diseases. J Biol Chem 279:13256-13264.

Chou JS, Impens F, Gevaert K, Davies PL (2011) m-Calpain activation in vitro does not require autolysis or subunit dissociation. Biochim Biophys Acta 1814:864-872.

Chu Y, Kompoliti K, Cochran EJ, Mufson EJ, Kordower JH (2002) Age-related decreases in Nurr1 immunoreactivity in the human substantia nigra. J Comp Neurol 450:203-214.

Chu Y, Kordower JH (2007) Age-associated increases of alpha-synuclein in monkeys and humans are associated with nigrostriatal dopamine depletion: Is this the target for Parkinson's disease? Neurobiol Dis 25:134-149.

Chung CY, Seo H, Sonntag KC, Brooks A, Lin L, Isacson O (2005) Cell type-specific gene expression of midbrain dopaminergic neurons reveals molecules involved in their vulnerability and protection. Hum Mol Genet 14:1709-1725.

Ciesielski-Treska J, Goetschy JF, Aunis D (1984) Proteolytic degradation of vimentin and glial fibrillary acidic protein in rat astrocytes in primary culture. Eur J Biochem 138:465-471.

Clarke LE, Liddelow SA, Chakraborty C, Munch AE, Heiman M, Barres BA (2018) Normal aging induces A1-like astrocyte reactivity. Proc Natl Acad Sci U S A 115:E1896-E1905.

Cliffer KD, Siuciak JA, Carson SR, Radley HE, Park JS, Lewis DR, Zlotchenko E, Nguyen T, Garcia K, Tonra JR, Stambler N, Cedarbaum JM, Bodine SC, Lindsay RM, DiStefano PS (1998) Physiological characterization of Taxol-induced large-fiber sensory neuropathy in the rat. Ann Neurol 43:46-55.

Cohen G, Farooqui R, Kesler N (1997) Parkinson disease: a new link between monoamine oxidase and mitochondrial electron flow. Proc Natl Acad Sci U S A 94:4890-4894.

Cohen J, D'Agostino L, Wilson J, Tuzer F, Torres C (2017) Astrocyte Senescence and Metabolic Changes in Response to HIV Antiretroviral Therapy Drugs. Front Aging Neurosci 9:281.

Cohen J, Torres C (2019) Astrocyte senescence: Evidence and significance. Aging Cell e12937.

Collier TJ, Kanaan NM, Kordower JH (2017) Aging and Parkinson's disease: Different sides of the same coin? Mov Disord 32:983-990.

Collier TJ, Kanaan NM, Kordower JH (2011) Ageing as a primary risk factor for Parkinson's disease: evidence from studies of non-human primates. Nat Rev Neurosci 12:359-366.

Collier TJ, Lipton J, Daley BF, Palfi S, Chu Y, Sortwell C, Bakay RA, Sladek JR,Jr, Kordower JH (2007) Aging-related changes in the nigrostriatal dopamine system and the response to MPTP in nonhuman primates: diminished compensatory mechanisms as a prelude to parkinsonism. Neurobiol Dis 26:56-65.

Collo G, Bono F, Cavalleri L, Plebani L, Merlo Pich E, Millan MJ, Spano PF, Missale C (2012) Pre-synaptic dopamine D(3) receptor mediates cocaine-induced structural plasticity in mesencephalic dopaminergic neurons via ERK and Akt pathways. J Neurochem 120:765-778.

Collo G, Bono F, Cavalleri L, Plebani L, Mitola S, Merlo Pich E, Millan MJ, Zoli M, Maskos U, Spano P, Missale C (2013) Nicotine-induced structural plasticity in mesencephalic dopaminergic neurons is mediated by dopamine D3 receptors and Akt-mTORC1 signaling. Mol Pharmacol 83:1176-1189.

Condorelli DF, Nicoletti VG, Barresi V, Conticello SG, Caruso A, Tendi EA, Giuffrida Stella AM (1999a) Structural features of the rat GFAP gene and identification of a novel alternative transcript. J Neurosci Res 56:219-228.

Condorelli DF, Nicoletti VG, Dell'Albani P, Barresi V, Caruso A, Conticello SG, Belluardo N, Giuffrida Stella AM (1999b) GFAPbeta mRNA expression in the normal rat brain and after neuronal injury. Neurochem Res 24:709-714.

Connolly BS, Lang AE (2014) Pharmacological treatment of Parkinson disease: a review. JAMA 311:1670-1683.

Cook C, Stetler C, Petrucelli L (2012) Disruption of protein quality control in Parkinson's disease. Cold Spring Harb Perspect Med 2:a009423.

Cottrell JS (2011) Protein identification using MS/MS data. J Proteomics 74:1842-1851.

Cowie AM, Sarty KI, Mercer A, Koh J, Kidd KA, Martyniuk CJ (2017) Molecular networks related to the immune system and mitochondria are targets for the pesticide dieldrin in the zebrafish (Danio rerio) central nervous system. J Proteomics 157:71-82.

Crocker SJ, Smith PD, Jackson-Lewis V, Lamba WR, Hayley SP, Grimm E, Callaghan SM, Slack RS, Melloni E, Przedborski S, Robertson GS, Anisman H, Merali Z, Park DS (2003) Inhibition of calpains prevents neuronal and behavioral deficits in an MPTP mouse model of Parkinson's disease. J Neurosci 23:4081-4091.

Curtin K, Fleckenstein AE, Robison RJ, Crookston MJ, Smith KR, Hanson GR (2015) Methamphetamine/amphetamine abuse and risk of Parkinson's disease in Utah: a population-based assessment. Drug Alcohol Depend 146:30-38.

Cutler AA, Dammer EB, Doung DM, Seyfried NT, Corbett AH, Pavlath GK (2017) Biochemical isolation of myonuclei employed to define changes to the myonuclear proteome that occur with aging. Aging Cell 16:738-749.

Dahl D (1975) Glial fibrillary acidic protein from bovine and rat brain degradation in tissues and homogenates. Biochim Biophys Acta 420:142-154.

Dahl D, Bignami A (1975) Glial fibrillary acidic protein from normal and gliosed human brain. Biochim Biophys Acta 386:41-51.

Damier P, Hirsch EC, Agid Y, Graybiel AM (1999) The substantia nigra of the human brain. II. Patterns of loss of dopamine-containing neurons in Parkinson's disease. Brain 122 (Pt 8):1437-1448.

Datta I, Ganapathy K, Razdan R, Bhonde R (2018) Location and Number of Astrocytes Determine Dopaminergic Neuron Survival and Function Under 6-OHDA Stress Mediated Through Differential BDNF Release. Mol Neurobiol 55:5505-5525.

Daubner SC, Le T, Wang S (2011) Tyrosine hydroxylase and regulation of dopamine synthesis. Arch Biochem Biophys 508:1-12.

Daviaud N, Garbayo E, Lautram N, Franconi F, Lemaire L, Perez-Pinzon M, Montero-Menei CN (2014) Modeling nigrostriatal degeneration in organotypic cultures, a new ex vivo model of Parkinson's disease. Neuroscience 256:10-22.

de Oliveira RM, Vicente Miranda H, Francelle L, Pinho R, Szego EM, Martinho R, Munari F, Lazaro DF, Moniot S, Guerreiro P, Fonseca-Ornelas L, Marijanovic Z, Antas P, Gerhardt E, Enguita FJ, Fauvet B, Penque D, Pais TF, Tong Q, Becker S, Kugler S, Lashuel HA, Steegborn C, Zweckstetter M, Outeiro TF (2017) The mechanism of sirtuin 2-mediated exacerbation of alpha-synuclein toxicity in models of Parkinson disease. PLoS Biol 15:e2000374.

De Pitta M, Brunel N (2016) Modulation of Synaptic Plasticity by Glutamatergic Gliotransmission: A Modeling Study. Neural Plast 2016:7607924.

de Vivo L, Landi S, Panniello M, Baroncelli L, Chierzi S, Mariotti L, Spolidoro M, Pizzorusso T, Maffei L, Ratto GM (2013) Extracellular matrix inhibits structural and functional plasticity of dendritic spines in the adult visual cortex. Nat Commun 4:1484.

DeArmond SJ, Fajardo M, Naughton SA, Eng LF (1983) Degradation of glial fibrillary acidic protein by a calcium dependent proteinase: an electroblot study. Brain Res 262:275-282.

Dekkers MP, Nikoletopoulou V, Barde YA (2013) Cell biology in neuroscience: Death of developing neurons: new insights and implications for connectivity. J Cell Biol 203:385-393.

DeLong M, Wichmann T (2009) Update on models of basal ganglia function and dysfunction. Parkinsonism Relat Disord 15 Suppl 3:S237-40.

DeLong MR (1990) Primate models of movement disorders of basal ganglia origin. Trends Neurosci 13:281-285.

DeMattei M, Levi AC, Fariello RG (1986) Neuromelanic pigment in substantia nigra neurons of rats and dogs. Neurosci Lett 72:37-42.

Derham BK, Harding JJ (1999) Alpha-crystallin as a molecular chaperone. Prog Retin Eye Res 18:463-509.

Devanna P, Chen XS, Ho J, Gajewski D, Smith SD, Gialluisi A, Francks C, Fisher SE, Newbury DF, Vernes SC (2018) Next-gen sequencing identifies non-coding variation disrupting miRNA-binding sites in neurological disorders. Mol Psychiatry 23:1375-1384.

Devi L, Raghavendran V, Prabhu BM, Avadhani NG, Anandatheerthavarada HK (2008) Mitochondrial import and accumulation of alpha-synuclein impair complex I in human dopaminergic neuronal cultures and Parkinson disease brain. J Biol Chem 283:9089-9100.

Di Lorenzo Alho AT, Suemoto CK, Polichiso L, Tampellini E, de Oliveira KC, Molina M, Santos GA, Nascimento C, Leite RE, de Lucena Ferreti-Rebustini RE, da Silva AV, Nitrini R, Pasqualucci CA, Jacob-Filho W, Heinsen H, Grinberg LT (2016) Three-dimensional and stereological characterization of the human substantia nigra during aging. Brain Struct Funct 221:3393-3403.

di Porzio U, Daguet MC, Glowinski J, Prochiantz A (1980) Effect of striatal cells on in vitro maturation of mesencephalic dopaminergic neurones grown in serum-free conditions. Nature 288:370-373.

Ding YM, Jaumotte JD, Signore AP, Zigmond MJ (2004) Effects of 6-hydroxydopamine on primary cultures of substantia nigra: specific damage to dopamine neurons and the impact of glial cell line-derived neurotrophic factor. J Neurochem 89:776-787.

Djordjevic T, Pogrebniak A, BelAiba RS, Bonello S, Wotzlaw C, Acker H, Hess J, Gorlach A (2005) The expression of the NADPH oxidase subunit p22phox is regulated by a redox-sensitive pathway in endothelial cells. Free Radic Biol Med 38:616-630.

Dolle C, Flones I, Nido GS, Miletic H, Osuagwu N, Kristoffersen S, Lilleng PK, Larsen JP, Tysnes OB, Haugarvoll K, Bindoff LA, Tzoulis C (2016) Defective mitochondrial DNA homeostasis in the substantia nigra in Parkinson disease. Nat Commun 7:13548.

Dominguez M, de Oliveira E, Odena MA, Portero M, Pamplona R, Ferrer I (2016) Redox proteomic profiling of neuroketal-adducted proteins in human brain: Regional vulnerability at middle age increases in the elderly. Free Radic Biol Med 95:1-15.

Domowicz MS, Sanders TA, Ragsdale CW, Schwartz NB (2008) Aggrecan is expressed by embryonic brain glia and regulates astrocyte development. Dev Biol 315:114-124.

Donaldson AE, Marshall CE, Yang M, Suon S, Iacovitti L (2005) Purified mouse dopamine neurons thrive and function after transplantation into brain but require novel glial factors for survival in culture. Mol Cell Neurosci 30:108-117.

Donega V, Burm SM, van Strien ME, van Bodegraven EJ, Paliukhovich I, Geut H, van de Berg WDJ, Li KW, Smit AB, Basak O, Hol EM (2019) Transcriptome and proteome profiling of neural stem cells from the human subventricular zone in Parkinson's disease. Acta Neuropathol Commun 7:84-019-0736-0.

Dopeso-Reyes IG, Rico AJ, Roda E, Sierra S, Pignataro D, Lanz M, Sucunza D, Chang-Azancot L, Lanciego JL (2014) Calbindin content and differential vulnerability of midbrain efferent dopaminergic neurons in macaques. Front Neuroanat 8:146.

Downes N, Mullins P (2014) The development of myelin in the brain of the juvenile rat. Toxicol Pathol 42:913-922.

Dragicevic E, Poetschke C, Duda J, Schlaudraff F, Lammel S, Schiemann J, Fauler M, Hetzel A, Watanabe M, Lujan R, Malenka RC, Striessnig J, Liss B (2014) Cav1.3 channels control D2-autoreceptor responses via NCS-1 in substantia nigra dopamine neurons. Brain 137:2287-2302.

Duda P, Wojcicka O, Wisniewski JR, Rakus D (2018) Global quantitative TPA-based proteomics of mouse brain structures reveals significant alterations in expression of proteins involved in neuronal plasticity during aging. Aging (Albany NY) 10:1682-1697.

Dumitriu A, Golji J, Labadorf AT, Gao B, Beach TG, Myers RH, Longo KA, Latourelle JC (2016) Integrative analyses of proteomics and RNA transcriptomics implicate mitochondrial processes, protein folding pathways and GWAS loci in Parkinson disease. BMC Med Genomics 9:5-016-0164-y.

Eaton SL, Roche SL, Llavero Hurtado M, Oldknow KJ, Farquharson C, Gillingwater TH, Wishart TM (2013) Total protein analysis as a reliable loading control for quantitative fluorescent Western blotting. PLoS One 8:e72457.

Ebrahimi-Fakhari D, Cantuti-Castelvetri I, Fan Z, Rockenstein E, Masliah E, Hyman BT, McLean PJ, Unni VK (2011) Distinct roles in vivo for the ubiquitin-proteasome system and the autophagy-lysosomal pathway in the degradation of alpha-synuclein. J Neurosci 31:14508-14520.

Edgar D, Shabalina I, Camara Y, Wredenberg A, Calvaruso MA, Nijtmans L, Nedergaard J, Cannon B, Larsson NG, Trifunovic A (2009) Random point mutations with major effects on protein-coding genes are the driving force behind premature aging in mtDNA mutator mice. Cell Metab 10:131-138.

Ehringer H, Hornykiewicz O (1960) Verteilung von noradrenalin and dopamin im gehirn des menschen und ihr verhalten bei erkrankungen des extrapyramidalen systems Klin Wschr 38:1126-1239.

Elahy M, Jackaman C, Mamo JC, Lam V, Dhaliwal SS, Giles C, Nelson D, Takechi R (2015) Blood-brain barrier dysfunction developed during normal aging is associated with inflammation and loss of tight junctions but not with leukocyte recruitment. Immun Ageing 12:2-015-0029-9. eCollection 2015.

Elobeid A, Bongcam-Rudloff E, Westermark B, Nister M (2000) Effects of inducible glial fibrillary acidic protein on glioma cell motility and proliferation. J Neurosci Res 60:245-256.

Emborg ME, Ma SY, Mufson EJ, Levey AI, Taylor MD, Brown WD, Holden JE, Kordower JH (1998) Age-related declines in nigral neuronal function correlate with motor impairments in rhesus monkeys. J Comp Neurol 401:253-265.

Eng LF (1985) Glial fibrillary acidic protein (GFAP): the major protein of glial intermediate filaments in differentiated astrocytes. J Neuroimmunol 8:203-214.

Engel M, Maurel P, Margolis RU, Margolis RK (1996) Chondroitin sulfate proteoglycans in the developing central nervous system. I. cellular sites of synthesis of neurocan and phosphacan. J Comp Neurol 366:34-43.

Erdo F, Denes L, de Lange E (2017) Age-associated physiological and pathological changes at the blood-brain barrier: A review. J Cereb Blood Flow Metab 37:4-24.

Erturk A, Hellal F, Enes J, Bradke F (2007) Disorganized microtubules underlie the formation of retraction bulbs and the failure of axonal regeneration. J Neurosci 27:9169-9180.

Fabregat A, Jupe S, Matthews L, Sidiropoulos K, Gillespie M, Garapati P, Haw R, Jassal B, Korninger F, May B, Milacic M, Roca CD, Rothfels K, Sevilla C, Shamovsky V, Shorser S, Varusai T, Viteri G, Weiser J, Wu G, Stein L, Hermjakob H, D'Eustachio P (2018) The Reactome Pathway Knowledgebase. Nucleic Acids Res 46:D649-D655.

Fabregat A, Sidiropoulos K, Viteri G, Forner O, Marin-Garcia P, Arnau V, D'Eustachio P, Stein L, Hermjakob H (2017) Reactome pathway analysis: a high-performance in-memory approach. BMC Bioinformatics 18:142-017-1559-2.

Faulkner JR, Herrmann JE, Woo MJ, Tansey KE, Doan NB, Sofroniew MV (2004) Reactive astrocytes protect tissue and preserve function after spinal cord injury. J Neurosci 24:2143-2155.

Fearnley JM, Lees AJ (1991) Ageing and Parkinson's disease: substantia nigra regional selectivity. Brain 114 (Pt 5):2283-2301.

Fedorow H, Tribl F, Halliday G, Gerlach M, Riederer P, Double KL (2005) Neuromelanin in human dopamine neurons: comparison with peripheral melanins and relevance to Parkinson's disease. Prog Neurobiol 75:109-124.

Feinstein DL, Weinmaster GA, Milner RJ (1992) Isolation of cDNA clones encoding rat glial fibrillary acidic protein: expression in astrocytes and in Schwann cells. J Neurosci Res 32:1-14.

Feng J, Naiman DQ, Cooper B (2007) Probability-based pattern recognition and statistical framework for randomization: modeling tandem mass spectrum/peptide sequence false match frequencies. Bioinformatics 23:2210-2217.

Fenn JB, Mann M, Meng CK, Wong SF, Whitehouse CM (1989) Electrospray ionization for mass spectrometry of large biomolecules. Science 246:64-71.

Ferreira JG, Del-Fava F, Hasue RH, Shammah-Lagnado SJ (2008) Organization of ventral tegmental area projections to the ventral tegmental area-nigral complex in the rat. Neuroscience 153:196-213.

Figueroa-Masot XA, Hetman M, Higgins MJ, Kokot N, Xia Z (2001) Taxol induces apoptosis in cortical neurons by a mechanism independent of Bcl-2 phosphorylation. J Neurosci 21:4657-4667.

Filippov V, Kronenberg G, Pivneva T, Reuter K, Steiner B, Wang LP, Yamaguchi M, Kettenmann H, Kempermann G (2003) Subpopulation of nestin-expressing progenitor cells in the adult murine hippocampus shows electrophysiological and morphological characteristics of astrocytes. Mol Cell Neurosci 23:373-382.

Firbank MJ, Yarnall AJ, Lawson RA, Duncan GW, Khoo TK, Petrides GS, O'Brien JT, Barker RA, Maxwell RJ, Brooks DJ, Burn DJ (2017) Cerebral glucose metabolism and cognition in newly diagnosed Parkinson's disease: ICICLE-PD study. J Neurol Neurosurg Psychiatry 88:310-316.

Fitzmaurice AG, Rhodes SL, Lulla A, Murphy NP, Lam HA, O'Donnell KC, Barnhill L, Casida JE, Cockburn M, Sagasti A, Stahl MC, Maidment NT, Ritz B, Bronstein JM (2013) Aldehyde dehydrogenase inhibition as a pathogenic mechanism in Parkinson disease. Proc Natl Acad Sci U S A 110:636-641.

Fliegner KH, Kaplan MP, Wood TL, Pintar JE, Liem RK (1994) Expression of the gene for the neuronal intermediate filament protein alpha-internexin coincides with the onset of neuronal differentiation in the developing rat nervous system. J Comp Neurol 342:161-173.

Floor E, Wetzel MG (1998) Increased protein oxidation in human substantia nigra pars compacta in comparison with basal ganglia and prefrontal cortex measured with an improved dinitrophenylhydrazine assay. J Neurochem 70:268-275.

Flowers A, Bell-Temin H, Jalloh A, Stevens SM,Jr, Bickford PC (2017) Proteomic anaysis of aged microglia: shifts in transcription, bioenergetics, and nutrient response. J Neuroinflammation 14:96-017-0840-7.

Freeman WM, Hemby SE (2004) Proteomics for protein expression profiling in neuroscience. Neurochem Res 29:1065-1081.

Frewen BE, Merrihew GE, Wu CC, Noble WS, MacCoss MJ (2006) Analysis of peptide MS/MS spectra from large-scale proteomics experiments using spectrum libraries. Anal Chem 78:5678-5684.

Froyset AK, Edson AJ, Gharbi N, Khan EA, Dondorp D, Bai Q, Tiraboschi E, Suster ML, Connolly JB, Burton EA, Fladmark KE (2018) Astroglial DJ-1 overexpression up-regulates proteins involved in redox regulation and is neuroprotective in vivo. Redox Biol 16:237-247.

Fu Y, Yuan Y, Halliday G, Rusznak Z, Watson C, Paxinos G (2012) A cytoarchitectonic and chemoarchitectonic analysis of the dopamine cell groups in the substantia nigra, ventral tegmental area, and retrorubral field in the mouse. Brain Struct Funct 217:591-612.

Fujita K, Kato T, Yamauchi M, Ando M, Honda M, Nagata Y (1998) Increases in fragmented glial fibrillary acidic protein levels in the spinal cords of patients with amyotrophic lateral sclerosis. Neurochem Res 23:169-174.

Fuller HR, Hurtado ML, Wishart TM, Gates MA (2014) The rat striatum responds to nigro-striatal degeneration via the increased expression of proteins associated with growth and regeneration of neuronal circuitry. Proteome Sci 12:20-5956-12-20. eCollection 2014.

Fuller HR, Morris GE (2012) Quantitative proteomics using iTRAQ labeling and mass spectrometry. Integrative Proteomics 18:347-362.

Fuller HR, Slade R, Jovanov-Milosevic N, Babic M, Sedmak G, Simic G, Fuszard MA, Shirran SL, Botting CH, Gates MA (2015) Stathmin is enriched in the developing corticospinal tract. Mol Cell Neurosci 69:12-21.

Gagne JJ, Power MC (2010) Anti-inflammatory drugs and risk of Parkinson disease: a meta-analysis. Neurology 74:995-1002.

Gao J, Miao H, Xiao CH, Sun Y, Du X, Yuan HH, Yu HL, Gao DS (2011) Influence of aging on the dopaminergic neurons in the substantia nigra pars compacta of rats. Curr Aging Sci 4:19-24.

Gao L, Hidalgo-Figueroa M, Escudero LM, Diaz-Martin J, Lopez-Barneo J, Pascual A (2013) Age-mediated transcriptomic changes in adult mouse substantia nigra. PLoS One 8:e62456.

Gardner RC, Byers AL, Barnes DE, Li Y, Boscardin J, Yaffe K (2018) Mild TBI and risk of Parkinson disease: A Chronic Effects of Neurotrauma Consortium Study. Neurology 90:e1771-e1779.

Gassmann M, Grenacher B, Rohde B, Vogel J (2009) Quantifying Western blots: pitfalls of densitometry. Electrophoresis 30:1845-1855.

Gaven F, Marin P, Claeysen S (2014) Primary culture of mouse dopaminergic neurons. J Vis Exp (91):e51751. doi:e51751.

GBD 2016 Parkinson's Disease Collaborators (2018) Global, regional, and national burden of Parkinson's disease, 1990-2016: a systematic analysis for the Global Burden of Disease Study 2016. Lancet Neurol 17:939-953.

Ge WP, Jia JM (2016) Local production of astrocytes in the cerebral cortex. Neuroscience 323:3-9.

Geller HM, Cheng KY, Goldsmith NK, Romero AA, Zhang AL, Morris EJ, Grandison L (2001) Oxidative stress mediates neuronal DNA damage and apoptosis in response to cytosine arabinoside. J Neurochem 78:265-275.

Genoud C, Quairiaux C, Steiner P, Hirling H, Welker E, Knott GW (2006) Plasticity of astrocytic coverage and glutamate transporter expression in adult mouse cortex. PLoS Biol 4:e343.

German DC, Manaye K, Smith WK, Woodward DJ, Saper CB (1989) Midbrain dopaminergic cell loss in Parkinson's disease: computer visualization. Ann Neurol 26:507-514.

German DC, Manaye KF (1993) Midbrain dopaminergic neurons (nuclei A8, A9, and A10): three-dimensional reconstruction in the rat. J Comp Neurol 331:297-309.

Geschwind DH, Konopka G (2009) Neuroscience in the era of functional genomics and systems biology. Nature 461:908-915.

Giguere N, Burke Nanni S, Trudeau LE (2018) On Cell Loss and Selective Vulnerability of Neuronal Populations in Parkinson's Disease. Front Neurol 9:455.

Gillet LC, Navarro P, Tate S, Rost H, Selevsek N, Reiter L, Bonner R, Aebersold R (2012) Targeted data extraction of the MS/MS spectra generated by data-independent acquisition: a new concept for consistent and accurate proteome analysis. Mol Cell Proteomics 11:O111.016717.

Glinka Y, Gassen M, Youdim MB (1997) Mechanism of 6-hydroxydopamine neurotoxicity. J Neural Transm Suppl 50:55-66.

Glish GL, Vachet RW (2003) The basics of mass spectrometry in the twenty-first century. Nat Rev Drug Discov 2:140-150.

Goetschy JF, Ulrich G, Aunis D, Ciesielski-Treska J (1986) The organization and solubility properties of intermediate filaments and microtubules of cortical astrocytes in culture. J Neurocytol 15:375-387.

Gokulrangan G, Zaidi A, Michaelis ML, Schoneich C (2007) Proteomic analysis of protein nitration in rat cerebellum: effect of biological aging. J Neurochem 100:1494-1504.

Goldstein DS, Sullivan P, Holmes C, Kopin IJ, Basile MJ, Mash DC (2011) Catechols in post-mortem brain of patients with Parkinson disease. Eur J Neurol 18:703-710.

Gonzalez-Burguera I, Ricobaraza A, Aretxabala X, Barrondo S, Garcia del Cano G, Lopez de Jesus M, Salles J (2016) Highly efficient generation of glutamatergic/cholinergic NT2-derived postmitotic human neurons by short-term treatment with the nucleoside analogue cytosine beta-D-arabinofuranoside. Stem Cell Res 16:541-551.

Goodall EF, Wang C, Simpson JE, Baker DJ, Drew DR, Heath PR, Saffrey MJ, Romero IA, Wharton SB (2018) Age-associated changes in the blood-brain barrier: comparative studies in human and mouse. Neuropathol Appl Neurobiol 44:328-340.

Gornstein E, Schwarz TL (2014) The paradox of paclitaxel neurotoxicity: Mechanisms and unanswered questions. Neuropharmacology 76 Pt A:175-183.

Gornstein EL, Schwarz TL (2017) Neurotoxic mechanisms of paclitaxel are local to the distal axon and independent of transport defects. Exp Neurol 288:153-166.

Graham LC, Naldrett MJ, Kohama SG, Smith C, Lamont DJ, McColl BW, Gillingwater TH, Skehel P, Urbanski HF, Wishart TM (2019) Regional Molecular Mapping of Primate Synapses during Normal Healthy Aging. Cell Rep 27:1018-1026.e4.

Greene JG, Dingledine R, Greenamyre JT (2005) Gene expression profiling of rat midbrain dopamine neurons: implications for selective vulnerability in parkinsonism. Neurobiol Dis 18:19-31.

Grillner S, Robertson B (2016) The Basal Ganglia Over 500 Million Years. Curr Biol 26:R1088-R1100.

Gu XL, Long CX, Sun L, Xie C, Lin X, Cai H (2010) Astrocytic expression of Parkinson's disease-related A53T alpha-synuclein causes neurodegeneration in mice. Mol Brain 3:12-6606-3-12.

Gu Z, Gu L, Eils R, Schlesner M, Brors B (2014) circlize Implements and enhances circular visualization in R. Bioinformatics 30:2811-2812.

Guillot TS, Miller GW (2009) Protective actions of the vesicular monoamine transporter 2 (VMAT2) in monoaminergic neurons. Mol Neurobiol 39:149-170.

Guingab-Cagmat JD, Newsom K, Vakulenko A, Cagmat EB, Kobeissy FH, Zoltewicz S, Wang KK, Anagli J (2012) In vitro MS-based proteomic analysis and absolute quantification of neuronal-glial injury biomarkers in cell culture system. Electrophoresis 33:3786-3797.

Guo JD, Zhao X, Li Y, Li GR, Liu XL (2018) Damage to dopaminergic neurons by oxidative stress in Parkinson's disease (Review). Int J Mol Med 41:1817-1825.

Gurevich EV, Gainetdinov RR, Gurevich VV (2016) G protein-coupled receptor kinases as regulators of dopamine receptor functions. Pharmacol Res 111:1-16.

Gygi SP, Rist B, Gerber SA, Turecek F, Gelb MH, Aebersold R (1999) Quantitative analysis of complex protein mixtures using isotope-coded affinity tags. Nat Biotechnol 17:994-999.

Hafkemeijer A, Altmann-Schneider I, de Craen AJ, Slagboom PE, van der Grond J, Rombouts SA (2014) Associations between age and gray matter volume in anatomical brain networks in middle-aged to older adults. Aging Cell 13:1068-1074.

Hagemann TL, Boelens WC, Wawrousek EF, Messing A (2009) Suppression of GFAP toxicity by alphaB-crystallin in mouse models of Alexander disease. Hum Mol Genet 18:1190-1199.

Haj-Yasein NN, Vindedal GF, Eilert-Olsen M, Gundersen GA, Skare O, Laake P, Klungland A, Thoren AE, Burkhardt JM, Ottersen OP, Nagelhus EA (2011) Glial-conditional deletion of aquaporin-4 (Aqp4) reduces blood-brain water uptake and confers barrier function on perivascular astrocyte endfeet. Proc Natl Acad Sci U S A 108:17815-17820.

Halliday GM, Blumbergs PC, Cotton RG, Blessing WW, Geffen LB (1990) Loss of brainstem serotonin- and substance P-containing neurons in Parkinson's disease. Brain Res 510:104-107.

Halnes G, Ostby I, Pettersen KH, Omholt SW, Einevoll GT (2013) Electrodiffusive model for astrocytic and neuronal ion concentration dynamics. PLoS Comput Biol 9:e1003386.

Hamezah HS, Durani LW, Ibrahim NF, Yanagisawa D, Kato T, Shiino A, Tanaka S, Damanhuri HA, Ngah WZW, Tooyama I (2017) Volumetric changes in the aging rat brain and its impact on cognitive and locomotor functions. Exp Gerontol 99:69-79.

Hamezah HS, Durani LW, Yanagisawa D, Ibrahim NF, Aizat WM, Bellier JP, Makpol S, Ngah WZW, Damanhuri HA, Tooyama I (2018) Proteome profiling in the hippocampus, medial prefrontal cortex, and striatum of aging rat. Exp Gerontol 111:53-64.

Hassler R (1938) Zur Pathologie der Paralysis agitans und des postenzephalitischen Parkinsonismus. J Psychol Neurol 48:387-476.

Haynes PA, Yates JR,3rd (2000) Proteome profiling-pitfalls and progress. Yeast 17:81-87.

Henneberger C, Papouin T, Oliet SH, Rusakov dopamine (2010) Long-term potentiation depends on release of D-serine from astrocytes. Nature 463:232-236.

Herculano-Houzel S (2009) The human brain in numbers: a linearly scaled-up primate brain. Front Hum Neurosci 3:31.

Herculano-Houzel S (2007) Encephalization, neuronal excess, and neuronal index in rodents. Anat Rec (Hoboken) 290:1280-1287.

Herculano-Houzel S, Collins CE, Wong P, Kaas JH (2007) Cellular scaling rules for primate brains. Proc Natl Acad Sci U S A 104:3562-3567.

Herculano-Houzel S, Messeder DJ, Fonseca-Azevedo K, Pantoja NA (2015) When larger brains do not have more neurons: increased numbers of cells are compensated by decreased average cell size across mouse individuals. Front Neuroanat 9:64.

Hernan MA, Takkouche B, Caamano-Isorna F, Gestal-Otero JJ (2002) A meta-analysis of coffee drinking, cigarette smoking, and the risk of Parkinson's disease. Ann Neurol 52:276-284.

Hernandez-Baltazar D, Zavala-Flores LM, Villanueva-Olivo A (2017) The 6-hydroxydopamine model and parkinsonian pathophysiology: Novel findings in an older model. Neurologia 32:533-539.

Herrera A, Munoz P, Paris I, Diaz-Veliz G, Mora S, Inzunza J, Hultenby K, Cardenas C, Jana F, Raisman-Vozari R, Gysling K, Abarca J, Steinbusch HW, Segura-Aguilar J (2016) Aminochrome induces dopaminergic neuronal dysfunction: a new animal model for Parkinson's disease. Cell Mol Life Sci 73:3583-3597.

Herrera A, Munoz P, Steinbusch HWM, Segura-Aguilar J (2017) Are Dopamine Oxidation Metabolites Involved in the Loss of Dopaminergic Neurons in the Nigrostriatal System in Parkinson's Disease? ACS Chem Neurosci 8:702-711.

Hirsch E, Graybiel AM, Agid YA (1988) Melanized dopaminergic neurons are differentially susceptible to degeneration in Parkinson's disease. Nature 334:345-348.

Hirsch L, Jette N, Frolkis A, Steeves T, Pringsheim T (2016) The Incidence of Parkinson's Disease: A Systematic Review and Meta-Analysis. Neuroepidemiology 46:292-300.

Hol EM, Capetanaki Y (2017) Type III Intermediate Filaments Desmin, Glial Fibrillary Acidic Protein (GFAP), Vimentin, and Peripherin. Cold Spring Harb Perspect Biol 9:10.1101/cshperspect.a021642.

Hol EM, Pekny M (2015) Glial fibrillary acidic protein (GFAP) and the astrocyte intermediate filament system in diseases of the central nervous system. Curr Opin Cell Biol 32:121-130.

Holtz WA, O'Malley KL (2003) Parkinsonian mimetics induce aspects of unfolded protein response in death of dopaminergic neurons. J Biol Chem 278:19367-19377.

Hornykiewicz O (2006) The discovery of dopamine deficiency in the parkinsonian brain. J Neural Transm Suppl (70):9-15.

Hornykiewicz O (1963) Die topische Lokalisation und das Verhalten von Noradrenalin und Dopamin (3-Hydroxytyramin) in the Substantia nigra des normalen und Parkinsonkranken Menschen. Wien. Klin Wochenschr 75:309-312.

Hosp F, Mann M (2017) A Primer on Concepts and Applications of Proteomics in Neuroscience. Neuron 96:558-571.

Huang da W, Sherman BT, Lempicki RA (2009) Systematic and integrative analysis of large gene lists using DAVID bioinformatics resources. Nat Protoc 4:44-57.

Huang DW, Sherman BT, Tan Q, Collins JR, Alvord WG, Roayaei J, Stephens R, Baseler MW, Lane HC, Lempicki RA (2007) The DAVID Gene Functional Classification Tool: a novel biological module-centric algorithm to functionally analyze large gene lists. Genome Biol 8:R183-2007-8-9-r183.

Huehnchen P, Boehmerle W, Springer A, Freyer D, Endres M (2017) A novel preventive therapy for paclitaxel-induced cognitive deficits: preclinical evidence from C57BL/6 mice. Transl Psychiatry 7:e1185.

Huenchuguala S, Sjodin B, Mannervik B, Segura-Aguilar J (2019) Novel Alpha-Synuclein Oligomers Formed with the Aminochrome-Glutathione Conjugate Are Not Neurotoxic. Neurotox Res 35:432-440.

Hughes KC, Gao X, Kim IY, Wang M, Weisskopf MG, Schwarzschild MA, Ascherio A (2017) Intake of dairy foods and risk of Parkinson disease. Neurology 89:46-52.

Hui CW, Zhang Y, Herrup K (2016) Non-Neuronal Cells Are Required to Mediate the Effects of Neuroinflammation: Results from a Neuron-Enriched Culture System. PLoS One 11:e0147134.

Humpel C (2015) Organotypic brain slice cultures: A review. Neuroscience 305:86-98.

Imai S, Koyanagi M, Azimi Z, Nakazato Y, Matsumoto M, Ogihara T, Yonezawa A, Omura T, Nakagawa S, Wakatsuki S, Araki T, Kaneko S, Nakagawa T, Matsubara K (2017) Taxanes and platinum derivatives impair Schwann cells via distinct mechanisms. Sci Rep 7:5947-017-05784-1.

Inoue KI, Miyachi S, Nishi K, Okado H, Nagai Y, Minamimoto T, Nambu A, Takada M (2019) Recruitment of calbindin into nigral dopamine neurons protects against MPTP-Induced parkinsonism. Mov Disord 34:200-209.

Inyushin MY, Huertas A, Kucheryavykh YV, Kucheryavykh LY, Tsydzik V, Sanabria P, Eaton MJ, Skatchkov SN, Rojas LV, Wessinger WD (2012) L-DOPA Uptake in Astrocytic Endfeet Enwrapping Blood Vessels in Rat Brain. Parkinsons Dis 2012:321406.

Islam MS, Nolte H, Jacob W, Ziegler AB, Putz S, Grosjean Y, Szczepanowska K, Trifunovic A, Braun T, Heumann H, Heumann R, Hovemann B, Moore DJ, Kruger M (2016) Human R1441C LRRK2 regulates the synaptic vesicle proteome and phosphoproteome in a Drosophila model of Parkinson's disease. Hum Mol Genet 25:5365-5382.

Ivenshitz M, Segal M (2010) Neuronal density determines network connectivity and spontaneous activity in cultured hippocampus. J Neurophysiol 104:1052-1060.

Jakel S, Dimou L (2017) Glial Cells and Their Function in the Adult Brain: A Journey through the History of Their Ablation. Front Cell Neurosci 11:24.

Jang HJ, Hwang S, Cho KY, Kim DK, Chay KO, Kim JK (2008) Taxol induces oxidative neuronal cell death by enhancing the activity of NADPH oxidase in mouse cortical cultures. Neurosci Lett 443:17-22.

Janzer RC, Raff MC (1987) Astrocytes induce blood-brain barrier properties in endothelial cells. Nature 325:253-257.

Jeon S, Kim YJ, Kim ST, Moon W, Chae Y, Kang M, Chung MY, Lee H, Hong MS, Chung JH, Joh TH, Lee H, Park HJ (2008) Proteomic analysis of the neuroprotective mechanisms of acupuncture treatment in a Parkinson's disease mouse model. Proteomics 8:4822-4832.

Jessen KR, Morgan L, Stewart HJ, Mirsky R (1990) Three markers of adult non-myelin-forming Schwann cells, 217c(Ran-1), A5E3 and GFAP: development and regulation by neuron-Schwann cell interactions. Development 109:91-103.

Jin J, Hulette C, Wang Y, Zhang T, Pan C, Wadhwa R, Zhang J (2006) Proteomic identification of a stress protein, mortalin/mthsp70/GRP75: relevance to Parkinson disease. Mol Cell Proteomics 5:1193-1204.

Jin J, Park J, Kim K, Kang Y, Park SG, Kim JH, Park KS, Jun H, Kim Y (2009) Detection of differential proteomes of human beta-cells during islet-like differentiation using iTRAQ labeling. J Proteome Res 8:1393-1403.

Jones AW, Cooper HJ (2011) Dissociation techniques in mass spectrometry-based proteomics. Analyst 136:3419-3429.

Jones LL, Margolis RU, Tuszynski MH (2003) The chondroitin sulfate proteoglycans neurocan, brevican, phosphacan, and versican are differentially regulated following spinal cord injury. Exp Neurol 182:399-411.

Jyothi HJ, Vidyadhara DJ, Mahadevan A, Philip M, Parmar SK, Manohari SG, Shankar SK, Raju TR, Alladi PA (2015) Aging causes morphological alterations in astrocytes and microglia in human substantia nigra pars compacta. Neurobiol Aging 36:3321-3333.

Kamphuis W, Kooijman L, Orre M, Stassen O, Pekny M, Hol EM (2015) GFAP and vimentin deficiency alters gene expression in astrocytes and microglia in wild-type mice

and changes the transcriptional response of reactive glia in mouse model for Alzheimer's disease. Glia 63:1036-1056.

Kamphuis W, Mamber C, Moeton M, Kooijman L, Sluijs JA, Jansen AH, Verveer M, de Groot LR, Smith VD, Rangarajan S, Rodriguez JJ, Orre M, Hol EM (2012) GFAP isoforms in adult mouse brain with a focus on neurogenic astrocytes and reactive astrogliosis in mouse models of Alzheimer disease. PLoS One 7:e42823.

Kamphuis W, Middeldorp J, Kooijman L, Sluijs JA, Kooi EJ, Moeton M, Freriks M, Mizee MR, Hol EM (2014) Glial fibrillary acidic protein isoform expression in plaque related astrogliosis in Alzheimer's disease. Neurobiol Aging 35:492-510.

Kanaan NM, Kordower JH, Collier TJ (2010) Age-related changes in glial cells of dopamine midbrain subregions in rhesus monkeys. Neurobiol Aging 31:937-952.

Kanaan NM, Kordower JH, Collier TJ (2008) Age-related changes in dopamine transporters and accumulation of 3-nitrotyrosine in rhesus monkey midbrain dopamine neurons: relevance in selective neuronal vulnerability to degeneration. Eur J Neurosci 27:3205-3215.

Kanaan NM, Kordower JH, Collier TJ (2007) Age-related accumulation of Marinesco bodies and lipofuscin in rhesus monkey midbrain dopamine neurons: relevance to selective neuronal vulnerability. J Comp Neurol 502:683-700.

Kanehisa M, Goto S (2000) KEGG: kyoto encyclopedia of genes and genomes. Nucleic Acids Res 28:27-30.

Kaneko A, Sankai Y (2014) Long-term culture of rat hippocampal neurons at low density in serum-free medium: combination of the sandwich culture technique with the three-dimensional nanofibrous hydrogel PuraMatrix. PLoS One 9:e102703.

Karas M, Bachmann D, Bahr U, Hillenkamp F (1987) Matrix-assisted ultraviolet laser desorption of non-volatile compounds. Int J Mass Spectrom 78:53-68.

Karve TM, Cheema AK (2011) Small changes huge impact: the role of protein posttranslational modifications in cellular homeostasis and disease. J Amino Acids 2011:207691.

Kasap M, Akpinar G, Kanli A (2017) Proteomic studies associated with Parkinson's disease. Expert Rev Proteomics 14:193-209.

Kaushik S, Cuervo AM (2018) The coming of age of chaperone-mediated autophagy. Nat Rev Mol Cell Biol 19:365-381.

Kee N, Volakakis N, Kirkeby A, Dahl L, Storvall H, Nolbrant S, Lahti L, Bjorklund AK, Gillberg L, Joodmardi E, Sandberg R, Parmar M, Perlmann T (2017) Single-Cell Analysis Reveals a Close Relationship between Differentiating Dopamine and Subthalamic Nucleus Neuronal Lineages. Cell Stem Cell 20:29-40.

Keeney PM, Xie J, Capaldi RA, Bennett JP,Jr (2006) Parkinson's disease brain mitochondrial complex I has oxidatively damaged subunits and is functionally impaired and misassembled. J Neurosci 26:5256-5264.

Keil JM, Qalieh A, Kwan KY (2018) Brain Transcriptome Databases: A User's Guide. J Neurosci 38:2399-2412.

Kelley KW, Nakao-Inoue H, Molofsky AV, Oldham MC (2018) Variation among intact tissue samples reveals the core transcriptional features of human CNS cell classes. Nat Neurosci 21:1171-1184.

Kerr CW, Lee LJ, Romero AA, Stull ND, Iacovitti L (1994) Purification of dopamine neurons by flow cytometry. Brain Res 665:300-306.

Khudoerkov RM, Voronkov DN, Dikalova YV (2014) Quantitative morphochemical characterization of the neurons in substantia nigra of rat brain and its volume reconstruction. Bull Exp Biol Med 156:861-864.

Kim H, Kang H, Lee Y, Park CH, Jo A, Khang R, Shin JH (2017a) Identification of transketolase as a target of PARIS in substantia nigra. Biochem Biophys Res Commun 493:1050-1056.

Kim J, Chen CH, Yang J, Mochly-Rosen D (2017b) Aldehyde dehydrogenase 2*2 knock-in mice show increased reactive oxygen species production in response to cisplatin treatment. J Biomed Sci 24:33-017-0338-8.

Kim JM, Cha SH, Choi YR, Jou I, Joe EH, Park SM (2016) DJ-1 deficiency impairs glutamate uptake into astrocytes via the regulation of flotillin-1 and caveolin-1 expression. Sci Rep 6:28823.

Kim Y, Zheng X, Ansari Z, Bunnell MC, Herdy JR, Traxler L, Lee H, Paquola ACM, Blithikioti C, Ku M, Schlachetzki JCM, Winkler J, Edenhofer F, Glass CK, Paucar AA,

Jaeger BN, Pham S, Boyer L, Campbell BC, Hunter T, Mertens J, Gage FH (2018) Mitochondrial Aging Defects Emerge in Directly Reprogrammed Human Neurons due to Their Metabolic Profile. Cell Rep 23:2550-2558.

Kitamura Y, Kojima M, Kurosawa T, Sasaki R, Ichihara S, Hiraku Y, Tomimoto H, Murata M, Oikawa S (2018) Proteomic Profiling of Exosomal Proteins for Blood-based Biomarkers in Parkinson's Disease. Neuroscience 392:121-128.

Kitsou E, Pan S, Zhang J, Shi M, Zabeti A, Dickson DW, Albin R, Gearing M, Kashima DT, Wang Y, Beyer RP, Zhou Y, Pan C, Caudle WM, Zhang J (2008) Identification of proteins in human substantia nigra. Proteomics Clin Appl 2:776-782.

Kleiger G, Mayor T (2014) Perilous journey: a tour of the ubiquitin-proteasome system. Trends Cell Biol 24:352-359.

Klettner A, Tholey A, Wiegandt A, Richert E, Nolle B, Deuschl G, Roider J, Schneider SA (2017) Reduction of GAPDH in lenses of Parkinson's disease patients: A possible new biomarker. Mov Disord 32:459-462.

Klopstein A, Santos-Nogueira E, Francos-Quijorna I, Redensek A, David S, Navarro X, Lopez-Vales R (2012) Beneficial effects of alphaB-crystallin in spinal cord contusion injury. J Neurosci 32:14478-14488.

Koopmans F, Ho JTC, Smit AB, Li KW (2018) Comparative Analyses of Data Independent Acquisition Mass Spectrometric Approaches: DIA, WiSIM-DIA, and Untargeted DIA. Proteomics 18:10.1002/pmic.201700304.

Koprich JB, Reske-Nielsen C, Mithal P, Isacson O (2008) Neuroinflammation mediated by IL-1beta increases susceptibility of dopamine neurons to degeneration in an animal model of Parkinson's disease. J Neuroinflammation 5:8-2094-5-8.

Kordower JH, Olanow CW, Dodiya HB, Chu Y, Beach TG, Adler CH, Halliday GM, Bartus RT (2013) Disease duration and the integrity of the nigrostriatal system in Parkinson's disease. Brain 136:2419-2431.

Kramer A, Green J, Pollard J,Jr, Tugendreich S (2014) Causal analysis approaches in Ingenuity Pathway Analysis. Bioinformatics 30:523-530.

Kramer BC, Goldman AD, Mytilineou C (1999) Glial cell line derived neurotrophic factor promotes the recovery of dopamine neurons damaged by 6-hydroxydopamine in vitro. Brain Res 851:221-227.

Kraytsberg Y, Kudryavtseva E, McKee AC, Geula C, Kowall NW, Khrapko K (2006) Mitochondrial DNA deletions are abundant and cause functional impairment in aged human substantia nigra neurons. Nat Genet 38:518-520.

Kril JJ, Flowers D, Butterworth RF (1997) Distinctive pattern of Bergmann glial pathology in human hepatic encephalopathy. Mol Chem Neuropathol 31:279-287.

Krishnan KJ, Reeve AK, Samuels DC, Chinnery PF, Blackwood JK, Taylor RW, Wanrooij S, Spelbrink JN, Lightowlers RN, Turnbull DM (2008) What causes mitochondrial DNA deletions in human cells? Nat Genet 40:275-279.

Kristensen BK, Askerlund P, Bykova NV, Egsgaard H, Moller IM (2004) Identification of oxidised proteins in the matrix of rice leaf mitochondria by immunoprecipitation and two-dimensional liquid chromatography-tandem mass spectrometry. Phytochemistry 65:1839-1851.

Kujoth GC, Hiona A, Pugh TD, Someya S, Panzer K, Wohlgemuth SE, Hofer T, Seo AY, Sullivan R, Jobling WA, Morrow JD, Van Remmen H, Sedivy JM, Yamasoba T, Tanokura M, Weindruch R, Leeuwenburgh C, Prolla TA (2005) Mitochondrial DNA mutations, oxidative stress, and apoptosis in mammalian aging. Science 309:481-484.

Kumar A, Tamjar J, Waddell AD, Woodroof HI, Raimi OG, Shaw AM, Peggie M, Muqit MM, van Aalten DM (2017) Structure of PINK1 and mechanisms of Parkinson's disease-associated mutations. Elife 6:10.7554/eLife.29985.

Kuter K, Kratochwil M, Marx SH, Hartwig S, Lehr S, Sugawa MD, Dencher NA (2016) Native DIGE proteomic analysis of mitochondria from substantia nigra and striatum during neuronal degeneration and its compensation in an animal model of early Parkinson's disease. Arch Physiol Biochem 122:238-256.

Kwon YH, Jang SH, Yeo SS (2014) Age-related changes of lateral ventricular width and periventricular white matter in the human brain: a diffusion tensor imaging study. Neural Regen Res 9:986-989.

La Manno G, Gyllborg D, Codeluppi S, Nishimura K, Salto C, Zeisel A, Borm LE, Stott SRW, Toledo EM, Villaescusa JC, Lonnerberg P, Ryge J, Barker RA, Arenas E,

Linnarsson S (2016) Molecular Diversity of Midbrain Development in Mouse, Human, and Stem Cells. Cell 167:566-580.e19.

Lachen-Montes M, Gonzalez-Morales A, Iloro I, Elortza F, Ferrer I, Gveric D, Fernandez-Irigoyen J, Santamaria E (2019) Unveiling the olfactory proteostatic disarrangement in Parkinson's disease by proteome-wide profiling. Neurobiol Aging 73:123-134.

Lange SC, Bak LK, Waagepetersen HS, Schousboe A, Norenberg MD (2012) Primary cultures of astrocytes: their value in understanding astrocytes in health and disease. Neurochem Res 37:2569-2588.

Langston JW, Ballard P, Tetrud JW, Irwin I (1983) Chronic Parkinsonism in humans due to a product of meperidine-analog synthesis. Science 219:979-980.

Langston JW, Forno LS, Tetrud J, Reeves AG, Kaplan JA, Karluk D (1999) Evidence of active nerve cell degeneration in the substantia nigra of humans years after 1-methyl-4-phenyl-1,2,3,6-tetrahydropyridine exposure. Ann Neurol 46:598-605.

Lasiene J, Matsui A, Sawa Y, Wong F, Horner PJ (2009) Age-related myelin dynamics revealed by increased oligodendrogenesis and short internodes. Aging Cell 8:201-213.

Lautenschlager J, Mosharov EV, Kanter E, Sulzer D, Kaminski Schierle GS (2018) An Easy-to-Implement Protocol for Preparing Postnatal Ventral Mesencephalic Cultures. Front Cell Neurosci 12:44.

Lee HJ, Suk JE, Patrick C, Bae EJ, Cho JH, Rho S, Hwang D, Masliah E, Lee SJ (2010) Direct transfer of alpha-synuclein from neuron to astroglia causes inflammatory responses in synucleinopathies. J Biol Chem 285:9262-9272.

Lee YB, Du S, Rhim H, Lee EB, Markelonis GJ, Oh TH (2000) Rapid increase in immunoreactivity to GFAP in astrocytes in vitro induced by acidic pH is mediated by calcium influx and calpain I. Brain Res 864:220-229.

Leeds P, Leng Y, Chalecka-Franaszek E, Chuang DM (2005) Neurotrophins protect against cytosine arabinoside-induced apoptosis of immature rat cerebellar neurons. Neurochem Int 46:61-72.

Lemaitre H, Goldman AL, Sambataro F, Verchinski BA, Meyer-Lindenberg A, Weinberger DR, Mattay VS (2012) Normal age-related brain morphometric changes:

nonuniformity across cortical thickness, surface area and gray matter volume? Neurobiol Aging 33:617.e1-617.e9.

Lessner G, Schmitt O, Haas SJ, Mikkat S, Kreutzer M, Wree A, Glocker MO (2010) Differential proteome of the striatum from hemiparkinsonian rats displays vivid structural remodeling processes. J Proteome Res 9:4671-4687.

Letourneau PC, Ressler AH (1984) Inhibition of neurite initiation and growth by taxol. J Cell Biol 98:1355-1362.

Lewis SA, Balcarek JM, Krek V, Shelanski M, Cowan NJ (1984) Sequence of a cDNA clone encoding mouse glial fibrillary acidic protein: structural conservation of intermediate filaments. Proc Natl Acad Sci U S A 81:2743-2746.

Lewy FH (1912) Paralysis agitans. 1. Pathologische Anatomie. Handbuch der Neurologie, Dritter Band, Spezielle Neurologie I 920-933.

Li KW, Ganz AB, Smit AB (2018a) Proteomics of neurodegenerative diseases: analysis of human post-mortem brain. J Neurochem

Li Y, North RY, Rhines LD, Tatsui CE, Rao G, Edwards DD, Cassidy RM, Harrison DS, Johansson CA, Zhang H, Dougherty PM (2018b) DRG Voltage-Gated Sodium Channel 1.7 Is Upregulated in Paclitaxel-Induced Neuropathy in Rats and in Humans with Neuropathic Pain. J Neurosci 38:1124-1136.

Li X, Li W, Liu G, Shen X, Tang Y (2015a) Association between cigarette smoking and Parkinson's disease: A meta-analysis. Arch Gerontol Geriatr 61:510-516.

Li Y, Adamek P, Zhang H, Tatsui CE, Rhines LD, Mrozkova P, Li Q, Kosturakis AK, Cassidy RM, Harrison DS, Cata JP, Sapire K, Zhang H, Kennamer-Chapman RM, Jawad AB, Ghetti A, Yan J, Palecek J, Dougherty PM (2015b) The Cancer Chemotherapeutic Paclitaxel Increases Human and Rodent Sensory Neuron Responses to TRPV1 by Activation of TLR4. J Neurosci 35:13487-13500.

Li Z, Hogan EL, Banik NL (1996) Role of calpain in spinal cord injury: increased calpain immunoreactivity in rat spinal cord after impact trauma. Neurochem Res 21:441-448.

Li Z, Hogan EL, Banik NL (1995) Role of calpain in spinal cord injury: increased mcalpain immunoreactivity in spinal cord after compression injury in the rat. Neurochem Int 27:425-432.

Li Z, Liu P, Zhang H, Zhao S, Jin Z, Li R, Guo Y, Wang X (2017) Role of GABAB receptors and p38MAPK/NF-kappaB pathway in paclitaxel-induced apoptosis of hippocampal neurons. Pharm Biol 55:2188-2195.

Liang CL, Wang TT, Luby-Phelps K, German DC (2007) Mitochondria mass is low in mouse substantia nigra dopamine neurons: implications for Parkinson's disease. Exp Neurol 203:370-380.

Licker V, Cote M, Lobrinus JA, Rodrigo N, Kovari E, Hochstrasser DF, Turck N, Sanchez JC, Burkhard PR (2012) Proteomic profiling of the substantia nigra demonstrates CNDP2 overexpression in Parkinson's disease. J Proteomics 75:4656-4667.

Licker V, Turck N, Kovari E, Burkhardt K, Cote M, Surini-Demiri M, Lobrinus JA, Sanchez JC, Burkhard PR (2014) Proteomic analysis of human substantia nigra identifies novel candidates involved in Parkinson's disease pathogenesis. Proteomics 14:784-794.

Liddelow SA, Barres BA (2017) Reactive Astrocytes: Production, Function, and Therapeutic Potential. Immunity 46:957-967.

Liddelow SA, Guttenplan KA, Clarke LE, Bennett FC, Bohlen CJ, Schirmer L, Bennett ML, Munch AE, Chung WS, Peterson TC, Wilton DK, Frouin A, Napier BA, Panicker N, Kumar M, Buckwalter MS, Rowitch DH, Dawson VL, Dawson TM, Stevens B, Barres BA (2017) Neurotoxic reactive astrocytes are induced by activated microglia. Nature 541:481-487.

Liedtke W, Edelmann W, Bieri PL, Chiu FC, Cowan NJ, Kucherlapati R, Raine CS (1996) GFAP is necessary for the integrity of CNS white matter architecture and long-term maintenance of myelination. Neuron 17:607-615.

Linder J, Stenlund H, Forsgren L (2010) Incidence of Parkinson's disease and parkinsonism in northern Sweden: a population-based study. Mov Disord 25:341-348.

Lindstrom V, Gustafsson G, Sanders LH, Howlett EH, Sigvardson J, Kasrayan A, Ingelsson M, Bergstrom J, Erlandsson A (2017) Extensive uptake of alpha-synuclein oligomers in astrocytes results in sustained intracellular deposits and mitochondrial damage. Mol Cell Neurosci 82:143-156.

Liu G, Yu J, Ding J, Xie C, Sun L, Rudenko I, Zheng W, Sastry N, Luo J, Rudow G, Troncoso JC, Cai H (2014) Aldehyde dehydrogenase 1 defines and protects a nigrostriatal dopaminergic neuron subpopulation. J Clin Invest 124:3032-3046.

Liu HM, Gao J, Miao H, Xiao CH, Sun Y, Du X, Yuan HH, Yu HL, Gao DS (2010) Influence of aging on the calbindin-D-28k immunoreactive positive dopaminergic neurons in the substantia nigra pars compacta of rats. Neurosci Lett 468:3-6.

Liu M, Qin L, Wang L, Tan J, Zhang H, Tang J, Shen X, Tan L, Wang C (2018) alphasynuclein induces apoptosis of astrocytes by causing dysfunction of the endoplasmic reticulumGolgi compartment. Mol Med Rep 18:322-332.

Liu SY, Chan P, Stoessl AJ (2017) The underlying mechanism of prodromal PD: insights from the parasympathetic nervous system and the olfactory system. Transl Neurodegener 6:4-017-0074-8. eCollection 2017.

Liu Y, Zhou Q, Tang M, Fu N, Shao W, Zhang S, Yin Y, Zeng R, Wang X, Hu G, Zhou J (2015) Upregulation of alphaB-crystallin expression in the substantia nigra of patients with Parkinson's disease. Neurobiol Aging 36:1686-1691.

Llorca O, Martin-Benito J, Ritco-Vonsovici M, Grantham J, Hynes GM, Willison KR, Carrascosa JL, Valpuesta JM (2000) Eukaryotic chaperonin CCT stabilizes actin and tubulin folding intermediates in open quasi-native conformations. EMBO J 19:5971-5979.

Lu X, Kim-Han JS, Harmon S, Sakiyama-Elbert SE, O'Malley KL (2014) The Parkinsonian mimetic, 6-OHDA, impairs axonal transport in dopaminergic axons. Mol Neurodegener 9:17-1326-9-17.

Lucius R, Mentlein R (1995) Development of a culture system for pure rat neurons: advantages of a sandwich technique. Ann Anat 177:447-454.

Lucking CB, Durr A, Bonifati V, Vaughan J, De Michele G, Gasser T, Harhangi BS, Meco G, Denefle P, Wood NW, Agid Y, Brice A, French Parkinson's Disease Genetics Study Group,European Consortium on Genetic Susceptibility in Parkinson's Disease (2000) Association between early-onset Parkinson's disease and mutations in the parkin gene. N Engl J Med 342:1560-1567.

Ma SY, Roytt M, Collan Y, Rinne JO (1999) Unbiased morphometrical measurements show loss of pigmented nigral neurones with ageing. Neuropathol Appl Neurobiol 25:394-399.

Maasz G, Zrinyi Z, Reglodi D, Petrovics D, Rivnyak A, Kiss T, Jungling A, Tamas A, Pirger Z (2017) Pituitary adenylate cyclase-activating polypeptide (PACAP) has a

neuroprotective function in dopamine-based neurodegeneration in rat and snail parkinsonian models. Dis Model Mech 10:127-139.

Mabud MA, Dekrey MJ, Graham Cooks R (1985) Surface-induced dissociation of moelcular ions. Int J Mass Spectrom 67:285-294.

Madeira F, Park YM, Lee J, Buso N, Gur T, Madhusoodanan N, Basutkar P, Tivey ARN, Potter SC, Finn RD, Lopez R (2019) The EMBL-EBI search and sequence analysis tools APIs in 2019. Nucleic Acids Res 47:W636-W641.

Magdalinou NK, Noyce AJ, Pinto R, Lindstrom E, Holmen-Larsson J, Holtta M, Blennow K, Morris HR, Skillback T, Warner TT, Lees AJ, Pike I, Ward M, Zetterberg H, Gobom J (2017) Identification of candidate cerebrospinal fluid biomarkers in parkinsonism using quantitative proteomics. Parkinsonism Relat Disord 37:65-71.

Magidson V, He J, Ault JG, O'Connell CB, Yang N, Tikhonenko I, McEwen BF, Sui H, Khodjakov A (2016) Unattached kinetochores rather than intrakinetochore tension arrest mitosis in taxol-treated cells. J Cell Biol 212:307-319.

Mak SK, McCormack AL, Langston JW, Kordower JH, Di Monte dopamine (2009) Decreased alpha-synuclein expression in the aging mouse substantia nigra. Exp Neurol 220:359-365.

Mallajosyula JK, Kaur D, Chinta SJ, Rajagopalan S, Rane A, Nicholls DG, Di Monte dopamine, Macarthur H, Andersen JK (2008) MAO-B elevation in mouse brain astrocytes results in Parkinson's pathology. PLoS One 3:e1616.

Manadas B, Mendes VM, English J, Dunn MJ (2010) Peptide fractionation in proteomics approaches. Expert Rev Proteomics 7:655-663.

Mancardi GL, Cadoni A, Tabaton M, Schenone A, Zicca A, De Martini I, Bianchini D, Damiani G, Zaccheo D (1991) Schwann cell GFAP expression increases in axonal neuropathies. J Neurol Sci 102:177-183.

Mann M (2006) Functional and quantitative proteomics using SILAC. Nat Rev Mol Cell Biol 7:952-958.

Mannervik B, Danielson UH (1988) Glutathione transferases--structure and catalytic activity. CRC Crit Rev Biochem 23:283-337.

Mao L, Zabel C, Wacker MA, Nebrich G, Sagi D, Schrade P, Bachmann S, Kowald A, Klose J (2006) Estimation of the mtDNA mutation rate in aging mice by proteome analysis and mathematical modeling. Exp Gerontol 41:11-24.

Marchitti SA, Deitrich RA, Vasiliou V (2007a) Neurotoxicity and metabolism of the catecholamine-derived 3,4-dihydroxyphenylacetaldehyde and 3,4-dihydroxyphenylglycolaldehyde: the role of aldehyde dehydrogenase. Pharmacol Rev 59:125-150.

Marchitti SA, Orlicky DJ, Vasiliou V (2007b) Expression and initial characterization of human ALDH3B1. Biochem Biophys Res Commun 356:792-798.

Mariani LL, Doulazmi M, Chaigneau V, Brefel-Courbon C, Carriere N, Danaila T, Defebvre L, Defer G, Dellapina E, Doe de Maindreville A, Geny C, Maltete D, Meissner WG, Rascol O, Thobois S, Torny F, Tranchant C, Vidailhet M, Corvol JC, Degos B,NS-Park/F-CRIN Network study group (2019) Descriptive analysis of the French NS-Park registry: Towards a nation-wide Parkinson's disease cohort? Parkinsonism Relat Disord

Markram H, Muller E, Ramaswamy S, Reimann MW, Abdellah M, Sanchez CA, Ailamaki A, Alonso-Nanclares L, Antille N, Arsever S, Kahou GA, Berger TK, Bilgili A, Buncic N, Chalimourda A, Chindemi G, Courcol JD, Delalondre F, Delattre V, Druckmann S, Dumusc R, Dynes J, Eilemann S, Gal E, Gevaert ME, Ghobril JP, Gidon A, Graham JW, Gupta A, Haenel V, Hay E, Heinis T, Hernando JB, Hines M, Kanari L, Keller D, Kenyon J, Khazen G, Kim Y, King JG, Kisvarday Z, Kumbhar P, Lasserre S, Le Be JV, Magalhaes BR, Merchan-Perez A, Meystre J, Morrice BR, Muller J, Munoz-Cespedes A, Muralidhar S, Muthurasa K, Nachbaur D, Newton TH, Nolte M, Ovcharenko A, Palacios J, Pastor L, Perin R, Ranjan R, Riachi I, Rodriguez JR, Riquelme JL, Rossert C, Sfyrakis K, Shi Y, Shillcock JC, Silberberg G, Silva R, Tauheed F, Telefont M, Toledo-Rodriguez M, Trankler T, Van Geit W, Diaz JV, Walker R, Wang Y, Zaninetta SM, DeFelipe J, Hill SL, Segev I, Schurmann F (2015) Reconstruction and Simulation of Neocortical Microcircuitry. Cell 163:456-492.

Marron Fernandez de Velasco E, Zhang L, N Vo B, Tipps M, Farris S, Xia Z, Anderson A, Carlblom N, Weaver CD, Dudek SM, Wickman K (2017) GIRK2 splice variants and neuronal G protein-gated K(+) channels: implications for channel function and behavior. Sci Rep 7:1639-017-01820-2.

Marsden CD (1961) Pigmentation in the nucleus substantiae nigrae of mammals. J Anat 95:256-261.

Martin DP, Wallace TL, Johnson EM,Jr (1990) Cytosine arabinoside kills postmitotic neurons in a fashion resembling trophic factor deprivation: evidence that a deoxycytidine-dependent process may be required for nerve growth factor signal transduction. J Neurosci 10:184-193.

Martinez J, Malireddi RK, Lu Q, Cunha LD, Pelletier S, Gingras S, Orchard R, Guan JL, Tan H, Peng J, Kanneganti TD, Virgin HW, Green DR (2015) Molecular characterization of LC3-associated phagocytosis reveals distinct roles for Rubicon, NOX2 and autophagy proteins. Nat Cell Biol 17:893-906.

Marton RM, Ioannidis JPA (2019) A Comprehensive Analysis of Protocols for Deriving Dopaminergic Neurons from Human Pluripotent Stem Cells. Stem Cells Transl Med 8:366-374.

Matsuda W, Furuta T, Nakamura KC, Hioki H, Fujiyama F, Arai R, Kaneko T (2009) Single nigrostriatal dopaminergic neurons form widely spread and highly dense axonal arborizations in the neostriatum. J Neurosci 29:444-453.

Matthews L, Gopinath G, Gillespie M, Caudy M, Croft D, de Bono B, Garapati P, Hemish J, Hermjakob H, Jassal B, Kanapin A, Lewis S, Mahajan S, May B, Schmidt E, Vastrik I, Wu G, Birney E, Stein L, D'Eustachio P (2009) Reactome knowledgebase of human biological pathways and processes. Nucleic Acids Res 37:D619-22.

Maxwell MM, Tomkinson EM, Nobles J, Wizeman JW, Amore AM, Quinti L, Chopra V, Hersch SM, Kazantsev AG (2011) The Sirtuin 2 microtubule deacetylase is an abundant neuronal protein that accumulates in the aging CNS. Hum Mol Genet 20:3986-3996.

McBean GJ (2017) Cysteine, Glutathione, and Thiol Redox Balance in Astrocytes. Antioxidants (Basel) 6:10.3390/antiox6030062.

McCarroll SA, Feng G, Hyman SE (2014) Genome-scale neurogenetics: methodology and meaning. Nat Neurosci 17:756-763.

McClatchy DB, Liao L, Lee JH, Park SK, Yates JR,3rd (2012) Dynamics of subcellular proteomes during brain development. J Proteome Res 11:2467-2479.

McCormack AL, Di Monte dopamine, Delfani K, Irwin I, DeLanney LE, Langston WJ, Janson AM (2004) Aging of the nigrostriatal system in the squirrel monkey. J Comp Neurol 471:387-395.

McCormack AL, Mak SK, Di Monte dopamine (2012) Increased alpha-synuclein phosphorylation and nitration in the aging primate substantia nigra. Cell Death Dis 3:e315.

McGinn MJ, Colello RJ, Sun D (2012) Age-related proteomic changes in the subventricular zone and their association with neural stem/progenitor cell proliferation. J Neurosci Res 90:1159-1168.

McLafferty FW (1981) Tandem mass spectrometry. Science 214:280-287.

McLuckey SA (1992) Principles of collisional activation in analytical mass spectrometry. J Am Soc Mass Spectrom 3:599-614.

McNaught KS, Belizaire R, Isacson O, Jenner P, Olanow CW (2003) Altered proteasomal function in sporadic Parkinson's disease. Exp Neurol 179:38-46.

McRitchie dopamine, Cartwright HR, Halliday GM (1997) Specific A10 dopaminergic nuclei in the midbrain degenerate in Parkinson's disease. Exp Neurol 144:202-213.

McRitchie dopamine, Halliday GM, Cartwright H (1995) Quantitative analysis of the variability of substantia nigra pigmented cell clusters in the human. Neuroscience 68:539-551.

McRitchie dopamine, Hardman CD, Halliday GM (1996) Cytoarchitectural distribution of calcium binding proteins in midbrain dopaminergic regions of rats and humans. J Comp Neurol 364:121-150.

Meles SK, Tang CC, Teune LK, Dierckx RA, Dhawan V, Mattis PJ, Leenders KL, Eidelberg D (2015) Abnormal metabolic pattern associated with cognitive impairment in Parkinson's disease: a validation study. J Cereb Blood Flow Metab 35:1478-1484.

Mendez I, Sanchez-Pernaute R, Cooper O, Vinuela A, Ferrari D, Bjorklund L, Dagher A, Isacson O (2005) Cell type analysis of functional fetal dopamine cell suspension transplants in the striatum and substantia nigra of patients with Parkinson's disease. Brain 128:1498-1510.

Meng F, Hlady V, Tresco PA (2012) Inducing alignment in astrocyte tissue constructs by surface ligands patterned on biomaterials. Biomaterials 33:1323-1335.

Mengler L, Khmelinskii A, Diedenhofen M, Po C, Staring M, Lelieveldt BP, Hoehn M (2014) Brain maturation of the adolescent rat cortex and striatum: changes in volume and myelination. Neuroimage 84:35-44.

Menon V (2018) Extracting new insights from bulk transcriptomics. Nat Neurosci 21:1142-1144.

Mercado-Gomez O, Ferrera P, Arias C (2004) Histopathologic changes induced by the microtubule-stabilizing agent Taxol in the rat hippocampus in vivo. J Neurosci Res 78:553-562.

Meredith GE, Rademacher DJ (2011) MPTP mouse models of Parkinson's disease: an update. J Parkinsons Dis 1:19-33.

Merlini M, Meyer EP, Ulmann-Schuler A, Nitsch RM (2011) Vascular beta-amyloid and early astrocyte alterations impair cerebrovascular function and cerebral metabolism in transgenic arcAbeta mice. Acta Neuropathol 122:293-311.

Michel PP, Hefti F (1990) Toxicity of 6-hydroxydopamine and dopamine for dopaminergic neurons in culture. J Neurosci Res 26:428-435.

Middeldorp J, Hol EM (2011) GFAP in health and disease. Prog Neurobiol 93:421-443.

Mink JW (1996) The basal ganglia: focused selection and inhibition of competing motor programs. Prog Neurobiol 50:381-425.

Mironov SL, Ivannikov MV, Johansson M (2005) Ca2+ signaling between mitochondria and endoplasmic reticulum in neurons is regulated by microtubules. From mitochondrial permeability transition pore to Ca2+-induced Ca2+ release. J Biol Chem 280:715-721.

Mirza B, Hadberg H, Thomsen P, Moos T (2000) The absence of reactive astrocytosis is indicative of a unique inflammatory process in Parkinson's disease. Neuroscience 95:425-432.

Mitchison T, Kirschner M (1984) Dynamic instability of microtubule growth. Nature 312:237-242.

Mitulovic G, Mechtler K (2006) HPLC techniques for proteomics analysis--a short overview of latest developments. Brief Funct Genomic Proteomic 5:249-260.

Moeendarbary E, Weber IP, Sheridan GK, Koser DE, Soleman S, Haenzi B, Bradbury EJ, Fawcett J, Franze K (2017) The soft mechanical signature of glial scars in the central nervous system. Nat Commun 8:14787.

Mohammed S, Heck A,Jr (2011) Strong cation exchange (SCX) based analytical methods for the targeted analysis of protein post-translational modifications. Curr Opin Biotechnol 22:9-16.

Molnar I, Horvath C (1976) Reverse-phase chromatography of polar biological substances: separation of catechol compounds by high-performance liquid chromatography. Clin Chem 22:1497-1502.

Moon LD, Asher RA, Rhodes KE, Fawcett JW (2002) Relationship between sprouting axons, proteoglycans and glial cells following unilateral nigrostriatal axotomy in the adult rat. Neuroscience 109:101-117.

Morawski M, Bruckner MK, Riederer P, Bruckner G, Arendt T (2004) Perineuronal nets potentially protect against oxidative stress. Exp Neurol 188:309-315.

Mori S, Sugama S, Nguyen W, Michel T, Sanna MG, Sanchez-Alavez M, Cintron-Colon R, Moroncini G, Kakinuma Y, Maher P, Conti B (2017) Lack of interleukin-13 receptor alpha1 delays the loss of dopaminergic neurons during chronic stress. J Neuroinflammation 14:88-017-0862-1.

Mortera P,Herculano-Houzel S (2012) Age-related neuronal loss in the rat brain starts at the end of adolescence. Front Neuroanat 6:45.

Mouatt-Prigent A, Karlsson JO, Agid Y, Hirsch EC (1996) Increased M-calpain expression in the mesencephalon of patients with Parkinson's disease but not in other neurodegenerative disorders involving the mesencephalon: a role in nerve cell death? Neuroscience 73:979-987.

Mouser PE, Head E, Ha KH, Rohn TT (2006) Caspase-mediated cleavage of glial fibrillary acidic protein within degenerating astrocytes of the Alzheimer's disease brain. Am J Pathol 168:936-946.

Moustafa AA, Chakravarthy S, Phillips JR, Gupta A, Keri S, Polner B, Frank MJ, Jahanshahi M (2016) Motor symptoms in Parkinson's disease: A unified framework. Neurosci Biobehav Rev 68:727-740.

Munoz P, Cardenas S, Huenchuguala S, Briceno A, Couve E, Paris I, Segura-Aguilar J (2015) DT-Diaphorase Prevents Aminochrome-Induced Alpha-Synuclein Oligomer Formation and Neurotoxicity. Toxicol Sci 145:37-47.

Muthuraman M, Koirala N, Ciolac D, Pintea B, Glaser M, Groppa S, Tamas G, Groppa S (2018) Deep Brain Stimulation and L-DOPA Therapy: Concepts of Action and Clinical Applications in Parkinson's Disease. Front Neurol 9:711.

Nahirnyj A, Livne-Bar I, Guo X, Sivak JM (2013) ROS detoxification and proinflammatory cytokines are linked by p38 MAPK signaling in a model of mature astrocyte activation. PLoS One 8:e83049.

Nair-Roberts RG, Chatelain-Badie SD, Benson E, White-Cooper H, Bolam JP, Ungless MA (2008) Stereological estimates of dopaminergic, GABAergic and glutamatergic neurons in the ventral tegmental area, substantia nigra and retrorubral field in the rat. Neuroscience 152:1024-1031.

Nakata Y, Yasuda T, Fukaya M, Yamamori S, Itakura M, Nihira T, Hayakawa H, Kawanami A, Kataoka M, Nagai M, Sakagami H, Takahashi M, Mizuno Y, Mochizuki H (2012) Accumulation of alpha-synuclein triggered by presynaptic dysfunction. J Neurosci 32:17186-17196.

Namihira M, Kohyama J, Semi K, Sanosaka T, Deneen B, Taga T, Nakashima K (2009) Committed neuronal precursors confer astrocytic potential on residual neural precursor cells. Dev Cell 16:245-255.

Navarrete M, Perea G, Maglio L, Pastor J, Garcia de Sola R, Araque A (2013) Astrocyte calcium signal and gliotransmission in human brain tissue. Cereb Cortex 23:1240-1246.

Neilson KA, Ali NA, Muralidharan S, Mirzaei M, Mariani M, Assadourian G, Lee A, van Sluyter SC, Haynes PA (2011) Less label, more free: approaches in label-free quantitative mass spectrometry. Proteomics 11:535-553.

Nelson EL, Liang CL, Sinton CM, German DC (1996) Midbrain dopaminergic neurons in the mouse: computer-assisted mapping. J Comp Neurol 369:361-371.

Nesvizhskii AI (2010) A survey of computational methods and error rate estimation procedures for peptide and protein identification in shotgun proteomics. J Proteomics 73:2092-2123.

Nesvizhskii AI (2007) Protein identification by tandem mass spectrometry and sequence database searching. Methods Mol Biol 367:87-119.

Neuropathology-web Chapter 9. Degenerative diseases. Neuropathology 2016:

Nicolini G, Rigolio R, Scuteri A, Miloso M, Saccomanno D, Cavaletti G, Tredici G (2003) Effect of trans-resveratrol on signal transduction pathways involved in paclitaxel-induced apoptosis in human neuroblastoma SH-SY5Y cells. Neurochem Int 42:419-429.

Nogales E, Wang HW (2006) Structural mechanisms underlying nucleotide-dependent self-assembly of tubulin and its relatives. Curr Opin Struct Biol 16:221-229.

Nogales E, Wolf SG, Khan IA, Luduena RF, Downing KH (1995) Structure of tubulin at 6.5 A and location of the taxol-binding site. Nature 375:424-427.

Nshanian M, Lakshmanan R, Chen H, Ogorzalek Loo RR, Loo JA (2018) Enhancing Sensitivity of Liquid Chromatography-Mass Spectrometry of Peptides and Proteins Using Supercharging Agents. Int J Mass Spectrom 427:157-164.

Olsen JV, Ong SE, Mann M (2004) Trypsin cleaves exclusively C-terminal to arginine and lysine residues. Mol Cell Proteomics 3:608-614.

Oo TF, Burke RE (1997) The time course of developmental cell death in phenotypically defined dopaminergic neurons of the substantia nigra. Brain Res Dev Brain Res 98:191-196.

Orimo S, Uchihara T, Kanazawa T, Itoh Y, Wakabayashi K, Kakita A, Takahashi H (2011) Unmyelinated axons are more vulnerable to degeneration than myelinated axons of the cardiac nerve in Parkinson's disease. Neuropathol Appl Neurobiol 37:791-802.

Ouchi Y, Yoshikawa E, Sekine Y, Futatsubashi M, Kanno T, Ogusu T, Torizuka T (2005) Microglial activation and dopamine terminal loss in early Parkinson's disease. Ann Neurol 57:168-175.

Ousman SS, Tomooka BH, van Noort JM, Wawrousek EF, O'Connor KC, Hafler dopamine, Sobel RA, Robinson WH, Steinman L (2007) Protective and therapeutic role for alphaB-crystallin in autoimmune demyelination. Nature 448:474-479.

Pabba M, Scifo E, Kapadia F, Nikolova YS, Ma T, Mechawar N, Tseng GC, Sibille E (2017) Resilient protein co-expression network in male orbitofrontal cortex layer 2/3 during human aging. Neurobiol Aging 58:180-190.

Pacelli C, Giguere N, Bourque MJ, Levesque M, Slack RS, Trudeau LE (2015) Elevated Mitochondrial Bioenergetics and Axonal Arborization Size Are Key Contributors to the Vulnerability of Dopamine Neurons. Curr Biol 25:2349-2360.

Pan J, Yu J, Sun L, Xie C, Chang L, Wu J, Hawes S, Saez-Atienzar S, Zheng W, Kung J, Ding J, Le W, Chen S, Cai H (2019) ALDH1A1 regulates postsynaptic mu-opioid receptor expression in dorsal striatal projection neurons and mitigates dyskinesia through transsynaptic retinoic acid signaling. Sci Rep 9:3602-019-40326-x.

Pan Q, Shai O, Lee LJ, Frey BJ, Blencowe BJ (2008) Deep surveying of alternative splicing complexity in the human transcriptome by high-throughput sequencing. Nat Genet 40:1413-1415.

Panneton WM, Kumar VB, Gan Q, Burke WJ, Galvin JE (2010) The neurotoxicity of DOPAL: behavioral and stereological evidence for its role in Parkinson disease pathogenesis. PLoS One 5:e15251.

Papa L, Lewis LM, Falk JL, Zhang Z, Silvestri S, Giordano P, Brophy GM, Demery JA, Dixit NK, Ferguson I, Liu MC, Mo J, Akinyi L, Schmid K, Mondello S, Robertson CS, Tortella FC, Hayes RL, Wang KK (2012) Elevated levels of serum glial fibrillary acidic protein breakdown products in mild and moderate traumatic brain injury are associated with intracranial lesions and neurosurgical intervention. Ann Emerg Med 59:471-483.

Park M, Kitahama K, Geffard M, Maeda T (2000) Postnatal development of the dopaminergic neurons in the rat mesencephalon. Brain Dev 22 Suppl 1:S38-44.

Park SB, Lin CS, Krishnan AV, Friedlander ML, Lewis CR, Kiernan MC (2011) Early, progressive, and sustained dysfunction of sensory axons underlies paclitaxel-induced neuropathy. Muscle Nerve 43:367-374.

Parker JG, Marshall JD, Ahanonu B, Wu YW, Kim TH, Grewe BF, Zhang Y, Li JZ, Ding JB, Ehlers MD, Schnitzer MJ (2018) Diametric neural ensemble dynamics in parkinsonian and dyskinetic states. Nature 557:177-182.

Parker WH, Rhea EM, Qu ZC, Hecker MR, May JM (2016) Intracellular ascorbate tightens the endothelial permeability barrier through Epac1 and the tubulin cytoskeleton. Am J Physiol Cell Physiol 311:C652-C662.

Parkinson's UK (2017) the incidence and prevalence of Parkinson's in the UK: Results from the Clinica Practice Research Datalink reference report. Parkinson's UK

Patel S, Sinha A, Singh MP (2007) Identification of differentially expressed proteins in striatum of maneb-and paraquat-induced Parkinson's disease phenotype in mouse. Neurotoxicol Teratol 29:578-585.

Pekny M, Wilhelmsson U, Pekna M (2014) The dual role of astrocyte activation and reactive gliosis. Neurosci Lett 565:30-38.

Peng L, Zhao Y, Li Y, Zhou Y, Li L, Lei S, Yu S, Zhao Y (2019) Effect of DJ-1 on the neuroprotection of astrocytes subjected to cerebral ischemia/reperfusion injury. J Mol Med (Berl) 97:189-199.

Perng MD, Wen SF, Gibbon T, Middeldorp J, Sluijs J, Hol EM, Quinlan RA (2008) Glial fibrillary acidic protein filaments can tolerate the incorporation of assembly-compromised GFAP-delta, but with consequences for filament organization and alphaB-crystallin association. Mol Biol Cell 19:4521-4533.

Perry TL, Godin DV, Hansen S (1982) Parkinson's disease: a disorder due to nigral glutathione deficiency? Neurosci Lett 33:305-310.

Perry VH, Teeling J (2013) Microglia and macrophages of the central nervous system: the contribution of microglia priming and systemic inflammation to chronic neurodegeneration. Semin Immunopathol 35:601-612.

Peters CM, Jimenez-Andrade JM, Kuskowski MA, Ghilardi JR, Mantyh PW (2007) An evolving cellular pathology occurs in dorsal root ganglia, peripheral nerve and spinal cord following intravenous administration of paclitaxel in the rat. Brain Res 1168:46-59.

Peters R (2006) Ageing and the brain. Postgrad Med J 82:84-88.

Pfisterer U, Khodosevich K (2017) Neuronal survival in the brain: neuron type-specific mechanisms. Cell Death Dis 8:e2643.

Piacentini R, Li Puma DD, Mainardi M, Lazzarino G, Tavazzi B, Arancio O, Grassi C (2017) Reduced gliotransmitter release from astrocytes mediates tau-induced synaptic dysfunction in cultured hippocampal neurons. Glia 65:1302-1316.

Pickrell AM, Fukui H, Wang X, Pinto M, Moraes CT (2011) The striatum is highly susceptible to mitochondrial oxidative phosphorylation dysfunctions. J Neurosci 31:9895-9904.

Picotti P, Aebersold R (2012) Selected reaction monitoring-based proteomics: workflows, potential, pitfalls and future directions. Nat Methods 9:555-566.

Pierson J, Norris JL, Aerni HR, Svenningsson P, Caprioli RM, Andren PE (2004) Molecular profiling of experimental Parkinson's disease: direct analysis of peptides and proteins on brain tissue sections by MALDI mass spectrometry. J Proteome Res 3:289-295.

Piguet O, Double KL, Kril JJ, Harasty J, Macdonald V, McRitchie dopamine, Halliday GM (2009) White matter loss in healthy ageing: a postmortem analysis. Neurobiol Aging 30:1288-1295.

Ping L, Duong DM, Yin L, Gearing M, Lah JJ, Levey AI, Seyfried NT (2018) Global quantitative analysis of the human brain proteome in Alzheimer's and Parkinson's Disease. Sci Data 5:180036.

Pissadaki EK, Bolam JP (2013) The energy cost of action potential propagation in dopamine neurons: clues to susceptibility in Parkinson's disease. Front Comput Neurosci 7:13.

Pizzorusso T, Medini P, Berardi N, Chierzi S, Fawcett JW, Maffei L (2002) Reactivation of ocular dominance plasticity in the adult visual cortex. Science 298:1248-1251.

Poewe W, Seppi K, Tanner CM, Halliday GM, Brundin P, Volkmann J, Schrag AE, Lang AE (2017) Parkinson disease. Nat Rev Dis Primers 3:17013.

Pollard A, Shephard F, Freed J, Liddell S, Chakrabarti L (2016) Mitochondrial proteomic profiling reveals increased carbonic anhydrase II in aging and neurodegeneration. Aging (Albany NY) 8:2425-2436.

Polymeropoulos MH, Lavedan C, Leroy E, Ide SE, Dehejia A, Dutra A, Pike B, Root H, Rubenstein J, Boyer R, Stenroos ES, Chandrasekharappa S, Athanassiadou A, Papapetropoulos T, Johnson WG, Lazzarini AM, Duvoisin RC, Di Iorio G, Golbe LI, Nussbaum RL (1997) Mutation in the alpha-synuclein gene identified in families with Parkinson's disease. Science 276:2045-2047.

Pomaznoy M, Ha B, Peters B (2018) GOnet: a tool for interactive Gene Ontology analysis. BMC Bioinformatics 19:470-018-2533-3.

Poon HF, Castegna A, Farr SA, Thongboonkerd V, Lynn BC, Banks WA, Morley JE, Klein JB, Butterfield dopamine (2004) Quantitative proteomics analysis of specific protein expression and oxidative modification in aged senescence-accelerated-prone 8 mice brain. Neuroscience 126:915-926.

Poon HF, Vaishnav RA, Getchell TV, Getchell ML, Butterfield dopamine (2006) Quantitative proteomics analysis of differential protein expression and oxidative modification of specific proteins in the brains of old mice. Neurobiol Aging 27:1010-1019.

Potokar M, Kreft M, Li L, Daniel Andersson J, Pangrsic T, Chowdhury HH, Pekny M, Zorec R (2007) Cytoskeleton and vesicle mobility in astrocytes. Traffic 8:12-20.

Pouchieu C, Piel C, Carles C, Gruber A, Helmer C, Tual S, Marcotullio E, Lebailly P, Baldi I (2018) Pesticide use in agriculture and Parkinson's disease in the AGRICAN cohort study. Int J Epidemiol 47:299-310.

Powell EM, Meiners S, DiProspero NA, Geller HM (1997) Mechanisms of astrocyte-directed neurite guidance. Cell Tissue Res 290:385-393.

Pringsheim T, Jette N, Frolkis A, Steeves TD (2014) The prevalence of Parkinson's disease: a systematic review and meta-analysis. Mov Disord 29:1583-1590.

Qamhawi Z, Towey D, Shah B, Pagano G, Seibyl J, Marek K, Borghammer P, Brooks DJ, Pavese N (2015) Clinical correlates of raphe serotonergic dysfunction in early Parkinson's disease. Brain 138:2964-2973.

Qi H,Li S (2014) Dose-response meta-analysis on coffee, tea and caffeine consumption with risk of Parkinson's disease. Geriatr Gerontol Int 14:430-439.

Raghunathan R, Polinski NK, Klein JA, Hogan JD, Shao C, Khatri K, Leon D, McComb ME, Manfredsson FP, Sortwell CE, Zaia J (2018) Glycomic and Proteomic Changes in Aging Brain Nigrostriatal Pathway. Mol Cell Proteomics 17:1778-1787.

Raicevic N, Mladenovic A, Perovic M, Miljkovic D, Trajkovic V (2005) The mechanisms of 6-hydroxydopamine-induced astrocyte death. Ann N Y Acad Sci 1048:400-405.

Ramsay RR, Kowal AT, Johnson MK, Salach JI, Singer TP (1987) The inhibition site of MPP+, the neurotoxic bioactivation product of 1-methyl-4-phenyl-1,2,3,6-tetrahydropyridine is near the Q-binding site of NADH dehydrogenase. Arch Biochem Biophys 259:645-649.

Ransom BR, Kunis DM, Irwin I, Langston JW (1987) Astrocytes convert the parkinsonism inducing neurotoxin, MPTP, to its active metabolite, MPP+. Neurosci Lett 75:323-328.

Reeve AK, Grady JP, Cosgrave EM, Bennison E, Chen C, Hepplewhite PD, Morris CM (2018) Mitochondrial dysfunction within the synapses of substantia nigra neurons in Parkinson's disease. NPJ Parkinsons Dis 4:9-018-0044-6. eCollection 2018.

Reeves SA, Helman LJ, Allison A, Israel MA (1989) Molecular cloning and primary structure of human glial fibrillary acidic protein. Proc Natl Acad Sci U S A 86:5178-5182.

Ren Y, Wang X, Lou Z, Huang S, Zhuang H, Wang Y, Weng G, Wang P (2017) Induction of cell cycle arrest by increasing GTPRhoA levels via Taxolinduced microtubule polymerization in renal cell carcinoma. Mol Med Rep 15:4273-4279.

Reyes S, Fu Y, Double K, Thompson L, Kirik D, Paxinos G,Halliday GM (2012) GIRK2 expression in dopamine neurons of the substantia nigra and ventral tegmental area. J Comp Neurol 520:2591-2607.

Rizzi G, Tan KR (2017) Dopamine and Acetylcholine, a Circuit Point of View in Parkinson's Disease. Front Neural Circuits 11:110.

Rizzo G, Copetti M, Arcuti S, Martino D, Fontana A, Logroscino G (2016) Accuracy of clinical diagnosis of Parkinson disease: A systematic review and meta-analysis. Neurology 86:566-576.

Rochester L, Yarnall AJ, Baker MR, David RV, Lord S, Galna B, Burn DJ (2012) Cholinergic dysfunction contributes to gait disturbance in early Parkinson's disease. Brain 135:2779-2788.

Rodriguez JJ, Yeh CY, Terzieva S, Olabarria M, Kulijewicz-Nawrot M, Verkhratsky A (2014) Complex and region-specific changes in astroglial markers in the aging brain. Neurobiol Aging 35:15-23.

Rodriguez M, Rodriguez-Sabate C, Morales I, Sanchez A, Sabate M (2015) Parkinson's disease as a result of aging. Aging Cell 14:293-308.

Roelofs RF, Fischer DF, Houtman SH, Sluijs JA, Van Haren W, Van Leeuwen FW, Hol EM (2005) Adult human subventricular, subgranular, and subpial zones contain astrocytes with a specialized intermediate filament cytoskeleton. Glia 52:289-300.

Ross PL, Huang YN, Marchese JN, Williamson B, Parker K, Hattan S, Khainovski N, Pillai S, Dey S, Daniels S, Purkayastha S, Juhasz P, Martin S, Bartlet-Jones M, He F, Jacobson A, Pappin DJ (2004) Multiplexed protein quantitation in Saccharomyces cerevisiae using amine-reactive isobaric tagging reagents. Mol Cell Proteomics 3:1154-1169.

Rudow G, O'Brien R, Savonenko AV, Resnick SM, Zonderman AB, Pletnikova O, Marsh L, Dawson TM, Crain BJ, West MJ, Troncoso JC (2008) Morphometry of the human substantia nigra in ageing and Parkinson's disease. Acta Neuropathol 115:461-470.

Safavi-Abbasi S, Wolff JR, Missler M (2001) Rapid morphological changes in astrocytes are accompanied by redistribution but not by quantitative changes of cytoskeletal proteins. Glia 36:102-115.

Saggu H, Cooksey J, Dexter D, Wells FR, Lees A, Jenner P, Marsden CD (1989) A selective increase in particulate superoxide dismutase activity in parkinsonian substantia nigra. J Neurochem 53:692-697.

Sampson TR, Debelius JW, Thron T, Janssen S, Shastri GG, Ilhan ZE, Challis C, Schretter CE, Rocha S, Gradinaru V, Chesselet MF, Keshavarzian A, Shannon KM, Krajmalnik-Brown R, Wittung-Stafshede P, Knight R, Mazmanian SK (2016) Gut Microbiota Regulate Motor Deficits and Neuroinflammation in a Model of Parkinson's Disease. Cell 167:1469-1480.e12.

Sanchez HL, Silva LB, Portiansky EL, Herenu CB, Goya RG, Zuccolilli GO (2008) Dopaminergic mesencephalic systems and behavioral performance in very old rats. Neuroscience 154:1598-1606.

Sanchez-Guajardo V, Febbraro F, Kirik D, Romero-Ramos M (2010) Microglia acquire distinct activation profiles depending on the degree of alpha-synuclein neuropathology in a rAAV based model of Parkinson's disease. PLoS One 5:e8784.

Sanders LH, Timothy Greenamyre J (2013) Oxidative damage to macromolecules in human Parkinson disease and the rotenone model. Free Radic Biol Med 62:111-120.

Sandhu JK, Gardaneh M, Iwasiow R, Lanthier P, Gangaraju S, Ribecco-Lutkiewicz M, Tremblay R, Kiuchi K, Sikorska M (2009) Astrocyte-secreted GDNF and glutathione antioxidant system protect neurons against 6-OHDA cytotoxicity. Neurobiol Dis 33:405-414.

Santos AL, Lindner AB (2017) Protein Posttranslational Modifications: Roles in Aging and Age-Related Disease. Oxid Med Cell Longev 2017:5716409.

Santos DM, Xavier JM, Morgado AL, Sola S, Rodrigues CM (2012) Distinct regulatory functions of calpain 1 and 2 during neural stem cell self-renewal and differentiation. PLoS One 7:e33468.

Sarath Babu N, Murthy C, Kakara S, Sharma R, Brahmendra Swamy CV, Idris MM (2016) 1-Methyl-4-phenyl-1,2,3,6-tetrahydropyridine induced Parkinson's disease in zebrafish. Proteomics 16:1407-1420.

Sasaki M, Shibata E, Tohyama K, Takahashi J, Otsuka K, Tsuchiya K, Takahashi S, Ehara S, Terayama Y, Sakai A (2006) Neuromelanin magnetic resonance imaging of locus ceruleus and substantia nigra in Parkinson's disease. Neuroreport 17:1215-1218.

Savaryn JP, Toby TK, Kelleher NL (2016) A researcher's guide to mass spectrometry-based proteomics. Proteomics 16:2435-2443.

Scahill RI, Frost C, Jenkins R, Whitwell JL, Rossor MN, Fox NC (2003) A longitudinal study of brain volume changes in normal aging using serial registered magnetic resonance imaging. Arch Neurol 60:989-994.

Schawkat K, Di Santo S, Seiler S, Ducray AD, Widmer HR (2015) Loss of Nogo-A-expressing neurons in a rat model of Parkinson's disease. Neuroscience 288:59-72.

Schichor C, Kerkau S, Visted T, Martini R, Bjerkvig R, Tonn JC, Goldbrunner R (2005) The brain slice chamber, a novel variation of the Boyden Chamber Assay, allows time-dependent quantification of glioma invasion into mammalian brain in vitro. J Neurooncol 73:9-18.

Schiff PB, Horwitz SB (1980) Taxol stabilizes microtubules in mouse fibroblast cells. Proc Natl Acad Sci U S A 77:1561-1565.

Schlaepfer WW, Zimmerman UP (1981) Calcium-mediated breakdown of glial filaments and neurofilaments in rat optic nerve and spinal cord. Neurochem Res 6:243-255.

Schneider CA, Rasband WS, Eliceiri KW (2012) NIH Image to ImageJ: 25 years of image analysis. Nat Methods 9:671-675.

Scholz B, Svensson M, Alm H, Skold K, Falth M, Kultima K, Guigoni C, Doudnikoff E, Li Q, Crossman AR, Bezard E, Andren PE (2008) Striatal proteomic analysis suggests that first L-dopa dose equates to chronic exposure. PLoS One 3:e1589.

Schweinhuber SK, Messerschmidt T, Hansch R, Korte M, Rothkegel M (2015) Profilin isoforms modulate astrocytic morphology and the motility of astrocytic processes. PLoS One 10:e0117244.

Schwieger J, Esser KH, Lenarz T, Scheper V (2016) Establishment of a long-term spiral ganglion neuron culture with reduced glial cell number: Effects of AraC on cell composition and neurons. J Neurosci Methods 268:106-116.

Scuteri A, Nicolini G, Miloso M, Bossi M, Cavaletti G, Windebank AJ, Tredici G (2006) Paclitaxel toxicity in post-mitotic DRG cells. Anticancer Res 26:1065-1070.

Seki T, Sato T, Toda K, Osumi N, Imura T, Shioda S (2014) Distinctive population of Gfap-expressing neural progenitors arising around the dentate notch migrate and form the granule cell layer in the developing hippocampus. J Comp Neurol 522:261-283.

Sengottuvel V, Leibinger M, Pfreimer M, Andreadaki A, Fischer D (2011) Taxol facilitates axon regeneration in the mature CNS. J Neurosci 31:2688-2699.

Sengupta B, Faisal AA, Laughlin SB, Niven JE (2013) The effect of cell size and channel density on neuronal information encoding and energy efficiency. J Cereb Blood Flow Metab 33:1465-1473.

Sengupta P (2013) The laboratory rat: relating its age with human's. Int J Prev Med 4:624-630.

Sethi S, Chourasia D, Parhar IS (2015) Approaches for targeted proteomics and its potential applications in neuroscience. J Biosci 40:607-627.

Sgobio C, Wu J, Zheng W, Chen X, Pan J, Salinas AG, Davis MI, Lovinger DM, Cai H (2017) Aldehyde dehydrogenase 1-positive nigrostriatal dopaminergic fibers exhibit distinct projection pattern and dopamine release dynamics at mouse dorsal striatum. Sci Rep 7:5283-017-05598-1.

Sharma S, Ray B, Bhardwaj D, Dwivedi AK, Roy TS (2009) Age changes in the human oculomotor nerve - a stereological study. Ann Anat 191:260-266.

Shemesh OA, Spira ME (2010) Paclitaxel induces axonal microtubules polar reconfiguration and impaired organelle transport: implications for the pathogenesis of paclitaxel-induced polyneuropathy. Acta Neuropathol 119:235-248.

Shilov IV, Seymour SL, Patel AA, Loboda A, Tang WH, Keating SP, Hunter CL, Nuwaysir LM, Schaeffer dopamine (2007) The Paragon Algorithm, a next generation search engine that uses sequence temperature values and feature probabilities to identify peptides from tandem mass spectra. Mol Cell Proteomics 6:1638-1655.

Shimoda K, Sauve Y, Marini A, Schwartz JP, Commissiong JW (1992) A high percentage yield of tyrosine hydroxylase-positive cells from rat E14 mesencephalic cell culture. Brain Res 586:319-331.

Shokolenko I, Venediktova N, Bochkareva A, Wilson GL, Alexeyev MF (2009) Oxidative stress induces degradation of mitochondrial DNA. Nucleic Acids Res 37:2539-2548.

Shulman JM, De Jager PL, Feany MB (2011) Parkinson's disease: genetics and pathogenesis. Annu Rev Pathol 6:193-222.

Sidiropoulos K, Viteri G, Sevilla C, Jupe S, Webber M, Orlic-Milacic M, Jassal B, May B, Shamovsky V, Duenas C, Rothfels K, Matthews L, Song H, Stein L, Haw R, D'Eustachio P, Ping P, Hermjakob H, Fabregat A (2017) Reactome enhanced pathway visualization. Bioinformatics 33:3461-3467.

Sievers F, Wilm A, Dineen D, Gibson TJ, Karplus K, Li W, Lopez R, McWilliam H, Remmert M, Soding J, Thompson JD, Higgins DG (2011) Fast, scalable generation of high-quality protein multiple sequence alignments using Clustal Omega. Mol Syst Biol 7:539.

Sihag RK, Inagaki M, Yamaguchi T, Shea TB, Pant HC (2007) Role of phosphorylation on the structural dynamics and function of types III and IV intermediate filaments. Exp Cell Res 313:2098-2109.

Silbergeld DL, Chicoine MR, Madsen CL (1995) In vitro assessment of Taxol for human glioblastoma: chemosensitivity and cellular locomotion. Anticancer Drugs 6:270-276.

Singh R, Brewer MK, Mashburn CB, Lou D, Bondada V, Graham B, Geddes JW (2014) Calpain 5 is highly expressed in the central nervous system (CNS), carries dual nuclear localization signals, and is associated with nuclear promyelocytic leukemia protein bodies. J Biol Chem 289:19383-19394.

Singh S, Brocker C, Koppaka V, Chen Y, Jackson BC, Matsumoto A, Thompson DC, Vasiliou V (2013) Aldehyde dehydrogenases in cellular responses to oxidative/electrophilic stress. Free Radic Biol Med 56:89-101.

Sinha A, Srivastava N, Singh S, Singh AK, Bhushan S, Shukla R, Singh MP (2009) Identification of differentially displayed proteins in cerebrospinal fluid of Parkinson's disease patients: a proteomic approach. Clin Chim Acta 400:14-20.

Smidak R, Sialana FJ, Kristofova M, Stojanovic T, Rajcic D, Malikovic J, Feyissa DD, Korz V, Hoeger H, Wackerlig J, Mechtcheriakova D, Lubec G (2017) Reduced Levels of the Synaptic Functional Regulator FMRP in Dentate Gyrus of the Aging Sprague-Dawley Rat. Front Aging Neurosci 9:384.

Smith AM, Depp C, Ryan BJ, Johnston GI, Alegre-Abarrategui J, Evetts S, Rolinski M, Baig F, Ruffmann C, Simon AK, Hu MTM, Wade-Martins R (2018) Mitochondrial dysfunction and increased glycolysis in prodromal and early Parkinson's blood cells. Mov Disord 33:1580-1590.

Smith LM, Kelleher NL, Consortium for Top Down Proteomics (2013) Proteoform: a single term describing protein complexity. Nat Methods 10:186-187.

Smith ME, Perret V, Eng LF (1984) Metabolic studies in vitro of the CNS cytoskeletal proteins: synthesis and degradation. Neurochem Res 9:1493-1507.

Snyder JM, Hagan CE, Bolon B, Keene CD (2018) Nervous system. Comparative Anatomy and Histology 403-444.

Sofroniew MV (2009) Molecular dissection of reactive astrogliosis and glial scar formation. Trends Neurosci 32:638-647.

Soltic D, Bowerman M, Stock J, Shorrock HK, Gillingwater TH, Fuller HR (2018) Multi-Study Proteomic and Bioinformatic Identification of Molecular Overlap between Amyotrophic Lateral Sclerosis (ALS) and Spinal Muscular Atrophy (SMA). Brain Sci 8:10.3390/brainsci8120212.

Song YJ, Halliday GM, Holton JL, Lashley T, O'Sullivan SS, McCann H, Lees AJ, Ozawa T, Williams DR, Lockhart PJ, Revesz TR (2009) Degeneration in different parkinsonian syndromes relates to astrocyte type and astrocyte protein expression. J Neuropathol Exp Neurol 68:1073-1083.

Sorensen A, Moffat K, Thomson C, Barnett SC (2008) Astrocytes, but not olfactory ensheathing cells or Schwann cells, promote myelination of CNS axons in vitro. Glia 56:750-763.

Spear LP (2000) The adolescent brain and age-related behavioral manifestations. Neurosci Biobehav Rev 24:417-463.

Spillantini MG, Schmidt ML, Lee VM, Trojanowski JQ, Jakes R, Goedert M (1997) Alpha-synuclein in Lewy bodies. Nature 388:839-840.

Spinelli JB, Haigis MC (2018) The multifaceted contributions of mitochondria to cellular metabolism. Nat Cell Biol 20:745-754.

Spittau B (2017) Aging Microglia-Phenotypes, Functions and Implications for Age-Related Neurodegenerative Diseases. Front Aging Neurosci 9:194.

Stauch KL, Purnell PR, Villeneuve LM, Fox HS (2015) Data for mitochondrial proteomic alterations in the aging mouse brain. Data Brief 4:127-129.

Stauch KL, Villeneuve LM, Purnell PR, Ottemann BM, Emanuel K, Fox HS (2016) Loss of Pink1 modulates synaptic mitochondrial bioenergetics in the rat striatum prior to motor symptoms: concomitant complex I respiratory defects and increased complex II-mediated respiration. Proteomics Clin Appl 10:1205-1217.

Stefanis L (2012) alpha-Synuclein in Parkinson's disease. Cold Spring Harb Perspect Med 2:a009399.

Steinbach S, Marcus K, Wolters D (2018) A proteomic investigation of the ageing substantia nigra and the selective neuronal vulnerability of its neurons. Ruhr-Universitat Bochum

Stepkowski TM, Wasyk I, Grzelak A, Kruszewski M (2015) 6-OHDA-Induced Changes in Parkinson's Disease-Related Gene Expression are not Affected by the Overexpression of PGAM5 in In Vitro Differentiated Embryonic Mesencephalic Cells. Cell Mol Neurobiol 35:1137-1147.

Stern MB, Lang A, Poewe W (2012) Toward a redefinition of Parkinson's disease. Mov Disord 27:54-60.

Stothard P (2000) The sequence manipulation suite: JavaScript programs for analyzing and formatting protein and DNA sequences. BioTechniques 28:1102, 1104.

Sulzer D, Cassidy C, Horga G, Kang UJ, Fahn S, Casella L, Pezzoli G, Langley J, Hu XP, Zucca FA, Isaias IU, Zecca L (2018) Neuromelanin detection by magnetic resonance imaging (MRI) and its promise as a biomarker for Parkinson's disease. NPJ Parkinsons Dis 4:11-018-0047-3. eCollection 2018.

Sulzer D, Surmeier DJ (2013) Neuronal vulnerability, pathogenesis, and Parkinson's disease. Mov Disord 28:41-50.

Surmeier DJ, Obeso JA, Halliday GM (2017) Selective neuronal vulnerability in Parkinson disease. Nat Rev Neurosci 18:101-113.

Swartz HM, Sarna T, Zecca L (1992) Modulation by neuromelanin of the availability and reactivity of metal ions. Ann Neurol 32 Suppl:S69-75.

Syka JE, Coon JJ, Schroeder MJ, Shabanowitz J, Hunt DF (2004) Peptide and protein sequence analysis by electron transfer dissociation mass spectrometry. Proc Natl Acad Sci U S A 101:9528-9533.

Szklarczyk D, Gable AL, Lyon D, Junge A, Wyder S, Huerta-Cepas J, Simonovic M, Doncheva NT, Morris JH, Bork P, Jensen LJ, Mering CV (2019) STRING v11: protein-protein association networks with increased coverage, supporting functional discovery in genome-wide experimental datasets. Nucleic Acids Res 47:D607-D613.

Takeshima T, Johnston JM, Commissiong JW (1994) Mesencephalic type 1 astrocytes rescue dopaminergic neurons from death induced by serum deprivation. J Neurosci 14:4769-4779.

Tanaka K, Watase K, Manabe T, Yamada K, Watanabe M, Takahashi K, Iwama H, Nishikawa T, Ichihara N, Kikuchi T, Okuyama S, Kawashima N, Hori S, Takimoto M, Wada K (1997) Epilepsy and exacerbation of brain injury in mice lacking the glutamate transporter GLT-1. Science 276:1699-1702.

Tang Y, Nyengaard JR, Pakkenberg B, Gundersen HJ (1997) Age-induced white matter changes in the human brain: a stereological investigation. Neurobiol Aging 18:609-615.

Tanimukai H, Kanayama D, Omi T, Takeda M, Kudo T (2013) Paclitaxel induces neurotoxicity through endoplasmic reticulum stress. Biochem Biophys Res Commun 437:151-155.

Tapia-Gonzalez S, Giraldez-Perez RM, Cuartero MI, Casarejos MJ, Mena MA, Wang XF, Sanchez-Capelo A (2011) Dopamine and alpha-synuclein dysfunction in Smad3 null mice. Mol Neurodegener 6:72-1326-6-72.

Tatton WG, Greenwood CE, Salo PT, Seniuk NA (1991) Transmitter synthesis increases in substantia nigra neurons of the aged mouse. Neurosci Lett 131:179-182.

Tawfik VL, Lacroix-Fralish ML, Bercury KK, Nutile-McMenemy N, Harris BT, Deleo JA (2006) Induction of astrocyte differentiation by propentofylline increases glutamate transporter expression in vitro: heterogeneity of the quiescent phenotype. Glia 54:193-203.

Taylor-Whiteley TR, Le Maitre CL, Duce JA, Dalton CF, Smith DP (2019) Recapitulating Parkinson's disease pathology in a three-dimensional human neural cell culture model. Dis Model Mech 12:10.1242/dmm.038042.

Tepper JM, Damlama M, Trent F (1994) Postnatal changes in the distribution and morphology of rat substantia nigra dopaminergic neurons. Neuroscience 60:469-477.

The M, Tasnim A, Kall L (2016) How to talk about protein-level false discovery rates in shotgun proteomics. Proteomics 16:2461-2469.

Thompson A, Schafer J, Kuhn K, Kienle S, Schwarz J, Schmidt G, Neumann T, Johnstone R, Mohammed AK, Hamon C (2003) Tandem mass tags: a novel quantification strategy for comparative analysis of complex protein mixtures by MS/MS. Anal Chem 75:1895-1904.

Thompson L, Barraud P, Andersson E, Kirik D, Bjorklund A (2005) Identification of dopaminergic neurons of nigral and ventral tegmental area subtypes in grafts of fetal ventral mesencephalon based on cell morphology, protein expression, and efferent projections. J Neurosci 25:6467-6477.

Tickle JA, Jenkins SI, Pickard MR, Chari DM (2015) Influence of amplitude of oscillating magnetic fields on magnetic nanoparticle-mediated gene transfer to astrocytes. Nano LIFE 4:

Tien AC, Tsai HH, Molofsky AV, McMahon M, Foo LC, Kaul A, Dougherty JD, Heintz N, Gutmann DH, Barres BA, Rowitch DH (2012) Regulated temporal-spatial astrocyte precursor cell proliferation involves BRAF signalling in mammalian spinal cord. Development 139:2477-2487.

Tisserand DJ, Pruessner JC, Sanz Arigita EJ, van Boxtel MP, Evans AC, Jolles J, Uylings HB (2002) Regional frontal cortical volumes decrease differentially in aging: an MRI study to compare volumetric approaches and voxel-based morphometry. Neuroimage 17:657-669.

Toby TK, Fornelli L, Kelleher NL (2016) Progress in Top-Down Proteomics and the Analysis of Proteoforms. Annu Rev Anal Chem (Palo Alto Calif) 9:499-519.

Tofthagen C, McAllister RD, Visovsky C (2013) Peripheral neuropathy caused by Paclitaxel and docetaxel: an evaluation and comparison of symptoms. J Adv Pract Oncol 4:204-215.

Tong J, Ang LC, Williams B, Furukawa Y, Fitzmaurice P, Guttman M, Boileau I, Hornykiewicz O, Kish SJ (2015) Low levels of astroglial markers in Parkinson's disease: relationship to alpha-synuclein accumulation. Neurobiol Dis 82:243-253.

Tosato M, Zamboni V, Ferrini A, Cesari M (2007) The aging process and potential interventions to extend life expectancy. Clin Interv Aging 2:401-412.

Trezzi JP, Galozzi S, Jaeger C, Barkovits K, Brockmann K, Maetzler W, Berg D, Marcus K, Betsou F, Hiller K, Mollenhauer B (2017) Distinct metabolomic signature in cerebrospinal fluid in early parkinson's disease. Mov Disord 32:1401-1408.

Triolo D, Dina G, Lorenzetti I, Malaguti M, Morana P, Del Carro U, Comi G, Messing A, Quattrini A, Previtali SC (2006) Loss of glial fibrillary acidic protein (GFAP) impairs Schwann cell proliferation and delays nerve regeneration after damage. J Cell Sci 119:3981-3993.

Triplett JC, Tramutola A, Swomley A, Kirk J, Grimes K, Lewis K, Orr M, Rodriguez K, Cai J, Klein JB, Perluigi M, Buffenstein R, Butterfield dopamine (2015) Age-related changes in the proteostasis network in the brain of the naked mole-rat: Implications promoting healthy longevity. Biochim Biophys Acta 1852:2213-2224.

Troncoso-Escudero P, Parra A, Nassif M, Vidal RL (2018) Outside in: Unraveling the Role of Neuroinflammation in the Progression of Parkinson's Disease. Front Neurol 9:860.

Tseng SH, Bobola MS, Berger MS, Silber JR (1999) Characterization of paclitaxel (Taxol) sensitivity in human glioma- and medulloblastoma-derived cell lines. Neuro Oncol 1:101-108.

Tysnes OB, Storstein A (2017) Epidemiology of Parkinson's disease. J Neural Transm (Vienna) 124:901-905.

Uchikubo Y, Hasegawa T, Mitani S, Kim HS, Wataya Y (2002) Mechanisms of cell death induced by 5-fluoro-2'-deoxyuridine (FUdR)--necrosis or apoptosis after treated with FUdR. Nucleic Acids Res Suppl (2):245-246.

Ullrich C, Daschil N, Humpel C (2011) Organotypic vibrosections: novel whole sagittal brain cultures. J Neurosci Methods 201:131-141.

Uman LS (2011) Systematic reviews and meta-analyses. J Can Acad Child Adolesc Psychiatry 20:57-59.

Unger MM, Spiegel J, Dillmann KU, Grundmann D, Philippeit H, Burmann J, Fassbender K, Schwiertz A, Schafer KH (2016) Short chain fatty acids and gut microbiota differ between patients with Parkinson's disease and age-matched controls. Parkinsonism Relat Disord 32:66-72.

Ungerstedt U (1968) 6-Hydroxy-dopamine induced degeneration of central monoamine neurons. Eur J Pharmacol 5:107-110.

Ustinova EE, Shurin GV, Gutkin DW, Shurin MR (2013) The role of TLR4 in the paclitaxel effects on neuronal growth in vitro. PLoS One 8:e56886.

Valente EM, Abou-Sleiman PM, Caputo V, Muqit MM, Harvey K, Gispert S, Ali Z, Del Turco D, Bentivoglio AR, Healy DG, Albanese A, Nussbaum R, Gonzalez-Maldonado R, Deller T, Salvi S, Cortelli P, Gilks WP, Latchman DS, Harvey RJ, Dallapiccola B, Auburger G, Wood NW (2004) Hereditary early-onset Parkinson's disease caused by mutations in PINK1. Science 304:1158-1160.

Valikangas T, Suomi T, Elo LL (2018) A comprehensive evaluation of popular proteomics software workflows for label-free proteome quantification and imputation. Brief Bioinform 19:1344-1355.

van Dijk KD, Berendse HW, Drukarch B, Fratantoni SA, Pham TV, Piersma SR, Huisman E, Breve JJ, Groenewegen HJ, Jimenez CR, van de Berg WD (2012) The proteome of the locus ceruleus in Parkinson's disease: relevance to pathogenesis. Brain Pathol 22:485-498.

Vasile F, Dossi E, Rouach N (2017) Human astrocytes: structure and functions in the healthy brain. Brain Struct Funct 222:2017-2029.

Venkateshappa C, Harish G, Mythri RB, Mahadevan A, Bharath MM, Shankar SK (2012) Increased oxidative damage and decreased antioxidant function in aging human substantia nigra compared to striatum: implications for Parkinson's disease. Neurochem Res 37:358-369.

Vidyadhara DJ, Yarreiphang H, Abhilash PL, Raju TR, Alladi PA (2016) Differential expression of calbindin in nigral dopaminergic neurons in two mice strains with differential susceptibility to 1-methyl-4-phenyl-1,2,3,6-tetrahydropyridine. J Chem Neuroanat 76:82-89.

Visscher M, De Henau S, Wildschut MHE, van Es RM, Dhondt I, Michels H, Kemmeren P, Nollen EA, Braeckman BP, Burgering BMT, Vos HR, Dansen TB (2016) Proteome-wide Changes in Protein Turnover Rates in C. elegans Models of Longevity and Age-Related Disease. Cell Rep 16:3041-3051.

Vizcaino JA, Foster JM, Martens L (2010) Proteomics data repositories: providing a safe haven for your data and acting as a springboard for further research. J Proteomics 73:2136-2146.

Vogt Weisenhorn DM, Giesert F, Wurst W (2016) Diversity matters - heterogeneity of dopaminergic neurons in the ventral mesencephalon and its relation to Parkinson's Disease. J Neurochem 139 Suppl 1:8-26.

von Mering C, Huynen M, Jaeggi D, Schmidt S, Bork P, Snel B (2003) STRING: a database of predicted functional associations between proteins. Nucleic Acids Res 31:258-261.

Voutsinos-Porche B, Bonvento G, Tanaka K, Steiner P, Welker E, Chatton JY, Magistretti PJ, Pellerin L (2003) Glial glutamate transporters mediate a functional metabolic crosstalk between neurons and astrocytes in the mouse developing cortex. Neuron 37:275-286.

Wallace TL, Johnson EM,Jr (1989) Cytosine arabinoside kills postmitotic neurons: evidence that deoxycytidine may have a role in neuronal survival that is independent of DNA synthesis. J Neurosci 9:115-124.

Wang MS, Davis AA, Culver DG, Glass JD (2002) WldS mice are resistant to paclitaxel (taxol) neuropathy. Ann Neurol 52:442-447.

Wang Q, Zhou Q, Zhang S, Shao W, Yin Y, Li Y, Hou J, Zhang X, Guo Y, Wang X, Gu X, Zhou J (2016) Elevated Hapln2 Expression Contributes to Protein Aggregation and Neurodegeneration in an Animal Model of Parkinson's Disease. Front Aging Neurosci 8:197.

Wang S, Kojima K, Mobley JA, West AB (2019) Proteomic analysis of urinary extracellular vesicles reveal biomarkers for neurologic disease. EBioMedicine

Wang SF, Liu LF, Wu MY, Cai CZ, Su H, Tan J, Lu JH, Li M (2017) Baicalein prevents 6-OHDA/ascorbic acid-induced calcium-dependent dopaminergic neuronal cell death. Sci Rep 7:8398-017-07142-7.

Wang XF, Cynader MS (1999) Effects of astrocytes on neuronal attachment and survival shown in a serum-free co-culture system. Brain Res Brain Res Protoc 4:209-216.

Wanner IB, Deik A, Torres M, Rosendahl A, Neary JT, Lemmon VP, Bixby JL (2008) A new in vitro model of the glial scar inhibits axon growth. Glia 56:1691-1709.

Weaver BA (2014) How Taxol/paclitaxel kills cancer cells. Mol Biol Cell 25:2677-2681.

Weinert M, Selvakumar T, Tierney TS, Alavian KN (2015) Isolation, culture and long-term maintenance of primary mesencephalic dopaminergic neurons from embryonic rodent brains. J Vis Exp (96). doi:10.3791/52475.

Weisskopf MG, Weuve J, Nie H, Saint-Hilaire MH, Sudarsky L, Simon DK, Hersh B, Schwartz J, Wright RO, Hu H (2010) Association of cumulative lead exposure with Parkinson's disease. Environ Health Perspect 118:1609-1613.

Werner CJ, Heyny-von Haussen R, Mall G, Wolf S (2008) Proteome analysis of human substantia nigra in Parkinson's disease. Proteome Sci 6:8-5956-6-8.

Wichmann T (2018) Models of Parkinson's disease revisited. Nature 557:169-170.

Wiese S, Reidegeld KA, Meyer HE, Warscheid B (2007) Protein labeling by iTRAQ: a new tool for quantitative mass spectrometry in proteome research. Proteomics 7:340-350.

Wille M, Schumann A, Wree A, Kreutzer M, Glocker MO, Mutzbauer G, Schmitt O (2015) The Proteome Profiles of the Cerebellum of Juvenile, Adult and Aged Rats--An Ontogenetic Study. Int J Mol Sci 16:21454-21485.

Willis AW, Evanoff BA, Lian M, Galarza A, Wegrzyn A, Schootman M, Racette BA (2010) Metal emissions and urban incident Parkinson disease: a community health study of Medicare beneficiaries by using geographic information systems. Am J Epidemiol 172:1357-1363.

Wilson RS, Nairn AC (2018) Cell-Type-Specific Proteomics: A Neuroscience Perspective. Proteomes 6:10.3390/proteomes6040051.

Winkelman MD, Hines JD (1983) Cerebellar degeneration caused by high-dose cytosine arabinoside: a clinicopathological study. Ann Neurol 14:520-527.

Witte H, Neukirchen D, Bradke F (2008) Microtubule stabilization specifies initial neuronal polarization. J Cell Biol 180:619-632.

Wohlan K, Goy S, Olling A, Srivaratharajan S, Tatge H, Genth H, Gerhard R (2014) Pyknotic cell death induced by Clostridium difficile TcdB: chromatin condensation and nuclear blister are induced independently of the glucosyltransferase activity. Cell Microbiol 16:1678-1692.

Xia Y, Zhang G, Han C, Ma K, Guo X, Wan F, Kou L, Yin S, Liu L, Huang J, Xiong N, Wang T (2019) Microglia as modulators of exosomal alpha-synuclein transmission. Cell Death Dis 10:174-019-1404-9.

Xiao WH, Zheng H, Zheng FY, Nuydens R, Meert TF, Bennett GJ (2011) Mitochondrial abnormality in sensory, but not motor, axons in paclitaxel-evoked painful peripheral neuropathy in the rat. Neuroscience 199:461-469.

Xie H, Huang H, Tang M, Wu Y, Huang R, Liu Z, Zhou M, Liao W, Zhou J (2018) iTRAQ-Based Quantitative Proteomics Suggests Synaptic Mitochondrial Dysfunction in the Hippocampus of Rats Susceptible to Chronic Mild Stress. Neurochem Res 43:2372-2383.

Xin H, Sha X, Jiang X, Zhang W, Chen L, Fang X (2012) Anti-glioblastoma efficacy and safety of paclitaxel-loading Angiopep-conjugated dual targeting PEG-PCL nanoparticles. Biomaterials 33:8167-8176.

Xing L, Wang D, Wang L, Lan W, Pan S (2015) Differential proteomics analysis of mononuclear cells in cerebrospinal fluid of Parkinson's disease. Int J Clin Exp Pathol 8:15462-15466.

Xing Y, Sapuan A, Dineen RA, Auer DP (2018) Life span pigmentation changes of the substantia nigra detected by neuromelanin-sensitive MRI. Mov Disord 33:1792-1799.

Xiong Y, Zhang Y, Iqbal J, Ke M, Wang Y, Li Y, Qing H, Deng Y (2014) Differential expression of synaptic proteins in unilateral 6-OHDA lesioned rat model-A comparative proteomics approach. Proteomics 14:1808-1819.

Xu B, Gao Y, Zhan S, Xiong F, Qiu W, Qian X, Wang T, Wang N, Zhang D, Yang Q, Wang R, Bao X, Dou W, Tian R, Meng S, Gai WP, Huang Y, Yan XX, Ge W, Ma C (2016a) Quantitative protein profiling of hippocampus during human aging. Neurobiol Aging 39:46-56.

Xu B, Xiong F, Tian R, Zhan S, Gao Y, Qiu W, Wang R, Ge W, Ma C (2016b) Temporal lobe in human aging: A quantitative protein profiling study of samples from Chinese Human Brain Bank. Exp Gerontol 73:31-41.

Xu L, Pu J (2016) Alpha-Synuclein in Parkinson's Disease: From Pathogenetic Dysfunction to Potential Clinical Application. Parkinsons Dis 2016:1720621.

Xu Q, Park Y, Huang X, Hollenbeck A, Blair A, Schatzkin A, Chen H (2010) Physical activities and future risk of Parkinson disease. Neurology 75:341-348.

Xuan Q, Xu SL, Lu DH, Yu S, Zhou M, Ueda K, Cui YQ, Zhang BY, Chan P (2011) Increased expression of alpha-synuclein in aged human brain associated with neuromelanin accumulation. J Neural Transm (Vienna) 118:1575-1583.

Yamada T, McGeer PL, Baimbridge KG, McGeer EG (1990) Relative sparing in Parkinson's disease of substantia nigra dopamine neurons containing calbindin-D28K. Brain Res 526:303-307.

Yang AC, Tsai SJ, Liu ME, Huang CC, Lin CP (2016) The Association of Aging with White Matter Integrity and Functional Connectivity Hubs. Front Aging Neurosci 8:143.

Yang F, Shen Y, Camp DG, Smith RD (2012) High-pH reversed-phase chromatography with fraction concatenation for 2D proteomic analysis. Expert Rev Proteomics 9:129-134.

Yang H, Cong R, Na L, Ju G, You SW (2010) Long-term primary culture of highly-pure rat embryonic hippocampal neurons of low-density. Neurochem Res 35:1333-1342.

Yang H, Hao D, Liu C, Huang D, Chen B, Fan H, Liu C, Zhang L, Zhang Q, An J, Zhao J (2019) Generation of functional dopaminergic neurons from human spermatogonial stem cells to rescue parkinsonian phenotypes. Stem Cell Res Ther 10:195-019-1294-x.

Yang IH, Siddique R, Hosmane S, Thakor N, Hoke A (2009) Compartmentalized microfluidic culture platform to study mechanism of paclitaxel-induced axonal degeneration. Exp Neurol 218:124-128.

Yang S, Liu T, Li S, Zhang X, Ding Q, Que H, Yan X, Wei K, Liu S (2008) Comparative proteomic analysis of brains of naturally aging mice. Neuroscience 154:1107-1120.

Yang Z, Wang KK (2015) Glial fibrillary acidic protein: from intermediate filament assembly and gliosis to neurobiomarker. Trends Neurosci 38:364-374.

Yetnikoff L, Lavezzi HN, Reichard RA, Zahm DS (2014) An update on the connections of the ventral mesencephalic dopaminergic complex. Neuroscience 282C:23-48.

Yoritaka A, Hattori N, Uchida K, Tanaka M, Stadtman ER, Mizuno Y (1996) Immunohistochemical detection of 4-hydroxynonenal protein adducts in Parkinson disease. Proc Natl Acad Sci U S A 93:2696-2701.

Yuan HH, Chen RJ, Zhu YH, Peng CL, Zhu XR (2013) The neuroprotective effect of overexpression of calbindin-D(28k) in an animal model of Parkinson's disease. Mol Neurobiol 47:117-122.

Zanchi D, Giannakopoulos P, Borgwardt S, Rodriguez C, Haller S (2017) Hippocampal and Amygdala Gray Matter Loss in Elderly Controls with Subtle Cognitive Decline. Front Aging Neurosci 9:50.

Zecca L, Casella L, Albertini A, Bellei C, Zucca FA, Engelen M, Zadlo A, Szewczyk G, Zareba M, Sarna T (2008a) Neuromelanin can protect against iron-mediated oxidative damage in system modeling iron overload of brain aging and Parkinson's disease. J Neurochem 106:1866-1875.

Zecca L, Wilms H, Geick S, Claasen JH, Brandenburg LO, Holzknecht C, Panizza ML, Zucca FA, Deuschl G, Sievers J, Lucius R (2008b) Human neuromelanin induces

neuroinflammation and neurodegeneration in the rat substantia nigra: implications for Parkinson's disease. Acta Neuropathol 116:47-55.

Zecca L, Fariello R, Riederer P, Sulzer D, Gatti A, Tampellini D (2002) The absolute concentration of nigral neuromelanin, assayed by a new sensitive method, increases throughout the life and is dramatically decreased in Parkinson's disease. FEBS Lett 510:216-220.

Zecca L, Tampellini D, Gerlach M, Riederer P, Fariello RG, Sulzer D (2001) Substantia nigra neuromelanin: structure, synthesis, and molecular behaviour. Mol Pathol 54:414-418.

Zelenika D, Grima B, Brenner M, Pessac B (1995) A novel glial fibrillary acidic protein mRNA lacking exon 1. Brain Res Mol Brain Res 30:251-258.

Zhang S, Wang R, Wang G (2019) Impact of Dopamine Oxidation on Dopaminergic Neurodegeneration. ACS Chem Neurosci 10:945-953.

Zhang X, Yin X, Yu H, Liu X, Yang F, Yao J, Jin H, Yang P (2012) Quantitative proteomic analysis of serum proteins in patients with Parkinson's disease using an isobaric tag for relative and absolute quantification labeling, two-dimensional liquid chromatography, and tandem mass spectrometry. Analyst 137:490-495.

Zhang Y, Fonslow BR, Shan B, Baek MC, Yates JR (2013) Protein analysis by shotgun/bottom-up proteomics. Chem Rev 113:2343-2394.

Zhang Y, Sloan SA, Clarke LE, Caneda C, Plaza CA, Blumenthal PD, Vogel H, Steinberg GK, Edwards MS, Li G, Duncan JA, Cheshier SH, Shuer LM, Chang EF, Grant GA, Gephart MG, Barres BA (2016) Purification and Characterization of Progenitor and Mature Human Astrocytes Reveals Transcriptional and Functional Differences with Mouse. Neuron 89:37-53.

Zhang Z, Zoltewicz JS, Mondello S, Newsom KJ, Yang Z, Yang B, Kobeissy F, Guingab J, Glushakova O, Robicsek S, Heaton S, Buki A, Hannay J, Gold MS, Rubenstein R, Lu XC, Dave JR, Schmid K, Tortella F, Robertson CS, Wang KK (2014) Human traumatic brain injury induces autoantibody response against glial fibrillary acidic protein and its breakdown products. PLoS One 9: e92698.

Zhao X, Xiao WZ, Pu XP, Zhong LJ (2010) Proteome analysis of the sera from Chinese Parkinson's disease patients. Neurosci Lett 479:175-179.

Zimprich A, Biskup S, Leitner P, Lichtner P, Farrer M, Lincoln S, Kachergus J, Hulihan M, Uitti RJ, Calne DB, Stoessl AJ, Pfeiffer RF, Patenge N, Carbajal IC, Vieregge P, Asmus F, Muller-Myhsok B, Dickson DW, Meitinger T, Strom TM, Wszolek ZK, Gasser T (2004) Mutations in LRRK2 cause autosomal-dominant parkinsonism with pleomorphic pathology. Neuron 44:601-607.

Zoltewicz JS, Mondello S, Yang B, Newsom KJ, Kobeissy F, Yao C, Lu XC, Dave JR, Shear dopamine, Schmid K, Rivera V, Cram T, Seaney J, Zhang Z, Wang KK, Hayes RL, Tortella FC (2013) Biomarkers track damage after graded injury severity in a rat model of penetrating brain injury. J Neurotrauma 30:1161-1169.

Zoltewicz JS, Scharf D, Yang B, Chawla A, Newsom KJ, Fang L (2012) Characterization of Antibodies that Detect Human GFAP after Traumatic Brain Injury. Biomark Insights 7:71-79.

Zubarev RA, Kelleher NL, McLafferty FW (1998) Electron capture dissociation of multiply charged protein cations. A nonergodic process. J Am Chem Soc 120:3265-3266.

Zucca FA, Vanna R, Cupaioli FA, Bellei C, De Palma A, Di Silvestre D, Mauri P, Grassi S, Prinetti A, Casella L, Sulzer D, Zecca L (2018) Neuromelanin organelles are specialized autolysosomes that accumulate undegraded proteins and lipids in aging human brain and are likely involved in Parkinson's disease. NPJ Parkinsons Dis 4:17-018-0050-8. eCollection 2018.

Zuchero JB (2014) Purification and culture of dorsal root ganglion neurons. Cold Spring Harb Protoc 2014:813-814.

Zweig RM, Jankel WR, Hedreen JC, Mayeux R, Price DL (1989) The pedunculopontine nucleus in Parkinson's disease. Ann Neurol 26:41-46.

Appendices

Annex 1

Table 1: Gene Ontology analysis of the 608 dysregulated proteins in the juvenile SN compared to old in rats, showing the 50 most enriched terms according to their p-value. BP: biological process. CC: Cellular component. MF: molecular function. KEGG pathway. Proteins are presented with the uniprot accession number. The entire list of terms and proteins associated to each term can be consulted in Supplementary Table 3b.

BP	Count	%	PValue	Genes
translation	54	8.881578947	8.84E-19	P20280, P35427, P62859, P62755, P62278, P24050, P61354, P62752, P27952, P09895, Q63507, P62850, P16036, P24049, P62268, P04644, P62425, P50878, P23358, P68101, P61928, P62282, P2153
tricarboxylic acid cycle	15	2.467105263	1.12E-13	P41565, P41562, O88989, Q8VHF5, P49432, P26284, Q63270, P14408, Q9ER34, Q06437, P08461, Q68FX0, P04636, P13086, Q99NA5
cell-cell adhesion	33	5.427631579	1.09E-12	Q68FR6, P30427, Q6AXS5, Q6IE36, P06761, P61980, Q68FR9, Q5PPJ9, O88767, Q9QZR6, P34058, Q66HR2, Q2HWF0, P61314, O35244, Q9QY17, P12785, P41562, Q9QWN8, Q99MZ8, Q8NYB7, Q8
substantia nigra development	16	2.631578947	2.96E-11	P02688, Q05175, P62161, Q8VBU2, P07335, P60203, P13233, P19643, P06761, P23565, P19511, Q5RJQ4, P20717, P68255, P07722, P68511
glutathione metabolic process	15	2.467105263	1.24E-09	Q9ZOW7, Q68FR6, P41562, P04906, P07632, P04904, P04041, P51650, Q9Z1B2, O35952, P57113, P02091, P07895, P08009, Q91XR8
cell adhesion	32	5.263157895	1.36E-09	Q5I6B8, P55068, P97603, P40241, Q05546, Q05695, P97686, Q63374, P07897, Q63372, P32736, P22063, P07340, Q68FQ2, Q64605, P08592, Q99P82, Q9ESM2, P15800, Q9WU82, P03994, P13596, P
response to drug	47	7.730263158	4.89E-09	Q9JIS4, P04904, B2GV06, O35274, P19643, P63159, P31652, P68403, P18266, P04762, P12232, O88767, Q9WVK7, P09034, P34058, P07897, P70645, P06687, P07895, P06685, P16970, P05369, P18
brain development	33	5.427631579	1.36E-08	Q9JIS4, P11030, P07335, B2GV06, P21588, P10687, P17764, B5DF41, P31652, P40241, Q9QXU9, P13668, O08875, P30009, Q9ESI7, P84076, P50878, Q5XI22, Q4V8C3, P45479, O35263, P63090, P16
ribosomal small subunit biogenesis	9	1.480263158	3.11E-08	P62850, P13084, P17074, P04644, P62859, P62755, P62083, P62250, P62845
neurotransmitter secretion	11	1.809210526	1.60E-07	P45479, P09951, P61765, Q91Z79, Q9QUL6, Q63374, Q05140, Q63372, P60881, P29101, Q63537
learning	14	2.302631579	2.72E-07	P22063, Q9Z2L0, P63090, O35274, Q62889, P10687, O54701, P61751, P12369, Q63228, P04177, P31424, Q63372, Q9R1Z0
NADH metabolic process	7	1.151315789	1.16E-06	P41565, Q68FX0, P04636, Q99NA5, O88989, O35077, P46462
aging	30	4.934210526	1.19E-06	P04904, P02688, Q99376, P04904, O35274, P04041, P61980, P62630, P18266, Q6P6R2, P04762, P09034, P07895, Q91XR8, P22062, P68101, P07632, P02650, O35458, Q3T1J1, P13233, P11915, P31
response to estradiol	23	3.782894737	1.39E-06	Q9JIS4, P04094, P14925, P04906, P63090, O35274, P07323, P04041, P31652, Q9WU82, P11915, P29147, P18266, P18418, P04762, P31000, P04177, P09034, Q6P6V0, P23928, P05197, Q91XR8, Q6
response to ethanol	22	3.618421053	2.64E-06	P04094, P22062, Q07439, P16975, P07632, P02650, P04906, P49242, B2GV06, P19643, P68403, P11598, P00507, P27952, P29147, P04762, P04177, P05197, P62703, P61314, P50554, P62907
response to toxic substance	17	2.796052632	2.67E-06	P04094, P02688, P04906, P21708, P13233, P04041, P19527, P19643, P14173, P31652, P29147, P04762, P09034, P70545, O35331, Q80XF7, P63086
cellular oxidant detoxification	13	2.138157895	3.14E-06	O88767, P04762, P11232, Q9R063, Q6AXX6, P04906, P02650, Q9ZOV6, P04041, P57113, O35244, P08009, Q91XR8
locomotory behavior	16	2.631578947	3.22E-06	Q01066, P04094, Q04400, P07632, P08592, O35430, P31652, P60881, P07171, P43425, Q63228, P04177, P31424, P59215, P07895, P50554
rRNA processing	13	2.138157895	3.67E-06	P62850, Q63507, P12749, P62914, P17074, P04644, P62859, P62755, P62083, P05426, P62250, P62845, P09895
glycolytic process	10	1.644736842	4.78E-06	P05708, Q9JJH5, P47858, Q6P6V0, P04797, P07323, P48500, P16617, P11980, P25113
liver development	18	2.960526316	8.69E-06	Q9JIS4, Q9JIL3, Q63413, P63090, P17764, Q09167, Q63270, P61980, Q9ER34, Q9WU82, P29147, P17425, P09034, P97532, P07895, P11348, Q5XI22, P11980
neuron projection development	18	2.960526316	9.53E-06	P0C5H9, P22063, Q9Z270, P08592, O35274, P15800, P63159, Q9ER24, P16884, Q05695, Q8K4Y5, P13596, P13668, P59215, P97846, Q641Z6, Q63198, Q91Y81
negative regulation of neuron projection development	12	1.973684211	1.06E-05	P18266, Q05546, Q00657, P31000, Q04400, P49911, Q62952, P07722, P61265, Q62950, P47819, Q62718
ribosomal small subunit assembly	10	1.644736842	1.13E-05	P17074, P04644, P62859, P62755, P24050, P63326, P62853, P38983, P27952, P62845
response to hydrogen peroxide	13	2.138157895	1.17E-05	O88767, P04762, P07632, P10686, Q9ZOV6, P59215, P01946, P04041, P07895, P23928, P02091, P05197, Q01728
2-oxoglutarate metabolic process	7	1.151315789	1.34E-05	P41565, Q6P6R2, P13221, P41562, Q68FX0, Q99NA5, P00507
liver regeneration	11	1.809210526	1.38E-05	P13383, P62850, P13084, P41123, Q09167, P84100, P05426, P62250, P62845, Q6PDV7, P12001
nervous system development	21	3.453947368	1.50E-05	P45479, Q8R511, P08592, Q8VBU2, P47875, P63159, Q9ER24, P23565, Q05546, P19234, O08875, Q07266, Q62952, Q62696, P07722, P31596, Q80ZA5, P07936, Q62936, Q2HWF0, Q63227
Bergmann glial cell differentiation	6	0.986842105	1.72E-05	P31000, P21708, P47819, P41499, Q01986, P63086
isocitrate metabolic process	5	0.822368421	1.86E-05	P41565, P41562, Q68FX0, Q99NA5, Q9ER34
hydrogen peroxide catabolic process	7	1.151315789	1.95E-05	P04762, Q9R063, Q9ZOV6, P01946, P04041, P02091, O35244
response to reactive oxygen species	7	1.151315789	5.22E-05	P04762, P07632, P04906, Q63259, P04041, P07895, O35244
actin filament organization	12	1.973684211	6.19E-05	Q912N1, Q9Z1P2, P45592, Q9Z0W5, Q07266, P30009, Q5RJL0, Q5U301, Q62696, O35274, P97710, O35413
oxaloacetate metabolic process	6	0.986842105	6.86E-05	P13221, P04636, P52873, O88989, Q8VHF5, P00507
ribosomal large subunit assembly	8	1.315789474	8.03E-05	P21531, P21533, P62914, P83732, P23358, P62752, Q6PDV7, P09895
hippocampus development	13	2.138157895	8.73E-05	P18266, Q62656, D3ZPX4, Q64605, O35458, P55068, Q9ESI7, O35274, Q7TQ16, P16884, P19527, P12839, P61980
gluconeogenesis	8	1.315789474	9.90E-05	Q6P6V0, P04797, P07323, P52873, O35077, P48500, P16617, P25113
cellular response to drug	13	2.138157895	1.07E-04	Q01062, Q99376, O35274, P13852, P06761, P14173, P20651, P62630, P63329, P11232, P04177, P34058, P11348
protein homooligomerization	19	3.125	1.20E-04	P14925, P14668, P17764, P35559, P13852, P47863, P84586, P31652, P62630, Q9Z1E1, P09606, Q8K4Y5, Q03344, P13084, Q62952, P07895, P23928, Q641Z6, P46462
response to oxidative stress	16	2.631578947	1.34E-04	Q812D1, P41562, P02650, P07632, P08592, Q9ZOV6, P13852, P04041, Q01986, P04762, O88767, Q9R063, P07895, P62909, P28075, Q91XR8
response to amphetamine	9	1.480263158	1.40E-04	Q01066, P07632, P04177, Q6J4I0, P62161, O35274, P47942, P20651, P63329
relaxation of cardiac muscle	5	0.822368421	1.44E-04	P07340, P11507, P15791, P06686, P06685
central nervous system development	13	2.138157895	1.58E-04	P22063, P02688, P14925, P55068, Q9ESM2, P51650, P61980, P03994, O08719, P97686, Q5RJQ4, P07897, Q9ERB4
response to gravity	6	0.986842105	1.95E-04	P16975, P10686, P07897, P32851, P33124, P11980
acetyl-CoA biosynthetic process from pyruvate	5	0.822368421	2.34E-04	Q6P6R2, P49432, P26284, Q06437, P08461
neurofilament cytoskeleton organization	5	0.822368421	2.34E-04	P07632, P16884, P19527, P12839, P23565
cellular response to interleukin-4	7	1.151315789	2.40E-04	P21531, Q912N1, P12785, P19945, P34058, P06761, P27952
response to activity	12	1.973684211	2.79E-04	Q8CGU9, P18266, Q9WVK7, P04762, P11232, P04177, Q07266, P63090, B2GV06, P07895, P61980, Q9WU82
cell redox homeostasis	10	1.644736842	2.92E-04	P04785, Q5XIK2, P11232, Q6P6R2, Q9R063, Q9Z0V6, P04041, P11598, O35244, Q63081
positive regulation of translation	10	1.644736842	2.92E-04	Q9JIS4, P13084, Q63413, P49242, P21708, Q7TP47, P02401, P05197, P62703, P63086

CC	Count	%	PValue	Genes
extracellular exosome	309	50.82236842	2.96E-105	Q7TPB1, D3ZAF6, Q6P502, B5DEH2, P50408, P62859, P24050, Q6IRE4, P62752, P27952, P40241, Q5BKB1, P09895, P43425, Q63507, Q4FZT9, F1LMZ8, P13086, Q9JI66, P61765, Q9QX69, P06685, P
myelin sheath	88	14.47368421	4.28E-78	P02688, Q9Z2L0, P42123, Q6P502, P63322, P37805, Q6IE36, P54313, P23565, P26284, P08461, P12075, P16036, Q6P6R2, P09034, P61765, Q99NA5, Q6P6V0, P97685, P19804, P06686, Q63357, P0
membrane	210	34.53947368	4.08E-50	P50408, P62755, P24050, P27952, P40241, P09895, Q63507, P62850, Q4FZT9, F1LMZ8, P13084, P62268, Q6JP77, P06686, P06685, Q9QYJ6, Q641Y0, P12785, P68101, Q9Z270, P13852, P13596, P41
cytoplasm	334	54.93421053	4.03E-45	Q7TPB1, Q6P502, B5DEH2, P62859, P62755, Q6IRE4, P62752, P27952, Q9QXY2, P09895, Q63507, P62850, P13084, Q9JHU0, P13086, P61765, P62268, Q6JP77, P06686, Q9QX69, P06687, Q4KMA2,
focal adhesion	84	13.81578947	1.74E-43	Q5I6B8, Q9EPH8, P35427, P63322, P19945, P62278, P63326, P54313, P24050, P61354, P27952, P40241, P09895, Q9QXY2, Q05695, Q9Z1P2, P13084, P04644, P19804, P62425, P97685, P50878, P23
mitochondrion	146	24.01315789	5.57E-31	D3ZAF6, Q9Z2L0, P42123, P26284, Q5BKB1, P12075, P09034, P13086, P61765, P19804, Q8CG45, Q8AYE2, P41565, P12785, P29266, P41562, P16975, P07632, Q5I0P2, Q9Z0V6, P16884, Q9QYU2, Q
cytosol	144	23.68421053	3.14E-30	P47858, P49911, Q6IE36, F1LMZ8, P13084, P13086, P61765, Q6P6V0, Q6JP77, Q9QY17, P12785, P45479, Q9Z5N3, P41562, P07632, P63041, Q9Z0V6, Q5U211, P34925, Q63270, Q6NYB7, P27139,
neuronal cell body	66	10.85526316	4.52E-20	P04094, P02688, Q7TP47, B5DF41, P97839, Q9ER24, P14173, P97603, P35053, A7VJC2, Q9QXY2, Q05695, P11232, Q9JHU0, Q6J4I0, P09034, Q63357, Q80ZA5, Q63259, Q9QYJ6, Q62936, P55051, P
neuron projection	53	8.717105263	5.11E-18	B5DF41, P63159, A7VJC2, Q9QXY2, O88767, P09034, Q6P6V0, Q9ESI7, P06686, Q63357, P12839, Q9WVC0, Q9ZZI6, P45479, P07632, O88871, P07323, P32851, P07171, P60881, P31000, O88778, P
axon	49	8.059210526	8.31E-17	P04094, P14173, Q9QXY2, Q05695, O88767, P11232, P97686, P97685, P06687, Q63357, P84076, P12839, P18088, Q912N1, P45479, P16884, P07171, P27139, Q01986, P60881, P29101, P11275, P31
cell-cell adherens junction	41	6.743421053	1.90E-16	Q68FR6, P30427, Q6AXS5, Q6IE36, P04218, P06761, P61980, Q68FR9, Q5PPJ9, O88767, Q9QZR6, P34058, Q66HR2, Q2HWF0, P61314, O35244, Q9QY17, Q1WIM3, P12785, P41562, Q9QWN8, Q95
proteasome complex	21	3.453947368	1.23E-15	Q9JIP9, Q63570, B0BN93, P60901, P40307, P18421, P62198, P18420, Q9JHW0, Q63569, P17220, P48004, P40112, Q4FZT9, F1LMZ8, Q63347, Q4KMA2, O88761, P28075, P62193, P46462
perinuclear region of cytoplasm	65	10.69078947	1.51E-15	P0C5H9, Q5RKI1, P49911, P62755, Q6IE36, P54313, Q9ER24, O88767, P11507, P19804, Q925N3, Q9Z270, Q63560, P63090, O35430, Q5XIT1, P60881, P05964, Q01986, P68182, Q63569, P18418, P3
cytosolic large ribosomal subunit	32	5.263157895	7.40E-15	P20280, P35427, P62902, P19945, P02401, P61354, P62752, P84100, P05426, P63174, P09895, Q63507, P24049, P62425, P62832, P50878, P23358, P61314, P12001, P62907, P83732, P61928, P2153
intracellular ribonucleoprotein complex	27	4.440789474	1.18E-14	Q9JIS4, Q9EPH8, P35427, P49242, P19945, P04797, P62755, Q7TP47, P24050, P61354, P27952, P05426, A7VJC2, P09895, P18266, P13084, P62425, P50878, P62909, P62703, Q5SGE0, P62243, P620
synapse	41	6.743421053	1.87E-14	Q9Z0W5, P84060, P55068, P62483, P97839, Q9QXY2, P97686, P30009, P06686, P06687, Q63259, Q62936, P18088, P22063, Q9WVC0, P45479, P25304, O35458, P08592, P63041, Q62889, P15800, P
ribosome	28	4.605263158	3.64E-13	P20280, P35427, P68101, P62755, P61354, P62752, P62083, P05426, P27952, P62282, P21531, P62850, Q63507, P21533, P62914, P17074, P62268, P04644, P62425, P17077, P62832, P23358, P6285
cytosolic small ribosomal subunit	24	3.947368421	4.85E-13	P49242, P62859, P62755, P62278, P24050, P63326, P62083, P27952, P62282, P62850, P62246, P17074, P04644, P62268, P01946, P62853, P29314, P38983, P62250, P62909, P62703, P62845, P60868
nucleus	238	39.14473684	7.21E-13	D3ZAF6, P37805, Q641X8, Q8K3E7, P62755, Q6IRE4, P62752, P27952, P26284, P09895, P62850, P24049, Q4FZT9, F1LMZ8, P13084, Q6JP77, P06687, P62853, O08629, P16975, P68101, P07632, P84
membrane raft	36	5.921052632	2.24E-12	Q04400, Q9Z2L0, P42123, Q01062, B5DEH2, P31652, P35053, P16617, P18266, Q05546, P85125, Q05695, O88767, P11167, P08050, P61227, P06685, Q9JI19, P29457, P10824, P45479, P26431, P085
small ribosomal subunit	14	2.302631579	5.10E-12	P62850, P13084, P62268, P62859, P62755, P24050, P63245, P29314, P62853, P38983, P62250, P62703, P62845, P60868
microtubule	33	5.427631579	8.89E-12	Q7TPB1, Q5PPN5, Q6P502, Q6IE36, P62483, Q9QXU8, P18266, P13668, P30009, Q9ESI7, Q9QZR6, Q66HR2, P69897, Q63525, Q99JD4, Q5SGE0, Q4V8C3, Q01728, P02650, Q63560, P37285, Q5XIM
melanosome	20	3.289473684	7.32E-11	P04785, Q7TPB1, P12785, P60905, O35783, Q63584, Q99376, P13233, P06761, P11598, Q9QZA2, Q6NYB7, Q9Z1E1, Q63081, P24368, P11167, Q66X93, P34058, Q66HD0, P07153
synaptic vesicle	23	3.782894737	1.92E-10	Q9Z2I6, P60905, P11030, P45479, Q9Z2L0, O35458, P08592, Q9QWN8, O35430, P14668, P32851, Q05140, P14173, P60881, P29101, P81155, P09951, O08839, P04177, P61265, Q63259, Q9R1Z0, Q
extracellular matrix	32	5.263157895	2.82E-10	P30427, P62278, P24050, P06761, P61980, P48679, P45592, P69897, P07897, P62832, P62703, P62804, P04785, P25304, P07632, P02650, P15800, Q5XIM9, P62282, P61751, P03994, P18418, P3100
cell body	20	3.289473684	2.87E-10	Q9WVC0, Q7TPB1, P55051, Q07439, P02696, Q6P502, P62755, Q5XIM9, P54313, P07171, P18266, O88767, P09606, P31000, Q62952, P69897, Q9R066, P59215, P63245, P47819
terminal bouton	22	3.618421053	3.03E-10	P60905, Q9Z0W5, P63041, P08592, Q05140, P09527, P07171, P60881, P29101, P02625, Q05695, P12749, P09951, P04177, Q9QUL6, P61765, P84087, Q9Z2P6, P47942, P47728, P54921, Q63537
cortical actin cytoskeleton	14	2.302631579	8.69E-10	Q912N1, Q99MZ8, O35274, Q08163, Q7M0E3, P62630, Q9Z1E1, Q9Z1P2, P45592, P11167, Q9Z2S9, Q9Z1Y3, P52481, Q63327
mitochondrial inner membrane	35	5.756578947	8.92E-10	P13437, D3ZAF6, Q9Z2L0, P52873, P17764, P19643, P00507, Q68FX9, P12075, P16036, Q9WVK7, P13086, P97521, P16970, P07895, P62909, Q91XR8, P38718, Q3KR86, P13233, P29147, P81155, P
protein complex	51	8.388157895	2.43E-09	Q9Z2L0, P04906, B5DEH2, P54313, P11507, Q9JHU0, P61765, P13086, Q6JP77, P69897, P06685, Q641Y0, Q6AYE2, Q912N1, Q9WVC0, P09456, P07632, P63041, O35430, P32851, P20651, P18418, P
mitochondrial matrix	23	3.782894737	1.11E-08	P13437, Q01062, B2GV06, P52873, P17764, Q8VHF5, P49432, Q9QYU2, P00507, Q06437, Q68FX9, P08461, P29147, Q9WVK7, Q6P6R2, O88767, P04636, P15650, P14604, O35952, P05369, P62909,
postsynaptic density	28	4.605263158	1.96E-08	O35274, P62483, P61980, Q9QXY2, P18266, O08875, P31424, P31422, P12839, P06685, Q62936, P16884, Q05140, P34926, P11275, Q05764, P09951, O88778, Q07266, D4A208, Q9QUL6, Q62696, C
dendrite	42	6.907894737	2.25E-08	P04094, Q9EPH8, Q01062, P55068, P19945, P07335, P62755, P97839, Q9ER24, Q9QXY2, P18266, Q05695, P11232, Q9JHU0, Q9ESI7, Q62950, Q99PF5, P62909, Q5UZ23, P45479, Q925N3, P02650, C
proteasome accessory complex	9	1.480263158	2.32E-08	Q4FZT9, F1LMZ8, Q63570, B0BN93, Q63347, P62198, O88761, P62193, Q63569
intercalated disc	13	2.138157895	6.56E-08	Q7M730, P07340, P26431, P14668, Q9WU82, P11507, P15791, P08050, Q9R066, P06686, P06685, Q9Z1Y3, Q01728
growth cone	21	3.453947368	7.72E-08	Q05175, P37285, P62161, P08592, Q8VBU2, O35274, P19527, P60881, P18266, P13596, Q62656, Q07266, Q5RUQ4, P30009, Q62952, Q9R066, A0MZ67, Q62950, P07936, P47942, Q62936
perikaryon	21	3.453947368	8.65E-08	P04094, P22062, P14925, P07323, P14668, P16884, P00507, Q01986, A7VJC2, P09606, P04177, Q5RUQ4, P09034, A0MZ67, Q63259, P84076, P63245, P12839, P23928, Q9QYJ6, P63086
proteasome core complex	9	1.480263158	1.73E-07	P17220, P48004, P40112, P60901, P40307, P18421, P18420, Q9JHW0, P28075
smooth endoplasmic reticulum	10	1.644736842	2.23E-07	P18418, P24368, P04177, P08592, Q63357, P05761, P11598, Q66HD0, Q63617, Q63081
proteasome regulatory particle, base subcomplex	7	1.151315789	9.26E-07	Q4FZT9, Q63570, Q63347, P62198, O88761, P62193, Q63569
cell junction	34	5.592105263	1.93E-06	Q05175, Q9Z0W5, P62483, B5DF41, P61980, Q9QXY2, Q9Z1P2, P08050, Q63372, Q63259, Q9ZI6, P25304, D3ZPX4, O88871, Q9QWN8, Q62889, P32851, P62024, P60881, P29101, P11275, Q9WU8
cell projection	15	2.467105263	2.75E-06	P02688, P55051, P10686, P14668, P13233, Q00657, Q9Z1P2, P09606, P31000, Q66HR2, O35964, O88831, P47819, Q01728, Q91Y81
lamellipodium	19	3.125	3.24E-06	Q912N1, P10686, O35274, Q9Z1E1, P60881, Q9WU82, Q9QXY2, P45592, Q9Z1P2, Q62656, O08719, Q07266, D4A208, Q62952, P19804, A0MZ67, Q9Z2S9, O35413, Q9Z1Y3
cell-cell junction	21	3.453947368	3.99E-06	Q9QY17, Q912N1, Q9Z0W7, Q1WIM3, P55051, Q68FQ2, P10686, P08592, P47863, Q7TT49, Q9WU82, Q9Z1P2, P13596, P45592, P11167, Q07266, P08050, Q9R066, Q62696, Q62936, Q9Z1Y3
extracellular vesicle	11	1.809210526	4.06E-06	P22062, P07340, P02650, Q99376, P06686, P06687, P06685, Q9QZA2, P40241, P47727, P11980
basolateral plasma membrane	22	3.618421053	4.51E-06	P22062, P07340, Q07439, P26431, Q99376, P06907, P47863, P27139, Q9Z1E1, Q9WU82, P11167, Q9JI66, Q9R066, Q62696, P34058, Q63357, Q80ZA5, P06685, Q9Z2S9, Q62936, Q9Z1Y3, Q01728
presynaptic membrane	13	2.138157895	4.57E-06	Q05695, Q01062, Q05683, Q62696, P31596, B5DF41, P31422, P61265, P32851, Q05140, Q63372, P60881, P11275
nuclear matrix	14	2.302631579	6.94E-06	Q9ZOW7, P70615, P16975, Q63413, P60901, P49911, Q9QWN8, P48679, P31000, P45592, P13084, Q62826, P43244, Q5FVM4
dendritic spine	18	2.960526316	7.02E-06	P08592, O35274, O35430, P61980, P18266, P61751, Q9Z1P2, Q62656, P12369, Q07266, P30009, P31424, Q6GMN2, P31596, P06686, P31422, P23928, Q01728

MF	Count	%	PValue	Genes
protein binding	189	31.08552632	3.67E-54	Q9Z2L0, P42123, Q8R511, Q8K3E7, P62859, P24050, O35550, P35053, P40241, A7VJC2, P09895, Q9QXY2, O88453, Q9IHU0, P13084, P61765, P62268, Q6JP77, P06686, P06687, P50878, P06685, Q8
poly(A) RNA binding	138	22.69736842	3.30E-39	Q7TPB1, Q5P502, P49911, P62859, P62755, P24050, P62752, P27952, D3ZBN0, A7VJC2, P09895, O88453, P62850, Q63507, P24049, P13084, P09034, P13086, P61765, P62268, P50878, P62853, O0
structural constituent of ribosome	58	9.539473684	1.28E-18	P20280, P35427, P19945, P62859, P62755, P62278, P63326, P24050, P61354, P62752, P27952, P09895, Q63507, P62850, P16036, P24049, P62268, P04644, P50878, P23358, P62853, P61314, P6192
cadherin binding involved in cell-cell adhesion	35	5.756578947	3.63E-13	Q68FR6, P30427, Q6AXS5, Q6JE36, P06761, P61980, Q68FR9, Q5PPJ9, O88767, Q9QZR6, P34058, Q66HR2, Q2HWF0, P61314, O35244, Q9QY17, P12785, P41562, Q9QWN8, Q99MZ8, Q6NYB7, Q9
protein domain specific binding	35	5.756578947	4.43E-09	Q05175, Q9JJP9, P97839, P06761, P14173, P61980, Q9QXY2, Q9Z1P2, P63100, P61765, P08050, P97685, Q6JP77, P69897, Q63357, P61265, P61227, P06685, Q62936, P62804, Q9JIJ9, Q9Z270, P62
enzyme binding	39	6.414473684	1.49E-08	P04797, P10687, P17764, Q9ER24, P06761, P14173, P00507, P27952, P63329, Q9Z1B2, P33124, P04762, P11232, O88767, P11507, P13084, P19804, P07895, Q8VHV7, P62909, P08009, P04785, Q6A
identical protein binding	53	8.717105263	2.74E-08	P42123, Q8R511, P47858, Q8K3E7, Q9ER24, Q9Z1B2, Q05695, O88767, P11167, P61765, P09034, Q66HR2, Q6AYE2, Q91ZN1, Q9QY17, Q9WVC0, P12785, P02650, P07632, Q92DV6, P13852, Q5XIT
protein homodimerization activity	61	10.03289474	3.60E-08	P47858, Q8K3E7, P17764, Q6IRE4, P04218, O35077, O35550, Q9Z1B2, O88767, Q9Z1P2, Q03344, P13084, Q6AYE2, Q91ZN1, P12785, Q68FQ2, Q66H12, P41562, P02650, P07323, Q9QZA2, P05964,
mRNA binding	22	3.618421053	6.39E-08	Q9JIJ4, Q9EPH8, P35427, Q6URK4, P49242, P62755, P62278, P24050, P84586, P27952, Q68A21, Q63270, P62630, P05426, P09895, P18418, O88767, P21533, P04256, Q99PF5, P17078, P62909
drug binding	19	3.125	8.37E-08	P85973, P12785, P07340, Q01062, P04906, P04904, P09812, P20651, P62630, P63329, P17425, Q62658, P34058, P19804, P06686, P53534, O35331, Q9QYJ6, P02770
kinase binding	17	2.796052632	1.07E-07	Q9JJP9, P42123, P47858, Q92DV6, O35274, P32851, Q9WU82, O88767, P31000, P11167, Q9JJH5, P34058, P84076, P47819, Q62936, Q07647, P62909
RNA binding	41	6.743421053	2.02E-07	Q9JJ54, Q9EPH8, Q32PX7, P62859, P24050, Q09167, P61980, P27952, A7VJC2, P63174, O88453, P13084, P62425, Q99PF5, Q8VHV7, P62909, P12001, Q55GE0, P62907, P60901, Q3TJJ1, P84586, P
calmodulin binding	21	3.453947368	6.95E-07	Q01066, Q05175, Q63560, P26431, P10687, P20651, Q63092, P63329, P11275, Q05764, Q03344, P97756, P30009, Q9ES17, P15791, P31424, Q63357, P07936, O88831, Q9EPH2, Q01728
threonine-type endopeptidase activity	9	1.480263158	1.03E-06	P17220, P48004, P40122, P60901, P40307, P18421, P18420, Q9IHW0, P28075
calcium-dependent protein binding	14	2.302631579	1.22E-06	P62161, P26431, Q6IRE4, P32851, Q9QZA2, P05964, P60881, P09951, P04631, P84087, Q63357, Q63372, Q62826, Q63537
actin filament binding	19	3.125	1.96E-06	Q912N1, Q99MZ8, O35274, Q63598, Q7M0E3, Q99PD4, P31652, Q05764, Q9Z1P2, P45592, O08839, Q07266, Q5RIL0, Q92DG8, A0MZ67, Q63357, Q99JD4, P05197, Q5SGE0
ion channel binding	18	2.960526316	2.37E-06	Q7M730, Q9Z2L0, P25304, P62161, O35274, P62483, P32851, P13852, P60881, Q9WU82, Q9Z1P2, Q62658, P68255, P15791, P68511, Q62696, P34058, Q01728
NAD binding	12	1.973684211	3.41E-06	P41565, Q6P6R2, P29266, Q9ILJ3, P41562, Q68FX0, P42123, Q99NA5, P04797, O88989, O35077, P51650
5S rRNA binding	6	0.986842105	6.05E-06	P21531, P50878, P63159, P05197, P05426, P09895
protein kinase binding	36	5.921052632	6.18E-06	Q9Z2L0, P04906, P10686, P62755, P62630, Q9QXY2, P18266, Q00657, P13084, Q9JJH5, P61765, Q9ESI7, P34058, Q6JP77, P61265, P06685, P62909, P14925, P62161, Q9Z0V6, P16884, Q05140, Q01
large ribosomal subunit rRNA binding	7	1.151315789	1.12E-05	P24049, P19945, P62832, P02401, P23358, P62752, P84100
unfolded protein binding	13	2.138157895	1.32E-05	P18418, Q7TPB1, P29457, Q07439, P13084, Q6P502, P34058, Q5XIM9, Q63525, P27682, P06761, P23928, Q66HD0
proteasome-activating ATPase activity	5	0.822368421	2.18E-05	Q63570, Q63347, P62198, P62193, Q63569
nucleotide binding	28	4.605263158	3.08E-05	Q9JJ54, Q9EPH8, Q04400, Q9Z2L0, Q6URK4, Q794E4, P21588, Q7TP47, Q09167, P62752, P62630, Q6PDU1, A7VJC2, P08461, Q8K3P7, O88453, P62850, P06685, Q8VHV7, Q5FVM4, P84586, P8115
5.8S rRNA binding	5	0.822368421	9.62E-05	P62919, P21533, P62278, P84100, P29314
pyruvate dehydrogenase (NAD+) activity	5	0.822368421	9.62E-05	Q6P6R2, P49432, P26284, Q06437, P08461
syntaxin-1 binding	7	1.151315789	1.14E-04	P61765, Q9QUL6, P63041, P84087, B5DF41, P31652, P60881
potassium ion binding	6	0.986842105	1.21E-04	O54701, P07340, P06686, O35331, P06685, P11980
pyridoxal phosphate binding	10	1.644736842	1.82E-04	P13221, Q05683, P53534, P09812, O35331, P14173, P00507, P02770, P18088, P50554
integrin binding	13	2.138157895	2.08E-04	P04785, Q68FQ2, P49911, Q9QZA6, P15800, P40241, P18266, Q05546, Q05695, P18418, Q9Z1P2, Q9R066, P47819
ATP-dependent protein binding	5	0.822368421	2.73E-04	P60905, Q63413, Q9QUL6, P13852, P32851
protein complex binding	28	4.605263158	3.01E-04	Q9Z0W7, Q9Z2L0, P49242, O35274, P54313, P27952, P62850, P16036, P69897, P62870, Q9JJ19, Q63584, Q63413, O35430, Q9WU82, P05708, Q91V33, P24368, P83941, O08839, P17074, Q9QUL6,
glycoprotein binding	11	1.809210526	3.64E-04	P18418, P22063, P31000, P60905, Q99376, P34058, P35559, P32851, P06761, P47819, Q63198
ionotropic glutamate receptor binding	7	1.151315789	3.67E-04	P18266, Q9QUL6, Q62696, Q9Z2S9, Q62936, Q9Z1E1, Q9WU82
ATPase activity	17	2.796052632	5.85E-04	P07340, Q07439, D3ZAF6, Q5RKI1, Q63570, Q63413, P35559, P62198, P06761, P19511, P05708, Q9QUL6, P06686, Q63347, P16970, P62193, P46462
glutathione peroxidase activity	6	0.986842105	6.87E-04	P04906, P04041, P57113, O35244, P08009, Q91XR8
ubiquitin protein ligase binding	23	3.782894737	7.53E-04	P09456, Q07439, Q4FZX7, P63322, P07335, B5DEH2, Q5XIM9, Q6IRE4, P06761, P68182, P18266, P18418, P12369, Q09073, Q6P6V0, P69897, P48500, Q62936, O08629, O35244, P62870, Q5SGE0, P
amino acid binding	7	1.151315789	7.82E-04	Q8CGU9, Q6MG60, P04177, P09034, O08557, P14173, P00507
peroxiredoxin activity	4	0.657894737	8.09E-04	O88767, Q9R063, Q9Z0V6, O35244
cell adhesion molecule binding	10	1.644736842	8.50E-04	Q1WIM3, P49911, Q9R066, Q62889, Q63374, A0MZ67, P04218, Q63372, P41499, Q1WIM1
TBP-class protein binding	6	0.986842105	8.63E-04	Q63570, Q794E4, Q63347, P62198, P62193, Q63569
receptor binding	26	4.276315789	0.001100275	P62198, P04218, O88767, P04762, P08050, P61265, P12839, Q63372, Q5XIG8, P08009, Q9JJ19, Q1WIM3, Q07439, P41562, P02650, P08592, P35559, P11915, Q1WIM1, P13383, Q8K4Y5, Q9R063, P
structural molecule activity	17	2.796052632	0.001115749	P70615, B0BN93, Q99PB2, P60203, Q4AEF8, P16884, P23565, P48679, P03994, Q05764, P31000, F1LMZ8, P12839, P47819, P23514, P38983, O35142
cytoskeletal protein binding	9	1.480263158	0.001169667	Q9QY17, Q912N1, P13596, Q9ZDW5, Q07266, P30427, P23928, Q01728, Q63537
rRNA binding	8	1.315789474	0.001217803	P13084, P62914, P17077, P24050, P29314, P62282, P62703, P61928
SNARE binding	9	1.480263158	0.001305396	P61765, Q9QUL6, P63041, P84087, P61265, P32851, Q5EGY4, P60881, P54921
translation elongation factor activity	6	0.986842105	0.001313838	Q68FR6, Q3TJJ1, P05197, P62630, Q9QYU2, Q68FR9
actin binding	20	3.289473684	0.001395285	Q912N1, Q9QWN8, P30427, O35274, Q08163, Q63598, P34926, P62024, Q05764, P45592, Q63228, O08719, P09951, Q07266, P30009, P68511, P84076, Q9EPH2, Q63327, P52481
protein C-terminus binding	18	2.960526316	0.001417252	Q912N1, Q9EPH8, P07340, P47858, Q9ZDV6, P49911, O35274, P19527, Q01986, Q9WU82, P31000, P13383, P11507, Q9QUL6, P68255, Q6JP77, Q62696, Q62936
sodium ion binding	5	0.822368421	0.001996424	O54701, P07340, P06686, O35331, P06685

KEGG	Count	%	PValue	Genes
Ribosome	55	9.046052632	1.98E-29	P20280, P35427, P19945, P62859, P62755, P62278, P24050, P63326, P61354, P62752, P27952, P09895, Q63507, P62850, P24049, P62268, P04644, P62425, P50878, P23358, P62853, P61314, P6192
Carbon metabolism	33	5.427631579	2.53E-15	P47858, P04797, P52873, O88989, P17764, Q8VHF5, P26284, P00507, P08461, P16617, Q6P6R2, P04762, Q68FX0, P13086, Q6P6V0, Q99NA5, P14604, P48500, Q5XI22, P41565, P41562, P07323, P4
Biosynthesis of antibiotics	43	7.072368421	2.26E-14	P13437, P42123, P47858, P04797, O88989, P17764, Q8VHF5, P00507, P26284, P08461, P16617, P04762, Q6P6R2, Q9WVK7, Q68FX0, P13086, P09034, Q6P6V0, Q99NA5, P19804, P14604, P48500,
Citrate cycle (TCA cycle)	17	2.796052632	3.59E-13	P41565, P41562, O88989, P52873, Q8VHF5, P49432, P14408, P26284, Q63270, Q9ER34, Q06437, P08461, Q6P6R2, Q68FX0, P04636, P13086, Q99NA5
Proteasome	18	2.960526316	4.13E-11	Q63570, B0BN93, P60901, P40307, P18421, P62198, P18420, Q9IHW0, Q63569, P17220, P40122, P48004, Q4FZT9, F1LMZ8, Q63347, O88761, P28075, P62193
Pyruvate metabolism	15	2.467105263	3.72E-09	Q9IJI3, P42123, O88989, P52873, P17764, P49432, P14408, P26284, Q06437, P08461, Q6P6R2, P04636, O35952, Q5XI22, P11980
Biosynthesis of amino acids	20	3.289473684	1.19E-08	P41565, P41562, P47858, P04797, P52873, P07323, Q8VHF5, Q63270, P00507, Q9ER34, P16617, P09606, P13221, Q68FX0, P09034, Q99NA5, P48500, Q6AY57, P11980, P25113
2-Oxocarboxylic acid metabolism	10	1.644736842	1.11E-07	P41565, P13221, P41562, Q68FX0, Q99NA5, Q8VHF5, Q6AY57, Q63270, P00507, Q9ER34
Glyoxylate and dicarboxylate metabolism	11	1.809210526	3.63E-07	P09606, P04762, Q6P6R2, P04636, Q5IOP2, O88989, P17764, Q8VHF5, Q63270, Q9ER34, Q5XI22
Butanoate metabolism	11	1.809210526	5.40E-07	Q9WVK7, P17425, Q05683, B2GV06, P14604, P17764, P51650, P18088, P50554, Q5XI22, P29147
Glycolysis / Gluconeogenesis	16	2.631578947	1.46E-06	Q9IJI3, P42123, P47858, P04797, P07323, P49432, P26284, Q06437, P08461, P16617, P05708, Q6P6R2, Q6P6V0, P48500, P25113, P11980
HIF-1 signaling pathway	18	2.960526316	1.12E-05	P10686, Q99376, P04797, P21708, P07323, P62755, P49432, P68403, P26284, Q01986, Q06437, P11275, P05708, P11167, P83941, P15791, P62870, P63086
Amphetamine addiction	14	2.302631579	1.37E-05	Q04400, P62161, P32851, P19643, P14173, P68403, P20651, P63329, P11275, P68182, P63100, P04177, Q6JAI0, P15791
Glucagon signaling pathway	17	2.796052632	3.43E-05	P42123, P62161, P10687, P09812, P49432, P20651, P26284, Q06437, P63329, P68182, P11275, P63100, P11167, P15791, P53534, P25113, P11980
Alanine, aspartate and glutamate metabolism	10	1.644736842	4.15E-05	Q9R1T5, P70627, P09606, P13221, P09034, Q05683, P51650, P00507, P18088, P50554
Gastric acid secretion	14	2.302631579	5.96E-05	P10824, Q04400, P07340, P26431, P62161, P15791, P10687, P06686, P06687, P06685, P68403, P27139, P68182, P11275
Long-term potentiation	13	2.138157895	7.94E-05	P62161, P21708, P10687, P68403, P20651, Q01986, P63329, P68182, P11275, P63100, P15791, P31424, P63086
GABAergic synapse	15	2.467105263	9.90E-05	P10824, Q04400, O88871, O35458, P54313, P68403, P68182, P43425, P09606, Q9QUL6, Q05683, P59215, Q62688, P50554, P18088
Metabolic pathways	93	15.29605263	1.61E-04	P70627, Q5I6B8, D3ZAF6, P42123, P47858, P50408, P17764, P14173, P26284, P08461, P12075, Q6P6R2, Q9WVK7, P09034, P13086, P25093, Q6P6V0, Q99NA5, P19804, P14604, P18088, O35244, C
cGMP-PKG signaling pathway	21	3.453947368	1.70E-04	P10824, Q04400, P07340, Q9Z2L0, Q01062, P62161, P21708, P10687, P20651, Q01986, P63329, P81155, P63100, P11507, Q09073, P06686, P06687, P06685, Q9R120, Q01728, P63086
Glutamatergic synapse	17	2.796052632	1.91E-04	P10824, Q04400, P21708, P10687, P54313, P68403, P20651, P63329, P68182, P43425, P09606, P63100, P31424, P31596, P31422, P59215, P63086
Dopaminergic synapse	18	2.960526316	2.37E-04	P10824, Q04400, P62161, P10687, P54313, P19643, P14173, P68403, P20651, P63329, P68182, P11275, P18266, P43425, P04177, Q6JAI0, P15791, P59215
Valine, leucine and isoleucine degradation	11	1.809210526	3.55E-04	P13437, Q9WVK7, Q6P6R2, P29266, Q9ILJ3, P17425, B2GV06, P14604, P17764, P50554, Q5XI22
Proximal tubule bicarbonate reclamation	7	1.151315789	5.86E-04	P07340, Q9JI66, O88989, P06686, P06687, P06685, P27139
Thyroid hormone signaling pathway	16	2.631578947	6.68E-04	P07340, P10686, P26431, P21708, P10687, P68403, Q01986, Q9WU82, P68182, P18266, P11167, Q9JJH5, P06686, P06687, P06685, P63086
Protein processing in endoplasmic reticulum	20	3.289473684	7.49E-04	P04785, P60905, Q07439, Q9JIP9, P68101, P54319, P06761, P11598, Q63081, P18418, P0C0A9, P34058, Q5HZY2, Q4KMA2, P23928, Q66HD0, Q63617, P07153, Q641Y0, P46462
Prion diseases	8	1.315789474	0.001060558	P13596, P07632, P21708, P13852, P06761, Q01986, P63086, P68182
Insulin secretion	13	2.138157895	0.001159698	Q04400, P07340, P11167, P15791, P10687, P06686, P32851, P06687, P06685, P68403, P60881, P68182, P11275
Central carbon metabolism in cancer	11	1.809210526	0.001227459	P05708, P11167, P47858, P21708, P49432, P26284, Q01986, Q06437, P63086, P11980, P25113
Melanogenesis	14	2.302631579	0.001302974	P10824, Q04400, P62161, P21708, P10687, P68403, Q01986, Q9WU82, P11275, P68182, P18266, P15791, P59215, P63086
Serotonergic synapse	16	2.631578947	0.001341878	P10824, Q8CGU9, Q04400, P08592, P21708, P10687, P54313, P19643, P14173, P68403, P31652, Q01986, P68182, P43425, P59215, P63086
Synthesis and degradation of ketone bodies	5	0.822368421	0.001571655	P17425, B2GV06, P17764, Q5XI22, P29147
Oxytocin signaling pathway	18	2.960526316	0.001586081	P10824, Q04400, P62161, P10687, P21708, P68403, P20651, Q01986, P63329, P68182, P11275, P63100, P97756, P15791, P59215, O88831, P05197, P63086
Tryptophan metabolism	9	1.480263158	0.001854525	Q8CGU9, Q9WVK7, P04762, Q9ILJ3, P14604, P17764, P19643, P14173, Q5XI22
Alzheimer's disease	20	3.289473684	0.001951984	P02650, P62161, P08592, P04797, P21708, P10687, P35559, P20651, P63329, P12075, P18266, P19511, P19234, P63100, P11507, Q5XIF3, Q5M9I5, Q7TQ16, P20788, P63086
Thyroid hormone synthesis	11	1.809210526	0.001970059	Q04400, P07340, P10687, P06686, P06687, P04041, P06761, Q66HD0, P06685, P68403, P68182
Propanoate metabolism	7	1.151315789	0.002290079	Q6AYG5, P42123, P13086, P14604, P17764, P50554, Q5XI22
Bile secretion	11	1.809210526	0.002736307	Q04400, P07340, P11167, Q9JI66, P26431, P06686, P06687, P47863, P06685, P27139, P68182
Estrogen signaling pathway	13	2.138157895	0.00301396	P10824, Q04400, Q07439, O88871, P62161, P34058, P10687, P21708, P59215, Q66HD0, Q01986, P68182, P63086
Circadian entrainment	13	2.138157895	0.003287656	P10824, Q04400, P62161, P21708, P10687, P54313, P68403, P68182, P11275, P43425, P15791, P59215, P63086
Synaptic vesicle cycle	10	1.644736842	0.003579093	O35458, P61765, Q9QUL6, P63041, P50408, P84087, P61265, P32851, P60881, P54921
Parkinson's disease	17	2.796052632	0.003982884	P10824, Q04400, Q9Z2L0, P68182, P12075, P19511, P81155, O88767, P19234, P04177, Q09073, Q5U300, Q5XIF3, Q7TQ16, Q5M9I5, P20788, Q9R1Z0
Gap junction	12	1.973684211	0.004433256	P10824, Q5XIF6, Q04400, P08050, P31424, P69897, P10687, P21708, P68403, Q01986, P63086, P68182
Fatty acid metabolism	9	1.480263158	0.005209446	P13437, Q9WVK7, P12785, P45479, P15650, P14604, P17764, Q5XI22, P33124
Cell adhesion molecules (CAMs)	18	2.960526316	0.005787532	P22063, Q1WIM3, Q68FQ2, Q62889, Q99PB2, P06907, P97603, Q05695, P13596, P97685, P07722, Q63374, Q63372, P97846, Q9Z1Y3, Q9ERB4, Q63198
Amyotrophic lateral sclerosis (ALS)	9	1.480263158	0.0058358	P04762, P63100, P07632, P31596, P16884, P19527, P12839, P20651, P63329
Morphine addiction	12	1.973684211	0.006224525	P10824, Q01066, P43425, Q04400, Q01062, O35458, O88871, P54313, P59215, P68403, Q9QYJ6, P68182
Cocaine addiction	8	1.315789474	0.007575064	P10824, Q04400, P04177, Q6JAI0, P31422, P19643, P14173, P68182
Endocrine and other factor-regulated calcium reabsorption	8	1.315789474	0.008526383	P07340, P10687, P06686, P06687, P06685, P68403, P07171, P68182

Table 2: Gene Ontology analysis of the 598 dysregulated proteins in the juvenile SN compared to young in rats, showing the 50 most enriched terms according to their p-value. BP: biological process. CC: Cellular component. MF: molecular function. KEGG pathway. Proteins are presented with the uniprot accession number. The entire list of proteins associated to each term can be consulted in Supplementary Table 3d.

BP	Count	%	PValue	Genes
translation	52	8.710218	9.78E-18	P20280, P35427, P62755, P62278, P24050, P61354, P62752, P27952, P09895, Q63507, P62850, P16
tricarboxylic acid cycle	15	2.512563	8.67E-14	P41565, P41562, O88989, Q8VHF5, P49432, P26284, Q63270, P14408, Q9ER34, Q06437, P08461, Q
cell-cell adhesion	31	5.19263	1.87E-11	Q9WTT7, Q68FR6, P30427, Q6AXS5, Q6JE36, P06761, P61980, Q68FR9, O88767, P34058, Q66HR2,
substantia nigra development	15	2.512563	3.01E-10	P02688, Q05175, Q8VBU2, P07335, P60203, P13233, P19643, P06761, P23565, Q5RJQ4, P60711, P2
glutathione metabolic process	14	2.345059	1.05E-08	Q9Z0W7, Q68FR6, P41562, P04906, P07632, P04904, P04041, P51650, O35952, P57113, P02091, P0
cell adhesion	30	5.025126	1.40E-08	Q5I6B8, P55068, P55067, P97603, P40241, Q05546, Q05695, P97686, Q63374, Q63372, P32736, P2
brain development	32	5.360134	3.12E-08	Q9JJ54, P11030, P07335, B2GV06, P21588, P10687, P17764, B5DF41, P31652, P40241, Q9QXU9, P1
response to ethanol	24	4.020101	1.25E-07	P04094, P22062, P16975, P07632, P04906, P49242, P20272, B2GV06, Q9Z0U4, P19643, P68403, P1
neurotransmitter secretion	11	1.842546	1.35E-07	P45479, Q63475, P09951, P61765, Q91Z79, Q9QUL6, Q63374, Q63372, Q62768, P29101, Q63537
response to drug	43	7.20268	1.77E-07	Q9JJ54, P04904, B2GV06, P19643, P31652, P68403, P37377, P04762, O88767, P11232, P23593, P09
NADH metabolic process	7	1.172529	1.04E-06	P41565, Q68FX0, P04636, Q99NA5, O88989, O35077, P46462
liver development	19	3.18258	1.60E-06	Q9JJ54, Q9JLJ3, Q63413, P63090, P17764, Q09167, Q63270, P61980, Q9ER34, Q9WU82, P29147, P1
response to oxidative stress	19	3.18258	1.77E-06	P41562, P07632, P08592, Q9Z0V6, P04041, P14141, Q6DGG0, Q01986, Q921A4, P04762, O88767, (
aging	29	4.857621	2.50E-06	P04094, P02688, Q99376, P04904, P04041, P61980, P62630, P37377, Q6P6R2, P04762, P05982, P23
cellular oxidant detoxification	13	2.177554	2.59E-06	Q921A4, O88767, P04762, P11232, Q9R063, Q6AXX6, P04906, Q9Z0V6, P04041, P57113, O35244, I
response to reactive oxygen species	8	1.340034	3.39E-06	P04762, P23593, P07632, P04906, Q63259, P04041, P07895, O35244
glycolytic process	10	1.675042	4.11E-06	P05708, P47858, Q6P6V0, P04797, P07323, P48500, P05065, P16617, P11980, P25113
response to toxic substance	16	2.680067	9.73E-06	P04094, P02688, P04906, P13233, P04041, P19527, P19643, P14173, P31652, P29147, P04762, P09
liver regeneration	11	1.842546	1.18E-05	P13383, P62850, P13084, P41123, Q09167, P84100, P05426, P62250, Q6PDV7, P12001, Q63009
2-oxoglutarate metabolic process	7	1.172529	1.20E-05	P41565, Q6P6R2, P13221, P41562, Q68FX0, Q99NA5, P00507
response to estradiol	21	3.517588	1.33E-05	Q9JJ54, P04094, P14925, P04906, P63090, P07323, P04041, P31652, Q9WU82, P11915, P29147, P1
isocitrate metabolic process	5	0.837521	1.73E-05	P41565, P41562, Q68FX0, Q99NA5, Q9ER34
hydrogen peroxide catabolic process	7	1.172529	1.75E-05	P04762, Q9R063, Q9Z0V6, P01946, P04041, P02091, O35244
positive regulation of translation	11	1.842546	4.66E-05	Q9JJ54, P13084, Q63413, Q3B8Q2, P49242, Q7TP47, P02401, P42346, P05197, P62703, P63086
response to hydrogen peroxide	12	2.01005	5.23E-05	O88767, P04762, P10686, P07632, Q9Z0V6, P01946, P04041, P05197, P07895, P23928, P02091, Q0
RNA splicing	13	2.177554	5.32E-05	Q9EPH8, Q794E4, Q63413, Q3B8Q2, Q6URK4, P04256, Q7TP47, Q99PF5, Q09167, P61980, Q8VHV
negative regulation of neuron projection devel	11	1.842546	5.34E-05	Q05546, P31000, Q04400, Q9JMC1, P49911, Q62952, P07722, P61265, Q62950, P47819, Q5QJC9
learning	11	1.842546	6.11E-05	P22063, O35116, P61751, P12369, Q63228, Q9Z2L0, P04177, P63090, P10687, Q63372, Q9R1Z0
oxaloacetate metabolic process	6	1.005025	6.28E-05	P13221, P04636, P52873, O88989, Q8VHF5, P00507
ribosomal large subunit assembly	8	1.340034	7.14E-05	P21531, P21533, P62914, P83732, P23358, P62752, Q6PDV7, P09895
ribosomal small subunit assembly	9	1.507538	7.47E-05	P17074, P04644, P13471, P62755, P24050, P63326, P62853, P38983, P27952
gluconeogenesis	8	1.340034	8.81E-05	Q6P6V0, P04797, P07323, P52873, O35077, P48500, P16617, P25113
rRNA processing	11	1.842546	1.02E-04	P62850, Q63507, P12749, Q3B8Q2, P62914, P17074, P04644, P62755, P05426, P62250, P09895
response to hypoxia	23	3.852596	1.08E-04	P04094, P07340, P14925, Q99376, P09812, P68403, P11598, P31652, P05065, P33124, Q921A4, P0
central nervous system development	13	2.177554	1.33E-04	P22063, P02688, P14925, P55068, P55067, Q9ESM2, P51650, P61980, P03994, O08719, P97686, Q5
relaxation of cardiac muscle	5	0.837521	1.34E-04	P07340, P11507, P15791, P06686, P06685
ribosomal small subunit biogenesis	6	1.005025	1.79E-04	P62850, P13084, P17074, P04644, P62755, P62250
response to nutrient	15	2.512563	1.94E-04	P20272, Q99376, B2GV06, P30427, P31652, P33124, P29147, P10888, P05982, P10760, P09034, Q6
cellular response to interleukin-4	7	1.172529	2.17E-04	P21531, Q91ZN1, P12785, P19945, P34058, P06761, P27952
neurofilament cytoskeleton organization	5	0.837521	2.18E-04	P07632, P16884, P19527, P12839, P23565
acetyl-CoA biosynthetic process from pyruvate	5	0.837521	2.18E-04	Q6P6R2, P49432, P26284, Q06437, P08461
cellular response to cAMP	11	1.842546	2.29E-04	P04094, P35427, P09034, P08592, P19945, Q6JP77, P29994, P02401, O35077, P06761, Q01728
locomotory behavior	13	2.177554	2.31E-04	Q01066, P04094, P43425, Q04400, Q63228, P07632, P04177, P08592, O35430, P07895, P31652, P0
cell redox homeostasis	10	1.675042	2.55E-04	P04785, Q5XIK2, P11232, Q6P6R2, Q9R063, Q9Z0V6, P04041, P11598, O35244, Q63081
negative regulation of translation	10	1.675042	2.55E-04	P18418, P35427, Q3B8Q2, Q5M9G3, P52759, P04797, Q7TP47, P63245, Q68A21, P62909
cellular response to oxidative stress	11	1.842546	2.55E-04	O88767, P11232, P04094, Q4V8C7, P11507, Q5RJQ4, P07632, Q9Z0V6, P16884, P12839, P37377
actin filament organization	11	1.842546	2.55E-04	Q91ZN1, Q9Z1P2, P45592, Q9Z0W5, Q07266, Q5RJL0, Q5U301, Q62696, P97710, P63312, P85845
negative regulation of neuron apoptotic proces	16	2.680067	2.63E-04	Q91ZN1, P60905, P45479, P63055, P07632, Q9Z0V6, Q63945, P19527, P37377, O88767, P13084, P6
regulation of neuronal synaptic plasticity	7	1.172529	2.68E-04	P22063, Q62639, P55068, P04631, P14200, P11275, P37377
response to selenium ion	6	1.005025	3.18E-04	P31000, P11232, P19945, P04041, P19643, P07895

CC	Count	%	PValue	Genes
extracellular exosome	301	50.41876	2.80E-101	Q7TPB1, D3ZAF6, B5DEH2, P24050, Q6PEC4, P26772, P62752, P27952, P40241, P09895, P43425, Q
myelin sheath	84	14.07035	5.06E-73	P02688, Q9Z2L0, Q5RKI0, P42123, P63322, Q6JE36, P23565, P26284, P08461, P12075, P16036, Q6F
membrane	213	35.67839	1.58E-53	Q9Z0U4, P62755, P24050, P26772, P27952, P40241, P09895, Q9Z2G8, Q63507, P62850, Q4FZT9, F1
cytoplasm	332	55.61139	2.07E-46	Q7TPB1, B5DEH2, Q9Z0U4, P62755, Q6PEC4, P26772, P62752, P27952, Q9Z2G8, Q9QXY2, P09895,
focal adhesion	77	12.89782	1.46E-37	Q5I6B8, Q9EPH8, P35427, P63322, P19945, P62278, P63326, P24050, P61354, P27952, P40241, P0
cytosol	151	25.29313	3.84E-35	P63055, P47858, P49911, Q6JE36, Q6PEC4, F1LMZ8, P13084, P13086, P61765, Q6P6V0, Q6JP77, Q
mitochondrion	142	23.78559	1.12E-29	D3ZAF6, Q9Z2L0, P42123, Q5EB81, P26772, P26284, P12075, P11951, Q5XIE6, P09034, P13086, P6
neuronal cell body	68	11.39028	8.03E-22	P04094, P02688, Q9Z0U4, Q7TP47, B5DF41, P97839, P14173, P97603, P35053, A7VJC2, Q9QXY2, C
axon	54	9.045226	9.57E-21	P04094, P04775, P63055, P63012, P14173, Q9QXY2, Q05695, O88767, P11232, P97686, P97685, Q6
neuron projection	54	9.045226	4.61E-19	O35116, P04775, P63055, Q9Z0U4, B5DF41, A7VJC2, Q9Z2G8, Q9QXY2, O88767, P10760, P09034, (
intracellular ribonucleoprotein complex	28	4.690117	8.66E-16	P38656, Q9JJ54, Q9EPH8, P35427, P49242, P19945, P04797, P62755, Q7TP47, P24050, P61354, P2
cytosolic large ribosomal subunit	32	5.360134	4.56E-15	P20280, P35427, P62902, P19945, P02401, P61354, P62752, P84100, P05426, P63174, P09895, Q63
ribosome	29	4.857621	3.25E-14	P20280, P35427, P62755, P61354, P62752, P27952, P05426, P37377, Q63507, P62850, P04644, P62
synapse	40	6.700168	5.12E-14	Q9Z0W5, P55068, P62483, P97839, Q9QXY2, P37377, P97686, P06686, P06687, Q63259, Q62936, P
cytosolic small ribosomal subunit	24	4.020101	3.31E-13	P49242, P13471, P62755, P62278, P24050, P63326, P27952, P62282, P62850, P62246, P17074, P04
cell-cell adherens junction	36	6.030151	5.99E-13	Q9WTT7, Q68FR6, P30427, Q6AXS5, Q6JE36, P04218, P06761, P61980, Q68FR9, O88767, P34058, (
melanosome	22	3.685092	6.46E-13	P04785, Q7TPB1, P12785, P60905, O35783, Q63584, Q99376, P13233, P06761, P11598, Q9QZA2, C
terminal bouton	24	4.020101	4.22E-12	P60905, Q63475, Q9Z0W5, P63041, P08592, P63012, P09527, P07171, Q8K3M6, P29101, P37377, P
perinuclear region of cytoplasm	57	9.547739	1.07E-11	P49911, P62755, Q6JE36, O88767, P11507, P29994, Q925N3, Q9Z270, Q63560, P63090, O35430, Q
dendrite	48	8.040201	1.12E-11	O35116, P04094, Q9EPH8, Q01062, P55068, P07335, P19945, P62755, P97839, Q9QXY2, Q05695, P
synaptic vesicle	24	4.020101	2.01E-11	Q9Z2I6, P60905, P11030, P45479, Q9Z2L0, O35458, P08592, Q9QWN8, Q9Z0U4, O35430, P14668, I
mitochondrial inner membrane	37	6.197655	3.36E-11	D3ZAF6, Q9Z2L0, P52873, P17764, P19643, Q5XHZ0, P00507, P12075, P11951, P16036, P10888, P3
membrane raft	33	5.527638	1.33E-10	Q04400, Q9Z2L0, P42123, Q01062, B5DEH2, Q9Z0U4, P31652, P35053, P16617, Q05546, P85125, Q
postsynaptic density	31	5.19263	1.60E-10	O35116, P62483, P61980, Q9QXY2, O08875, P31422, P29994, P12839, P06685, Q9QW07, Q62936, (
proteasome complex	16	2.680067	3.55E-10	Q9JJP9, Q63570, B0BN93, P60901, P40307, P62198, P17220, P40112, P48004, Q4FZT9, F1LMZ8, Q4
protein complex	52	8.710218	4.47E-10	Q9Z2L0, P04906, B5DEH2, P63012, P11507, Q9JHU0, P61765, P13086, Q6JP77, P69897, P29994, P0
nucleus	223	37.35343	6.45E-10	D3ZAF6, Q641X8, Q8K3E7, P62755, Q6PEC4, P62752, P26284, P27952, P09895, Q9Z2G8, P62850, P
cell junction	40	6.700168	1.47E-09	Q63475, Q05175, Q9Z0W5, Q5RKI0, Q9Z0U4, P62483, B5DF41, P61980, Q9QXY2, P37377, Q9Z1P2,
small ribosomal subunit	12	2.01005	1.59E-09	P62850, P13084, P62268, P62755, P24050, P63245, P62853, P29314, P38983, P62250, P62703, P60
intercalated disc	14	2.345059	5.19E-09	Q7M730, P07340, P04775, P26431, P14668, Q9WU82, P11507, P15791, P08050, Q9R066, P06686, F
mitochondrial matrix	23	3.852596	8.01E-09	Q01062, B2GV06, P52873, P17764, Q8VHF5, P49432, P26772, Q5XHZ0, P00507, Q06437, P08461, F
microtubule	28	4.690117	1.12E-08	Q5PPN5, Q7TPB1, Q6JE36, P62483, Q68FR8, P13668, Q6P6T4, Q9ESI7, Q66HR2, P69897, Q63525, (
smooth endoplasmic reticulum	11	1.842546	1.23E-08	P18418, P24368, P04177, P08592, Q63357, P06761, P11598, Q66HD0, Q63617, Q9QW07, Q63081
perikaryon	22	3.685092	1.25E-08	O35116, P04094, P22062, P14925, P07323, P14668, P16884, P00507, Q01986, A7VJC2, P09606, P0
extracellular matrix	28	4.690117	5.32E-08	P30427, P62278, P24050, P06761, P61980, P45592, P69897, P62832, P62703, P62804, P04785, P07
growth cone	21	3.517588	5.72E-08	Q05175, Q9JMC1, P37285, P08592, P20272, Q8VBU2, P19527, Q8K3M6, P37377, P13596, Q62656,
cortical actin cytoskeleton	12	2.01005	9.87E-08	Q91ZN1, Q9Z1P2, P45592, Q5RKI0, P11167, Q99MZ8, Q08163, Q7M0E3, P62630, Q9Z1Y3, P52481,
cell-cell junction	23	3.852596	1.88E-07	Q9QY17, Q91ZN1, Q9Z0W7, Q1WIM3, P55051, Q68FQ2, Q5RKI0, P10686, P08592, P47863, Q9WU
cell projection	16	2.680067	3.89E-07	P02688, P55051, Q5RKI0, P10686, P14668, P13233, P24942, Q9Z1P2, P09606, P31000, Q66HR2, O3
presynaptic membrane	14	2.345059	5.80E-07	Q01062, Q9Z0U4, P32851, B5DF41, Q8K3M6, P11275, Q05695, Q05683, Q62696, P31596, P61265, I
cytoplasmic ribonucleoprotein granule	9	1.507538	7.13E-07	P13383, Q9EPH8, P21533, P60711, P19945, P69897, P62755, P23565, P62703
axon terminus	15	2.512563	1.00E-06	Q9WVC0, P04094, Q9Z0W5, O54800, P14668, P62483, P61980, P37377, P06300, P09606, P13221, (
Golgi apparatus	54	9.045226	1.36E-06	P11030, Q8K3E7, P97603, Q9QXU9, Q66HR2, P06687, Q63259, P06685, P43278, P12785, P45479, C
T-tubule	12	2.01005	1.63E-06	P04775, O08839, P26431, P15791, Q62696, Q6JP77, P06686, P47863, P06685, P20651, Q9Z1Y3, Q0
cell body	15	2.512563	2.52E-06	Q9WVC0, Q7TPB1, P55051, P02696, P62755, Q5XIM9, P07171, O88767, P09606, P31000, Q62952,
paranode region of axon	7	1.172529	4.15E-06	P04775, Q5RJQ4, Q5RJL0, P97685, Q62696, P07722, P97846
endoplasmic reticulum	52	8.710218	5.06E-06	Q9Z0W7, P11030, Q9JJP9, Q68FR6, Q01062, P49911, B5DEH2, Q7TP47, Q7TPJ0, P06761, Q6AY41,
nuclear matrix	14	2.345059	5.69E-06	Q9Z0W7, P70615, P16975, Q63413, P60901, P49911, Q9QWN8, P97690, P31000, P45592, P13084,
proteasome accessory complex	7	1.172529	9.71E-06	Q4FZT9, F1LMZ8, Q63570, B0BN93, P62198, O88761, P62193
endoplasmic reticulum chaperone complex	6	1.005025	2.19E-05	P04785, P24368, P06761, Q66HD0, Q63617, Q63081

MF	Count	%	PValue	Genes
protein binding	191	31.9933	9.79E-57	O35116, Q9Z2L0, P42123, Q8K3E7, Q9Z0U4, P24050, P35053, P40241, A7VJC2, P09895, Q9QXY2, C
poly(A) RNA binding	133	22.27806	1.06E-36	Q7TPB1, P49911, P62755, P24050, P26772, P62752, D3ZBN0, P27952, A7VJC2, P09895, O88453, Q
structural constituent of ribosome	57	9.547739	2.94E-18	P20280, P35427, P19945, P62755, P62278, P63326, P24050, P61354, P62752, P27952, P09895, Q63
cadherin binding involved in cell-cell adhesion	33	5.527638	6.43E-12	Q9WTT7, Q68FR6, P30427, Q6AXS5, Q6JE36, P06761, P61980, Q68FR9, O88767, P34058, Q66HR2,
mRNA binding	25	4.187605	3.41E-10	Q9JJ54, Q9EPH8, P35427, Q6URK4, P49242, P62278, P62755, P24050, P27952, P62630, P05426, P0
protein domain specific binding	35	5.862647	3.00E-09	Q05175, Q9JJP9, P97839, P06761, P14173, P61980, P37377, Q9QXY2, Q9Z1P2, P63100, P61765, P0
enzyme binding	39	6.532663	9.85E-09	P04797, P10687, P27615, P17764, P06761, P14173, P00507, P27952, Q6DGG0, P63329, Q63009, P3
drug binding	20	3.350084	1.15E-08	P85973, P12785, P07340, Q01062, P04906, P20272, P04904, P09812, P20651, P62630, P63329, P17
identical protein binding	53	8.877722	1.64E-08	P42123, P47858, Q8K3E7, Q05695, O88767, P05982, P10760, P11167, P54690, P09034, P61765, Q6
actin filament binding	21	3.517588	7.21E-08	Q91ZN1, Q5RKI0, P31232, Q99MZ8, Q63598, Q7M0E3, Q99PD4, P31652, Q05764, Q9Z1P2, P45592
protein kinase binding	40	6.700168	7.80E-08	Q9Z2L0, P04906, P10686, P62755, Q5XHZ0, P62630, Q9QXY2, Q4V8C7, P13084, P61765, Q9ESI7, P
kinase binding	17	2.847571	8.64E-08	Q9JJP9, P42123, P47858, Q9Z0V6, P32851, Q9WU82, Q9Z2G8, O88767, P31000, P11167, P34058, F
NAD binding	13	2.177554	3.85E-07	P41565, Q6P6R2, P29266, Q9JLJ3, P10760, P41562, Q68FX0, P42123, Q99NA5, P04797, O88989, O
calmodulin binding	21	3.517588	5.46E-07	Q01066, Q05175, P63055, Q63560, P26431, P10687, P20651, Q63092, Q63862, P63329, P11275, Q0
protein homodimerization activity	57	9.547739	5.93E-07	P47858, Q8K3E7, P17764, P04218, O35077, O88767, Q9Z1P2, P13084, Q62768, Q6AYE2, Q91ZN1, I
RNA binding	39	6.532663	9.98E-07	Q9JJ54, P38656, Q9EPH8, P63055, P13471, P24050, Q09167, P61980, P27952, A7VJC2, P63174, O8
nucleotide binding	29	4.857621	8.54E-06	Q9JJ54, P38656, Q9EPH8, Q04400, Q4G061, Q9Z2L0, Q6URK4, Q794E4, P21588, Q7TP47, Q09167,
large ribosomal subunit rRNA binding	7	1.172529	1.02E-05	P24049, P19945, P62832, P02401, P23358, P62752, P84100
unfolded protein binding	13	2.177554	1.13E-05	Q7TPB1, Q5XIM9, P26772, Q5XHZ0, P06761, P18418, P13084, P34058, Q63525, P27682, Q66HD0, I
protein C-terminus binding	22	3.685092	1.66E-05	Q91ZN1, Q9EPH8, P07340, P47858, Q9Z0V6, P49911, P63012, P19527, O55164, Q01986, Q9WU82,
pyridoxal phosphate binding	11	1.842546	2.77E-05	P13221, P54690, Q05683, P53534, P09812, O35331, P14173, P00507, P02770, P18088, P50554
5.8S rRNA binding	5	0.837521	9.06E-05	P62919, P21533, P62278, P84100, P29314
pyruvate dehydrogenase (NAD+) activity	5	0.837521	9.06E-05	Q6P6R2, P49432, P26284, Q06437, P08461
syntaxin-1 binding	7	1.172529	1.05E-04	P61765, Q9QUL6, P63041, P84087, B5DF41, P31652, Q62768
5S rRNA binding	5	0.837521	1.59E-04	P21531, P50878, P05197, P05426, P09895
calcium-dependent protein binding	11	1.842546	1.84E-04	P09951, P26431, P04631, P84087, P32851, Q63357, Q63372, Q62826, Q9QZA2, P05964, Q63537
cytoskeletal protein binding	10	1.675042	2.12E-04	Q9QY17, Q91ZN1, P13596, Q9Z0W5, Q07266, P30427, P23928, P05065, Q01728, Q63537
glycoprotein binding	11	1.842546	3.23E-04	P18418, P22063, P31000, P60905, Q99376, P34058, P35559, P32851, P06761, P47819, Q63198
ion channel binding	14	2.345059	4.81E-04	Q7M730, Q9Z2L0, P62483, P32851, Q9WU82, Q9Z1P2, Q62658, P15791, P68255, Q62696, P34058,
peroxidase activity	6	1.005025	5.02E-04	Q921A4, Q9R063, Q9Z0V6, P01946, P02091, O35244
glutathione peroxidase activity	6	1.005025	6.40E-04	P04906, P04041, P57113, O35244, P08009, Q91XR8
peroxiredoxin activity	4	0.670017	7.73E-04	O88767, Q9R063, Q9Z0V6, O35244
structural constituent of cytoskeleton	10	1.675042	8.45E-04	Q5XIF6, Q05764, P31000, Q9QWN8, P69897, P30427, P16884, P19527, P47819, Q68FR8
hyaluronic acid binding	6	1.005025	9.99E-04	P03994, P55068, P55067, Q9ESM2, O35796, Q9ERB4
actin binding	20	3.350084	0.001167	Q91ZN1, Q9QWN8, P30427, Q08163, Q63598, P34926, P62024, Q63862, Q05764, P45592, Q63228,
protein complex binding	26	4.355109	0.001197	Q9Z0W7, Q9Z2L0, P49242, P27952, P62850, P16036, Q9ES53, P69897, P29994, P62870, Q9JJ19, Q6
threonine-type endopeptidase activity	6	1.005025	0.001227	P17220, P48004, P40112, P60901, P40307, P28075
potassium ion binding	5	0.837521	0.001455	P07340, P06686, O35331, P06685, P11980
sodium ion binding	5	0.837521	0.001887	P07340, P04775, P06686, O35331, P06685
receptor binding	25	4.187605	0.001937	Q1WIM3, P41562, P08592, P35559, P04218, P62198, P11915, P04762, Q8K4Y5, O88767, P13383, Q
SH3 domain binding	11	1.842546	0.001993	Q91V33, Q9JMC1, O08719, P08050, Q9Z0G8, Q62952, P97710, Q9QX69, P04041, P97846, Q9QZA2
fatty acid binding	6	1.005025	0.002138	P55051, P55053, P02770, P22057, Q6AYE2, P37377
integrin binding	11	1.842546	0.002501	P18418, P04785, Q05695, Q05546, Q9Z1P2, Q68FQ2, P49911, Q9R066, P15800, P47819, P40241
PDZ domain binding	12	2.01005	0.002541	Q05695, Q811U3, Q9QUL6, P08050, Q62696, O35430, Q9R066, Q6GMN2, Q62936, Q8K3M6, Q636
structural molecule activity	16	2.680067	0.002552	P70615, B0BN93, Q99P82, P60203, Q4AEF8, P16884, P23565, P03994, Q05764, P31000, F1LMZ8, P
oxygen binding	6	1.005025	0.003464	Q921A4, P04177, P01946, P07895, P02091, P02770
protein self-association	8	1.340034	0.003474	P22063, Q05695, P10760, P04636, P11167, P0C0A9, P16970, Q9JJ19
glutamate decarboxylase activity	3	0.502513	0.003538	P09606, Q05683, P18088
ATPase activity	15	2.512563	0.003792	P07340, D3ZAF6, P35435, Q63570, Q63413, P35559, P62198, P06761, P05708, P31399, Q9QUL6, P(
ATP-dependent protein binding	4	0.670017	0.004181	P60905, Q63413, Q9QUL6, P32851

KEGG	Count	%	PValue	Genes
Ribosome	55	9.21273	5.14E-30	P20280, P35427, P19945, P62755, P62278, P24050, P63326, P61354, P62752, P27952, P09895, Q63
Carbon metabolism	35	5.862647	1.66E-17	P47858, P04797, P52873, O88989, P17764, Q8VHF5, P26284, P00507, P08461, P16617, Q6P6R2, Q5
Biosynthesis of antibiotics	43	7.20268	9.10E-15	P42123, P47858, P04797, O88989, P17764, Q8VHF5, P00507, P26284, P08461, P16617, P04762, Q6
Citrate cycle (TCA cycle)	17	2.847571	2.40E-13	P41565, P41562, O88989, P52873, Q8VHF5, P49432, P14408, P26284, Q63270, Q9ER34, Q06437, P(
Biosynthesis of amino acids	22	3.685092	1.66E-10	P41565, P41562, P47858, P04797, P52873, P07323, Q8VHF5, P00507, Q63270, Q9ER34, P05065, P1
Pyruvate metabolism	15	2.512563	2.65E-09	Q9JLJ3, P42123, O88989, P52873, P17764, P49432, P14408, P26284, Q06437, P08461, Q6P6R2, P04
2-Oxocarboxylic acid metabolism	11	1.842546	4.45E-09	P41565, P13221, P41562, Q68FX0, P54690, Q99NA5, Q8VHF5, Q6AYS7, Q63270, P00507, Q9ER34
Glycolysis / Gluconeogenesis	17	2.847571	1.78E-07	Q9JLJ3, P42123, P47858, P04797, P07323, P49432, P26284, P05065, Q06437, P08461, P16617, P05
Glyoxylate and dicarboxylate metabolism	11	1.842546	2.85E-07	P09606, P04762, Q6P6R2, P04636, Q5I0P2, O88989, P17764, Q8VHF5, Q63270, Q9ER34, Q5XI22
Glucagon signaling pathway	19	3.18258	1.36E-06	P42123, P10687, P09812, P49432, P20651, P26284, Q06437, Q63009, P63329, P68182, P11275, P63
Proteasome	13	2.177554	1.79E-06	Q63570, B0BN93, P60901, P40307, P62198, P40112, P48004, P17220, Q4FZT9, F1LMZ8, O88761, P2
Butanoate metabolism	10	1.675042	4.49E-06	P17425, Q05683, B2GV06, P14604, P17764, P51650, P18088, P50554, Q5XI22, P29147
Gastric acid secretion	15	2.512563	9.59E-06	P10824, Q04400, P07340, P26431, P15791, P10687, P06686, P29994, P06687, P06685, P68403, Q9C
Amphetamine addiction	14	2.345059	1.04E-05	Q04400, P32851, P19643, P14173, P68403, P20651, P63329, P68182, P06300, P11275, P63100, P04
Metabolic pathways	96	16.0804	1.14E-05	P70627, Q5I6B8, D3ZAF6, P42123, P47858, P17764, P14173, P26284, P08461, P12075, P11951, Q6F
HIF-1 signaling pathway	17	2.847571	3.21E-05	P10686, Q99376, P04797, P07323, P62755, P49432, P68403, P26284, Q01986, Q06437, P11275, P05
Alanine, aspartate and glutamate metabolism	10	1.675042	3.38E-05	Q9R1T5, P70627, P09606, P13221, P09034, Q05683, P51650, P00507, P18088, P50554
cGMP-PKG signaling pathway	22	3.685092	3.92E-05	P10824, Q04400, P07340, Q9Z2L0, Q01062, P10687, P20651, Q01986, P63329, P81155, P63100, P1
Parkinson's disease	21	3.517588	4.82E-05	P10824, Q04400, P35435, Q9Z2L0, P68182, P37377, P12075, P81155, P11951, O88767, P10888, P19
Thyroid hormone synthesis	13	2.177554	9.77E-05	Q04400, P07340, P10687, P06686, P29994, P06687, P04041, P06761, Q66HD0, P06685, P68403, Q9
Thyroid hormone signaling pathway	17	2.847571	1.57E-04	P07340, P10686, P26431, P10687, P68403, Q01986, Q9WU82, P68182, P11167, Q62639, P60711, P(
Protein processing in endoplasmic reticulum	21	3.517588	1.97E-04	P04785, P60905, Q9JJP9, P54319, Q6PEC4, Q7TPJ0, P06761, P11598, Q63081, P18418, Q9ES53, P0
Insulin secretion	14	2.345059	2.57E-04	Q04400, P07340, P11167, P15791, P10687, P06686, P32851, P06687, P63012, P06685, P68403, Q9C
Long-term potentiation	12	2.01005	2.79E-04	P63100, P15791, P10687, P29994, P68403, Q9QW07, P20651, Q01986, P63329, P63086, P11275, P(
Valine, leucine and isoleucine degradation	11	1.842546	2.88E-04	Q6P6R2, Q5XIE6, P29266, Q9JLJ3, P17425, P54690, B2GV06, P14604, P17764, P50554, Q5XI22
GABAergic synapse	14	2.345059	2.90E-04	P10824, Q04400, O35458, O88871, Q9Z0U4, P68403, P68182, P09606, P43425, Q05683, Q9QUL6, C
Propanoate metabolism	8	1.340034	3.12E-04	Q5XIE6, Q6AYG5, P42123, P13086, P14604, P17764, P50554, Q5XI22
Glutamatergic synapse	16	2.680067	4.64E-04	P10824, Q04400, P10687, P24942, P68403, P20651, P63329, P68182, P43425, P09606, P63100, P31
Proximal tubule bicarbonate reclamation	7	1.172529	5.10E-04	P07340, Q9JI66, O88989, P06686, P06687, P06685, P27139
Alzheimer's disease	21	3.517588	5.71E-04	P35435, P08592, P04797, P10687, P35559, P20651, P63329, P37377, P12075, P11951, P10888, P19
Central carbon metabolism in cancer	11	1.842546	0.001007	P05708, P11167, P47858, P49432, P42346, P26284, Q01986, Q06437, P63086, P11980, P25113
Gap junction	13	2.177554	0.001138	P10824, Q5XIF6, Q04400, P08050, P69897, P10687, P29994, P68403, Q9QW07, Q01986, Q68FR8, P
Oxytocin signaling pathway	18	3.015075	0.001196	P10824, Q04400, P10687, P68403, P20651, Q01986, P63329, P68182, P11275, P63100, P97756, P6C
Synthesis and degradation of ketone bodies	5	0.837521	0.001427	P17425, B2GV06, P17764, Q5XI22, P29147
Dopaminergic synapse	16	2.680067	0.00155	P10824, Q04400, P10687, P19643, P14173, P68403, P20651, P63329, P68182, P11275, P43425, P04
Cocaine addiction	9	1.507538	0.001572	P10824, Q04400, P04177, Q6J4I0, P31422, P19643, P14173, P68182, P06300
Endocrine and other factor-regulated calcium r	9	1.507538	0.001815	P07340, P10687, P06686, P06687, P06685, P68403, Q9QW07, P07171, P68182
Bile secretion	11	1.842546	0.002263	Q04400, P07340, P11167, Q9JI66, P26431, P06686, P06687, P47863, P06685, P27139, P68182
Pancreatic secretion	13	2.177554	0.002433	Q04400, P07340, P11507, P26431, Q9JI66, P10687, P06686, P29994, P06687, P06685, P68403, Q9C
Oocyte meiosis	14	2.345059	0.002934	Q04400, Q6PEC4, P97690, P20651, Q01986, P63329, P68182, P11275, P63100, P15791, P68255, P6
Salivary secretion	11	1.842546	0.003766	Q04400, P07340, P26431, P10687, P06686, P29994, P06687, P06685, P68403, Q9QW07, P68182
Calcium signaling pathway	19	3.18258	0.004126	Q01066, Q9Z2L0, P10686, P10687, P68403, P20651, P63329, P68182, P11275, P81155, P63100, P11
Amyotrophic lateral sclerosis (ALS)	9	1.507538	0.004998	P04762, P63100, P07632, P31596, P16884, P19527, P12839, P20651, P63329
Renin secretion	10	1.675042	0.005115	P10824, Q01066, Q04400, P63100, P10687, P29994, Q9QW07, P20651, P63329, P68182
Estrogen signaling pathway	12	2.01005	0.00708	P10824, Q04400, O88871, P10687, Q9Z0U4, P34058, P29994, Q66HD0, Q9QW07, Q01986, P63086,
Serotonergic synapse	14	2.345059	0.007561	P10824, P43425, Q04400, P08592, P10687, P29994, P19643, P31652, P68403, P14173, Q9QW07, Q
Synaptic vesicle cycle	9	1.507538	0.010315	O35458, P61765, Q9QUL6, P63041, P84087, P61265, P32851, P63012, Q62768
Huntington's disease	19	3.18258	0.010617	P35435, Q9Z2L0, P07632, P10687, P12075, P81155, P11951, P10888, P19234, P31399, Q09073, Q5X
Tyrosine metabolism	7	1.172529	0.011042	P13221, P04177, P25093, P19643, P57113, P14173, P00507
Cysteine and methionine metabolism	7	1.172529	0.012469	P10760, P13221, P04636, P42123, P97532, O88989, P00507

ANNEX 2

Table S1. Differentially expressed proteins that change in the same direction (downregulated) in at least three different proteomic studies related to the ageing nervous system. The first column shows the gene name of the 44 proteins downregulated (red cells) with ageing. Numbers indicate the reference number that can be checked in Table 6.1.

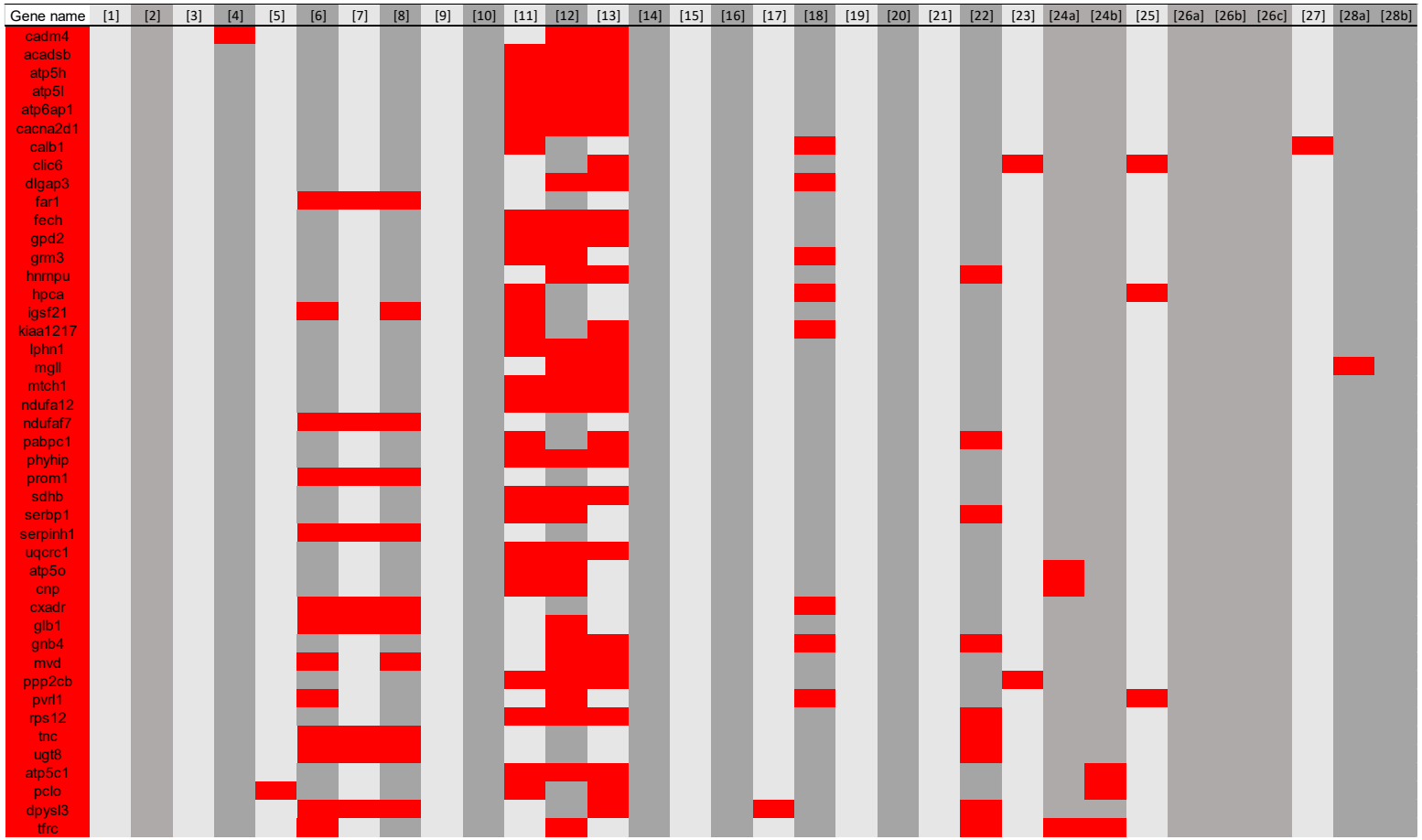

Table S2. Differentially expressed proteins that change in the same direction (upregulated) in at least three different proteomic studies about the ageing nervous system. The first column shows the gene name of the 103 proteins upregulated (green cells) with ageing. Numbers indicate the reference number that can be checked in Table 6.1.

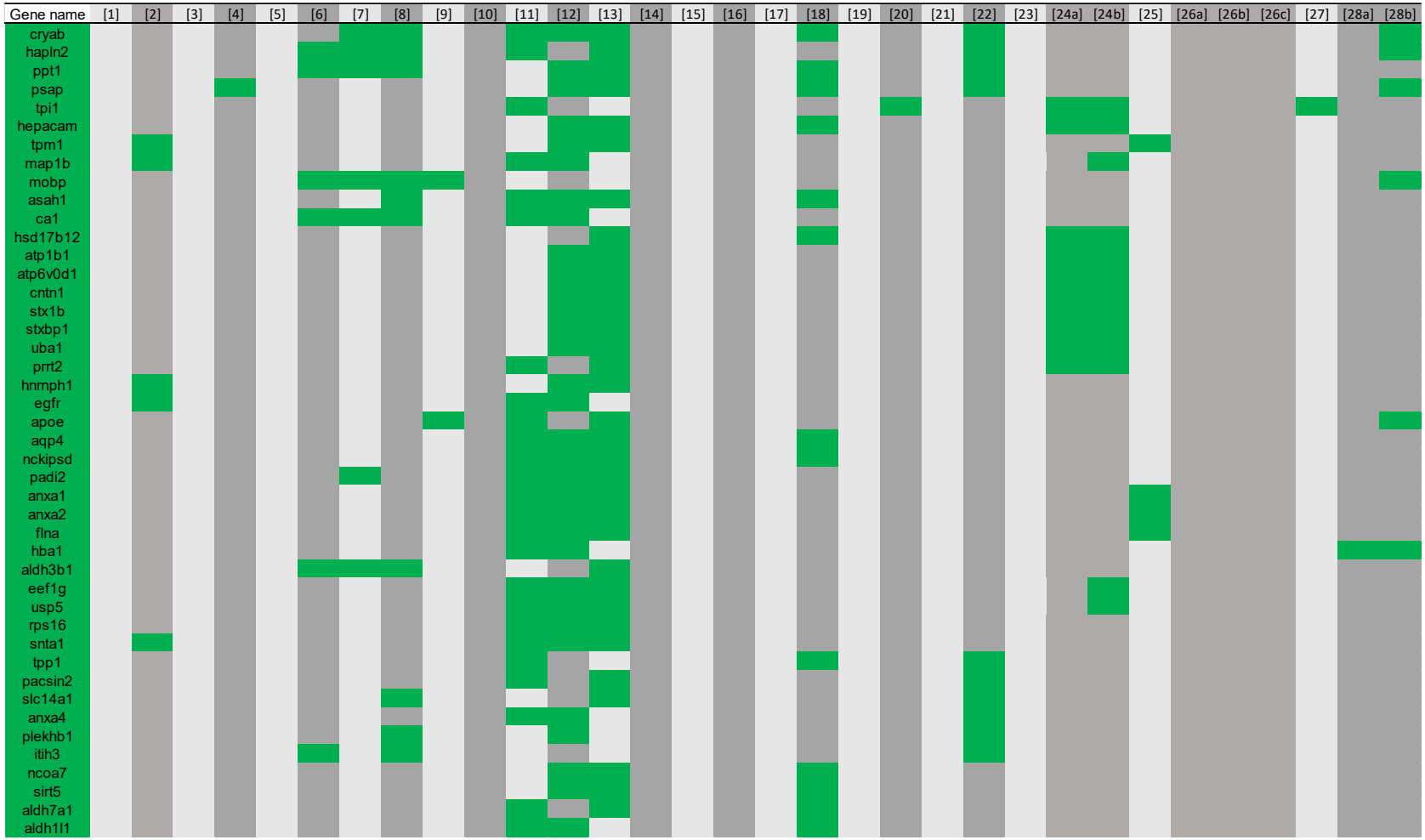

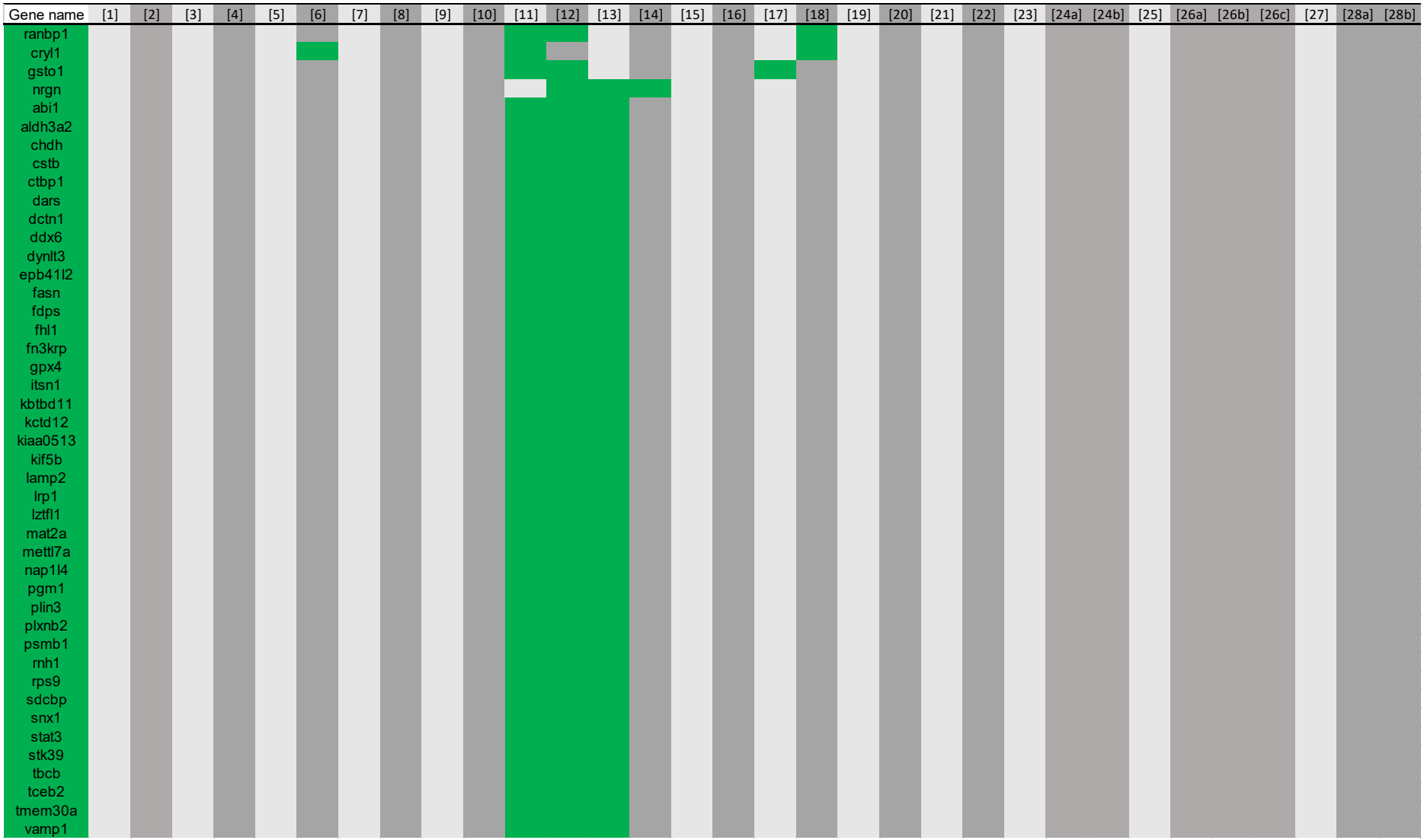
Gene name
[1] [2] [3] [4] [5] [6] [7] [8] [9] [10] [11] [12] [13] [14] [15] [16] [17] [18] [19] [20] [21] [22] [23] [24a] [24b] [25] [26a] [26b] [26c] [27] [28a] [28b]
ranbp1
cryl1
gsto1
nrgn
abi1
aldh3a2
chdh
cstb
ctbp1
dars
dctn1
ddx6
dynlt3
epb41l2
fasn
fdps
fhl1
fn3krp
gpx4
itsn1
kbtbd11
kctd12
kiaa0513
kif5b
lamp2
lrp1
lztfl1
mat2a
mettl7a
nap1l4
pgm1
plin3
plxnb2
psmb1
rnh1
rps9
sdcbp
snx1
stat3
stk39
tbcb
tceb2
tmem30a
vamp1

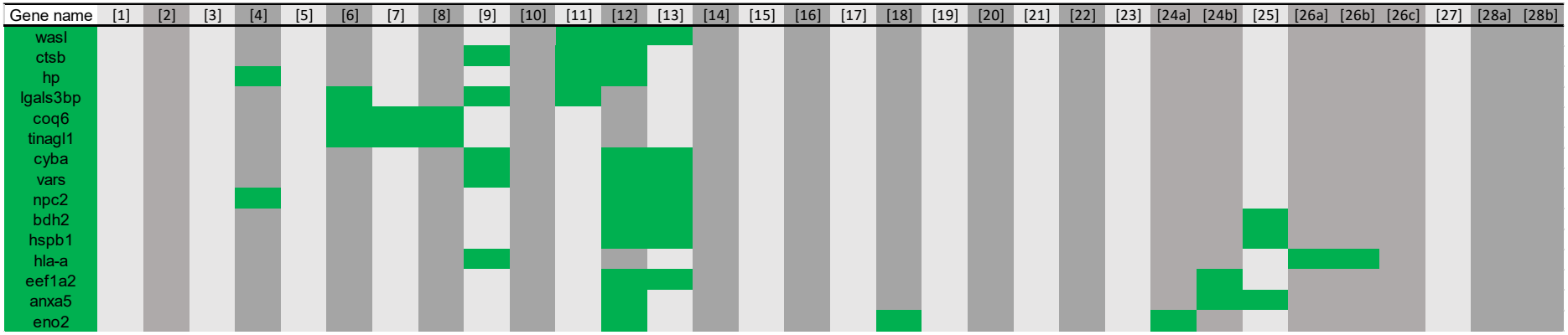
Gene name
[1]
[2]
[3]
[4]
[5]
[6]
[7]
[8]
[9]
[10]
[11]
[12]
[13]
[14]
[15]
[16]
[17]
[18]
[19]
[20]
[21]
[22]
[23]
[24a]
[24b]
[25]
[26a]
[26b]
[26c]
[27]
[28a]
[28b]
wasl
ctsb
hp
lgals3bp
coq6
tinagl1
cyba
vars
npc2
bdh2
hspb1
hla-a
eef1a2
anxa5
eno2

Table S3. Differentially expressed proteins that change in different direction (down- and upregulated) in at least three different proteomic studies about the ageing nervous system. The first column shows the gene name of the 501 proteins downregulated (red cells) or upregulated (green cells) with ageing. Numbers indicate the reference number that can be checked in Table 6.1.

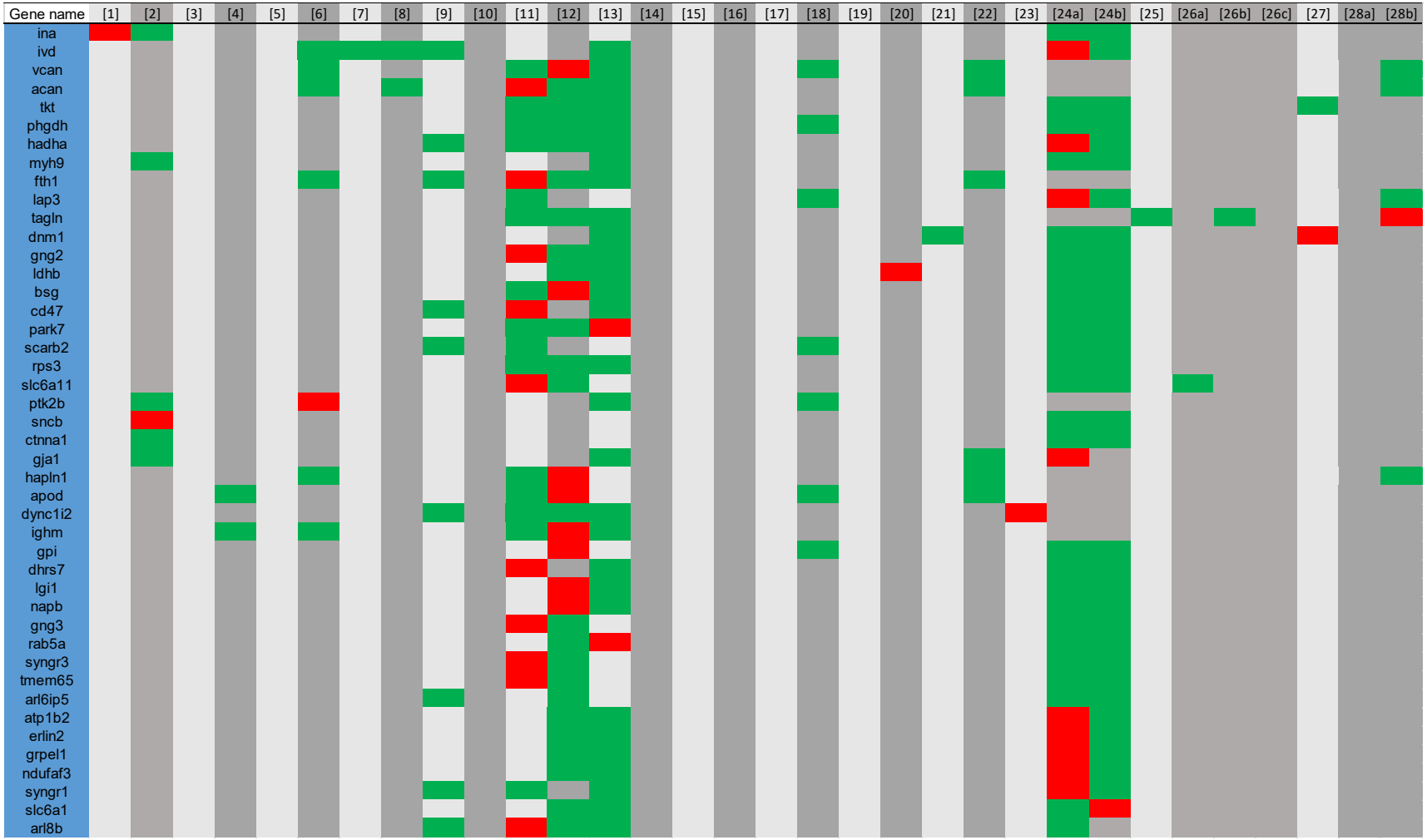

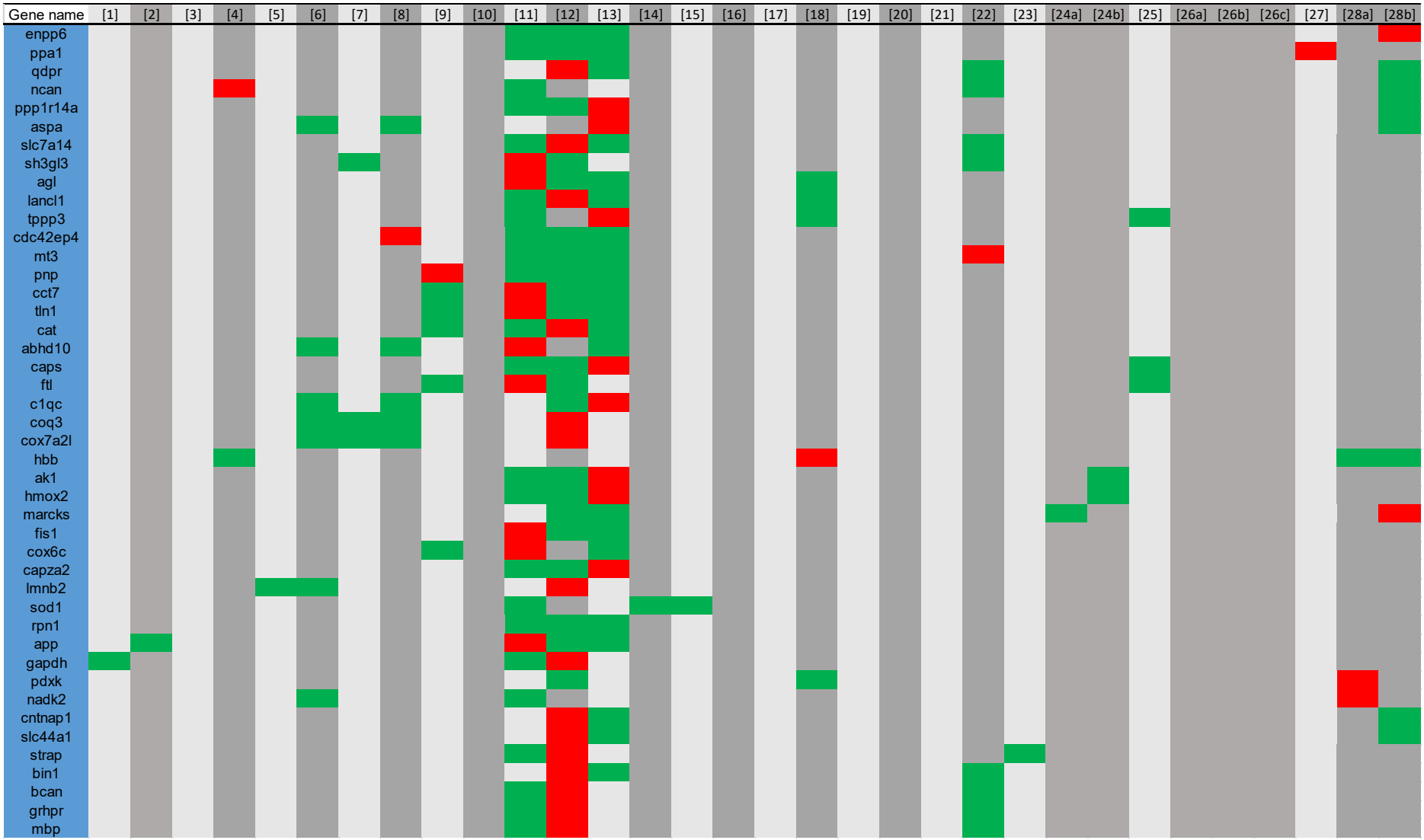
Gene name
[1] [2] [3] [4] [5] [6] [7] [8] [9] [10] [11] [12] [13] [14] [15] [16] [17] [18] [19] [20] [21] [22] [23] [24a] [24b] [25] [26a] [26b] [26c] [27] [28a] [28b]
enpp6
ppa1
qdpr
ncan
ppp1r14a
aspa
slc7a14
sh3gl3
agl
lancl1
tppp3
cdc42ep4
mt3
pnp
cct7
tln1
cat
abhd10
caps
ftl
c1qc
coq3
cox7a2l
hbb
ak1
hmox2
marcks
fis1
cox6c
capza2
lmnb2
sod1
rpn1
app
gapdh
pdxk
nadk2
cntnap1
slc44a1
strap
bin1
bcan
grhpr
mbp

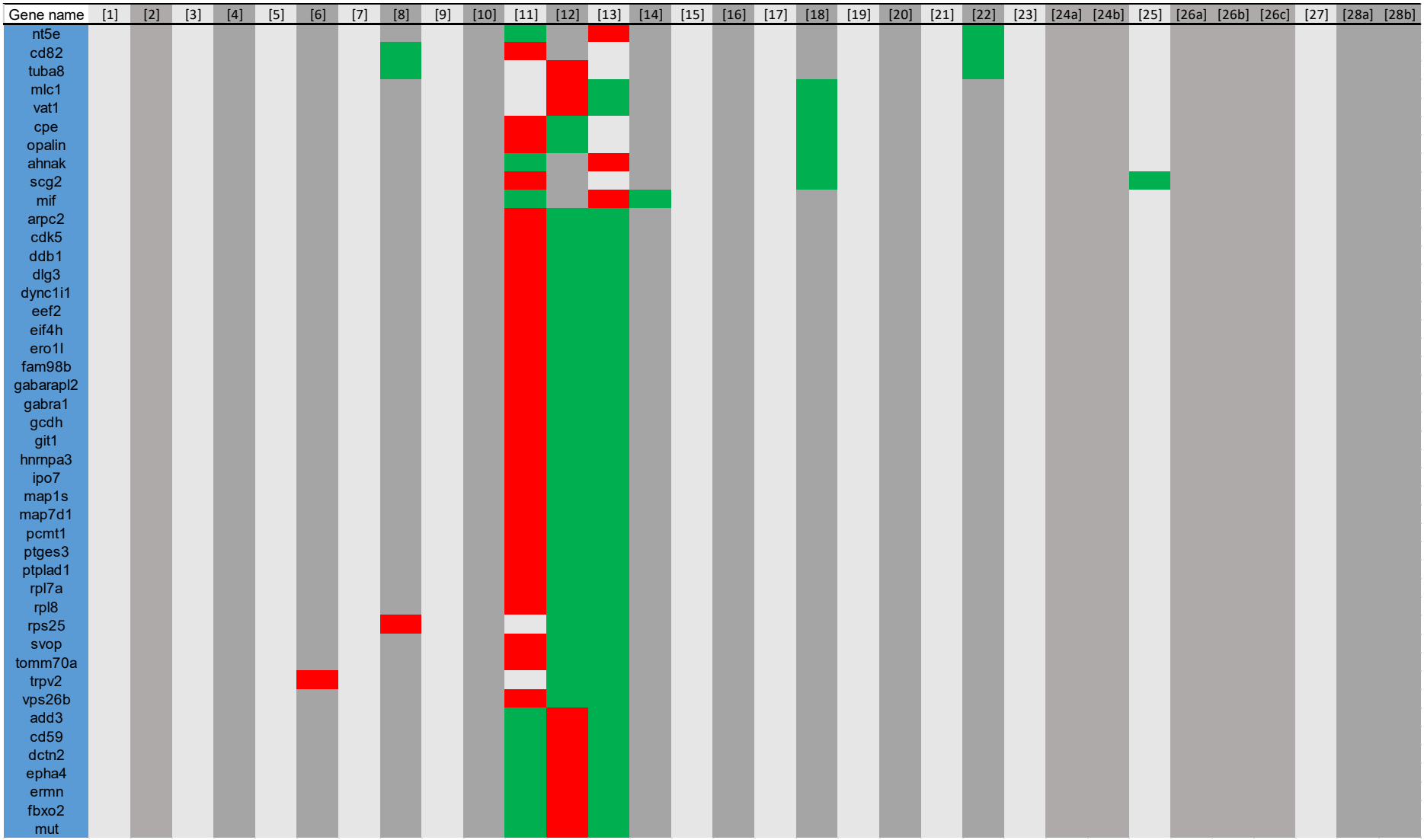
Gene name
[1] [2] [3] [4] [5] [6] [7] [8] [9] [10] [11] [12] [13] [14] [15] [16] [17] [18] [19] [20] [21] [22] [23] [24a] [24b] [25] [26a] [26b] [26c] [27] [28a] [28b]
nt5e
cd82
tuba8
mlc1
vat1
cpe
opalin
ahnak
scg2
mif
arpc2
cdk5
ddb1
dlg3
dync1i1
eef2
eif4h
ero1l
fam98b
gabarapl2
gabra1
gcdh
git1
hnrnpa3
ipo7
map1s
map7d1
pcmt1
ptges3
ptplad1
rpl7a
rpl8
rps25
svop
tomm70a
trpv2
vps26b
add3
cd59
dctn2
epha4
ermn
fbxo2
mut

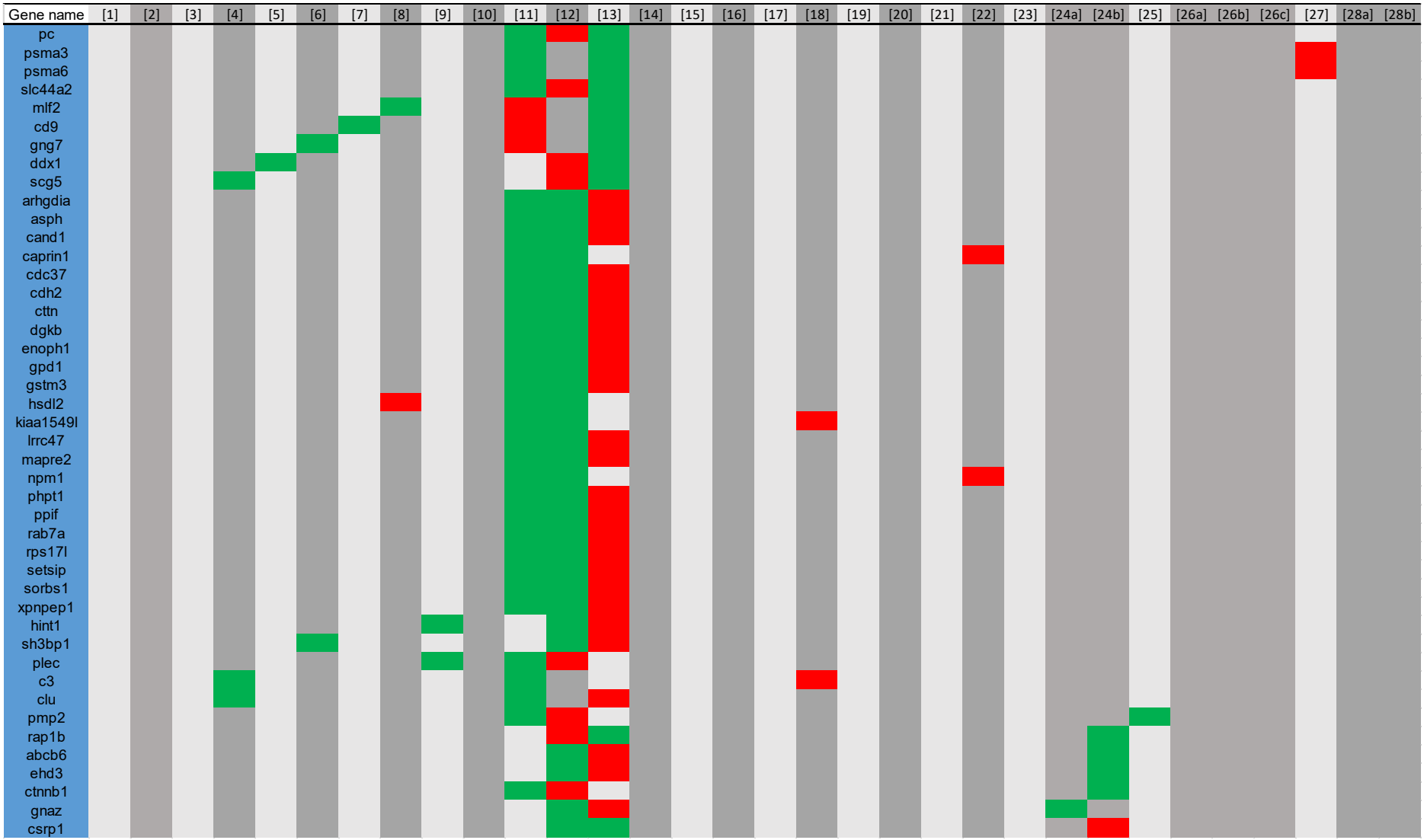
Gene name
[1] [2] [3] [4] [5] [6] [7] [8] [9] [10] [11] [12] [13] [14] [15] [16] [17] [18] [19] [20] [21] [22] [23] [24a] [24b] [25] [26a] [26b] [26c] [27] [28a] [28b]
pc
psma3
psma6
slc44a2
mlf2
cd9
gng7
ddx1
scg5
arhgdia
asph
cand1
caprin1
cdc37
cdh2
cttn
dgkb
enoph1
gpd1
gstm3
hsdl2
kiaa1549l
lrrc47
mapre2
npm1
phpt1
ppif
rab7a
rps17l
setsip
sorbs1
xpnpep1
hint1
sh3bp1
plec
c3
clu
pmp2
rap1b
abcb6
ehd3
ctnnb1
gnaz
csrp1

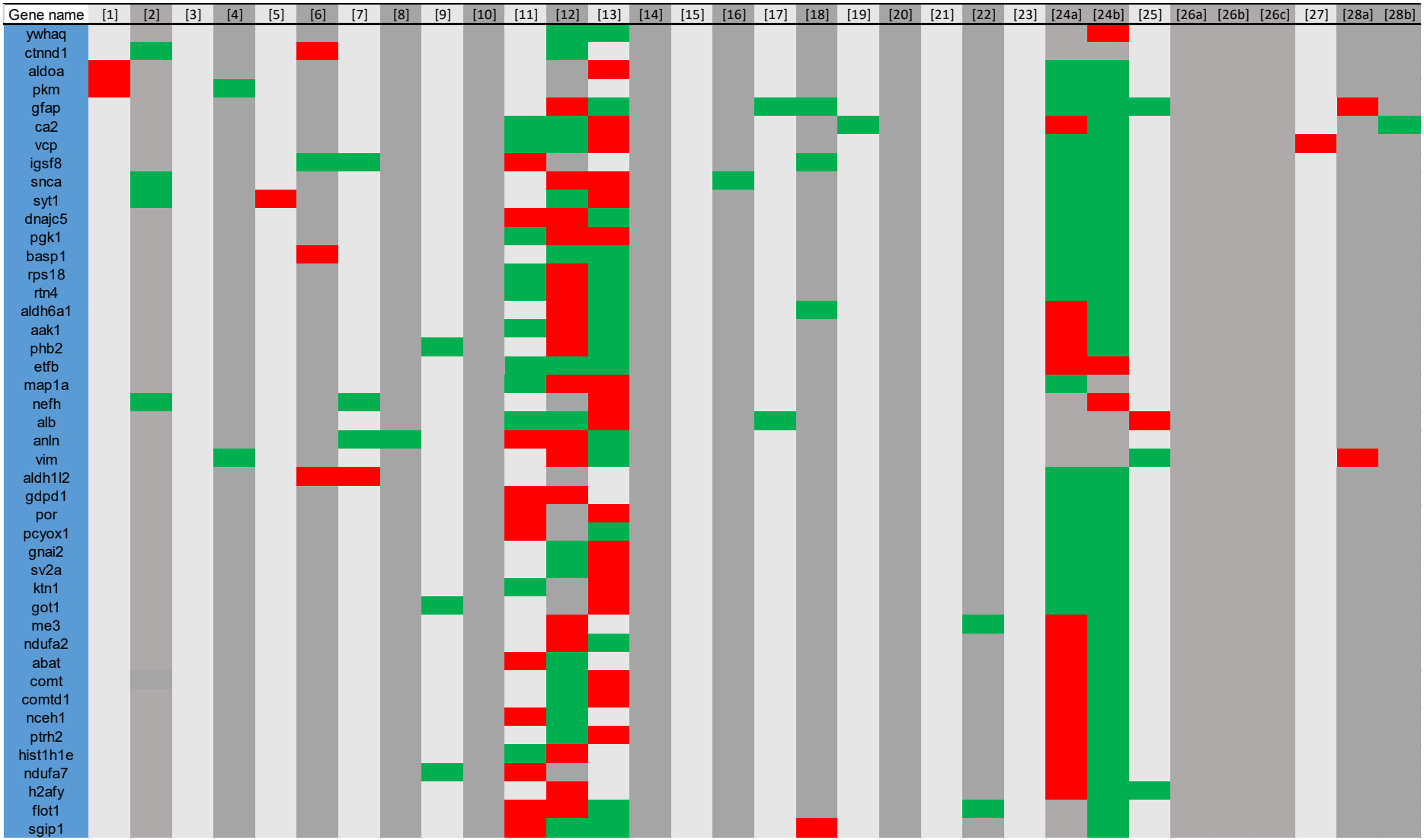
Gene name
[1]
[2]
[3]
[4]
[5]
[6]
[7]
[8]
[9]
[10]
[11]
[12]
[13]
[14]
[15]
[16]
[17]
[18]
[19]
[20]
[21]
[22]
[23]
[24a]
[24b]
[25]
[26a]
[26b]
[26c]
[27]
[28a]
[28b]
ywhaq
ctnnd1
aldoa
pkm
gfap
ca2
vcp
igsf8
snca
syt1
dnajc5
pgk1
basp1
rps18
rtn4
aldh6a1
aak1
phb2
etfb
map1a
nefh
alb
anln
vim
aldh1l2
gdpd1
por
pcyox1
gnai2
sv2a
ktn1
got1
me3
ndufa2
abat
comt
comtd1
nceh1
ptrh2
hist1h1e
ndufa7
h2afy
flot1
sgip1

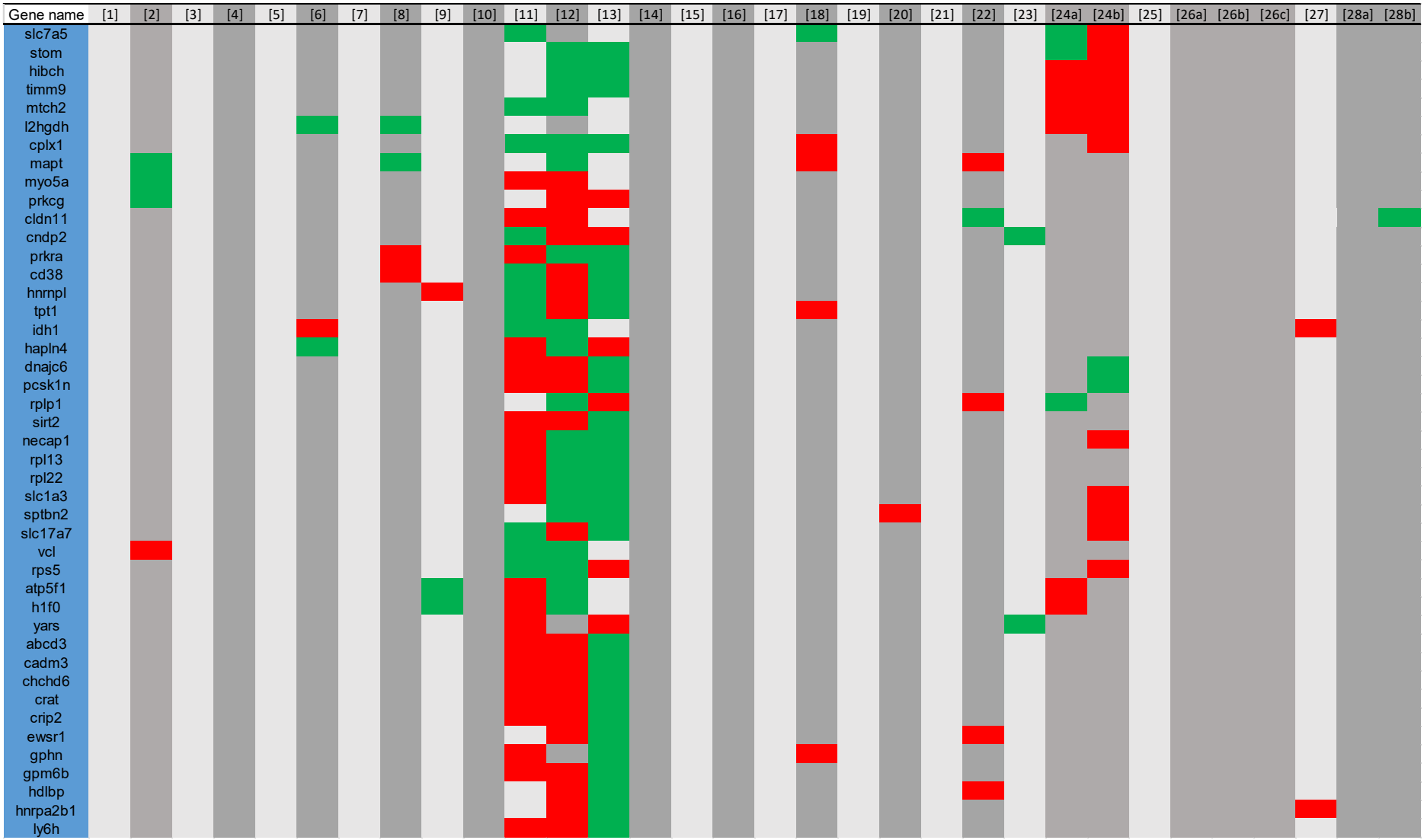
Gene name
[1]
[2]
[3]
[4]
[5]
[6]
[7]
[8]
[9]
[10]
[11]
[12]
[13]
[14]
[15]
[16]
[17]
[18]
[19]
[20]
[21]
[22]
[23]
[24a]
[24b]
[25]
[26a]
[26b]
[26c]
[27]
[28a]
[28b]
slc7a5
stom
hibch
timm9
mtch2
l2hgdh
cplx1
mapt
myo5a
prkcg
cldn11
cndp2
prkra
cd38
hnrnpl
tpt1
idh1
hapln4
dnajc6
pcsk1n
rplp1
sirt2
necap1
rpl13
rpl22
slc1a3
sptbn2
slc17a7
vcl
rps5
atp5f1
h1f0
yars
abcd3
cadm3
chchd6
crat
crip2
ewsr1
gphn
gpm6b
hdlbp
hnrpa2b1
ly6h

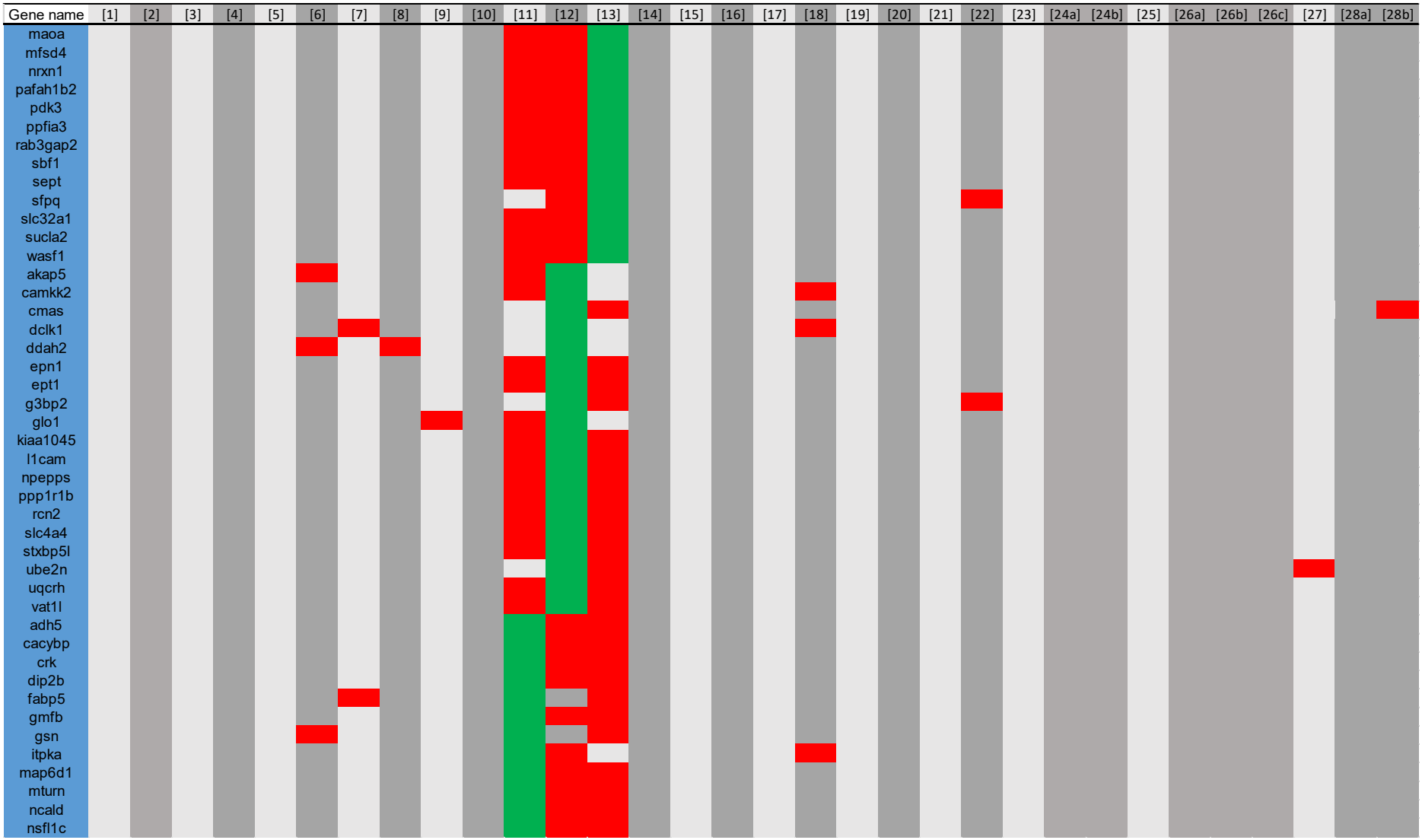
Gene name
[1] [2] [3] [4] [5] [6] [7] [8] [9] [10] [11] [12] [13] [14] [15] [16] [17] [18] [19] [20] [21] [22] [23] [24a] [24b] [25] [26a] [26b] [26c] [27] [28a] [28b]
maoa
mfsd4
nrxn1
pafah1b2
pdk3
ppfia3
rab3gap2
sbf1
sept
sfpq
slc32a1
sucla2
wasf1
akap5
camkk2
cmas
dclk1
ddah2
epn1
ept1
g3bp2
glo1
kiaa1045
l1cam
npepps
ppp1r1b
rcn2
slc4a4
stxbp5l
ube2n
uqcrh
vat1l
adh5
cacybp
crk
dip2b
fabp5
gmfb
gsn
itpka
map6d1
mturn
ncald
nsfl1c

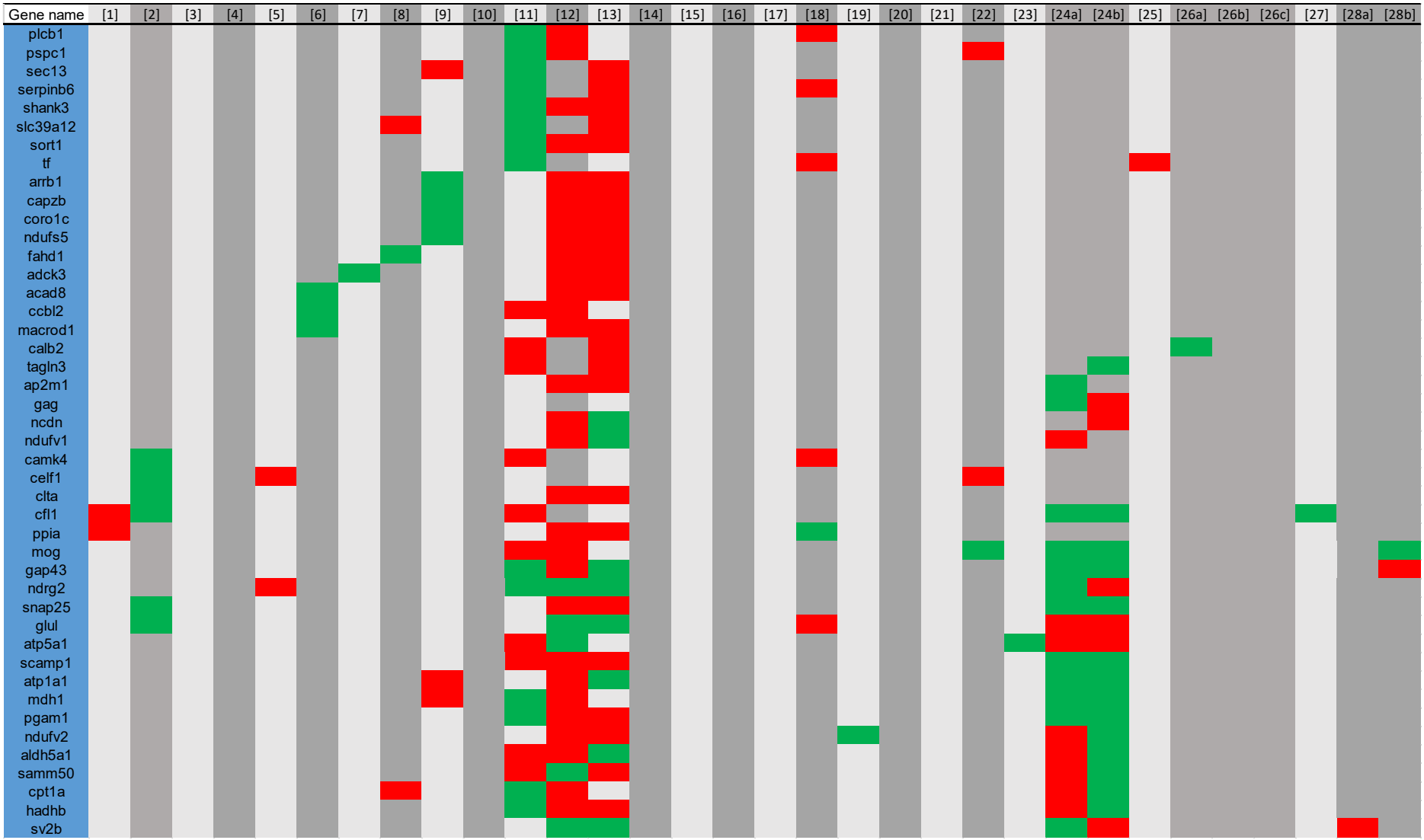
Gene name
[1]
[2]
[3]
[4]
[5]
[6]
[7]
[8]
[9]
[10]
[11]
[12]
[13]
[14]
[15]
[16]
[17]
[18]
[19]
[20]
[21]
[22]
[23]
[24a]
[24b]
[25]
[26a]
[26b]
[26c]
[27]
[28a]
[28b]
plcb1
pspc1
sec13
serpinb6
shank3
slc39a12
sort1
tf
arrb1
capzb
coro1c
ndufs5
fahd1
adck3
acad8
ccbl2
macrod1
calb2
tagln3
ap2m1
gag
ncdn
ndufv1
camk4
celf1
clta
cfl1
ppia
mog
gap43
ndrg2
snap25
glul
atp5a1
scamp1
atp1a1
mdh1
pgam1
ndufv2
aldh5a1
samm50
cpt1a
hadhb
sv2b

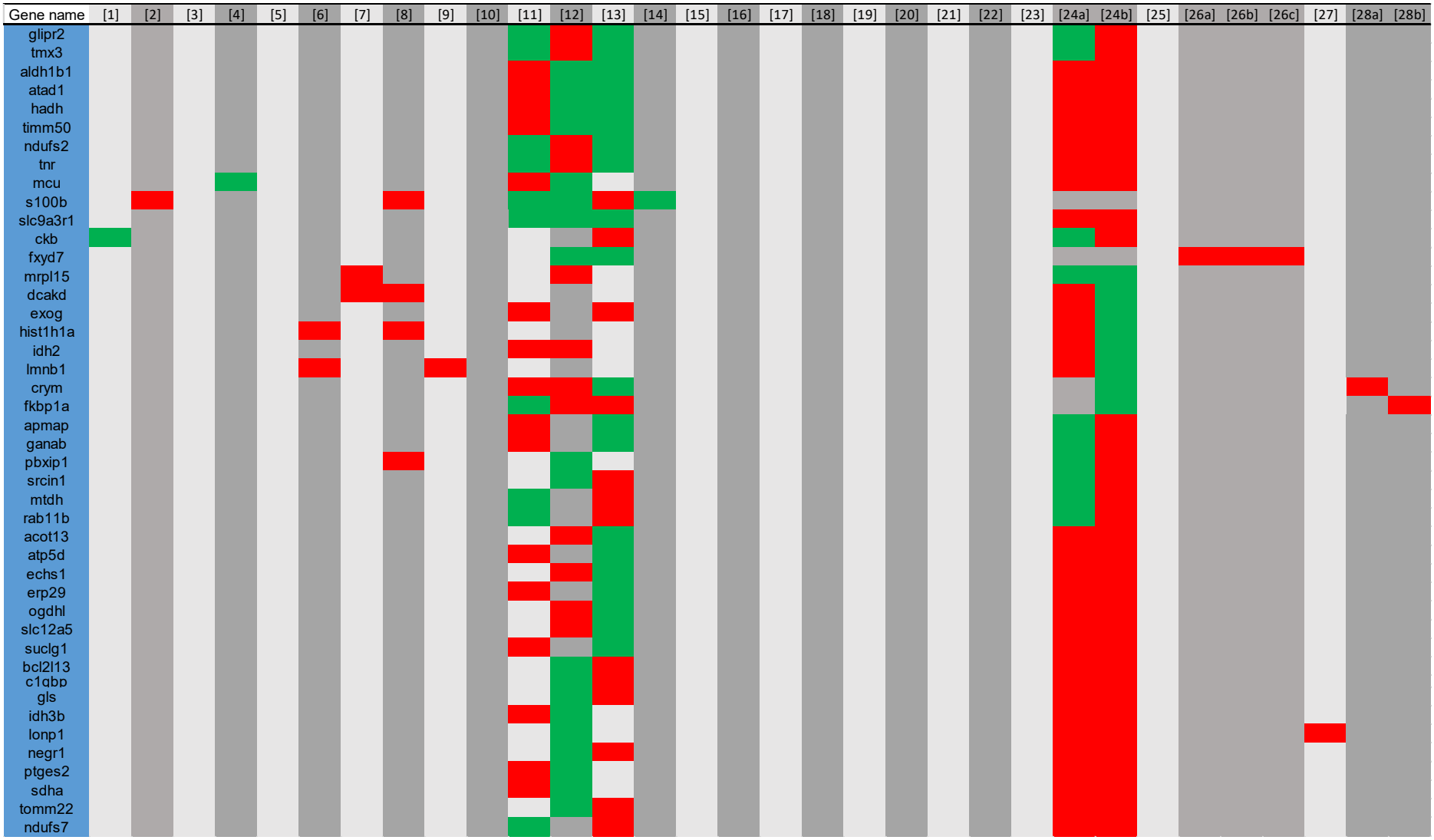
Gene name
[1]
[2]
[3]
[4]
[5]
[6]
[7]
[8]
[9]
[10]
[11]
[12]
[13]
[14]
[15]
[16]
[17]
[18]
[19]
[20]
[21]
[22]
[23]
[24a]
[24b]
[25]
[26a]
[26b]
[26c]
[27]
[28a]
[28b]
glipr2
tmx3
aldh1b1
atad1
hadh
timm50
ndufs2
tnr
mcu
s100b
slc9a3r1
ckb
fxyd7
mrpl15
dcakd
exog
hist1h1a
idh2
lmnb1
crym
fkbp1a
apmap
ganab
pbxip1
srcin1
mtdh
rab11b
acot13
atp5d
echs1
erp29
ogdhl
slc12a5
suclg1
bcl2l13
c1qbp
gls
idh3b
lonp1
negr1
ptges2
sdha
tomm22
ndufs7

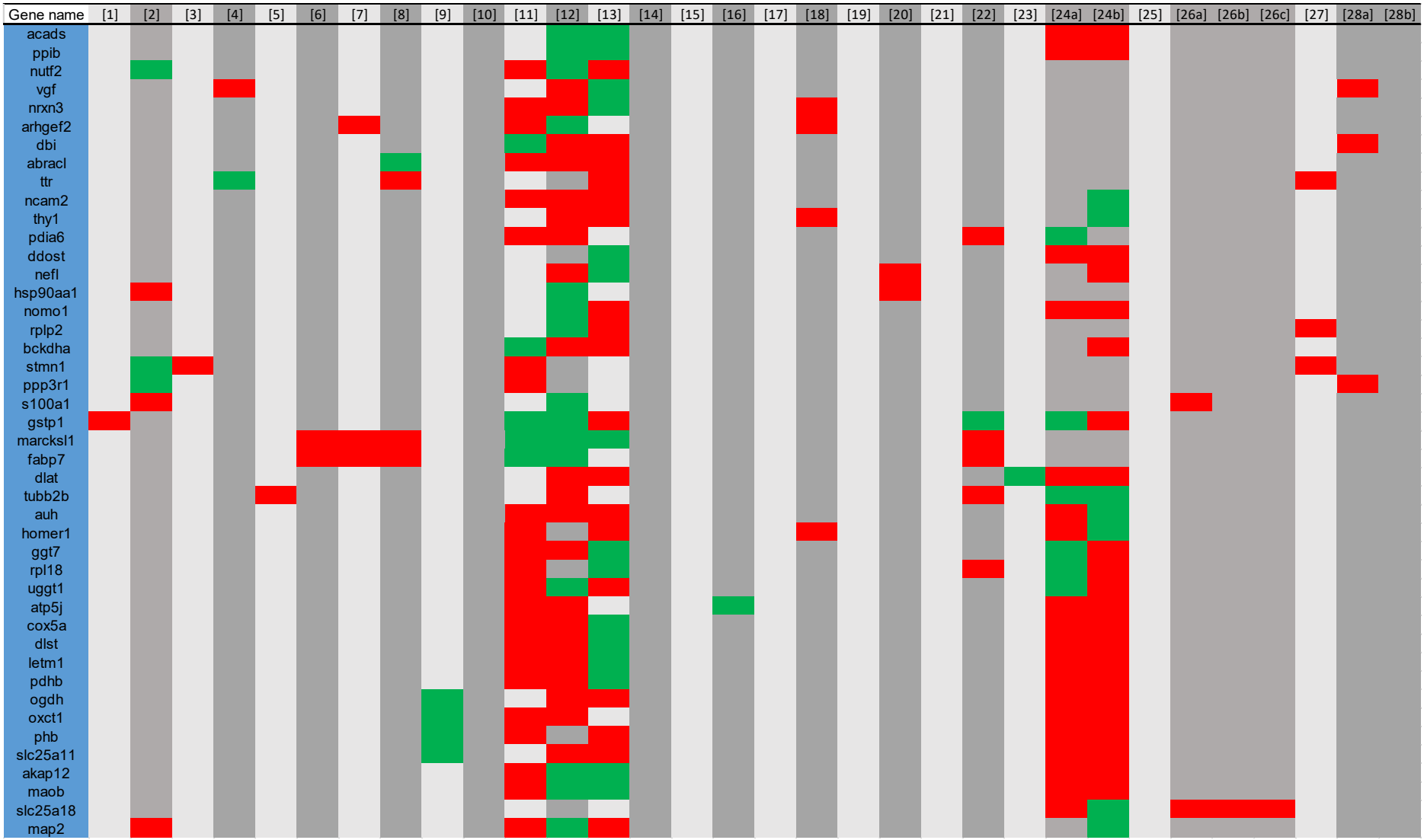
Gene name
[1] [2] [3] [4] [5] [6] [7] [8] [9] [10] [11] [12] [13] [14] [15] [16] [17] [18] [19] [20] [21] [22] [23] [24a] [24b] [25] [26a] [26b] [26c] [27] [28a] [28b]
acads
ppib
nutf2
vgf
nrxn3
arhgef2
dbi
abracl
ttr
ncam2
thy1
pdia6
ddost
nefl
hsp90aa1
nomo1
rplp2
bckdha
stmn1
ppp3r1
s100a1
gstp1
marcksl1
fabp7
dlat
tubb2b
auh
homer1
ggt7
rpl18
uggt1
atp5j
cox5a
dlst
letm1
pdhb
ogdh
oxct1
phb
slc25a11
akap12
maob
slc25a18
map2

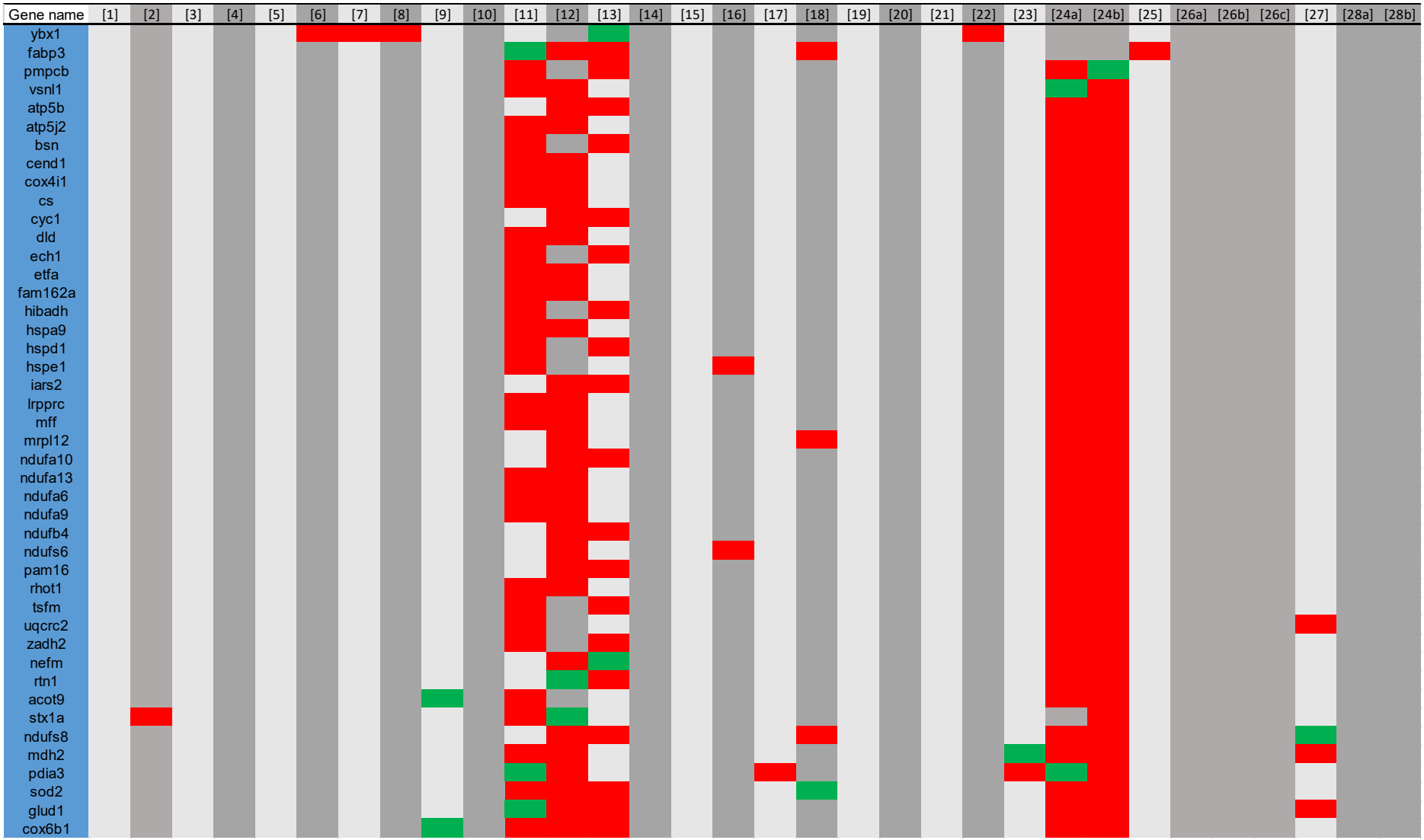
Gene name
[1] [2] [3] [4] [5] [6] [7] [8] [9] [10] [11] [12] [13] [14] [15] [16] [17] [18] [19] [20] [21] [22] [23] [24a] [24b] [25] [26a] [26b] [26c] [27] [28a] [28b]
ybx1
fabp3
pmpcb
vsnl1
atp5b
atp5j2
bsn
cend1
cox4i1
cs
cyc1
dld
ech1
etfa
fam162a
hibadh
hspa9
hspd1
hspe1
iars2
lrpprc
mff
mrpl12
ndufa10
ndufa13
ndufa6
ndufa9
ndufb4
ndufs6
pam16
rhot1
tsfm
uqcrc2
zadh2
nefm
rtn1
acot9
stx1a
ndufs8
mdh2
pdia3
sod2
glud1
cox6b1

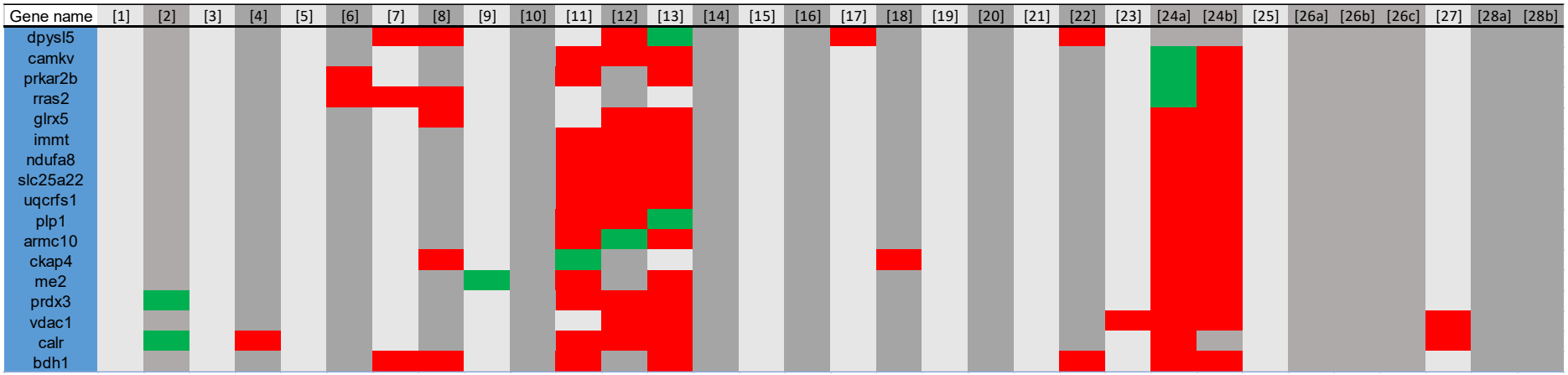
Gene name
[1]
[2]
[3]
[4]
[5]
[6]
[7]
[8]
[9]
[10]
[11]
[12]
[13]
[14]
[15]
[16]
[17]
[18]
[19]
[20]
[21]
[22]
[23]
[24a]
[24b]
[25]
[26a]
[26b]
[26c]
[27]
[28a]
[28b]
dpysl5
camkv
prkar2b
rras2
glrx5
immt
ndufa8
slc25a22
uqcrfs1
plp1
armc10
ckap4
me2
prdx3
vdac1
calr
bdh1

Table S4. Gene Ontology (GO) and KEGG pathway analyses of the differentially expressed proteins that change in the same direction (downregulated, Table S1) in the ageing nervous system proteomic studies.

GO enriched term	Count	Proteins
Biological process		
Mitochondrial ATP synthesis coupled proton transport	4	ATP5C1, ATP5H, ATP5L, ATP5O
ATP synthesis coupled proton transport	4	ATP5C1, ATP5H, ATP5L, ATP5O
ATP biosynthetic process	4	ATP5C1, ATP5H, ATP5L, ATP5O
Cellular component		
Extracellular exosome	21	CACNA2D1, CADM4, ATP5C1, GLB1, CLIC6, TFRC, SERBP1, ACADSB, GNB4, CALB1, PROM1, PCLO, PPP2CB, ATP5H, ATP5L, SDHB, ATP5O, ATP6AP1, SERPINH1, CNP, PABPC1
Membrane	12	NDUFA12, ATP5C1, TFRC, SERBP1, TNC, HNRNPU, RPS12, CNP, MTCH1, PABPC1, MGLL, PCLO
Mitochondrial inner membrane	11	NDUFA12, FECH, ATP5C1, ATP5H, SDHB, ATP5L, ATP5O, CNP, MTCH1, UQCRC1, GPD2
Mitochondrion	10	FECH, ATP5C1, ATP5H, SDHB, ATP5L, ATP5O, ACADSB, NDUFAF7, MTCH1, UQCRC1
Extracellular space	9	CXADR, GLB1, TFRC, TNC, SERPINH1 NDUFAF7, CNP, DPYSL3, PROM1
Mitochondrial proton-transporting ATP synthase complex	4	ATP5C1, ATP5H, ATP5L, ATP5O
Mitochondrial matrix	4	FECH, ATP5C1, ACADSB,NDUFAF7
Myelin sheath	3	ATP5C1, GNB4, UQCRC1
Molecular function		
Poly(A) RNA binding	7	ATP5C1, TFRC, SERBP1, HNRNPU, RPS12, SERPINH1, PABPC1
Proton-transporting ATP synthase activity, rotational mechanism	5	ATP5C1, ATP5H, ATP5L, ATP5O, ATP6AP1
Transmembrane transporter activity	4	ATP5C1, ATP5H, ATP5L, ATP5O
ATPase activity	4	ATP5C1, ATP5H, ATP5L, ATP5O
Electron carrier activity	3	NDUFA12, SDHB, ACADSB

KEGG enriched pathway	Count	Proteins
Metabolic pathways	14	ATP5C1, GLB1, ACADSB, FECH, NDUFA12, MVD, ATP5H, ATP5L, SDHB, ATP5O, ATP6AP1, UGT8, MGLL, UQCRC1
Oxidative phosphorylation	8	NDUFA12, ATP5C1, ATP5H, SDHB, ATP5L, ATP5O, ATP6AP1, UQCRC1
Parkinson's disease	6	NDUFA12, ATP5C1, ATP5H, SDHB, ATP5O, UQCRC1

Table S5. Gene Ontology (GO) and KEGG pathway analyses of the differentially expressed proteins that change in the same direction (upregulated, Table S2) in the ageing nervous system proteomic studies.

GO enriched term	Count	Proteins
Biological process		
Oxidation-reduction process	13	ALDH3B1, CTBP1, ALDH3A2, GSTO1, COQ6, ALDH7A1, ALDH1L1, CHDH, CRYL1, FASN, GPX4, HSD17B12, CYBA
Cell-cell adhesion	11	FASN, ANXA2, DDX6, ABI1, SDCBP, EEF1G, SNX1, PLIN3, PACSIN2, RANBP1, KIF5B
Negative regulation of apoptotic process	9	CRYAB, STAT3, ANXA1, EGFR, FLNA, ANXA5, ANXA4, PPT1, HSPB1
Receptor-mediated endocytosis	8	HBA1, HP, EGFR, LRP1, TINAGL1, PPT1, LGALS3BP, APOE
Nervous system development	8	TBCB, NRGN, DCTN1, STAT3, TPP1, PPT1, MAP1B, MOBP
Platelet degranulation	6	STXBP1, ITIH3, FLNA, LAMP2, PSAP, LGALS3BP
Viral process	6	FDPS, PSMB1, STAT3, ABI1, HLA-A, RANBP1
Cellular oxidant detoxification	5	HBA1, HP, GSTO1, GPX4, APOE
Movement of cell or subcellular component	5	TPM1, WASL, STAT3, ABI1, HSPB1
Positive regulation of neuron projection development	5	CNTN1, PLXNB2, TMEM30A, NCKIPSD, RANBP1
Negative regulation of neuron apoptotic process	5	STXBP1, ITSN1, LRP1, PPT1, APOE
Epithelial cell differentiation	4	BDH2, TPP1, ANXA4, CTSB
Negative regulation of catalytic activity	4	ANXA2, RNH1, ANXA5, ANXA4
Protein stabilization	4	STXBP1, ATP1B1, FLNA, LAMP2
Positive regulation of vesicle fusion	3	ANXA2, ANXA1, KIF5B
Positive regulation of potassium ion transport	3	FHL1, STK39, KIF5B
Cellular aldehyde metabolic process	3	ALDH3B1, ALDH3A2, ALDH7A1
Positive regulation of phosphorylation	3	ITSN1, SDCBP, EGFR
One-carbon metabolic process	3	MAT2A, CA1, ALDH1L1
Glycolytic process	3	TPI1, PGM1, ENO2
Platelet aggregation	3	STXBP1, FLNA, HSPB1
Long-chain fatty-acyl-CoA biosynthetic process	3	FASN, HSD17B12, PPT1
Gluconeogenesis	3	TPI1, PGM1, ENO2
Proteolysis involved in cellular protein catabolic process	3	PSMB1, TINAGL1, CTSB
Response to hydrogen peroxide	3	CRYAB, HBA1, HP
IRE1-mediated unfolded protein response	3	DCTN1, ATP6V0D1, TPP1
Cellular component		
Extracellular exosome	57	CRYAB, HP, CSTB, EEF1G, PLXNB2, PPT1, CRYL1, FASN, TPI1, ATP1B1, LAMP2, PACSIN2,

		TCEB2, HLA-A, HBA1, ITSN1, ANXA2, WASL, ANXA1, GSTO1, RPS16, TINAGL1, ANXA5, ANXA4, ALDH7A1, APOE, PSMB1, DARS, NPC2, BDH2, ATP6V0D1, ABI1, PADI2, RNH1, LGALS3BP, CNTN1, FLNA, PSAP, HSPB1, METTL7A, ITIH3, GPX4, ENO2, CTSB, STXBP1, ALDH3B1, ALDH3A2, UBA1, CA1, ALDH1L1, RPS9, ASAH1, KCTD12 TPP1, SDCBP, PGM1, EPB41L2
Cytoplasm	57	CRYAB, CSTB, STAT3, EEF1G, CRYL1, FASN, PACSIN2, CTBP1, ANXA1, GSTO1, LRP1, TINAGL1, ANXA5, ANXA4, ALDH7A1, APOE, HNRNPH1, PSMB1, DARS, BDH2, DDX6, ABI1, PADI2, RNH1, EGFR, EEF1A2, FLNA, PLIN3, AQP4, PSAP, HSPB1, FDPS, METTL7A, FHL1, DYNLT3, SNX1, NAP1L4, SNTA1, MAP1B, KIF5B, STXBP1,TBCB, ALDH3B1, UBA1, HEPACAM, CA1, ALDH1L1, RANBP1, RPS9, DCTN1, KIAA0513, SDCBP, PGM1, STK39, EPB41L2, PLEKHB1, STX1B
Cytosol	50	CRYAB, STAT3, EEF1G, PPT1, CRYL1, FASN, TPM1, SIRT5, TPI1, PACSIN2, TCEB2, HBA1, ANXA2, ITSN1, WASL, GSTO1, RPS16, VARS, ALDH7A1, BDH2, DARS, PSMB1, DDX6, ABI1, PADI2, FLNA, PLIN3, VAMP1, HSPB1, FDPS, FHL1, GPX4, SNX1, ENO2, NCKIPSD, MAP1B, STXBP1, ALDH3B1, LZTFL1, UBA1, CA1, ALDH1L1, RPS9, DCTN1, SDCBP, PGM1, STK39, MAT2A,STX1B, FN3KRP
Membrane	31	CNTN1, EGFR, EEF1G, FLNA, PLIN3, PPT1, AQP4, METTL7A, FASN, ATP1B1, SNX1, LAMP2, HLA-A, KIF5B, HBA1, ANXA2, RPS16, TMEM30A, ANXA5, APOE, RPS9, HNRNPH1, DARS, DDX6, DCTN1, ATP6V0D1, SDCBP, STX1B, CYBA, PRRT2, LGALS3BP
Mitochondrion	18	STXBP1, CRYAB, UBA1, VARS, COQ6, ALDH7A1, PSAP, ALDH1L1, FDPS, BDH2, FASN, SIRT5, DDX6, TPP1, GPX4, CYBA, CTSB, MOBP
Extracellular space	17	HP, CSTB, ANXA2, ANXA1, EGFR, TINAGL1, PPT1, PSAP, HSPB1, APOE, ASAH1, TPI1, SDCBP, LAMP2, ENO2, CTSB, LGALS3BP
Cell-cell adherens junction	14	ANXA2, ANXA1, EGFR, EEF1G, FLNA, PLIN3, RANBP1, FASN, DDX6, ABI1, SDCBP, SNX1, PACSIN2, KIF5B
Focal adhesion	13	RPS9, FHL1, ANXA1, EGFR, SDCBP, LRP1, RPS16, FLNA, EPB41L2, ANXA5, PACSIN2, CYBA, HSPB1
Golgi apparatus	11	CRYL1, CRYAB, FASN, SNX1, TMEM30A, PLIN3, COQ6, PPT1, CYBA, HLA-A, APOE
Lysosome	9	ASAH1, USP5, NPC2, TPP1, TINAGL1, LAMP2, PPT1, PSAP, CTSB
Cytoskeleton	8	TPM1, ABI1, SDCBP, STK39, EPB41L2, PACSIN2, SNTA1, HSPB1

Cell surface	8	CRYAB, ANXA2, ANXA1, EGFR, PLXNB2, VAMP1, ANXA4, HLA-A
Myelin sheath	7	STXBP1, CRYAB, CNTN1, ATP1B1, EEF1A2, ENO2, MOBP
Basolateral plasma membrane	7	ANXA2, ANXA1, EGFR, ATP1B1, STK39, SLC14A1, AQP4
Apical plasma membrane	7	ATP6V0D1, ANXA1, EGFR, ATP1B1, STK39, TMEM30A, CYBA
Extracellular matrix	7	ANXA2, FLNA, RPS16, TINAGL1, HSPB1, LGALS3BP, APOE
Neuronal cell body	7	NRGN, LRP1, FLNA, EEF1A2, PPT1, CYBA, APOE
Cell junction	7	KCTD12, ITSN1, EPB41L2, VAMP1, SNTA1, MAP1B, PRRT2
Endosome	6	ANXA2, ANXA1, EGFR, LRP1, PLIN3, CYBA
Lysosomal membrane	6	ANXA2, ATP6V0D1, LRP1, UBA1, LAMP2, PSAP
Extrinsic component of membrane	5	ANXA1, STK39, SNX1, EPB41L2, PACSIN2
Lysosomal lumen	5	ASAH1, TPP1, LAMP2, PPT1, PSAP
Melanosome	5	FASN, ANXA2, TPP1, SDCBP, CTSB
Vesicle	5	ALDH3B1, ANXA2, ANXA1, SNX1, KIF5B
Blood microparticle	5	HBA1, HP, SDCBP, LGALS3BP, APOE
Endosome membrane	5	ATP6V0D1, EGFR, SNX1, UBA1, PLIN3
Membrane raft	5	CNTN1, ANXA2, SDCBP, EGFR, PPT1
Phagocytic vesicle membrane	4	ATP6V0D1, LAMP2, CYBA, HLA-A
Sarcolemma	4	ANXA2, ANXA1, ATP1B1, SNTA1
Early endosome membrane	4	ANXA1, EGFR, SNX1, HLA-A
Endocytic vesicle lumen	3	HBA1, HP, APOE
Cytosolic small ribosomal subunit	3	RPS9, HBA1, RPS16
Extracellular vesicle	3	SDCBP, ATP1B1, APOE
Endocytic vesicle	3	ITSN1, EGFR, KIF5B
Molecular function		
Cadherin binding involved in cell-cell adhesion	14	ANXA2, ANXA1, EGFR, EEF1G, FLNA, PLIN3, RANBP1, FASN, DDX6, ABI1, SDCBP, SNX1, PACSIN2, KIF5B
Identical protein binding	13	STXBP1, CRYAB, STAT3, LZTFL1, EGFR, ANXA4, HSPB1, APOE, DYNLT3, SDCBP, SNX1, MAT2A, PACSIN2
Oxidoreductase activity	9	ALDH3B1, BDH2, FASN, ALDH3A2, GSTO1, HSD17B12, COQ6, ALDH7A1, ALDH1L1
Cytoskeletal protein binding	5	TPM1, ANXA2, ABI1, PACSIN2, NCKIPSD
Aldehyde dehydrogenase (NAD) activity	4	ALDH3B1, ALDH3A2, ALDH7A1, ALDH1L1
Glycoprotein binding	4	CNTN1, SDCBP, EGFR, FLNA
SNARE binding	3	STXBP1, VAMP1, STX1B
Calcium-dependent protein binding	3	ANXA2, ANXA1, ANXA4
Cysteine-type endopeptidase activity	3	USP5, TINAGL1, CTSB

KEGG enriched pathway	Count	Proteins
Metabolic pathways	17	ALDH3B1, ALDH3A2, COQ6, PPT1, ALDH7A1, CRYL1, FDPS, CHDH, ASAH1, BDH2, FASN, ATP6V0D1, TPI1, PGM1, HSD17B12, MAT2A, ENO2
Lysosome	8	ASAH1, NPC2, ATP6V0D1, TPP1, LAMP2, PPT1, PSAP, CTSB
Glycolysis / Gluconeogenesis	6	ALDH3B1, ALDH3A2, TPI1, PGM1, ENO2, ALDH7A1
Biosynthesis of antibiotics	6	FDPS, ALDH3A2, TPI1, PGM1, ENO2, ALDH7A1
Histidine metabolism	3	ALDH3B1, ALDH3A2, ALDH7A1

References used for the comparison analysis of the ageing nervous system (Table 6.1) (these references appear in the main reference section, but appear here for easy consultation of the data)

[1] Argüelles S, Cano M, Machado A, Ayala A. Effect of aging and oxidative stress on elongation factor-2 in hypothalamus and hypophysis. Mechanisms of ageing and development. 2011 Feb 28;132(1):55-64.

[2] Chadwick W, Martin B, Park SS, Wang L, Daimon CM, Brenneman R, Maudsley S. GIT2 acts as a potential keystone protein in functional hypothalamic networks associated with age-related phenotypic changes in rats. PLoS One. 2012 May 14;7(5):e36975.

[3] Chen W, Ji J, Xu X, He S, Ru B. Proteomic comparison between human young and old brains by two-dimensional gel electrophoresis and identification of proteins. International journal of developmental neuroscience. 2003 Jun 30;21(4):209-16.

[4] Chen CP, Preston JE, Zhou S, Fuller HR, Morgan DG, Chen R. Proteomic analysis of age-related changes in ovine cerebrospinal fluid. Experimental gerontology. 2018 Jul 15;108:181-8.

[5] Cutler AA, Dammer EB, Doung DM, Seyfried NT, Corbett AH, Pavlath GK. Biochemical isolation of myonuclei employed to define changes to the myonuclear proteome that occur with aging. Aging cell. 2017 Aug 1;16(4):738-49.

[6] [7] [8] Duda P, Wójcicka O, Wiśniewski JR, Rakus D. Global quantitative TPA-based proteomics of mouse brain structures reveals significant alterations in expression of proteins involved in neuronal plasticity during aging. Aging (Albany NY). 2018 Jul;10(7):1682.

[9] Flowers A, Bell-Temin H, Jalloh A, Stevens SM, Bickford PC. Proteomic analysis of aged microglia: shifts in transcription, bioenergetics, and nutrient response. Journal of neuroinflammation. 2017 May 3;14(1):96.

[10] [11] [12] [13] Graham LC, Naldrett MJ, Kohama SG, Smith C, Lamont DJ, McColl BW, Gillingwater TH, Skehel P, Urbanski HF, Wishart TM. Regional Molecular Mapping of Primate Synapses during Normal Healthy Aging. Cell reports. 2019 Apr 23;27(4):1018-26.

[14] [15] Hamezah HS, Durani LW, Yanagisawa D, Ibrahim NF, Aizat WM, Bellier JP, Makpol S, Ngah WZ, Damanhuri HA, Tooyama I. Proteome profiling in the hippocampus,

medial prefrontal cortex, and striatum of aging rat. Experimental gerontology. 2018 Oct 1;111:53-64.

[16] Mao L, Zabel C, Wacker MA, Nebrich G, Sagi D, Schrade P, Bachmann S, Kowald A, Klose J. Estimation of the mtDNA mutation rate in aging mice by proteome analysis and mathematical modeling. Experimental gerontology. 2006 Jan 1;41(1):11-24.

[17] McGinn MJ, Colello RJ, Sun D. Age-related proteomic changes in the subventricular zone and their association with neural stem/progenitor cell proliferation. Journal of neuroscience research. 2012 Jun 1;90(6):1159-68.

[18] Pabba M, Scifo E, Kapadia F, Nikolova YS, Ma T, Mechawar N, Tseng GC, Sibille E. Resilient protein co-expression network in male orbitofrontal cortex layer 2/3 during human aging. Neurobiology of aging. 2017 Oct 1;58:180-90.

[19] Pollard A, Shephard F, Freed J, Liddell S, Chakrabarti L. Mitochondrial proteomic profiling reveals increased carbonic anhydrase II in aging and neurodegeneration. Aging (Albany NY). 2016 Oct;8(10):2425.

[20] Poon HF, Castegna A, Farr SA, Thongboonkerd V, Lynn BC, Banks WA, Morley JE, Klein JB, Butterfield DA. Quantitative proteomics analysis of specific protein expression and oxidative modification in aged senescence-accelerated-prone 8 mice brain. Neuroscience. 2004 Dec 31;126(4):915-26.

[21] Poon HF, Vaishnav RA, Getchell TV, Getchell ML, Butterfield DA. Quantitative proteomics analysis of differential protein expression and oxidative modification of specific proteins in the brains of old mice. Neurobiology of aging. 2006 Jul 31;27(7):1010-9.

[22] Smidak RS, Sialana FJ, Kristofova M, Stojanovic T, Rajcic D, Malikovic J, Feyissa DD, Korz V, Hoeger H, Wackerlig J, Mechtcheriakova D. Reduced levels of the synaptic functional regulator FMRP in dentate gyrus of the aging Sprague-Dawley rat. Frontiers in aging neuroscience. 2017; 9:384.

[23] Wille M, Schümann A, Wree A, Kreutzer M, Glocker MO, Mutzbauer G, Schmitt O. The Proteome Profiles of the Cerebellum of Juvenile, Adult and Aged Rats—An Ontogenetic Study. International journal of molecular sciences. 2015 Sep 7;16(9):21454-85.

[24] Stauch KL, Purnell PR, Villeneuve LM, Fox HS. Proteomic analysis and functional characterization of mouse brain mitochondria during aging reveal alterations in energy metabolism. Proteomics. 2015 May 1;15(9):1574-86.

[25] Xu B, Gao Y, Zhan S, Xiong F, Qiu W, Qian X, Wang T, Wang N, Zhang D, Yang Q, Wang R. Quantitative protein profiling of hippocampus during human aging. Neurobiology of aging. 2016 Mar 31;39:46-56.

[26] Xu B, Xiong F, Tian R, Zhan S, Gao Y, Qiu W, Wang R, Ge W, Ma C. Temporal lobe in human aging: A quantitative protein profiling study of samples from Chinese Human Brain Bank. Experimental gerontology. 2016 Jan 31;73:31-41.

[27] Yang S, Liu T, Li S, Zhang X, Ding Q, Que H, Yan X, Wei K, Liu S. Comparative proteomic analysis of brains of naturally aging mice. Neuroscience. 2008 Jun 26;154(3):1107-20.

[28] Chapter 3 of this Thesis.

ANNEX 3

Table S1. Comparison of the differentially expressed proteins in humans with PD and PD models, using proteins that appeared in at least two different studies.

Differentially expressed proteins in humans with PD and PD models
Four proteins commonly expressed in humans with PD and PD models
ALDH1A1, EEF2, GAPDH, VIM
64 proteins expressed only in humans with PD
A2M, AK1, ALB, ANXA1, APOA1, APOA2, APOC3, APOH, APOM, ARHGDIB, ATP5PD, AZGP1, BBOX1, BSCL2, C3, C4B, CACNA2D1, CALB1, CHGB, CLU, CP, DLG2, EEF1A2, EIF5A, EPDR1, ERAP1, ERP29, EZR, FTL, GAD1, GC, GNAO1, GSN, GSTO1, HEBP2, HLA-DRB1, HP, INA, ITGB1, LAP3, LGALS3, MPP2, NCAN, NUTF2, OAT, ORM1, PEA15, PFN1, PGRMC1, PKM, PRNP, PTGES3, RBP4, RPL3, RTN4, SAA1, SEC23A, SLC32A1, STXBP1, TF, TLN1, TTR, TUBA8, UGGT1
109 proteins expressed only in PD models
UGGT1, ACADL, ACO2, ADH5, AKAP5, ALDH1L1, ALDH2, ALDH4A1, ALDH5A1, ALDOA, ALDOC, ANXA5, ANXA6, ANXA7, ATP5B, ATP5J2, ATP6V1B2, CALM1, CAMK2D, CANX, CAP1, CAPZA2, CCT2, CCT4, CKB, CLTA, CLTC, CNP, COL4A2, COPS4, CST3, CTSD, CYC1, DHRS1, DLD, DST, ECHS1, EHD3, ENO2, FSCN1, GDA, GFAP, GLUD1, GM237, GNAI3, GOT1, GPM6B, GSTM1, GSTM5, H2AFV, HIST2H3C2, HK1, HNRPAB, HSPA5, HSPA8, IGSF8, INPP1, IVD, KIF2A, MARCK2, MBP, MT-ATP8, NCDN, NDUFA10, NDUFS2, NDUFS3, NDUFS7, NEFL, NIT2, NSF, OMG, P4HB, PCP4, PDE10A, PDE1B, PDHB, PDIA3, PGM2, PHB, PLP1, PPP1R9A, PPP2R1A, PRDX6, PREI3, PRKCC, PROSC, RAB21, RAB3A, RTN1, SFRS7, SIRT2, SLC25A5, SLC2A3, SNAP25, SRM, STX1A, SYN1, SYN2, SYT2, TOLLIP, TPM3, TUBA4A, UCHL1, UQCRC1, USP14, VAPB, VCP, VDAC1, YWHAE, YWHAZ

Table S2. Comparison of the differentially expressed proteins in PD (humans and PD models) and ageing of the nervous system, using proteins that appeared in at least two different studies in the case of PD and three studies in the case of the ageing nervous system.

Differentially expressed proteins in PD and ageing nervous system
70 proteins commonly expressed in PD and ageing nervous system
ADH5, AK1, AKAP5, ALB, ALDH1L1, ALDH5A1, ALDOA, ANXA1, ANXA5, ATP5B, ATP5J2, C3, CACNA2D1, CALB1, CAPZA2, CKB, CLTA, CLU, CNP, CYC1, DLD, ECHS1, EEF1A2, EEF2, EHD3, ENO2, ERP29, FTL, GAPDH, GFAP, GLUD1, GOT1, GPM6B, GSN, GSTO1, HP, IGSF8,INA, IVD, LAP3, MBP, NCAN, NCDN, NDUFA10, NDUFS2, NDUFS7, NEFL, NUTF2, PDHB, PDIA3, PHB, PKM, PLP1, PTGES3, RTN1, RTN4, SIRT2, SLC32A1, SNAP25, STX1A, STXBP1, TF, TLN1, TTR, TUBA8, UGGT1, UQCRC1, VCP, VDAC1, VIM
578 proteins expressed only in ageing nervous system
AAK1, ABAT, ABCB6, ABCD3, ABHD10, ABI1, ABRACL, ACAD8, ACADS, ACADSB, ACAN, ACOT13, ACOT9, ADCK3, ADD3, AGL, AHNAK, AKAP12, ALDH1B1, ALDH1L2, ALDH3A2, ALDH3B1, ALDH6A1, ALDH7A1, ANLN, ANXA2, ANXA4, AP2M1, APMAP, APOD, APOE, APP, AQP4, ARHGDIA, ARHGEF2, ARL6IP5 ARL8B, ARMC10, ARPC2, ARRB1, ASAH1, ASPA, ASPH, ATAD1, ATP1A1, ATP1B1, ATP1B2, ATP5A1, ATP5C1, ATP5D, ATP5F1, ATP5H, ATP5J, ATP5L, ATP5O, ATP6AP1, ATP6V0D1, AUH, BASP1, BCAN, BCKDHA, BCL2L13, BDH1, BDH2, BIN1, BSG, BSN, C1QBP, C1QC, CA1, CA2,CACYBP, CADM3, CADM4, CALB2, CALR, CAMK4, CAMKK2, CAMKV,CAND1, CAPRIN1, CAPS, CAPZB, CAT, CCBL2, CCT7, CD38, CD47, CD59, CD82, CD9, CDC37, CDC42EP4, CDH2, CDK5, CELF1, CEND1, CFL1, CHCHD6, CHDH, CKAP4, CLDN11, CLIC6, CMAS, CNDP2, CNTN1, CNTNAP1, COMT, COMTD1, COQ3, COQ6, CORO1C, COX4I1, COX5A, COX6B1, COX6C, COX7A2L, CPE, CPLX1, CPT1A, CRAT, CRIP2, CRK, CRYAB, CRYL1, CRYM, CS, CSRP1, CSTB, CTBP1, CTNNA1, CTNNB1, CTNND1, CTSB, CTTN, CXADR, CYBA, DARS, DBI, DCAKD, DCLK1, DCTN1, DCTN2, DDAH2, DDB1, DDOST, DDX1, DDX6, DGKB, DHRS7, DIP2B, DLAT, DLG3, DLGAP3, DLST, DNAJC5, DNAJC6, DNM1, DPYSL3,DPYSL5, DYNC1I1, DYNC1I2, DYNLT3, ECH1, EEF1G, EGFR, EIF4H, ENOPH1, ENPP6, EPB41L2, EPHA4, EPN1, EPT1, ERLIN2, ERMN, ERO1L, ETFA, ETFB, EWSR1, EXOG, FABP3, FABP5, FABP7, FAHD1, FAM162A, FAM98B, FAR1, FASN, FBXO2, FDPS, FECH, FHL1, FIS1, FKBP1A, FLNA, FLOT1, FN3KRP, FTH1, FXYD7, G3BP2, GABARAPL2, GABRA1, GAG, GANAB, GAP43, GCDH, GDPD1, GGT7, GIT1, GJA1, GLB1, GLIPR2, GLO1, GLRX5, GLS, GLUL, GMFB, GNAI2, GNAZ, GNB4, GNG2, GNG3, GNG7, GPD1, GPD2, GPHN, GPI, GPX4, GRHPR, GRM3, GRPEL1, GSTM3, GSTP1, H1F0, H2AFY, HADH, HADHA, HADHB, HAPLN1, HAPLN2, HAPLN4, HBA1, HBB, HDLBP, HEPACAM, HIBADH, HIBCH, HINT1, HIST1H1A, HIST1H1E, HLA-A, HMOX2, HNRNPA3, HNRNPH1, HNRNPL, HNRNPU, HNRPA2B1, HOMER1, HPCA, HSD17B12, HSDL2, HSP90AA1,HSPA9, HSPB1, HSPD1, HSPE1, IARS2, IDH1, IDH2, IDH3B, IGHM, IGSF21, IMMT, IPO7, ITIH3, ITPKA, ITSN1, KBTBD11, KCTD12, KIAA0513, KIAA1045, KIAA1217, KIAA1549L, KIF5B, KTN1, L1CAM, L2HGDH, LAMP2, LANCL1, LDHB, LETM1, LGALS3BP, LGI1, LMNB1, LMNB2, LONP1, LPHN1, LRP1, LRPPRC, LRRC47, LY6H, LZTFL1, MACROD1, MAOA, MAOB, MAP1A, MAP1B, MAP1S, MAP2, MAP6D1, MAP7D1, MAPRE2, MAPT, MARCKS, MARCKSL1, MAT2A, MCU, MDH1, MDH2, ME2, ME3, METTL7A, MFF, MFSD4, MGLL, MIF, MLC1, MLF2, MOBP, MOG, MRPL12, MRPL15, MT3, MTCH1, MTCH2, MTDH, MTURN, MUT, MVD, MYH9, MYO5A, NADK2, NAP1L4, NAPB, NCALD, NCAM2, NCEH1, NCKIPSD, NCOA7, NDRG2, NDUFA12, NDUFA13, NDUFA2, NDUFA6, NDUFA7, NDUFA8, NDUFA9, NDUFAF3, NDUFAF7, NDUFB4, NDUFS5, NDUFS6, NDUFS8, NDUFV1, NDUFV2, NECAP1, NEFH, NEFM, NEGR1, NOMO1, NPC2, NPEPPS, NPM1, NRGN, NRXN1, NRXN3, NSFL1C, NT5E, OGDH, OGDHL, OPALIN, OXCT1, PABPC1, PACSIN2, PADI2, PAFAH1B2,

PAM16, PARK7, PBXIP1, PC, PCLO, PCMT1, PCSK1N, PCYOX1, PDIA6, PDK3, PDXK, PGAM1, PGK1, PGM1, PHB2, PHGDH, PHPT1, PHYHIP, PLCB1, PLEC, PLEKHB1, PLIN3, PLXNB2, PMP2, PMPCB, PNP, POR, PPA1, PPFIA3, PPIA, PPIB, PPIF, PPP1R14A, PPP1R1B, PPP2CB, PPP3R1, PPT1, PRDX3, PRKAR2B, PRKCG, PRKRA, PROM1, PRRT2, PSAP, PSMA3, PSMA6, PSMB1, PSPC1, PTGES2, PTK2B, PTPLAD1, PTRH2, PVRL1, QDPR, RAB11B, RAB3GAP2, RAB5A, RAB7A, RANBP1, RAP1B, RCN2, RHOT1, RNH1, RPL13, RPL18, RPL22, RPL7A, RPL8, RPLP1, RPLP2, RPN1, RPS12, RPS16, RPS17L, RPS18, RPS25, RPS3, RPS5, RPS9, RRAS2, S100A1, S100B, SAMM50, SBF1, SCAMP1, SCARB2, SCG2, SCG5, SDCBP, SDHA, SDHB, SEC13, SEPT, SERBP1, SERPINB6, SERPINH1, SETSIP, SFPQ, SGIP1, SH3BP1, SH3GL3, SHANK3, SIRT5, SLC12A5, SLC14A1, SLC17A7, SLC1A3, SLC25A11, SLC25A18, SLC25A22, SLC39A12, SLC44A1, SLC44A2, SLC4A4, SLC6A1, SLC6A11, SLC7A14, SLC7A5, SLC9A3R1, SNCA, SNCB, SNTA1, SNX1, SOD1, SOD2, SORBS1, SORT1, SPTBN2, SRCIN1, STAT3, STK39, STMN1, STOM, STRAP, STX1B, STXBP5L, SUCLA2, SUCLG1, SV2A, SV2B, SVOP, SYNGR1, SYNGR3, SYT1, TAGLN, TAGLN3, TBCB, TCEB2, TFRC, THY1, TIMM50, TIMM9, TINAGL1, TKT, TMEM30A, TMEM65, TMX3, TNC, TNR, TOMM22, TOMM70A, TPI1, TPM1, TPP1, TPPP3, TPT1, TRPV2, TSFM, TUBB2B, UBA1, UBE2N, UGT8, UQCRC2, UQCRFS1, UQCRH, USP5, VAMP1, VARS, VAT1, VAT1L, VCAN, VCL, VGF, VPS26B, VSNL1, WASF1, WASL, XPNPEP1, YARS, YBX1, YWHAQ, ZADH2
107 proteins expressed only in PD and PD models
A2M, ACADL, ACO2, ALDH1A1, ALDH2, ALDH4A1, ALDOC, ANXA6, ANXA7, APOA1, APOA2, APOC3, APOH, APOM, ARHGDIB, ATP5PD, ATP6V1B2, AZGP1, BBOX1, BSCL2, C4B, CALM1, CAMK2D, CANX, CAP1, CCT2, CCT4, CHGB, CLTC, COL4A2, COPS4, CP, CST3, CTSD, DHRS1, DLG2, DST, EIF5A, EPDR1, ERAP1, EZR, FSCN1, GAD1, GC, GDA, GM237, GNAI3, GNAO1, GSTM1, GSTM5, H2AFV, HEBP2, HIST2H3C2, HK1, HLA-DRB1, HNRPAB, HSPA5, HSPA8, INPP1, ITGB1, KIF2A, LGALS3, MARCK2, MPP2, MT-ATP8, NDUFS3, NIT2, NSF, OAT, OMG, ORM1, P4HB, PCP4, PDE10A, PDE1B, PEA15, PFN1, PGM2, PGRMC1, PPP1R9A, PPP2R1A, PRDX6, PREI3, PRKCC, PRNP, PROSC, RAB21, RAB3A, RBP4, RPL3, SAA1, SEC23A, SFRS7, SLC25A5, SLC2A3, SRM, SYN1, SYN2, SYT2, TOLLIP, TPM3, TUBA4A, UCHL1, USP14, VAPB, YWHAE, YWHAZ

Table S3. Gene Ontology (GO) analysis of the differentially expressed proteins that change in the same direction (downregulated, Table 6.12) in human PD proteomic studies.

GO enriched term	Count	Proteins
Biological process		
Retinoid metabolic process	3	RBP4, APOC3, APOM
Cellular component		
Extracellular exosome	13	RTN4, PTGES3, RBP4, LGALS3, EPDR1, C3, ERP29, STXBP1, PKM, SAA1, APOC3, APOM, GAPDH
Extracellular region	7	RBP4, EPDR1, SAA1, C3, APOC3, NCAN, APOM
Extracellular space	5	RBP4, LGALS3, SAA1, C3, APOC3
Extracellular matrix	3	PKM, LGALS3, GAPDH

Table S4. Gene Ontology (GO) analysis of the differentially expressed proteins that change in the same direction (upregulated, Table 6.13) in human PD proteomic studies.

GO enriched term	Count	Proteins
Cellular component		
Extracellular exosome	12	LAP3, PFN1, TTR, CACNA2D1, EZR, AK1, VIM, ERAP1, ITGB1, BBOX1, FTL, ARHGDIB
Cytosol	9	PFN1, PEA15, EZR, AK1, VIM, ERAP1, BBOX1, FTL, ARHGDIB
Cytoplasm	9	LAP3, PFN1, TTR, EZR, AK1, VIM, ITGB1, FTL, ARHGDIB
Membrane	6	PFN1, EZR, ERAP1, ITGB1, FTL, ARHGDIB
Focal adhesion	5	LAP3, PFN1, EZR, VIM, ITGB1
Cytoskeleton	4	PFN1, EZR, VIM, ARHGDIB
Molecular function		
Identical protein binding	4	TTR, VIM, BBOX1, FTL
Actin binding	3	PFN1, EZR, ITGB1
Cadherin binding involved in cell-cell adhesion	3	PFN1, EZR, ITGB1

Table S5. Gene Ontology (GO) and KEGG pathway analyses of the differentially expressed proteins that change in the same direction (downregulated, Table 6.15) in PD models proteomic studies.

GO enriched term	Count	Proteins
Biological process		
Neurotransmitter secretion	4	RAB3A, STX1A, SYT2, SNAP25
Regulation of exocytosis	3	STX1A, NSF, RAB21
Glutamate secretion	3	RAB3A, STX1A, SNAP25
Protein targeting	3	YWHAZ, AKAP5, YWHAE
Regulation of insulin secretion	3	STX1A, SLC25A5, SNAP25
Vesicle-mediated transport	3	STX1A, CLTC, NSF
Cellular component		
Extracellular exosome	22	PPP2R1A, COL4A2, YWHAZ, ATP5J2, GNAI3, SLC25A5, PHB, CST3, ECHS1, PROSC, CLTC, YWHAE, PDHB, TPM3, ALDH1A1, ANXA6, PGM2, IGSF8, SLC2A3, CAP1, NSF, RAB21
Cytosol	18	INPP1, PPP2R1A, RAB3A, YWHAZ, STX1A, NCDN, PDE10A, CLTC, YWHAE, SIRT2, TPM3, PGM2, ALDH1A1, PPP1R9A, PCP4, AKAP5, SNAP25, NSF
Plasma membrane	15	RAB3A, STX1A, GNAI3, PHB, SYT2, GPM6B, CLTC, SIRT2, IGSF8, SLC2A3, AKAP5, CAP1, OMG, SNAP25, NSF
Membrane	13	ANXA6, PPP2R1A, RAB3A, IGSF8, GNAI3, NCDN, SLC25A5, SYT2, PHB, PDE10A, CLTC, SNAP25, YWHAE
Mitochondrion	12	ANXA6, PPP2R1A, YWHAZ, SLC25A5, PHB, ALDH4A1, ECHS1, PROSC, CLTC, YWHAE, NDUFS2, PDHB
Myelin sheath	6	SLC25A5, PHB, CLTC, SNAP25, NSF, SIRT2
Focal adhesion	6	ANXA6, YWHAZ, CAP1, CLTC, YWHAE, RAB21
Mitochondrial matrix	5	NDUFS7, ALDH4A1, ECHS1, NDUFS2, PDHB
Synaptic vesicle	4	RAB3A, STX1A, SYT2, SNAP25
Melanosome	4	ANXA6, YWHAZ, CLTC, YWHAE
Axon	4	RAB3A, NCDN, CST3, YWHAE
Neuronal cell body	4	NDUFS7, PPP1R9A, NCDN, CST3
Cytoplasmic vesicle membrane	3	YWHAZ, YWHAE, RAB21
Molecular function		
Protein binding	29	RAB3A, YWHAZ, GNAI3, VAPB, SYT2, ECHS1, CLTC, PDHB, TPM3, NDUFS7, ANXA6, PCP4, NDUFS2, SNAP25, NSF, RAB21, PPP2R1A, STX1A, COL4A2, NCDN, SLC25A5, PHB, CST3, YWHAE, SIRT2, PGM2, PPP1R9A, IGSF8, AKAP5
Protein domain specific binding	5	PPP1R9A, STX1A, YWHAZ, GNAI3, YWHAE
Ubiquitin protein ligase binding	4	YWHAZ, SLC25A5, YWHAE, NDUFS2

Protein kinase binding	4	PPP1R9A, YWHAZ, CLTC, NSF
GTP binding	4	ANXA6, RAB3A, GNAI3, RAB21
Calcium-dependent protein binding	3	ANXA6, STX1A, SNAP25
Histone deacetylase binding	3	PHB, YWHAE, SIRT2
Ion channel binding	3	PPP1R9A, STX1A, YWHAE

KEGG enriched pathway	Count	Proteins
Metabolic pathways	9	ALDH1A1, INPP1, PGM2, NDUFS7, ATP5J2, ALDH4A1, ECHS1, NDUFS2, PDHB
Synaptic vesicle cycle	5	RAB3A, STX1A, CLTC, SNAP25, NSF
Parkinson's disease	4	NDUFS7, GNAI3, SLC25A5, NDUFS2
Huntington's disease	4	NDUFS7, SLC25A5, CLTC, NDUFS2
Insulin secretion	3	RAB3A, STX1A, SNAP25
Oocyte meiosis	3	PPP2R1A, YWHAZ, YWHAE

Table S6. Gene Ontology (GO) and KEGG pathway analyses of the differentially expressed proteins that change in the same direction (upregulated, Table 6.16) in PD models proteomic studies.

GO enriched term	Count	Proteins
Biological process		
Epithelial cell differentiation	4	ANXA7, TOLLIP, ALDOC, VDAC1
Antigen processing and presentation of exogenous peptide antigen via MHC class II	3	CLTA, CTSD, KIF2A
Autophagy	3	ANXA7, TOLLIP, CTSD
Protein folding	3	CCT4, PDIA3, CCT2
Cellular component		
Extracellular exosome	20	GDA, ALDH1L1, PDIA3, NIT2, TOLLIP, ALDOC, COPS4, VIM, ADH5, CCT2, EEF2, ANXA5, VDAC1, CKB, ANXA7, CCT4, H2AFV, CTSD, DST, USP14
Cytosol	18	GDA, CLTA, ALDH1L1, SRM, TOLLIP, ALDOC, COPS4, VIM, ADH5, HK1, CCT2, EEF2, CKB, ANXA7, CCT4, DST, EHD3, KIF2A
Mitochondrion	9	ALDH1L1, NIT2, IVD, ALDOC, DLD, ADH5, HK1, VDAC1, CKB
Myelin sheath	7	PDIA3, SYN2, DLD, CCT2, EHD3, VDAC1, CKB
Focal adhesion	5	PDIA3, VIM, ANXA5, DST, EHD3
Membrane raft	4	HK1, CTSD, EEF2, VDAC1
Extracellular matrix	4	VIM, CTSD, CCT2, EEF2
Synaptic vesicle	3	SYN2, COPS4, VDAC1
Melanosome	3	CCT4, PDIA3, CTSD
Cytoplasmic, membrane-bounded vesicle	3	CLTA, DST, USP14
Molecular function		

Protein binding	21	CLTA, SRM, PDIA3, TOLLIP, ALDOC, COPS4, VIM, HK1, CCT2, EEF2, ANXA5, VDAC1, CKB, DHRS1, ANXA7, CCT4, CTSD, DST, USP14, EHD3, KIF2A
ATP binding	7	CCT4, SYN2, HK1, CCT2, EHD3, KIF2A, CKB
Cysteine-type endopeptidase activity	3	PDIA3, CTSD, USP14
Oxidoreductase activity	3	DHRS1, ALDH1L1, ADH5

KEGG enriched pathway	Count	Proteins
Metabolic pathways	8	GDA, SRM, IVD, ALDOC, DLD, ADH5, HK1, CKB
Glycolysis / Gluconeogenesis	4	ALDOC, DLD, ADH5, HK1
Carbon metabolism	4	ALDOC, DLD, ADH5, HK1
Biosynthesis of antibiotics	4	ALDOC, DLD, ADH5, HK1

Table S7. Gene Ontology (GO) analysis of the commonly differentially expressed proteins in human PD and PD models proteomic studies (Table S1 of this Annex)

GO enriched term	Count	Proteins
Cellular component		
Extracellular exosome	4	ALDH1A1, VIM, EEF2, GAPDH
Cytosol	4	ALDH1A1, VIM, EEF2, GAPDH
Cytoplasm	4	ALDH1A1, VIM, EEF2, GAPDH
Extracellular matrix	3	VIM, EEF2, GAPDH

Table S8. Gene Ontology (GO) and KEGG enriched pathway analyses of the commonly differentially expressed proteins in PD and the ageing nervous system proteomic studies (Table S2 of this Annex).

GO enriched term	Count	Proteins
Biological process		
Substantia nigra development	7	INA, PLP1, GLUD1, CNP, SIRT2, MBP, CKB
Oxidation-reduction process	7	NDUFS7, UQCRC1, ALDH1L1, PDIA3, GLUD1, GSTO1, NDUFA10
Platelet degranulation	6	ALDOA, TF, TLN1, ALB, CLU, STXBP1
Chemical synaptic transmission	2	PLP1, AKAP5, CNP, SNAP25, MBP
Positive regulation of gene expression	2	PLP1, GSN, PHB, VIM, ERP29
Canonical glycolysis	4	ALDOA, PKM, ENO2, GAPDH
Gluconeogenesis	4	ALDOA, GOT1, ENO2, GAPDH
ATP biosynthetic process	4	ALDOA, PKM, ATP5J2, ATP5B
Mitochondrial electron transport, NADH to ubiquinone	4	NDUFS7, DLD, NDUFA10, NDUFS2
Neurotransmitter secretion	4	SLC32A1, STX1A, STXBP1, SNAP25

Movement of cell or subcellular component	4	IGSF8, TLN1, CAPZA2, VIM
Protein stabilization	4	PHB, CLU, STXBP1, GAPDH
Aging	4	SLC32A1, DLD, CNP, EEF2
Intermediate filament organization	3	GFAP, VIM, NEFL
Astrocyte development	3	GFAP, PLP1, VIM
Mitochondrial ATP synthesis coupled proton transport	3	ATP5J2, ATP5B, CYC1
Glutamate secretion	3	STX1A, STXBP1, SNAP25
ATP metabolic process	3	VCP, AK1, ATP5B
Glycolytic process	3	ALDOA, ENO2, GAPDH
Mitochondrial respiratory chain complex I assembly	3	NDUFS7, NDUFA10, NDUFS2
Positive regulation of proteasomal ubiquitin-dependent protein catabolic process	3	VCP, CLU, SIRT2
Glucose metabolic process	3	ALDH5A1, GAPDH, PDHB
Cellular oxidant detoxification	3	ALB, HP, GSTO1
Microtubule cytoskeleton organization	3	CNP, NEFL, GAPDH
Response to toxic substance	3	CNP, NEFL, MBP
Cellular component		
Extracellular exosome	43	RTN4, ALDOA, PTGES3, TF, TLN1, ALDH1L1, PDIA3, C3, ATP5B, CAPZA2, VIM, CLU, ADH5, ECHS1, HP, CNP, CALB1, PDHB, CKB, PKM, TTR, GOT1, GSN, ALB, ENO2, GSTO1, GAPDH, FTL, CACNA2D1, ATP5J2, AK1, PHB, ERP29, ANXA1, STXBP1, EEF2, ANXA5, VDAC1, LAP3, IGSF8, VCP, NUTF2, UGGT1
Cytosol	31	ALDOA, PTGES3, TLN1, CLTA, GFAP, ALDH1L1, CAPZA2, VIM, CLU, ADH5, CALB1, CKB, PKM, GOT1, GSN, ENO2, GSTO1, SNAP25, GAPDH, NEFL, EHD3, FTL, STX1A, NCDN, AK1, STXBP1, EEF2, SIRT2, VCP, AKAP5, NUTF2
Cytoplasm	30	PTGES3, TLN1, GFAP, ALDH1L1, GLUD1, VIM, CLU, CNP, CKB, PKM, TTR, GOT1, GSN, GSTO1, SNAP25, GAPDH, NEFL, EHD3, FTL, AK1, EEF1A2, PHB, ANXA1, STXBP1, EEF2, ANXA5, SIRT2, LAP3, TUBA8, VCP
Plasma membrane	27	RTN4, TLN1, CLTA, C3, ATP5B, VIM, GPM6B, CNP, MBP, PKM, SLC32A1, GSN, ENO2, GAPDH, SNAP25, CACNA2D1, PLP1, STX1A, PHB, AK1, ANXA1, STXBP1, EEF2, SIRT2, VDAC1, IGSF8, AKAP5
Myelin sheath	21	INA, GFAP, PLP1, UQCRC1, PDIA3, PHB, EEF1A2, ATP5B, STXBP1, NDUFA10, SIRT2, VDAC1, CKB, PKM, VCP, ALB, DLD, ENO2, SNAP25, NEFL, EHD3

Mitochondrion	20	ALDH1L1, UQCRC1, ALDH5A1, PHB, GLUD1, ATP5B, CYC1, CLU, STXBP1, ADH5, ECHS1, PDHB, VDAC1, CKB, LAP3, PKM, GOT1, IVD, DLD, NDUFS2
Membrane	16	ALDOA, CLTA, NCDN, ATP5B, CAPZA2, PHB, ERP29, CYC1, CNP, EEF2, ANXA5, VDAC1, IGSF8, SNAP25, GAPDH, FTL
Extracellular space	13	ALDOA, INA, TF, C3, CLU, ANXA1, CNP, HP, CKB, TTR, GSN, ALB, ENO2
Extracellular region	13	ALDOA, TF, TTR, TLN1, STX1A, ALB, C3, GSN, CAPZA2, CLU, ANXA1, HP, NCAN
Mitochondrial matrix	10	NDUFS7, ALDH5A1, IVD, ATP5B, GLUD1, DLD, ECHS1, NDUFA10, NDUFS2, PDHB
Mitochondrial inner membrane	9	NDUFS7, ATP5J2, UQCRC1, ATP5B, PHB, CYC1, CNP, NDUFA10, VDAC1
Focal adhesion	8	LAP3, TLN1, PDIA3, GSN, VIM, ANXA1, ANXA5, EHD3
Cell surface	8	TF, TLN1, PDIA3, ATP5B, PHB, ERP29, CLU, ANXA1
Perinuclear region of cytoplasm	8	TF, VCP, CLU, CNP, SNAP25, GAPDH, EHD3, SIRT2
Blood microparticle	6	TF, ALB, C3, GSN, CLU, HP
Extracellular matrix	6	PKM, ATP5B, VIM, CLU, EEF2, GAPDH
Cell-cell adherens junction	6	ALDOA, PKM, RTN4, TLN1, ANXA1, EEF2
Vesicle	5	PKM, TF, ANXA1, SNAP25, GAPDH
Neuron projection	5	SLC32A1, NDUFS7, STX1A, VIM, SNAP25
Neuronal cell body	5	NDUFS7, NCDN, EEF1A2, CALB1, MBP
Protein complex	5	TTR, ALB, CLU, ANXA1, STXBP1
Mitochondrial membrane	4	IVD, ATP5B, CLU, ANXA1
Mitochondrial respiratory chain complex I	3	NDUFS7, NDUFA10, NDUFS2
Intermediate filament cytoskeleton	3	INA, GFAP, VIM
Platelet alpha granule lumen	3	ALDOA, ALB, CLU
Synaptic vesicle	3	STX1A, SNAP25, VDAC1
Melanosome	3	PDIA3, ERP29, CNP
Growth cone	3	NEFL, SNAP25, SIRT2
Molecular function		
Protein binding	49	PTGES3, RTN4, GFAP, CLTA, TLN1, PDIA3, ATP5B, HP, RTN1, CALB1, PDHB, MBP, CKB, NDUFS7, PKM, TTR, GSN, NDUFS2, FTL, STX1A, STXBP1, EEF2, IGSF8, AKAP5, UGGT1, ALDOA, TF, C3, GLUD1, CLU, VIM, ECHS1, ALB, ENO2, GSTO1, GAPDH, NEFL, SNAP25, EHD3, PLP1, NCDN, PHB, EEF1A2, ANXA1, ANXA5, SIRT2, VDAC1, VCP, NUTF2
Identical protein binding	12	ALDOA, TTR, GFAP, GOT1, VCP, ALB, GLUD1, VIM, STXBP1, NEFL, GAPDH, FTL
Structural constituent of cytoskeleton	6	INA, GFAP, TLN1, TUBA8, VIM, NEFL
Structural molecule activity	6	GFAP, PLP1, CLTA, VIM, ANXA1, NEFL
Cadherin binding involved in cell-cell adhesion	6	ALDOA, PKM, RTN4, TLN1, ANXA1, EEF2

Protein domain specific binding	5	STX1A, VCP, GSN, STXBP1, NEFL
Ubiquitin protein ligase binding	5	UQCRC1, VCP, CLU, NDUFS2, CKB
ATPase activity	4	ATP5J2, VCP, ATP5B, CLU
Oxidoreductase activity, acting on the aldehyde or oxo group of donors, NAD or NADP as acceptor	3	ALDH1L1, ALDH5A1, GAPDH
ADP binding	3	PKM, VCP, GLUD1
NAD binding	3	DLD, GAPDH, NDUFS2
NADH dehydrogenase (ubiquinone) activity	3	NDUFS7, NDUFA10, NDUFS2
Calcium-dependent protein binding	3	STX1A, ANXA1, SNAP25
Glycoprotein binding	3	GFAP, STX1A, VIM
Protein binding, bridging	3	STX1A, ANXA1, NEFL
Chaperone binding	3	ALB, ERP29, CLU

KEGG enriched pathway	Count	Proteins
Metabolic pathways	23	ALDOA, PTGES3, ATP5J2, UQCRC1, ALDH5A1, GLUD1, AK1, ATP5B, CYC1, ADH5, ECHS1, NDUFA10, PDHB, CKB, NDUFS7, LAP3, PKM, GOT1, IVD, DLD, ENO2, GAPDH, NDUFS2
Carbon metabolism	10	ALDOA, PKM, GOT1, GLUD1, DLD, ENO2, ADH5, ECHS1, GAPDH, PDHB
Biosynthesis of antibiotics	10	ALDOA, PKM, GOT1, AK1, DLD, ENO2, ADH5, ECHS1, GAPDH, PDHB
Huntington's disease	8	NDUFS7, CLTA, UQCRC1, ATP5B, CYC1, NDUFA10, NDUFS2, VDAC1
Glycolysis / Gluconeogenesis	7	ALDOA, PKM, DLD, ENO2, ADH5, GAPDH, PDHB
Oxidative phosphorylation	7	NDUFS7, ATP5J2, UQCRC1, ATP5B, CYC1, NDUFA10, NDUFS2
Parkinson's disease	7	NDUFS7, UQCRC1, ATP5B, CYC1, NDUFA10, NDUFS2, VDAC1
Alzheimer's disease	7	NDUFS7, UQCRC1, ATP5B, CYC1, NDUFA10, GAPDH, NDUFS2
Synaptic vesicle cycle	5	SLC32A1, CLTA, STX1A, STXBP1, SNAP25
Biosynthesis of amino acids	5	ALDOA, PKM, GOT1, ENO2, GAPDH
Non-alcoholic fatty liver disease (NAFLD)	5	NDUFS7, UQCRC1, CYC1, NDUFA10, NDUFS2
HIF-1 signaling pathway	4	TF, ENO2, GAPDH, PDHB
Alanine, aspartate and glutamate metabolism	3	GOT1, ALDH5A1, GLUD1
Pyruvate metabolism	3	PKM, DLD, PDHB
Valine, leucine and isoleucine degradation	3	IVD, DLD, ECHS1
Arginine and proline metabolism	3	LAP3, GOT1, CKB

References used for the comparison analysis of the PD nervous system (these references appear in the main reference section, but appear here for easy consultation of the data)

PD in humans:

[1] Bereczki E, Branca RM, Francis PT, Pereira JB, Baek JH, Hortobágyi T, Winblad B, Ballard C, Lehtiö J, Aarsland D. Synaptic markers of cognitive decline in neurodegenerative diseases: a proteomic approach. Brain. 2018 Jan 9;141(2):582-95.

[2] van Dijk KD, Berendse HW, Drukarch B, Fratantoni SA, Pham TV, Piersma SR, Huisman E, Brevé JJ, Groenewegen HJ, Jimenez CR, van de Berg WD. The proteome of the locus ceruleus in Parkinson's disease: relevance to pathogenesis. Brain Pathology. 2012 Jul 1;22(4):485-98.

[3] Licker V, Turck N, Kövari E, Burkhardt K, Côte M, Surini-Demiri M, Lobrinus JA, Sanchez JC, Burkhard PR. Proteomic analysis of human substantia nigra identifies novel candidates involved in P arkinson's disease pathogenesis. Proteomics. 2014 Mar;14(6):784-94

[4] Boerger M, Funke S, Leha A, Roser AE, Wuestemann AK, Maass F, Bähr M, Grus F, Lingor P. Proteomic analysis of tear fluid reveals disease-specific patterns in patients with Parkinson's disease–A pilot study. Parkinsonism & related disorders. 2019 Mar 6.

[5] Lachén-Montes M, González-Morales A, Iloro I, Elortza F, Ferrer I, Gveric D, Fernández-Irigoyen J, Santamaría E. Unveiling the olfactory proteostatic disarrangement in Parkinson's disease by proteome-wide profiling. Neurobiology of aging. 2019 Jan 1;73:123-34.

[6] Kitamura Y, Kojima M, Kurosawa T, Sasaki R, Ichihara S, Hiraku Y, Tomimoto H, Murata M, Oikawa S. Proteomic profiling of exosomal proteins for blood-based biomarkers in Parkinson's disease. Neuroscience. 2018 Nov 10;392:121-8.

[7] Magdalinou NK, Noyce AJ, Pinto R, Lindstrom E, Holmén-Larsson J, Holtta M, Blennow K, Morris HR, Skillbäck T, Warner TT, Lees AJ. Identification of candidate cerebrospinal fluid biomarkers in parkinsonism using quantitative proteomics. Parkinsonism & related disorders. 2017 Apr 1;37:65-71.

[8] Klettner A, Tholey A, Wiegandt A, Richert E, Nölle B, Deuschl G, Roider J, Schneider SA. Reduction of GAPDH in lenses of Parkinson's disease patients: A possible new biomarker. Movement Disorders. 2017 Mar 1;32(3):459-62.

[9] Chiu CC, Yeh TH, Lai SC, Weng YH, Huang YC, Cheng YC, Chen RS, Huang YZ, Hung J, Chen CC, Lin WY. Increased Rab35 expression is a potential biomarker and implicated in the pathogenesis of Parkinson's disease. Oncotarget. 2016 Aug 23;7(34):54215.

[10] Xing L, Wang D, Wang L, Lan W, Pan S. Differential proteomics analysis of mononuclear cells in cerebrospinal fluid of Parkinson's disease. International journal of clinical and experimental pathology. 2015;8(11):15462.

[11] Dumitriu A, Golji J, Labadorf AT, Gao B, Beach TG, Myers RH, Longo KA, Latourelle JC. Integrative analyses of proteomics and RNA transcriptomics implicate mitochondrial processes, protein folding pathways and GWAS loci in Parkinson disease. BMC medical genomics. 2015 Dec;9(1):5.

[12] Liu Y, Zhou Q, Tang M, Fu N, Shao W, Zhang S, Yin Y, Zeng R, Wang X, Hu G, Zhou J. Upregulation of alphaB-crystallin expression in the substantia nigra of patients with Parkinson's disease. Neurobiology of aging. 2015 Apr 1;36(4):1686-91.

[13] Wang S, Kojima K, Mobley JA, West AB. Proteomic analysis of urinary extracellular vesicles reveal biomarkers for neurologic disease. EBioMedicine. 2019 Jun 20.

[14] Donega V, Burm SM, van Strien ME, van Bodegraven EJ, Paliukhovich I, Geut H, van de Berg WD, Li KW, Smit AB, Basak O, Hol EM. Transcriptome and proteome profiling of neural stem cells from the human subventricular zone in Parkinson's disease. Acta neuropathologica communications. 2019 Dec;7(1):4.

[15] Alberio T, Pippione AC, Zibetti M, Olgiati S, Cecconi D, Comi C, Lopiano L, Fasano M. Discovery and verification of panels of T-lymphocyte proteins as biomarkers of Parkinson's disease. Scientific reports. 2012 Dec 11; 2:953.

[16] Licker V, Côte M, Lobrinus JA, Rodrigo N, Kövari E, Hochstrasser DF, Turck N, Sanchez JC, Burkhard PR. Proteomic profiling of the substantia nigra demonstrates CNDP2 overexpression in Parkinson's disease. Journal of proteomics. 2012 Aug 3;75(15):4656-67.

[17] Zhang X, Yin X, Yu H, Liu X, Yang F, Yao J, Jin H, Yang P. Quantitative proteomic analysis of serum proteins in patients with Parkinson's disease using an isobaric tag for relative and absolute quantification labeling, two-dimensional liquid chromatography, and tandem mass spectrometry. Analyst. 2012;137(2):490-5.

[18] Zhao X, Xiao WZ, Pu XP, Zhong LJ. Proteome analysis of the sera from Chinese Parkinson's disease patients. Neuroscience letters. 2010 Jul 26;479(2):175-9.

[19] Sinha A, Srivastava N, Singh S, Singh AK, Bhushan S, Shukla R, Singh MP. Identification of differentially displayed proteins in cerebrospinal fluid of Parkinson's disease patients: a proteomic approach. Clinica chimica acta. 2009 Feb 1;400(1-2):14-20.

[20] Werner CJ, Heyny-von Haussen R, Mall G, Wolf S. Proteome analysis of human substantia nigra in Parkinson's disease. Proteome science. 2008 Dec;6(1):8.

[21] Abdi F, Quinn JF, Jankovic J, McIntosh M, Leverenz JB, Peskind E, Nixon R, Nutt J, Chung K, Zabetian C, Samii A. Detection of biomarkers with a multiplex quantitative proteomic platform in cerebrospinal fluid of patients with neurodegenerative disorders. Journal of Alzheimer's Disease. 2006 Jan 1;9(3):293-348.

[22] Basso M, Giraudo S, Corpillo D, Bergamasco B, Lopiano L, Fasano M. Proteome analysis of human substantia nigra in Parkinson's disease. Proteomics. 2004 Dec;4(12):3943-52.

[23] Choi J, Levey AI, Weintraub ST, Rees HD, Gearing M, Chin LS, Li L. Oxidative modifications and down-regulation of ubiquitin carboxyl-terminal hydrolase L1 associated with idiopathic Parkinson's and Alzheimer's diseases. Journal of Biological Chemistry. 2004 Mar 26;279(13):13256-64.

[24] Jin J, Hulette C, Wang Y, Zhang T, Pan C, Wadhwa R, Zhang J. Proteomic identification of a stress protein, mortalin/mthsp70/GRP75: relevance to Parkinson disease. Molecular & Cellular Proteomics. 2006 Jul 1;5(7):1193-204.

PD models in other mammals:

[1] Triplett JC, Zhang Z, Sultana R, Cai J, Klein JB, Büeler H, Butterfield DA. Quantitative expression proteomics and phosphoproteomics profile of brain from PINK1 knockout mice: insights into mechanisms of familial Parkinson's disease. Journal of neurochemistry. 2015 Jun 1;133(5):750-65.

[2] [3] [4] Kim H, Kang H, Lee Y, Park CH, Jo A, Khang R, Shin JH. Identification of transketolase as a target of PARIS in substantia nigra. Biochemical and biophysical research communications. 2017 Nov 18;493(2):1050-6.

[5] Maasz G, Zrinyi Z, Reglodi D, Petrovics D, Rivnyak A, Kiss T, Jungling A, Tamas A, Pirger Z. Pituitary adenylate cyclase-activating polypeptide (PACAP) has a neuroprotective function in dopamine-based neurodegeneration in rat and snail parkinsonian models. Disease models & mechanisms. 2017 Feb 1;10(2):127-39.

[6] Stauch KL, Villeneuve LM, Purnell PR, Ottemann BM, Emanuel K, Fox HS. Loss of Pink1 modulates synaptic mitochondrial bioenergetics in the rat striatum prior to motor symptoms: concomitant complex I respiratory defects and increased complex II-mediated respiration. PROTEOMICS-Clinical Applications. 2016 Dec 1;10(12):1205-17.

[7] Kuter K, Kratochwil M, Marx SH, Hartwig S, Lehr S, Sugawa MD, Dencher NA. Native DIGE proteomic analysis of mitochondria from substantia nigra and striatum during neuronal degeneration and its compensation in an animal model of early Parkinson's disease. Archives of physiology and biochemistry. 2016 Oct 19;122(5):238-56.

[8] Xiong Y, Zhang Y, Iqbal J, Ke M, Wang Y, Li Y, Qing H, Deng Y. Differential expression of synaptic proteins in unilateral 6-OHDA lesioned rat model—A comparative proteomics approach. Proteomics. 2014 Aug;14(15):1808-19.

[9] Fuller HR, Hurtado ML, Wishart TM, Gates MA. The rat striatum responds to nigro-striatal degeneration via the increased expression of proteins associated with growth and regeneration of neuronal circuitry. Proteome science. 2014 Dec;12(1):20.

[10] Lessner G, Schmitt O, Haas SJ, Mikkat S, Kreutzer M, Wree A, Glocker MO. Differential proteome of the striatum from hemiparkinsonian rats displays vivid structural remodeling processes. Journal of proteome research. 2010 Aug 16;9(9):4671-87.

[11] Jeon S, Kim YJ, Kim ST, Moon W, Chae Y, Kang M, Chung MY, Lee H, Hong MS, Chung JH, Joh TH. Proteomic analysis of the neuroprotective mechanisms of acupuncture treatment in a Parkinson's disease mouse model. Proteomics. 2008 Nov;8(22):4822-32.

[12] Scholz B, Svensson M, Alm H, Sköld K, Fälth M, Kultima K, Guigoni C, Doudnikoff E, Li Q, Crossman AR, Bezard E. Striatal proteomic analysis suggests that first L-dopa dose equates to chronic exposure. PLoS One. 2008 Feb 13;3(2):e1589.

[13] [14] Chin MH, Qian WJ, Wang H, Petyuk VA, Bloom JS, Sforza DM, Lacan G, Liu D, Khan AH, Cantor RM, Bigelow DJ. Mitochondrial dysfunction, oxidative stress, and apoptosis revealed by proteomic and transcriptomic analyses of the striata in two mouse models of Parkinson's disease. Journal of proteome research. 2008 Jan 4;7(2):666-77.

[15] Patel S, Sinha A, Singh MP. Identification of differentially expressed proteins in striatum of maneb-and paraquat-induced Parkinson's disease phenotype in mouse. Neurotoxicology and teratology. 2007 Sep 1;29(5):578-85.

[16] Pierson J, Norris JL, Aerni HR, Svenningsson P, Caprioli RM, Andrén PE. Molecular profiling of experimental Parkinson's disease: direct analysis of peptides and proteins on brain tissue sections by MALDI mass spectrometry. Journal of proteome research. 2004 Apr 12;3(2):289-95.